COVALENT & SUPRAMOLECULAR PHOSPHORUS LIGANDS FOR LINEAR-SELECTIVE HYDROFORMYLATIONS

Andrés Romero Navarro

UNIVERSITAT ROVIRA i VIRGILI

Covalent & Supramolecular Phosphorus Ligands for Linear-Selective Hydroformylations

---

Andrés Romero Navarro

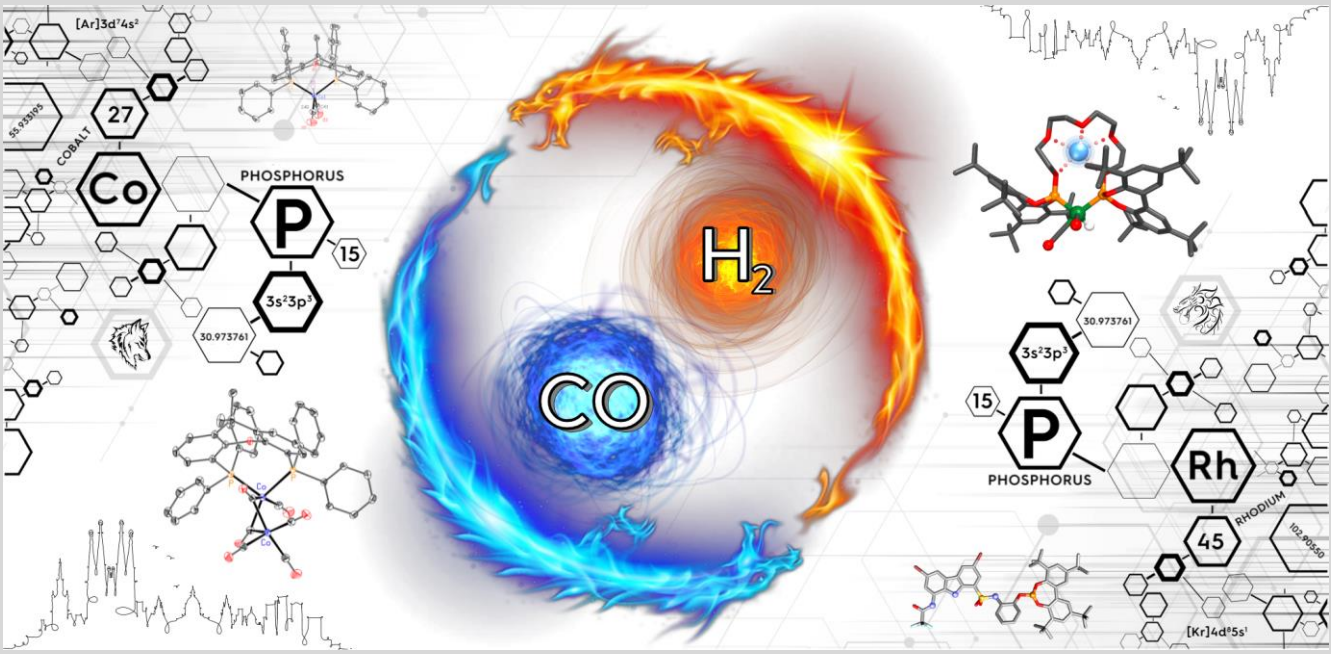

DOCTORAL THESIS

2023

Andrés Romero Navarro

Covalent & Supramolecular Phosphorus Ligands for Linear-Selective Hydroformylations

Doctoral Thesis

Supervised by Prof. Dr. Anton Vidal Ferran

Institut Català d'Investigació Química (ICIQ)

Tarragona 2023

ICIQ
Institute of Chemical Research of Catalonia

UNIVERSITAT ROVIRA i VIRGILI
Dept. de Química Analítica i Química Orgànica

Prof. Dr. Anton Vidal i Ferran, former Group Leader of the Institute of Chemical Research of Catalonia (ICIQ) and Research Professor of the Catalan Institution for Research and Advance Studies (ICREA).

I STATE that the present Doctoral Thesis entitled: "**Covalent & Supramolecular Phosphorus Ligands for Linear-Selective Hydroformylations**", that Andrés Romero Navarro presents to obtain the PhD degree in chemistry, has been carried out under my supervision, in the corresponding research group at the Institute of Chemical Research of Catalonia (ICIQ).

Tarragona, 4th of May 2023.

PhD Thesis Supervisor

Prof. Dr. Anton Vidal i Ferran

II

ACKNOWLEDGEMENTS

La principal persona a la que va dedicada aquesta tesi doctoral és al meu supervisor, el **Prof. Anton Vidal i Ferran**. Moltes gràcies per donar-me l´oportunitat de fer la tesi al teu grup de recerca, on he après i madurat científicament gràcies a tu. Ha sigut un plaer treballar amb tu colze a colze durant tots aquest anys. Gràcies per apostar per mi des del principi i per la paciència en la meva formació com a doctor en química.

Vull agrair també a l´Institut Català d`Investigació Química (ICIQ). Ha sigut un honor treballar en un centre de recerca tant important a nivell nacional e internacional. Gràcies per tractar-me tant bé a nivell personal, especialment després del meu accident del 2018 on em vau fer sentir una seguretat laboral la qual agraeixo molt. Agradecer a **Israel** y **Kerman** por siempre brindarme su ayuda y soporte con los estudios de RMN realizados en esta tesis. Siempre agradeceré el amable mensaje que me escribisteis cuando estaba en el hospital después de sufrir el accidente para saber cómo estaba y darme vuestro apoyo. A la **Noelia**, gràcies per els teus bons consells i suport durant tots aquest anys. A la Facultat de Química de la Universitat de Barcelona, la meva *alma mater*, gràcies per la vostra hospitalitat i ha sigut un honor acabar la meva tesi a un lloc que sento com si fos casa meva. És pot dir que ha sigut un principi i final de la meva tesi ideal.

En mi opinión, el logro de una tesis doctoral depende en gran medida del grupo de trabajo que compartes día a día en el laboratorio. Cada una de las presentes personas me han aportado su experiencia científica y sobre todo su apoyo a lo largo de estos años. **Héctor F.**, lo que más te agradezco es que siempre que acudía para hablar contigo de química, siempre tenías tiempo a pesar de la cantidad de trabajo que tenías. Los principios fueron duros y tú siempre estuviste ahí para echarme una mano. Ha sido un placer trabajar contigo pucelano y una suerte haber podido aprender de ti. **Rajesh**, even after only six months of working together, it was clear to see how genuine you are as a person and as a scientist. **Lucas**, gràcies per acollir-me tant be al grup, ha sigut un plaer poder treballar amb tu dia a dia. Ets una de les persones més intel·ligents que he conegut i de la que he après més, tant de química com de la vida. Sempre he admirat la teva habilitat d'entendre qualsevol tema de química i ràpidament fer preguntes o raonaments tant intel·ligents. També he rigut molt amb tu amb les teves bromes o curiositats de la vida. Compartir el dia a dia en el laboratori amb tu ha sigut una de les millors experiències d'aquests anys. **Alicia**, mi mentora en el campo de la hidroformilación, gracias por enseñarme todos tus conocimientos y tener la paciencia de enseñarme. Ha sido un placer haber trabajado en el mismo campo, donde siempre has tenido tiempo para discutir resultados. **Ester**, siempre te

consideraré como una hermana mayor, eres una de las personas más buenas y sensibles que he conocido. Gracias por protegerme y animarme cuando más lo necesitaba. **Juanjo**, has sido un pilar muy importante durante estos años de tesis y un amigo el cual me llevo para toda la vida. Has sido de los mejores compañeros de laboratorio que he tenido, el cual siempre ha estado para apoyarme tanto científicamente como personalmente. **Paula**, gracias a ti también por la ayuda de los primeros años en el ICIQ y posteriores en la UB con el trabajo administrativo. **Arnald**, qui em diria quan em vas donar classe de Química Bàsica II que acabaria treballant amb tu durant els últims anys de la meva tesi. Ha sigut un plaer treballar amb tu, sempre amb un somriure per donar un cop de mà, no canviïs mai! Espero que quan et faci alguna visita a la facultat hi hagi una foto meva al sistema de pressurització que vaig instal·lar. **Guti**, gràcies per la teva feina de punxar mostres al cromatògraf de gasos. T'he donat moltes mostres a analitzar i hi havia dies que et tornava boig. T'agreixo molt la teva ajuda durant aquest anys i la teva bona predisposició en ajudar-me en tot el que et demanava. **Dani**, también ha sido un placer trabajar contigo, siempre dispuesto a ayudar cuando se te necesitaba y de la que he aprendido mucho de sistemas de alta presión. **José Luis**, "JLo" para los amigos, eres la persona más curiosa y perfeccionista que he conocido y que vive de su profesión con una pasión increíble. He aprendido mucho de tu experiencia, de que la seguridad en el laboratorio es esencial. Eres un ejemplo de profesionalidad como químico, tanto en el laboratorio como en la parte docente. **Edgar**, has sido de los últimos de unirte al grupo y en menos de un año he podido comprobar lo buena persona que eres. ¡Qué jocundo eres tío! Este último año ha sido genial compartir y colaborar contigo en el proyecto de hidroformilación, gracias por estar ahí en cualquier momento que te necesitaba y siempre colaborar con una sonrisa. Ha sido muy fácil y un placer compartir laboratorio contigo. **Alba**, has sido con la que he compartido más tiempo en el laboratorio. Nuestra relación ha ido de menos a más, hasta tener una bonita amistad. ¡Qué maravilla! Sigue con esa pasión y ganas que pones en sacar las cosas y la bondad que te caracteriza para ayudar a quien lo necesita. Ha sido un auténtico placer compartir todos estos años de laboratorio contigo.

Siempre digo que puedes aprender de cualquiera, independientemente de los años de experiencia o edad. ¡Qué suerte que lo he podido comprobar durante estos años! **Javier**, el químic que és també informàtic. De tu he aprés sobretot d'informàtica, una eina indispensable avui en dia a la nostra feina i que destaques per sobre de la resta. T'agraeixo molt que sempre hagis compartit amb mi els programes de bibliografia que creaves per facilitar-te la feina. **Ignasi**, una persona ideal per compartir el dia a dia, ja que de lo difícil o fa fàcil. També he tingut l'oportunitat d'aprendre de tu camps de la química que no coneixia i que he aprés gràcies a tu. **Yuzelfy**, una persona que siempre

tener buen humor es su filosofía, y que es muy importante en ciencia ya que siempre hay días muy duros. **Hannah**, der jüngste Neuzugang in unserer Gruppe! Es war mir ein Vergnügen die letzten Monate der Doktorarbeit mit dir zu teilen. Danke, dass du mir neue deutsche Wörter beigebracht hast und vor allem wie man Xantphos richtig ausspricht. Ich bewundere deine Professionalität im Labor und deine Passion für die Wissenschaft seit Anfang an. Das hat mich an meinen Beginn im chemischen Labor erinnert.

I also want to thank **Prof. Clark R. Landis** for welcoming me to a research stay at University of Wisconsin-Madison. You and your group always treated me so well to make my experience in Madison (Wisconsin, USA) one I will never forget. To all the members of the group: **Spencer**, **Nick**, **Andrew**, **Katie,** and **Megan**, thank you for your collaboration and expertise. My stay in Madison would not have been the same without **Asmaul** and **Sabnam**. Thank you both for opening the doors to your home and beyond. You are amazing people with huge hearts who taught me all about your wonderful culture, I cannot wait to visit your hometown in India and have great memories.

Durante un doctorado también se hacen grandes amigos los cuales mantienes la relación durante muchos años y que es el mayor tesoro que me llevo de estos años. **Juanjo**, he tenido la gran suerte de poder compartir contigo el día a día en el laboratorio y tener una gran amistad. Siempre te voy a agradecer el apoyo científico y moral de estos años. Desde el primer día me demostraste la gran persona que eres. Has sido, eres y serás un gran amigo que siempre tendré presente. **Cristina**, tienes un corazón que no te cabe en el pecho. Empezamos como compañeros de piso en nuestros inicios en Tarragona a amigos viviendo en ciudades distintas. Has sido un gran apoyo durante estos años y siempre has estado en los malos momentos que es cuando los amigos se demuestran. Como una vez me dijiste: *"Quién tiene un amigo catalán, es un amigo para toda la vida"*, así que siempre vas a tener a tu amigo catalán para lo que necesites. **Mabel**, te conocí durante los últimos meses que estuve en el ICIQ y rápidamente me di cuenta del enorme corazón que tienes. Ha sido una suerte que nuestros caminos se hayan cruzado y que hayamos compartidos grandes momentos juntos.

La finalización de una tesis es la culminación de una etapa que ha sido precedida por anteriores. Este logro no hubiera sido posible sin las personas que apostaron y creyeron en mí. **Francesc**, vas ser el primer professor que va creure i apostar per mi. Em vas insistir i guiar pel camí correcte amb el principal objectiu de créixer com a persona. De la mateixa manera, em vas ensenyar que amb esforç i dedicació tot és possible. También quiero agradecer a **Carlos H.**, quién fue la primera persona en enseñarme la pasión por la química orgánica y él que me motivo para hacer un doctorado. **Héctor C.**,

gracias por enseñarme y tratarme tan bien durante mi trabajo final de grado del cual aprendí mucho. Por último, a todos mis ex compañeros de trabajo del departamento de química medica de Almirall S. A.: **Lluís**, **Carles**, **Marta**, **Joan**, **Laura**, **Sonia**, **Montse**, **Silvia**, **Nuria**, **Jordi**, **Jacob**, **Laia**, **Imma**, **Josep Maria** y **Yolanda**. De todos ellos me gustaría agradecer especialmente a **Elena** y **Joan C.**, mis supervisores durante mi estancia en Almirall. Muchas gracias por enseñarme de lo que consiste el trabajo en un laboratorio de química en el mundo industrial. Sobre todo, agradezco la formación y habilidades que me enseñasteis, y que me han servido muchísimo para lograr la finalización de esta tesis doctoral. Todos los miembros del departamento de química médica me demostrasteis que el trabajo de equipo es esencial para tener éxito en el mundo de la investigación científica.

Durante estos años también ha habido varios altibajos. En diciembre de 2018 viví la peor experiencia de mi vida con el atropello de una motocicleta y la posterior cirugía que padecí. Vull agrair la professionalitat i gran treball del **Dr. Victor** i el seu equip mèdic de l'hospital de Bellvitge i del centre mèdic Teknon. M'heu salvat la cama esquerra i la meva qualitat de vida. Mai em cansaré d'agrair-vos el que vau fer per mi. La superación y total recuperación de esta lesión es de lo que más orgulloso estoy de estos últimos años, ya que con voluntad y esfuerzo no hay nada imposible en esta vida. A parte de la salud física, la salud metal es igual o más importante. Quiero agradecer a la **Dra. Sandra** por el apoyo psicológico recibido durante estos años tan duros. Me has ayudado a crecer y a madurar como persona. Gracias a ti he recuperado la seguridad, la confianza y la felicidad conmigo mismo.

Los amigos son el mayor tesoro que una persona puede tener en esta vida, como bien dice la frase: *"Quién tiene un amigo tiene un tesoro"*. Sin lugar a duda me considero un afortunado al tener a tantos tesoros a mi lado. Este logro va por todos vosotros, ya que sin vuestro apoyo no hubiera llegado donde estoy y parte de esta tesis también es vuestra. **Francisco**, desde el colegio que compartimos una amistad que sigue y seguirá intacta. Te agradezco tu sinceridad y honestidad que siempre has tenido conmigo. Siempre has estado en los malos momentos desinteresadamente y siempre te lo agradeceré. Un tiempo después vino la universidad y con ello un grupo de personas que siempre estaré agradecido de haber conocido. **Álvaro**, fuiste el primero del grupo que conocí durante la primera semana de universidad y de la cual nació una amistad que será para siempre. Me siento muy orgulloso de tenerte como amigo ya que durante todos estos años me has ayudado a crecer como persona. Gracias por ser tan buen amigo a través de los años y estar siempre presente en los malos momentos. **Pol**, aún recuerdo el día que nos conocimos en clases de problemas de Física I y me hiciste la típica pregunta: ¿De qué equipo eres? Y al responderte que era del RCD Espanyol, pusiste una cara

tremenda de sorpresa como si hubieras visto un unicornio. Han sido 13 años de grandísimos momentos que quedarán para siempre en el recuerdo y espero que durante los próximos vivamos más momentos juntos. Gracias por demostrarme día a día que eres un amigo de verdad. Y como no, la persona más inteligente y culta que he conocido, **Alberto**, al lado tuyo la Wikipedia no sirve para nada. Gracias por darme siempre tan buenos consejos y apoyarme siempre. Eres un gran amigo que quiero conservar para siempre. **Alba F.**, eres una gran amiga que siempre has estado a mi lado tanto en los buenos como en los malos momentos. Valoro mucho que siempre me hayas dicho tanto las cosas buenas como malas directamente. Espero que durante los próximos años siga siendo así ya que me has ayudado mucho a crecer como persona y llegar donde estoy. **Pedro**, eres una grandísima persona y amigo. Siempre dispuesto a ayudar a quien tienes alrededor desinteresadamente. Y obviamente, siempre que quedamos el grupo siempre aportas un gran humor y buen ambiente que hace que te lo pases mejor. Y tanto a ti como a tu pareja, **Mireia**, os tengo que agradecer vuestra hospitalidad en vuestra casa durante mi primer mes en Tarragona. Me tratasteis como uno más y siempre con amabilidad, nunca lo olvidaré. **Aleix**, ets de les persones més bones que conec i amb un cor enorme. Gràcies pel teu suport i amistat en el bons i malts moments. **Lluc**, gràcies per la teva amistat i suport de tots aquests anys. Hem viscut grans moments junts i encara queden molts per gaudir. Ets tot un exemple: campió en atletisme i doctor en química. Poques persones he conegut que siguin tant humils i amables com tu. Sempre he admirat la teu desig de ser millor cada dia sense trepitjar a ningú del teu entorn, no canviïs mai! **Marc**, el primer que va obtenir el títol de doctor en el grup i el qual també es mereix un títol de doctor de festes. Moltes gràcies per creure en mi i el suport durant aquest anys. Va ser el primer de marxar fora, però sempre hem mantingut una bona amistat que espero que sigui durant molts anys. **Bernat**, un altre membre del grup que mereix un doctorat en festes. Anar a qualssevol lloc amb tu es sinònim de passar-s'ho bé. Et vas marxar fora fa uns anys i quina sort que encara mantinguem l'amistat i que ens podem veure de tant en quan i passar bons moments amb tots els del grup. Moltes gràcies per donar-me el teu suport i ajuda durant tots aquest anys. **Èric**, quantes vegades he hagut d'aguantar i hauré d'aguantar els teus comentaris en contra del meu estimat RCD Espanyol, però això és la bellesa de la rivalitat entre pericos i culés. Ets un amic amb un cor que no et cap al pit i espero que aquesta amistat duri molts anys. **Iván**, un altre membre del grup que va marxar fora a fer la tesi i una vegada acabada ha tornat a casa. Durant aquest temps hem mantingut l'amistat i hem seguit fent plans, ja sigui quan venies a Barcelona o planejàvem un viatge per Europa amb tot el grup. Gràcies per estar en els bons i mal moments i pel teu suport durant aquest anys. **Ferran**, vas marxar també a fora i al cap d'uns anys vas rebre el títol de doctor. Moltes

gràcies pels ànims i les bones paraules que m'has donat durant aquest anys. I també, lo més important, gràcies per la teva amistat i per estar en els bons i mals moments. **Maria**, et vaig conèixer a primer de carrera, però fins el viatge de Milà de fa 5 anys no vam començar a tenir un relació d'amistat que encara perdura i perdurarà. Gràcies per aquests anys de bons moments i per la teva amistat. **Carla**, vam començar a tenir més relació durant el màster i des de llavors som amics. Gràcies per la teva amistat durant aquest anys i els bons moments que hem passat junts.

Pour ma copine, **Marlene**, merci que tu es entrée dans ma vie. Tu es la raison principale grâce à laquelle j'ai une meilleure vie et tu es la personne qui me rend le plus heureux. J'ai hâte d'habiter avec toi et de partager plus de moments avec toi maintenant et dans le futur. Je suis reconnaissant pour ton support pendant toutes ces années et cette thèse de doctorat est dédié à toi. Je suis tellement fier de toi et c'est un privilège d'être à tes côtés. Merci de me pousser à faire le maximum possible chaque jour, je t'aime.

Otro pilar que ha sido esencial durante este camino ha sido mi familia, compuesta por mi hermano y mis padres. Sin vuestro apoyo y amor de estos años, este logro no hubiera sido imposible. A mi hermano, **Carlos R.**, no podía haber deseado un hermano mejor. Gracias por protegerme siempre ante las personas que me menospreciaban y me hacían daño, sin ti mi infancia no hubiera sido la misma. A mi madre, **Mª Pilar**, la madre perfecta que cualquier hijo/a quisiera tener, tú eres la razón de como soy y llegaré a ser. Gracias por educarme y criarme con tanto amor como lo has hecho. Como también, gracias por motivarme día tras día para poder lograr mis objetivos e ilusiones que tengo. Tu vida es el claro ejemplo de superación y entereza, de la cual admiro mucho y de la que siento un orgullo tremendo como hijo. Al meu pare, **Andrés**, el qual comparteixo nom i del qual em sento molt orgullós de portar. Gràcies per ser un dels meus referents d'esforç, constància, sacrifici i resiliència. Uns valors que m'has inculcat des de petit amb el teu exemple. Em sento molt orgullós de ser el teu fill, i tot el que sóc, també és gràcies a tu. Me siento un afortunado y orgulloso de teneros como padres, esta tesis va dedicada especialmente a vosotros.

The research work developed in the present PhD thesis has been possible thanks to the MICINN for an FPI-SO predoctoral fellowship (BES-2017-080405), and the financial support provided by the ICIQ foundation, MCINN (CTQ2017-89814-P and PID2020-115658GB-I00) and Severo Ochoa Excellence Accreditation (SEV-2013-0319-17-2).

X

A mis padres, Andrés y Mª Pilar.

XII

"To do things right,
first you need love,
then technique"

Antoni Gaudí

"Out of the night that covers me
Black as the pit from pole to pole,
I thank whatever gods may be
For my unconquerable soul.

In the fell clutch of circumstance,
I have not winced nor cried aloud.
Under the bludgeonings of chance
My head is bloody, but unbowed.

Beyond this place of wrath and tears
Looms but the Horror of the shade,
And yet the menace of the years
Finds, and shall find, me unafraid.

It matters not how strait the gate,
How charged with punishments the scroll,
I am the master of my fate
I am the captain of my soul."

William Ernest Henley

XIV

LIST OF PUBLICATIONS

At the moment of the submission of this doctoral thesis, the results contained herein have so far resulted in the following publications:

- "Efficient modular phosphorus-containing ligands for stereoselective catalysis" Llorente, N.; Fernández-Pérez, H.; Núñez-Rico, J. L.; Carreras, L.; Martínez-Carrión, A.; Iniesta, E.; **Romero-Navarro, A.**; Martínez-Bascuñana, A.; Vidal-Ferran, A. *Pure Appl. Chem.* **2019**, *91*, 3-15.

- "Valorisation of mixtures of linear alkenes using cobalt-mediated isomerisation and hydroformylation chemistries" Martínez-Carrión, A.; **Romero-Navarro, A.**; Núñez-Rico, J. L.; Gutiérrez, A.; Grabulosa, A.; Vidal-Ferran, A. *Catal. Sci. Technol.* **2022**, *12*, 3219-3227.

- "Supramolecular Hydroformylation Catalyst" **Romero-Navarro, A.**; Vidal-Ferran, A.; EP23382305, **2023**. Filed on 30th of March 2023.

XVI

Table of Contents

LIST OF ACRONYMS AND ABBREVIATIONS

The acronyms and abbreviations used in this doctoral thesis have been used following the recommendations given by the American Chemical Society. Additional abbreviations and acronyms used in this thesis are listed below:

º	Angle
Å	Angstrom(s)
Ac	Acetyl
ACN	Acetonitrile
acac	Acetylacetonate
AHF	Asymmetric hydroformylation
aq.	Aqueous
ATR	Attenuate Total Reflection
BArF	Tetrakis[3,5-bis(trifluoromethyl)phenyl]borate
BINOL	1,1'-Bi-2-naphtol
b.p.	Boiling point
br	Broad (spectrum)
Bu, *n*Bu	*Normal* butyl
ºC	Degrees, Celsius
C_n	Undetermined metal complex(es)
ca.	*Circa* (about)
calcd	Calculated
cat	Catalyst
cm	Centimetre(s)
cm^{-1}	Wavenumber(s)
cod	1,5-Cyclooctadiene
conv.	Conversion

Cy	Cyclohexane (solvent)
δ	Chemical shift in ppm
d	Doublet
DCM	Dichloromethane
DIPEA	*N*,*N*-Diisopropylethylamine
DFT	Density-functional theory
DMF	Dimethylformamide
DMSO	Dimethyl sulfoxide
DReaM	Dynamic Reaction Monitoring
dppe	(Ethane-1,2-diyl)bis(diphenylphosphane)
dppb	(Butane-1,4-diyl)bis(diphenylphosphane)
dppp	(Propane-1,3-diyl)bis(diphenylphosphane)
dppv	1,1'-(1*Z*)-1,2-Ethenediylbis[1,1-diphenylphosphine]
ee	Enantiomeric excess
e.g.	*Exempli gratia* (for example)
eq–eq	Equatorial-equatorial (coordination)
eq–ax	Equatorial-axial (coordination)
equiv.	Equivalent(s)
er	Enantiomeric ratio
ESI	Electrospray ionization
et al.	*Et alii* (and co-workers)
Et	Ethyl
EWG	Electro-withdrawing group
EDG	Electro-donating group
EtOH	Ethanol
EtOAc	Ethyl acetate
GC	Gas chromatography

h	Hour(s)
g	Gram(s)
HF	Hydroformylation
HPLC	High performance liquid chromatography
HRMS	High resolution mass spectrometry
Hz	Hertz
Hydrog.	Hydrogenation
i.e.	*Id est* (in other words)
iPr	iso-Propyl
IS	Internal standard
Isom.	Isomerisation
IR	Infrared spectroscopy
IUPAC	International Union of Pure and Applied Chemistry
J	Coupling constant (expressed in Hz)
L	Litre
L_n	Undetermined ligand(s)
l/*b*	Linear/branched
μ	Micro- (prefix)
m	Multiplet (spectrum); Milli- (prefix)
MALDI	Matrix-Assisted Laser Desorption/Ionization
mg	Milligram(s)
MHz	Megahertz
min	Minute(s)
mM	Millimolar (millimoles per litre)
mol	Mole(s), molecular
mp	Melting point
MS	Mass spectroscopy, Molecular sieves

m/*z*	Mass-to-charge ratio
nbd	Norbornadiene
nm	Nanometre
NMR	Nuclear Magnetic Resonance
OAc	Acetate
ORTEP	Oak Ridge Thermal Ellipsoid Plot Program
OTs	Tosylate group
Ph	Phenyl
ppm	Part(s) per million
ref	Reference
rpm	Revolution per minute
PhMe	Toluene
RA	Regulation Agent
s	Singlet (spectrum); second(s)
Select.	Selectivity
SPS	Solvent purification system
Subs.	Substrate
t	Triplet (spectrum); Time
T	Temperature
TADDOL	α,α,α',α'-Tetraaryl-2,2-disubstituted-1,3-dioxolane-4,5-dimethanol
tbp	Trigonal bipyramid (geometry)
*t*Bu	*tert*-Butyl
TEA	Triethylamine
THF	Tetrahydrofuran
TMB	1,3,5-Trimethoxybenzene
TMS	Trimethylsilyl group

TOF	Time-Of-Flight
Tol	Toluene
TPhP	Triphenyl phosphate
Ts	Tosyl group
v/v	Volume per unit volume
vol	Volume
vs.	*Versus* (against, in contrast to)
VTNA	Variable Time Normalization Analysis
Xantphos	(9,9-Dimethyl-9*H*-xanthene-4,5-diyl)bis(diphenylphosphane)
XRD	X-ray diffraction

XXVI

INTRODUCTION

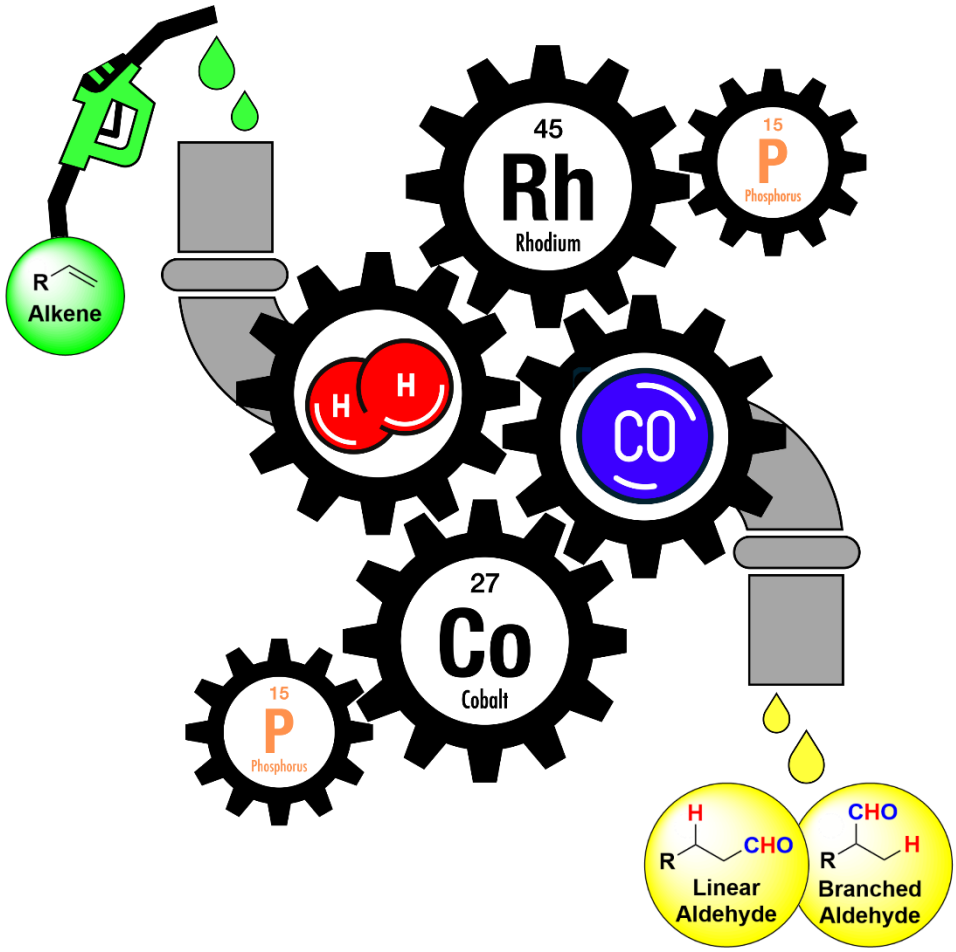

2 *Introduction & Objectives*

Introduction & Objectives

I.1. Hydroformylation reaction

The hydroformylation reaction is an atom-economic addition of a mixture of hydrogen (H_2) and carbon monoxide (CO), commonly called syngas[1]; across an unsaturated C–C bond. In this transformation, a hydrogen atom (H) and a formyl group (CHO) are added across the C=C bond of an alkene[2] in the presence of a catalyst to produce value-added aldehydes. The reaction may generate (except for symmetric (cyclo)alkenes) a mixture of isomeric products. For instance, for a monosubstituted terminal alkene, a branched or *iso*-aldehyde (with a stereogenic centre) and a linear or *n*-aldehyde can be formed, depending on the position at which the H and CHO groups are bonded (Scheme 1).

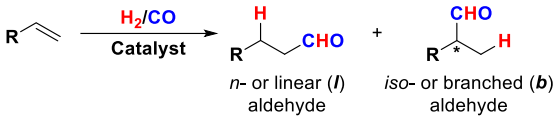

Scheme 1. General scheme of hydroformylation reaction.

Otto Roelen serendipitously discovered the hydroformylation reaction in 1938[3] during an attempt to return ethylene, produced by the Fischer–Tropsch synthesis (Scheme 2a),[4] back into the reaction to improve the yield. As ammonia (NH_3) was present in the reaction mixture that contained the solid Fischer–Tropsch catalyst, which consisted of a mixture silica (66%), cobalt (30%), thorium oxide (2%) and magnesium oxide (2%), Roelen found the corresponding imine (CH_3CH_2-C=NH) of propionaldehyde (CH_3CH_2-CHO) as a white solid product.[5] In his patent of 1938, Roelen confirmed the reaction of ethylene under syngas pressure using a silica-based cobalt-thorium contact as a catalysts, in which propionaldehyde and diethyl ketone were obtained as main products (Scheme 2b).[6] At the beginning, hydroformylation was named *oxo*-synthesis or *oxo*-process and this name is still widely used in industrial settings.[7]

---

[1] Syngas is mixture of hydrogen (H_2) and carbon monoxide (CO) in various ratios. The most common ratio used in hydroformylation is 1:1 (H_2/CO).
[2] Most examples of hydroformylation refer to alkenes, although addition of a H and CHO groups across the C-C unsaturated bond of alkynes and allenes can also take place.
[3] Roelen, O. Verfahren zur Herstellung von sauerstoffhaltigen Verbindungen. Germany DE849548C, **1938/1952**.
[4] Roelen, O. *Erdoel Kohle, Erdgas, Petrochem.* **1978**, *31*, 524.
[5] Cornils, B.; Herrmann, W. A.; Rasch, M. *Angew. Chem. Int. Ed. Eng.* **1994**, *33*, 2144-2163.
[6] Zhang, B.; Peña Fuentes, D.; Börner, A. *ChemTexts* **2021**, *8*, 2.
[7] Adkins, H.; Krsek, G. *J. Am. Chem. Soc.* **1949**, *71*, 3051-3055.

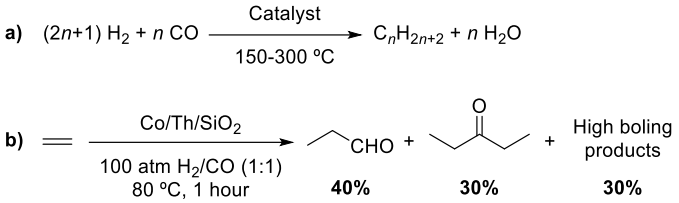

Scheme 2. a) Fischer–Tropsch synthesis. b) Hydroformylation discovered by Otto Roelen.

The discovery of this catalytic transformation was one of the greatest achievements in the field of homogenous catalysis and it is nowadays one of the largest processes in the industry. Its development is considered one of the premier achievements of the 20th century industrial chemistry. Nowadays, every year, nearly 10 million metric tons of aldehydes are produced using hydroformylation reactions as the method of synthesis. Several large companies, such as SHELL, BASF,[8a] Eastman, BP,[8b] DOW and Evonik, have plants. The main reason for which hydroformylation is a valuable method is because aldehydes (branched and linear) are extremely versatile building blocks in synthesis, considering that the formyl group (CHO) can be transformed into a wide variety of functional groups (Figure 1).[9]

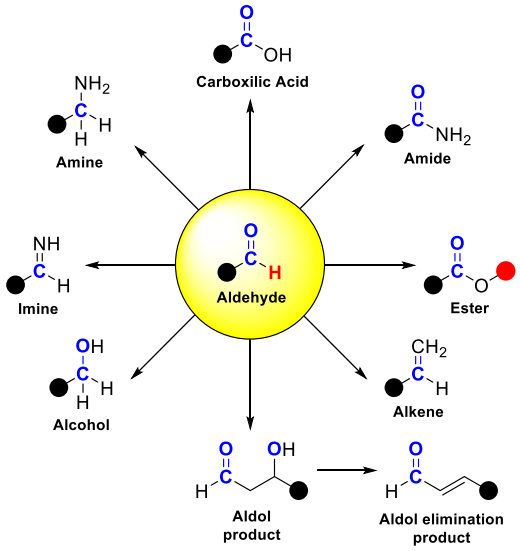

Figure 1. Transformation of aldehydes to other molecules.

[8] a) BASF is the acronym that refers to Badische Anilin und Sodafabrik. b) BP is the acronym that refers to British Petroleum.
[9] a) Franke, R.; Selent, D.; Börner, A. *Chem. Rev.* **2012**, *112*, 5675-5732. b) de Vries, J. G. Hydroformylation of Alkenes: Industrial Applications. In *C-1 Building Blocks in Organic Synthesis*, Science of Synthesis, Vol. 1; Georg Thieme Verlag KG, 2014; pp 193-227. c) Cornils, B.; Börner, A.; Franke, R.; Zhang, B.; Wiebus, E.; Schmid, K. *Applied Homogeneous Catalysis with Organometallic Compounds* **2017**, 23-90.

Not only are aldehydes important intermediates or starting materials in organic synthesis, but they are also valuable chemicals for applications in the chemical industry at the large scale. Applications of hydroformylation at the large scale mainly focus on the production of the linear aldehydes due to their commodity. These products are key intermediates to produce solvents, plasticizers, and detergents.[9b] Moreover, they are important products for the production of scents and fragrances, which are used in perfume manufacturing.[10] On other hand, branched aldehydes are important to produce enantiopure aldehydes for the fine chemical or pharmaceutical industry.[9c]

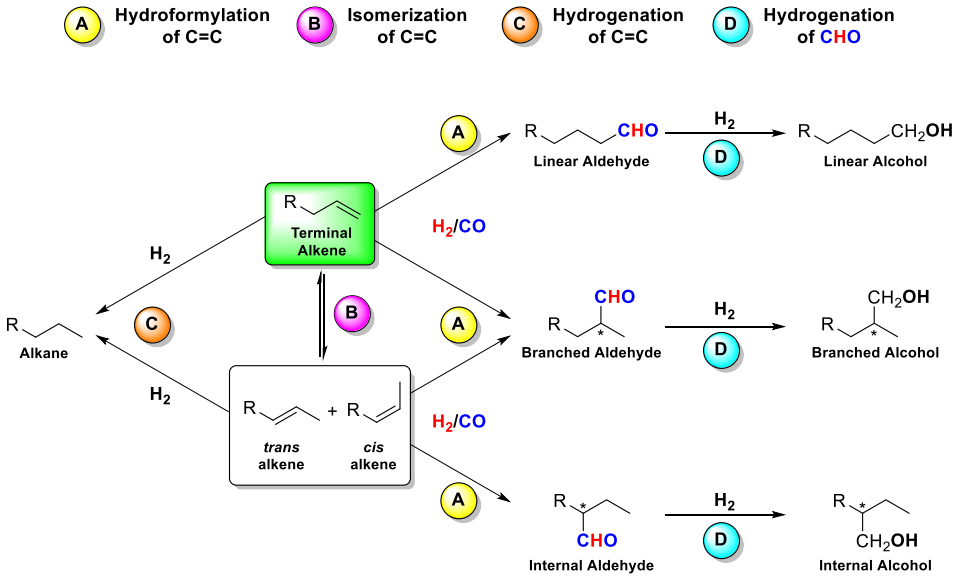

Scheme 3. Set of possible reaction alternatives in the hydroformylation reaction.

Controlling the chemo-, regio- and stereo-selectivity in hydroformylation is the main challenge, since the hydroformylation reaction may lead to numerous products. The main reaction is the hydroformylation process, by which the branched and/or linear aldehydes are formed depending on the position of the alkene at which the CHO and H groups are bonded (see Scheme 3A as a representative example of hydroformylation from a terminal alkene). The regio-selectivity (branched or linear aldehydes) and stereo-selectivity (*R* or *S* enantiomers of the branched aldehyde) is influenced by the structure of the alkene, the catalytic system (metal precursor & ligand)

[10] a) Sell, C. *The Chemistry of Fragrances: From Perfumer to Consumer*; The Royal Society of Chemistry, 2006. b) Sell, C. S. *Fundamentals of Fragrance Chemistry*; Wiley-VCH Verlag GmbH & Co. KGaA, 2019. c) Gusevskaya, E. V.; Jiménez-Pinto, J.; Börner, A. *ChemCatChem* **2014**, *6*, 382-411.

and the reaction conditions such as the temperature, time, pressure of syngas and relative ratio of H_2 and CO in syngas.[11]

Furthermore, there are several by-products that can be formed during the hydroformylation reactions. The terminal alkene can isomerize (Scheme 3B) under catalytic conditions to form the thermodynamically more favoured internal alkenes (*cis*- & *trans*-) that can be in turn hydroformylated to internal aldehydes (Scheme 3A). Moreover, hydrogen (H_2) is present under hydroformylation conditions, therefore the C=C bond in the substrate and/or the C=O bond in the products can be hydrogenated to the alkane and/or alcohol derivatives, respectively (Scheme 3C and D).[11]

Another aspect that is important is the reactivity of the substrate in hydroformylation. Terminal alkenes are more reactive than internal alkenes towards hydroformylation. The rate of hydroformylation decreases when increasing the steric hindrance of the double bond C=C (Figure 2).[12] For instance, the reaction of disubstituted terminal alkenes requires harsher reaction conditions (*e.g.*, higher temperatures and pressures). According to the *Keulemans' rule*,[13] hydroformylation of doubly substituted alkene carbons is unfavourable.

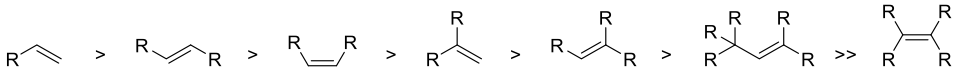

Figure 2. Rate of the hydroformylation according to the steric hindrance of the alkene.

Regarding the metal precursor, cobalt (Co) and rhodium (Rh) are the most common metals in hydroformylation, both in industry and academia. However, there are other metals that are active in this transformation and are being investigated in academia and/or industry in order to find new, more efficient and cheaper hydroformylation catalysts. The following trend of metal activity as catalysts in hydroformylation, with unmodified metal carbonyl complexes, is shown below:[14]

$$Rh \gg Co > Ir > Ru > Os \sim Tc > Pt > Pd > Mn > Fe > Ni \gg Re$$

Species which play an active role in hydroformylation chemistry are the hydrido complex of the type $[M(CO)_xH_y(P)_z]$ in which P is representing an organic phosphorus ligand and M is the metal. The metals Co and Rh are

[11] a) van Leeuwen, P. W. N. M.; Claver, C. *Rhodium Catalyzed Hydroformylation*; Springer Dordrecht, 2002. b) Kamer, P. C. J.; Reek, J. N. H.; van Leeuwen, P. W. N. M. *Rhodium Catalyzed Hydroformylation*; Wiley-VCH Verlag GmbH & Co. KGaA, 2005.
[12] Frey, G. D. *J. Organomet. Chem.* **2014**, *754*, 5-7.
[13] Keulemans, A. I. M.; Kwantes, A.; van Bavel, T. *Recl. Trav. Chim. Pays-Bas* **1948**, *67*, 298-308.
[14] Pruchnik, F. P.; Duraj, S. A. Application of Organometallic Compounds in Homogeneous Catalysis. In *Organometallic Chemistry of the Transition Elements*, Pruchnik, F. P., Duraj, S. A. Eds.; Springer US, 1990; pp 647-743.

widely used in academia and industry. This research work will only focus on these two metals.

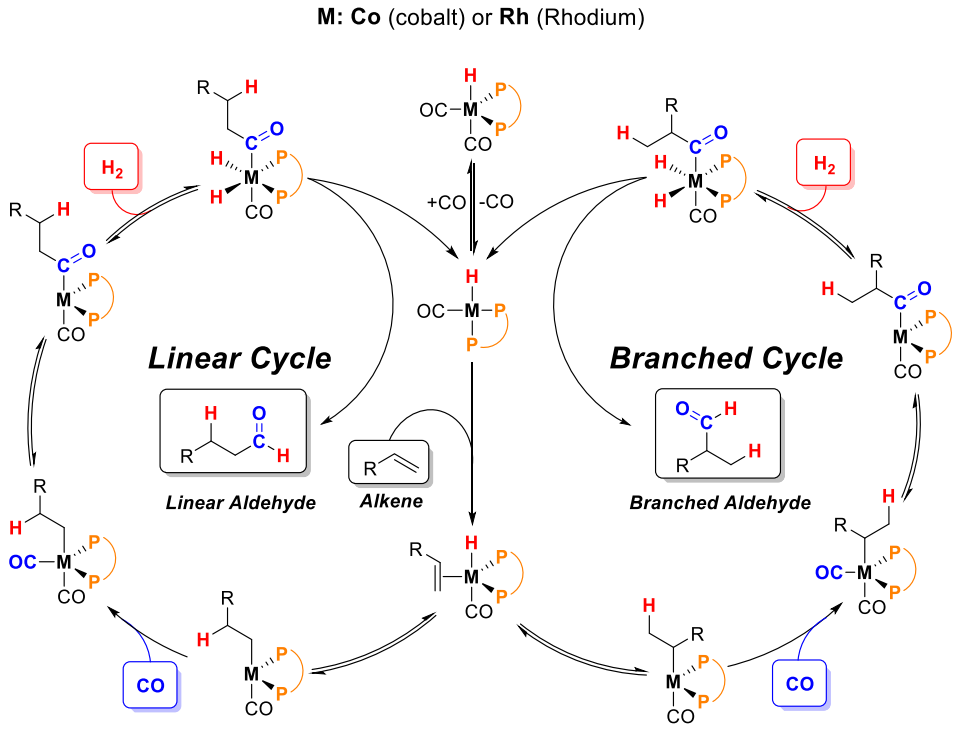

Scheme 4. Hydroformylation mechanism proposed by Heck and Breslow for rhodium- and cobalt-catalysed processes in the presence of phosphorus bidentate ligands.

Heck and Breslow proposed a mechanism of the cobalt-catalysed hydroformylation in 1960, which is still accepted today (Scheme 4, with M=Co).[15a] The active species $[M(CO)H(P)_2]$ is formed from the resting state $[M(CO)_2H(P)_2]$ by losing a CO ligand. The catalytic cycle involves the coordination of the alkene, the transfer of a hydrido ligand to provide the linear alkyl species (and the isomeric branched one), followed by CO coordination, migratory CO insertion, and lastly oxidative addition of H_2 followed by the reductive elimination of the aldehyde which regenerates the metal active species.[15b]

[15] a) Heck, R. F.; Breslow, D. S. *J. Am. Chem. Soc.* **1961**, *83*, 4023-4027. b) Hebrard, F.; Kalck, P. *Chem. Rev.* **2009**, *109*, 4272-4282.

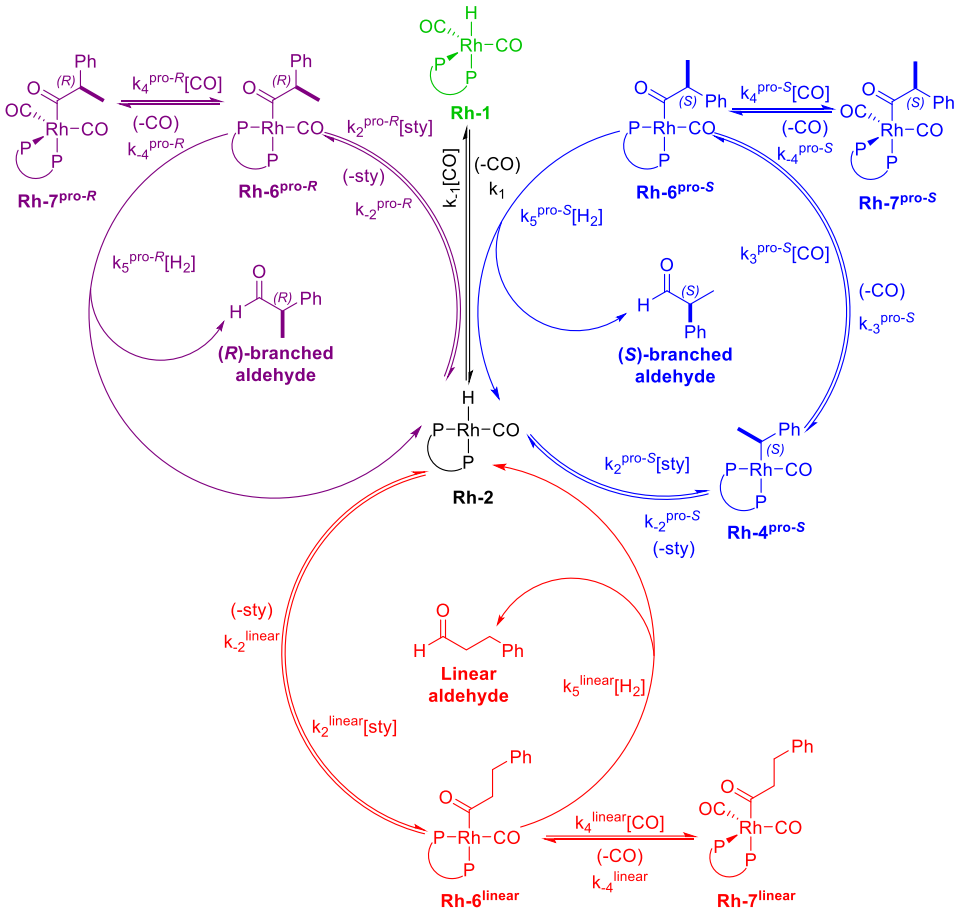

Scheme 5. Full kinetic model for asymmetric hydroformylation of styrene published by Landis and co-workers. For the sake of simplicity, the transformation of one complex into another may imply few organometallic elementary steps.

Studying the kinetics of a reaction can help improving its rate, selectivity, and even enantioselectivity. Landis and co-workers examined the micro-kinetics of the asymmetric hydroformylation of styrene using the (*S*,*S*,*S*)-BisDiazoPhos ligand (**L22**, Figure 15). In fact, for the asymmetric hydroformylation of styrene, there are three possible catalytic reaction manifolds: one leading to the linear and the two enantiomeric routes to the branched products (Scheme 5). The main goal of this study was to find the step in which the enantioselectivity was determined. The authors found that, in the majority of scenarios for their ligand, the hydrogenolysis was the rate-determining step. However, the enantioselectivity was determined in the alkene insertion step as the rhodium-alkyl complex **Rh-4** very rapidly inserted CO leading to **Rh-6**. This complex bound a second CO molecule to form the stable acyl complex **Rh-7**. Because of this, the alkene insertion step became irreversible when the CO pressure was high enough. Therefore, Landis and

co-workers found that there is a dependence of the regioselectivity and the enantioselectivity on the CO pressure.[16]

I.2. Cobalt-catalysed hydroformylation

As mentioned before, the cobalt-catalysed hydroformylation is directly connected to the discovery of Otto Roelen in his patent of 1938.[3] Therefore, the first hydroformylation catalysts were based on $[Co_2(CO)_8]$ as a metal precursor without using ligands. In this chemistry, the hydrido complex $[Co(CO)_4H]$ was found to be the active catalyst in hydroformylation.[15b] For the reaction using the unmodified cobalt catalysts, severe reaction conditions involving 100–300 bar of syngas and 100–180 °C were required, as the CO partial pressure had to be increased as the temperature rose in order to avoid the decomposition of the catalyst into cobalt metal.[4,6,17]

Generally speaking, organic phosphorus-based ligands decrease the hydroformylation activity of cobalt catalysts. However, they lead to higher ratios of the linear aldehyde than those obtained with the unmodified catalyst. Furthermore, phosphane ligands improve the hydrogenation activity of the catalyst, which translates into the hydrogenation of alkenes to alkanes and aldehydes to alcohols (Scheme 3C and D).[18a] Among common trivalent phosphorus compounds, only phosphanes can be used as a ligands. As alcohols are frequently formed under hydroformylation conditions with cobalt catalyst, phosphoramidite and phosphite ligands would be unstable due to P–O or P–N cleavage induced by the alcohol produced from the alkene.[18b]

The most common ligands in cobalt-catalysed hydroformylation are substituted phosphanes. They have a strong σ-donor character, which leads to strong coordination to the metal centre. The donicity of the phosphanes towards the metal centre greatly affects the ratio of linear aldehydes (Figure 3).[19] The higher the donicity of the phosphane, the less active the metal complexes derived from it are in hydroformylation. Strong donor phosphanes are only active at high temperatures in hydroformylation, which is possible due to the higher thermal stability of the ligand-modified cobalt catalysts. For example, tributylphosphane (PBu_3) is one preferred phosphane in hydroformylation as it gives good results in the production of linear aldehydes

[16] Brezny, A. C.; Landis, C. R. *ACS Catal.* **2019**, *9*, 2501-2513.
[17] Ungvary, F.; Marko, L. *Organometallics* **1982**, *1*, 1120-1125.
[18] a) Slaugh, L. H.; Mullineaux, R. D. *J. Organometal. Chem.* **1968**, *13*, 469-477. b) Kamer, P. C. J.; van Leeuwen, P. W. N. M. *Phosphorus(III) Ligands in Homogeneous Catalysis: Design and Synthesis*; John Wiley & Sons Ltd., 2012.
[19] Tucci, E. R. *Ind. Eng. Chem., Prod. Res. Develop.* **1970**, *9*, 516-521.

with low amounts of isomerisation products. Interestingly, this ligand has been used at the technical scale by the Shell Plc company since 1966.[20]

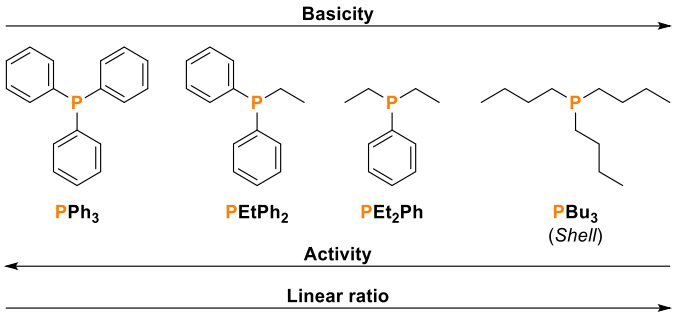

Figure 3. Dependence of the activity and linear regioselectivity in the hydroformylation.

Nonetheless, a few years later, more stable, and selective phosphanes were developed by chemical companies (Figure 4). Phobanes, which derive from 1,5-cyclooctadiene, were developed by Shell.[21] On the other hand, bicyclic limonene-based ligands (LIM) and 4-vinyl-cyclohexene-based ligands (VCH) were developed by Sasol.[22] All these phosphane ligands have bulky groups which assist in the generation of the active catalyst from the precatalyst, as well as at the level of the Co–acyl complex, by enhancement of the dissociation of one CO ligand due to the relief of steric congestion.

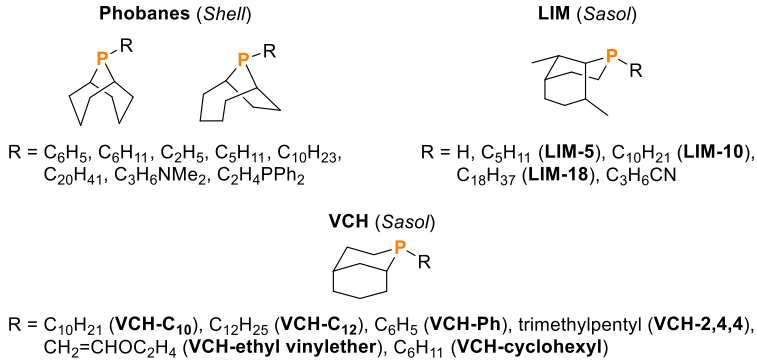

Figure 4. Byciclic monophosphanes ligands used in cobalt-catalysed hydroformylation.

[20] Slaugh, L. H.; Mullineaux, R. D. Hydroformylation of olefins. US3239569, **1966**.
[21] a) Mason, R. F.; van Winkle, J. L. Bicyclic heterocyclic sec- and tert-phosphines. US3400163A, **1968**. b) van Winkle, J. L.; Morris, R. C.; Mason, R. F. Single Stage Hydroformylation of Olefins to Alcohols. US3420898A, **1969**.
[22] a) Steynberg, J. P.; Govender, K.; Steynberg, P. J. Hydroformylation process and [3.3.1]phosphabicyclononane-ligated catalysts for the manufacture of alcohols and aldehydes from alkenes and synthesis gas. WO2002014248, **2002**. b) Steynberg, P. J.; van Rensburg, H.; Grove, J. J. C.; Otto, S.; Crause, C. Hydroformylation process for the production of aldehydes and alcohols from alkenes using transition metals complexed with bicyclic phosphine ligands as catalysts. WO2003068719, **2003**.

Bisphosphanes were also applied in cobalt-catalysed hydroformylations. The first reports were published in the 1980s using bisphosphanes of the type dppe (**L1**), dppv (**L2**), dppp (**L3**) and dppb (**L4**) (Figure 5). The disadvantage is that they decrease the reactivity of the catalyst in hydroformylation, although the isomerisation of the alkene is supressed.[23]

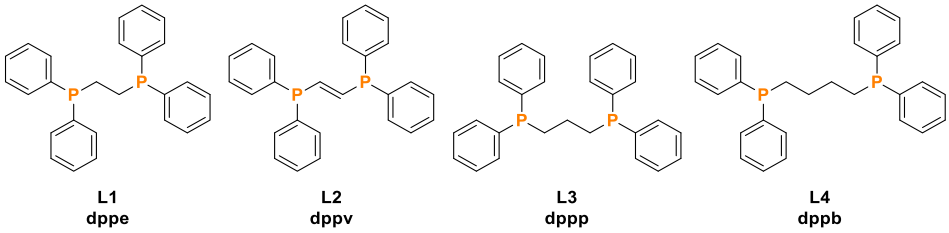

Figure 5. Bisphosphane ligands used in cobalt-catalysed hydroformylation.

Bisphosphite ligands are still under research in cobalt-catalysed hydroformylation nowadays. In 2020, Stanley and co-workers reported the synthesis of new cobalt (II) cationic complexes **C1**–**C4** (Scheme 6), which were described to be active in the hydroformylation of terminal and internal alkenes employing lower pressures than those using $[Co(CO)_4H]$, with the limitation that high temperatures are still needed. This cobalt (II) cationic catalyst appeared to have exceptional stability with respect to cobalt induced phosphane degradation reactions or decomposition to cobalt metal.[24a] Interestingly, two years later, Franke and co-workers reported that the cobalt(II) cationic complexes **C1**–**C4** synthesised by the procedure of Stanley and co-workers had extremely low activity under the published conditions.[24b] The results published by Franke and co-coworkers are in contradiction with those reported by Stanley *et al.*, which will probably motivate further studies in this area of research.

In 2020, Chirik and co-workers published a new enantiopure hydrido cobalt catalyst using iPrDuPhos as a bisphosphane ligand. The $[Co(CO)_2H((R,R)$-iPrDuPhos)] (**C5**) (Scheme 6) was tested in hydroformylation without success, as it only promoted the hydrogenation of styrene.[25] However, Chirik and co-workers recently reported the synthesis of alcohols from terminal alkenes and 1,1-disubstituted alkenes by cobalt-catalysed visible-light-driven reductive hydroformylation (Scheme 6)

[23] Cornely, W.; Fell, B. *J. Mol. Catal.* **1982**, *16*, 89-94.
[24] a) Hood, D. M.; Johnson, R. A.; Carpenter, A. E.; Younker, J. M.; Vinyard, D. J.; Stanley, G. G. *Science* **2020**, *367*, 542. b) Zhang, B.; Kubis, C.; Franke, R. *Science* **2022**, *377*, 1223-1227.
[25] a) MacNeil, C. S.; Mendelsohn, L. N.; Zhong, H.; Pabst, T. P.; Chirik, P. J. *Angew. Chem. Int. Ed.* **2020**, *59*, 8912-8916. b) MacNeil, C. S.; Mendelsohn, L. N.; Pabst, T. P.; Hierlmeier, G.; Chirik, P. J. *J. Am. Chem. Soc.* **2022**, *144*, 19219-19224.

using the cobalt catalyst **C5**, obtaining high yields and regioselectivities towards linear alcohols.

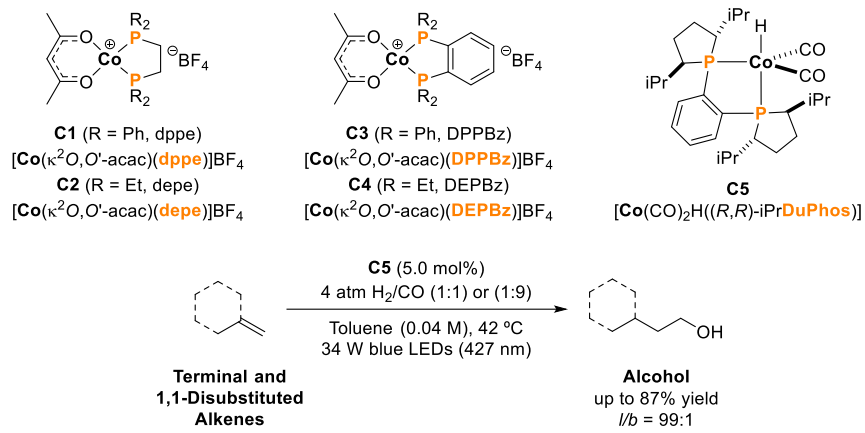

Scheme 6. Cobalt catalyst based on bisphosphanes and synthesis of alcohols from terminal and 1,1-disubstituted alkenes.

Phosphorus-based ligands are the most common in hydroformylation, but additionally, some NHC–cobalt[26] complexes have been explored in hydroformylation (Figure 6). The binuclear cobalt complex **C6** was tested in hydroformylation at 170 ºC under 60 bar of syngas with oct-1-ene as substrate. Interestingly, the expected formation of aldehydes did not take place.[27] Only the decomposition of the precatalyst to give the $[1,3\text{-bis}(2,4,6\text{-trimethyl-phenyl})\text{imidazolium}]^{+}[Co(CO)_4]^{-}$ derivative was observed. The hydrido-cobalt complex **C7** was active in the hydroformylation of oct-1-ene under mild conditions (8 bar of syngas at 50 ºC for 17 hours). The conversion of the reaction was moderate (47.3%) and the regioselectivity was favoured towards the branched aldehyde (*l*/*b*= 10:90).[28]

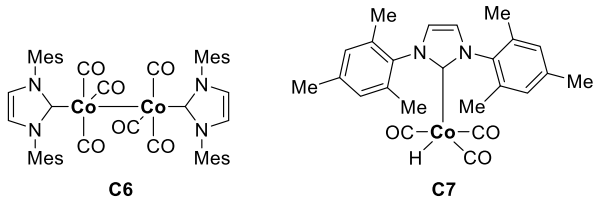

Figure 6. NHC-cobalt complexes.

[26] NHC is an acronym that refers to *N*-heterocyclic-carbene.
[27] van Rensburg, H.; Tooze, R. P.; Foster, D. F.; Slawin, A. M. Z. *Inorg. Chem.* **2004**, *43*, 2468-2470.
[28] Llewellyn, S. A.; Green, M. L. H.; Cowley, A. R. *Dalton Trans.* **2006**, 4164-4168.

I.3. Rhodium-catalysed hydroformylation

Rhodium is the other metal, besides cobalt, which is mostly used in industry and academic research in hydroformylation. The major advantages of rhodium catalysts are: i) high activity, ii) low syngas pressure required, iii) lower reaction temperatures than those required in cobalt catalysts and iv) high chemoselectivities towards aldehydes.[9] The main disadvantage of rhodium catalysts is its increased price over the years.

Nowadays, [Rh(κ^2*O,O'*-acac)(CO)$_2$] and trivalent phosphorus ligands are mostly employed for the generation of phosphorus-modified catalysts in lab-scale hydroformylation reactions. Through the years, several kinds of phosphorus-ligands have been studied (Figure 7).[9a] Phosphane ligands are usually characterized by three carbon substituents bonded to one phosphorus atom. The substitution of one, two or three carbon substituents in phosphines by an oxygen-containing substituent leads to phosphinites, phosphonites or phosphites, respectively. They can also incorporate nitrogen-containing substituents, which lead to aminophosphines, diaminophosphines or triaminophosphines, respectively. Additionally, there is the chance to combine different heteroatom-containing substituents, such as phosphoramidite ligands, which are widely used in asymmetric hydroformylation.[6,9]

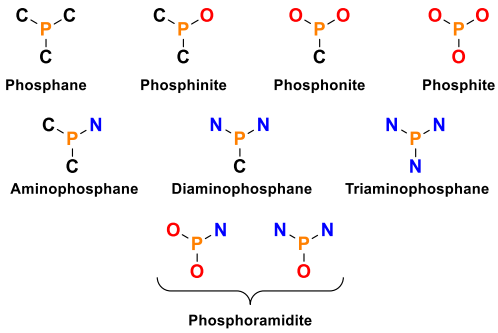

Figure 7. Types of organophosphorus ligands applied in hydroformylation.

The first monodentate phosphorus ligand used with rhodium was PPh_3, because it is a readily available, inexpensive, and air-stable ligand. The use of trialkyl phosphanes, such as PEt_3 or PBu_3, has also been reported in the literature.[29] However, rhodium alkyl phosphane catalysts promote high amounts of hydrogenation products (*i.e.* alkanes and alcohols).[30] Andreetta

[29] a) Franks, S.; Hartley, F. R. *J. Mol. Catal.* **1981**, *12*, 121-124. b) MacDougall, J. K.; Simpson, M. C.; Green, M. J.; Cole-Hamilton, D. J. *J. Chem. Soc., Dalton Trans.* **1996**, 1161-1172. c) Simpson, M. C.; Cole-Hamilton, D. J. *Coord. Chem. Rev.* **1996**, *155*, 163-207.
[30] Evans, D.; Osborn, J. A.; Wilkinson, G. *J. Chem. Soc. A* **1968**, 3133-3142.

and Wilkinson reported that a high excess of PPh_3 increased the concentration of the species $[Rh(CO)H(PPh_3)_2]$ in the reaction.[31] This species contains two triphenylphosphane units which lead to higher concentrations of linear aldehydes.

Therefore, the use of suitable bidentate phosphorus-based ligands promotes the formation of stable $[Rh(P)_2]$ complexes. The exact composition of the first-coordination sphere of the metal depends on the nature of the ligands (steric and electronic properties), the Rh/ligand ratio, and the CO partial pressure during the hydroformylation reaction. When bidentate ligands are bound to the rhodium centre, the resulting complex adopts a trigonal bipyramidal (tbp) geometry. The bidentate ligand can be coordinated in an equatorial–equatorial (eq–eq) (Figure 8a) or equatorial-axial (eq–ax) (Figure 8b) fashion in the rhodium complex.[11a] Bidentate ligands with large bite angles coordinate in an eq–eq fashion and those which have small bite angles lead to eq–ax complexes.

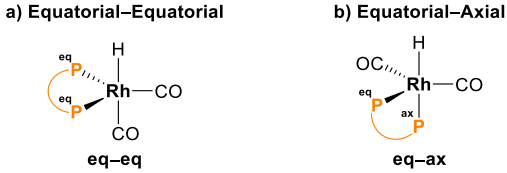

Figure 8. Coordination of bidentate phosphorus ligands in trigonal bipyramidal rhodium complexes.

Several chelating α,ω-bisphosphanes such as dppe (**L1**), dppp (**L3**) or dppb (**L4**) (Figure 5) with small bite angles have been tested in rhodium hydroformylation and showed poor results towards the linear aldehydes.[11a] Although the resulting rhodium complexes derived from **L1**, **L3** and **L4** are active in hydroformylation, these catalysts suffer from providing mixtures of linear and branched aldehydes, with a small preference for the linear or branched aldehyde being observed. However, in order to increase the regioselectivity towards linear aldehydes, van Leeuwen and Kamer developed the "Xantphos family" of ligands (Figure 9a), such as Xantphos (**L5**), DPEphos (**L6**), Sixantphos (**L7**) and Thixantphos (**L8**). In all the cases, the phosphane groups are in a rigid scaffold.[32] By varying the xanthene backbone, the P–Rh–P bite angles can be modified. The natural bite angle (α)[33] has helped in rationalising the relationship between the activity and

[31] a) Gregorio, G.; Montrasi, G.; Tampieri, M.; Cavalieri d'Oro, P.; Pagani, G.; Andreetta, A. *Chim. Ind. (Milan)* **1980**, *62*, 389. b) Brown, C. K.; Wilkinson, G. *J. Chem. Soc. A* **1970**, 2753-2764.
[32] Kamer, P. C. J.; Kranenburg, M.; van Leeuwen, P. W. N. M.; de Vries, J. G. Bidentate phosphine ligand. WO9530680, **1995**.
[33] Natural bite angle (α) is the bond angle formed by the coordination of a bidentate ligand to a metal centre (see Figure 9b).

regioselectivity in homogeneous rhodium catalysis (Figure 9b).[34] The ligands with a bite angle near 110º showed high regioselectivities (96–98% linear ratio) in the hydroformylation of oct-1-ene.[35] Furthermore, by modifying the substitution pattern in the phosphane groups[36], fine-tuning of the stereoelectronic properties of the ligand could be achieved. For instance, styrene was hydroformylated with Thixantphos ligands. When the substituents at the phosphane groups had an electron withdrawing character, an increase in the *l:b* ratio was observed (R = CF_3; *l/b* ratio = 64:34). In contrast, if the substituent had a donating character,[37] a decrease in the *l:b* ratio (R = NMe_2; *l/b* ratio = 43:57) was observed (Figure 9a).[38]

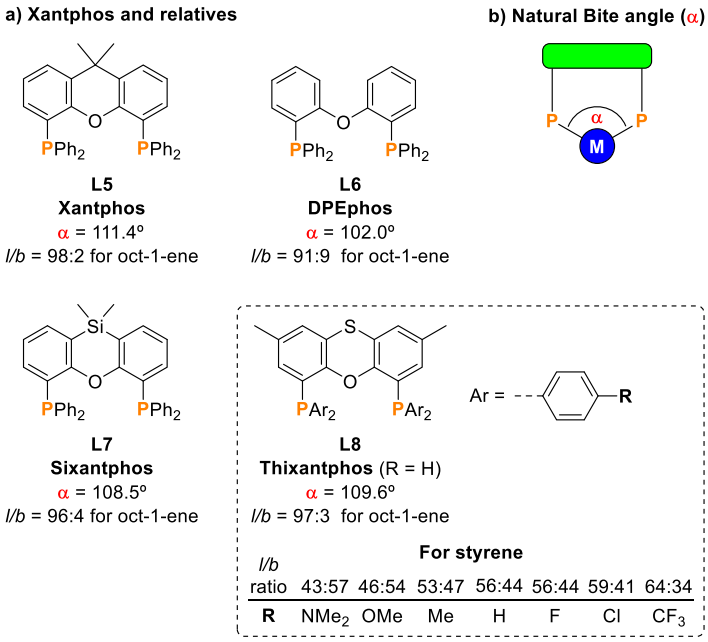

Figure 9. a) Xantphos and analogous ligands. Thixantphos ligands bearing electronically different P–aryl substituents. b) Natural Bite angle (**α**).

Another important discovery for achieving high linear ratios in hydroformylation was the use of bidentate bisphosphanes such as BISBI (**L9**)

[34] a) Goertz, W.; C. J. Kamer, P.; W. N. M. van Leeuwen, P.; Vogt, D. *Chem. Commun.* **1997**, 1521-1522. b) van der Veen, L. A.; Boele, M. D. K.; Bregman, F. R.; Kamer, P. C. J.; van Leeuwen, P. W. N. M.; Goubitz, K.; Fraanje, J.; Schenk, H.; Bo, C. *J. Am. Chem. Soc.* **1998**, *120*, 11616-11626. c) Birkholz, M.-N.; Freixa, Z.; van Leeuwen, P. W. N. M. *Chem. Soc. Rev.* **2009**, *38*, 1099-1118.
[35] Kranenburg, M.; van der Burgt, Y. E. M.; Kamer, P. C. J.; van Leeuwen, P. W. N. M.; Goubitz, K.; Fraanje, J. *Organometallics* **1995**, *14*, 3081-3089.
[36] EWG is an acronym that refers to electron-withdrawing group.
[37] EDG is an acronym that refers to electron-donating group.
[38] van der Veen, L. A.; Boele, M. D. K.; Bregman, F. R.; Kamer, P. C. J.; van Leeuwen, P. W. N. M.; Goubitz, K.; Fraanje, J.; Schenk, H.; Bo, C. *J. Am. Chem. Soc.* **1998**, *120*, 11616-11626.

and NAPHOS (**L10**) (Figure 10).[39] These ligands favoured the obtention of linear aldehydes in high yields in the hydroformylation of terminal alkenes. Beller and co-workers introduced fluoro-substituted aryl groups, in the ligand named IPHOS (**L11**), instead of phenyl substituents (Figure 10). The increase in the regioselectivity towards the linear aldehyde of internal alkenes as substrates was attribute by the authors to electronic effects of the ligand.[40]

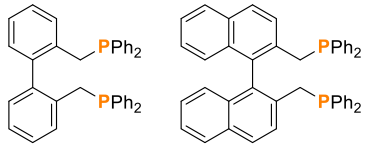

L9
BISBI

L10
NAPHOS

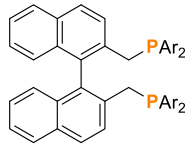

L11
IPHOS
Ar = 3,5-$(CF_3)_2C_6H_3$

Substrate	*l/b* ratio aldehydes
Pent-1-ene	96:4
Pent-2-ene	91:9
Oct-2-ene	86:14
Oct-4-ene	66:34

Figure 10. BISBI, NAPHOS and IPHOS ligands in Rh-catalysed hydroformylations.

The first studies using phosphites as ligands in Rh-hydroformylation reactions showed a considerable increase in the reaction rate in comparison with phosphanes. That is because phosphites (P–O bonds) are stronger π-acceptors but weaker σ-donors than phosphanes (P–C bonds) (Figure 11).[41] This feature makes the Rh–CO bond weaker in phosphites than phosphanes, thus promoting the dissociation of the CO ligand from the Rh and facilitating the coordination of the alkene to the metal centre.[42] Moreover, another advantage of using phosphites instead of phosphines is that they are less sensitive towards oxidation, despite being water-sensitive compounds.

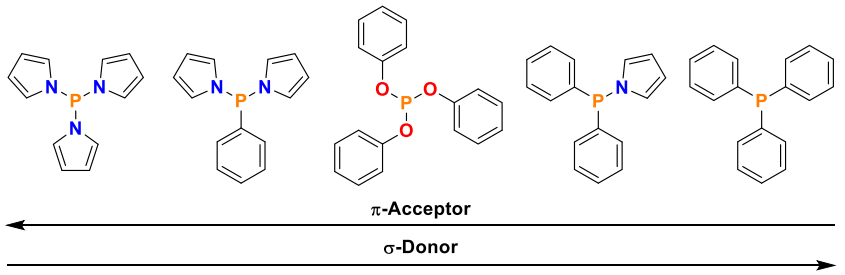

Figure 11. π-Acceptor and σ-donor characteristics of phosphorus ligands with different P–X bonds.

[39] Casey, C. P.; Paulsen, E. L.; Beuttenmueller, E. W.; Proft, B. R.; Petrovich, L. M.; Matter, B. A.; Powell, D. R. *J. Am. Chem. Soc.* **1997**, *119*, 11817-11825.
[40] Klein, H.; Jackstell, R.; Wiese, K.-D.; Borgmann, C.; Beller, M. *Angew. Chem. Int. Ed.* **2001**, *40*, 3408-3411.
[41] M. Trzeciak, A.; Głowiak, T.; Grzybek, R.; J. Ziółkowski, J. *J. Chem. Soc., Dalton Trans.* **1997**, 1831-1838.
[42] van Leeuwen, P. W. N. M.; Roobeek, C. F. *J. Organomet. Chem.* **1983**, *258*, 343-350.

The introduction of bulky alkyl groups close to the P–O bond of the phosphite group improved the *l*/*b* ratio of the reaction and the stability of the ligand towards hydrolysis.[43] Phosphites with a *tert*-butyl group in *ortho*-position of the P–O bond (**L12a**, **L12b** and **L12c**) were designed by Piet van Leeuwen[44] and developed by Shell and Union Carbide Chemicals & Plastics (UCC, since 2001 Dow Chemical).[45] Interestingly, these ligands are still used in academia and industry (Figure 12). These monophosphite ligands show high rates in the hydroformylation of internal alkenes and moderate regioselectivities towards the linear isomer for terminal alkenes.

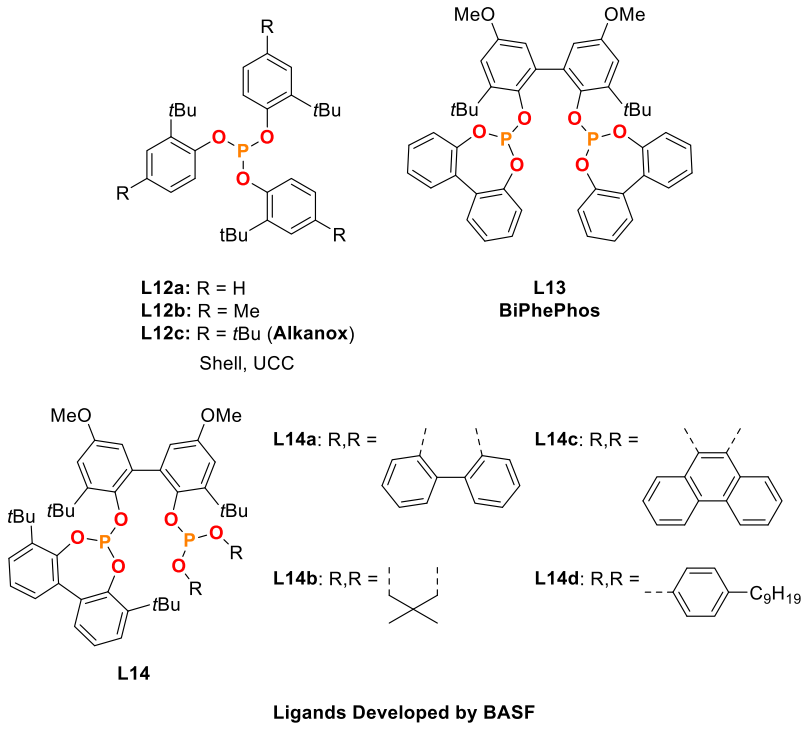

Figure 12. Phosphite ligands frequently used in Rh-catalysed hydroformylation.

Sterically hindered, chelating bidentate phosphorus ligands favour the formation of linear aldehydes. BiPhePhos ligand (**L13**), reported by Bryant and co-workers,[46] showed excellent results towards the formation of linear aldehydes. The authors identified that the bulky groups present in the ligand played an important role in the high regioselectivities observed.[47] Ligand **L13**

[43] van Rooy, A.; Orij, E. N.; Kamer, P. C. J.; van Leeuwen, P. W. N. M. *Organometallics* **1995**, *14*, 34-43.
[44] van Leeuwen, P. W. N. M.; Roobeek, C. F. Olefin hydroformylation. EP54986, **1982**.
[45] Abatjoglou, A. G.; Bryant, D. R.; Maher, J. M. Stabilization of phosphite ligands in hydroformylation process. EP697391, **1996**.
[46] Billig, E.; Abatjoglou, A. G.; Bryant, D. R. Homogeneous rhodium carbonyl compound-phosphite ligand catalysts and process for olefin hydroformylation. US4769498, **1988**.
[47] Cuny, G. D.; Buchwald, S. L. *J. Am. Chem. Soc.* **1993**, *115*, 2066-2068.

became the prototype in the subsequently developed phosphite ligands. Moreover, Röper and Paciello (BASF) correlated product linearity in Rh-catalysed hydroformylation of oct-1-ene with structural data of closely related bisphosphite ligands (Figure 12).[48] The explanation was that ligands that stabilize the P–Rh–P angle around 120° lead to a higher *l/b* ratio, with ligand **L14a** providing the best results.[49]

I.4. Asymmetric rhodium-catalysed hydroformylation

A molecule whose mirror image is non-superimposable with the original molecule is called a *chiral molecule*. The molecule and mirror image (if non-superimposable) are called *enantiomers* or *optical isomers*.[50] This concept is very important in chemistry because the two enantiomers may have different biological properties. The synthesis or obtention of enantiomerically pure compounds is in high demand from the fragrance and pharmaceutical industries.[51] As shown in Figure 13, the enantiomers may have completely different biological activity and it is important to know their effects for biological purposes. For example, the smell of carvone depends on the enantiomer.[52] On the other hand, (*S*)-thalidomide has an embryo-toxic and teratogenic effects, whereas the (*R*)-thalidomide has a sedative effect.[53] In other cases, one enantiomer is active and the other does not show any biological activity (like for (*R*)-citalopram).[54]

---

[48] Paciello, R.; Siggel, L.; Kneuper, H.-J.; Walker, N.; Roper, M. *J. Mol. Catal. A: Chem.* **1999**, *143*, 85-97.
[49] a) Paciello, R.; Siggel, L.; Röper, M. *Angew. Chem. Int. Ed.* **1999**, *38*, 1920-1923. b) Kunze, C.; Selent, D.; Neda, I.; Schmutzler, R.; Spannenberg, A.; Börner, A. *Heteroat. Chem.* **2001**, *12*, 577-585. c) Monnereau, L.; Sémeril, D.; Matt, D. *Eur. J. Org. Chem.* **2010**, *2010*, 3068-3073.
[50] IUPAC. *Compendium of Chemical Terminology*, 2nd Ed. (the "Gold Book"). Blackwell Scientific Publications, Oxford, **1997**.
[51] Evans, P. A. Stereoselective Synthesis 3. 1st Edition ed.; Science of Synthesis, Vol. Volume 3; Georg Thieme Verlag KG, 2011.
[52] Leitereg, T. J.; Guadagni, D. G.; Harris, J.; Mon, T. R.; Teranishi, R. *J. Agric. Food. Chem.* **1971**, *19*, 785-787.
[53] Kim, J. H.; Scialli, A. R. *Toxicol. Sci.* **2011**, *122*, 1-6.
[54] Aronson, J. K. *Meyler's Side Effects of Drugs: The International Encyclopedia of Adverse Drug Reactions and Interactions*; Elsevier, 2016.

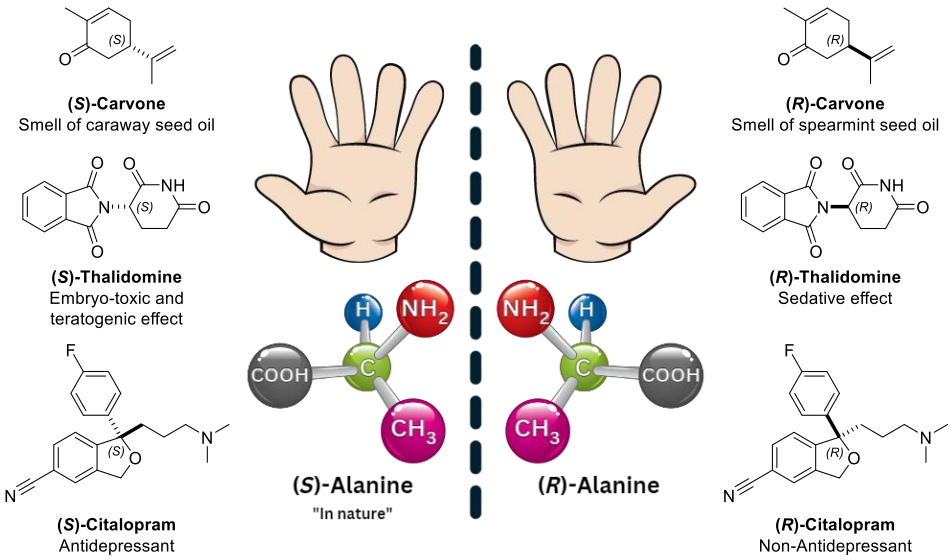

Figure 13. Chiral molecules and their biological properties of the enantiomers.

Asymmetric hydroformylation (AHF) has become an important tool to produce optically pure (or highly enantioenriched) aldehydes from alkenes.[55] Enantiopure aldehydes possess high value in the fragrance and pharmaceutical industries. Aldehydes, as previously mentioned, present a huge synthetic versality, as they can be easily transformed into other classes of organic compounds such as alcohols, imines, carboxylic acids, *etc.* (Figure 1).

Key aspects to consider for developing efficient chiral catalysts providing high conversions, regioselectivities and enantioselectivities must take into account i) the ligand skeleton, ii) the bite angle, iii) the electronic properties of the phosphorus atom and iv) the steric elements of the ligand.[56] In hydroformylation, enantiopure phosphorus ligands can be divided into two groups i) *P*-stereogenic ligands[57] (Figure 14) and ii) ligands with a stereogenic elements in the backbone (Figures 15 and 16).

[55] Chakrabortty, S.; Almasalma, A. A.; de Vries, J. G. *Catal. Sci. Technol.* **2021**, *11*, 5388-5411.
[56] Gillespie, J. A.; Dodds, D. L.; Kamer, P. C. J. *Dalton Trans.* **2010**, *39*, 2751-2764.
[57] Grabulosa, A. *P-Stereogenic Ligands in Enantioselective Catalysis*; Royal Society of Chemistry Publishing, 2011.

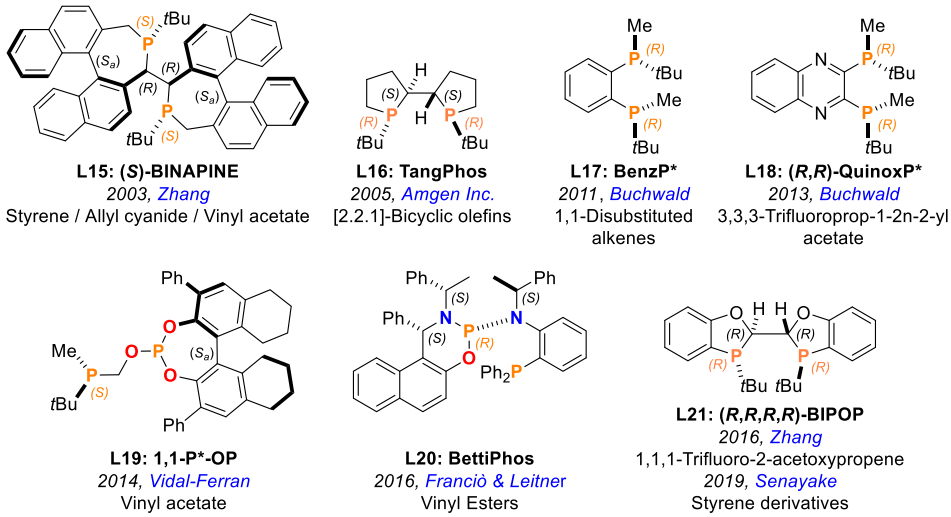

Figure 14. Selected enantiopure *P*-stereogenic ligands for asymmetric rhodium-catalysed hydroformylation.

In 1972, Ogata and Ikeda were the first to report the use of *P*-stereogenic phosphanes in asymmetric hydroformylation (AHF), but the enantioselectivity was moderate in the hydroformylation of styrene.[58] In subsequent studies, structurally diverse enantiopure *P*-stereogenic ligands were developed (for the structure of the ligands, see Figure 14). In 2003, Zhang reported high enantioselectivities for styrene (94% *ee*), allyl cyanide (94% *ee*) and vinyl acetate (87% *ee*) with (*S*)-BINAPINE (**L15**) as the ligand, although the regioselectivities were low.[59] TangPhos (**L16**), which was developed by Amgen Inc., is one of the best ligands for the AHF of norbornene (92% *ee* of the *exo*-product).[60] In 2011 and 2013, Buchwald and co-workers applied BenzP* (**L17**) and (*R*,*R*)-QuinoxP* (**L18**) in the AHF of 1,1-disubstituted alkenes (81–94% *ee*, 54–91% yields) and 3,3,3-trifluoroprop-1-en-2-yl acetate (92% *ee*) respectively.[61] Vidal-Ferran and co-workers reported several examples with mixed donor P–OP enantiopure ligands such as **L19** with a narrow bite angle and a *P*-stereogenic phosphane group (AHF of vinyl acetate *l*:*b* = 5:95, 61% *ee*).[62] For vinyl esters, Franciò, Leitner and co-workers reported the ligand BettiPhos (**L20**) (up to 82–95% *ee*).[63] Finally, in 2016, Zhang and co-workers reported the use of ligand (*R*,*R*,*R*,*R*)-BIPOP (**L21**) for

[58] Ogata, I.; Ikeda, Y. *Chem. Lett.* **1972**, 487-488.
[59] Tang, W.; Wang, W.; Chi, Y.; Zhang, X. *Angew. Chem. Int. Ed.* **2003**, *42*, 3509-3511.
[60] Huang, J.; Bunel, E.; Allgeier, A.; Tedrow, J.; Storz, T.; Preston, J.; Correll, T.; Manley, D.; Soukup, T.; Jensen, R.; *et al. Tetrahedron Lett.* **2005**, *46*, 7831-7834.
[61] a) Wang, X.; Buchwald, S. L. *J. Am. Chem. Soc.* **2011**, *133*, 19080-19083. b) Wang, X.; Buchwald, S. L. *J. Org. Chem.* **2013**, *78*, 3429-3433.
[62] Lao, J. R.; Benet-Buchholz, J.; Vidal-Ferran, A. *Organometallics* **2014**, *33*, 2960-2963.
[63] Schmitz, C.; Holthusen, K.; Leitner, W.; Franciò, G. *ACS Catal.* **2016**, *6*, 1584-1589.

1,1,1-trifluoro-2-acetoxypropene, which is a challenging substrate in AHF, and obtained high enantioselectivity (*l*/*b* = 1:8.5, 80% *ee*).[64] On the other hand, Senanayake reported the use of the same ligand **L21** for styrene derivatives providing high enantioselectivities (79–90% *ee*).[65]

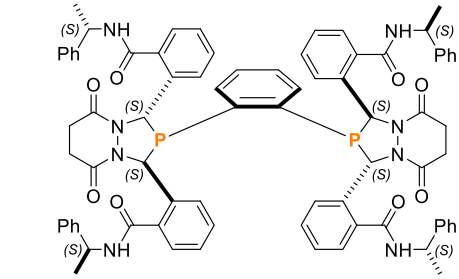

L22: (*S*,*S*,*S*)-BisDiazoPhos
2005, Landis
Styrene / Allyl cyanide / Vinyl acetate
2010, Landis & Stahl
Monosubstituted enamides / Allyl ethers / Allyl carbamates
2013, Landis
Z-Enamides / *Z*-Enol esters
2018, Landis
1,1'-Disubstituted acrylates

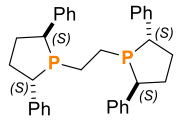

L23: (*S*,*S*)-Ph-BPE
2015, Morken
Terminal alkenes

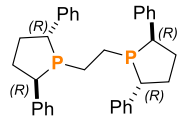

L24: (*R*,*R*)-Ph-BPE
2015, Morken
Internal alkenes

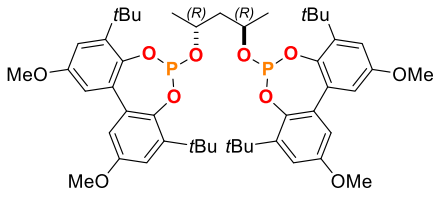

L25: (*R*,*R*)-Chiraphite
1993, Union Carbide Chemicals (UCC)
Vinyl arenes

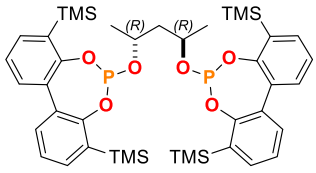

L26: (*R*,*R*)-Bisphosphite
1997, Kamer & van Leeuwen
Styrene

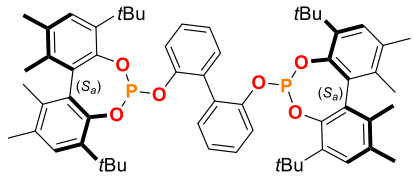

L27: (S_a,S_a)-Kelliphite
2004, Chirotec
Vinyl acetate / Vinyl cyanide

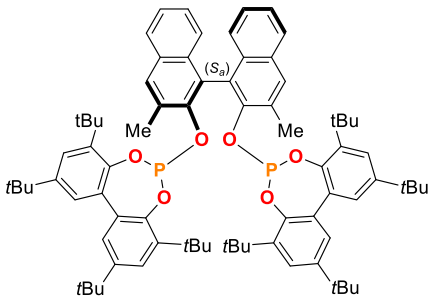

L28: (S_a)-Bisphosphite
2007, Zhang
Vinyl acetate

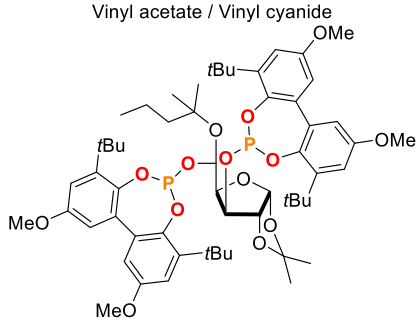

L29: Sugar-based Bisphosphite
2019, Claver & Godard
Norborenes

Figure 15. Selected enantiopure bisphosphanes (**L22**–**L24**) and bisphosphites (**L25**–**L28**) ligands for asymmetric rhodium-catalysed hydroformylation.

[64] Tan, R.; Zheng, X.; Qu, B.; Sader, C. A.; Fandrick, K. R.; Senanayake, C. H.; Zhang, X. *Org. Lett.* **2016**, *18*, 3346-3349.
[65] Qu, B.; Tan, R.; Herling, M. R.; Haddad, N.; Grinberg, N.; Kozlowski, M. C.; Zhang, X.; Senanayake, C. H. *J. Org. Chem.* **2019**, *84*, 4915-4920.

Selected enantiopure bidentate phosphorus ligands for AHF have been summarised in Figures 15 and 16. Enantiopure bisphosphane ligands are useful for some selected substrates (Figure 15, *ee*'s ranging from 73–99%). Between 2005 and 2018, Landis and co-workers reported several AHFs on an array of structurally diverse alkenes using (*S*,*S*,*S*)-BisDiazoPhos (**L22**) as the ligand. For styrene, allyl cyanide and vinyl acetate, the desired products were obtained in high regio- and enantio-selectivities (styrene *l:b* = 1:30 & 89% *ee*; allyl cyanide *l:b* = 1:4.8 & 87% *ee*; vinyl acetate *l:b* = 1:40 & 95% *ee*).[66] An excellent result for monosubstituted enamides (*ee* up to 99%), and allyl ethers and carbamates (*ee* up to 97%) were reported in 2010 by the same authors.[67] Internal alkenes are challenging substrates in AHF and the use of ligand **L22** provided high regio- and enantio-selectivities for (*Z*)-enamides (α:β = >50:1 and 92-99% *ee*) and (*Z*)-enol-esters (α:β = 6.3-99 and (α) = 85-94% *ee*), high regio- and enantio-selectivities were obtained.[68] In 2018, the AHF of 1,1′-disubstituted acrylates was achieved with high enantioselectivities when the substrate incorporated electron-withdrawing substituents at the 2-position, such as F (85% *ee*), OAc (73% *ee*) or OMe (90% *ee*), were reported.[69] Other important enantiopure bisphosphanes are (*S*,*S*)-Ph-BPE (**L23**) and (*R*,*R*)-Ph-BPE (**L24**) which were used by Morken and co-workers in the AHF of terminal (ligand **L23**, 90-99% *ee*) and internal alkenes (ligand **L24**, 82% *ee*).[70]

Other bidentate enantiopure ligands for AHF are structurally diverse bisphosphites. Through the years, these ligands have provided promising enantioselectivities in the AHF of different substrates (Figure 15). Union Carbide Chemicals (UCC) reported in a patent that (*R*,*R*)-Chiraphite (**L25**), which was developed by Babin and co-workers, was one of the first enantiopure bisphosphites used in the AHF of vinyl arenes obtaining good enantioselectivities (*ee*'s up to 90%).[71] In 1997, the ligand **L26** was developed by Kamer and van Leeuwen. Good enantioselectivities were obtained for styrene (*ee*'s up to 87%) with this ligand.[72] (S_a,S_a)-Kelliphite (**L27**), which incorporates a biphenol backbone, is a ligand developed by Chirotec. This ligand provided favourable enantioselectivities for vinyl acetate (88% *ee*) and

[66] Clark, T. P.; Landis, C. R.; Freed, S. L.; Klosin, J.; Abboud, K. A. *J. Am. Chem. Soc.* **2005**, *127*, 5040-5042.
[67] McDonald, R. I.; Wong, G. W.; Neupane, R. P.; Stahl, S. S.; Landis, C. R. *J. Am. Chem. Soc.* **2010**, *132*, 14027-14029.
[68] Abrams, M. L.; Foarta, F.; Landis, C. R. *J. Am. Chem. Soc.* **2014**, *136*, 14583-14588.
[69] Eshon, J.; Foarta, F.; Landis, C. R.; Schomaker, J. M. *J. Org. Chem.* **2018**, *83*, 10207-10220.
[70] Yu, Z.; Eno, M. S.; Annis, A. H.; Morken, J. P. *Org. Lett.* **2015**, *17*, 3264-3267.
[71] Babin, J. E.; Whiteker, G. T. Preparation of catalyst ligands for asymmetric synthesis. WO9303839, **1993**.
[72] Buisman, G. J. H.; van der Veen, L. A.; Klootwijk, A.; de Lange, W. G. J.; Kamer, P. C. J.; van Leeuwen, P. W. N. M.; Vogt, D. *Organometallics* **1997**, *16*, 2929-2939.

vinyl cyanide (78% *ee*).[73] In 2007, Zhang and co-workers reported the preparation and use of the enantiopure bisphosphite **L28**, which was applied in the AHF of vinyl acetate, obtaining good results in regioselectivity (*l*/*b* = 2:98) and enantioselectivity (80% *ee*).[74] Claver and Godard reported a sugar-based bisphosphite ligand (**L29**) for the AHF of norbornenes obtaining 96% of *exo*-selectivity and 71% *ee*.[75]

Furthermore, phosphane-phosphoramidite (**L30**), phosphane-phosphites (**L31**-**L34**) and bisphosphonite (**L35**) were used in AHF as well, as summarised in Figure 16. Zhang and co-workers reported high regio- and enantioselectivities, using (S_a,R_a)-*N*-Bn-YanPhos (**L30**) as a ligand for the AHF of substituted cyclopentene derivatives (up to *l*/*b* = 1:99 and 97% *ee*) and (*Z*)-alkenylsilanes (β:α = 99:1[76] and 91-96% *ee*).[77] There are more examples on the use of phosphane-phosphites in AHF, one of the first being related to enantiopure ligands (R_a,S_a)-Binaphos (**L31**), as reported in 1993 by Takaya and co-workers as one of the most versatile and high enantioselectivity in the AHF of a broad array of substrates.[78] The (S_a)-phosphane-phosphonite **L32** was developed by Reek and co-workers. Interestingly, this ligand is based on the Xantphos skeleton and was used in the AHF of dihydrofuran with up to 99% of regioselectivity and 91% of *ee*.[79] In 2014, Vidal-Ferran and co-workers applied the enantiopure ligand (S_a,R)-P–OP' **L33** in AHF. This ligand provides a short bite-angle upon binding with the metal centre and has the two ligating phosphorus atoms connected by a stereogenic carbon centre. This ligand **L33** gave moderate enantioselectivities for vinyl acetate (*l*/*b* = 1:99 with 74% *ee*) and 2,2-dihydrofurans (50/50 mixture of regioisomers with up to 80% *ee*).[80] Clarke and co-workers developed the ligand (S_a,*S*,*S*)-BOBPhos (**L34**) that was applied in AHF of styrene (*l*/*b* = 2:98 in 92% *ee*) and allylbenzenes (*l*/*b* = 14:86 and 92% *ee*).[81] Bisphosphonites were also studied in hydroformylation. For instance, (*R*,*R*,*R*,*R*)-bisphosphonite **L35**, which incorporates the TADDOL[82] fragment, was developed by Breit and

[73] Cobley, C. J.; Gardner, K.; Klosin, J.; Praquin, C.; Hill, C.; Whiteker, G. T.; Zanotti-Gerosa, A.; Petersen, J. L.; Abboud, K. A. *J. Org. Chem.* **2004**, *69*, 4031-4040. b) Cobley, C. J.; Klosin, J.; Qin, C.; Whiteker, G. T. *Org. Lett.* **2004**, *6*, 3277-3280.
[74] Zou, Y.; Yan, Y.; Zhang, X. *Tetrahedron Lett.* **2007**, *48*, 4781-4784.
[75] Cunillera, A.; Blanco, C.; Gual, A.; Marinkovic, J. M.; Garcia-Suarez, E. J.; Riisager, A.; Claver, C.; Ruiz, A.; Godard, C. *ChemCatChem* **2019**, *11*, 2195-2205.
[76] β position refers to the relative position to the silicon heteroatom.
[77] a) You, C.; Wei, B.; Li, X.; Yang, Y.; Liu, Y.; Lv, H.; Zhang, X. *Angew. Chem. Int. Ed.* **2016**, *55*, 6511-6514. b) You, C.; Li, X.; Yang, Y.; Yang, Y.-S.; Tan, X.; Li, S.; Wei, B.; Lv, H.; Chung, L.-W.; Zhang, X. *Nat. Commun.* **2018**, *9*, 2045.
[78] Sakai, N.; Mano, S.; Nozaki, K.; Takaya, H. *J. Am. Chem. Soc.* **1993**, *115*, 7033-7034.
[79] Chikkali, S. H.; Bellini, R.; Berthon-Gelloz, G.; van der Vlugt, J. I.; de Bruin, B.; Reek, J. N. H. *Chem. Commun.* **2010**, *46*, 1244-1246.
[80] Fernández-Pérez, H.; Benet-Buchholz, J.; Vidal-Ferran, A. *Chem. Eur. J.* **2014**, *20*, 15375-15384.
[81] Noonan, G. M.; Cobley, C. J.; Mahoney, T.; Clarke, M. L. *Chem. Commun.* **2014**, *50*, 1475-1477.
[82] TADDOL is an acronym that refers to α,α,α,α-tetraaryl-1,3-dioxolane-4,5-dimethanol.

co-workers and used in the AHF of styrene derivatives (*l*/*b* = 16:84 and 91% *ee*).[83]

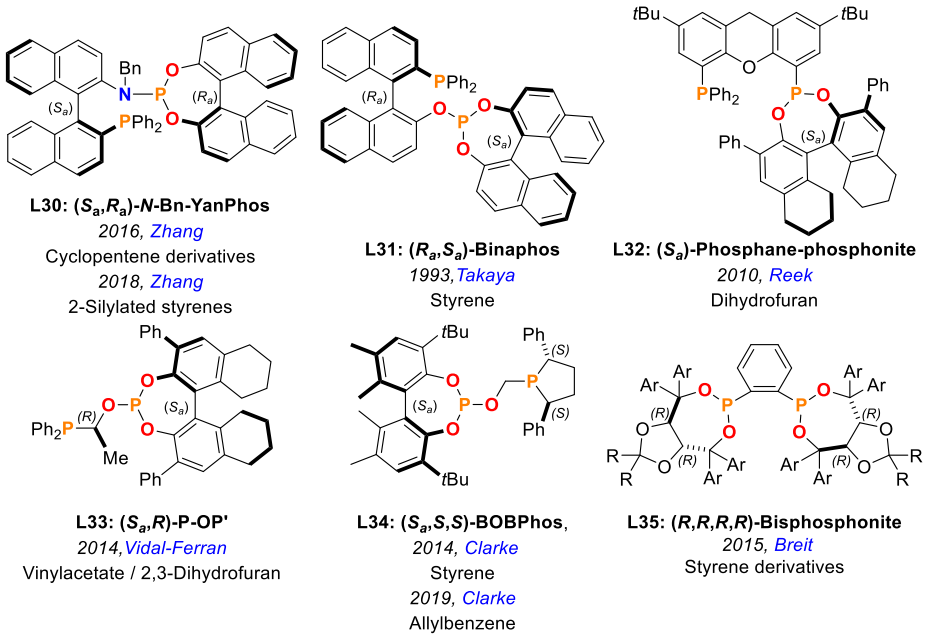

Figure 16. Selected enantiopure phosphane-phosphoramidite (**L30**), phosphane-phosphites (**L31**–**L34**) and bisphosphonite (**L35**) ligands for asymmetric rhodium-catalysed hydroformylations.

I.5. Supramolecular approaches in catalysis

The field of supramolecular catalysis was inspired by the enzymatic machinery in nature, which involves the participation of reversible interactions, such as hydrogen bonding, cation-π interaction, hydrophobic forces, *etc.*, in the catalytic event in order to increase the rate of a chemical reaction and/or its selectivity.[84] Therefore, the term of supramolecular catalysis refers to a catalytic system involving supramolecular interactions[85] with a recognition site capable of binding the components of the catalytic reaction.[86] The different supramolecular chemistry interactions have been summarised according to their nature and strength (kJ/mol) in the Figure 17.

[83] Allmendinger, S.; Kinuta, H.; Breit, B. *Adv. Synth. Catal.* **2015**, *357*, 41-45.
[84] a) Raynal, M.; Ballester, P.; Vidal-Ferran, A.; van Leeuwen, P. W. N. M. *Chem. Soc. Rev.* **2014**, *43*, 1660-1733. b) Raynal, M.; Ballester, P.; Vidal-Ferran, A.; van Leeuwen, P. W. N. M. *Chem. Soc. Rev.* **2014**, *43*, 1734-1787.
[85] Cragg, P. J. *A Practical Guide to Supramolecular Chemistry*; John Wiley & Sons, Ltd, 2005.
[86] van Leeuwen, P. W. N. M.; Raynal, M. *Supramolecular Catalysis: New Directions and Developments*; Wiley-VCH GmbH, 2022.

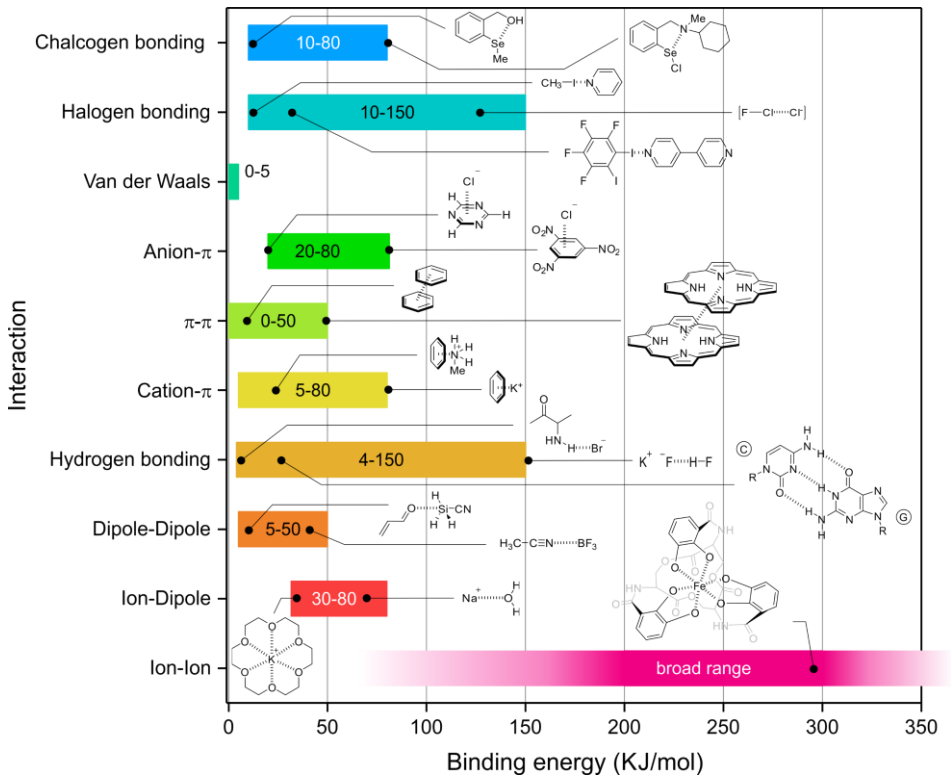

Figure 17. Schematic representation of supramolecular interactions.

Supramolecular interactions have become an alternative and powerful tool in catalysis in the recent years. They have contributed to achieve excellent results in the chemo-, regio- and enantio-selectivities in diverse catalytic reactions. Four strategies have been developed for the design and synthesis of supramolecular catalysts:[84,85,86]

a) Ligand-ligand interactions: The ligands contain the building blocks for the supramolecular assembly through supramolecular interactions to generate the catalyst (Figure 18a).

b) Ligand-additive interactions: The ligand interacts through supramolecular interactions with an external agent (regulation agent, allosteric effector, or cofactor, among other names in the literature). As a result, the performance of the catalyst is improved (Figure 18b).

c) Catalyst-substrate interactions: The catalytic system contains binding sites capable of establishing supramolecular interactions with the substrate(s). The chemo-, regio- and/or enantio-selectivity of the reaction is improved as a result of the pre-organization of the substrate within the catalytic site (Figure 18c).

d) Multiple reactions: Supramolecular interactions between the components of the catalytic system (*i.e.*, metal centres, substrates, anionic or cationic counterparts, *etc.*) help in improving the performance of the catalyst (Figure 18d).

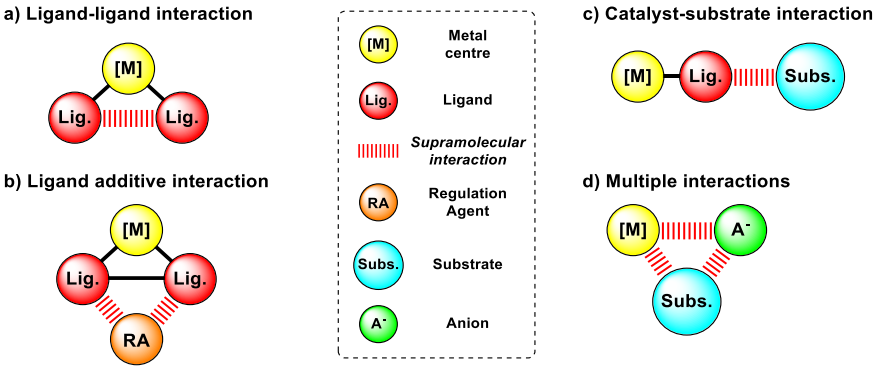

Figure 18. Schematic representation of supramolecular interactions for catalysis.

The supramolecular regulation approach involves the maximization of the performance of the catalyst by an external agent (the so-called regulation agent or RA) that binds away from the catalytic site, but has an effect in the outcome of the catalytic process (Figure 19). This strategy was inspired by the phenomenon called *allosterism*, which is observed in enzyme catalysis. *Allosterism* is described by the change in the affinity for binding process of a molecule, or the change in the outcome of a catalytic event, that is caused by the binding of another molecule or allosteric effector away from the active site.[87] Ito and co-workers pioneered the field of supramolecular regulation in non-natural systems in enantioselective allylation reactions of α-nitro ketones and α-nitro esters with allyl acetate.[88]

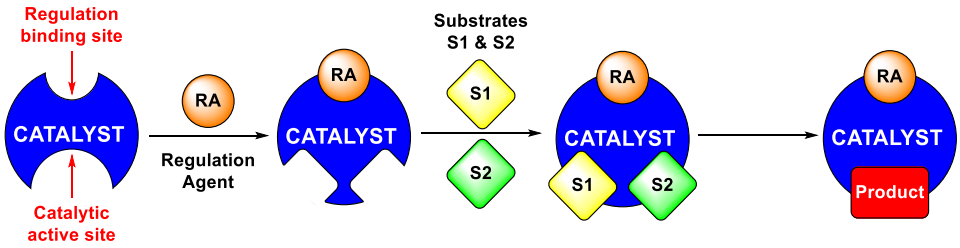

Figure 19. Schematic representation of the supramolecular regulation approach.

Research activities of our group have focussed and still focus on supramolecularly regulated catalysis. Our group's approach is going to be

[87] Pelley, J. W. 3 - Protein Structure and Function. In *Elsevier's Integrated Review Biochemistry (Second Edition)*, Pelley, J. W. Ed.; W.B. Saunders, 2012; pp 19-28.
[88] Sawamura, M.; Nakayama, Y.; Tang, W.-M.; Ito, Y. *J. Org. Chem.* **1996**, *61*, 9090-9096.

summarised in this introduction. Our group has already published a few modular designs of the catalytic system, in which the supramolecular ligand contains a polyether chain as the regulation site bonded to metal ligating groups (G) for catalysis. In some supramolecular ligands, a linking group (X) was included in the regulation site in order to: i) have additional stereogenic motifs; and/or ii) limit the flexibility of the polyether chain (Figure 20).[89]

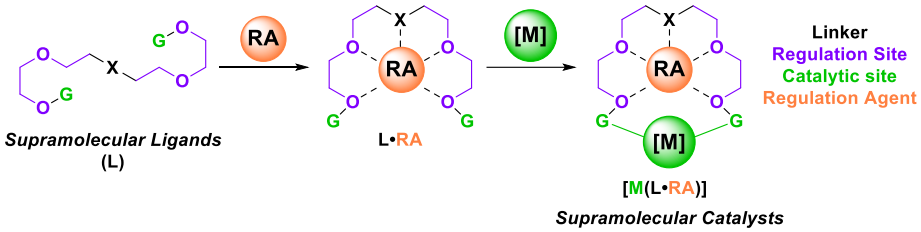

Figure 20. Schematic representation of the supramolecular approach in Vidal-Ferran's group.

The regulation agent (RA) in our supramolecular approach is a salt derived from alkali metals, alkaline earth metals, lanthanides, or organic amines.[90] The RA interacts with the regulation site through non-covalent interactions producing a change in the three-dimensional structure of the catalytic site depending on the size and shape of the regulation agent. Regarding the catalytic site, the group has mainly focused on metal complexes of ligands containing monophosphite, bisphosphite or bisoxazoline ligating groups (G) and rhodium(I), palladium(II), gold(I) and copper(I) as metal centres ([M]). These supramolecularly regulated catalysts have been applied in different catalytic transformations of interest.[91]

Our group has successfully applied the regulation strategy to rhodium asymmetric hydroformylation reactions (AHF) of several alkenes obtaining excellent results. For vinyl esters, the combined use of RbBArF as the RA and ligand **L36** provides an increase up to 81% in the conversion, an improvement in the *l*/*b* ratio from 90:10 to 99:1 and an increase up to 64% in the enantiomeric excess in the AHF of vinyl acetate **S1** (Scheme 7). Based on computational studies, Vidal-Ferran and co-workers proposed that RbBArF adjusts the P–Rh–P bond angle of the catalytic site to the optimal value for achieving almost perfect enantioselectivity in the AHF reaction. The combination of ligand **L36** with RbBArF as the RA led to a high increase in enantioselectivity for the vinyl esters **S2** and **S3** (63% and 82%, respectively).

---

[89] Vaquero, M.; Rovira, L.; Vidal-Ferran, A. *Chem. Commun.* **2016**, *52*, 11038-11051.
[90] Carreras, L.; Rovira, L.; Vaquero, M.; Mon, I.; Martin, E.; Benet-Buchholz, J.; Vidal-Ferran, A. *RSC Adv.* **2017**, *7*, 32833-32841.
[91] Llorente, N.; Fernández-Pérez, H.; Núñez-Rico, J. L.; Carreras, L.; Martínez-Carrión, A.; Iniesta, E.; Romero-Navarro, A.; Martínez-Bascuñana, A.; Vidal-Ferran, A. *Pure Appl. Chem.* **2019**, *91*, 3-15.

The ligand **L36** was also tested in the AHF of styrene and allyloxytrimethylsilane as substrates.[92]

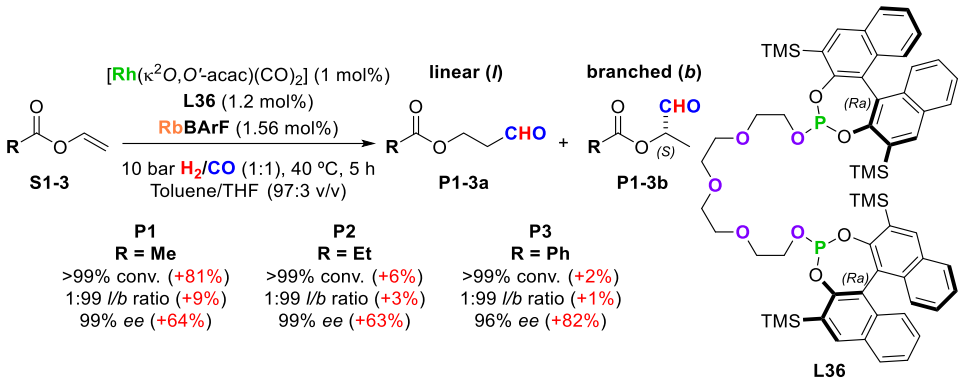

Scheme 7. Supramolecular regulation in the asymmetric hydroformylation of vinyl esters (**S1-3**) with Rh(I)-complexes derived from bisphosphite **L36** (values in brackets denote the difference between the results with and without a RA).

Furthermore, kinetic studies on the AHF of vinyl acetate (**S1a**) employing the supramolecular ligand **L36** and RbBArF as the RA were performed. The kinetic studies were carried out employing FlowNMR under the reaction conditions indicated in Scheme 7. Variable Time Normalization Analysis (VTNA)[93] was used to extract relevant kinetic parameters from the raw concentration data against time measured by NMR spectrometry. This simplified kinetic analysis demonstrated first-order kinetics for the catalyst and substrate (Figure 21).[94]

[92] Mon, I.; Jose, D. A.; Vidal-Ferran, A. *Chem. Eur. J.* **2013**, *19*, 2720-2725.
[93] Burés, J. *Angew. Chem. Int. Ed.* **2016**, *55*, 16084-16087.
[94] Martínez-Carrión, A.; Howlett, M. G.; Alamillo-Ferrer, C.; Clayton, A. D.; Bourne, R. A.; Codina, A.; Vidal-Ferran, A.; Adams, R. W.; Burés, J. *Angew. Chem. Int. Ed.* **2019**, *58*, 10189-10193.

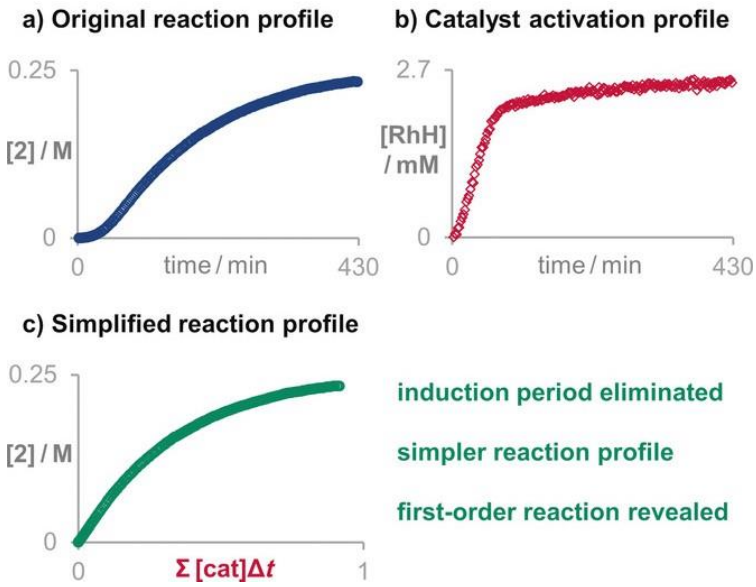

Figure 21. a) The original reaction profile of the asymmetric hydroformylation reaction catalysed of vinyl acetate under the reaction conditions of scheme 6 is corrected by b) the profile of the active catalyst to reveal c) a simple first-order reaction profile.

Our research group also published the AHF of heterocyclic alkenes such as 2,3,6,7-tetrahydrooxepine (**S4**) and 2,3-dihydrofuran (**S5**). For these substrates, the group developed new supramolecularly regulated bisphosphites, such as **L37**, with a stereogenic motif incorporated in the linker in the regulation site. The addition of KBArF as a RA led to an increase of 76% in the conversion and 83% in the enantioselectivity for the heterocyclic alkene **S4**. On the other hand, for the heterocyclic alkene **S5**, the addition of KBArF provided an increase of 33% in the conversion, an improvement in the ratio of the α:β aldehydes from 38:62 to 80:20 and, finally, an increase of 68% in the enantiomeric excess of the aldehyde **P5-α** (Scheme 8).[95]

[95] Rovira, L.; Vaquero, M.; Vidal-Ferran, A. *J. Org. Chem.* **2015**, *80*, 10397-10403.

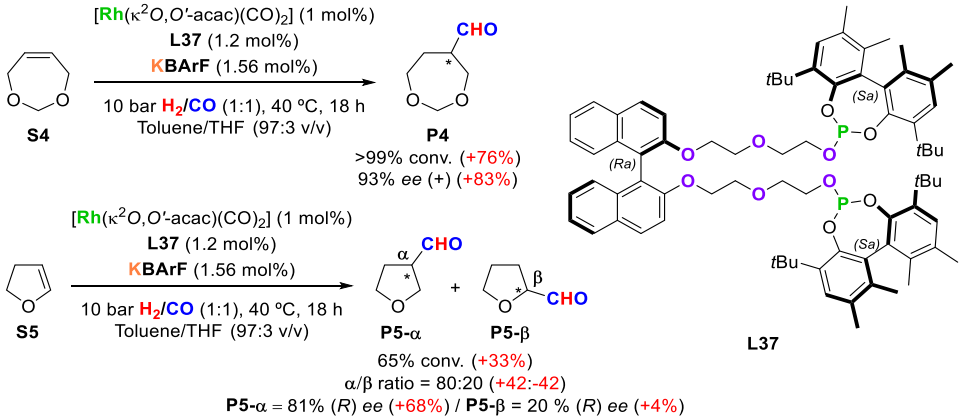

Scheme 8. Supramolecular regulation of AHF of heterocyclic alkenes employing Rh(I)-complexes derived from bisphosphite **L37** (values in brackets denote the difference between the results with and without an RA).

The supramolecular regulation of the AHF for aryl vinyl ethers (**S6-13**) was performed using the bisphosphite ligand **L38** (Scheme 9). This supramolecular ligand has a conformationally labile biphenyl group as a linker in order to limit the flexibility of the polyether chain. The best RA for phenyl vinyl ether (**S6**) was LiBArF, whose use led to an increase in the conversion by 70%, in the *l*/*b* ratio from 8:92 to 1:99 and in the enantiomeric ratio (*S*:*R*) from 78:22 to 92:8 for **P6a** at 40ºC. The reaction was optimized at 25ºC with an increase in the enantiomeric ratio from 92:8 to 94:6, but at the expense of a lower conversion. It was also applied to a set of structurally diverse aryl vinyl ethers (**S7-13**). The substrates studied have been summarized in Scheme 9, with conversions being up to 83%, and enantiomeric ratios up to 97:3 (*S*:*R*).[96]

[96] Martínez-Carrión, A. The Hydroformylation Reaction: from Covalent to Supramolecular Approaches and *Operando* Kinetic Studies. *Univertitat Rovira i Virgili*, **2020**.

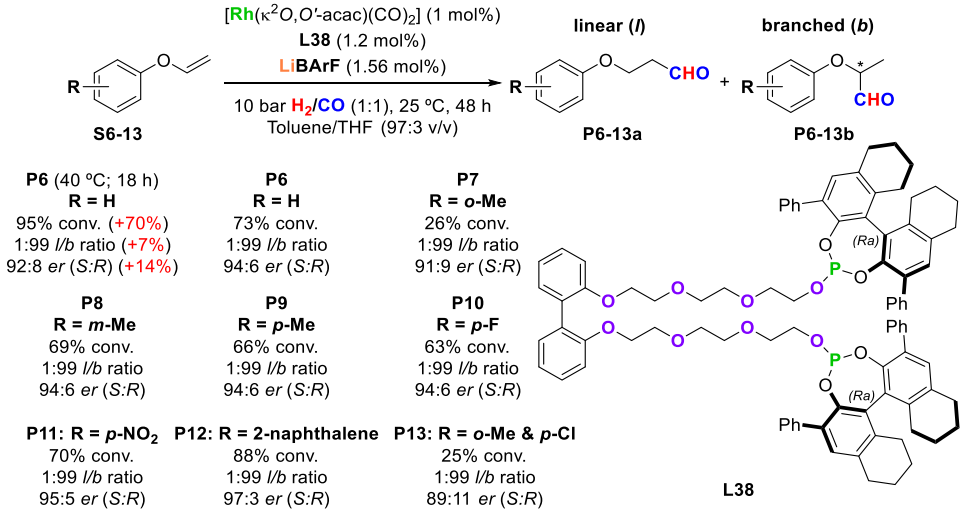

Scheme 9. Supramolecular regulation of asymmetric hydroformylation of aryl vinyl ether derivatives with Rh(I)-complexes derived from bisphosphite **L38** (values in brackets denote the difference between the results with and without an RA).

Encouraged by the performance of the supramolecular ligands with a distal regulation site in AHF, the group studied other transformations of interest.

The supramolecular regulation strategy was also applied in the AHs of functionalised alkenes **S14-17** using the bisphosphite **L39** as the supramolecular ligand (Scheme 10). For this reaction, an enantiomeric ammonium BArF salt proved to be the most efficient RA. The ammonium BArF salt increased the enantioselectivity by 3% and the conversion by 2% for the substrates **S14-16**. However, CsBArF as the RA provided the best results for the alkene **P17**, increasing the enantioselectivity by 5%.[97] A similar regulation strategy for rhodium-mediated asymmetric hydrogenations was also reported by Fan and co-workers.[98]

[97] Vidal-Ferran, A.; Mon, I.; Bauzá, A.; Frontera, A.; Rovira, L. *Chem. Eur. J.* **2015**, *21*, 11417-11426.
[98] Li, Y.; Ma, B.; He, Y.; Zhang, F.; Fan, Q.-H. *Chem. Asian J.* **2010**, *5*, 2454-2458.

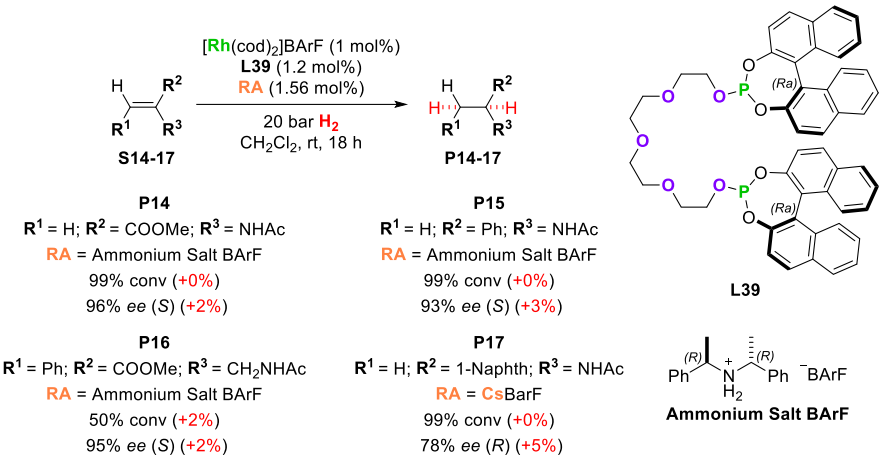

Scheme 10. Supramolecular regulation of asymmetric hydrogenations of functionalised alkenes with Rh(I)-complexes derived from bisphosphite **L39** (values in brackets denote the difference between the results with and without an RA).

In 2016, a study of allylic substitutions with Pd(II)-complexes derived from the supramolecular ligand **L40** was published by members of our research group (Scheme 11). The allylic acetate **S18** was reacted with C-nucleophiles derived from DMM[99] and with benzylamine (BZA)[100], each nucleophile requiring its own optimal palladium precursor and RA for obtaining the allylic substitution product with the highest possible enantioselectivity. For DMM, the combined use of RbOAc with [$PdCl_2$(cod)] and ligand **L40** provided the best results in terms of enantioselectivity of the final compound (increase up to 6% in the ee; Scheme 10). On the contrary, the indistinct use of $Mg(OTf)_2$, $La(OTf)_3$ or $Ho(OTf)_3$ in combination with [{Pd(η^3-allyl)(μ-Cl)}$_2$] and ligand **L40** provided the best results for the nucleophilic substitution of **S18** with BZA (increase in the *ee* up to 16%).[101]

[99] DMM refers to dimethyl malonate.
[100] BZA refers to benzylamine.
[101] Rovira, L.; Fernández-Pérez, H.; Vidal-Ferran, A. *Organometallics* **2016**, *35*, 528-533.

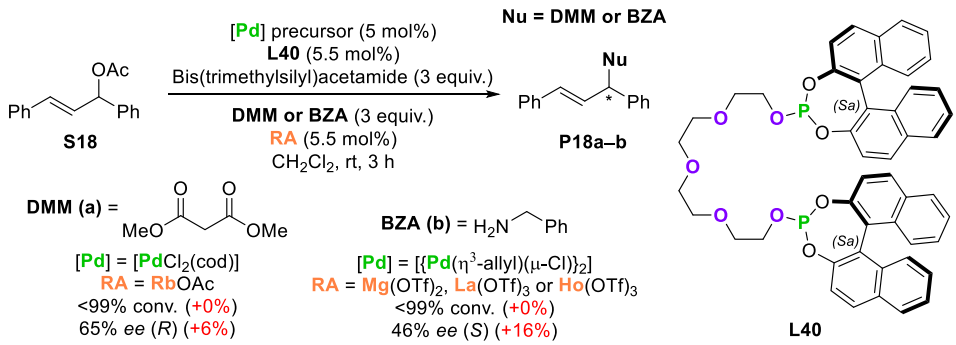

Scheme 11. Supramolecular regulation of allylic substitutions with Pd(II)-complexes derived from bisphosphite **L40** (values in brackets denote the difference between the results with and without an RA).

In 2020, our research group published a supramolecularly regulated Au(I)-catalyst with a monophosphite ligand. The Au(I)-complex **C8** was successfully applied in the selective *para*-C–H functionalization of phenols **S19-24** and related derivatives with gold carbenes derived from diazo derivatives (Scheme 12). The addition of the RA improved the yield up to 20% for product **P20** when RbBArF was employed as the RA. The reaction took place quantitatively for **P22**. DFT calculations suggested that the use of regulation agents derived from cations with a large size, like RbBArF or CsBArF, favoured the insertion of the gold-carbene into the *para*-position of the phenols **S19-24**.[102]

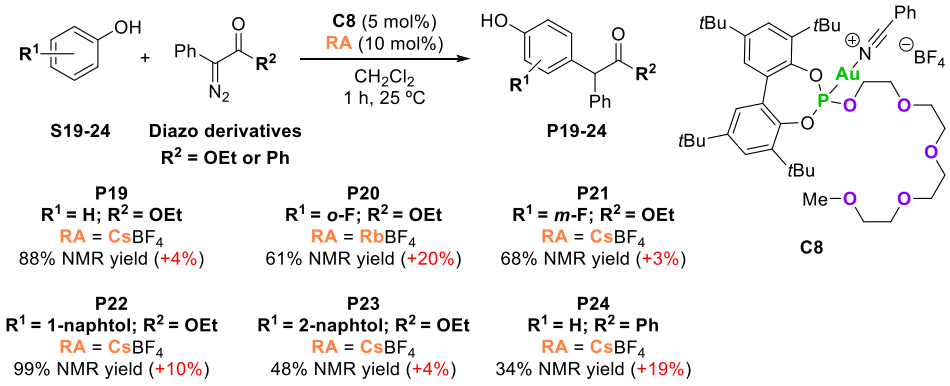

Scheme 12. Supramolecular regulation of *para*-C–H functionalization of aromatic alcohols with gold(I)-complex **C8** (values in brackets denote the difference between the results with and without an RA).

On the other hand, the group also published the functionalization of O–H bonds of substituted phenols (**S25-30**) employing supramolecularly regulated

[102] Carreras, L.; Franconetti, A.; Grabulosa, A.; Frontera, A.; Vidal-Ferran, A. *Org. Chem. Front.* **2020**, *7*, 1626-1634.

catalysts (Scheme 13). In this case, the group designed supramolecular ligand **L41** with a polyether chain as a regulation site and two oxazoline motifs as ligating groups towards copper(I) centres. The addition of NaBArF increased the yield up to 55% for the insertion of the corresponding Cu-carbenoids into O–H bond of substrate **S26**. For this reaction, the group discovered the optimal RA, such as NaBArF, KBArF or RbBArF, for the different combinations of phenol and diazo derivatives. The use of the optimal RA increased the yield in all the cases, achieving final yield up to 99%.[103]

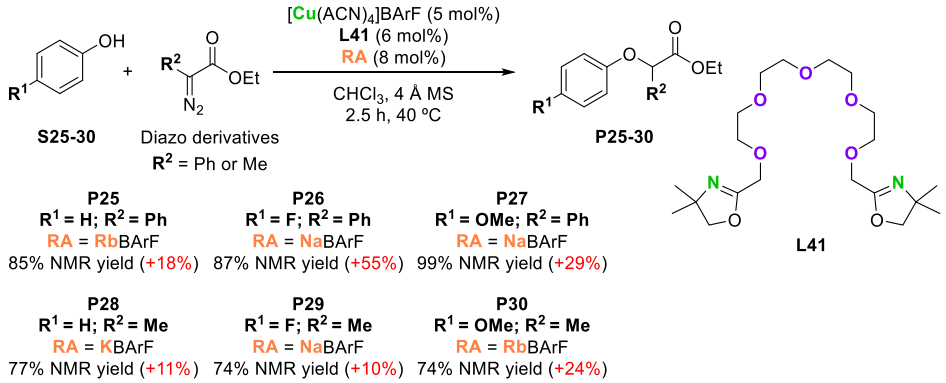

Scheme 13. Supramolecular regulation of copper carbenoid insertion reactions into O–H bonds with Cu(I)-complexes derived from bisoxazoline **L41** (values in brackets denote the difference between the results with and without an RA).

X-Ray analysis confirmed the coordination of both oxazoline units to the copper centre and the coordination of sodium within the polyether chain as regulation site of the supramolecular catalyst (Figure 22).[103]

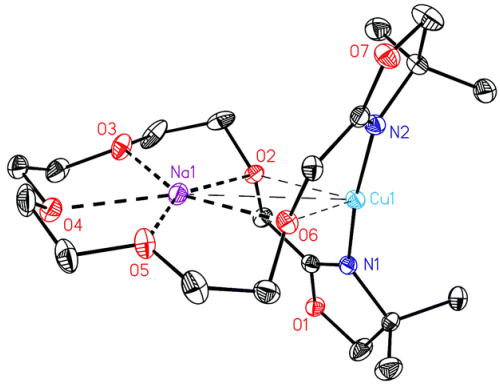

Figure 22. ORTEP drawing of the crystal structure of [Cu(**L41**•$NaPF_6$)]PF_6. Hydrogen and PF_6 groups have been omitted for clarity. Colour scheme: C: black, Cu: turquoise, N: blue, O: red, Na: purple.

[103] Iniesta, E.; Vidal-Ferran, A. *Chem. Commun.* **2020**, *56*, 6364-6367.

Hydrogen-bonding (H-bond) is an interesting supramolecular interaction that can be applied in catalysis as detailed in chapter 3 of this doctoral thesis.[104] Hydrogen-bonding is an electrostatic attractive force between a hydrogen (H) atom which is covalently bonded to a more electronegative donor atom or group (**Dn**), and another electronegative atom bearing a lone pair of electrons (the so-called hydrogen bond acceptor (**Ac**)). The most common **Dn** and **Ac** atoms are oxygen (O), nitrogen (N), fluorine (F) and bromine (Br). Some examples of hydrogen bonds have been drawn in Figure 23a. It is interesting to note that the bifluoride derivative (**1**) present one of the strongest H-Bond energies ever observed ($E_{(H-F)}$ = 60-120 kJ/mol), whereas one of the weakest has been found in the interaction between an aminic proton in compound **2** and the H of hydrogen bromide ($E_{(H-Br)}$ = 4.6 kJ/mol).[105] Furthermore, the interaction between the two strands in DNA *via* hydrogen bonding is the main responsible of the DNA's double helical structure. Scientist have observed that the sequence of nucleobases within DNA strands plays a significant role in dictating the self-assembled structure by association of complementary nucleobases (*e.g.*, cytosine (C) and guanine (G), with a hydrogen bonding energy in complex **3** of 23.8 kJ/mol).[106]

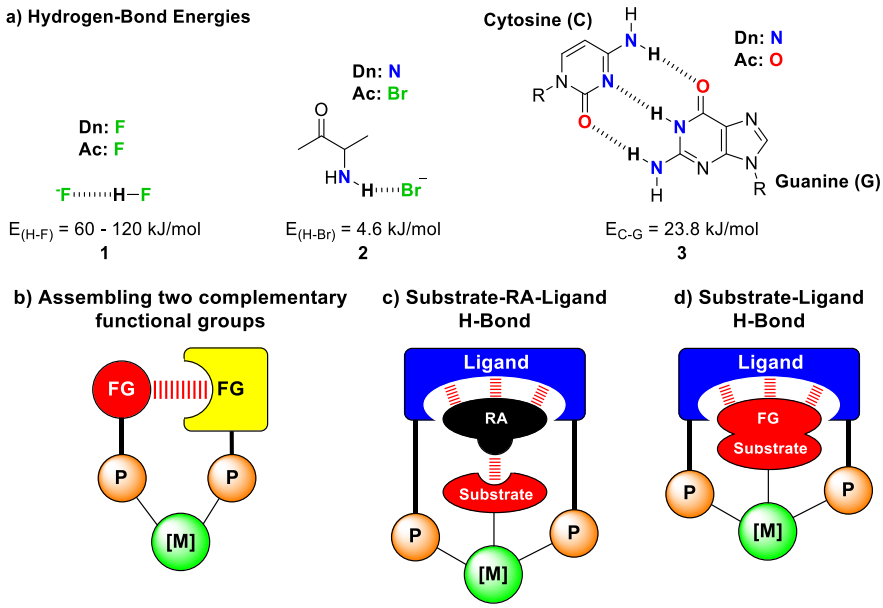

Figure 23. Examples of the hydrogen bonded assemblies in catalysis.

Hydrogen bonding has been used in different ways in supramolecular catalysis. Figure 23b shows the assembly between two building blocks that

[104] Reek, J. N. H.; De Bruin, B.; Pullen, S.; Mooibroek, T. J.; Kluwer, A. M.; Caumes, X. *Chem. Rev.* **2022**, *122*, 12308-12369.
[105] *Core Concepts in Supramolecular Chemistry and Nanochemistry*; John Wiley & Sons Ltd., 2007.
[106] Biedermann, F.; Schneider, H.-J. *Chem. Rev.* **2016**, *116*, 5216-5300.

behave as a hydrogen-bonded bisphosphane, with the formation of the corresponding supramolecular metal complex. Breit and co-workers pioneered the self-assembly of monodentate ligands *via* hydrogen bonding interactions in order to build bidentate ligands. One seminal example is presented in Scheme 14a, in which the monophosphanes **L42** (6-DPPA) and **L43** (3-DPPICon) assembled through hydrogen bonding to form the supramolecular bisphosphane rhodium complex **C9**. This approach is inspired by the A–T[107] DNA pairs. This supramolecular rhodium catalyst incorporating an assembled bidentate bisphosphane was tested in the hydroformylation reaction of oct-1-ene (**S31a**), with an overall increase in the regioselectivity towards the linear aldehyde up to 94:6 (Scheme 14b).[108]

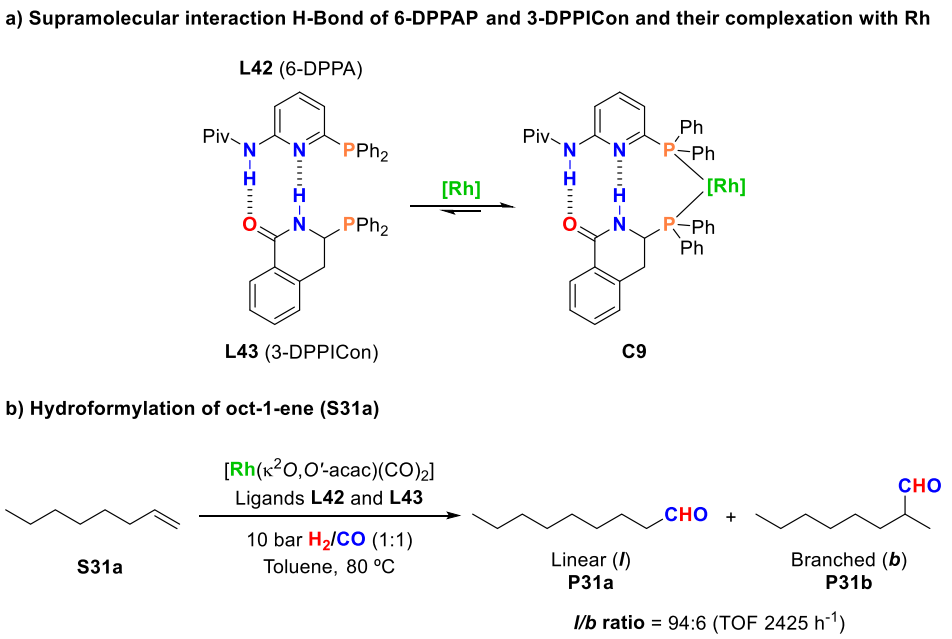

Scheme 14. a) Self-assembled monodentate ligands 6-DPPAP (**L42**) and 3-DPPICon (**L43**). b) Hydroformylation using ligands **L42** and **L43**.

Secondly, Figure 23b summarizes another elegant example of the use of hydrogen bonding in catalysis developed by Reek and co-workers The addition of an enantiopure molecule **4** favours the formation of a chiral conformation of **L44** through the formation of hydrogen bonds. The enantiopure anion of the regulation agent plays an important role in preventing the interconversion of conformations derived from the resulting complex and in conferring chiral properties to the resulting complex **L44•4**. This complex was tested in asymmetric hydrogenations (Scheme 15). The enantiopure molecule **4** was the regulation agent (called co-factor by the

[107] A and T refer to adenosine and thymine, respectively.
[108] Breit, B.; Seiche, W. *Angew. Chem. Int. Ed.* **2005**, *44*, 1640-1643.

authors) that led to the highest conversions and enantioselectivities (up to 93% conversion and 98% *ee*) in the asymmetric hydrogenations of substrates **S32-34**.[109]

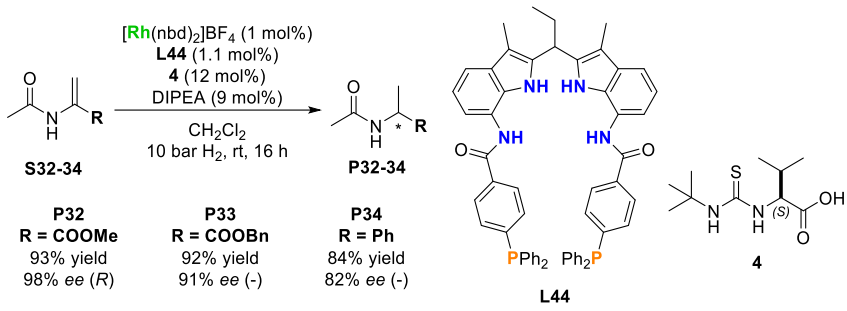

Scheme 15. Asymmetric hydrogenation of alkenes with a supramolecular catalyst generated *via* hydrogen-bonding interactions.

Another elegant strategy was developed by Reek and co-workers for hydroformylating hydroxycarbonyl-substituted styrenes in a selective manner (see Figure 23c for the design principle and Scheme 16 for the results). The catalytic system and substrate contained complementary binding motifs that allowed for the preorganization of the substrate within the catalytic system through the formation of hydrogen bonds. The ligand designed (DIMPhos2, structure **L45** in Scheme 16) was tested in the hydroformylation of internal alkenes and derivatives of styrene, with all substrates incorporating a COOH group placed at a strategic position of the molecule that favoured addition of the CHO group at a specific carbon of the C=C bond (See Scheme 16). The alkenes studied were converted to the corresponding aldehydes with high conversions and *ex/in* aldehyde ratios up to 19:81.[110] The same ligand was tested in the hydroformylation of hydroxycarbonyl-substituted styrenes **S14a-i**. The terminal aldehyde is usually the disfavoured product in the hydroformylation of styrenes, but the use of DIMPhos2 (**L45**) pre-organized the substrate in such a way that the CHO group was bonded to the terminal position of the vinyl group throughout the hydroformylation process. Most remarkably, *l/b* ratios up to >99:<1 towards the linear aldehyde were achieved in a set of substituted styrenes (Scheme 16).[111]

[109] Dydio, P.; Rubay, C.; Gadzikwa, T.; Lutz, M.; Reek, J. N. H. *J. Am. Chem. Soc.* **2011**, *133*, 17176-17179.
[110] Dydio, P.; Detz, R. J.; Reek, J. N. H. *J. Am. Chem. Soc.* **2013**, *135*, 10817-10828.
[111] a) Dydio, P.; Reek, J. N. H. *Angew. Chem. Int. Ed.* **2013**, *52*, 3878-3882. b) Dydio, P.; Detz, R. J.; de Bruin, B.; Reek, J. N. H. *J. Am. Chem. Soc.* **2014**, *136*, 8418-8429.

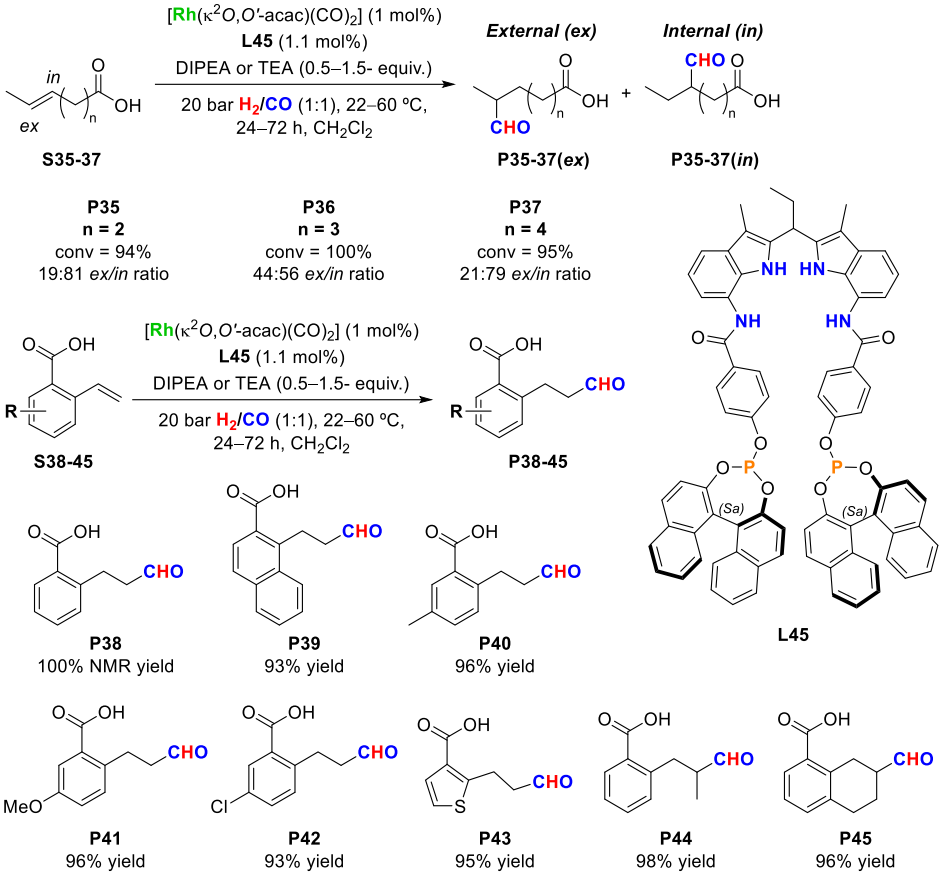

Scheme 16. Hydroformylations of alkenes with a supramolecular catalyst *via* hydrogen-bonding interactions.

OBJECTIVES

Overall, the previous discussion shows that cobalt and rhodium complexes are privileged catalysts in homogenous hydroformylation. Previous results in this area of research demonstrate that the use of phosphorus-based ligands improves the selectivity of the reaction. The chemo-, regio- and enantio-selectivity of a specific substrate can be controlled if the right ligand is used.

Taking into account the past research activities of the group in the design and development of efficient and stereoselective hydroformylation catalysts, the objectives of the present thesis are the:

1. Design, synthesis, and application of cobalt-Xantphos complexes for the valorisation of mixtures of alkenes, majorly leading to the linear aldehyde through the isomerisation-hydroformylation tandem reactions.

2. Design, synthesis, and application of supramolecularly bisphosphite ligands, with a polyether chain as regulation site, in rhodium catalysed hydroformylations in order to maximise the *l*/*b* ratio by means of the addition of a regulation agent (alkali metal BArF salts).

Application of supramolecularly regulated catalysts for the preparation of valuable aldehydes for the fragrance industry.

3. Design, synthesis, and application of new supramolecularly regulated hydroformylation catalyst operating with anionic regulation agents.

CHAPTER I

Valorisation of Mixtures of Linear Alkenes using Cobalt-Mediated Isomerisation and Hydroformylation Chemistries

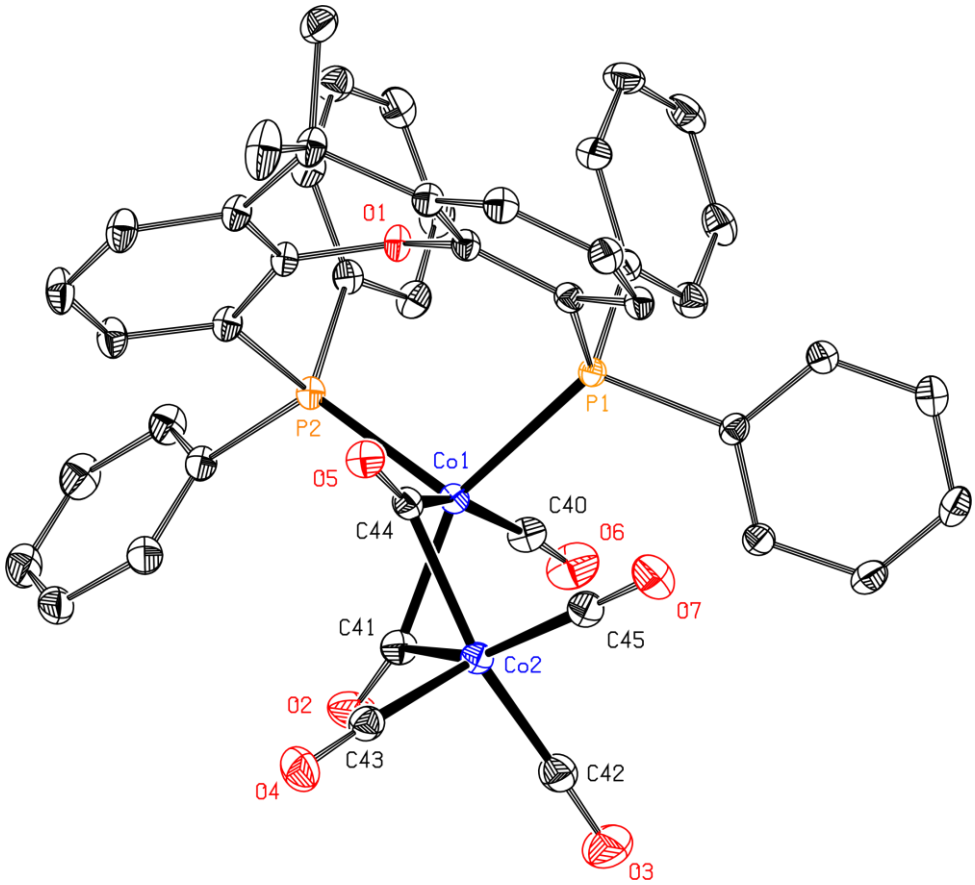

Valorisation of Mixtures of Linear Alkenes using Cobalt-Mediated Isomerisation and Hydroformylation Chemistries

Catal. Sci. Techno., **2022**, *12*, 3219-3227

Alicia Martínez-Carrión,[a] **Andrés Romero-Navarro**,[a,b] José Luis Núñez-Rico,[b,c] Albert Gutiérrez,[b,c] Arnald Grabulosa[b,c] and Anton Vidal-Ferran[b,c,d*]

[a] Institute of Chemical Research of Catalonia (ICIQ), Av. Països Catalans 16, 43007 Tarragona, Spain.

[b] Department of Inorganic and Organic Chemistry, University of Barcelona, C. Martí i Franquès 1-11, 08028 Barcelona, Spain.

[c] Institut de Nanociència i Nanotecnologia (IN2UB), Universitat de Barcelona, 08028 Barcelona, Spain.

[d] Institució Catalana de Recerca i Estudis Avançats (ICREA), Pg. Lluís Companys 23, 08010 Barcelona, Spain.

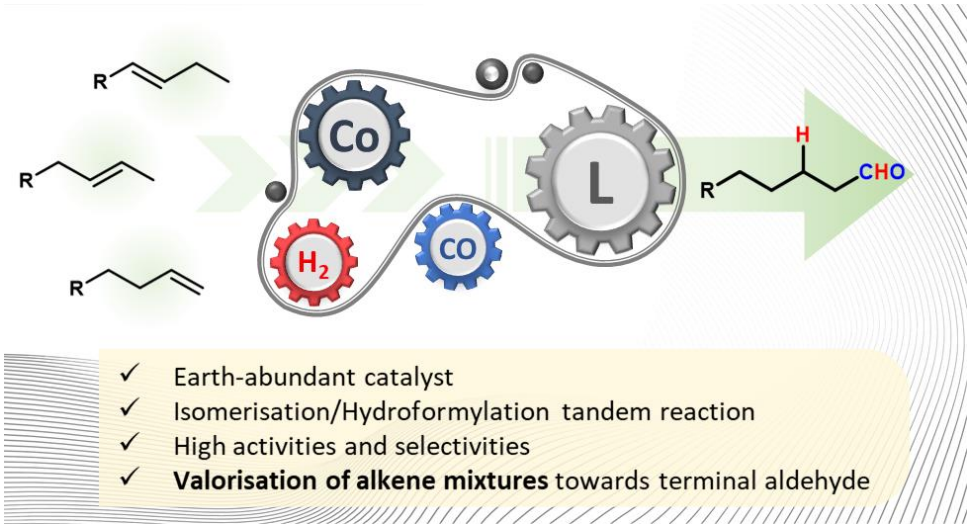

1.1. ABSTRACT

Active catalysts derived from cobalt and the Xantphos ligand were synthesised, characterised, and tested in the hydroformylation of pure linear alkenes or their mixtures. The preformed complex $[(OC)_3Co(\mu\text{-}CO)_2Co(CO)(\kappa^2P,P\text{-Xantphos})]$ (**C11**) showed similar reactivity

and selectivity towards aldehydes as the active catalyst formed *in situ* from equimolar amounts of $[Co_2(CO)_8]$ and Xantphos (**L5**). In the case of oct-1-ene, the linear aldehyde was obtained with good chemo- and regio-selectivity (linear to branched ratio was up to 75:25). For all octene isomers, tandem isomerisation-hydroformylation processes took place. Regioselectivities for all the studied octene isomers remained practically constant, independently of the position or geometry of the C=C double bond in the starting material. Moreover, by-products were formed in similarly small amounts for all the octene isomers. We also demonstrated that this chemistry is an interesting strategy for valorising mixtures of linear hexenes, heptenes or octenes by transforming the initial mixture into one major aldehyde (addition of a CHO group to the C_1 carbon of the alkene skeleton, up to 73% selectivity). Moreover, these mixtures of alkenes were hydroformylated with low final amounts of non-hydroformylated alkenes, hydrogenated alkenes, and alcohols.

1.2. INTRODUCTION

Cobalt-catalysed hydroformylations were discovered by Otto Roelen in 1938.[3] First reports of cobalt-catalysed hydroformylations avoided the use of ligands and operated at high temperatures and pressures.[112] The introduction of ligands produced important milestones in this chemistry, such as catalyst stabilisation,[19] increased activity of the catalyst,[15b] smoothing of the reaction conditions,[113] and/or improved chemo- and/or regio-selectivities.[114]

Alkenes, under cobalt-catalysed hydroformylation reaction conditions, can undergo several transformations in addition to hydroformylation (mainly C=C isomerisation and hydrogenation).[15b,25a,115,116] Moreover, depending on the reaction conditions and the catalyst employed, the hydroformylation products are unstable and evolve into the corresponding alcohols through the hydrogenation of the C=O double bond.[15b,7,9] Up to a certain extent, the complexity of the outcome of cobalt-catalysed hydroformylations can be reduced by tuning the reaction conditions (mainly H_2 and CO partial pressures and the temperature, but also the catalyst concentration, the choice of solvent

---

[112] a) Duembgen, G.; Neubauer, D. *Chem. Ing. Tech.* **1969**, *41*, 974-980. b) Cornils, B. *React. Struct.: Concepts Org. Chem.* **1980**, *11*, 1-225.
[113] Murata, K.; Matsuda, A.; Masuda, T. *J. Mol. Catal.* **1984**, *23*, 121-132.
[114] a) Slaugh, L. H.; Mullineaux, R. D. *J. Organometal. Chem.* **1968**, *13*, 469-477. b) Achonduh, G.; Yang, Q.; Alper, H. *Tetrahedron* **2015**, *71*, 1241-1246. c) Crause, C.; Bennie, L.; Damoense, L.; Dwyer, C. L.; Grove, C.; Grimmer, N.; Rensburg, W. J. v.; Kirk, M. M.; Mokheseng, K. M.; Otto, S.; *et al. Dalton Trans.* **2003**, 2036-2042. d) Bungu, P. N.; Otto, S. *Dalton Trans.* **2007**, 2876-2884. e) Bungu, P. N.; Otto, S. *J. Organomet. Chem.* **2007**, *692*, 3370-3379.
[115] Cornils, B.; Herrmann, W. A.; Beller, M.; Paciello, R. *Applied Homogeneous Catalysis with Organometallic Compounds*; Wiley-VCH Verlag GmbH & Co. KGaA, 2017.
[116] Boerner, A.; Franke, R. *Hydroformylation: Fundamentals, Processes, and Applications in Organic Synthesis*; Wiley-VCH Verlag GmbH & Co. KGaA, 2016.

or the use of additives).[3,15b,117] The use of organic ligands in cobalt-catalysed hydroformylations simplifies the complexity of the reaction mixtures, shifting the outcome of the reaction towards the products of interest. For instance, tertiary trialkyl monophosphanes have been exploited in hydroformylations as useful ligands for increasing the regioselectivity towards linear products (Shell process).[114a,118]

Bisphosphane ligands (for instance, $Ph_2P(CH_2)_nPPh_2$, with n = 2, 4 or 5) were introduced in cobalt-catalysed hydroformylations at the early stages of the application of this chemistry.[114a] Regioselectivity towards *n*-hexanal in the hydroformylation of pent-1-ene drops with the size of the cobalt chelate (regioselectivity towards the linear aldehyde for n = 5 ≈ n = 4 > n = 2, see Table 1).[23,113,114a]

Table 1. Hydroformylation of pent-1-ene.

Entry	Ligand	Conv. (%)	*l*/*b* ratio (%)
1	$Ph_2P(CH_2)_2PPh_2$	96	56:44
2	$Ph_2P(CH_2)_4PPh_2$	99	75:25
3	$Ph_2P(CH_2)_5PPh_2$	99	74:26

Catalysts were prepared *in situ* by adding the corresponding ligand to $[Co_2(CO)_8]$.

The use of bisphosphane ligands with a well-defined rigid backbone improves the catalytic results in the hydroformylation of terminal alkenes to aldehydes.[119,120] Stanley and co-workers[24] reported highly active cationic cobalt(II) catalysts for hydroformylation. These authors noted that the activity of the monometallic catalyst precursor $[Co(\kappa^2O,O'\text{-acac})(DEPBz)]BF_4$ (**C4**, DEPBz = 1,2-bis(diethylphos-phaneyl)benzene) approached that of rhodium[9a,11,121] catalysts (see Table 2). Interestingly, two years later, Franke and co-workers reported that the cobalt(II) cationic complexes **C1**–**C4** synthesised by the procedure of Stanley and co-workers had extremely low activity under the published conditions.[24b] The results published by Franke and co-coworkers are in contradiction with those reported by Stanley *et al.*, which will probably motivate further studies in this area of research.

[117] Bartik, T.; Bartik, B.; Hanson, B. E. *J. Mol. Catal.* **1993**, *85*, 121-129.
[118] Bohnen, H.-W.; Cornils, B. *Adv. Catal.* **2002**, *47*, 1-64.
[119] Kluwer, A. M.; Krafft, M. J.; Hartenbach, I.; de Bruin, B.; Kaim, W. *Topics in Catalysis* **2016**, *59*, 1787-1792.
[120] Hood, D. M.; Johnson, R. A.; Carpenter, A. E.; Younker, J. M.; Vinyard, D. J.; Stanley, G. G. *Science* **2020**, *367*, 542-548.
[121] For selected examples of rhodium hydroformylation, see the references that follow and those cited therein: a) Kamer, P. C. J.; Reek, J. N. H.; van Leeuwen, P. W. N. M. Mechanisms in Homogeneous Catalysis. A Spectroscopic Approach. In *Rhodium Catalyzed Hydroformylation*, Wiley Online Books, 2005; pp 231-269. b) Nurttila, S. S.; Linnebank, P. R.; Krachko, T.; Reek, J. N. H. *ACS Catal.* **2018**, *8*, 3469-3488.

Table 2. Results of the hydroformylation of 3,3-dimethylbut-1-ene with cobalt and rhodium catalysts.

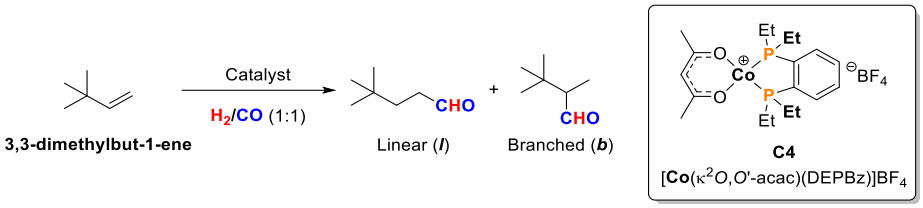

Entry	Catalyst	Aldehyde (%)	*l*/*b* ratio (%)
1	**C4**	85	51 : 49
2	Rh + BiPhePhos (**L13**)	96	99 : 1
3	Rh + PPh_3	91	34 : 66

The Rh metal precursor used is [Rh(κ^2*O*,*O'*-acac)$(CO)_2$]. In entries 2 and 3, the catalysts were prepared *in situ*. BiPhePhos = 6,6′-[(3,3′-Di-*tert*-butyl-5,5′-dimethoxy-[1,1′-biphenyl]-2,2′-diyl)bis(oxy)]bis(6*H*-dibenzo[d,f][1,3,2]dioxaphosphepine).

The isomerisation of C=C double bonds and the hydroformylation reaction itself are competing processes under cobalt-catalysed hydroformylation reaction conditions.

The formation of a complex mixture of aldehydes is the main consequence of the isomerisation processes under hydroformylation conditions. Interestingly, if C=C isomerisations are faster than the hydroformylations, the net addition of the H and CHO groups will take place, irrespective of the position and geometry of the C=C bond in the starting material, at the most reactive and/or favourable position of the C=C double bond after isomerisation. Although it has been reported that unmodified hydrido carbonyl cobalt complexes such as $[Co(CO)_4H]$ play an important role in C=C isomerisations,[25a,116,122] examples of cobalt-based hydroformylations of long chain internal alkenes are scarce in the literature.[114b,123]

The main objective of this work was to develop cobalt-based catalysts for the selective production of C_l-aldehydes irrespective of the position and geometry of the C=C bond in a given hydrocarbon skeleton. In terms of the ligand to be used, we hypothesised that cobalt catalysts incorporating the

[122] a) Taylor, P.; Orchin, M. *J. Am. Chem. Soc.* **1971**, *93*, 6504-6506. b) Hendrix, W. T.; Von Rosenberg, J. L. *J. Am. Chem. Soc.* **1976**, *98*, 4850-4852.
[123] For examples, see: a) Fell, B.; Rupilius, W.; Asinger, F. *Tetrahedron Lett.* **1968**, *9*, 3261-3266. b) Asinger, F.; Fell, B.; Rupilius, W. *Ind. Eng. Chem., Prod. Res. Develop.* **1969**, *8*, 214. c) Kniese, W.; Nienburg, H. J.; Fischer, R. *J. Organomet. Chem.* **1969**, *17*, 133-141; d) Beller, M.; Krauter, J. G. E. *J. Mol. Catal. A: Chem.* **1999**, *143*, 31-39. e) Dabbawala, A. A.; Parmar, J. N.; Jasra, R. V.; Bajaj, H. C.; Monflier, E. *Catal. Commun.* **2009**, *10*, 1808-1812. f) Delolo, F. G.; Yang, J.; Neumann, H.; dos Santos, E. N.; Gusevskaya, E. V.; Beller, M. *ACS Sustainable Chem. Eng.* **2021**, *9*, 5148-5154.

Xantphos ligand[124] (Xantphos = (9,9-dimethyl-9*H*-xanthene-4,5-diyl)bis(diphenylphosphane); **L5**) could be appropriate given its wide bite angle[124] (bite angle with Rh as metal centre = 111.4º) that could favour the preferential formation of C_1-aldehydes. While rhodium-catalysed hydroformylations using Xantphos-type ligands[124,125] have been well studied, their use in cobalt-catalysed hydroformylation remains unexplored. We also hypothesised that the use of an excess of cobalt centres (as a tool to mediate C=C bond isomerisations) with respect to the ligand could lead to the discovery of selective catalysts for the addition of a CHO group to the C_1 carbon of the alkene skeleton (Scheme 17).

Herein, we describe the results obtained in the tandem isomerisation/hydroformylation reactions of linear alkenes employing cobalt catalysts. We also demonstrate that mixtures of alkenes differing in the position and geometry of the C=C double bond can be transformed into one major aldehyde.

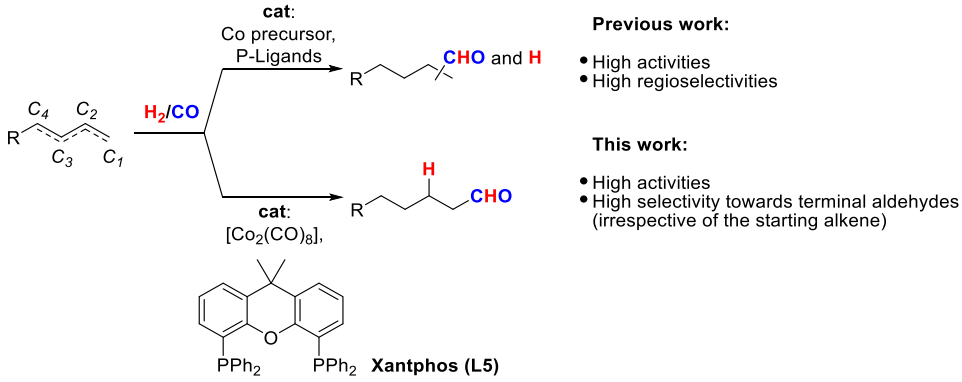

Scheme 17. Overview of the hydroformylation process.

[124] van Leeuwen, P. W. N. M.; Kamer, P. C. J. *Catal. Sci. Technol.* **2018**, *8*, 26-113.
[125] a) van der Veen, L. A.; Keeven, P. K.; Kamer, P. C. J.; van Leeuwen, P. W. N. M. *J. Chem. Soc., Dalton Trans.* **2000**, 2105-2112. b) Landis, C. R.; Uddin, J. *J. Chem. Soc., Dalton Trans.* **2002**, 729-742. c) Bronger, R. P. J.; Kamer, P. C. J.; van Leeuwen, P. W. N. M. *Organometallics* **2003**, *22*, 5358-5369. d) Ohtsuka, Y.; Kobayashi, O.; Yamakawa, T. *J. Fluorine Chem.* **2014**, *161*, 34-40. e) Vieira, G. M.; Granato, A. V.; Gusevskaya, E. V.; dos Santos, E. N.; Dixneuf, P. H.; Fischmeister, C.; Bruneau, C. *Appl. Catal. A* **2020**, *598*, 117583.

1.3. RESULTS AND DISCUSSION

1.3.1. Synthesis of Xantphos-Cobalt Complexes

Our investigations began with the synthesis and characterisation of suitable cobalt complexes derived from the Xantphos ligand for the hydroformylation reactions. The line of reasoning behind the ligand design included standard cobalt complexes in hydroformylation[15b,25a,115,116] (for instance, the hydrido dicarbonyl complex of cobalt(I) (**C10**[126]; Scheme 18) and other complexes with different ratios of the number of Xantphos units to the number of cobalt centres. For instance, we hypothesised that in complexes with **L5**/[Co] ratios lower than 1:1 (such as **C11**[127]; Scheme 18), one cobalt centre could be responsible for the hydroformylation and the other for the C=C isomerisation.

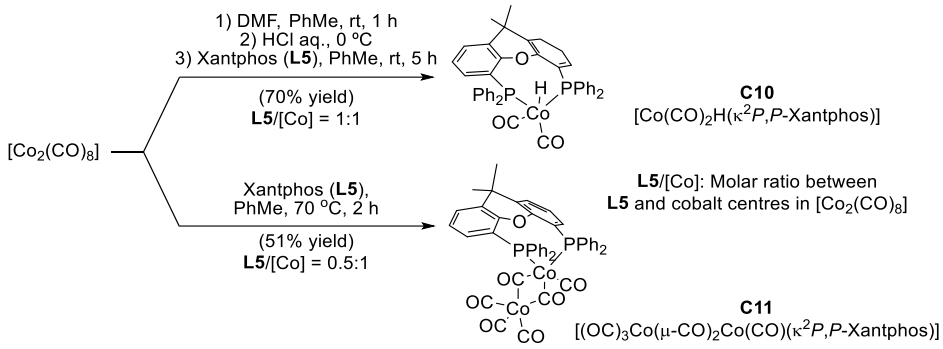

Scheme 18. Synthesis of cobalt-Xantphos complexes.

We envisaged that **C10** could be prepared from $[Co(CO)_4H]$ and Xantphos through the displacement of two CO ligands. The $[Co(CO)_4H]$ complex was prepared following the methodology developed by Roodt[128] and Kluwer[119] and co-workers, which consisted of disproportionating $[Co_2(CO)_8]$ into $[Co(DMF)_6]^{2+}$ and $[Co(CO)_4]^-$ species. The complex **C10** was isolated in a 70% yield after acidification of $[Co(CO)_4]^-$ with the formation of $[Co(CO)_4H]$ followed by the reaction with Xantphos (Figure 18). As expected, the IR spectrum showed two strong C≡O bands at 1910 and 1971 cm^{-1}. ^1H NMR spectroscopy showed a triplet signal at –11.23 ppm, corresponding to the hydrido ligand coupled to two equivalent phosphorus nuclei from the ligand ($^2J_{P-H}$ = 23.3 Hz). The multiplicity of the signal and the magnitude of the coupling constants suggested that both P–groups were coordinated in equatorial positions and the hydrido ligand in an axial position in a trigonal-bipyramidal cobalt geometry.[123a] The structure of **C10** was confirmed

[126] **C10** complex refers to $[Co(CO)_2H(Xantphos)]$, see structure in Scheme 18.
[127] **C11** complex refers to $[(CO)_3Co(\mu\text{-}CO)_2Co(CO)(Xantphos)]$, see structure in Scheme 18.
[128] Haumann, M.; Meijboom, R.; Moss, J. R.; Roodt, A. *Dalton Trans.* **2004**, 1679-1686.

by single-crystal X-Ray diffraction analysis,[129] which confirmed the axial position of the hydrido ligand at a distorted trigonal-bipyramidal cobalt centre (Figure 24 shows the IR and ^{31}P NMR spectra and the X-Ray structure of **C10**). The bisequatorial binding mode of the two phosphino groups at the trigonal-bipyramidal metal centre was also demonstrated by X-Ray analysis (P–Co–P bond angle = 110.2º).

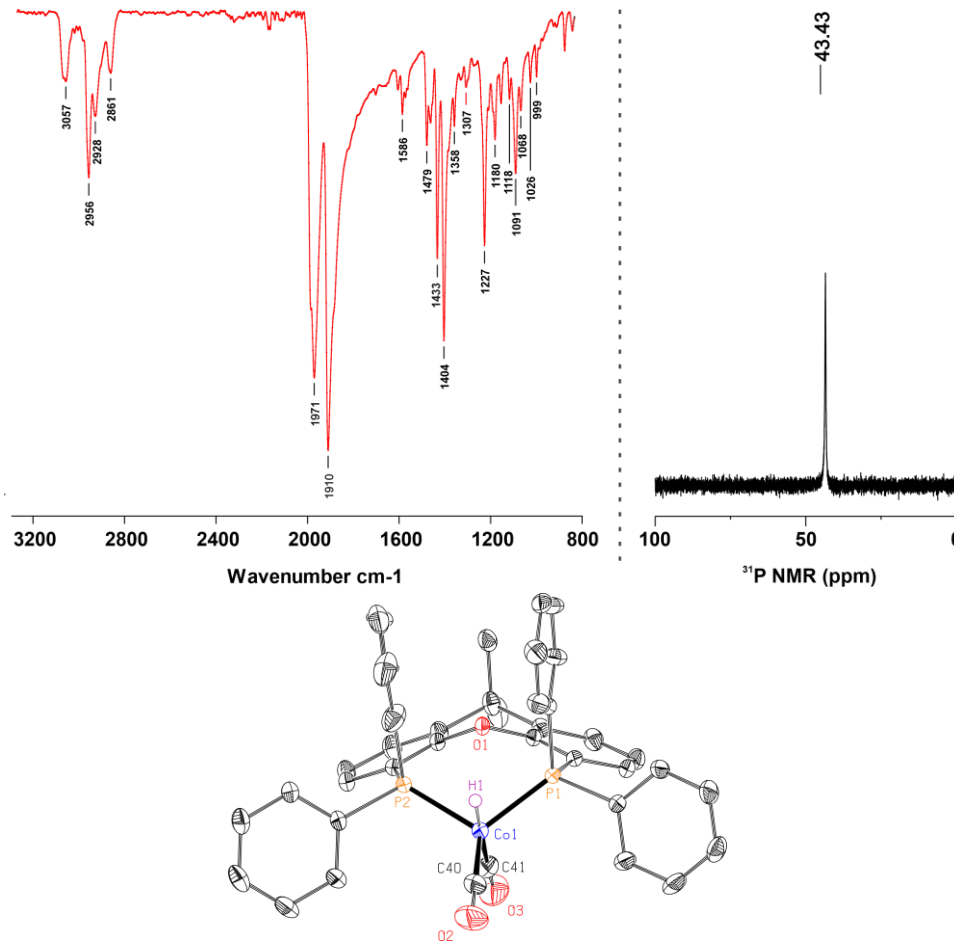

Figure 24. IR and ^{31}P MMR spectra (top) and ORTEP plot of the crystal structure of **C10** (bottom). Hydrogen atoms have been omitted for clarity. Colour scheme: C: black, Hydride: violet, Co: blue, O: red, P: orange.

[129] For details of the X-Ray structures of **C10** and **C11**, see the experimental section 1.5.2.1 and 1.5.2.2, respectively.

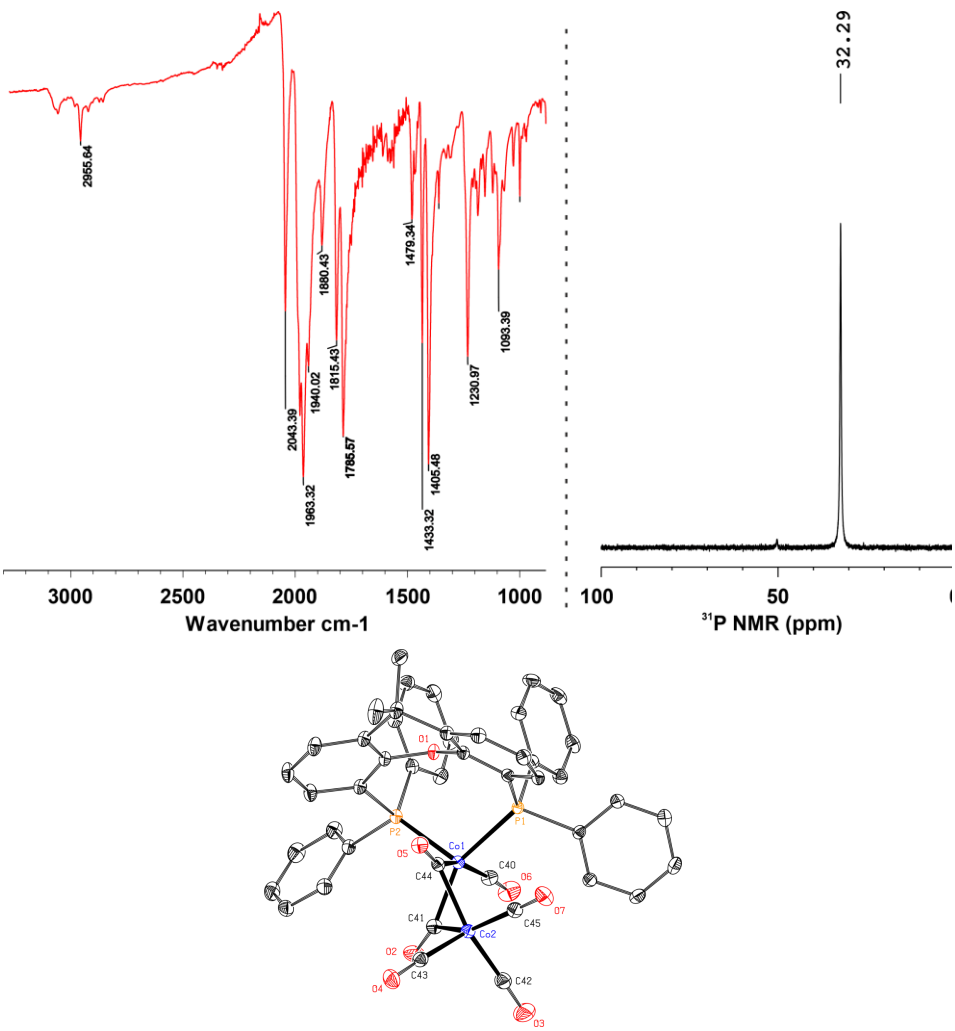

Figure 25. IR and ^{31}P MMR spectra (top), and ORTEP plot of the crystal structure of **C11** (bottom). Hydrogen atoms have been omitted for clarity. Colour scheme: C: black, Co: blue, O: red, P: orange.

The cobalt(0) complex **C11** was prepared by reacting equimolar amounts of $[Co_2(CO)_8]$ with Xantphos. The complex crystallised out from the reaction mixture, which allowed for a practical preparation protocol. Complex **C11** was characterised with standard spectroscopic techniques and X-ray analysis unequivocally confirmed the structure of **C11** as $[(OC)_3Co(\mu\text{-}CO)_2Co(CO)(\kappa^2P,P\text{-Xantphos})]$[129] (Scheme 18 shows the synthesis and Figure 25 shows the IR and ^{31}P NMR spectra and the X-ray structure of **C11**). Interestingly, the Xantphos ligand was coordinated with the same cobalt atom ($d_{Co\text{-}Co}$ = 2.51 Å; $d_{P\text{-}Co}$ = 2.258 and 2.308 Å), with the other cobalt atom

being coordinated only with CO ligands.[130] The coordination of both phosphino groups from Xantphos (**L5**) to the same cobalt centre was confirmed with X-Ray analysis (P–Co–P bond angle = 105.06º).

1.3.2. Development of optimal hydroformylation reaction conditions for oct-1-ene as a model substrate

We envisioned that the combination of a metal centre, such as cobalt, with a wide bite angle bisphosphane ligand, such as Xantphos, would be a suitable starting point in developing efficient hydroformylation reaction conditions for oct-1-ene (**S31a**).[131] The hydroformylation of oct-1-ene can potentially lead to a mixture of different products. The main aldehydes nonanal (**P31a**) and 2-methyloctanal (**P31b**) are obtained by direct hydroformylation, while 2-ethylheptanal (**P31c**) and 2-propylhexanal (**P31d**) can only be derived from a C=C bond isomerisation process followed by hydroformylation. The corresponding alcohols nonan-1-ol (**5a**), 2-methyloctan-1-ol (**5b**), 2-ethylheptan-1-ol (**5c**) and 2-propylhexan-1-ol (**5d**) are obtained after the hydrogenation of the aldehydes **P31a-d**. Other potential products are the hydrogenation product **6** (octane) and non-hydroformylated octenes **S31b-d** arising from the isomerisation of **S31a** (for the structures, see Scheme to Table 3).

Initial studies focussed on the identification of active and selective cobalt catalysts derived from Xantphos. The activity of the cobalt complexes **C10** and **C11** in the hydroformylation of **S31a** was initially studied (Table 3, entries 1 and 2). With the aim of following a rational process to discover catalysts for hydroformylation and to minimise the number of experiments, typical temperatures (140 ºC) and partial H_2 and CO pressures (40 bar H_2/CO at a ratio of 1:1) were used throughout the catalyst discovery process.[132] **C10** provided high selectivity towards aldehydes (abbreviated as "HF selectivity" in the discussion that follows; 73%, Table 3, entry 1), although there were considerable amounts of **6** formed (10%) as well as non-hydroformylated octenes (**S31b-d**, 15%). **C11** proved to be a more selective catalyst than **C10** (HF selectivity of 89%; Table 3, entry 2). To increase the practicality of the hydroformylation by avoiding the necessity of synthesising the cobalt catalyst,

[130] This terminal coordination mode of the bisphosphane to $[Co_2(CO)_8]$ has also been reported for BINAP (2,2′-bis(diphenylphosphaneyl)-1,1′-binaphthalene); for example, see: Gibson, S. E.; Lewis, S. E.; Loch, J. A.; Steed, J. W.; Tozer, M. J. *Organometallics* **2003**, *22*, 5382-5384. A bridging coordination mode with the bisphosphane being coordinated with both cobalt centres has also been reported, for example, see: Chang; Lee, J.-C.; Hong, F.-E. *Organometallics* **2005**, *24*, 5686-5695.

[131] For efficient cobalt-catalysed hydroformylations for oct-1-ene employing other ligands, see ref. 114b and 123e–f.

[132] 40 bars refer to the H_2/CO pressure at room temperature. The pressure increased up to 45 bar after heating the reaction mixture at the desired temperature (45 bar at 140 ºC).

we also studied the *in situ* generation of catalysts using different **L5**/[Co] ratios (Scheme 2) by varying the relative molar amounts of the ligand and cobalt precursor. **L5**/[Co] ratios ranging from 0:1 (*i.e.* absence of ligand) to 2:1 were studied. The results are indicated in Table 3 (entries 3-7). As previously observed for other bisphosphane ligands and substrates,[113] changes in the **L5**/[Co] ratio led to different outcomes in the hydroformylation of oct-1-ene. The conversion decreased with the **L5**/[Co] ratio, with a 51% conversion at an **L5**/[Co] ratio of 2:1 (Table 3, entry 7). The regioselectivity towards the linear aldehyde **P31a** was not appreciably affected by the different *in situ* generated catalysts studied (Table 3). The amounts of **P31a** with respect to all the aldehydes ranged from 62% to 70% throughout the whole study. Interestingly, the **L5**/[Co] ratio of 0.5:1 (*i.e.* equimolar amounts of ligand **L5** and $[Co_2(CO)_8]$) led to high HF selectivities (85%). It is interesting to highlight that the relative ratio of **L5** units to Co centres in **C11** was the same as that in the complex generated *in situ* with an **L5**/[Co] ratio of 0.5:1, leading to similar results in the hydroformylation of oct-1-ene (compare entries 2 and 5 in Table 3). As indicated in Table 3, **C10**, **C11** and the ligand-free system are equally active (conversions are in all cases ≥ 99%). In terms of selectivity towards aldehydes, **C11** provides a higher selectivity than **C10** or the ligand-free system (89% *vs.* 73% or 71%, respectively). The main difference in the reactivity between **C11** and **C10**/ligand-free system is that **C10** provides much higher amounts of *n*-octane (**6**) and non-hydroformylated octenes (10% and 15%, respectively) than **C11**, whilst the ligand-free system leads to much higher amounts of alcohols **5a-d** (25%, Table 3, entry 3) than **C11**. Overall, **C11** and the catalyst generated *in situ* with an **L5**/[Co] ratio of 0.5:1 were the best performing catalysts, with the selectivities towards 1-nonanal being amongst the highest reported in the literature.[131]

Table 3. Screening of cobalt catalysts for the hydroformylation of oct-1-ene (**S31a**).

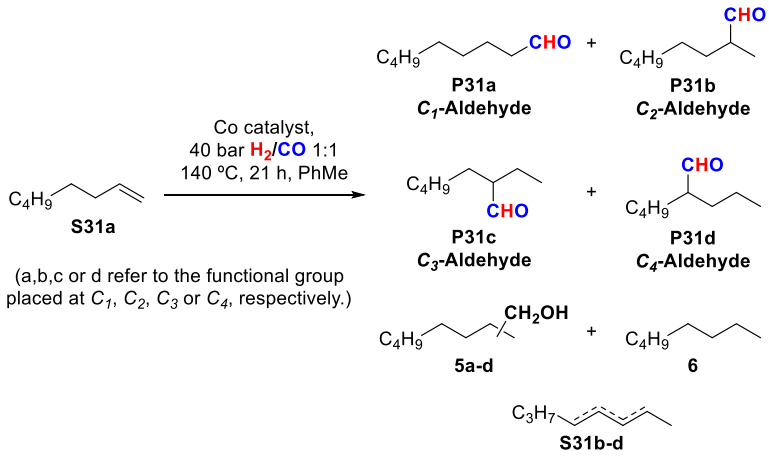

Entry	Co complex or L5/[Co] ratio[a]	Conv.[b] (%)	Selectivity (%)[b]			
			P31a-b	5	6	S31b-d
			Ratio $C_1/C_2/C_3/C_4$ (P31)			
1	**C10** (1 mol%)	99	73	2	10	15
			64:22:8:6			
2	**C11** (1 mol%)	> 99	89	2	4	5
			69:19:7:5			
3	0:1[c]	> 99	71	25	2	2
			66:19:8:7			
4	0.25:1	98	80	17	0	3
			70:19:6:5			
5	0.5:1	> 99	85	11	2	2
			65:21:8:6			
6	1:1	> 99	79	13	4	4
			62:23:8:7			
7	2:1	51	37	1	13	49
			64:26:6:4			

Reaction conditions: [alkene] = 0.26 M; reaction time = 21 h; stirring rate = 800 rpm. [a] **L5**/[Co] ratio refers to the molar ratio between **L5** and cobalt centres from $[Co_2(CO)_8]$, with [Co centres] = 5.2 mM (2 mol% with respect to oct-1-ene) unless otherwise indicated. [b] Conversion and product distribution were determined and quantified by GC analysis with dodecane as internal standard. [c] *In situ* generated $[Co(CO)_4H]$.

Hydroformylation is highly influenced by the reaction conditions.[15b,25a,116] A temperature screening study (90-160 °C) was also performed with oct-1-ene

and *in situ* generated cobalt catalysts incorporating Xantphos. That study[133] revealed that 140 °C was the temperature of choice for obtaining a high HF selectivity. As expected, low conversions were observed at 90 °C and 110 °C (< 50%), although the selectivity towards **P31a** was slightly higher at 90 °C (ratio **P31a**/(**P31b** + **P31c** + **P31d**) = 75:25; Table 4, entry 1) than at 140 °C (ratio **P31a**/(**P31b** + **P31c** + **P31d**) = 62:38; Table 4, entry 3). Temperatures above 140 °C (*e.g.* 160 °C) did not confer any advantage to the previously studied reaction conditions, as the amounts of alcohols **5a-d** surpassed the 12% yield. The catalyst screening study (Table 3) was performed with an H_2/CO ratio of 1:1 and H_2 and CO partial pressures of 20 bar. To study the effects of an excess of H_2 or CO on the outcome of the hydroformylation reactions, two experiments were conducted with H_2/CO ratios of 1:3 and 3:1, with the overall pressure maintained at 40 bar. In both cases, the cobalt catalysts were generated *in situ*.[133] An excess of CO (H_2/CO ratio = 1:3) led to a decrease in the conversion (52% with respect to > 99% for the H_2/CO ratio of 1:1) and in the HF selectivity (59% with respect to 79%).[133] Much higher amounts of non-hydroformylated octenes were generated from the isomerisation of **S31a** with an excess of CO (33% with respect to 2%). When an excess of H_2 with respect to CO was used (H_2/CO ratio = 3:1), increased amounts of non-hydroformylated octenes arising from the isomerisation of **S31a** (29% with respect to 2%) were observed.[133] The fact that significant amounts of non-hydroformylated octenes arising from the isomerisation of **S31a** remained unreacted towards hydroformylation for both the 1:3 and 3:1 H_2/CO ratios indicated that the hydroformylations did not proceed as efficiently at these H_2/CO ratios when compared to the H_2/CO ratio of 1:1. Overall, these optimisation studies confirmed that 40 bar of H_2/CO at a ratio of 1:1 at 140 °C were the optimal hydroformylation conditions for achieving high HF selectivities.

[133] For the complete set of results for the hydroformylations at temperatures ranging from 90–160 °C or employing H_2/CO ratios different to 1:1, see Table 13 in the experimental section 1.5.7.

Table 4. Screening of temperatures for the hydroformylation of oct-1-ene (**S31a**).

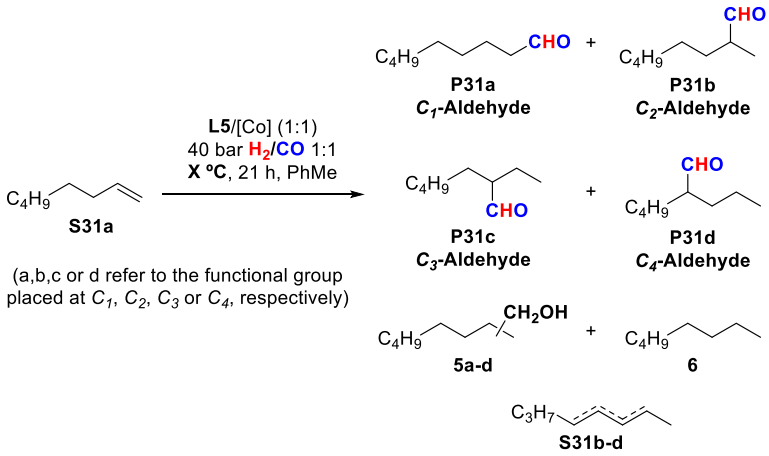

Entry	Temperature (ºC)	Conv.[a] (%)	Selectivity (%)[b]			
			P31a-b	5	6	S31b-d
			Ratio $C_1/C_2/C_3/C_4$ (P31)			
1	90	17	11	0	24	65
			64:22:8:6			
2	110	50	58	1	7	34
			73:18:5:4			
3	140	> 99	79	13	4	4
			62:23:8:7			

Reaction conditions: [alkene] = 0.26 M; reaction time = 21 h; stirring rate = 800 rpm. [a] Conversion and product distribution were determined and quantified by GC analysis with dodecane as internal standard. **L5**/[Co] ratio refers to the molar ratio between **L5** and cobalt centres from $[Co_2(CO)_8]$, with [Co centres] = 5.2 mM (2 mol% with respect to oct-1-ene).

The practicality of the method was demonstrated by performing the hydroformylation of **S31a** at the gram scale using **C11** as catalyst, with a 1.8 M concentration of alkene (*i.e.* 7-fold increase in the concentration with respect to standard experiments) and at a S/C ratio of 1000 (*i.e.* 10-fold reduction in the amount of catalyst with respect to standard experiments in Table 3, entry 2). Under these new reaction conditions, the hydroformylation showed a conversion of 99% and led to the target aldehydes in a 51% isolated yield after distillation. The regioselectivity of the hydroformylation (50% of nonanal) was lower than that obtained under more diluted reaction conditions and employing higher amounts of catalyst (61% of nonanal; Table 3, entry 2).

1.3.3. Cobalt-catalysed hydroformylation of oct-1-ene isomers

Having demonstrated that Xantphos-based cobalt catalysts were active and selective in the hydroformylation of **S31a**, we then broadened the substrate scope to its isomers with the C=C double bond at different positions and with different geometries. These substrates are inherently less reactive than the terminal isomer **S31a** and studies of their cobalt-catalysed hydroformylation are scarce.[134] The results of the hydroformylation of the octenes **(*Z*)-S31b**, **(*E*)-S31b**, **(*E*)-S31c**, **(*Z*)-S31d** and **(*E*)-S31d** are summarised in Table 5.

Hydroformylation of oct-1-ene isomers was performed under optimised catalytic conditions, forming the active catalyst *in situ*. In all cases, full conversion and high selectivities towards the aldehydes **P31a-d** were observed, producing better results than those for **P31a**. For **(*Z*)-S31b** and **(*E*)-S31b**, the aldehydes **P31a-d** were formed with an 89 and 86% selectivity, respectively. By-products such as **5a-d**, **6** and non-hydroformylated octenes were obtained in low amounts (selectivities of 3-4%, 4-5% and 3-6%, respectively; Table 5, entries 2 and 3). In the case of (*E*)-oct-3-ene (**(*E*)-S31c**), the corresponding aldehydes were obtained with a 91% selectivity, whilst the sum of all the by-products amounted to 9%. For **(*Z*)-S31d** and **(*E*)-S31d** (Table 5, entry 5 and 6), the results were similar, with a slightly higher HF selectivity for **(*Z*)-S31d** (91%) than for **(*E*)-S31d** (89%). Interestingly, for all the octene isomers studied (Table 5), a similar product distribution of **P31a-d** was observed, with the hydroformylation of **S31a** leading to the highest regioselectivity towards the linear aldehyde **P31a** (Table 5, entry 1).

[134] For the examples, see ref. 23, 114b, and 123b-f and Haymore, B. L.; van Asselt, A.; Beck, G. R. *Ann. N.Y. Acad. Sci.* **1983**, *415*, 159-175.

Table 5. Hydroformylation of the octene isomers.

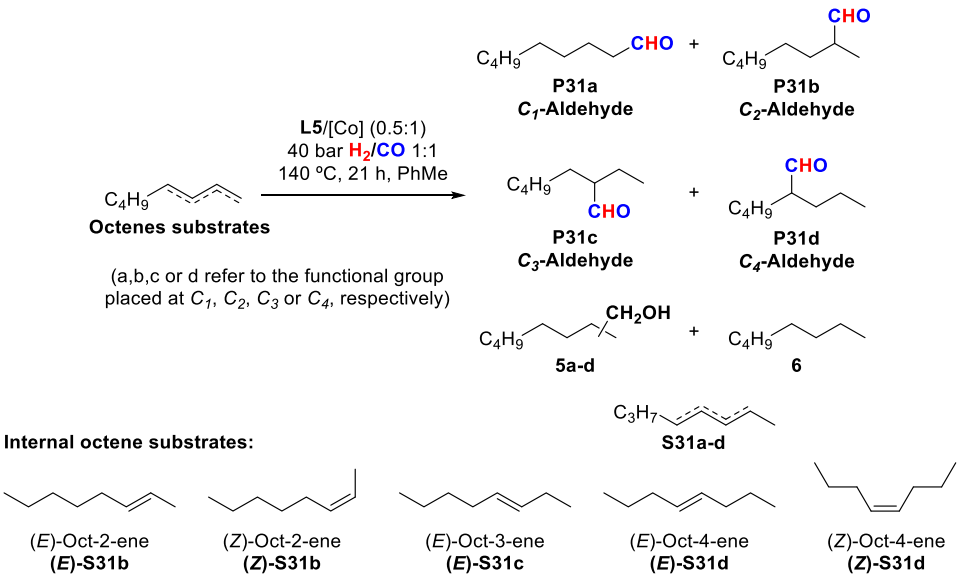

Entry	Alkene	Conv.[a] (%)	Selectivity (%)[a]			
			P31	5	6	S31a-d
			Ratio $C_1/C_2/C_3/C_4$ (P31)			
1	S31a[b]	>99	85	11	2	2
			65:21:8:6			
2	(*Z*)-S31b	99	89	4	4	3
			62:22:9:7			
3	(*E*)-S31b	>99	86	3	5	6
			62:22:9:7			
4	(*E*)-S31c	99	91	4	3	2
			60:21:10:9			
5	(*Z*)-S31d	>99	91	3	4	2
			59:21:10:10			
6	(*E*)-S31d	99	89	3	5	3
			60:21:9:10			

Reaction conditions: [alkene] = 0.26 M; reaction time = 21 h; stirring rate = 800 rpm. **L5**/[Co] ratio refers to the molar ratio between **L5** and cobalt centres from $[Co_2(CO)_8]$, with [Co centres] = 5.2 mM (2 mol% with respect to the substrate) unless otherwise indicated. [a] Conversion and product distribution were determined and quantified by GC analysis with dodecane as internal standard. [b] These results are already shown in Table 3, but are included here for comparison.

In general terms, very high aldehyde selectivities (from 85% to 91%) and low selectivities towards by-products were observed independently of the position or geometry of the C=C double bond (Figure 26). The selectivity towards **P31a-d** was slightly higher for the internal alkenes, with the highest

HF selectivity being obtained for **(*E*)-S31c** and **(*Z*)-S31d**. This behaviour is remarkable as the hydroformylation selectivities of internal alkenes are generally lower than those of the terminal analogues.[123f]

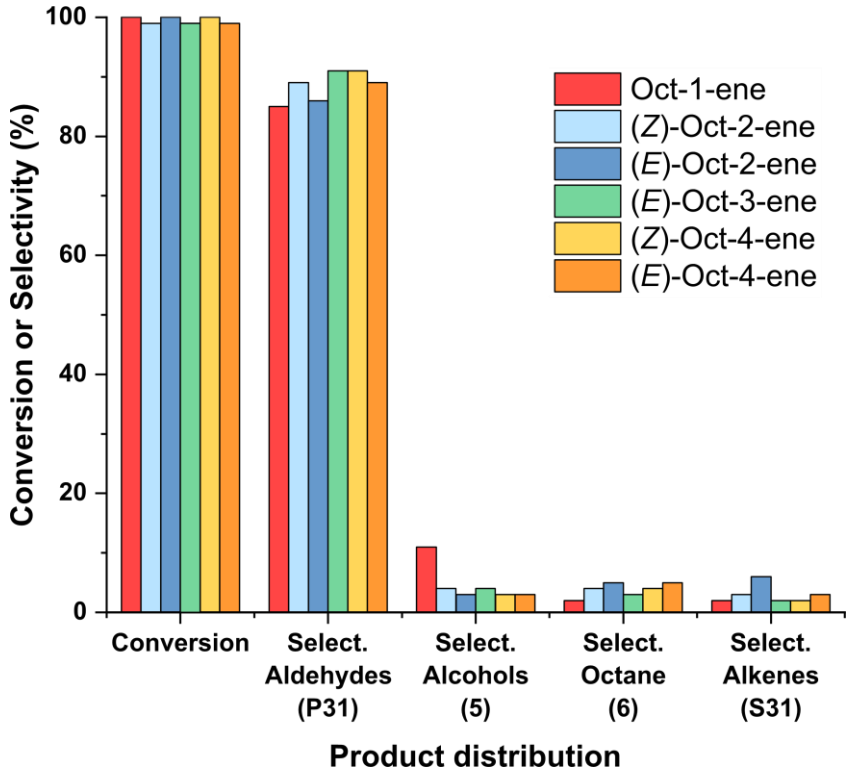

Figure 26. Cobalt-catalysed hydroformylation of octenes with Xantphos as the ligand.

1.3.4. Valorisation of mixtures of alkenes by cobalt-catalysed hydroformylations

In recent years, the valorisation of petrochemical feedstocks (generally available as non-separable mixtures of hydrocarbons) has emerged as a driving force in fundamental research to produce high value-added products derived from petrochemicals rather than higher performing fuels.[135] Researchers have found that hydroformylation is useful in transforming mixtures of unsaturated hydrocarbons into value-added products such as aldehydes. The valorisation of mixtures of alkenes into the corresponding aldehydes by cobalt-catalysed hydroformylations is a well-established process, both in academia and industry.[135] However, the hydroformylation of mixtures of isomeric C_6-, C_7- and C_8-alkenes retaining the same carbon connectivity but varying the position of the unsaturation has received less attention.[115,116,136] Taking into account the similar regioselectivities observed in the hydroformylation of terminal and internal octenes with our cobalt-Xantphos catalysts, we turned our attention to mixtures of linear alkenes in cobalt-catalysed hydroformylation. For practical reasons, we prepared equimolar mixtures of all available linear hexene, heptene and octene isomers. These mixtures were subjected to our optimised hydroformylation conditions (140 °C, 40 bar H_2/CO at a 1:1 ratio, preformed catalyst **C11** or catalyst generated *in situ* with an **L5**/[Co] ratio of 0.5:1).

Mixtures of linear hexenes, heptenes and octenes (see Table 6 for the components of the alkene mixtures) were successfully hydroformylated to the corresponding aldehydes, with low final amounts of by-products. The mixtures of linear hexenes, heptenes or octenes were hydroformylated with HF selectivities ranging from 82% to 91%, depending on the alkene mixture and the catalyst used (Table 6). In general, slightly higher HF selectivities were obtained with the *in situ* generated catalysts (85% *vs.* 82%, 87% *vs.* 85%, and 91% *vs.* 83% for the mixtures of linear hexenes, heptenes and octenes, respectively; Table 6, entries 1, 3 and 5). By contrast, the regioselectivity towards the hydroformylation at the terminal carbon C_1 was slightly higher for C_2 (up to a 4% increase in the regioselectivity towards the hydroformylation product at C_1 (*i.e.* the terminal aldehyde; Table 6, entry 6)). For each alkene mixture, selective hydroformylation conditions were discovered, with low amounts of alkanes or alcohols produced.

[135] Treese, S. A.; Pujadó, P. R.; J., J. D. S. *Handbook of Petroleum Processing*; Springer Dordrecht, 2006.
[136] To the best of our knowledge, only one heterogeneous cobalt catalytic system has been employed with this aim, reporting low conversions: Peng, Q.; He, D. *Catal. Lett.* **2007**, *115*, 19-22.

Table 6. Hydroformylation of mixtures of alkenes employing the cobalt complex **C11** or catalysts generated *in situ* with an **L5**/[Co] ratio of 0.5:1.

Entry	Alkene mixture	Co complex or L5/[Co] ratio	Selectivity (%)			
			Aldehydes	Alcohols	Alkanes	Alkenes
			Hydroformylation at $C_1/C_2/C_3/C_4$			
1	Hexenes[a]	**L5**/[Co] = 0.5:1	85	1	2	12
			72:20:8			
2	Hexenes[a]	**C11**	82	3	2	13
			73:19:8			
3	Heptenes[b]	**L5**/[Co] = 0.5:1	87	1	1	11
			69:20:8:3			
4	Heptenes[b]	**C11**	85	2	1	12
			70:19:8:3			
5	Octenes[c]	**L5**/[Co] = 0.5:1	91	3	3	3
			62:21:9:8			
6	Octenes[c]	**C11**	83	1	7	9
			66:19:8:7			

Reaction conditions: [alkene] = 0.26 M; reaction time = 21 h; stirring rate = 800 rpm. Product distribution was determined by GC analysis (area % results). **L5**/[Co] ratio refers to the molar ratio between **L5** and cobalt centres from $[Co_2(CO)_8]$, with [Co centres] = 5.2 mM (2 mol% with respect to the mixture of alkenes) unless otherwise indicated. Product distribution was determined by GC analysis (area % results). [a] Mixture of hexenes contained equimolar amounts of hex-1-ene, (*E*)-hex-2-ene, (*Z*)-hex-2-ene, (*E*)-hex-3-ene and (*Z*)-hex-3-ene. [b] Mixture of heptenes contained equimolar amounts of hept-1-ene, (*E*)-hept-2-ene, (*E*)-hept-3-ene and (*Z*)-hept-3-ene. [c] Mixture of octenes contained equimolar amounts of oct-1-ene, (*E*)-oct-2-ene, (*Z*)-oct-2-ene, (*E*)-oct-3-ene, (*E*)-oct-4-ene and (*Z*)-oct-4-ene.

These results illustrate that cobalt-catalysed hydroformylation could be a useful valorisation tool for mixtures of alkenes with the same carbon connectivity given the high regioselectivities towards addition of a CHO group to the C_1 carbon of the alkene skeleton (up to 73%) under the specific reaction conditions optimised for each mixture of alkenes.

1.3.5. Rationalisation of the hydroformylation results

As described in the previous sections, the ratios of terminal aldehydes (*i.e.* hydroformylation at C_1) with respect to their branched isomers (*i.e.* hydroformylation at C_2 and C_3 and also at C_4 for heptenes and octenes) remained practically constant. These results led us to hypothesise that under the effects of the Xantphos-based cobalt catalysts, a tandem isomerisation-hydroformylation process could be taking place, with the isomerisation process being faster than the hydroformylation reaction. The isomerisation of C=C bonds through the formation of cobalt-alkyl or cobalt-π-allyl complexes has been reported in the literature.[137] The final regioselectivity would

[137] a) Vilches-Herrera, M.; Domke, L.; Börner, A. *ACS Catal.* **2014**, *4*, 1706-1724. b) Molloy, J. J.; Morack, T.; Gilmour, R. *Angew. Chem. Int. Ed.* **2019**, *58*, 13654-13664.

correspond to the product distribution obtained after the isomerisation processes, with the hydroformylation products of the terminal alkene being the major aldehyde isomers obtained.

To confirm these observations, the progress of the hydroformylation of an equimolar mixture of linear octenes (for details, see caption to Figure 27) was monitored by running independent hydroformylations at different reactions times and analysing the composition of the resulting reaction mixtures. Changes in the concentration of all starting octene isomers and final aldehydes against time are shown in Figure 27a. An analysis of the concentration of oct-1-ene at short reaction times confirms that isomerisation is faster than hydroformylation: whilst *ca.* 9% of the initial amounts of oct-1-ene were consumed after 30 minutes, only 3% of the final amounts of the terminal hydroformylation product were formed. It is also interesting to note that the concentration of (*E*)-oct-2-ene in the reaction mixture at short reaction times was higher than the initial one (*ca.* 5% and 12% increase in the concentration after 30 and 90 min, respectively, with respect to the initial concentration of (*E*)-oct-2-ene). As for the formation of aldehydes (Figure 27b), the reaction rate slopes for hydroformylation at C_1 in the first 90 minutes (mmol L^{-1} min^{-1}) are 2.9, 7.4 and 8.2 times higher than for hydroformylation at C_2, C_3 and C_4, respectively, which is in agreement with the experimental results.

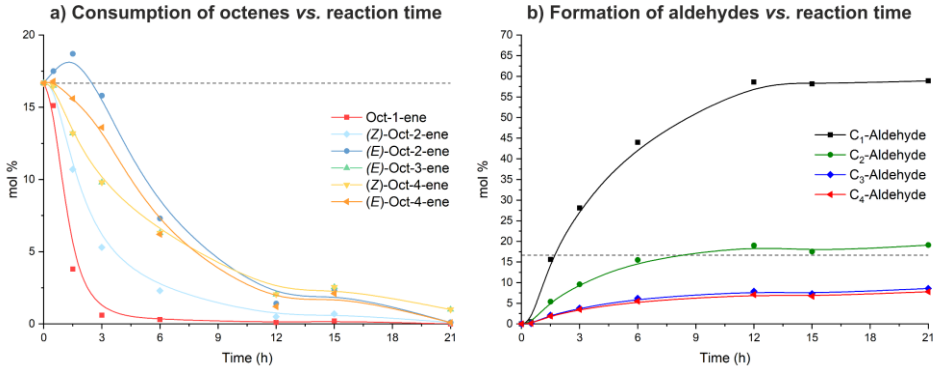

Figure 27. Reaction progress monitoring of the hydroformylation of a mixture of octenes (1 mol% **C11**, 140 °C, 40 bar H_2/CO (1:1), toluene, 43.3 mM in oct-1-ene, (*E*)-oct-2-ene, (*Z*)-oct-2-ene, (*E*)-oct-3-ene, (*E*)-oct-4-ene and (*Z*)-oct-4-ene).**a)** Consumption of each octene isomer with time (GC peaks of 3-*E*- and 4-*Z*-octene co-elute). **b)** Formation of the four possible aldehydes with time; the grey dotted line indicates the initial mol% amount of each octene isomer; the solid lines correspond to eye guidelines.

To identify catalytically active cobalt complexes in this chemistry, the *in situ* generated cobalt complexes (**L5**/[Co] ratio 0.5:1) and **C11** were reacted with 40 bar H_2/CO at a ratio of 1:1 at 140 °C in the absence of alkenes (Figure 28). Analysis of the mixture by ^{1}H and $^{31}P\{^{1}H\}$ NMR and ESI-MS indicated that **C10** was formed in both cases (Scheme 19). In addition to the formation

of **C10** (Scheme 19), NMR and ESI-MS indicated that $[Co(CO)_4(H)]$ was also formed (hydride signal in ^1H NMR for $[Co(CO)_4H]$ in PhMe-d_8: δ_{exp} = δ -11.58 ppm; δ_{lit} = δ -11.55 ppm;[138] HRMS ESI-MS *m/z*: $[M–H]^-$ calcd. for $C_4O_4Co^-$ 170.9129, found 170.9298). It is reported in the literature that $[Co(CO)_4H]$ plays an important role in C=C double bond isomerisation.[122]

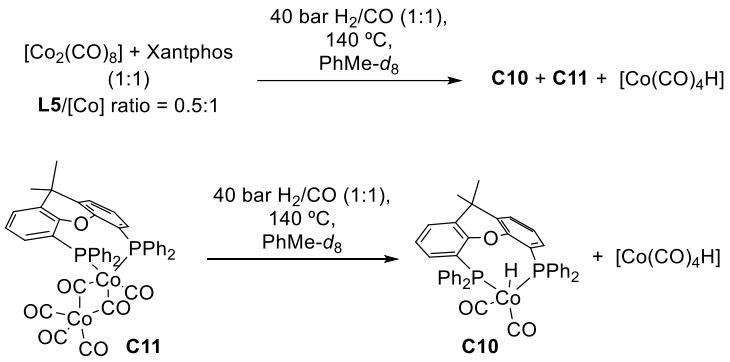

Scheme 19. Cobalt complexes generated under hydroformylation reaction conditions.

These results demonstrated that **C11** and the cobalt complexes generated *in situ* with an **L5**/[Co] ratio of 0.5:1 evolve into the same cobalt complexes (**C10** and $[Co(CO)_4H]$) under the hydroformylation reaction conditions. Whilst it is reasonable to assume that $[Co(CO)_4H]$ plays a major role in the C=C isomerisation processes, **C10** is associated with the addition of a CHO group to the C_1 carbon of the alkene skeleton, irrespective of the position and geometry of the C=C bond in the starting material.

[138] Mika, L. T.; Tuba, R.; Tóth, I.; Pitter, S.; Horváth, I. T. *Organometallics* **2011**, *30*, 4751-4764.

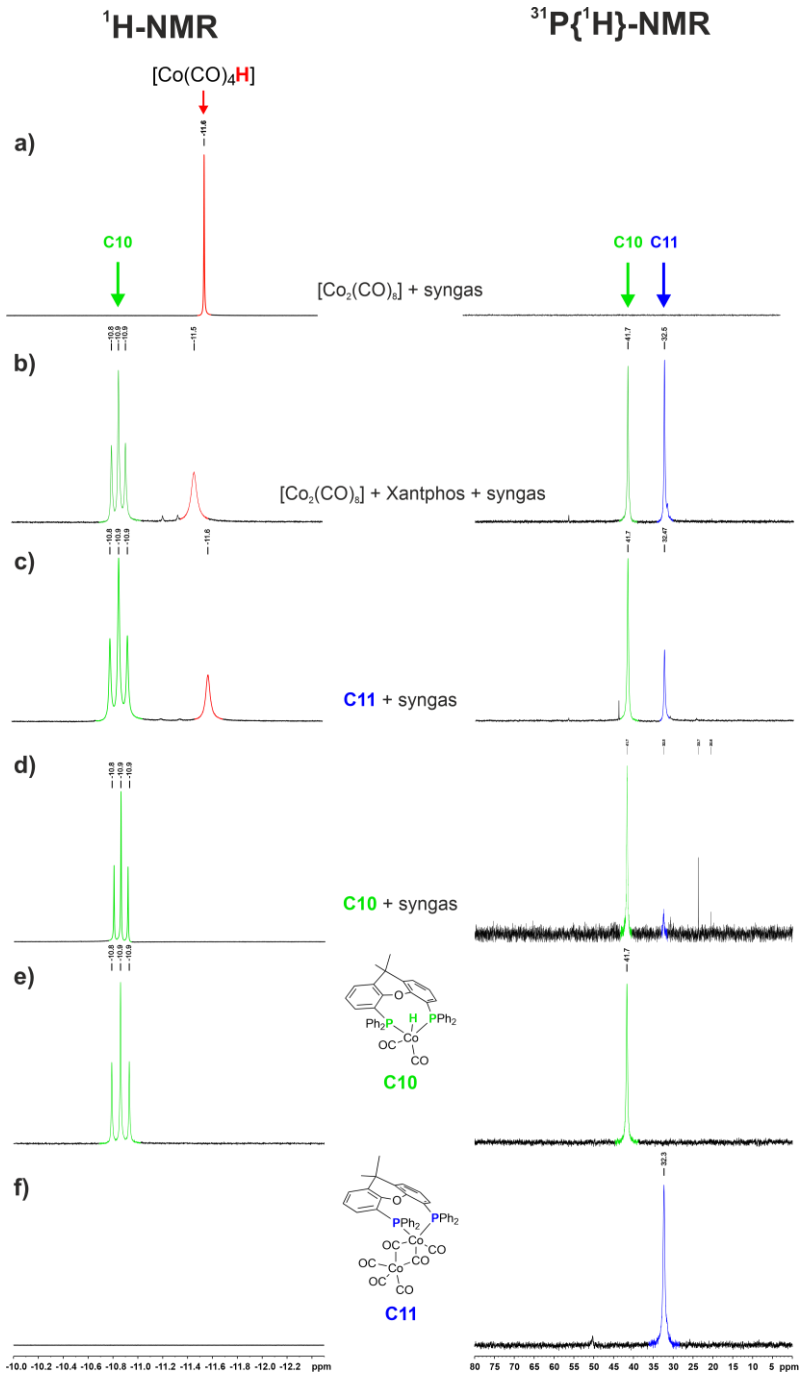

Figure 28. Regions of the ^{1}H NMR & ^{31}P{^{1}H} NMR spectrum of: **a)** $[Co_2(CO)_8]$ after treatment with 40 bar of H_2/CO (1:1) at 140 ºC for 1 hour in PhMe-d_8; **b)** $[Co_2(CO)_8]$ and Xantphos after treatment with 40 bar of H_2/CO (1:1) at 140 ºC for 1 hour in PhMe-d_8; **c) C11** after treatment with 40 bar of H_2/CO (1:1) at 140 ºC for 1 hour in PhMe-d_8; **d) C10** after treatment with 40 bar of H_2/CO (1:1) at 140 ºC for 6 hours in PhMe-d_8; **e) C10** in PhMe-d_8 under N_2. **f) C11** in PhMe-d_8 under N_2.

In terms of the stability of **C10** under hydroformylation reaction conditions (PhMe-d_8, 140 ºC, 40 bar H_2/CO 1:1, 21 h), $^{31}P\{^1H\}$ NMR analysis revealed that complex **C10** remains unchanged in solution (*ca.* 90%; Figure 29) under the above-mentioned reaction conditions, with free ligand not being detected. The role of **C10** in this chemistry is important (either because it is directly used, or it is formed *in situ* from **C11** in the presence of syngas as previously discussed) and this stability test confirms its catalytic role in hydroformylation as it remains mostly unchanged.

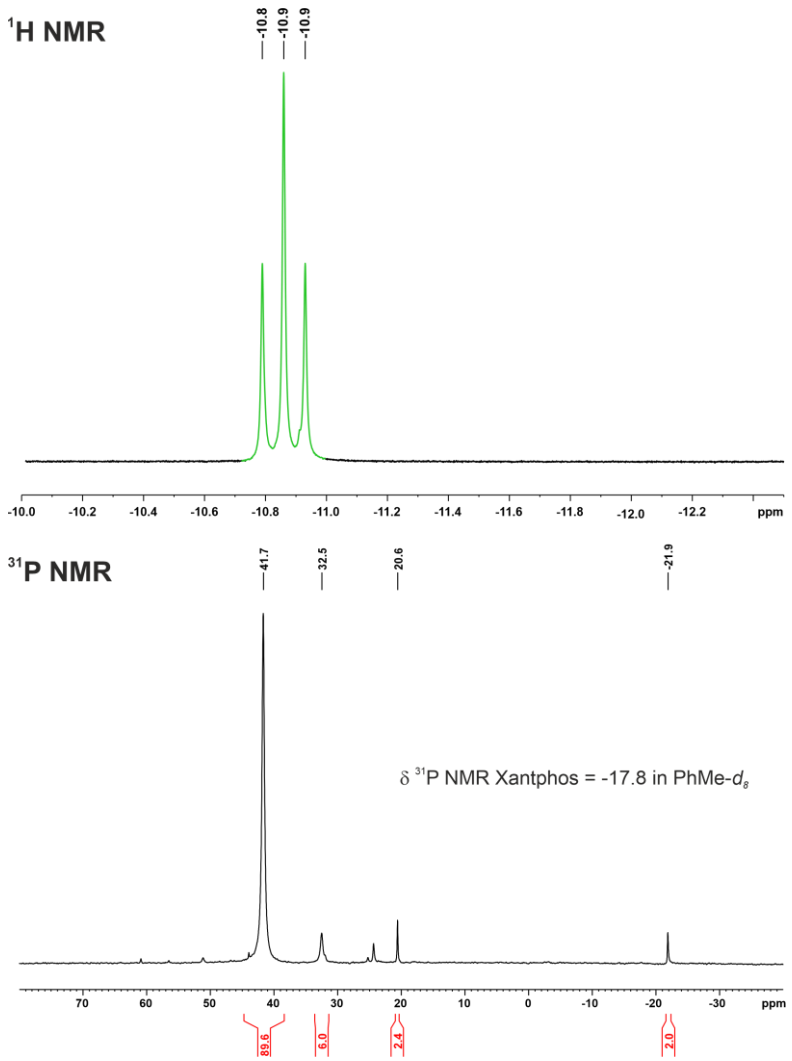

Figure 29. Hydride region in ^1H NMR (top) and $^{31}P\{^1H\}$ NMR spectrum (bottom) of $[Co(CO)_2H(\kappa^2P,P\text{-Xantphos})]$ (**C10**) after being under 40 bar of H_2/CO (1:1), 140 ºC for 21 h in PhMe-d_8.

1.4. CONCLUSIONS

Cobalt complexes [$Co(CO)_2H(\kappa^2P,P$-Xantphos)] (**C10**) and [$(OC)_3Co(\mu$-$CO)_2Co(CO)(\kappa^2P,P$-Xantphos)] (**C11**) were efficiently synthesised and characterised for their application in the hydroformylation of an array of structurally diverse alkenes, differing in the position of the unsaturation and the geometry of the C=C double bond. Complexes **C10** and **C11** showed high performance as catalysts in terms of conversion and selectivity towards aldehydes in the hydroformylation of alkenes. Comparative studies employing the preformed **C11,** or complexes formed *in situ* from Xantphos and [$Co_2(CO)_8$], indicated that the results obtained in the hydroformylation reactions were comparable, therefore demonstrating that the two strategies for the preparation of the catalysts were equally valid (*i.e.* synthesis of cobalt catalysts in advance or *in situ* generation).

The cobalt-catalysed hydroformylation of oct-1-ene employing Xantphos as a ligand was highly selective towards aldehydes under the optimised catalytic reaction conditions (**C11** or *in situ* generated catalyst with an **L5**/[Co] ratio of 0.5:1, 140 °C and 40 bar of H_2/CO at a 1:1 ratio). Furthermore, the formation of hydrogenated products, non-hydroformylated alkenes arising from the C=C isomerisation processes in the starting material and alcohol derivatives was minimised. Hydroformylations of other octenes were successfully carried out. High aldehyde selectivities were observed in all the cases. Regioselectivities for all the studied linear octene isomers remained practically constant, irrespective of the position and geometry of the double bond. These results lead us to suggest that under the effects of our Xantphos-cobalt-based catalyst, a tandem isomerisation-hydroformylation process takes place, with the isomerisation mediator [$Co(CO)_4H$] being formed in the reaction mixture from **C11** or Xantphos/[$Co_2(CO)_8$]. We also demonstrated that this chemistry is an interesting strategy for valorising mixtures of linear hexenes, heptenes or octenes by transforming the initial mixture into one major aldehyde (addition of a CHO group to the C_1 carbon of the alkene skeleton, up to 73% selectivity).

1.5. EXPERIMENTAL SECTION

1.5.1. General Considerations

All syntheses were carried out using chemicals purchased from commercial sources unless otherwise cited. Air- and moisture-sensitive manipulations and hydroformylation reactions were performed under inert atmosphere, either in a N_2-filled glove box or with standard Schlenk techniques. Hazards: Carbon monoxide (CO) is a very toxic gas by inhalation and this reagent or metal carbonyl complexes were always used in well-ventilated hoods. Glassware was dried in vacuo before use with a hot air gun. All solvents were dried and deoxygenated by using a Solvent Purification system (SPS). All solvents and reagents (liquids) have been degassed using freeze-pump-thaw cycles and stored at low temperature with activated molecular sieves (4 Å) under N_2 atmosphere prior to their use. NMR spectra were recorded at room temperature, unless otherwise cited, in 300 MHz, 400 MHz or 500 MHz spectrometers in CD_2Cl_2 and PhMe-d_8 unless otherwise noted. ^{1}H, $^{13}C\{^{1}H\}$ or $^{13}C\{^{1}H,^{31}P\}$ NMR chemical shifts were quoted in ppm relative to the residual solvent peaks. $^{31}P\{^{1}H\}$ NMR chemical shifts were quoted in ppm relative to 85% phosphoric acid in water. IR spectra were recorded using Attenuate Total Reflection (ATR) techniques unless otherwise cited. High-resolution mass spectrum (HRMS) was recorded by matrix-assisted laser desorption/ionization (MALDI) or ESI ionization methods.

1.5.2. General Structural Comments on X-Ray Crystals

1.5.2.1. X-Ray Crystal of [Co(CO)$_2$H(κ^2*P*,*P*-Xantphos)] (C10)

Crystals of the complex **C10** were grown by solvent diffusion, using toluene and *n*-pentane at –20 °C under inert atmosphere. The measured crystals were prepared under inert conditions and immersed in perfluoropolyether as protecting oil for manipulation.

Crystal structure determination for the complex **C10** was carried out using a Rigaku diffractometer equipped with a Pilatus 200K area detector, a Rigaku MicroMax-007HF microfocus rotating anode with MoK_α radiation, confocal Max Flux optics and an Oxford Cryosystems low temperature device Cryostream 700 plus (T = –173 °C). Full-sphere data collection was used with ω and φ scans. *Programs used:* Data collection and reduction with CrysAlisPro[139] V/60A and absorption correction with Scale3 Abspack scaling algorithm.[140] Crystal structure solution was achieved using the computer

[139] Data collection and reduction with CrysAlisPro 1.171.39.12b (Rigaku OD, 2015).
[140] Empirical absorption correction using spherical harmonics as implemented in Scale3 Abspack scaling algorithm, CrysAlisPro 1.171.39.12b (Rigaku OD, 2015).

program SHELXT.[141] Visualization was performed with the program SHELXle.[142] Missing atoms were subsequently located from difference Fourier synthesis and added to the atom list. Least-squares refinement on F^2 using all measured intensities was carried out using the program SHELXL 2015.[143] All non-hydrogen atoms were refined including anisotropic displacement parameters.

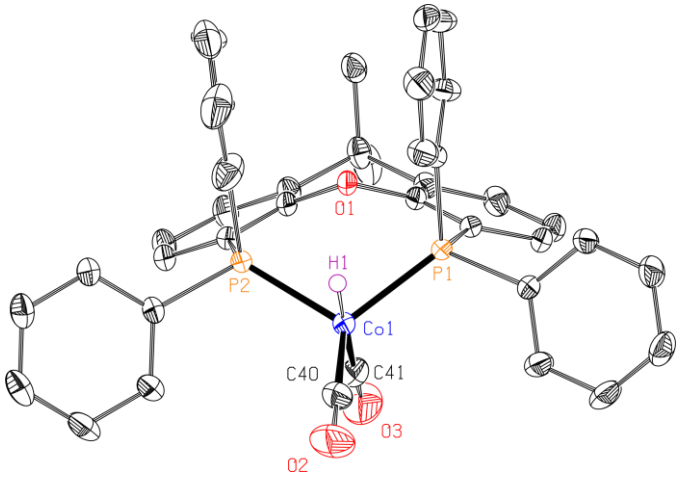

Figure 30. ORTEP drawing (thermal ellipsoids drawn at a 50% probability level) showing the structure of the complex **C10**. Colour Scheme: C: black, Hydride: violet, Co: blue, O: red, P: orange.

Comments to the crystal structure of complex **C10**: The asymmetric unit contains one molecule of the metal complex, one molecule of toluene and 0.5 molecules of pentane. The toluene molecule is disordered in three orientations with a ratio of 65:25:10. The half pentane molecule is disordered in two orientations and shared with the neighbouring asymmetric unit. The hydrogen atom attached to the cobalt atom was localized from the residual electron density and refined free on its position. The Co–H distance is of 1.50(2) Å, which is in the range for the expected distance for this type of bonds (a search in the CCDC for similar structures gave distances in the range 1.39-1.58 Å).

[141] Sheldrick, G. M. *Acta Crystallogr., Sect. A: Found. Adv.* **2015**, *71*, 3-8.
[142] Huebschle, C. B.; Sheldrick, G. M.; Dittrich, B. *J. Appl. Crystallogr.* **2011**, *44*, 1281-1284.
[143] Sheldrick, G. M. *Acta Crystallogr., Sect. C: Struct. Chem.* **2015**, *71*, 3-8.

Table 7. Crystal data and structural parameters for the complex **C10**

Compound	**Complex C10**
Formula	$C_{50}H_{47}CoO_3P_2$
Solvent	Toluene/Pentane
Formula weight	822.75
Temperature (K)	293(2)
Crystal system	Monoclinic
Space group	*P2*(1)/n
a (Å)	9.9652(3)
b (Å)	18.3490(5)
c (Å)	23.3602(9)
α (°)	90
β (°)	96.462(3)
γ (°)	90
Volume ($Å^3$)	4244.3(2)
Θ	4
ρ ($g \cdot cm^{-3}$)	1.288
μ (mm^{-1})	0.522
θmax (°)	34.798
Reflect. collected	76515
Unique reflect.	17442 [R(int) = 0.0548]
Absorpt. correction	Multi-scan
Parameters/restrains	678/739
R1/wR2 [I>2σ(I)]	0.0512/0.1233
R1/wR2 (all data)	0.1079/0.1468
Goodness-of-fit (F^2)	1.009
Peak/hole (e/$Å^{-3}$)	0.986/–0.643

Table 8. Bond lengths (Å) for complex **C10.**

Entry	Atoms	Length (Å)	Entry	Atoms	Length (Å)
1	Co1-C40	1.726(2)	**41**	C25-C26	1.377(3)
2	Co1-C41	1.750(2)	**42**	C26-C27	1.390(3)
3	Co1-P2	2.1899(5)	**43**	C28-C29	1.382(3)
4	Co1-P1	2.1927(5)	**44**	C28-C33	1.398(3)
5	P1-C16	1.8307(16)	**45**	C29-C30	1.395(3)
6	P1-C22	1.8311(16)	**46**	C30-C31	1.372(4)
7	P1-C2	1.8341(17)	**47**	C31-C32	1.376(4)
8	P2-C28	1.8287(18)	**48**	C32-C33	1.382(3)
9	P2-C12	1.8337(18)	**49**	C34-C39	1.389(3)
10	P2-C34	1.8343(17)	**50**	C34-C35	1.392(2)
11	O1-C13	1.3818(19)	**51**	C35-C36	1.393(3)
12	O1-C1	1.3848(19)	**52**	C36-C37	1.380(3)
13	O2-C40	1.156(3)	**53**	C37-C38	1.384(3)
14	O3-C41	1.151(3)	**54**	C38-C39	1.394(3)
15	C1-C6	1.384(2)	**55**	C1S-C2S	1.324(7)
16	C1-C2	1.396(2)	**56**	C1S-C6S	1.475(7)
17	C2-C3	1.399(2)	**57**	C1S-C7S	1.475(7)
18	C3-C4	1.389(3)	**58**	C2S-C3S	1.380(7)
19	C4-C5	1.394(3)	**59**	C3S-C4S	1.375(6)
20	C5-C6	1.394(2)	**60**	C3S-C7S'	1.483(8)
21	C6-C7	1.532(2)	**61**	C4S-C5S	1.379(7)
22	C7-C14	1.524(3)	**62**	C5S-C6S	1.338(7)
23	C7-C8	1.531(2)	**63**	C1S"-C2S"	1.318(8)
24	C7-C15	1.545(3)	**64**	C1S"-C6S"	1.471(8)
25	C8-C13	1.386(2)	**65**	C1S"-C7"	1.484(8)
26	C8-C9	1.401(2)	**66**	C2S"-C3S"	1.382(8)
27	C9-C10	1.396(3)	**67**	C3S"-C4S"	1.372(7)
28	C10-C11	1.387(3)	**68**	C4S"-C5S"	1.381(8)
29	C11-C12	1.401(2)	**69**	C5S"-C6S"	1.339(8)
30	C12-C13	1.398(2)	**70**	C1X-C2X	1.321(8)
31	C16-C17	1.386(2)	**71**	C1X-C6X	1.472(8)
32	C16-C21	1.394(2)	**72**	C1X-C7X	1.480(8)
33	C17-C18	1.390(3)	**73**	C2X-C3X	1.382(8)

Table 8. cont.

34	C18-C19	1.382(3)	**74**	C3X-C4X	1.377(8)
35	C19-C20	1.383(3)	**75**	C4X-C5X	1.381(8)
36	C20-C21	1.388(3)	**76**	C5X-C6X	1.339(8)
37	C22-C27	1.392(2)	**77**	C1T-C2T	1.523(7)
38	C22-C23	1.393(3)	**78**	C2T-C3T	1.534(7)
39	C23-C24	1.389(3)	**79**	C3T-C4T	1.509(7)
40	C24-C25	1.384(3)	**80**	C4T-C5T	1.559(8)

Table 9. Bond angles (º) for complex **C10**.

Entry	Atoms	Bond angles (º)	Entry	Atoms	Bond angles (º)
1	C40-Co1-C41	102.41(11)	**57**	C20-C21-C16	120.46(17)
2	C40-Co1-P2	117.45(7)	**58**	C27-C22-C23	118.19(16)
3	C41-Co1-P2	99.19(7)	**59**	C27-C22-P1	123.51(14)
4	C40-Co1-P1	123.08(7)	**60**	C23-C22-P1	118.30(13)
5	C41-Co1-P1	98.77(7)	**61**	C24-C23-C22	120.84(18)
6	P2-Co1-P1	110.196(18)	**62**	C25-C24-C23	120.23(19)
7	C16-P1-C22	102.52(8)	**63**	C26-C25-C24	119.45(18)
8	C16-P1-C2	101.45(7)	**64**	C25-C26-C27	120.52(18)
9	C22-P1-C2	102.16(7)	**65**	C26-C27-C22	120.74(18)
10	C16-P1-Co1	115.24(6)	**66**	C29-C28-C33	118.59(19)
11	C22-P1-Co1	118.25(5)	**67**	C29-C28-P2	123.69(16)
12	C2-P1-Co1	114.90(5)	**68**	C33-C28-P2	117.72(15)
13	C28-P2-C12	103.60(8)	**69**	C28-C29-C30	119.9(2)
14	C28-P2-C34	101.68(8)	**70**	C31-C30-C29	121.1(3)
15	C12-P2-C34	101.04(8)	**71**	C30-C31-C32	119.3(2)
16	C28-P2-Co1	116.87(6)	**72**	C31-C32-C33	120.4(3)
17	C12-P2-Co1	115.80(6)	**73**	C32-C33-C28	120.7(2)
18	C34-P2-Co1	115.58(6)	**74**	C39-C34-C35	118.74(16)
19	C13-O1-C1	113.41(12)	**75**	C39-C34-P2	118.86(13)
20	C6-C1-O1	119.65(14)	**76**	C35-C34-P2	122.37(13)
21	C6-C1-C2	124.70(15)	**77**	C34-C35-C36	120.50(18)
22	O1-C1-C2	115.65(14)	**78**	C37-C36-C35	120.28(18)
23	C1-C2-C3	116.74(15)	**79**	C36-C37-C38	119.71(18)
24	C1-C2-P1	117.04(12)	**80**	C37-C38-C39	120.14(19)

Table 9. cont.

25	C3-C2-P1	126.04(13)	**81**	C34-C39-C38	120.61(19)
26	C4-C3-C2	120.22(16)	**82**	O2-C40-Co1	176.6(2)
27	C3-C4-C5	120.96(16)	**83**	O3-C41-Co1	179.5(2)
28	C6-C5-C4	120.49(17)	**84**	C2S-C1S-C6S	118.9(5)
29	C1-C6-C5	116.85(16)	**85**	C2S-C1S-C7S	124.1(5)
30	C1-C6-C7	117.00(15)	**86**	C6S-C1S-C7S	117.1(5)
31	C5-C6-C7	126.11(16)	**87**	C1S-C2S-C3S	119.2(5)
32	C14-C7-C8	112.24(15)	**88**	C4S-C3S-C2S	122.8(5)
33	C14-C7-C6	111.74(16)	**89**	C4S-C3S-C7S'	116.9(7)
34	C8-C7-C6	106.34(14)	**90**	C2S-C3S-C7S'	120.3(6)
35	C14-C7-C15	109.58(16)	**91**	C3S-C4S-C5S	118.9(5)
36	C8-C7-C15	108.22(15)	**92**	C6S-C5S-C4S	119.9(5)
37	C6-C7-C15	108.56(14)	**93**	C5S-C6S-C1S	120.3(5)
38	C13-C8-C9	116.85(16)	**94**	C2S"-C1S"-C6S"	118.7(7)
39	C13-C8-C7	117.29(15)	**95**	C2S"-C1S"-C7S"	122.5(7)
40	C9-C8-C7	125.82(16)	**96**	C6S"-C1S"-C7S"	118.5(8)
41	C10-C9-C8	120.14(17)	**97**	C1S"-C2S"-C3S"	119.9(7)
42	C11-C10-C9	121.23(17)	**98**	C4S"-C3S"-C2S"	122.3(7)
43	C10-C11-C12	120.36(16)	**99**	C3S"-C4S"-C5S"	118.5(7)
44	C13-C12-C11	116.58(16)	**100**	C6S"-C5S"-C4S"	120.5(7)
45	C13-C12-P2	117.40(12)	**101**	C5S"-C6S"-C1S"	119.9(7)
46	C11-C12-P2	125.74(13)	**102**	C2X-C1X-C6X	118.3(7)
47	O1-C13-C8	119.30(14)	**103**	C2X-C1X-C7X	123.7(9)
48	O1-C13-C12	115.91(15)	**104**	C6X-C1X-C7X	117.2(9)
49	C8-C13-C12	124.78(15)	**105**	C1X-C2X-C3X	119.8(8)
50	C17-C16-C21	118.54(16)	**106**	C4X-C3X-C2X	122.5(8)
51	C17-C16-P1	119.36(13)	**107**	C3X-C4X-C5X	118.3(8)
52	C21-C16-P1	122.10(13)	**108**	C6X-C5X-C4X	120.3(9)
53	C16-C17-C18	120.78(18)	**109**	C5X-C6X-C1X	120.3(8)
54	C19-C18-C17	120.45(19)	**110**	C1T-C2T-C3T	109.3(5)
55	C18-C19-C20	119.14(17)	**111**	C4T-C3T-C2T	111.6(6)
56	C19-C20-C21	120.60(19)	**112**	C3T-C4T-C5T	108.3(6)

1.5.2.2. X-Ray Crystal of [(OC)$_3$Co(μ-CO)$_2$Co(CO)(κ^2*P*,*P*-Xantphos)] (C11)

Crystals of the complex **C11** were grown by solvent diffusion, using toluene and *n*-pentane under inert atmosphere. The measured crystals were prepared under inert conditions and immersed in perfluoropolyether as protecting oil for manipulation.

A yellow prism-like specimen of $C_{45}H_{32}Co_2O_7P_2$, approximate dimensions 0.060 mm x 0.149 mm x 0.348 mm, was used for the X-ray crystallographic analysis. The X-ray intensity data were measured on a D8 Venture system equipped with a multilayer monochromator and a Mo microfocus (λ = 0.71073 Å).

The frames were integrated with the Bruker SAINT software package using a narrow-frame algorithm. The integration of the data using a triclinic unit cell yielded a total of 63484 reflections to a maximum θ angle of 30.55° (0.70 Å resolution), of which 11551 were independent (average redundancy 5.496, completeness = 99.2%, Rint = 3.56%, Rsig = 2.51%) and 10051 (87.01%) were greater than 2σ(F2). The final cell constants of a = 10.8578(8) Å, b = 11.6947(9) Å, c = 17.4282(13) Å, α = 106.744(3)°, β = 95.840(3)°, γ = 112.496(3)°, volume = 1900.9(3) Å^3, are based upon the refinement of the XYZ-centroids of reflections above 20 σ(I). Data were corrected for absorption effects using the Multi-Scan method (SADABS). The calculated minimum and maximum transmission coefficients (based on crystal size) are 0.6883 and 0.7461.

The structure was solved and refined using the Bruker SHELXTL Software Package, using the space group P-1, with Z = 2 for the formula unit, $C_{45}H_{32}Co_2O_7P_2$. The final anisotropic full-matrix least-squares refinement on F2 with 507 variables converged at R1 = 2.92%, for the observed data and wR2 = 7.82% for all data. The goodness-of-fit was 1.034. The largest peak in the final difference electron density synthesis was 1.113 e/Å^3 and the largest hole was -0.724 e/Å^3 with an RMS deviation of 0.069 e/Å^3. On the basis of the final model, the calculated density was 1.510 g/cm^3 and F(000), 884 e.

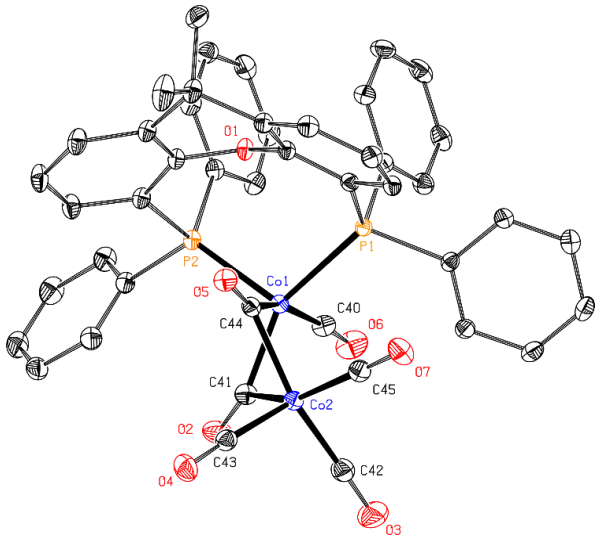

Figure 31. ORTEP drawing (thermal ellipsoids drawn at a 50% probability level) showing the structure of complex **C11**. Colour Scheme: C: black, Co: blue, O: red, P: orange.

Comments to the crystal structure of complex **C11**: The asymmetric unit contains one molecule of the metal complex.

Table 10. Crystal data and structural parameters for the complex **C11**.

Compound	Complex C11
Formula	$C_{45}H_{32}Co_2O_7P_2$
Solvent	Toluene/Pentane
Formula weight	864.50
Temperature (K)	100(2)
Crystal system	Triclinic
Space group	P -1
a (Å)	10.8578(8)
b (Å)	11.6947(9)
c (Å)	17.4282(13)
α (°)	106.744(3)
β (°)	95.840(3)
γ (°)	112.496(3)
Volume (Å^3)	1900.9(3)
Θ	2
ρ (g·cm^{-3})	1.510
μ (mm^{-1})	1.011
θmax (°)	30.548
Reflect. collected	63484
Unique reflect.	11551 [R(int) = 0.0356]
Absorpt. correction	Semi-empirical from equivalents
Parameters/restrains	507/0
R1/wR2 [I>2σ(I)]	0.0292/0.0719
R1/wR2 (all data)	0.0375/0.0782
Goodness-of-fit (F^2)	1.034
Peak/hole (e/Å^{-3})	-0.724

Table 11. Bond lengths (Å) for complex **C11**.

Entry	Atoms	Length (Å)	Entry	Atoms	Length (Å)
1	Co(1)-C(40)	1.7980(15)	**34**	C(7)-C(15)	1.532(2)
2	Co(1)-C(44)	1.8716(14)	**35**	C(7)-C(14)	1.547(2)
3	Co(1)-C(41)	1.8987(15)	**36**	C(8)-C(13)	1.3883(18)
4	Co(1)-P(2)	2.2578(4)	**37**	C(8)-C(9)	1.397(2)
5	Co(1)-P(1)	2.3082(4)	**38**	C(9)-C(10)	1.393(2)
6	Co(1)-Co(2)	2.5103(3)	**39**	C(10)-C(11)	1.392(2)
7	Co(2)-C(43)	1.7938(16)	**40**	C(11)-C(12)	1.3969(19)
8	Co(2)-C(42)	1.8122(17)	**41**	C(12)-C(13)	1.3925(18)
9	Co(2)-C(45)	1.8245(16)	**42**	C(16)-C(21)	1.3947(19)
10	Co(2)-C(41)	1.9733(14)	**43**	C(16)-C(17)	1.401(2)
11	Co(2)-C(44)	2.0306(14)	**44**	C(17)-C(18)	1.387(2)
12	P(1)-C(16)	1.8337(14)	**45**	C(17)-H(17)	0.9500
13	P(1)-C(1)	1.8374(14)	**46**	C(18)-C(19)	1.390(2)
14	P(1)-C(22)	1.8374(14)	**47**	C(19)-C(20)	1.383(2)
15	P(2)-C(12)	1.8289(14)	**48**	C(20)-C(21)	1.395(2)
16	P(2)-C(34)	1.8313(14)	**49**	C(22)-C(23)	1.390(2)
17	P(2)-C(28)	1.8414(14)	**50**	C(22)-C(27)	1.4031(19)
18	O(1)-C(6)	1.3831(15)	**51**	C(23)-C(24)	1.397(2)
19	O(1)-C(13)	1.3874(16)	**52**	C(24)-C(25)	1.384(2)
20	O(2)-C(41)	1.1740(18)	**53**	C(25)-C(26)	1.383(2)
21	O(3)-C(42)	1.138(2)	**54**	C(26)-C(27)	1.388(2)
22	O(4)-C(43)	1.1418(19)	**55**	C(28)-C(33)	1.396(2)
23	O(5)-C(44)	1.1717(17)	**56**	C(28)-C(29)	1.400(2)
24	O(6)-C(40)	1.1379(19)	**57**	C(29)-C(30)	1.391(2)
25	O(7)-C(45)	1.1364(19)	**58**	C(30)-C(31)	1.393(2)
26	C(1)-C(6)	1.3945(19)	**59**	C(31)-C(32)	1.381(3)
27	C(1)-C(2)	1.4024(18)	**60**	C(32)-C(33)	1.396(2)
28	C(2)-C(3)	1.3934(19)	**61**	C(34)-C(35)	1.392(2)
29	C(3)-C(4)	1.389(2)	**62**	C(34)-C(39)	1.3983(19)
30	C(4)-C(5)	1.3952(19)	**63**	C(35)-C(36)	1.396(2)
31	C(5)-C(6)	1.3928(18)	**64**	C(36)-C(37)	1.386(2)
32	C(5)-C(7)	1.5295(19)	**65**	C(37)-C(38)	1.389(2)
33	C(7)-C(8)	1.5263(19)	**66**	C(38)-C(39)	1.389(2)

Table 12. Bond angles (º) for complex **C11**.

Entry	Atoms	Bond angle (º)	Entry	Atoms	Bond angle (º)
1	C(40)-Co(1)-C(44)	159.97(6)	**58**	C(5)-C(7)-C(15)	110.94(12)
2	C(40)-Co(1)-C(41)	83.69(7)	**59**	C(8)-C(7)-C(14)	109.19(12)
3	C(44)-Co(1)-C(41)	86.00(6)	**60**	C(5)-C(7)-C(14)	109.00(12)
4	C(40)-Co(1)-P(2)	102.55(5)	**61**	C(15)-C(7)-C(14)	109.27(14)
5	C(44)-Co(1)-P(2)	96.56(4)	**62**	C(13)-C(8)-C(9)	116.41(13)
6	C(41)-Co(1)-P(2)	103.78(5)	**63**	C(13)-C(8)-C(7)	118.66(12)
7	C(40)-Co(1)-P(1)	90.98(5)	**64**	C(9)-C(8)-C(7)	124.93(12)
8	C(44)-Co(1)-P(1)	89.80(4)	**65**	C(10)-C(9)-C(8)	121.01(13)
9	C(41)-Co(1)-P(1)	151.15(5)	**66**	C(11)-C(10)-C(9)	120.57(14)
10	P(2)-Co(1)-P(1)	105.059(15)	**67**	C(10)-C(11)-C(12)	120.18(13)
11	C(40)-Co(1)-Co(2)	107.88(5)	**68**	C(13)-C(12)-C(11)	117.13(12)
12	C(44)-Co(1)-Co(2)	52.80(4)	**69**	C(13)-C(12)-P(2)	117.16(10)
13	C(41)-Co(1)-Co(2)	50.89(4)	**70**	C(11)-C(12)-P(2)	125.49(11)
14	P(2)-Co(1)-Co(2)	136.242(13)	**71**	O(1)-C(13)-C(8)	120.10(12)
15	P(1)-Co(1)-Co(2)	105.083(13)	**72**	O(1)-C(13)-C(12)	115.29(11)
16	C(43)-Co(2)-C(42)	104.91(7)	**73**	C(8)-C(13)-C(12)	124.60(13)
17	C(43)-Co(2)-C(45)	109.61(7)	**74**	C(21)-C(16)-C(17)	118.81(13)
18	C(42)-Co(2)-C(45)	95.61(7)	**75**	C(21)-C(16)-P(1)	121.27(11)
19	C(43)-Co(2)-C(41)	97.97(6)	**76**	C(17)-C(16)-P(1)	119.49(10)
20	C(42)-Co(2)-C(41)	88.30(7)	**77**	C(18)-C(17)-C(16)	120.77(14)
21	C(45)-Co(2)-C(41)	149.99(6)	**78**	C(17)-C(18)-C(19)	119.84(14)
22	C(43)-Co(2)-C(44)	93.10(6)	**79**	C(20)-C(19)-C(18)	119.96(14)
23	C(42)-Co(2)-C(44)	159.72(6)	**80**	C(19)-C(20)-C(21)	120.37(14)
24	C(45)-Co(2)-C(44)	86.83(6)	**81**	C(20)-C(21)-C(16)	120.19(14)
25	C(41)-Co(2)-C(44)	79.90(6)	**82**	C(23)-C(22)-C(27)	118.96(13)
26	C(43)-Co(2)-Co(1)	125.84(5)	**83**	C(23)-C(22)-P(1)	124.28(11)
27	C(42)-Co(2)-Co(1)	112.99(5)	**84**	C(27)-C(22)-P(1)	116.76(11)
28	C(45)-Co(2)-Co(1)	103.75(5)	**85**	C(22)-C(23)-C(24)	120.09(14)
29	C(41)-Co(2)-Co(1)	48.30(4)	**86**	C(25)-C(24)-C(23)	120.42(15)
30	C(44)-Co(2)-Co(1)	47.23(4)	**87**	C(26)-C(25)-C(24)	119.86(14)
31	C(16)-P(1)-C(1)	103.49(6)	**88**	C(25)-C(26)-C(27)	120.19(15)
32	C(16)-P(1)-C(22)	96.81(6)	**89**	C(26)-C(27)-C(22)	120.47(14)
33	C(1)-P(1)-C(22)	106.48(6)	**90**	C(33)-C(28)-C(29)	118.55(13)

Table 12. cont.

34	C(16)-P(1)-Co(1)	116.32(5)	**91**	C(33)-C(28)-P(2)	122.13(12)
35	C(1)-P(1)-Co(1)	114.86(5)	**92**	C(29)-C(28)-P(2)	119.24(11)
36	C(22)-P(1)-Co(1)	116.63(5)	**93**	C(30)-C(29)-C(28)	120.71(14)
37	C(12)-P(2)-C(34)	102.61(6)	**94**	C(29)-C(30)-C(31)	120.00(15)
38	C(12)-P(2)-C(28)	101.28(6)	**95**	C(32)-C(31)-C(30)	119.82(15)
39	C(34)-P(2)-C(28)	101.28(6)	**96**	C(31)-C(32)-C(33)	120.32(15)
40	C(12)-P(2)-Co(1)	115.33(5)	**97**	C(32)-C(33)-C(28)	120.56(15)
41	C(34)-P(2)-Co(1)	116.27(5)	**98**	C(35)-C(34)-C(39)	118.86(13)
42	C(28)-P(2)-Co(1)	117.65(5)	**99**	C(35)-C(34)-P(2)	122.59(11)
43	C(6)-O(1)-C(13)	114.75(10)	**100**	C(39)-C(34)-P(2)	118.45(11)
44	C(6)-C(1)-C(2)	116.73(12)	**101**	C(34)-C(35)-C(36)	120.51(13)
45	C(6)-C(1)-P(1)	117.22(10)	**102**	C(37)-C(36)-C(35)	120.27(14)
46	C(2)-C(1)-P(1)	125.32(11)	**103**	C(36)-C(37)-C(38)	119.47(14)
47	C(3)-C(2)-C(1)	120.23(13)	**104**	C(39)-C(38)-C(37)	120.48(14)
48	C(4)-C(3)-C(2)	120.93(13)	**105**	C(38)-C(39)-C(34)	120.37(14)
49	C(3)-C(4)-C(5)	120.76(13)	**106**	O(6)-C(40)-Co(1)	174.61(14)
50	C(6)-C(5)-C(4)	116.67(13)	**107**	O(2)-C(41)-Co(1)	143.48(13)
51	C(6)-C(5)-C(7)	118.73(12)	**108**	O(2)-C(41)-Co(2)	135.42(12)
52	C(4)-C(5)-C(7)	124.60(12)	**109**	Co(1)-C(41)-Co(2)	80.80(6)
53	O(1)-C(6)-C(5)	119.84(12)	**110**	O(3)-C(42)-Co(2)	178.71(16)
54	O(1)-C(6)-C(1)	115.48(11)	**111**	O(4)-C(43)-Co(2)	176.90(14)
55	C(5)-C(6)-C(1)	124.64(12)	**112**	O(5)-C(44)-Co(1)	149.36(12)
56	C(8)-C(7)-C(5)	107.58(11)	**113**	O(5)-C(44)-Co(2)	130.67(11)
57	C(8)-C(7)-C(15)	110.82(13)	**114**	Co(1)-C(44)-Co(2)	79.97(5)

1.5.3. Synthesis of metal complexes C10 and C11

1.5.3.1. Synthesis of [Co(CO)$_2$H(κ^2*P*,*P*-Xantphos)] (C10)

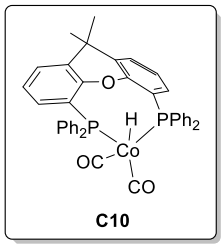

C10

The preparation of the complex **C10** was performed by modifying a reported procedure in the literature.[144] In a glove box filled with nitrogen, [$Co_2(CO)_8$] (94.8 mg, 0.25 mmol) was dissolved in anhydrous toluene (1.7 mL) in a 2 mL Schlenk flame-dried flask with stirring and anhydrous DMF (869 µL, 11.20 mmol) was added to the previous solution. After formation of a pink precipitate

[144] Kluwer, A. M.; Krafft, M. J.; Hartenbach, I.; de Bruin, B.; Kaim, W. *Top. Catal.* **2016**, *59*, 1787-1792.

(*ca.* 1 h), the reaction mixture was cooled down to 0 °C and aqueous HCl (2.5 mL, 6 M, 15.00 mmol) was added at once. After stirring for 2 minutes, two phases were formed: the aqueous phase (pink) and the organic phase (yellow). The organic phase (yellow) was separated under argon atmosphere at 0 °C and a solution of Xantphos (202 mg, 0.33 mmol) in anhydrous toluene (3.7 mL) was added. The reaction proceeded by CO bubbling, which led to the formation of a yellow precipitate. After 5 hours stirring at 0 °C, the crude mixture was stored in the freezer under N_2 for 2 hours. The liquid and precipitate were separated, the precipitate was washed with anhydrous *n*-pentane (5 mL) and solid was dried under vacuum. The complex **C10** was obtained as a yellow solid (161 mg, 70% yield). IR (neat, cm^{-1}) $\bar{\upsilon}$ 3057, 2956, 2928, 2861, 1917 ($\bar{\upsilon}_{CO}$), 1910 ($\bar{\upsilon}_{CO}$), 1586, 1479, 1433, 1404, 1358, 1307, 1227, 1180, 1154, 1118, 1091, 1068, 1026, 999, 794, 779, 748, 689, 655, 536, 509, 469, 441. ^{1}H NMR (500 MHz, CD_2Cl_2) δ 7.48 (dd, J = 7.9, 1.2 Hz, 2H), 7.36 (bs, 8H), 7.28–7.25 (m, 4H), 7.18 (t, J = 7.4 Hz, 8H), 7.02 (t, J = 7.7 Hz, 2H), 6.36–6.33 (m, 2H), 1.69 (s, 6H), –11.23 (t, J = 23.3 Hz, 1H) ppm. ^{13}C{^{1}H,^{31}P} NMR (126 MHz, CD_2Cl_2) δ 209.3 (2 C, *C*O), 155.9 (2 C, *Carom*O), 136.3 (4 C, *Carom*P), 135.5 (2 C, *Carom*C(CH_3)$_2$), 133.6 (8 C, *Carom*H), 129.7 (2 C, *Carom*H), 129.5 (4 C, *Carom*H), 128.3 (8 C, *Carom*H), 127.5 (2 C, *Carom*P), 126.2 (2 C, *Carom*H), 124.0 (2 C, *Carom*H), 37.0 (2 C, CH_3), 27.1 (1 C, *C*(CH_3)$_2$) ppm. ^{31}P{^{1}H} NMR (202 MHz, CD_2Cl_2) δ 43.4 ppm. HRMS (MALDI) *m/z* $[M–2CO–H]^+$ calcd for $C_{39}H_{32}CoOP_2$ 637.1255, found 637.1270.

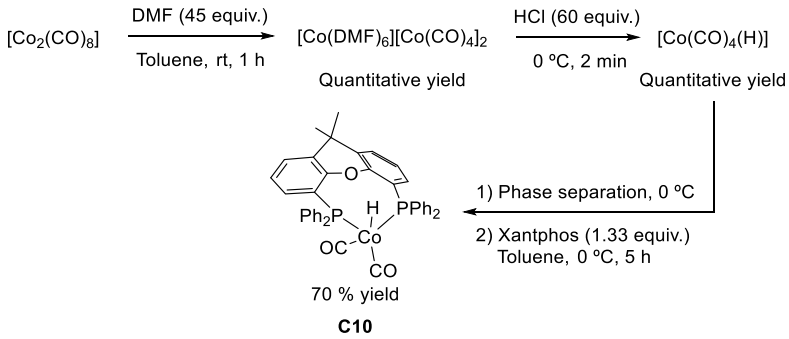

Scheme 20. Synthesis of complex **C10**.

1.5.3.2. Synthesis of [(OC)$_3$Co(μ-CO)$_2$Co(CO)(κ^2*P*,*P*-Xantphos)] (C11)

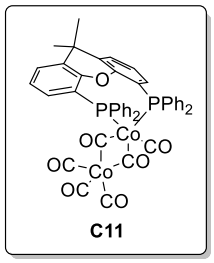

C11

In a glove box filled with nitrogen, [$Co_2(CO)_8$] (220 μmol, 83.8 mg) and Xantphos (220 μmol, 134.3 mg) were added into a 10 mL in a flame dried 10 mL ace pressure tube with a magnetic stirrer in 1.9 mL of anhydrous and deoxygenated toluene having a concentration of 0.115 M respect of the Xantphos. The reaction mixture was stirred at 70 ºC for 2 hours under nitrogen atmosphere. Following the reaction mixture was kept in the glove box and 5 mL of anhydrous and deoxygenated *n*-pentane was added into the glass tube, which led to the formation of a red orange precipitate. The vial was kept in the glove box for 48 hours to favour the precipitation of the product. Then, the liquid and precipitate were separated, the precipitate was washed twice with anhydrous *n*-pentane (2x5 mL) and solid was dried under vacuum. The complex **C11** was obtained as a red-orange solid (97 mg, 51% yield). IR (neat, cm^{-1}) ῡ 2955.64, 2043.39 ($\bar{\upsilon}_{CO}$), 1963.32 ($\bar{\upsilon}_{CO}$), 1940.02 ($\bar{\upsilon}_{CO}$), 1880.43 ($\bar{\upsilon}_{CO}$), 1815.43, 1785.57, 1479.34, 1433.32, 1405.48, 123.9.7, 1093.39, 747.79, 735.73, 686.25, 622.59, 603.46, 575.93. ^{1}H NMR (400 MHz, CD_2Cl_2) δ 7.62 (d, J = 7.3 Hz, 2H), 7.26 (bs, 12 H), 7.17 (bs, 10 H), 6,61 (bs, 2H), 1.72 (s, 6 H). ^{13}C{^{1}H} NMR (126 MHz, CD_2Cl_2) 155.22 (2 C, *Carom*O), 133.23 (4 C, *Carom*P), 132.89, 130.87, 129.58, 128.10, 128.06, 128.02, 126.91, 124.52, 118.54, 118.25, 36.28 (2 C, CH_3). ^{31}P{^{1}H} NMR (202 MHz, CD_2Cl_2) δ 32.29. HRMS (ESI$^+$) *m/z* [M–5CO–Co]$^+$ calcd for $C_{40}H_{32}CoO_2P_2$ 665.1210, found 665.1213.

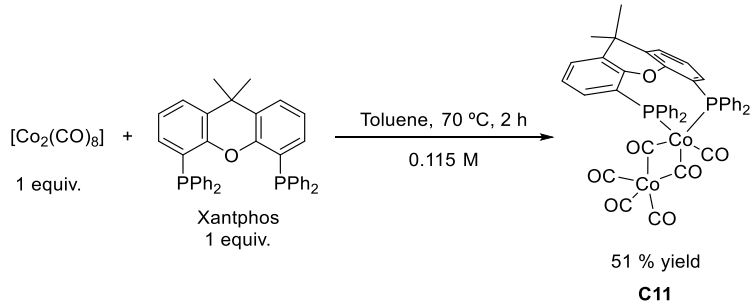

Scheme 21. Synthesis of complex **C11**.

1.5.4. General procedure for the cobalt-catalysed hydroformylation

Essays for screening catalysts:

In a glove box filled with nitrogen, Xantphos (*ca.* 2.7 μmol in 360 μL of toluene) and [$Co_2(CO)_8$] (*ca.* 2.7 μmol in 360 μL of toluene),

$[Co(CO)_2H(\kappa^2P,P\text{-Xantphos})]$ (**C10**) (*ca.* 2.3 μmol in 65 μL of toluene) or $[(OC)_3Co(\mu\text{-}CO)_2Co(CO)(\kappa^2P,P\text{-Xantphos})]$ (**C11**) (*ca.* 2.3 μmol in 65 μL of toluene) were added into a 2 mL vial equipped with a magnetic stirrer. Substrate (the corresponding octene, heptene or hexene or mixtures thereof; *ca.* 230 μmol), dodecane (*ca.* 69 μmol) and additional toluene were charged to provide the desired final solution having a 0.26 M concentration of substrate(s). The vial was transferred into an autoclave and taken out of the glove box. The autoclave was purged three times with syngas (1:1 H_2/CO ratio without stirring, at a pressure not higher than 10 bar) and, finally, the autoclave was pressurized with syngas to the desired pressure. The reaction mixture was stirred at the selected temperature (metallic block) for the selected reaction time. The reaction was cooled down to room temperature (ice bath) and the pressure was carefully released in a well-ventilated hood. Conversion, chemo- and regio-selectivity of the products arising from hydroformylation reaction conditions were determined by GC analysis on an achiral stationary phase (HP-5) using dodecane as the internal standard (IS).

Hydroformylation at the preparative scale (S/C = 500):

In a glove box filled with nitrogen, $[(OC)_3Co(\mu\text{-}CO)_2Co(CO)(\kappa^2P,P\text{-Xantphos})]$ (**C11**) (43.6 mg, 0.0505 mmol) was placed in a 25 mL autoclave with a magnetic stirrer. Oct-1-ene (**S31a**) (4.0 mL, 25.2 mmol) and toluene (10.4 mL) were added to provide the desired final solution, giving a 1.8 M concentration of oct-1-ene. The autoclave was purged three times with syngas (1:1 H_2/CO ratio without stirring, at a pressure not higher than 10 bar) and, finally, the autoclave was pressurised with syngas to 40 bar. The autoclave was connected to a five-litre steel reservoir filled with syngas to ensure that pressure was high enough during the whole hydroformylation process. The reservoir was isolated from the reactor by a valve, and the pressure inside the autoclave was restored to 40 bar by opening the valve when the pressure inside the autoclave dropped by 10% and closing it afterwards. The reaction mixture was stirred at 140 °C for 21 h. The reaction was cooled down to room temperature (ice bath) and the pressure was carefully released in a well-ventilated hood. The reaction mixture was distilled under reduced pressure to obtain the corresponding mixture of aldehydes (fraction 1, b.p. = 35-45 ºC, 25-30 mbar, 8.84 g, 2.3 mmol of aldehydes and fraction 2, b.p. = 75-80 ºC, 25-30 mbar, 1.57 g, 11.0 mmol of aldehydes; 53% overall yield).

Hydroformylation at the preparative scale (S/C = 1000):

In a glove box filled with nitrogen, $[(OC)_3Co(\mu\text{-}CO)_2Co(CO)(\kappa^2P,P\text{-Xantphos})]$ (**C11**) (21.8 mg, 0.0252 mmol) was placed in a 25 mL autoclave with a magnetic stirrer. Oct-1-ene (**S31a**) (4.0

mL, 25.2 mmol) and toluene (10.4 mL) were added to provide the desired final solution, giving a 1.8 M concentration of oct-1-ene. The hydroformylation process was carried out as indicated above for S/C = 500. The reaction mixture was distilled under reduced pressure to obtain the corresponding mixture of aldehydes (fraction 1, b.p. = 40-45 ºC, 25-30 mbar, 8.40 g, 1.72 mmol of aldehydes and fraction 2, b.p. = 75-80 ºC, 25 mbar, 2.16 g, 11.0 mmol of aldehydes; 51% overall yield).

1.5.5. Determination of the conversion, chemoselectivity and regioselectivity in hydroformylation reaction mixtures.

Conversion, chemo- and regio-selectivity of the products arising from hydroformylation reaction conditions were determined by GC analysis on an achiral stationary phase (HP-5) using dodecane as the internal standard. The conversion was determined using the response factor of the starting material. The selectivity was determined from area % data of the GC analysis.

GC analysis conditions for hydroformylation reaction mixtures of oct-1-ene, (*Z*)-oct-2-ene, (*E*)-oct-2-ene, (*E*)-oct-3-ene, (*E*)-oct-4-ene and (*Z*)-oct-4-ene: Conversion, chemo- and regio-selectivity in the mixtures arising from hydroformylation reaction conditions were determined by GC-FID analysis with a HP-5 column (5% phenyl methyl siloxane; 30 m x 320 µm x 0.25 µm). Flow rate: 2.3 mL/min. Temperature program: 35 °C for 5 min, then up to 150 °C at 20 °C/min and 10 min at 150 °C, then up to 320 °C at 20 °C/min and 5 min at 320 ºC. Retention times: 5.2 min for oct-1-ene, 5.3 min for (*E*)-oct-4-ene, 5.4 min for octane, 5.6 min for (*E*)-oct-3-ene, 5.7 min for (*Z*)-oct-4-ene, 5.9 min for (*E*)-oct-2-ene, 6.1 min for (*Z*)-oct-2-ene, 9.5 min for **P31d** (2-propylhexanal), 9.6 min for **P31c** (2-ethylheptanal), 9.7 min for **P31b** (2-methyloctanal), 10.2 min for **P31a** (nonanal) , 10.7 min for **5d** (2-propyl-hexan-1-ol), 10.8 min for **5c** (2-ethyl-heptan-1-ol), 10.9 min for **5b** (2-methyl-octan-1-ol), 11.1 min for the IS (dodecane), 11.3 min for **5a** (nonan-1-ol).

GC analysis conditions for hydroformylation reaction mixtures of hept-1-ene, (*Z*)-hept-2-ene, (*E*)-hept-2-ene, (*E*)-hept-3-ene: Conversion, chemo- and regio-selectivity in the mixtures arising from hydroformylation reaction conditions were determined by GC-FID analysis with a HP-5 column (5% phenyl methyl siloxane; 30 m x 320 µm x 0.25 µm). Flow rate: 2.6 mL/min. Temperature program: 40 °C for 5 min, then up to 150 °C at 20 °C/min and 10 min at 150 °C, then up to 275 °C at 20 °C/min and 5 min at 275 °C. Retention times: 2.74 min for hept-1-ene, 2.06 min for (*E*)-hept-3-ene, 2.89 min for heptane, 2.95 min for (*E*)-hept-2-ene, 3.07 min for (*Z*)-hept-2-ene, 7.88 min for 2-propylpentanal (**P46d**), 7.98 min for 2-ethylhexanal (**P46c**), 8.09 min

for 2-methylheptanal (**P46b**), 8.60 min for octanal (**P46a**), 10.39 min for the IS (dodecane).

GC analysis conditions for hydroformylation reaction mixtures of hex-1-ene, (*Z*)-hex-2-ene, (*E*)-hex-2-ene, (*E*)-hex-3-ene, (*Z*)-hex-3-ene: Conversion, chemo- and regio-selectivity in the mixtures arising from hydroformylation reaction conditions were determined by GC-FID analysis with a HP-5 column (5% phenyl methyl siloxane; 30 m x 320 µm x 0.25 µm). Flow rate: 2.6 mL/min. Temperature program: 40 °C for 5 min, then up to 150 °C at 20 °C/min and 10 min at 150 °C, then up to 275 °C at 20 °C/min and 5 min at 275 °C. Retention times: 1.95 min for hex-1-ene, 1.99 min for hexane, 2.03 min for (*E*)-hex-2-ene, (*Z*)-hex-3-ene, (*E*)-hex-3-ene, 2.09 min for (*Z*)-hex-2-ene), 6.38 min for 2-ethylpentanal (**P47c**), 6.52 min for 2-methylhexanal (**P47b**), 7.24 min for heptanal (**P47a**), 10.39 min for the IS (dodecane).

1.5.6. Selected GC chromatograms

Representative example of a GC chromatogram of the mixtures derived from oct-1-ene or its isomers under cobalt-catalysed hydroformylation reaction conditions.

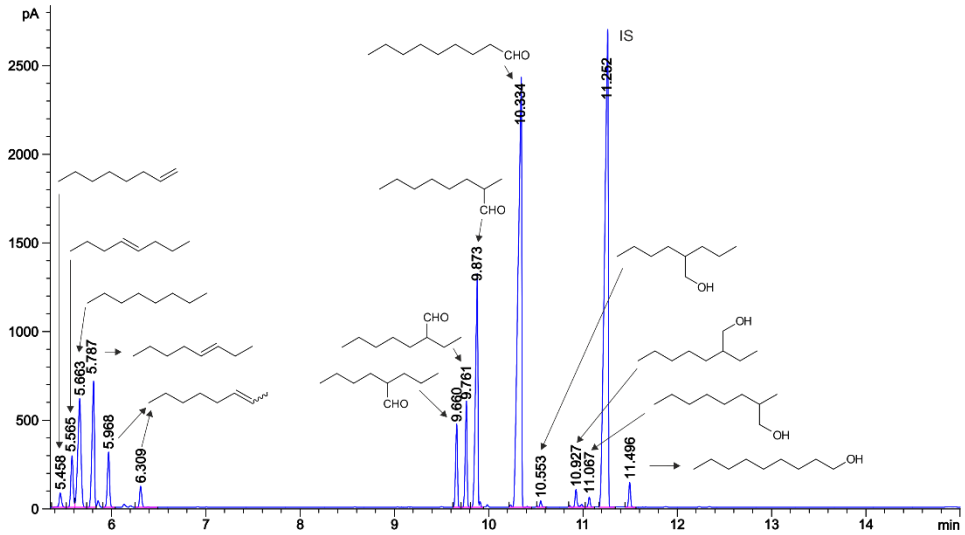

Figure 32. GC chromatogram of the mixtures derived from octenes after hydroformylation catalysis.

Representative example of a GC chromatogram of the mixtures derived from hept-1-ene or its isomers under cobalt-catalysed hydroformylation reaction conditions.

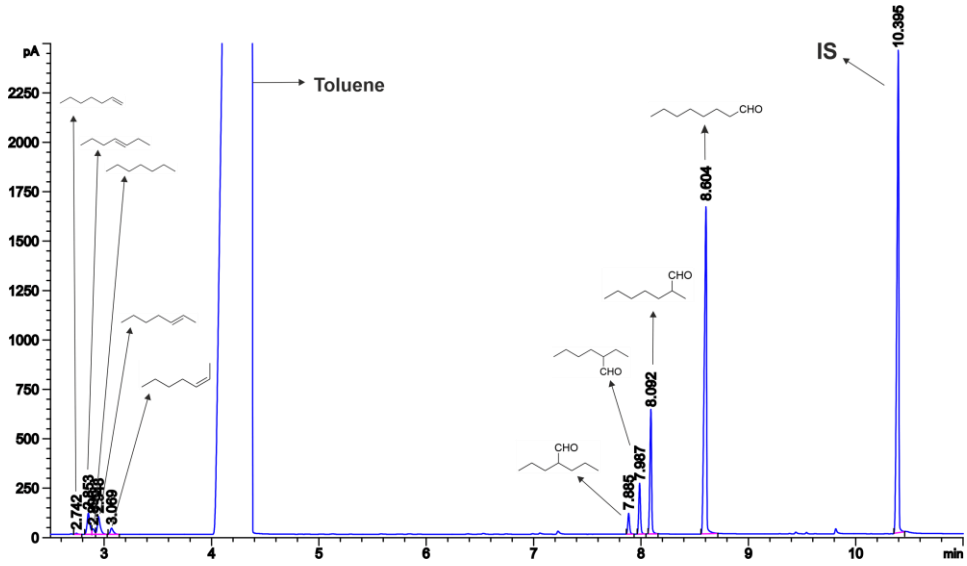

Figure 33.GC chromatogram of mixtures derived from heptenes after hydroformylation catalysis.

Representative example of a GC chromatogram of the mixtures derived from hex-1-ene or its isomers under cobalt-catalysed hydroformylation reaction conditions.

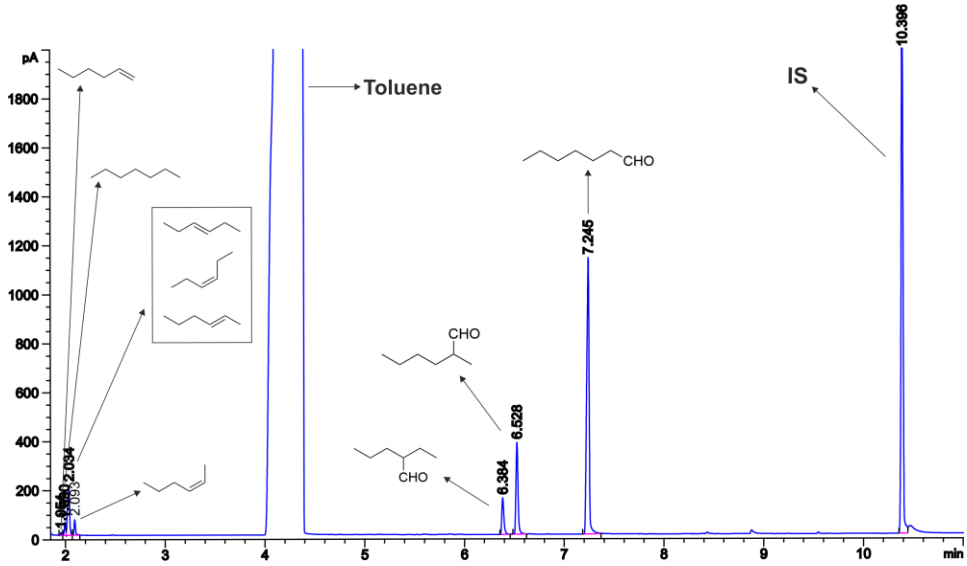

Figure 34. GC chromatogram of mixtures derived from hexenes after hydroformylation catalysis.

1.5.7. Complete set of results for cobalt-catalysed hydroformylation

Table 13. Complete set of results of cobalt-catalysed hydroformylation of oct-1-ene.

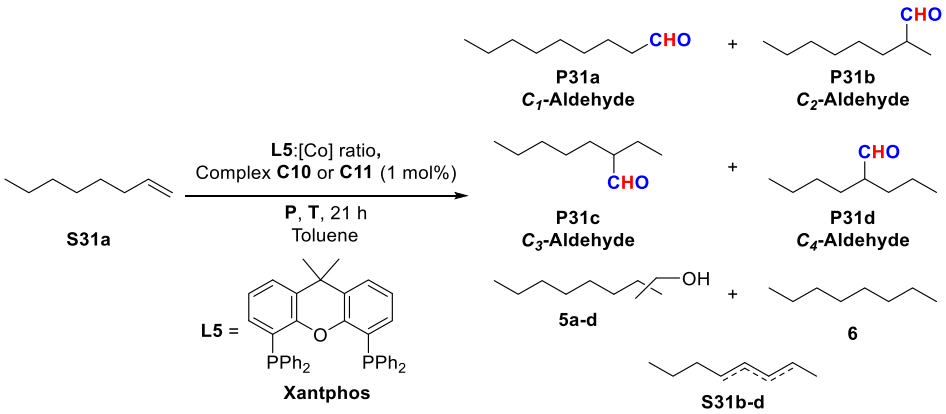

Entry	T (°C)	Pressure (H_2/CO) (bar)	L5:[Co] ratio[a], C10 or C11	[ ] (M)	Conv. (%)[a]	Selectivity (%)[b]				Regioselectivity[b] P31 C_1/C_2 ($C_1/C_2/C_3/C_4$)
						P31	5a–d	6	S31 b–d	
1	90	40 (1:1)	1:1	0.26	17	11	0	24	65	81:19 (75:18:4:3)
2	110	40 (1:1)	1:1	0.26	50	58	1	7	34	80:20 (73:18:5:4)
3	140	40 (1:1)	1:1	0.26	>99	79	13	4	4	73:27 (62:23:8:7)
4	160	40 (1:1)	1:1	0.26	>99	79	12	5	4	70:30 (56:24:11:9)
5	140	40 (1:3)	1:1	0.26	52	59	0	8	33	76:24 (68:21:6:5)
6	140	40 (3:1)	1:1	0.26	99	48	13	10	29	76:24 (67:21:7:5)
7	140	40 (1:1)	0.25:1	0.26	98	80	17	0	3	79:21 (70:19:6:5)
8	140	40 (1:1)	0:1	0.26	>99	71	25	2	2	77:23 (66:19:8:7)
9	140	40 (1:1)	0.5:1	0.26	>99	85	11	2	2	76:24 (65:21:8:6)
10	140	40 (1:1)	2:1	0.26	51	37	1	13	49	72:28 (64:26:6:4)
11	140	40 (1:1)	**C10**	0.26	99	73	2	10	15	74:26 (64:22:8:6)

Table 13. cont.

12	140	40 (1:1)	0.5:1	0.1	>99	85	5	3	7	75:25 (63:21:9:7)
13	140	40 (1:1)	0.5:1	0.5	>99	80	15	3	2	74:26 (61:21:10:8)
14	140	40 (1:1)	0.5:1	1	>99	67	31	0	2	69:31 (51:23:14:12)
15	140	40 (1:1)	**C11**	0.26	>99	89	2	4	5	78:22 (69:19:7:5)

The hydroformylations were performed in a parallel autoclave. Reaction conditions: [alkene] = 0.26 M; reaction time = 21 h; stirring rate = 800 rpm; H_2/CO in a 1:1 ratio, unless otherwise cited. [a] **L5**:[Co] Molar ratio between **L5** and cobalt centres in $[Co_2(CO)_8]$. [b] Conversion, regioselectivity and product distribution were determined by GC analysis on an achiral stationary phase (HP-5). Selectivities were calculated as mol of compound into mol of converted substrate.

Table 14. Complete set of results of cobalt-catalysed hydroformylation of octenes.

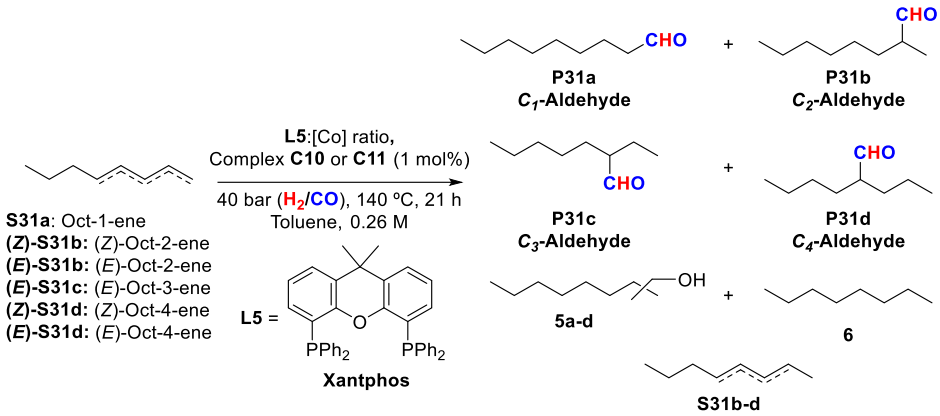

Entry	Substrate	T (°C)	Pressure (H_2/CO) (bar)	L5:[Co] ratio[a], C10 or C11	Conv. (%)[a]	Selectivity (%)[b]				Regioselectivity[b] P31 C_1/C_2 ($C_1/C_2/C_3/C_4$)
						P31	5a–d	6	S31 a–d	
1	(*Z*)-Oct-2-ene	140	40 (1:1)	0.5:1	99	89	4	4	3	74:26 (62:22:9:7)
2		140	40 (1:1)	**C10**	99	55	1	11	33	74:26 (63:22:8:7)
3	(*E*)-Oct-2-ene	140	40 (1:1)	0.5:1	>99	86	3	5	6	75:25 (62:22:9:7)
4		140	40 (1:1)	**C10**	>99	57	1	11	31	74:26 (63:22:8:7)
5	(*E*)-Oct-3-ene	140	40 (1:1)	0.5:1	99	91	4	3	2	74:26 (60:21:10:9)
6		140	40 (1:1)	**C10**	94	74	1	16	9	73:27 (60:22:9:9)
7	(*Z*)-Oct-4-ene	140	40 (1:1)	0.5:1	>99	91	3	4	2	74:26 (59:21:10:10)
8		140	40 (1:1)	**C10**	98	62	1	15	22	74:26 (61:21:9:9)
9	(*E*)-Oct-4-ene	140	40 (1:1)	0.5:1	99	89	3	5	3	75:25 (60:21:9:10)
10		140	40 (1:1)	**C10**	79	68	0	19	13	74:26 (60:21:9:10)

The hydroformylations were performed in a parallel autoclave. Reaction conditions: [alkene] = 0.26 M; reaction time = 21 h; stirring rate = 800 rpm; H_2/CO in a 1:1 ratio, unless otherwise cited. [a] **L5**:[Co] Molar ratio between **L5** and cobalt centres in [$Co_2(CO)_8$]. [b] Conversion, regioselectivity and product distribution were determined by GC analysis on an achiral stationary phase (HP-5). Selectivities were calculated as mol of compound into mol of converted substrate.

Table 15. Complete set of results of cobalt-catalysed hydroformylation of a mixture of octenes.

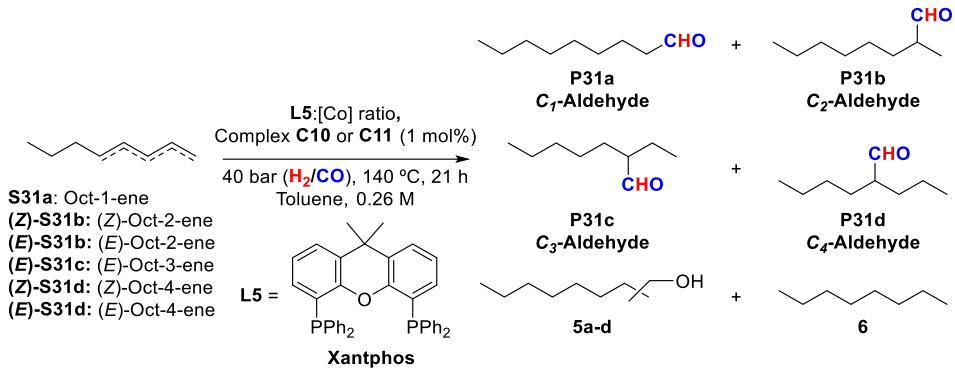

Entry	Substrate	T (ºC)	Pressure (H_2/CO) (bar)	L5:[Co] ratio[a], C10 or C11	Selectivity (%)[b]				Regioselectivity[b] P31 C_1/C_2 ($C_1/C_2/C_3/C_4$)
					P31	5a–d	6	S31 a–d	
1	Octenes mixture	140	40 (1:1)	0.5:1	91	3	3	3	74:26 (62:21:9:8)
2		140	40 (1:1)	**C10**	60	1	14	25	74:26 (62:21:9:8)
3		140	40 (1:1)	**C11**	83	1	7	9	77:23 (66:19:8:7)

The hydroformylations of octenes mixture were performed in a parallel autoclave. Reaction conditions: [alkene] = 0.26 M; reaction time = 21 h; stirring rate = 800 rpm; H_2/CO in a 1:1 ratio, unless otherwise cited. [a] **L5**:[Co] Molar ratio between **L5** and cobalt centres in $[Co_2(CO)_8]$. [b] regioselectivity and product distribution were determined by GC analysis on an achiral stationary phase (HP-5). Selectivities were calculated as mol of compound into mol of converted substrate.

Table 16. Complete set of results of cobalt-catalysed hydroformylation of a mixture of heptenes.

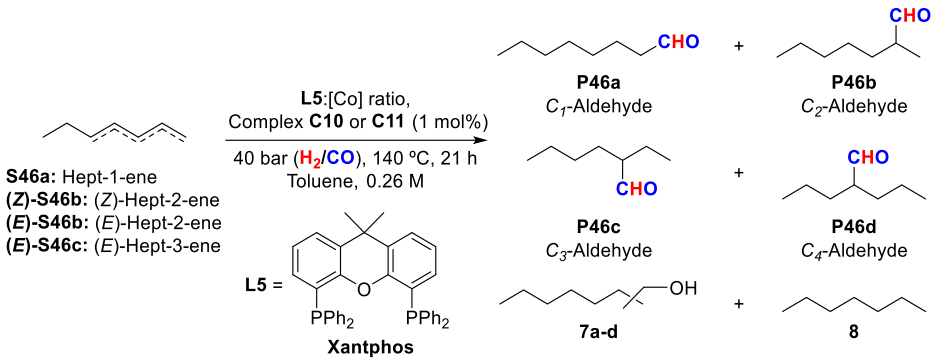

Entry	Substrate	T (ºC)	Pressure (H_2/CO) (bar)	L5:[Co] ratio[a], C10 or C11	Selectivity (%)[b]				Regioselectivity[b] C_1/C_2 ($C_1/C_2/C_3/C_4$)
					P46	7a-d	8	S46	
1	Heptenes mixture	140	40 (1:1)	0.5:1	87	1	1	11	77:23 (69:20:8:3)
2		140	40 (1:1)	**C10**	33	0	0	67	77:23 (69:20:8:3)
3		140	40 (1:1)	**C11**	85	2	1	12	78:22 (70:19:8:3)

The hydroformylations of heptenes mixture were performed in a parallel autoclave. Reaction conditions: [alkene] = 0.26 M; reaction time = 21 h; stirring rate = 800 rpm; H_2/CO in a 1:1 ratio, unless otherwise cited. [a] **L5**:[Co] Molar ratio between **L5** and cobalt centres in $[Co_2(CO)_8]$. [b] regioselectivity and product distribution were determined by GC analysis on an achiral stationary phase (HP-5). Selectivities were calculated as mol of compound into mol of converted substrate.

Table 17. Complete set of results of cobalt-catalysed hydroformylation of a mixture of hexenes.

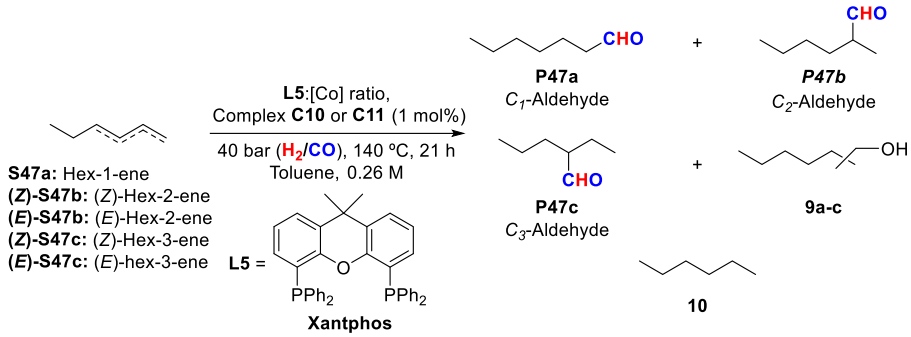

Entry	Substrate	T (ºC)	Pressure (H_2/CO) (bar)	L5:[Co] ratio[a], C10 or C11	Selectivity (%)[b]				Regioselectivity[b] C_1/C_2 ($C_1/C_2/C_3/C_4$)
					P47	9a-c	10	S47	
1		140	40 (1:1)	0.5:1	85	1	2	12	78:22 (72:20:8)
2	Hexenes Mixture	140	40 (1:1)	**C10**	36	0	1	63	77:23 (71:21:8)
3		140	40 (1:1)	**C11**	82	3	2	13	79:21 (73:19:8)

The hydroformylations of hexenes mixture were performed in a parallel autoclave. Reaction conditions: [alkene] = 0.26 M; reaction time = 21 h; stirring rate = 800 rpm; H_2/CO in a 1:1 ratio, unless otherwise cited. [a] **L5**:[Co] Molar ratio between **L5** and cobalt centres in $[Co_2(CO)_8]$. [b] regioselectivity and product distribution were determined by GC analysis on an achiral stationary phase (HP-5). Selectivities were calculated as mol of compound into mol of converted substrate.

1.5.8. NMR pressure experiments

General procedure: The corresponding solutions of cobalt catalysts/complexes were placed in an autoclave and pressurized and heated under the stated conditions in each case. After that, the autoclave was depressurized. The autoclave was opened in the glove box and *ca.* 0.6-0.7 mL of the solution were quickly placed in an NMR tube which was immediately closed with a septum. The required NMR experiments were run from this point within a few minutes (< 15 min.).

a. $[Co_2(CO)_8]$ (10.75 mg, 31.44 μmol) was dissolved in 1.75 mL of deuterated toluene (0.018 M). The solution was pressurised at 40 bar of H_2/CO (1:1) in an autoclave. The autoclave was heated 140 °C for 1 hour. ^1H NMR (126 MHz, PhMe-d_8) δ –11.59 (singlet) ppm. HRMS ESI-MS (negative mode) *m/z*: $[M–H]^-$ calcd. for C_4CoO_4 170.9129, found 170.9245.

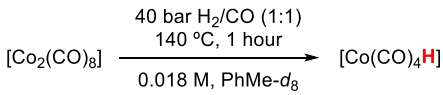

Scheme 22. Treatment of $[Co_2(CO)_8]$ with H_2/CO.

b. $[Co_2(CO)_8]$ (11.02 mg, 31.9 μmol) and Xantphos (18.80 mg, 31.9 μmol) were dissolved in 1.79 mL of deuterated toluene (0.018 M). The mixture was pressurized at 40 bar of H_2/CO (1:1) in an autoclave. The autoclave was heated 140 °C for 1 hour. ^1H NMR (126 MHz, PhMe-d_8) δ –10.86 (t, J = 28.2 Hz) and –11.47 (s) ppm. $^{31}P\{^1H\}$-NMR (202 MHz, PhMe-d_8) δ 32.47, 41.65 ppm. HRMS ESI-MS (negative mode) *m/z*: $[M–H]^-$ calcd. for C_4CoO_4 170.9129, found 170.9295. For the HRMS ESI-MS spectrum of **C1**, see section 1.5.3.1.

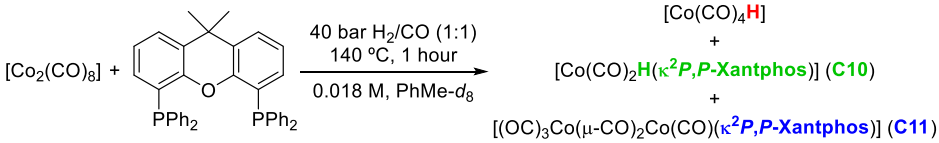

Scheme 23. Treatment of a mixture of $[Co_2(CO)_8]$ and Xantphos with H_2/CO.

c. $[(OC)_3Co(\mu\text{-}CO)_2Co(CO)(\kappa^2P,P\text{-Xantphos})]$ (**C11**) (16 mg, 18.51 μmol) was dissolved in 1.03 mL of deuterated toluene (0.018 M). The solution was pressurized at 40 bar of H_2/CO (1:1) in an autoclave. The autoclave was heated 140 °C for 1 hour. ^1H NMR (126 MHz, PhMe-d_8) δ –10.86 (triplet, J = 28.1 Hz) and –11.58 (singlet) ppm. $^{31}P\{^1H\}$-NMR (202 MHz, PhMe-d_8) δ 32.47 and 41.67 ppm. HRMS ESI-MS (negative mode) *m/z*:

[M–H]⁻ calcd. for C_4O_4Co 170.9129, found 170.9298. For the HRMS ESI-MS spectrum of **C10**, see section 1.5.3.1.

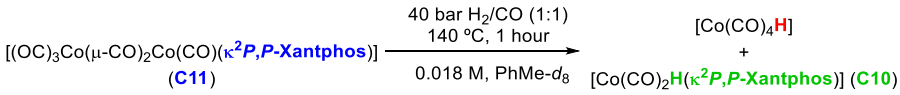

Scheme 24. Treatment of $[(CO)_3Co(\mu\text{-}CO)_2Co(CO)(Xantphos)]$ (**C11**) with H_2/CO.

d. $[Co(H)(CO)_2(\kappa^2P,P\text{-}Xantphos)]$ (**C10**) (12.85 mg, 18.51 μmol) was dissolved in 1.03 mL of deuterated toluene (0.018 M). The solution was pressurized at 40 bar of H_2/CO (1:1) in an autoclave. The autoclave was heated 140 ºC for 6 hours. ^1H NMR (126 MHz, PhMe-d_8) δ –10.86 (triplet, J = 28.1 Hz). $^{31}P\{^1H\}$-NMR (202 MHz, PhMe-d_8) δ 32.47 and 41.67 ppm.

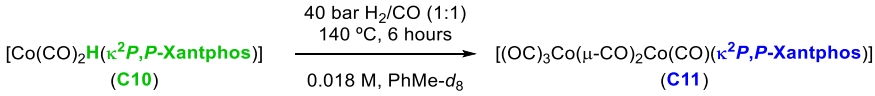

Scheme 25. Treatment of $[Co(CO)_2H(\kappa^2P,P\text{-}Xantphos)]$ (**C10**) with H_2/CO.

e. Complex **C10** $[Co(CO)_2(H)(\kappa^2P,P\text{-}Xantphos)]$ in deuterated toluene. ^1H NMR (126 MHz, PhMe-d_8) δ –10.86 (t, J = 28.3 Hz). $^{31}P\{^1H\}$ NMR (202 MHz, PhMe-d_8) δ 41.69 ppm.

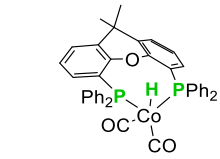

[Co(CO)2H(κ2P,P-Xantphos)]
(C10)

f. Complex **C11** $[(OC)_3Co(\mu\text{-}CO)_2Co(CO)(\kappa^2P,P\text{-}Xantphos)]$ in deuterated toluene. $^{31}P\{^1H\}$-NMR (202 MHz, PhMe-d_8) δ 32.30 ppm.

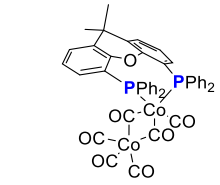

[(OC)3Co(μ-CO)2Co(CO)(κ2P,P-Xantphos)]
(C11)

1.5.9. Reaction progress monitoring

The progress of the hydroformylation of an equimolar mixture of octenes was monitored by running independent hydroformylations at different reactions times and analysing the composition of the resulting reaction mixtures. Reaction conditions: 1 mol% **C11**, 140 °C, 40 bar H_2/CO 1:1, toluene, 43.3 mM in oct-1-ene, (*E*)-oct-2-ene, (*Z*)-oct-2-ene, (*E*)-oct-3-ene, (*E*)-oct-4-ene and (*Z*)-oct-4-ene. Results are expressed in mol%.

Time (h)	Oct-1-ene	(*E*)-oct-4-ene	3-(*E*)- and 4-(*Z*)-Octene	(*E*)-Oct-2-ene	(*Z*)-Octe-2-ene
0.0	16.67	16.67	33.33	16.67	16.67
0.5	15.10	16.80	33.00	17.50	16.60
1.5	3.80	15.60	26.40	18.70	10.70
3.0	0.60	13.60	19.60	15.80	5.30
6.0	0.30	6.20	12.60	7.30	2.30
12.0	0.10	1.20	4.10	1.40	0.50
15.0	0.20	2.10	5.10	2.30	0.70
21.0	0.00	0.10	2.00	0.10	0.10

Time (h)	C_4-CHO	C_3-CHO	C_2-CHO	C_1-CHO	C_4-CH_2OH	C_3-CH_2OH	C_2-CH_2OH	C_1-CH_2OH
0.0	0.00	0.00	0.00	0.00	0.00	0.00	0.00	0.00
0.5	0.11	0.12	0.30	0.51	0.00	0.00	0.00	0.00
1.5	1.90	2.10	5.40	15.60	0.00	0.00	0.00	0.00
3.0	3.50	3.80	9.60	28.10	0.00	0.00	0.00	0.00
6.0	5.50	6.20	15.50	44.00	0.00	0.00	0.00	0.00
12.0	7.10	7.90	19.00	58.60	0.00	0.00	0.00	0.00
15.0	6.69	7.32	17.53	58.14	0.00	0.00	0.00	0.00
21.0	7.80	8.60	19.10	58.90	0.20	0.20	0.80	2.20

1.5.10. Spectroscopic Data

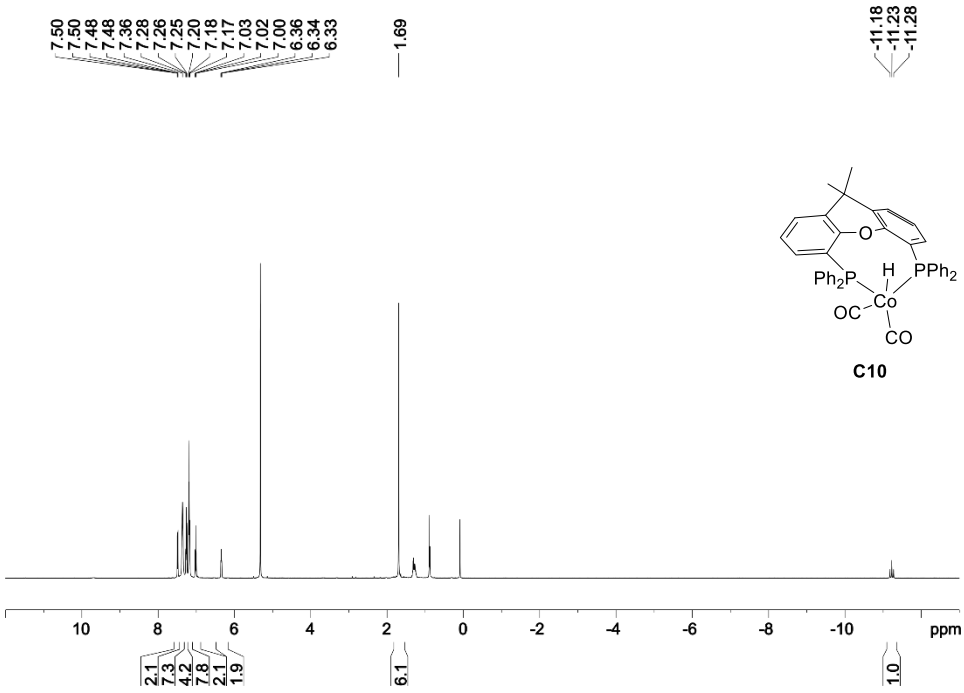

Figure 35. ^{1}H NMR spectrum (500 MHz, CD_2Cl_2) of complex **C10**.

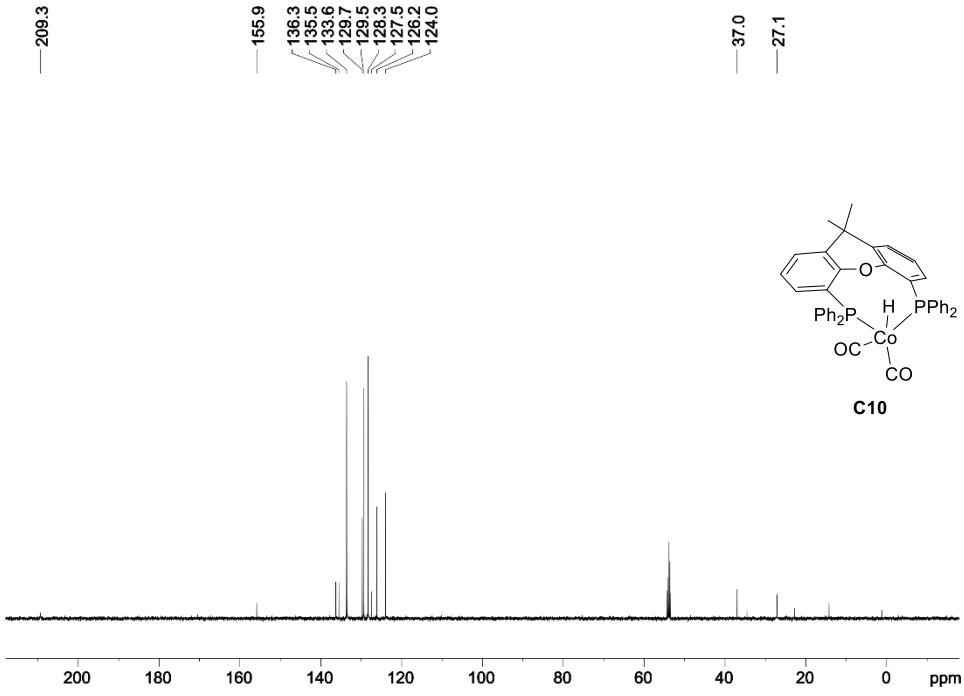

Figure 36. $^{13}C\{^{1}H,^{31}P\}$ NMR spectrum (126 MHz, CD_2Cl_2) of complex **C10**.

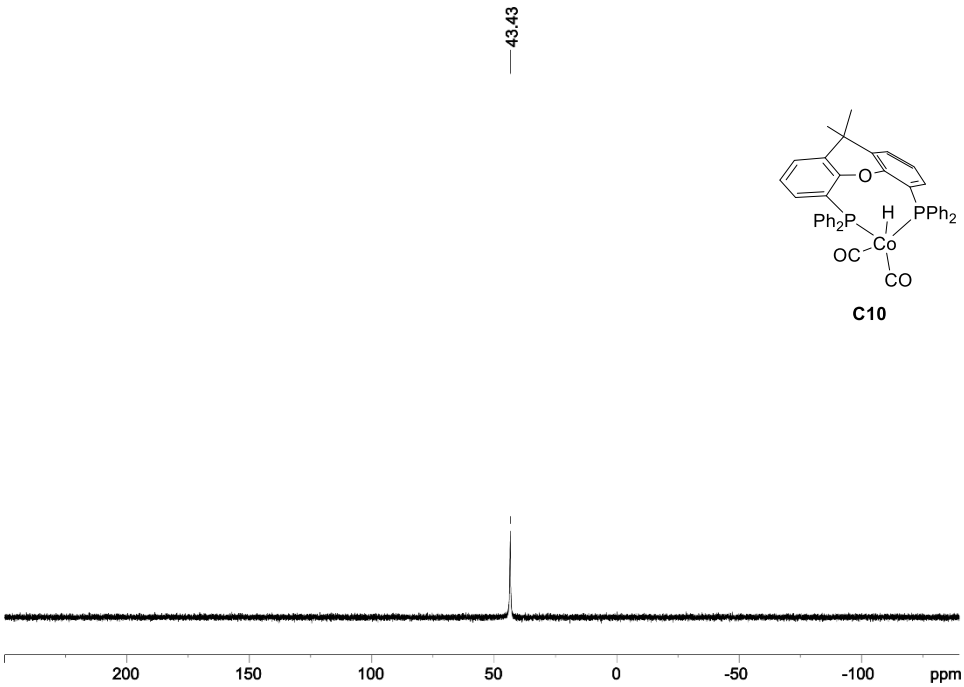

Figure 37. $^{31}P\{^{1}H\}$ NMR spectrum (202 MHz, CD_2Cl_2) of complex **C10**.

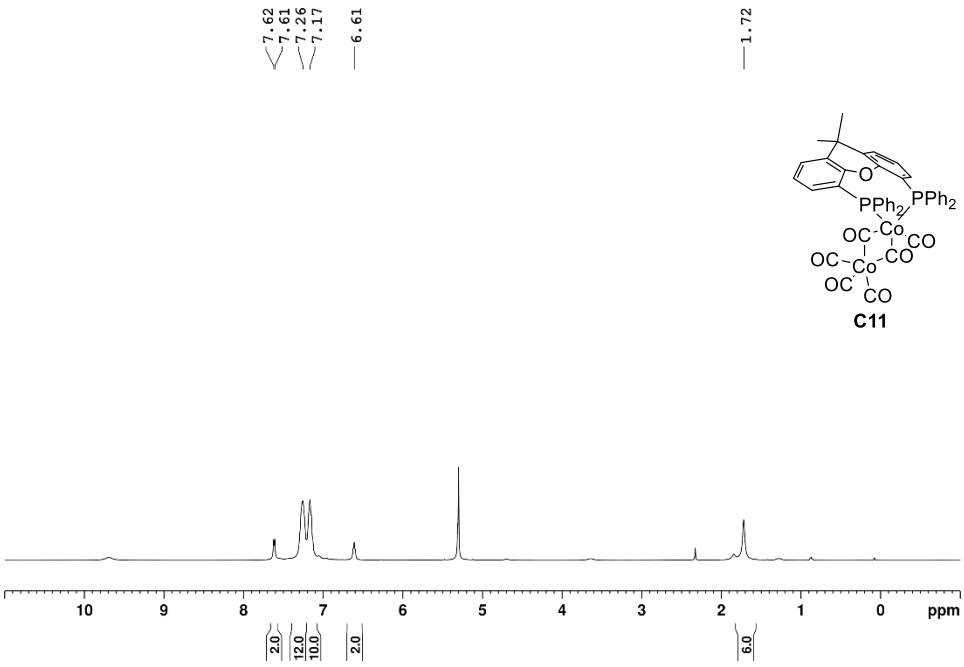

Figure 38. ^{1}H NMR spectrum (500 MHz, CD_2Cl_2) of complex **C11**.

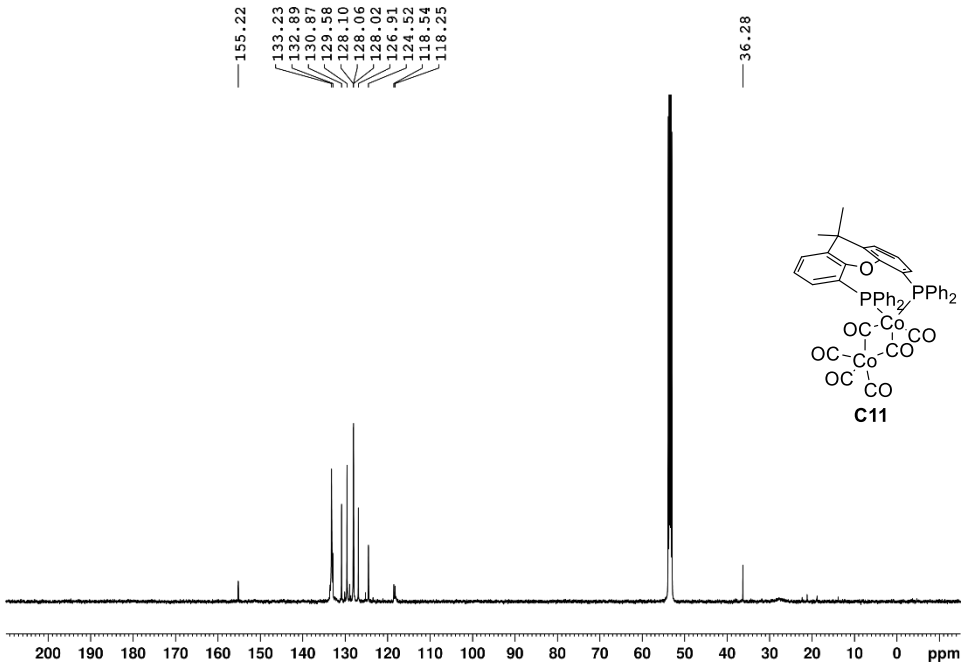

Figure 39. $^{13}C\{^{1}H\}$-NMR spectrum (126 MHz, CD_2Cl_2) of complex **C11**.

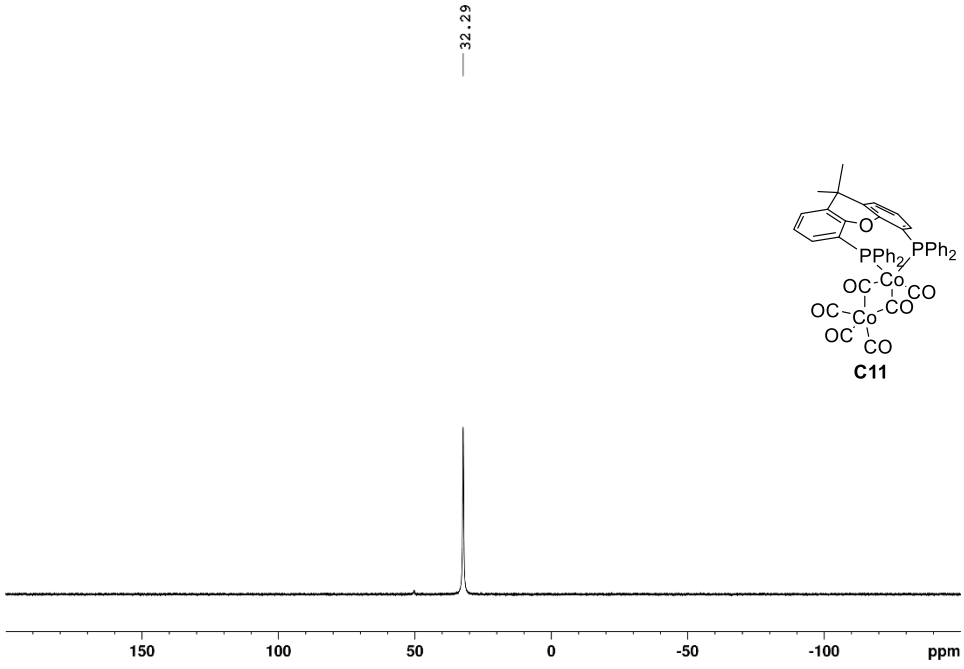

Figure 40. $^{31}P\{^{1}H\}$-NMR spectrum (202 MHz, CD_2Cl_2) of complex **C11**.

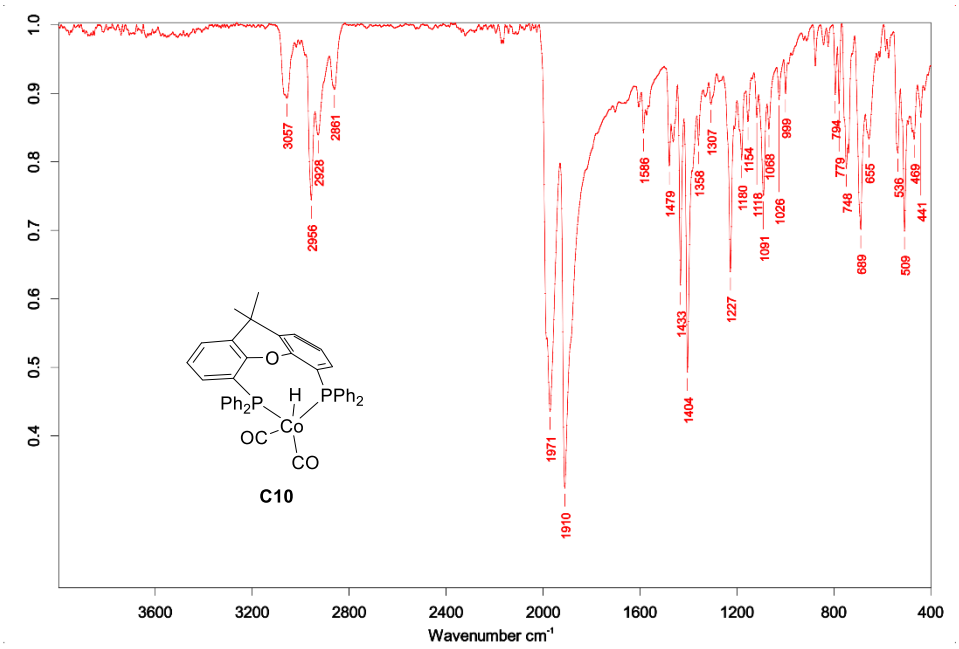

Figure 41. IR spectrum of complex **C10**.

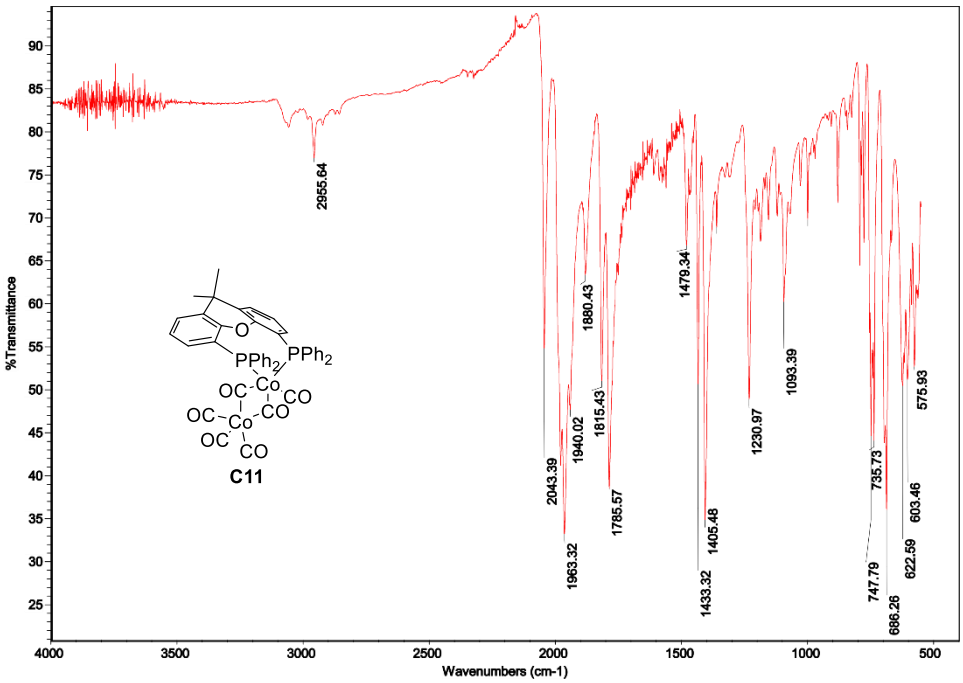

Figure 42. IR spectrum of complex **C11**.

CHAPTER II

Supramolecularly Maximised Regioselectivities: Towards Linear Aldehydes in Rhodium-Catalysed Hydroformylations

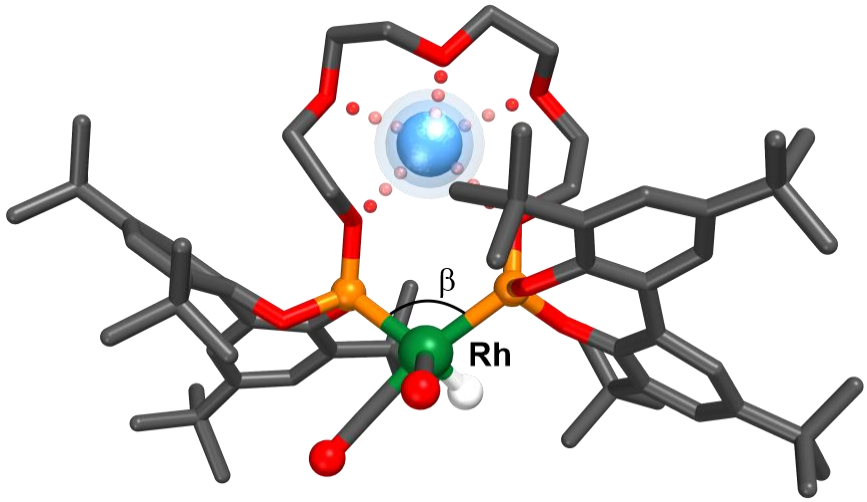

Supramolecularly Maximised Regioselectivities: Towards Linear Aldehydes in Rhodium-Catalysed Hydroformylations

Unpublished work[145]

Andrés Romero-Navarro[a,b] and Anton Vidal-Ferran[b,c,d*]

[a] Institute of Chemical Research of Catalonia (ICIQ), Av. Països Catalans 16, 43007 Tarragona, Spain.

[b] Department of Inorganic and Organic Chemistry, University of Barcelona, C. Martí i Franquès 1-11, 08028 Barcelona, Spain.

[c] Institució Catalana de Recerca i Estudis Avançats (ICREA), Pg. Lluís Companys 23, 08010 Barcelona, Spain

[d] Institut de Nanociència i Nanotecnologia (IN2UB), Universitat de Barcelona, 08028 Barcelona, Spain.

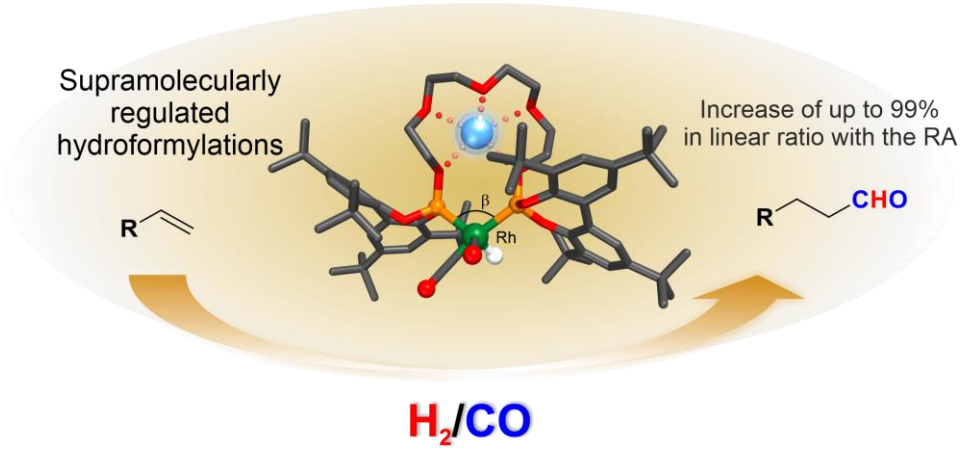

2.1. ABSTRACT

Herein we report the use of rhodium hydroformylation catalysts derived from supramolecular bisphosphite ligands, with a polyether chain as the regulation side, combined with an alkali metal BArF salt as the regulation agent (RA). This supramolecular approach for hydroformylation (HF)

[145] Romero-Navarro, A.; Vidal-Ferran, A. Supramolecular Hydroformylation Catalyst. EP23382305, **2023**. Filed on 30th of March 2023.

reactions of aliphatic terminal alkenes maximised the regioselectivity of the reaction towards the linear aldehydes. The highest regioselectivity in the hydroformylation of the aliphatic alkenes was achieved by using the ligand **L46** and RbBArF as the RA, with up to 99% linear ratio in the case of (+)-β-citronellene (Scheme 26). Supramolecularly regulated catalysts were also applied to obtain value-added aldehydes for the fragrance industries, such as lauric aldehyde, mefranal®, florhydral® and bourgeonal®. In addition, the supramolecular catalyst was combined with Pd(0) catalysts leading to efficient conditions for a tandem isomerisation-hydroformylation process in a mixture of alkenes. Finally, relevant catalytic species were studied and observed by High-Pressure NMR complexation studies and by FlowNMR *operando* spectroscopy.

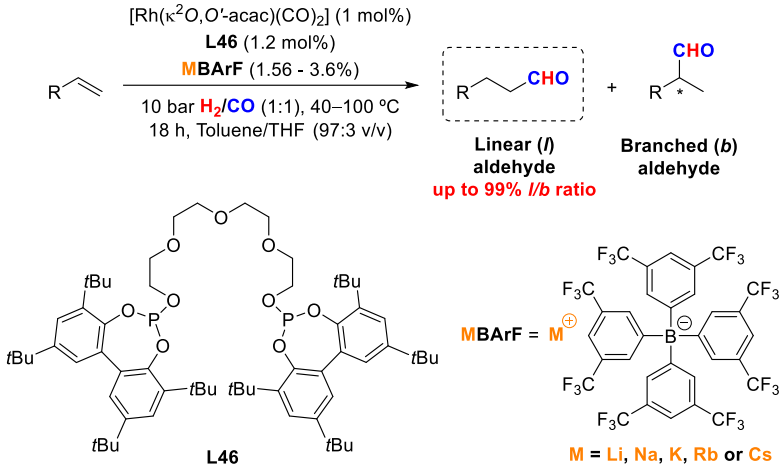

Scheme 26. Supramolecularly regulated catalysts for linear-selective hydroformylations.

Keywords: hydroformylation, alkenes, supramolecular bisphosphite ligands, *n*-aldehydes, linear aldehydes, supramolecular catalysis, high-pressure NMR, rhodium catalysis, regulation agent, regioselectivity maximisation.

2.2. INTRODUCTION

The hydroformylation reaction was discovered and patented by Otto Roelen in 1938.[3] Its discovery was one of the most important chemistry achievements of the 20th century related to the field of homogeneous catalysis. Hydroformylation consists of the addition of a hydrogen atom (H) and a formyl group (CHO) across an unsaturated C-C bond. In terms of atom economy, hydroformylation is the ideal reaction as all the atoms of the reagents end up in the products.[9a,112b] The reaction requires the use of a transition metal catalyst (mainly Co or Rh) and a mixture of H_2 and CO as the source of the "H" and "CHO" groups. The mixture of H_2 and CO is

commonly referred to as syngas[1]. Rhodium is the most common catalytic metal used in this transformation because of its high catalytic activity. Moreover, it requires milder conditions of pressure and temperature than its more abundant counterpart, cobalt. Rhodium is also able to control the chemo-, regio- and enantio-selectivity when combined with a phosphorus-based ligand.[11] However, each catalytic system and each set of structurally related substrates react in a particular manner providing a different ratio of linear and branched aldehydes.

The main goal of this work was the maximization of the regioselectivity of the reaction towards the linear aldehyde. Currently, the design and synthesis of regio- and enantio-selective ligands remain an important challenge in hydroformylation reactions.[146]After the discovery of the hydroformylation reaction, several phosphorus-based ligands have been published in rhodium-catalysed hydroformylation with high regioselectivities towards the linear aldehydes being observed (for some examples of ligands involved in the hydroformylation of oct-1-ene and pent-1-ene, see Figure 43).[116] The most common phosphorus-based ligands used in hydroformylation have been phosphites and phosphanes.[9a] BiPhePhos (**L13**) is one of the highest performing and regioselective phosphites ligands for obtaining the linear aldehydes. Its application for the hydroformylation of oct-1-ene yielded only the linear aldehyde.[147]

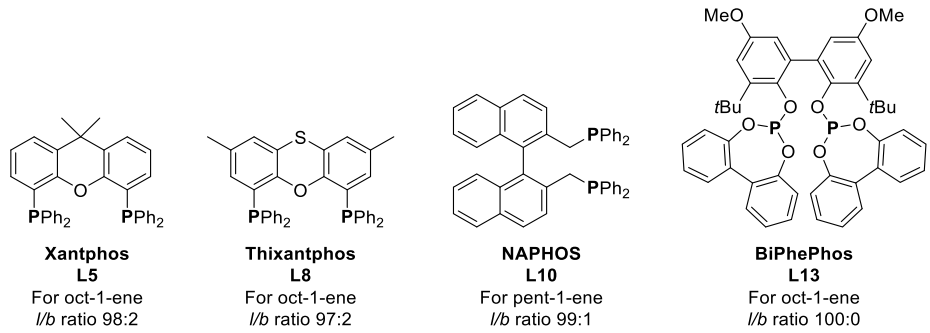

Figure 43. Phosphorus-based ligands providing high regioselectivities towards linear aldehydes in Rh-hydroformylations.

Our research group has designed and developed a strategy for regulating the geometry, rigidity, and/or conformational flexibility around the metal centre. The supramolecular catalysts developed by the group have a catalytic site with two identical phosphite fragments capable of binding a catalytically

[146] Cunillera, A.; Godard, C.; Ruiz, A. Asymmetric Hydroformylation Using Rhodium. In *Rhodium Catalysis*, Claver, C. Ed.; Springer International Publishing, 2018; pp 99-143.
[147] van Rooy, A.; Kamer, P. C. J.; van Leeuwen, P. W. N. M.; Goubitz, K.; Fraanje, J.; Veldman, N.; Spek, A. L. *Organometallics* **1996**, *15*, 835-847.

active metal centre (rhodium for hydroformylation) and a distal regulation site containing a polyether chain[148], which is capable of interacting with a regulation agent (RA) through ion-dipole interactions.[149] The use of diverse RAs translates into structural singularities in the catalytic site which depend on the size and the shape of the RA employed (Figure 44a).[92,97] Changes in the geometry and flexibility of the associated catalytic site constitute the basis of our proposed regulation mechanism. Thus, conversion, chemo-selectivity, regio-selectivity and enantioselectivity could be maximised by the choice of whether or not to use an RA (and if so, which one).[89]

This supramolecular approach was applied by our group in asymmetric hydroformylations, employing phosphite-based ligating groups for rhodium, a polyether chain as the regulation site and BArF salts as regulation agents. We have already reported the asymmetric hydroformylation of vinyl acetate and heterocyclic alkenes with *ee*'s up to 99%.[92] Furthermore, kinetic studies were performed for the supramolecularly regulated asymmetric hydroformylation of vinyl acetate with RbBArF as the RA obtaining a first-order reaction profile.[94]

[148] Gray, G. M. *Comments Inorg. Chem.* **1995**, *17*, 95-114.
[149] Kaisare, A. A.; Owens, S. B.; Valente, E. J.; Gray, G. M. *J. Organomet. Chem.* **2010**, *695*, 2658-2666.

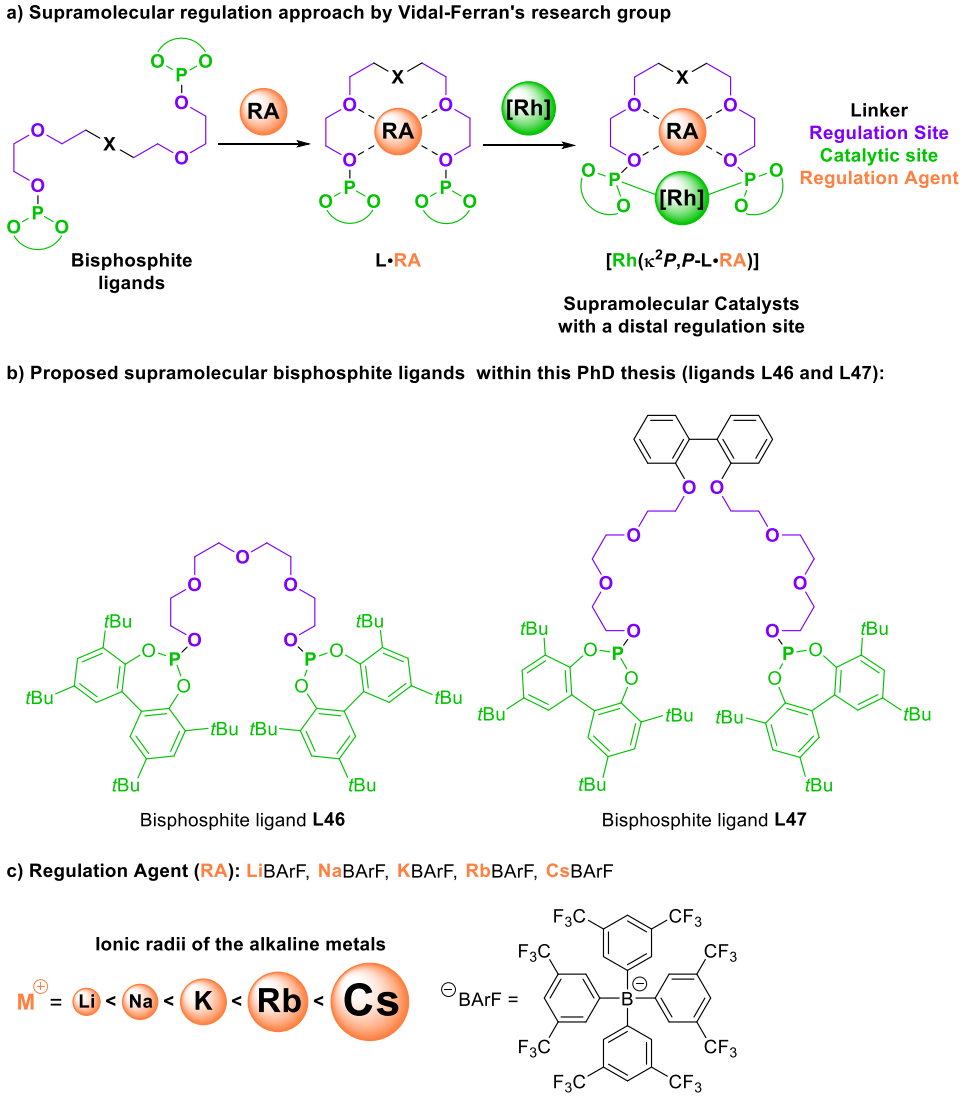

Figure 44. a) Scheme of the supramolecular regulation approach from Vidal-Ferran's group. b) Bisphosphite supramolecular ligands **L46** and **L47**. c) Alkali metal BArF salts. Ionic radii of Li^+, Na^+, K^+, Rb^+ and Cs^+ are 0.76 Å, 1.02 Å, 1.38 Å, 1.52 Å and 1.67 Å, respectively.[150]

Additionally, our research group has also applied the supramolecular regulation approach to other chemistries,[91] such as i) hydrogenation of alkenes,[97] ii) allylic substitutions,[101] iii) *para*-C–H functionalization of aromatic alcohols[102] and iv) insertion reactions into O–H bonds.[103] All these studies have demonstrated the versatility of our approach in supramolecular catalysis. In terms of the regulation agents used, we have mainly focussed on BArF[151] and

[150] Shannon, R. D. *Acta Crystallogr., Sect. A: Cryst. Phys, Diffr, Theor. Gen. Crystallogr.* **1976**, *A32*, 751-767.
[151] BArF is an acronym that refers to tetrakis[3,5-bis(trifluoromethyl)phenyl]borate anion; $[B(3,5\text{-}(CF_3)_2C_6H_3)_4]^-$.

BF_4[152] salts as RAs, mainly due to their adequate solubility profile and weakly-coordinating behaviour towards its cationic counterpart.[90,153]

Past research activities of our group focused on asymmetric hydroformylations. In this work, we aim to apply our supramolecular regulation approach to the maximization of the regioselectivities towards the formation of linear aldehydes (also called *n*-aldehydes). Herein, we describe the design, synthesis, and application of the new supramolecularly regulated bisphosphite ligands **L46** and **L47** (see the structures in Figure 44b), which incorporate a conformationally labile [1,1'-biphenyl]-2,2'-diol-based phosphite group and a five- and eight-oxygen-containing regulation site, respectively, capable of interacting with the RAs *via* ion-dipole interactions. It is also interesting to note that our ligand design incorporates bulky substituents (*i.e.*, *tert*-butyl groups) at the 3 and 3' positions of the biaryl fragment, as the placement of such substituents at the indicated positions have been reported to be beneficial for increasing the *l*/*b* ratio.[11,116]

Hydroformylation is the largest industrial process in the field of homogeneous catalysis, which is applied in the fragrance, bulk, pharmaceutical and fine chemical industries. Linear aldehydes find many applications,[154] as for instance the examples shown in Figure 45, which have found application in the fragrance industry.[155] It should also be noted that alcohols derived from linear aldehydes are important starting materials for plasticizers and detergents.[156]

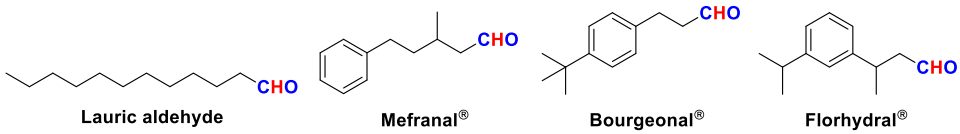

Figure 45. Examples of linear aldehydes in the fragrance industry.[157]

The first example is lauric aldehyde, also known as dodecanal. It is a colourless liquid which is present in several citrus oils and has been found in small amounts in essential oils produced from several *pinus* species. It is a

[152] BF_4 is the chemical formula that refers to the tetrafluoroborate anion $[BF_4]^-$.
[153] Nishida, H.; Takada, N.; Yoshimura, M.; Sonoda, T.; Kobayashi, H. *Bull. Chem. Soc. Jpn.* **1984**, *57*, 2600-2604.
[154] Kohlpaintner, C.; Schulte, M.; Falbe, J.; Lappe, P.; Weber, J.; Frey, G. D. *Aldehydes, Aliphatic*; Wiley-VCH Verlag GmbH & Co. KGaA, 2013.
[155] Surburg, H.; Panten, J. *Common Fragrance and Flavor Materials: Preparation, Properties and Uses*; Wiley-VCH Verlag GmbH & Co. KGaA, 2016.
[156] Barker, G. E.; Forster, D. Plasticizer and detergent alcohols. US4426542, **1984**.
[157] From the connectivity point of view, mefranal®, bourgeonal® and florhydral® are not linear aldehydes. However, in hydroformylation books and articles, authors have traditionally named as "linear" the aldehydes arising from the attachment of the CHO group to the terminal position of the C=C bond, independently of the fact that the resulting aldehyde is linear or contains ramifications. We have respected this nomenclature convention in this doctoral thesis.

component of several fragrances, such as the perfume Chanel N°5®, with a waxy odour reminiscent of violets in high dilution. Second, mefranal® is a colourless liquid which has a fresh, aldehydic, floral, citrus, lily of the valley[158] odour. The compound is mainly used in cosmetics, toiletries, and alcoholic fragrances to modify and lift floral notes. Third, bourgeonal® is an aromatic aldehyde that is a colourless to pale yellow liquid. The compound is used in perfumery since it has a powerful green, aquatic, aldehydic, and lily of the valley odour. Its usage is applied for toiletries, alcoholic fragrances, soaps, and detergents.[10] Besides, Hatt and co-workers reported in 2003 that bourgeonal® has an *in vitro* biological activity by regulating the mobility of the spermatozoa through the an olfactory receptor (OR) mediated by Ca^{+} channels.[159] Interestingly, Laska and co-workers reported that males have a higher sensitivity towards the odour of bourgeonal® than females.[160] Finally, florhydral® is a clear colourless to pale yellow liquid with a powerful fresh, green, floral, and lily of the valley odour. This aldehyde is recommended for use in all areas of perfumery.[10] In this work, these aldehydes have been successfully obtained from their corresponding alkene applying the supramolecular regulation approach in hydroformylation.

2.3. RESULTS AND DISCUSSION

2.3.1. Synthesis of supramolecular ligands

The bisphosphite ligands **L46** and **L47** were synthesised by *O*-phosphorylation of the corresponding diol derivatives in high yields (see the experimental section for the synthetic procedure and their characterization). Ligand **L46** was synthesised in only two steps. The first step consisted of the formation of the chlorophosphite **12** in quantitative yield from the corresponding diol **11** using PCl_3 as the *O*-phosphorylating agent and triethylamine as the base. Under our optimized conditions, the formation of **12** was highly selective and the reaction mixture was subsequently used in the next step without any further purification. Finally, the bisphosphite ligand **L46** was obtained in 92% isolated yield after the reaction of the 2,2'-[oxybis(2,1-ethanediyloxy)]diethanol[161] and the freshly prepared chlorophosphite **12** (Scheme 27a) under standard *O*-phosphorylation conditions.

[158] Lilly of the valley: a perennial plant of the lilly family, that grows in the shade and has a single pair of basal, oblong leaves and a single leafless raceme of very fragant, small, white, bell-shaped flowers.
[159] Spehr, M.; Gisselmann, G.; Poplawski, A.; Riffell, J. A.; Wetzel, C. H.; Zimmer, R. K.; Hatt, H. *Science* **2003**, *299*, 2054-2058.
[160] Olsson, P.; Laska, M. *Chem. Senses* **2010**, *35*, 427-432.
[161] Commonly called tetraethylene glycol.

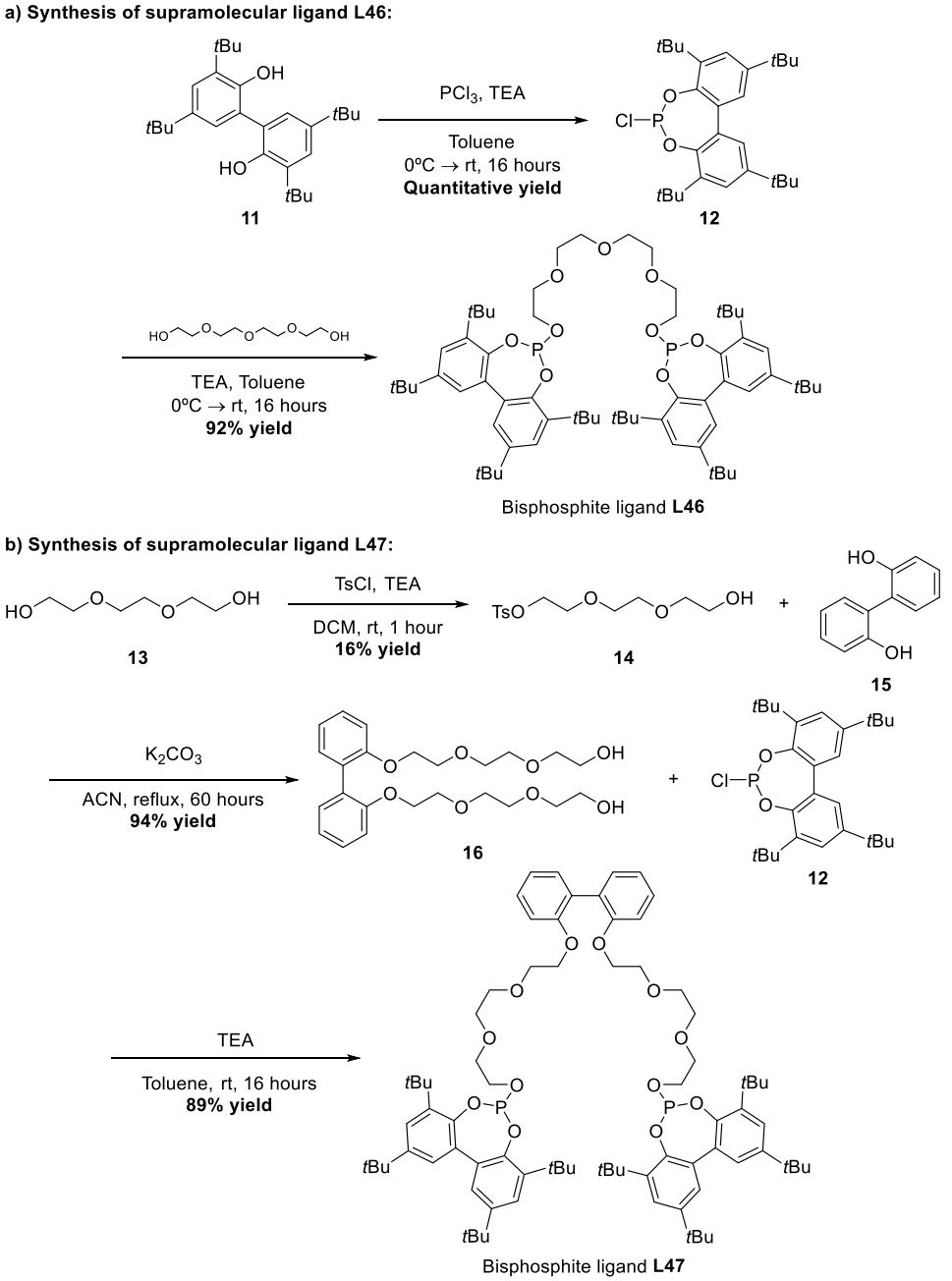

Scheme 27. a) Synthesis of supramolecular bisphosphite ligand **L46**.
b) Synthesis of supramolecular bisphosphite ligand **L47**.

As regards the synthesis of the ligand **L47**, mono-protection of the 2,2'-[1,2-ethanediylbis(oxy)]diethanol[162] with 0.25 eq. of tosyl chloride and

[162] Commonly called triethylene glycol.

triethylamine as auxiliary base led to the target product in 16% isolated yield. Subsequent reaction of **14** and **15** under Williamson etherification conditions led to diol **16** in 94% isolated yield. Finally, the reaction between the diol **16** and the freshly prepared chlorophosphite **12** under the above-mentioned *O*-phosphorylation conditions led to the supramolecular bisphosphite ligand **L47** in 89% isolated yield (Scheme 27b).

2.3.2. Catalytic studies for supramolecular regulation in hydroformylation reactions

The activity of both ligands in HF was evaluated for oct-1-ene as substrate. Oct-1-ene is a typical benchmark substrate for initial screenings in hydroformylation, keeping in mind that this substrate can isomerize to internal alkenes and hydrogenate to octane. Moreover, the newly formed alkenes by an isomerisation process can *a priori* be hydroformylated at two distinct positions, with which the aldehydes arising from attack at C_1, C_2, C_3 or C_4 of oct-1-ene can be expected when hydrido rhodium complexes are used as catalysts. Standard catalyst screening conditions were performed with [Rh(κ^2*O*,*O*'-acac)(CO)$_2$] (1.0 mol%) as metal precursor and the corresponding bisphosphite ligand **L46** or **L47** (1.20 mol%) at 60 °C under 10 bar H_2/CO (1:1) for 18 hours in a mixture of toluene and THF (v/v 97:3), with the minimum amount of THF to solubilize the RA (1.56 mol%). It should be noted that this mixture of solvents is capable of solubilizing the alkali BArF salts under the working conditions The alkali metal BArF salts were synthesised following optimised synthetic procedures developed by our group.[90] The catalytic results of the hydroformylation of oct-1-ene are summarised in Table 18 in the absence and presence of the whole set of regulation agents.

Table 18. Study of the effects of the RAs in the supramolecularly regulated hydroformylation of oct-1-ene (**S31a**).

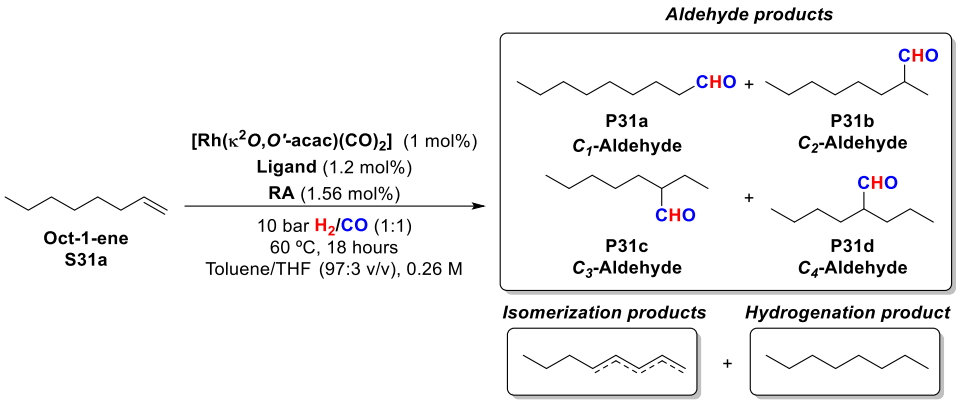

Entry	RA	Ligand	Conv. (%)	Select. (%)[a]		$C_1/C_2/C_3/C_4$ ratio (%)	$C_1/C_2/C_4/C_3$ yield (%)
				Isom.	Hydrog.		
1	None	L46	98	3	2	62:38:0:0	58:35:0:0
2	LiBArF	L46	99	2	1	61:39:0:0	59:37:0:0
3	NaBArF	L46	98	7	8	94:6:0:0	78:5:0:0
4	KBArF	L46	98	8	14	97:3:0:0	74:2:0:0
5	RbBArF	L46	98	6	10	94:6:0:0	77:5:0:0
6	CsBArF	L46	99	4	5	86:14:0:0	77:13:0:0
7	None	L47	99	2	0.3	60:38:2:0	58:37:2:0
8	LiBArF	L47	99	2	0.3	61:34:4:1	59:33:4:1
9	NaBArF	L47	99	2	0.3	61:34:4:1	59:33:4:1
10	KBArF	L47	99	2	0.5	66:30:3:1	64:29:3:1
11	RbBArF	L47	99	2	1	73:24:3:0	70:23:3:0
12	CsBArF	L47	99	2	1	75:22:3:0	72:21:3:0

The HF was performed in a parallel autoclave. Reaction conditions: [substrate] = 0.26 M; stirring rate = 800 rpm; 10 bar H_2/CO (1:1); 60 °C, 18h. Conversion was determined by GC using dodecane as an internal standard. Selectivity, ratio, and yield were determined by the area% values of the peaks in the GC chromatogram. [a] Selectivity of the isomerisation (Isom.) and hydrogenation (Hydrog.) processes.

The use of ligands **L46** and **L47** provided good results in the formation of linear aldehydes with high conversions. As expected, the addition of the regulation agent induced changes in the chemo- and regio-selectivity of the reaction. In the case of **L46**, excellent results were observed in the formation of the linear aldehyde using NaBArF, KBArF and RbBArF as RAs. The use of KBArF (entry 4, Table 18) as RA led to the highest regioselectivity with a *l*/*b* ratio of 97:3 towards the linear aldehyde. However, the use of NaBArF as

RA (entry 3, Table 18) provided almost the same *l*/*b* ratio (94:6 instead of 97:3) with the isomerisation and hydrogenation processes taking place at a lesser extent. On the other hand, despite the fact that the use of **L47** favoured the formation of the linear aldehyde **P31a**, its selectivity was lower than with **L46**. Additionally, the formation of internal aldehydes **P31c** and **P31d** was observed, a fact that did not occur when **L46** was used as the ligand. Moreover, under the standard catalytic conditions, both ligands led to low but measurable amounts of unreacted isomerisation and hydrogenation products. Therefore, ligand **L46** provided the better results in terms of regioselectivity towards **P31a** (also referred to as C_1-aldehyde) and yield than ligand **L47**.

Accordingly, bisphosphite ligands **L46** and **L47** were tested in the hydroformylation of an array of structurally diverse terminal alkenes to determine the activity of the catalytic systems derived from them. The set of substrates are indicated in Scheme 28. The structural diversity of the starting materials comprised linear unfunctionalized[163] (*i.e.*, **S31a**, **S46**, **S48** and **S51**; for the structures of the resulting linear aldehydes, see Scheme 28) and functionalized alkenes (*i.e.* **S49** and **S50**). All the selected alkenes contain the vinyl unit (*i.e.*, –CH=CH2), as we hypothesised that the HF would majorly take place at the least substituted position with formation of a non-stereogenic formyl-substituted carbon. Alkenes with a pro-stereogenic sp^2 carbon were not included in this study as our ligand design incorporating conformationally labile [1,1'-biphenyl]-2,2'-diol-based phosphite groups is intrinsically non-enantioselective.

[163] Linear unfunctionalized alkenes refer to unsaturated hydrocarbons that contain the –CH=CH_2 unit with hydrocarbon substituents. In contrast, linear functionalized alkenes also incorporate heteroatom-containing functional groups.

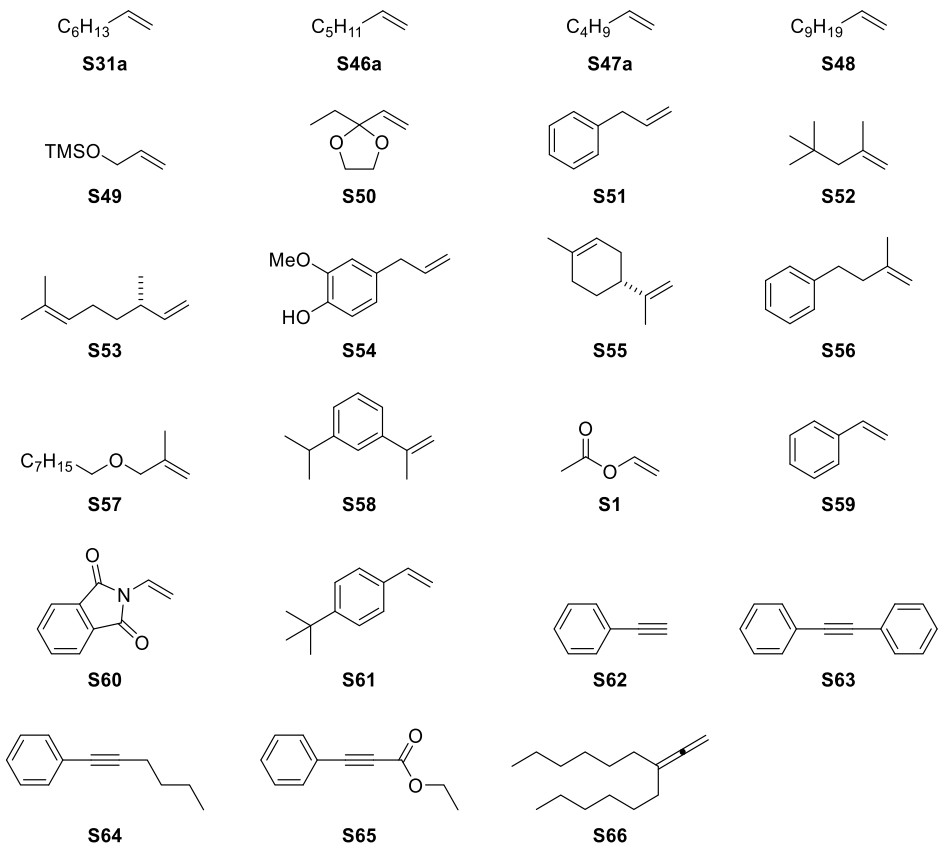

Scheme 28. Alkene and alkyne substrates hydroformylated.

Other substrates included in this study (*i.e.*, **S47**, **S52**, **S53**, **S54**, **S55**, **S56**, **S57** and **S58**) were selected because their hydroformylation at the least substituted olefinic carbon leads to relevant products for the fragrance industry.

Substrates **S56**, **S57** and **S58** are not commercially available and were prepared following well-stablished synthetic protocols. **S56** was synthesised through a Wittig reaction (see Scheme 29).[164] The corresponding triphenylphosphonium ylide was freshly prepared *in situ*[165] and the synthesis of alkene **S56** was continued by adding benzylacetone (**17**) to the ylide. Alkene **S56** was obtained in 82% yield.

[164] Fei, J.; Wang, Z.; Cai, Z.; Sun, H.; Cheng, X. *Adv. Synth. Catal.* **2015**, *357*, 4063-4068.
[165] Lee, K. C.; Lebel, H. Methyltriphenylphosphonium Bromide. *Encyclopedia of Reagents for Organic Synthesis (EROS)*, 2014; pp 1-2.

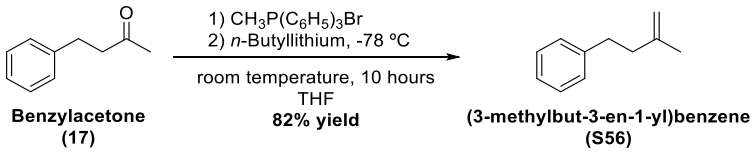

Scheme 29. Synthesis of (3-methylbut-3-en-1-yl)benzene (**S56**).

The alkene **S57** was prepared by a nucleophilic substitution reaction (see Scheme 30) by adapting a reported procedure.[166] The alcohol **18** was deprotonated with NaH to generate the corresponding alkoxide *in situ*, which was subsequently alkylated with *n*-octyl bromide (**19**). Alkene **S47** was obtained in 37% yield.

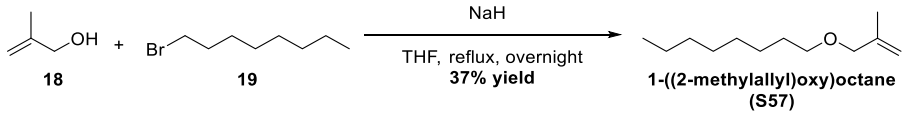

Scheme 30. Synthesis of 1-((2-mehylsllyl)oxy)octane (**S57**).

An optimised Suzuki cross-coupling reaction was used to synthesise the alkene **S58** (see Scheme 31).[167] The aryl halide **20** and the trifluoroborate potassium salt **21** were reacted with $[Pd(OAc)_2]$ and DPPF as catalyst to lead to the alkene **S58** in 65% yield.

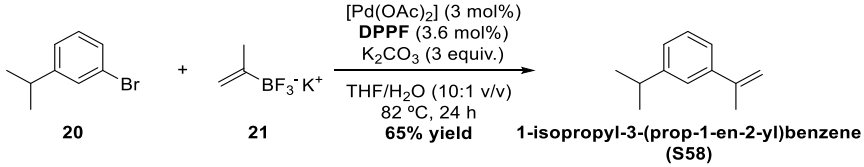

Scheme 31. Synthesis of 1-isopropyl-3-(prop-1-en-2-yl)benzene (**S58**).

With all substrates in hand and after having obtained good results in the HF of oct-1-ene (**S31a**) towards the linear aldehyde employing the ligand **L46** and our supramolecular regulation approach, alkenes with other alkyl substituents at the $–CH=CH_2$ unit were hydroformylated employing the same ligand and regulation approach. The hydroformylation of hept-1-ene (**S46a**) and hex-1-ene (**S47a**) under standard catalytic conditions showed high conversions (Scheme 32). In both cases, the use of NaBArF as RA maximised the regioselectivity towards the linear aldehyde (93% for **P46a** and 98% for

[166] Su, C.; Williard, P. G. *Org. Lett.* **2010**, *12*, 5378-5381.
[167] Yamamoto, Y.; Takada, S.; Miyaura, N.; Iyama, T.; Tachikawa, H. *Organometallics* **2009**, *28*, 152-160.

P47a with respect to the overall amount of aldehydes).[168] As for the hydroformylation of allylbenzene (**S51**), the highest performing HF catalyst incorporated KBArF as the RA, and a high *l*/*b* ratio was observed (95:5) with minimal amounts of isomerized substrate being recovered (Scheme 32). This is an interesting result for this challenging substrate, which may in principle evolve under the HF reaction conditions to the conjugated counterparts (*i.e.*, (*E*)- or (*Z*)-prop-1-en-1-ylbenzene) which could be in turn hydroformylated. The benefits of our regulation approach, which consists of screening a set of regulation agents to obtain the highest yield and/or selectivity for the substrate of interest, have been demonstrated in this example: the optimal catalytic system to a particular substrate was easily tailored.

As for the hydroformylation of alkenes leading to aldehydes with interest for the fragrance industry, the hydroformylation of lauric aldehyde (**P48a**), which is used in the fragrance industry in many perfumes such as Chanel N°5®, showed good regioselectivities when NaBArF was used in the construction of the hydroformylation catalyst. The yield and regioselectivity were increased up to 95% and 78%,[169] respectively (Scheme 32). It is interesting to note that the highest performing hydroformylation catalysts for linear terminal alkenes (**S31a**, **S46a**, **S47a** and **S48**) has consistently been that derived from NaBArF as the regulation agent.

[168] For the results obtained with the complete set of alkali metal BArF salts (*i.e.*, LiBArF, NaBArF, KBArF, RbBArF and CsBArF), see the experimental part, section 2.5.7 and 2.5.8.
[169] 80% of regioselectivity indicates 80% of the aldehyde derived from attachment of the CHO group to the C_1 carbon of the starting alkene with respect to the overall amount of aldehydes produced during the hydroformylation.

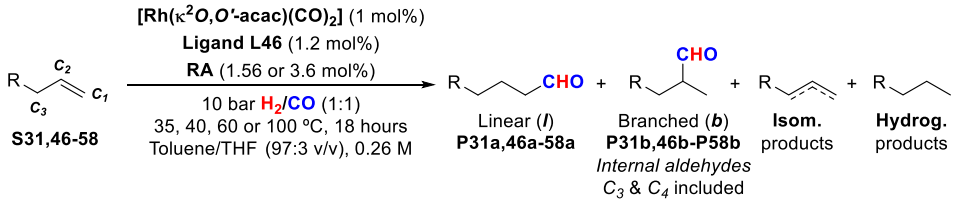

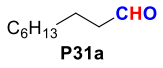

P31a

NaBArF / 60 ºC
98% conv. (0%)
94:6:0:0 *l/b* ratio (+32%)
7% Select. **Isom.** (+4%)
8% Select. **Hydro.** (+6%)
78% yield (+20%)

KBArF / 60 ºC
98% conv. (0%)
97:3:0:0 *l/b* ratio (+35%)
8% Select. **Isom.** (+5%)
14% Select. **Hydro.** (+12%)
74% yield (+16%)

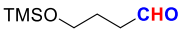

P49a

KBArF / 60 ºC
>99% conv. (0 %)
87:13 *l/b* ratio (+46%)
67% yield (+30%)

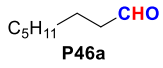

P46a

NaBArF/ 60 ºC
>99% conv. (0%)
93:6:1:0 *l/b* ratio (+31%)
3% Select. **Isom.** (+3%)
2% Select. **Hydro.** (+2%)
87% yield (+26%)

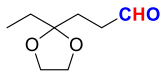

P50a

KBArF / 60 ºC
84% conv. (+65%)
96:4 *l/b* ratio (+20%)
57% yield (+50%)

RbBArF / 60 ºC
95% conv. (+76%)
92:8 *l/b* ratio (+16%)
82% yield (+75%)

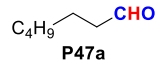

P47a

NaBArF / 60 ºC
>99% conv. (0%)
98:2:0 *l/b* ratio (+37%)
6% Select. **Isom.** (+5%)
1% Select. **Hydro.** (0%)
90% yield (+31%)

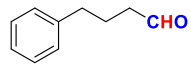

P51a

KBArF / 60 ºC
99% conv. (0%)
95:5 *l/b* ratio (+43%)
2% Select. **Isom.** (+2%)
6% Select. **Hydro.** (+6%)
87% yield (+36%)

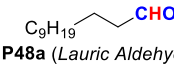

P48a (*Lauric Aldehyde*)

NaBArF / 60 ºC
95% conv. (0%)
95:5:0:0 *l/b* ratio (+33%)
8% Select. **Isom.** (+3%)
6% Select. **Hydro.** (+4%)
78% yield (+23%)

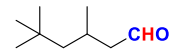

P52a

None / 100 ºC
98% conv.
>99:<1 *l/b* ratio
2% Select. **Isom.**
1% Select. **Hydro.**
95% yield

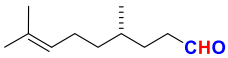

P53a

RbBArF / 35 ºC
75% conv. (+60%)
99:1:0 *l/b* ratio (+23%)
3% Select. **Isom.** (+2%)
3% Select. **Hydro.** (+2%)
71% yield (+60%)

CsBArF / 35 ºC
88% conv. (+73%)
95:3:2 *l/b* ratio (+19%)
3% Select. **Isom.** (+2%)
2% Select. **Hydro.** (+1%)
79% yield (+68%)

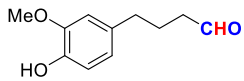

P54a

RbBArF / 60 ºC
99% conv. (0%)
91:9 *l/b* ratio (+39%)
4% Select. **Isom.** (+0%)
5% Select. **Hydro.** (+5%)
82% yield (+33%)

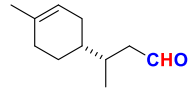

P55a

NaBArF / 60 ºC
96% conv. (-1%)
99:1 *l/b* ratio (0%)
14% Select. **Isom.** (+3%)
1% Select. **Hydro.** (-27%)
81% yield (+22%)

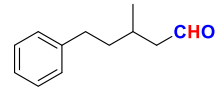

P56a (*Mefranal*®)

CsBArF / 100 ºC
98% conv. (+1%)
98:2 *l/b* ratio (+2%)
10% Select. **Isom.** (+4%)
5% Select. **Hydro.** (0%)
82% yield (-1%)

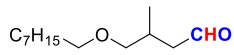

P57a

CsBArF / 100 ºC
>99% conv. (0%)
99:1 *l/b* ratio (+6%)
31% Select. **Isom.** (+14%)
5% Select. **Hydro.** (+2%)
63% yield (-11%)

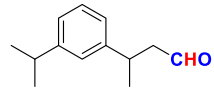

P58a (*Florhydral*®)

None / 100 ºC
98% conv.
>99:<1 *l/b* ratio
5% Select. **Hydro.**
93% yield

Scheme 32. Substrate scope of supramolecularly regulation in HF of terminal alkenes. The difference in the results when using a RA in the reaction compared to those in the absence of RA is shown in brackets.[170]

Another interesting substrate is the 2,4,4-trimethylpent-1-ene (**S52**), which can be structurally classified as a geminal disubstituted alkene. This alkene was hydroformylated under standard conditions and showed very low conversions at 60 ºC (10 bar H_2/CO (1:1) and 18 hours). This was due to the decreasing rate of hydroformylation when the steric hindrance of the C=C double bond increases.[12,13] In these cases, the hydroformylation requires stronger conditions to proceed, such as higher temperatures and/or pressures. An increase of the temperature up to 100 ºC was performed for **S52** in the hydroformylation studies. Moreover, 3.6 mol% of RA was added to the reaction in order to compensate the decrease of the binding affinity of the RA to the polyether chain of the ligand **L46** that was expected with increased temperatures. As envisioned, an increase of the temperature resulted in an increase of the conversion up to 98% with an excellent regioselectivity (*l*/*b* ratio higher than 99:1) and 95% yield for the linear aldehyde (**P52a**). In that case, the use of the ligand in the absence of RA was the optimal choice, as addition of a RA decreased conversion and increased the isomerisation and hydrogenation products (see Scheme 32 and the experimental section 2.5.13 for the catalytic results of the hydroformylation of **S52**).

The already mentioned supramolecular regulation approach with ligand **L46** was also applied to the hydroformylation of other alkenes commonly used in the fragrance industry such as (+)-β-citronellene (**S53**), eugenol (**S54**) and (*R*)-limonene (**S55**). Their corresponding aldehydes can have interesting odour and/or flavour properties, making them valuable ingredients for the fragrance industry. For all of them, the addition of a RA improved the regioselectivity and yield towards the linear aldehyde. In particular for (+)-β-citronellene (**S53**), there was an increase in the conversion up to 75% or 88% with RbBArF or CsBArF, respectively. The use of both RAs promoted an increase of the *l*/*b* ratio and yield. The hydroformylation of eugenol (**S54**) showed an increase of the ratio of the linear aldehyde and yield when RbBArF was added (91:9 *l*/*b* ratio and 82% yield). In the case of (*R*)-limonene, the addition of NaBArF did not change the value in the conversion or the *l*/*b* ratio, yet there was an increase of up to 24% in the hydroformylation selectivity when NaBArF was used as regulation agent (Scheme 32). Interestingly, the use of this RA almost suppressed the hydrogenation side-reaction.

The scents of mefranal® (**P56a**), 3-methyl-4-(octyloxy)butanal (**P57a**) and florhydral® (**P58a**) were also obtained in this work with our hydroformylation regulation strategy (Scheme 32). Since the starting alkenes (**S56**, **S57** and **S58**) are disubstituted alkenes, the hydroformylation temperature was increased to

[170] The scheme of the substrate scope shows the best RA for each substrate giving the highest *l*/*b* ratio. The results with the different RAs can be found in the experimental section 2.5.6 to 2.5.28.

100 ºC employing 3.6 mol% of RA. Positive regulation effects were observed for the hydroformylation of **S56** and **S57** with CsBArF as RA. For both cases, the regioselectivity towards the linear aldehyde increased (*l:b* ratio of 98:2 for **P56a** and 99:1 for **P57a**). As for florhydral® (**P58a**), the optimal hydroformylation catalyst involved not using a regulation agent, obtaining high conversion, regioselectivity and yield (98% conv., >99:<1 *l/b* ratio and 93% in yield).

Table 19. Study of H_2/CO partial pressure in the supramolecularly regulated hydroformylation of the substrates **S31a**, **S49**, **S50** and **S51**.

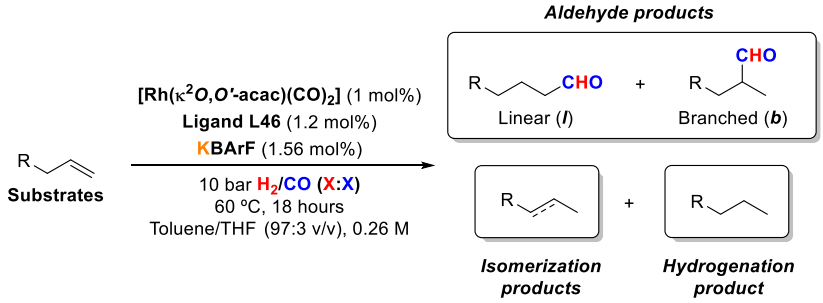

Entry	Substrate	10 bar H_2/CO (X:X)	Conv. (%)	Select. (%)[a]		*l/b* ratio (%)	*l/b* yield (%)
				Isom.	Hydrog.		
1	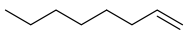	(1:1)	98	8	14	97:3	74:2
2	S31a	(3:7)	99	3	14	97:3	80:2
3		(7:3)	99	5	19	98:2	74:2
4	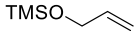	(1:1)	99	-	-	87:13	67:10
5	S49	(3:7)	99	-	-	86:14	68:11
6		(7:3)	99	-	-	89:11	70:9
7	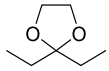	(1:1)	84	-	-	96:4	57:3
8		(3:7)	87	-	-	96:4	76:4
9	S50	(7:3)	99	-	-	97:3	89:3
10	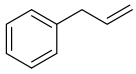	(1:1)	99	2	6	95:5	87:5
11		(3:7)	99	2	6	96:4	87:4
12	S51	(7:3)	99	6	9	98:2	82:2

The HF of substrates **S31a**, **S49**, **S50** and **S51** were performed in a parallel autoclave. Reaction conditions: [substrate] = 0.26 M; stirring rate = 800 rpm; 10 bar H_2/CO; 60 °C, 18h. For substrates **S31a** and **S51**, the conversion was determined by GC using dodecane as an internal standard. Selectivity, ratio, and yield were determined by the area% values of the peaks in the GC chromatogram. For the substrates **S49** and **S50**, the conversion, ratio, selectivity, and yield were determined by ^{1}H NMR using 1,3,5-trimethoxybenzene as internal standard. [a] Selectivity of the isomerisation (Isom.) and hydrogenation (Hydrog.) processes.

The variation of the relative molar ratios of the H_2/CO mixture is another parameter that can affect the conversion, chemo- and regio-selectivity of the hydroformylation reaction. Therefore, studies varying the H_2/CO molar ratio of syngas (overall pressure of 10 bar) were performed with the supramolecular catalyst derived from ligand **L46** and KBArF on the substrates **S31a**, **S49**, **S50** and **S51**. As it can be observed in Table 19, there is almost no difference between the outcome of the reaction employing H_2/CO 1:1 or 3:7. However, a slight increase in the *l*/*b* ratio (increases up to *l*/*b* ratios 98:2 from 95:5; entries 12 and 10, table 19) was observed when an excess of H_2 was used (H_2/CO molar ratio = 7:3). Unfortunately, the benefits on the *l*/*b* ratio by increasing the molar ratio of H_2 in the syngas mixture were diminished by the fact that increased amounts of hydrogenated products were observed for two out of four substrates.

The hydroformylation of substrates which tend to form the branched products instead of linear aldehydes was also studied. It is well known in the literature that substituted styrenes (*e.g.*, **S59a** and **S61a**; see Scheme 34 for the structures of the hydroformylation products that derive from them) and heteroatom substituted alkenes (such as enol acetate **S1a** and enamine **S60a**) majorly lead to the branched aldehydes due to electronic factors. This has been rationalized by the formation of a highly stable η^3-allyl intermediate previous to the formation of the rhodium acyl complexes in the catalytic cycle that involves the aryl group (or the oxygen or nitrogen groups in enols and enamines, respectively; for the structures of the Rh-species derived from styrene, see Scheme 33).[171]

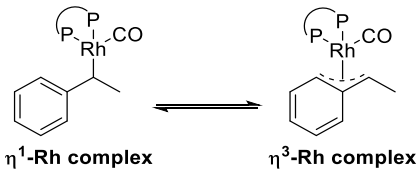

Scheme 33. Alkyl rhodium complexes derived from styrene.

The hydroformylation of these substrates was studied employing the supramolecularly regulated systems derived from **L46** under standard hydroformylation reaction conditions (1.0 mol% of precatalyst formed *in situ* from [Rh(κ^2*O*,*O'*-acac)$(CO)_2$] (1 mol%), ligand (1.2 mol%), and a slight excess of RA (1.56 mol%) under H_2/CO (1:1, 10 bar) in toluene and THF (97:3 v/v), at 60 ºC for 18 hours. The results for the hydroformylation of alkenes **S1a**, **S60a**, **S61a** and **S62a** are summarized in Scheme 34.

[171] Pignolet, L. M. *Homogeneous Catalysis with Metal Phosphine Complexes*; Springer Science & Business Media, 2013.

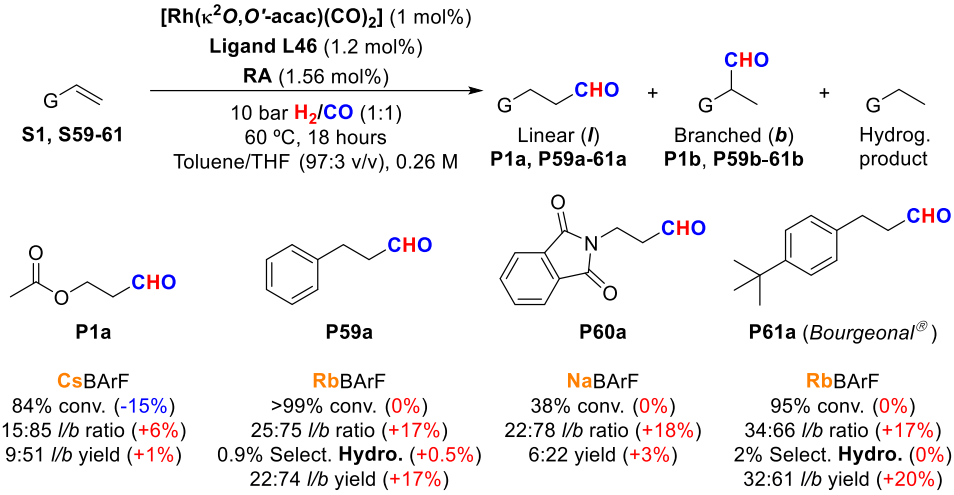

Scheme 34. Hydroformylation of alkenes **S1**, **S59**, **S60** and **S61** using **L46** as a ligand.

The most remarkable result in the hydroformylation of these functionalised alkenes is that the use of our supramolecular catalysts consistently led to an increase of the *l*/*b* ratio (increase of 17-18% of the linear product with respect to the overall amounts of aldehydes). Unfortunately, the regulation ability of our catalysts is not capable of overriding the electronic effects in the HF of these substrates that favour the formation of the branched aldehydes. As it can be observed in Scheme 34, the branched product is majorly obtained, with yields ranging from 22% to 74%. In the case of vinyl acetate (**S1**), the highest *l*/*b* ratio was obtained when CsBArF was used as the regulation agent (*l*/*b* ratio = 15:85), whilst for styrene (**S60**) and 1-(*tert*-butyl)-4-vinylbenzene (**S62**) RbBArF maximised the formation of the linear aldehyde (*l*/*b* ratios of 25:75 and 34:66, respectively). Lastly, enamine **S61a** was hydroformylated with low yield, even in the presence of the highest performing RA (NaBArF).

The hydroformylation of alkynes is a perfectly atom-economic transformation that leads to highly interesting synthetic intermediates, such as α,β-unsaturated aldehydes. However, high performing, chemo- and regio-selective catalysts that mediate this transformation are scarce in the literature.[172] α,β-Unsaturated aldehydes are versatile intermediates in organic synthesis,[173] which are widely employed in the agrochemical, pharmaceutical, flavour and fragrance industries. During the last few years, several methods of rhodium- and palladium-catalysed hydroformylation of internal alkynes have

[172] a) Johnson, J. R.; Cuny, G. D.; Buchwald, S. L. *Angew. Chem. Int. Ed. Eng.* **1995**, *34*, 1760-1761. b) Agabekov, V.; Seiche, W.; Breit, B. *Chem. Sci.* **2013**, *4*, 2418-2422. c) Zhang, Z.; Wang, Q.; Chen, C.; Han, Z.; Dong, X.-Q.; Zhang, X. *Org. Lett.* **2016**, *18*, 3290-3293. d) Fang, X.; Zhang, M.; Jackstell, R.; Beller, M. *Angew. Chem. Int. Ed.* **2013**, *52*, 4645-4649.
[173] a) Vchislo, N. V. *Asian J. Org. Chem* **2019**, *8*, 1207-1226. b) Keiko, N. A.; Vchislo, N. V. *Asian J. Org. Chem* **2016**, *5*, 439-461. c)Verochkina, E. A.; Vchislo, N. V.; Rozentsveig, I. B. *Molecules* **2021**, *26*, 4297.

been reported, demonstrating that the selective production of α,β-unsaturated aldehydes from internal alkynes is possible.[174] However, hydrogenation processes are difficult to suppress, resulting in the formation of multiple side products, such as saturated aldehydes, alkenes, and/or alkanes.

The hydroformylation of substrates **S62**-**S65** (for the structures of the aldehydes derived from them by hydroformylation, see Scheme 36) was studied employing the supramolecularly regulated systems derived from **L46** under standard reaction conditions. The internal alkyne **S64** is not commercially available, so it was synthesised following a reported procedure (Scheme 35).[175] Hex-1-yn-1-ylbenzene (**S64**) was synthesized by *C*-alkylation of phenylacetylene (**S62**). Deprotonation with *n*-butyllithium followed by the addition of the alkyl halide, 1-iodobutane, led to **S64** in 93% yield.

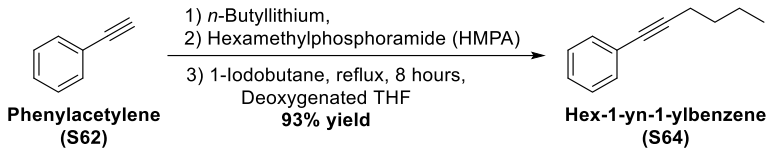

Scheme 35. Synthesis of **S64**.

The reactions of internal alkynes bearing bis-aryl (**S63**) and aryl-alkyl (**S64**) substituents employing the catalytic systems derived from **L46** provided α,β-unsaturated aldehydes in yields ranging from 74% to 94% (Scheme 36). NaBArF was the regulation agent of choice for both internal alkenes. Interestingly, the use of NaBArF and RbBArF led to an increase of the yield (73% and 41% for **S63** and **S64**, respectively) by suppressing the hydrogenation processes (reduction of the amounts of hydrogenated products down to 3% with respect to the starting material). Substrate **S63** is symmetric and the hydroformylation product is the same independently of the position at which the CHO group is attached. However, it is important to mention that the hydroformylation majorly leads to the *E*-configured α,β-unsaturated aldehydes (98% and 2% of the *E*- and *Z*-configured aldehyde, respectively). As for the asymmetrically substituted internal alkyne **S64**, the use of RbBArF as the RA led to highest regioselectivity, with a *ca.* 3:1 ratio in favour of the aldehyde with the phenyl group in a relative *trans*-position with respect to the CHO group. These hydroformylation reaction conditions are quite efficient and are amongst those providing the highest yields.[174,175] As for the

[174] a) Fan, C.; Hou, J.; Chen, Y.-J.; Ding, K.-L.; Zhou, Q.-L. *Org. Lett.* **2021**, *23*, 2074-2077. b). Zhang, Y.; Sigrist, M.; Dydio, P. *Eur. J. Org. Chem.* **2021**, *2021*, 5985-5997. c) Zhang, Y.; Torker, S.; Sigrist, M.; Bregović, N.; Dydio, P. *J. Am. Chem. Soc.* **2020**, *142*, 18251-18265. d) Fang, X.; Zhang, M.; Jackstell, R.; Beller, M. *Angew Chem Int Ed Engl* **2013**, *52*, 4645-4649. e) Agabekov, V.; Seiche, W.; Breit, B. *Chem. Sci.* **2013**, *4*, 2418-2422.
[175] Zhang, Y.; Torker, S.; Sigrist, M.; Bregović, N.; Dydio, P. *J. Am. Chem. Soc.* **2020**, *142*, 18251-18265.

hydroformylation of mono-substituted alkynes (such as ethynylbenzene, **S62**) or those incorporating electron withdrawing groups (such ethyl 3-phenylpropiolate, **S65**), catalysts derived from **L46** showed a lack of activity in the hydroformylation of these substrates.

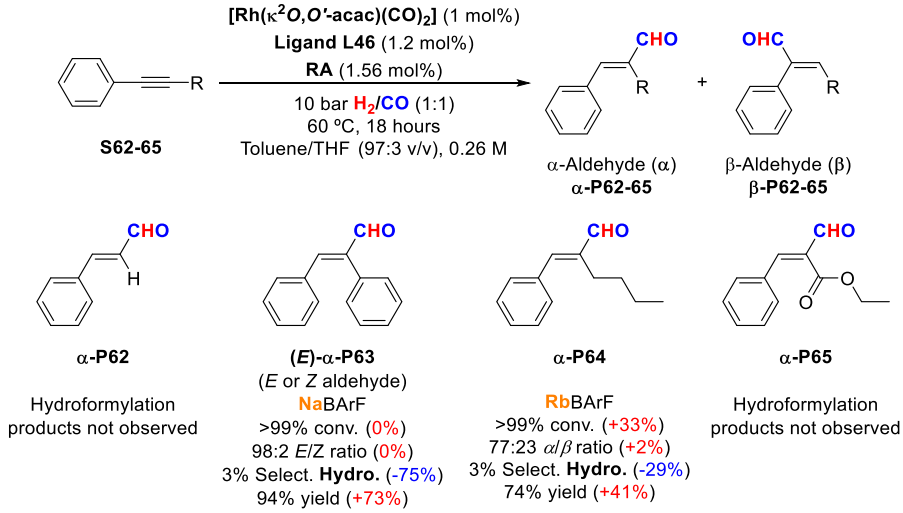

Scheme 36. Substrate scope of supramolecular regulation in hydroformylation of alkynes using **L46** as a ligand.

While alkene and alkyne hydroformylation have been studied for a broad array of substrates with a set of catalytic systems, the literature on the hydroformylation of allenes remains scarce. Hydroformylation of allenes has to address regioselectivity as well as chemo-selectivity issues, as a consequence of the multiple reaction pathways that are possible. The allene 7-vinylidenetridecane (**S66**) was selected as substrate to be hydroformylated with our supramolecularly regulated catalysts. The substrate **S66** was synthesized following a reported procedure (see Scheme 37).[176] Non-2-yl-1-ol **23** was synthesized from commercially available oct-1-yne **22** by deprotonation with *n*-butyllithium and subsequent reaction with paraformaldehyde obtaining **23** in almost quantitative yield (98% yield). Subsequent tosylation of **23** led to the formation of **24** in 66% yield. The final product **S66** was synthesized in 56% yield by copper-catalysed nucleophilic addition of *n*-hexyl magnesium bromide to tosylated product **24**.

[176] Guo, H.; Ma, S. *Adv. Synth. Catal.* **2008**, *350*, 1213-1217.

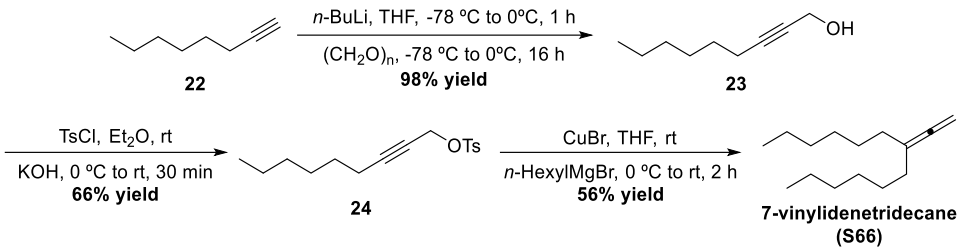

Scheme 37. Synthesis of 7-vinylidenetridecane (**S66**).

The supramolecular catalytic systems derived from **L46** were applied to the hydroformylation of the allene **S66**. In the absence of RA, aldehyde **P66a** was formed in 9% yield. When KBArF was used as the RA, a remarkable improvement in the yield was observed, obtaining the aldehyde **P66a** with a 69% yield (Table 20).

Table 20. Supramolecularly regulated hydroformylation of 7-vinylidenetridecane (**S66**).

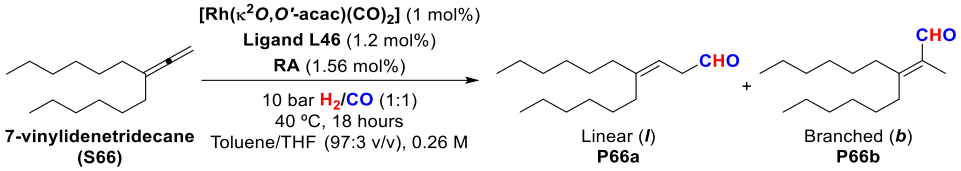

Entry	RA	Ligand	Conv. (%)	Select. (%)[a]		*l*/*b* ratio (%)	*l*/*b* yield (%)
				Isom.	Hydrog.		
1	None	L46	99	-	-	>99:<1	9:0
2	LiBArF	L46	99	-	-	>99:<1	11:0
3	NaBArF	L46	99	-	-	>99:<1	62:0
4	KBArF	L46	99	-	-	>99:<1	69:0
5	RbBArF	L46	99	-	-	>99:<1	43:0
6	CsBArF	L46	99	-	-	>99:<1	11:0

The HF was performed in a parallel autoclave. Reaction conditions: [substrate] = 0.26 M; stirring rate = 800 rpm; 10 bar H_2/CO (1:1); 40 °C, 18h. Conversion, ratio and yield were determined by ^{1}H NMR using 1,3,5-trimethoxybenzene as internal standard.

2.3.3. Linear selective isomerisation-hydroformylation tandem reactions of mixtures of alkenes employing supramolecularly regulated rhodium catalyst derived from bisphosphite ligands

One of the still unsolved challenges in hydroformylation chemistry is the selective hydroformylation of internal alkenes towards the linear aldehyde. In this chemistry, the issue of regioselectivity is addressed twice: first, regioselective isomerisation of the double bond and, second, regioselective hydroformylation. Thus, isomerisation-hydroformylation tandem reactions can be defined as the process in which the net addition of hydrogen (H) and formyl (CHO) groups take place away from the original alkene. It has to be mentioned that other migrations of the C=C double bond and its subsequent hydroformylation can take place in the process.

The isomerisation process towards the terminal alkene is a well-known process which is induced by hydrido complexes.[177] As hydroformylation catalysts are based on hydrido-carbonyl complexes, isomerisation is a transformation which may take place simultaneously with hydroformylation. Isomerisation is a well-known process in cobalt[178], rhodium[179], platinum[180], palladium[181] and ruthenium[182] chemistries. Hydroformylation practitioners have developed strategies for taking advantage of the isomerisation within hydroformylation chemistry. If isomerisation processes are much faster than the hydroformylation process, the latter transformation should take place at the most reactive and/or favourable position of the C=C double bond after isomerisation and not at the initial position of the C=C bond. For instance, our research group (amongst other groups[183]) reported the hydroformylation of mixture of octenes, heptenes and hexenes using cobalt catalysts (see Chapter I) with selective formation of the terminal aldehyde.[184] Our group demonstrated that cobalt hydroformylation chemistry was an interesting strategy for valorising mixtures of linear hexenes, heptenes or octenes by

---

[177] Vilches-Herrera, M.; Domke, L.; Börner, A. *ACS Catal.* **2014**, *4*, 1706-1724. b) Biswas, S. *Comments Inorg. Chem.* **2015**, *35*, 300-330.
[178] Liu, X.; Zhang, W.; Wang, Y.; Zhang, Z.-X.; Jiao, L.; Liu, Q. *J. Am. Chem. Soc.* **2018**, *140*, 6873-6882.
[179] a) Behr, A.; Obst, D.; Schulte, C.; Schosser, T. *J. Mol. Catal. A: Chem.* **2003**, *206*, 179-184. b) Edwards, D. R.; Crudden, C. M.; Yam, K. *Adv. Synth. Catal.* **2005**, *347*, 50-54.
[180] a) Gottardo, M.; Scarso, A.; Paganelli, S.; Strukul, G. *Adv. Synth. Catal.* **2010**, *352*, 2251-2262. b) Gelling, O. J.; Toth, I. Hydroformylation Process and Water-soluble catalysts for the preparation of a linear ω-formylcarboxylic acids and ω-formylnitriles. WO9518783, **1995**. c) Burke, P. M.; Gelling, O. J.; Oevering, H.; Toth, I. Process and Catalysts for the Hydroformylation of Internal Unsaturated Compounds. WO9708127, **1997**.
[181] Mamone, P.; Grünberg, M. F.; Fromm, A.; Khan, B. A.; Gooßen, L. J. *Org. Lett.* **2012**, *14*, 3716-3719.
[182] Fleischer, I.; Wu, L.; Profir, I.; Jackstell, R.; Franke, R.; Beller, M. *Chem. Eur. J.* **2013**, *19*, 10589-10594.
[183] Donohoe, T. J.; O'Riordan, T. J. C.; Rosa, C. P. *Angew. Chem. Int. Ed.* **2009**, *48*, 1014-1017.
[184] Martínez-Carrión, A.; Romero-Navarro, A.; Núñez-Rico, J. L.; Gutiérrez, A.; Grabulosa, A.; Vidal-Ferran, A. *Catal. Sci. Technol.* **2022**, *12*, 3219-3227.

transforming the initial mixture into one major aldehyde (addition of a CHO group to the C_1 carbon of the alkene skeleton, up to 73% selectivity).

Rhodium catalysts have also been studied for linear selective isomerisation-hydroformylation reactions. In 2001, Börner and co-workers reported the isomerisation-hydroformylation of mixtures of octenes using the electronically nonsymmetric acylphosphite-phosphite **L48** (Scheme 38).[185] Under 20 bar of H_2/CO (1:1) at 130 ºC, linear nonanal was obtained in 69% yield by hydroformylating mixtures of octenes with rhodium catalysts.

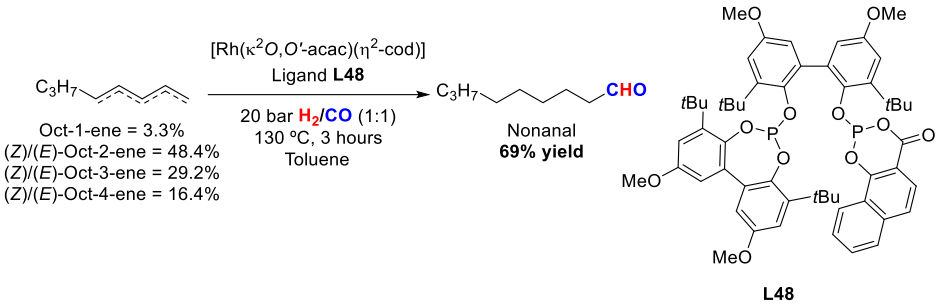

Scheme 38. Isomerisation-hydroformylation tandem reaction of mixtures of octenes.

The combination of two catalysts is another strategy to perform isomerisation-hydroformylation tandem reactions. One of the catalysts is for the isomerisation process and the other for the hydroformylation. In 2013, Nozaki and co-workers reported a dual rhodium and ruthenium catalyst based on a combination of a [Rh(κ^2*O,O'*-acac)$(CO)_2$]/**L49**, Shvo's catalyst (**C12**) and $[Ru_3(CO)_{12}]$ in isomerisation-hydroformylation-hydrogenation tandem reactions. The method was applied for the transformation of methyl oleate into the corresponding alcohol derived from hydroformylation with a 93% conversion, 82:18 *l/b* ratio and 53% isolated yield.[186] The authors claimed through control experiments that the isomerisation process was mediated by Rh and Ru and the coexistence of Rh and Ru was detrimental for the hydrogenation of the aldehyde under H_2/CO atmosphere.

[185] Selent, D.; Hess, D.; Wiese, K.-D.; Röttger, D.; Kunze, C.; Börner, A. *Angew. Chem. Int. Ed.* **2001**, *40*, 1696-1698.
[186] Yuki, Y.; Takahashi, K.; Tanaka, Y.; Nozaki, K. *J. Am. Chem. Soc.* **2013**, *135*, 17393-17400.

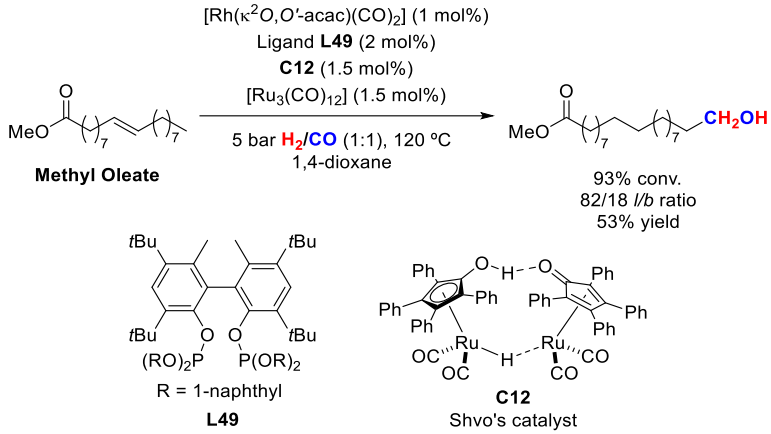

Scheme 39. Isomerisation-hydroformylation/hydrogenation tandem reactions of methyl oleate catalysed by Rh/Ru dual catalysis.

Thus, we decided to study whether the supramolecularly regulated rhodium catalysts already described in this section would be suitable for transforming a mixture of alkenes into one major aldehyde. For that reason, all commercially available linear octenes (**S31b-d**) were tested using **L46** as the ligand and [Rh(κ²*O*,*O'*-acac)(CO)$_2$] as the metal precursor under the standard hydroformylation conditions: 10 bar H_2/CO (1:1) at 60 ºC for 18 hours (Table 21). Generally, internal alkenes are less reactive than terminal alkenes because reactivity decreases when increasing the steric hindrance of the double bond C=C. Under these standard catalytic conditions, higher conversions were obtained for all the internal alkenes (Table 21). In terms of the selectivity towards hydroformylation products, this was > 95% for all the studied octenes, except for **(*Z*)-S31b**. Unfortunately, low selectivities towards the linear aldehyde (*i.e.*, C_1-aldehyde) were observed for all substrates studied (up to 14% molar amounts of C_1-aldehyde with respect to the overall aldehyde amount for **S31d**, see entry 10, Table 21).

The formation of a complex mixture of aldehydes is the main consequence of the isomerisation processes under hydroformylation conditions if the rates of the hydroformylation and isomerisation processes are similar. Regrettably, this appear to be case for the rhodium-based catalytic systems derived from **L46** and the RAs used.

Table 21. Selected results of the supramolecular regulated hydroformylation of the internal octenes (**S31b-d**).

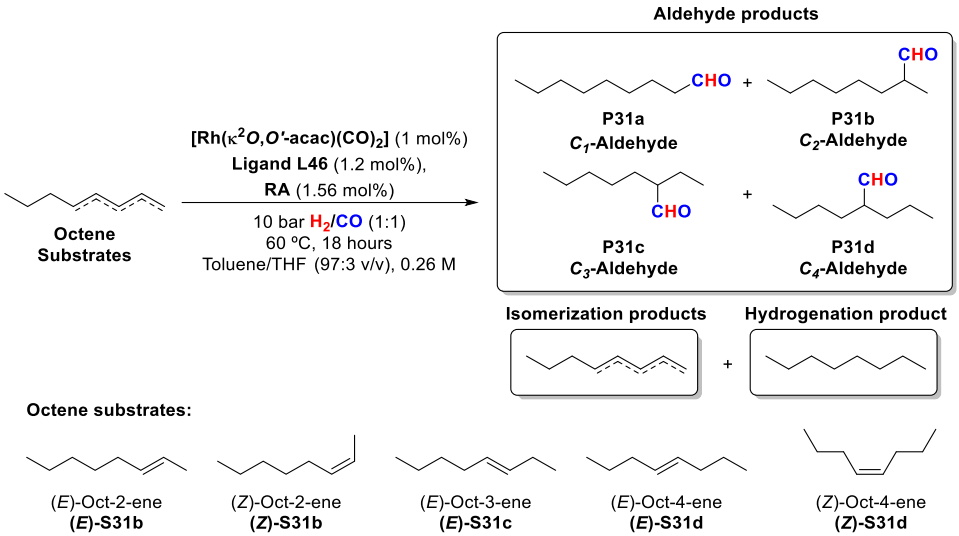

Entry	RA	Subs.	Conv. (%)	Select. (%)[a]		$C_1/C_2/C_3/C_4$ ratio (%)	$C_1/C_2/C_3/C_4$ yield (%)
				Isom.	Hydrog.		
1	-	(*E*)-S31b	99	2	0.3	3:54:33:11	3:52:31:11
2	RbBArF		99	3	1	8:51:27:14	8:48:26:13
3	-	(*Z*)-S31b	99	1	2	3:57:32:7	3:55:31:8
4	RbBArF		99	4	8	8:55:26:11	7:48:23:10
5	-	(*E*)-S31c	99	1	0.3	3:19:37:41	3:21:36:40
6	CsBArF		99	0	0.1	7:29:31:33	7:29:31:33
7	-	(*E*)-S31d	99	1	0.7	0:6:22:72	0:6:21:70
8	CsBArF		99	2	0.2	1:14:28:57	1:14:27:55
9	-	(*Z*)-S31d	99	1	2	3:20:28:49	3:19:27:47
10	NaBArF		99	2	2	14:35:25:26	13:33:24:25

The HF was performed in a parallel autoclave. Reaction conditions: [substrate] = 0.26 M; stirring rate = 800 rpm; 10 bar H_2/CO (1:1); 60 °C, 18h. Conversion was determined by GC using dodecane as an internal standard. Selectivity, ratio, and yield were determined by the area% values of the peaks in the GC chromatogram. [a] Selectivity of the isomerisation (Isom.) and hydrogenation (Hydrog.) processes. **(*E*)-S31b**: (*E*)-oct-2-ene; **(*Z*)-S31b**: (*Z*)-oct-2-ene; **(*E*)-S31c**: (*E*)-oct-3-ene; **(*E*)-S31d**: (*E*)-oct-4-ene; **(*Z*)-S31d**: (*Z*)-oct-4-ene.

Interestingly, if the C=C isomerisation is faster than the hydroformylation, the net addition of the H and CHO groups will take place at the most reactive and/or favourable position of the C=C double bond after isomerisation, irrespective of the position and geometry of the C=C bond in the starting

material. Therefore, the new goal in our research activities was to find an active catalyst in double-bond isomerisation with the aim of reaching high yields and high selectivities towards the terminal aldehydes. We turned our attention towards the use of a bimetallic catalytic systems, as we envisioned that one metal could be responsible of fast isomerisation processes, while our rhodium catalyst could be responsible of the hydroformylations. The overall transformation could thus be regarded as a tandem isomerisation-hydroformylation process (Scheme 40).

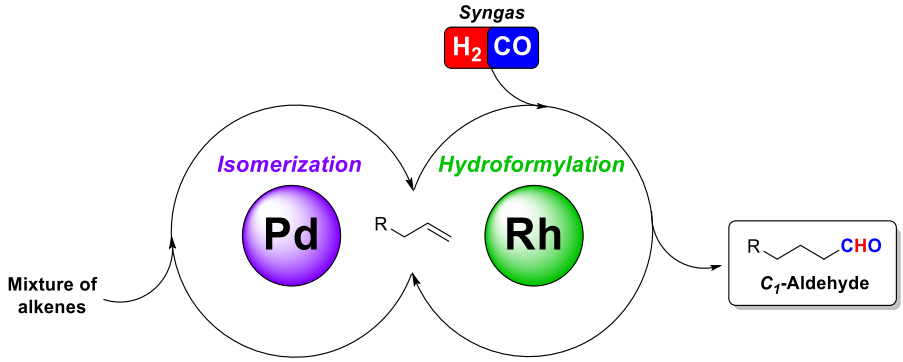

Scheme 40. General strategy for the bimetallic isomerisation-hydroformylation tandem reactions.

In 2017, Vorholt and co-workers reported a linear selective isomerisation-hydroformylation of unsaturated fatty acid methyl esters into asymmetric α,ω-functionalized aldehyde esters.[187] In this work, the authors combined a palladium catalyst and rhodium catalyst using the BiPhePhos ligand (**L13**) as a ligand. They studied different metal precursors (*i.e.,* Pd, Rh, Ir, Pt, Ru, Co, and Ni) for catalysing the isomerisation of C=C bonds under syngas atmosphere. The purpose of this method was to preferentially perform isomerisation rather than hydroformylation. Their findings concluded that the best isomerisation catalyst was the combined use of [Pd(*t*Bu$_3$P)$_2$] and PdI$_2$. In fact, palladium is a well-known transition metal for the isomerisation of C=C double bonds in alkenes. As a result, an orthogonal tandem catalytic system consisting of a palladium-based isomerisation catalyst and a rhodium-based hydroformylation catalyst derived from BiPhePhos (**L13**) as ligand was developed for the hydroformylation of methyl oleate with high yields (74%) and an *l/b* ratio of 91:9 (Scheme 41).[187] The same catalytic system was applied to the hydroformylation of methyl 3-hexenoate with an excellent *l/b* ratio of 98:2 and a yield of 81% for the linear aldehyde.

[187] Gaide, T.; Bianga, J.; Schlipköter, K.; Behr, A.; Vorholt, A. J. *ACS Catal.* **2017**, *7*, 4163-4171.

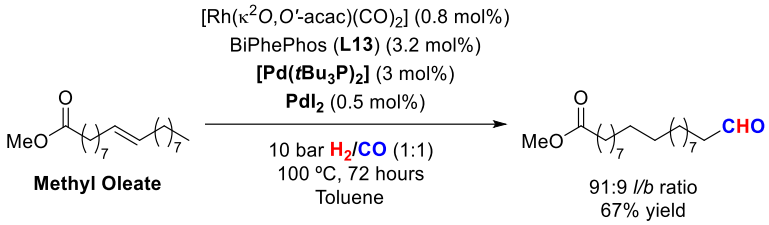

Scheme 41. Isomerisation-hydroformylation tandem reaction of methyl oleate catalysed by a Rh/Pd dual catalyst.

The authors claimed that the positive role of PdI_2 in isomerisation reactions could be attributed to the iodide group: it is well known that the nature of the halide influences the formation of the catalytically active, three-coordinated Pd-isomerisation species from a four-coordinated, halide-bridged dimeric resting state of the isomerisation catalyst (see Scheme 42; Gooßen and co-workers proposed the catalytic active species with the bromo as the halogen substituent).[181,188] However, an excess of PdI_2 promotes the complete deactivation of the rhodium hydroformylation catalyst because the iodide coordinates to the rhodium complex, which is inactive in hydroformylation. Thus, only up to 0.5 mol% of PdI_2 was considered to be an ideal amount to favour the isomerisation process without favouring the deactivation of the rhodium hydroformylation catalyst.[187]

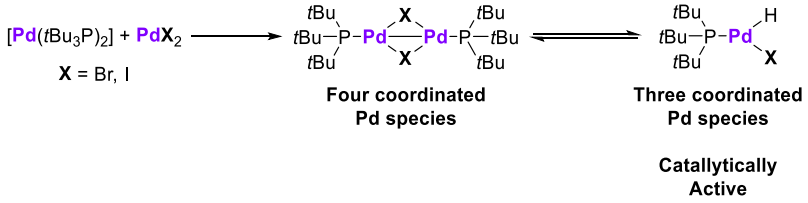

Scheme 42. Proposed catalytically active palladium species in the isomerisation of alkenes, according to Gooßen and co-workers.

We hypothesized that the use of our optimal hydroformylation conditions (*i.e.*, [Rh(κ^2*O*,*O*'-acac)(CO)$_2$] (1.0 mol%) and the corresponding bisphosphite ligand **L46** (1.20 mol%) at 100 °C under 10 bar H_2/CO (1:1) for 18 hours in toluene with the minimum amount of THF to solubilize the RA) in combination with catalytic amounts of [Pd(*t*Bu$_3$P)$_2$] and PdI_2 could constitute an optimal starting point for our studies aiming to achieve a isomerisation-hydroformylation tandem process. As the optimal relative amounts of RA, [Pd(*t*Bu$_3$P)$_2$] and PdI_2 were unknown, we performed a study

[188] Gooßen, L.; Arndt, M.; Mamone, P.; Gruenberg, M. Preparation of palladium(I) tri-tert-butylphosphine bromide dimer and its use in isomerization reactions. WO2013000874, **2013**.

in which the RA amounts ranged from (3.6 mol% to 10 mol%), [Pd(*t*Bu$_3$P)$_2$] from 0.5 mol% to 3 mol% and PdI$_2$ from 0 mol% to 0.5 mol%.

The results of this study clearly indicate that the presence of PdI$_2$ was beneficial for achieving a higher selectivity towards the C_1-aldehyde (compare entries 1 and 2 in Table 22, in which less than the half of the linear aldehyde was obtained when PdI$_2$ was not used). As for the other conditions assayed (entries 3-6 in Table 22), they involved the use of higher amounts of RA, [Pd(*t*Bu$_3$P)$_2$] or PdI$_2$. None of the conditions assayed was clearly better than using 3.6 mol% of RA, 0.5 mol% of [Pd(*t*Bu$_3$P)$_2$] and PdI$_2$ to justify the use of higher amounts of these derivatives (compare entries 2-6 with entry 1, Table 22). Thus, the use of 0.5 mol% of [Pd(*t*Bu$_3$P)$_2$], PdI$_2$ and 3.6 mol% of RA were chosen as the conditions of choice for future studies.

Table 22. Catalytic screening of palladium sources for isomerisation-hydroformylation tandem reaction of mixture of octenes.

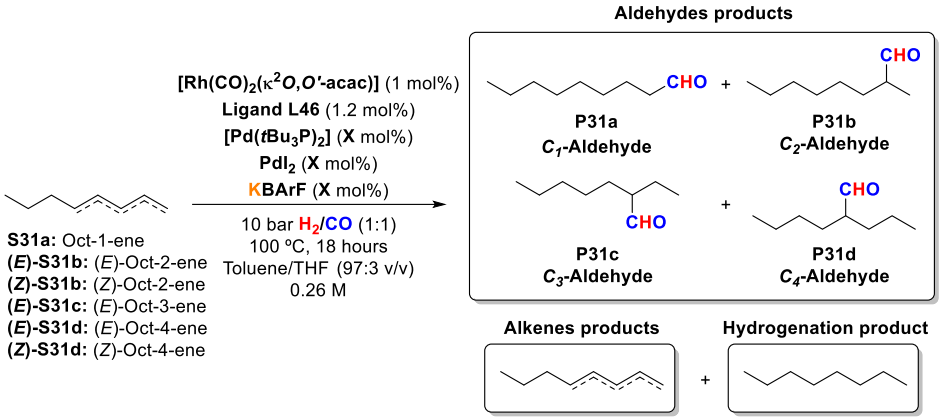

Entry	[Pd(*t*Bu$_3$P)$_2$] (mol%)	PdI$_2$ (mol%)	KBArF (mol%)	Molar amounts of unreacted alkene (%)	HF Selectivity (%)	$C_1/C_2/C_3/C_4$ ratio (%)
1	0.5	0.5	3.6	22	78	37:36:14:13
2	1	0	3.6	3	97	21:34:21:24
3	2.5	0	4.6	10	90	33:26:18:22
4	2.5	0.5	3.6	9	91	31:31:18:20
5	3	0	10	24	76	41:22:17:21
6	3	0.5	3.6	4	96	24:31:21:24

The HF of an equimolar mixture of octenes was performed in a parallel autoclave. Reaction conditions: [substrate] = 0.26 M; stirring rate = 800 rpm; 10 bar H$_2$/CO (1:1); 100 °C, 18h. Selectivity and ratio were determined by GC using dodecane as an internal standard. Mixture of octenes: oct-1-ene, (*E*)-oct-2-ene, (*Z*)-oct-2-ene, (*E*)-oct-3-ene, (*E*)-oct-4-ene, (*Z*)-oct-4-ene.

Table 23. Isomerisation-hydroformylation tandem reactions for a mixture of octenes, heptenes, hexenes and allylbenzenes.

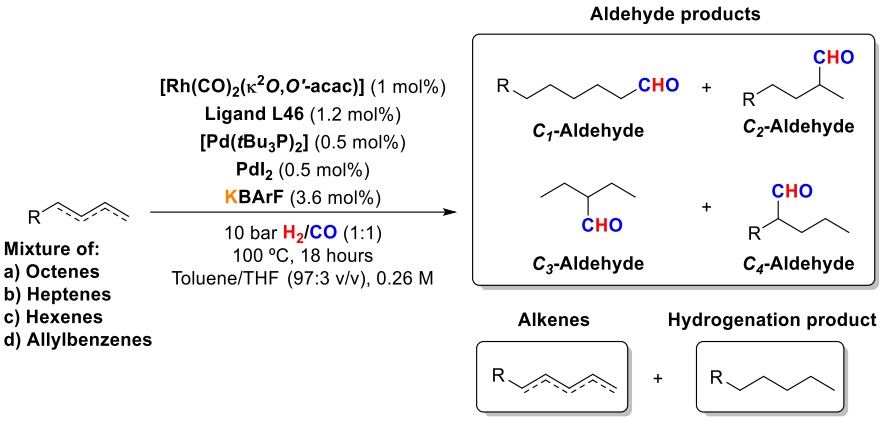

Entry	Substrate	Molar amounts of unreacted alkenes (%)	Selectivity (%)		$C_1/C_2/C_3/C_4$ ratio (%)
			Hydrog.	HF	
1[a]	Octenes[b]	22	0	78	37:36:14:13
2	Heptenes[c]	10	1	89	46:33:15:6
3	Hexenes[d]	11	2	87	58:28:14
4	Allylbenzenes[e]	68	2	30	86:14:0

The HF of an equimolar mixture of alkenes was performed in a parallel autoclave. Reaction conditions: [substrate] = 0.26 M; stirring rate = 800 rpm; 10 bar H_2/CO (1:1); 100 °C, 18h. Selectivity and ratio were determined by GC using dodecane as an internal standard. [a] These results have already been discussed in Table 22, but have been included again in this table to aid comparison. [b] Mixture of octenes: oct-1-ene, (*E*)-oct-2-ene, (*Z*)-oct-2-ene, (*E*)-oct-3-ene, (*E*)-oct-4-ene, (*Z*)-oct-4-ene. [c] Mixture of heptenes: hept-1-ene, (*E*)-hept-2-ene, (*Z*)-hept-2-ene, (*E*)-hept-3-ene. [d] Mixture of hexenes: hex-1-ene, (*E*)-hex-2-ene, (*Z*)-hex-2-ene, (*E*)-hex-3-ene, (*Z*)-hex-4-ene. [e] Mixture of allylbenzenes: allylbenzene, *trans*-β-methylstyrene, *cis*-β-methylstyrene.

After having studied the isomerisation-hydroformylation tandem reactions for a mixture of octenes and having developed satisfactory conditions for these substrates that led to the formation of the linear aldehyde as the most abundant product of the reaction (entry 1, Table 23), the same conditions were tested with equimolar mixtures of heptenes, hexenes and allylbenzenes (Table 23). For all the substrate mixtures, a higher regioselectivity towards the linear aldehyde was observed (heptenes 46%; hexenes 58% and allylbenzenes 86%). For the heptene and hexene mixtures, the selectivity towards the formation of

aldehydes (*i.e.*, HF selectivity) was high, 89% and 87% respectively. As for allylbenzenes, the HF selectivity was low (30%, see entry 4, Table 23) with important amounts of alkenes being non-hydroformylated. However, the terminal aldehyde was the most abundant product of the hydroformylation (86%; entry 4, Table 23).

Our supramolecularly regulated catalyst derived from **L46** combined with KBArF as RA showed low amounts of the linear aldehyde in the hydroformylation of the internal octenes. Therefore, the addition of palladium(0)-based catalysts was essential to increase the isomerisation process from the internal to the terminal alkenes for their subsequent hydroformylation. Only a 0.5 mol% of [Pd(*t*Bu$_3$P)$_2$] and PdI$_2$ was enough to promote an increase of the linear selectivity for the mixtures of octenes (37%), heptenes (46%), hexenes (58%) and allylbenzenes (86%). As a result, the mentioned supramolecularly catalyst was successfully combined with Pd(0)-isomerisation catalysts to perform isomerisation-hydroformylation tandem reactions of mixtures of alkenes.

2.3.4. NMR studies on the formation of catalytically active complexes for hydroformylations from ligand L46

Complexation studies were performed between the rhodium metal precursor, the ligand **L46**, and two high performing regulation agents providing high *l*/*b* ratios in the hydroformylation of several substrates: KBArF and CsBArF. The main goal was to elucidate the structure of the active rhodium complexes involved in the selective hydroformylation towards linear aldehydes (Figure 46 and Figure 47).

Our complexation studies started by analysing the coordination behaviour of equimolar amounts of [Rh(κ^2*O*,*O'*-acac)(CO)$_2$] and **L46** ([Rh]/**L46** = 1:1) at room temperature under inert atmosphere, but in the absence of syngas. These conditions led to the major formation of the complex [Rh(κ^2*O*,*O'*-acac)(CO)(κ*P*-**L46**)] by displacement of one of the CO groups from the initial rhodium precursor by one phosphite-binding group of ligand **L46** (see Figure 46a for the ^{31}P{^{1}H} spectrum).

The formation of this phosphorus-monodentate complex was confirmed by ^{31}P{^{1}H} NMR spectroscopy (Figure 46a), which revealed a singlet at δ = 135.8 ppm and a doublet centred at δ = 134.2 ppm ($^1J_{P–Rh}$ = 295.3 Hz), which were assigned to the unbound and bound phosphite groups, respectively. In a previous work, Vidal-Ferran and co-workers had observed the same type of complex with a different bisphosphite as ligand. In that case, the structure of

the complex was confirmed by IR studies and $^{31}P\{^{1}H\}$ exchange spectroscopy (EXSY[189]).[92]

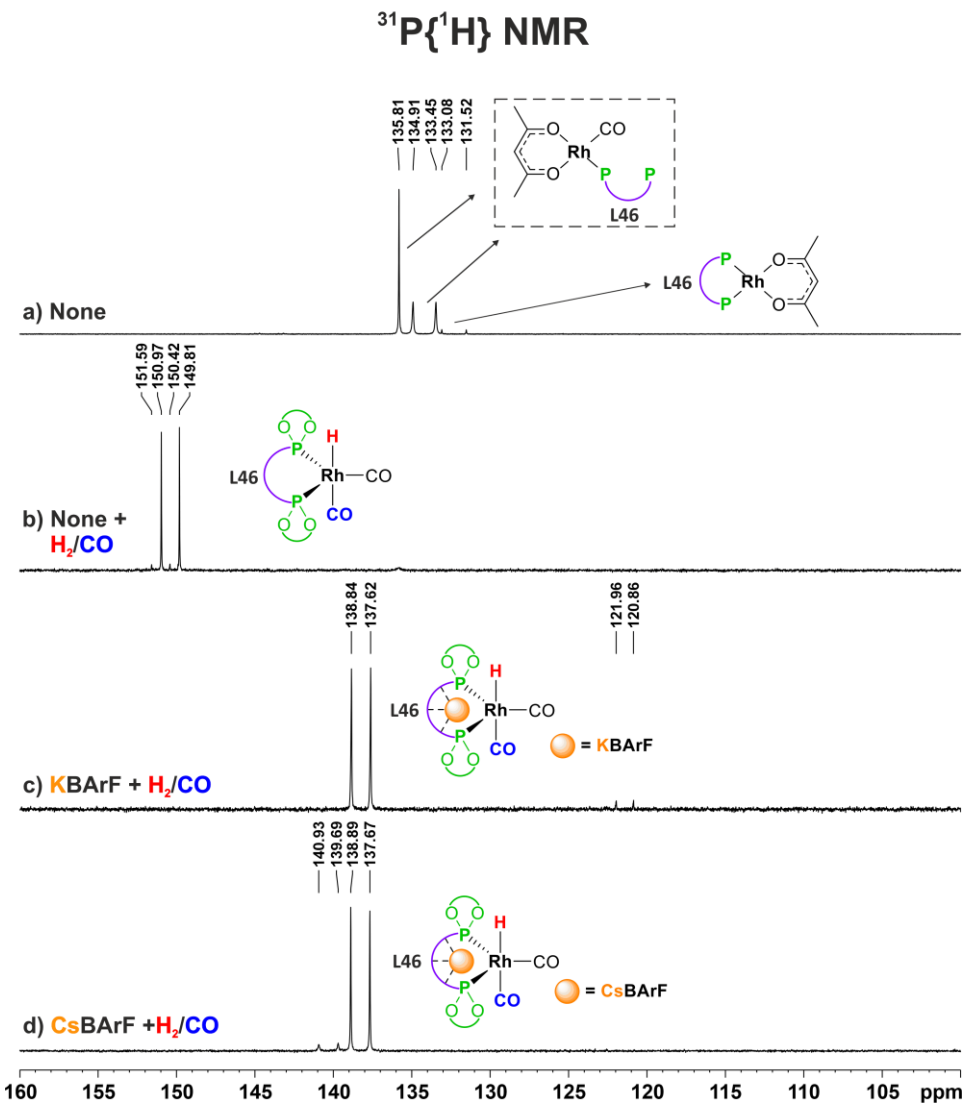

Figure 46. $^{31}P\{^{1}H\}$ NMR (202 MHz, PhMe-d_8/THF-d_8 (97:3 v/v)): a) [Rh]/**L1**; 1 bar N_2; 25 °C. b) [Rh]/**L46**; 10 bar H_2/CO (1:1); 25 °C. c) [Rh]/**L46**/KBArF; 10 bar H_2/CO (1:1); 25 °C. d) [Rh]/**L46**/CsBArF; 10 bar H_2/CO (1:1); 25 °C.

In our studies, a doublet with very low intensity centred at δ = 132.3 ppm ($^{1}J_{P-Rh}$ = 319.8 Hz) was also observed in the spectra, with the most likely structural hypothesis being the rhodium complex

[189] The exchange spectroscopy (EXSY) NMR experiment is a homonuclear shift correlated spectroscopy where coherence transfer takes place through chemical or conformational exchange.

[Rh(κ²*O*,*O*'-acac)(κ²*P*,*P*-**L46**)] arising from displacement of both carbonyl ligands from the initial rhodium complex by the two phosphorus ligating groups of **L46**.

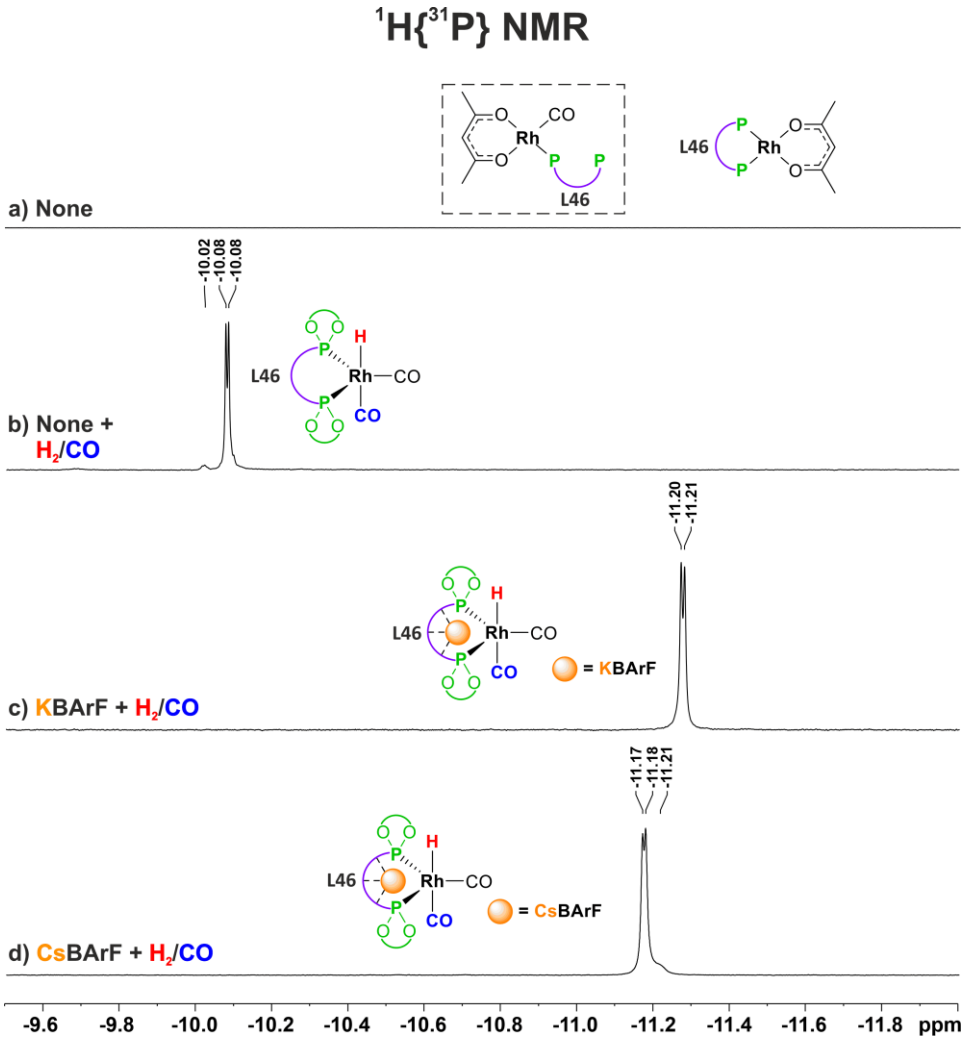

Figure 47. $^{1}H\{^{31}P\}$ NMR (500 MHz, PhMe-d_8/THF-d_8 (97:3 v/v)): a) [Rh]/**L46**; 1 bar N_2; 25 °C. b) [Rh]/**L46**; 10 bar H_2/CO (1:1); 25 °C. c) [Rh]/**L46**/KBArF; 10 bar H_2/CO (1:1); 25 °C. d) [Rh]/**L46**/CsBArF; 10 bar H_2/CO (1:1); 25 °C.

The solution of the previously mentioned complex was pressurised at 10 bar of H_2/CO (1:1) at 60 °C for 18 hours. The solution was subsequently put into a sapphire NMR tube, which was pressurised at 10 bar of H_2/CO (1:1), and the required NMR experiments were recorded at 25 °C. $^{31}P\{^{1}H\}$ NMR revealed a centred doublet at δ = 150.4 ppm ($^{1}J_{P-Rh}$ = 233.8 Hz) and $^{1}H\{^{31}P\}$ NMR a centred doublet at δ = –10.1 ppm ($^{1}J_{H-Rh}$ = 3.6 Hz) (see

Figure 46b and 47b).[190] Spectroscopic data clearly pointed to a bidentate coordination mode of **L46** to a trigonal bipyramidal rhodium centre [$Rh(CO)_2H(\kappa^2P,P$-**L46**)].[191] A magnitude of the $^2J_{P\text{-}H}$ coupling constant value of around 10 Hz is only in agreement with a *cis*-arrangement of the phosphorus and hydrido groups in the trigonal bipyramidal rhodium centre, with the hydrido ligand in the apical position of the trigonal bipyramid. Thus, the expected hydrido-dicarbonyl chelate [$Rh(CO)_2H(\kappa^2P,P$-**L46**)] was efficiently formed regardless of the absence of the RA

As for the preparation of the analogous complexes incorporating alkali metal BArF salts, these were straightforwardly prepared following analogous synthetic protocols, which started from the supramolecular complexes **L46**•RA rather than the ligand alone. Consequently, the rhodium complexes [$Rh(CO)_2H(\kappa^2P,P$-**L46**•KBArF)] and [$Rh(CO)_2H(\kappa^2P,P$-**L46**•CsBArF)] were formed by pressurising a solution of [$Rh(\kappa^2O,O'$-acac$)(CO)_2$] (1 mol%), **L46** (1 mol%) and the alkali metal BArF salt (1.3 mol%) at 10 bar of H_2/CO (1:1) at 60 ºC for 18 hours.

The chemical shifts and coupling constants of the new supramolecular rhodium complexes are summarised in Table 24. In general terms, the spectral data of the complexes differed only in the chemical shifts and magnitudes of the coupling constants. Further differences were found in the width of the signals of the complexes incorporating a RA, with broad doublets being observed in the spectra of the complexes derived from both BArF salts (Figure 46c-d and Figure 47c-d). The H–P coupling was further studied by $^1H–^{31}P$ HMBC spectroscopy[192] where a cross-peak signal was observed at the chemical shift of the hydrido and the phosphite groups. MALDI-TOF[193] MS indicated that [$Rh(CO)_2H(\kappa^2P,P$-**L46**•RA)]] complexes were formed in the absence or presence of the RA (HRMS (MALDI-TOF) *m/z* calcd. for $C_{64}H_{96}O_9P_2Rh^+$ $[M\text{-}RA\text{-}2CO\text{-}H]^+$ 1173.5579, found 1173.5569 (RA = none), 1173.5584 (RA = KBArF) and 1173.5583 (RA = CsBArF)). Mass

[190] When the ^1H NMR was recorded without ^{31}P decoupling, the two phosphite groups were observed as a doublet of triplets centred at δ = -10.1 ppm ($^2J_{H–P}$ = 12.8 Hz, $^1J_{H–Rh}$ = 3.5 Hz), with the larger coupling constant corresponding to the coupling of the proton to the two phosphorus nuclei. If the ^{31}P NMR spectrum is recorded without ^1H decoupling, the two phosphite groups are observed as only one doublet of doublets centred at δ = 150.4 ppm ($^1J_{P–Rh}$ = 233.8 Hz, $^2J_{P–H}$ = 11.1 Hz).

[191] To see the couplet ^1H NMR and ^{31}P NMR see the sections 2.5.39, 2.5.40 and 2.5.41 from the experimental section of this chapter II.

[192] The $^1H–^{31}P$ HMBC (Heteronuclear Multiple Bond Correlation) experiment gives correlations between phosphorus and protons that are separated by two, three, or sometimes in conjugated systems, four bonds. Direct one-bond correlations are suppressed.

[193] MALDI-TOF (Matrix-Assisted Laser Desorption/Ionization-Time of Flight) is a mass spectrometry technique. It works by ionizing the molecules of interest using a laser beam and then measuring their mass-to-charge ratio (*m/z*) using a time-of-flight mass analyser.

spectrometry and ^{13}C NMR studies excluded the formation under these conditions of rhodium oligomers incorporating ligand **L46**.

Table 24. Chemical shifts and coupling constants for complexes $[Rh(CO)_2H(\kappa^2P,P\text{-}\mathbf{L46}\bullet RA)]$.

Entry	RA	Chemical shifts & coupling constants (*J*)									
		^1H			$^1H\{^{31}P\}$		^{31}P			$^{31}P\{^1H\}$	
		ppm	$^1J_{H\text{-}Rh}$	$^2J_{H\text{-}P}$	ppm	$^1J_{H\text{-}Rh}$	ppm	$^1J_{P\text{-}Rh}$	$^2J_{P\text{-}H}$	ppm	$^1J_{P\text{-}Rh}$
1	**-**	–10.1	3.5	12.8	–10.1	3.6	150.4	233.7	11.1	150.4	233.8
2	**KBArF**	–11.2	4.3	n. o. [a]	–11.2	4.3	138.2	248.2	n. o. [a]	138.2	248.2
3	**CsBArF**	–11.2	2.8	n. o. [a]	–11.2	3.9	138.3	246.9	n. o. [a]	138.3	246.9

Chemical shifts and couplings constants of the species $[Rh(CO)_2H(\kappa^2P,P\text{-}\mathbf{L46}\bullet RA)]$ under 10 bar of H_2/CO (1:1) at 25 °C. [a] n. o. = not observed.

Interestingly, the complex $[Rh(CO)_2H(\kappa^2P,P\text{-}\mathbf{L46}\bullet KBArF)]$ could also be synthesized by the addition of KBArF to the chelated rhodium complex $[Rh(CO)_2H(\kappa^2P,P\text{-}\mathbf{L46})]$, which lacked the alkali metal BArF salt. The preparation and characterization of this complex has been previously described in this section. Spectral data for the newly formed complex was in agreement with those above mentioned for $[Rh(CO)_2H(\kappa^2P,P\text{-}\mathbf{L46}\bullet KBArF)]$. These results are a clear indication of the strength of the non-covalent interaction of the alkali metal BArF salt with the polyether chain of **L46** *via* ion-dipole interactions.[194]

The fact that both P groups have the same chemical shift and a small Rh–H and large P–H coupling constants indicated that the P atoms of **L46** had a strong preference for a *cis*- arrangements relative to the H ligand, which occupies the apical position of the trigonal bipyramidal rhodium centre according to literature precedents.[11, 195] Thus, the two P groups are coordinated in an equatorial–equatorial (eq–eq) fashion to a trigonal-bipyramidal rhodium centre (Scheme 43). It is interesting to note at this point that hydrido-dicarbonyl rhodium complexes having a bidentate phosphorus ligand bound to two equatorial positions of a trigonal bipyramidal rhodium centre, favour the formation of linear aldehydes in the hydroformylation of monosubstituted alkenes.[11,196,97]

It is interesting to highlight that all $^{31}P\{^1H\}$ NMR spectra of the rhodium complexes involving a chelating coordination mode for **L46** (*i.e.*, spectrum in

[194] Steed, J. W.; Atwood, J. L. *Supramolecular Chemistry, 2nd Edition*; John Wiley & Sons, Ltd., 2009.
[195] Diebolt, O.; van Leeuwen, P. W. N. M.; Kamer, P. C. J. *ACS Catal.* **2012**, *2*, 2357-2370.
[196] Damoense, L.; Datt, M.; Green, M.; Steenkamp, C. *Coord. Chem. Rev.* **2004**, *248*, 2393-2407.

Figure 46b when no alkali metal BArF salt is used and spectra in Figure 46c with KBArF and Figure 46d with CsBArF) showed an additional broad doublet of low intensity. In an analogous manner, unaccounted broad signals of low intensity were observed in the hydride region of the $^{1}H\{^{31}P\}$ NMR spectra (Figure 47b and Figure 47d). In order to investigate the potential structure of the rhodium complexes to which the above-mentioned low intensity signals could be attributed, $^{31}P\{^{1}H\}$ exchange spectroscopy (EXSY) experiments were performed. Interestingly, these experiments did not reveal any cross-peak attributable to chemical exchange processes between the phosphite groups.

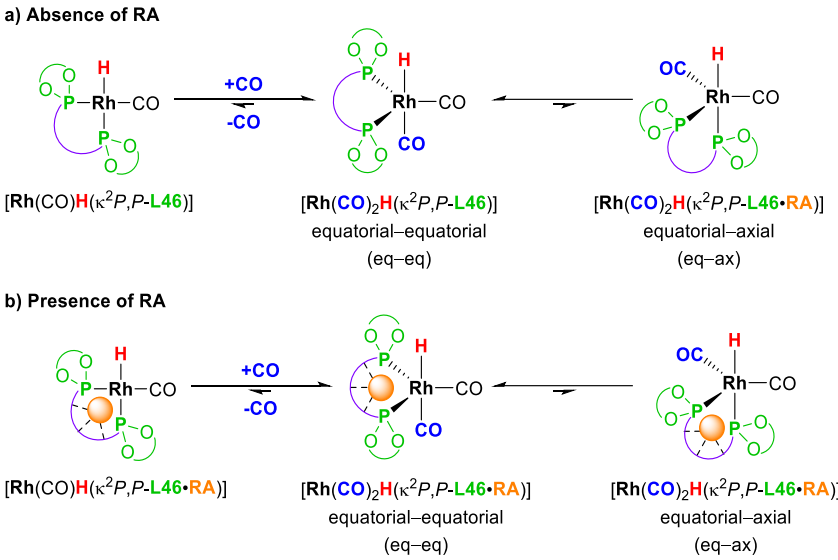

Scheme 43. Equilibrium of hydrido carbonyl rhodium complexes under 10 bar of H_2/CO (1:1) at 25 ºC.

This observation allows to confirm that equilibria due to the coordination of the ligand in an equatorial–equatorial (eq–eq) or equatorial–axial (eq–ax) fashion to the trigonal-bipyramidal rhodium centre are minor processes, if at all present (Scheme 43). For instance, the coordination of the phosphite groups in an axial position leads to a large coupling constant with the axial hydrido group through two bonds ($^{2}J_{P\text{-}H} > 150$ Hz), which for these cases were not observed. Unfortunately, no plausible structure for this minor Rh complex could be suggested.

2.3.5. FlowNMR studies of the supramolecularly regulated hydroformylation of hex-1-ene (S47a)

The monitoring of the concentration of active species is key in homogeneous catalysis for the understanding of the reaction under study. This monitoring process for transformations carried out under non-standard conditions, such as reactions under pressure, requires dedicated and specialized instrumentation. The research group from Prof. Hintermair at the University of Bath has developed the "*Dynamic Reaction Monitoring (*DReaM*) Facility*",[197] which combines several analytical techniques to monitor liquid-phase chemical reactions in real-time.[198] The DReaM facility at Bath includes online high-pressure NMR (HP-NMR) instrumentation, capable of recording multinuclear NMR spectra of real hydroformylation reaction mixtures under a flow regime. With the aim of following the progress of our hydroformylation reactions by ^{1}H and ^{31}P NMR spectroscopy, the hydroformylation of hex-1-ene in the presence of the supramolecular ligand **L46** was studied in the above-mentioned NMR laboratory.

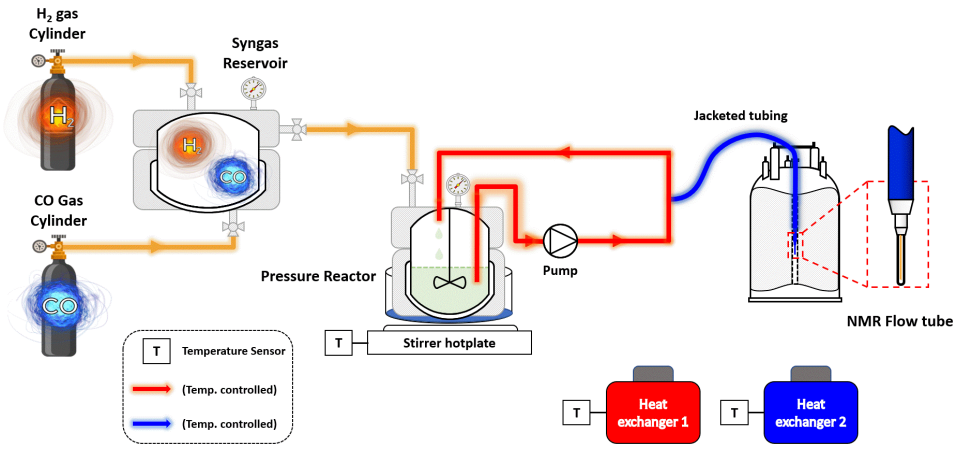

Figure 48. Schematic of the FlowNMR apparatus set up for hydroformylation reactions.

The NMR reaction monitoring equipment within the DReaM facilities consist of a 500 MHz spectrometer from Bruker® connected to a 50 mL thick-walled glass autoclave. The spectrometer and autoclave are connected through a tubbing in a closed loop with an aliquot of the reaction mixture recirculating from the autoclave to the spectrometer continuously and the temperature controlled in all the setup (Figure 48). Multinuclear NMR spectra can be

[197] Dynamic Reaction Monitoring (DReaM) Facility. https://www.bath.ac.uk/research-facilities/dynamic-reaction-monitoring-facility/ (accessed on 2023-04-10).
[198] a) Hall, A. M. R.; Chouler, J. C.; Codina, A.; Gierth, P. T.; Lowe, J. P.; Hintermair, U. *Catal. Sci. Technol.* **2016**, *6*, 8406-8417. b) Saib, A.; Bara-Estaún, A.; Harper, O. J.; Berry, D. B. G.; Thomlinson, I. A.; Broomfield-Tagg, R.; Lowe, J. P.; Lyall, C. L.; Hintermair, U. *React. Chem. Eng.* **2021**, *6*, 1548-1573.

recorded at all reaction times by means of the corresponding FlowNMR probe. Hintermair and co-workers have previously studied a number of hydroformylation reactions in the DReaM facilities.[199,200] Amongst numerous mechanistic and kinetic aspects within the studied hydroformylation reactions, Hintermair and co-workers have been able to elucidate the structure of reaction intermediates including Rh-hydride species and Rh-acyl complexes. The authors were also able to detect the formation of relevant reaction intermediates related with isomerisation processes of the alkene under study.[200]

Our hydroformylation reactions studies in the DReaM facilities consisted of monitoring the progress of the hydroformylation reaction of hex-1-ene employing the supramolecularly regulated catalyst derived from **L46** and CsBArF (Scheme 44). These studies were performed under 10 bar of H_2/CO (1:1) at 60 ºC, where the reactor was sequentially pressurised with CO (5 bar) and H_2 (5 bar). 1,3,5-Trimethoxybenzene (TMB) and triphenyl phosphate were also added to the reaction mixture as internal standards, with the aim of being able to determine the concentration of the alkenes, aldehydes, and relevant catalytic species by quantitative ^{1}H and ^{31}P NMR analysis.

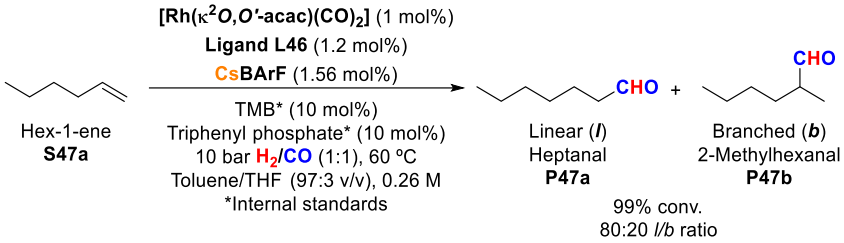

Scheme 44. Continuous monitoring of the supramolecularly regulated hydroformylation of hex-1-ene in the FlowNMR under 10 bar H_2/CO (1:1) at 60 ºC.

Figure 49a summarizes the conversion of the reaction, which was complete after two hours under the hydroformylation reaction conditions previously mentioned. From this reaction time, the concentration of the aldehydes (heptanal and 2-methylhexanal) remained constant, with no side-reaction taking place from the final products. The regioselectivity of the aldehydes could be reproduced with respect to hydroformylation conditions in a batch mode (*l*/*b* = 80:20 or 83:17[201] under flow or batch hydroformylation

[199] a) Bara-Estaún, A.; Lyall, C. L.; Lowe, J. P.; Pringle, P. G.; Kamer, P. C. J.; Franke, R.; Hintermair, U. *Faraday Discuss.* **2021**, *229*, 422-442. b) Bara-Estaún, A.; Lyall, C. L.; Lowe, J. P.; Pringle, P. G.; Kamer, P. C. J.; Franke, R.; Hintermair, U. *Catal. Sci. Technol.* **2022**, *12*, 5501-5516.
[200] Bara-Estaún, A.; Lyall, C. L.; Lowe, J. P.; Pringle, P. G.; Kamer, P. C. J.; Franke, R.; Hintermair, U. *Catal. Sci. Technol.* **2022**, *12*, 5501-5516.
[201] The *l*/*b* ratio was also determined by ^{1}H NMR in the batch reactions when the supramolecularly regulated hydroformylations with all the set of RAs were studied. The catalytic results under the batch conditions, which are shown in the experimental section 2.5.8, were determined by GC analysis.

conditions, respectively). Hex-2-ene and hex-3-ene were also observed in equal concentration (*ca.* 23 mM) which correspond to 8.9% molar amounts with respect to the initial amounts of alkene. Overall, the results of the hydroformylation reactions under flow conditions agreed with those obtained for batch reactions.

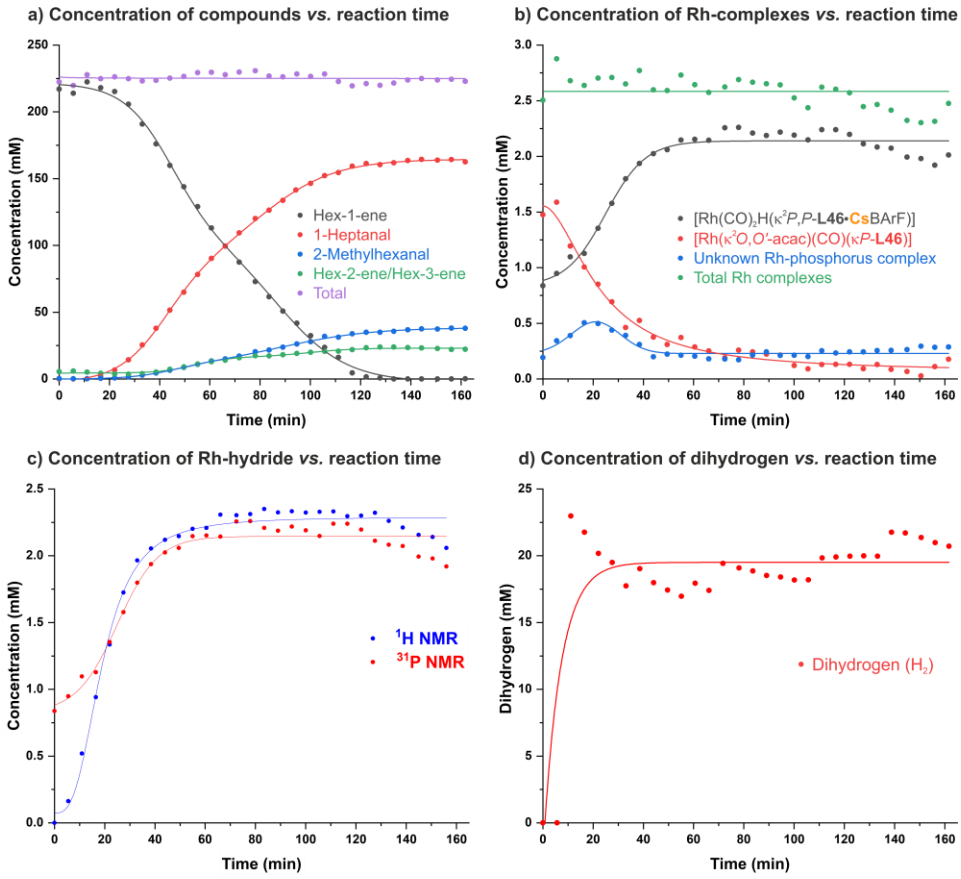

Figure 49. FlowNMR charts of the supramolecular hydroformylation of hex-1-ene with [Rh(κ^2*O*,*O'*-acac)(CO)$_2$] (1 mol%), **L46** (1.2 mol%) and CsBArF (1.56 mol%) under 10 bar of H$_2$/CO (1:1) at 60°C. **a)** Concentrations of hexenes and their corresponding aldehydes detected in ^{1}H NMR *vs.* reaction time. **b)** Concentrations of rhodium-phosphorus species in ^{31}P NMR *vs.* reaction time. **c)** Concentration of Rh-hydride complexes from ^{1}H and ^{31}P NMR data *vs.* reaction time. **d)** Dihydrogen concentration from ^{1}H NMR data *vs.* reaction time. Lines in graphics a-d correspond to eye guidelines

The concentration of rhodium-hydrides could be determined both by ^{1}H and ^{31}P NMR spectroscopy (see Figure 49c). It is interesting to note that the concentration of the [Rh(CO)$_2$H(κ^2*P*,*P*-**L46**•CsBArF] complex *vs.* reaction time calculated from ^{1}H NMR data was in agreement with that obtained from ^{31}P NMR experiments (*ca.* 2.15 mM at times higher than 60 min.). Another interesting aspect to highlight is that the reaction set-up minimized changes in

the pressure of H_2 (and hence CO, although this variable was not monitored) as it can be observed in Figure 49d. Minimizing changes in the H_2 pressure with respect to the target value (*i.e.*, H_2 pressure = 5 bar) was achieved by modifying the original setup by introducing a gas reservoir between the pressure reactor and the gas tanks of H_2 & CO in the original design (Figure 48).

As the progress of the hydroformylation reaction was monitored by NMR, ^{31}P NMR spectra at different reaction times were recorded. A selection of ^{31}P NMR spectra at t = 0, 15, 20 and 25 min are shown in Figure 50. ^{31}P NMR analysis revealed no major changes in the spectra from t = 30 min to the end of the experiment (t = 160 min). The ^{31}P NMR spectrum at t = 60 min has been included in Figure 50 as a representative spectrum for this period of time. As already discussed in the previous section (*i.e.*, 2.3.4), the complex [Rh(κ^2*O,O'*-acac)(CO)(κ*P*-**L46**)] arising from displacement of one CO group from [Rh(κ^2*O,O'*-acac)(CO)$_2$] by one *P*-ligating group of the ligand was detected at the very beginning of the experiment (t = 0). It is interesting to note that this is the most abundant rhodium complex at early stages of the reaction (up to 15 min). Spectroscopic data (a singlet at 138.9 ppm and a centred doublet at 129.0 ppm ($^1J_{P\text{-}Rh}$ = 295.9 Hz), Figure 50) were in agreement with those previously described for this compound (see Figure 46a). This rhodium complex is observed in the first 25 minutes of the reaction, after which it is no longer detected in measurable amounts. The active rhodium complex in hydroformylations [Rh(CO)$_2$H(κ^2*P,P*-**L46**•CsBArF] was first detected after 10 min. Spectroscopic data were in agreement with those already described for this complex (see Figure 46d). It is interesting to note that important amounts of this complex survive the hydroformylation process ([Rh(CO)$_2$H(κ^2*P,P*-**L46**•CsBArF]$_{160\ min}$ = 2.01 mM, 77% of the initial concentration of the rhodium precursor; [Rh(κ^2*O,O*-acac)(CO)$_2$] = 2.60 mM, 1.0% molar amount). This result paves the way to future experiments aiming to recover and reuse the hydroformylation catalysts derived from **L46**. It is interesting to note that a new phosphorus-complex leading to a doublet centred at 123.4 ppm ($^1J_{P\text{-}Rh}$ = 208.0 Hz) in ^{31}P NMR was formed. The concentration of this unknow compound remains constant after reaction times of 40 min. We have no clear structure for this compound, and we hypothesize that it could be a dead end in the hydroformylation catalytic cycle.

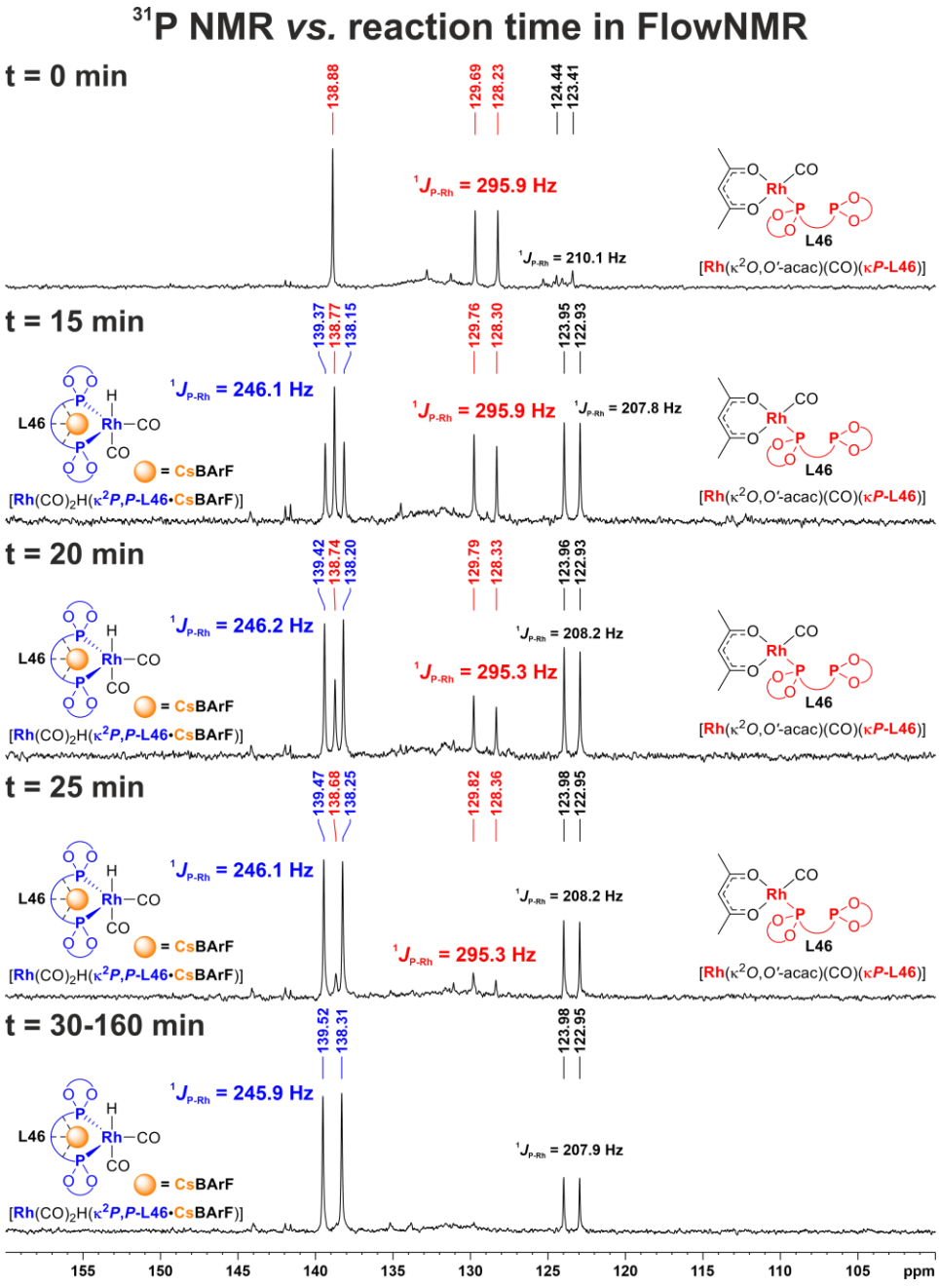

Figure 50. Selected ^{31}P NMR spectra *vs.* reaction times performed in FlowNMR. Colour figure: Blue: [Rh(CO)$_2$H(κ^2*P*,*P*-**L46**•CsBArF]; Red: [Rh(κ^2*O*,*O'*-acac)(CO)(κ*P*-**L46**)]; Black: unknown rhodium-phosphorus species.

2.4. CONCLUSIONS

Rhodium catalysts derived from supramolecular bisphosphite ligand **L46** were successfully used for linear selective hydroformylations of an array of structurally diverse alkenes and provided excellent linear ratios for terminal alkenes with aliphatic substituents (*l*/*b* ratios up to 99:1). For most of the alkenes studied, the use of a regulation agent (RA) maximised the regioselectivities of the hydroformylations (*l*/*b* ratios up to 98:2 for hex-1-ene with NaBArF as the RA). The benefits of our regulation approach, which consists of screening a set of regulation agents to obtain the highest yield and/or selectivity for the substrate of interest, has been demonstrated in this work: the optimal catalytic system to a particular substrate was easily tailored by the choice of the regulation agent. In this work, relevant aldehydes for the fragrance industry were prepared employing supramolecular catalysts derived from ligand **L46**. Such aldehydes comprise, lauric aldehyde (**P48a**), mefranal® (**P56a**), florhydral® (**P58a**), and bourgeonal® (**P61a**). For the case of alkenes with a strong preference towards branched hydroformylation products, the linear selectivity was moderate with an increase in the linear-selectivity due to the effects of the regulation agent. The hydroformylation of internal alkynes was also achieved with supramolecularly regulated catalysts derived from **L46** with decreased amounts of the hydrogenation products and increased yield of the α,β-unsaturated aldehyde being observed with the optimal catalyst. Finally, the abovementioned supramolecularly regulated catalyst was tested in the hydroformylation of a representative allene. The addition of KBArF as regulation agent provided a remarkable maximisation in the yield of the corresponding β,γ-unsaturated aldehyde (up to 60% increase), being the formation of side-products suppressed.

The linear selective hydroformylation catalysed by supramolecular complexes derived from **L46** was successfully combined with palladium(0)-based isomerisation catalysts in order to develop an isomerisation-hydroformylation tandem reaction. With the use of only 0.5 mol% of [Pd(*t*Bu$_3$P)$_2$] and PdI$_2$, a considerable increase of the linear selectivity (up to 86%) was observed for the mixtures of i) octenes, ii) heptenes, iii) hexenes and iv) allylbenzenes.

NMR studies of the hydroformylation reaction mixtures revealed the structure of the active complex [Rh(CO)$_2$H(κ^2*P*,*P*-**L46**•RA], with the RA supramolecularly interacting with the polyether chain and the two phosphite-ligating groups being coordinated at bis-equatorial positions of the trigonal bipyramidal rhodium centre.

The monitoring of the progress of the hydroformylation reaction of hex-1-ene employing the supramolecularly regulated catalyst derived from

L46 and CsBArF by FlowNMR allowed for the determination of the structure of relevant rhodium complexes in the hydroformylation of hex-1-ene. These studies also revealed that Rh-active complexes are stable throughout the hydroformylation process.

2.5. EXPERIMENTAL SECTION

2.5.1. General remarks

All syntheses were carried out using chemicals purchased from commercial sources unless otherwise cited. Air- and moisture-sensitive manipulations and hydroformylation reactions were performed under inert atmosphere, either in a N_2-filled glove box or with standard Schlenk techniques. Hazards: Carbon monoxide (CO) is a very toxic gas by inhalation and this reagent or metal carbonyl complexes were always used in well-ventilated hoods. Glassware was dried in vacuo before use with a hot air gun. All solvents were dried by using a Solvent Purification system (SPS). Air and moisture sensitive manipulations or reactions were run under inert atmosphere using anhydrous solvents, either in a glove box or with standard Schlenk techniques. All solvents were dried by using a Solvent Purification System (SPS). SiO_2 (230-400 mesh) was used for column chromatography. NMR spectra were recorded in $CDCl_3$, CD_2Cl_2, PhMe-d_8 or THF-d_8 unless otherwise cited, on a Bruker Avance 400 MHz or 500 MHz Ultrashield spectrometers. ^1H NMR and $^{13}C\{^1H\}$ NMR chemical shifts are quoted in ppm relative to residual solvent peaks. $^{31}P\{^1H\}$ NMR chemical shifts are quoted in ppm relative to 85% phosphoric acid in water. High-resolution mass spectrum (HRMS) was recorded by using ESI as ionization method in positive mode, unless otherwise stated. IR spectra were recorded using Attenuated Total Reflection (ATR) spectroscopy unless otherwise stated. Melting points were measured in open capillaries and are uncorrected. Selectivity of hydrogenation and isomerisation of the octenes substrates were determined by GC with a FID detector using achiral stationary phase, HP-5. The preparation and characterization of BArF salts such as LiBArF, KBArF, RbBArF, CsBArF and $EtNH_3$BArF have been previously described the preparation in the literature.[90] In the case of NaBArF is commercially available.

2.5.2. Synthesis of supramolecular bisphosphite ligand L46

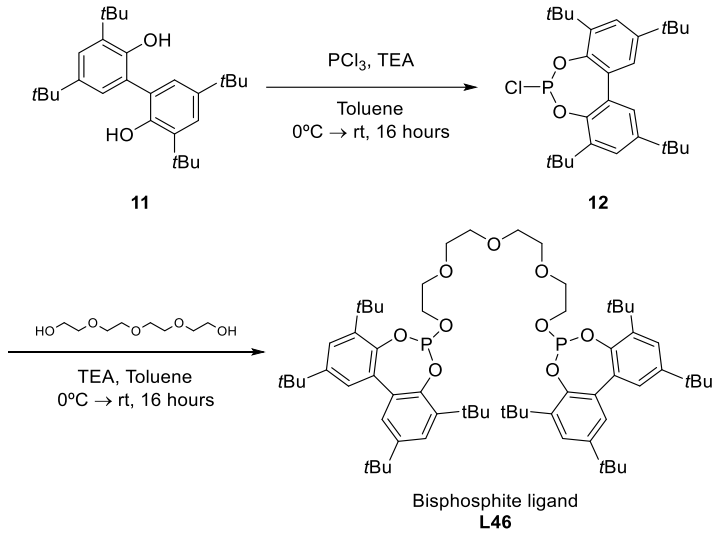

Scheme 45. Synthetic route towards bisphosphite **L46**.

2.5.2.1. Synthesis of 3,3',5,5'-tetra-*tert*-butylbiphenyl-2,2'-diyl chlorophosphite (12)

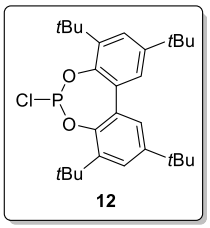

The preparation of 3,3',5,5'-tetra-*tert*-butylbiphenyl-2,2'-diyl chlorophosphite (**12**) was performed by slightly varying a reported procedure.[202] In a flame-dried Schlenk flask, 3,3',5,5'-tetra-*tert*-butyl-2,2'-dihydroxybiphenyl (**11**) (2.01 g, 4.8 mmol, 1.01 equiv.) was weighted, and then azeotropically dried with toluene (3 x 10 mL). 30 mL of anhydrous toluene (SPS[203]) were added to the flask. Another flame-dried Schlenk flask was placed in the glove box, and 0.51 mL of PCl_3 (5.82 mmol, 1.22 equiv.) were transferred to the flask. 30 mL of anhydrous toluene were also added to the Schlenk flask. Finally, triethylamine (1.75 mL, 12.6 mmol, 2.64 equiv.) was syringed into the solution. The "BIPOL" solution at room temperature was slowly (*ca.* 45-60 min) cannulated to the PCl_3 solution (0°C). Then, the mixture was stirred for 16 h at room temperature. After this, the reaction mixture was filtered with a cannula filter to another flame-dried Schlenk flask. The filtrate was evaporated to dryness by vacuum to give a yellow solid (1.97 g, quantitative yield). This chlorophosphite (**12**) was used with no purification in the next synthesis step. Spectroscopic data for this compound were in agreement with those already reported in the literature.[102] ^{1}H NMR (400 MHz, $CDCl_3$) δ 7.47 (d, J = 2.4 Hz,

[202] Buisman, G. J. H.; Kamer, P. C. J.; van Leeuwen, P. W. N. M. *Tetrahedron: Asymmetry* **1993**, *4*, 1625-1634.
[203] Abbreviation that refers to Solvent Purification System.

4H), 7.18 (d, J = 2.4, 4H), 1.48 (s, 18H), 1.36 (s, 18H) ppm; $^{31}P\{^{1}H\}$ NMR (162 MHz, $CDCl_3$) δ 171.5 ppm.

2.5.2.2. Synthesis of bisphosphite ligand L46

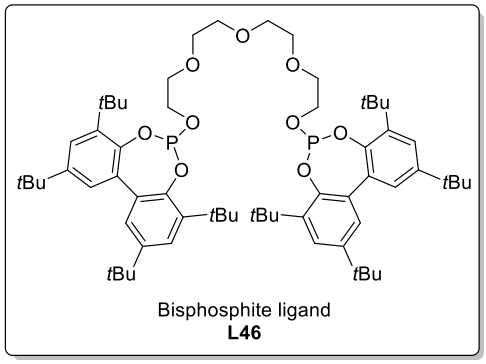

Bisphosphite ligand
L46

In a flame-dried Schlenk, a solution of the corresponding chlorophosphite **12** (1.97 g, 4.15 mmol, 2.2 equiv.) in 30 mL of anhydrous toluene (SPS) was prepared and then triethylamine (635 µL, 4.52 mmol, 2.4 equiv.) was added dropwise to the former solution. In another flame-dried Schlenk, a solution of tetraethylene glycol (331 mL, 1.89 mmol, 1.0 equiv.), previously azeotropically dried with toluene (3 x 5 mL), in 30 mL anhydrous toluene was prepared. Tetraethylene glycol was slowly added via cannula to the chlorophosphite solution (*ca.* 30 min) at room temperature. Then, the mixture was stirred for 16 hours. After this, the turbid reaction mixture was filtered through celite® and the filtrate was evaporated to dryness to give the crude as a white-yellow solid. The product was then purified by filtration through a pad of basic alumina, using dichloromethane as the solvent, to give the pure bisphosphite **L46** a white solid (1.86 g, 92% isolated yield). ^{1}H NMR (500 MHz, CD_2Cl_2) δ 7.46 (d, J = 2.4 Hz, 4H), 7.19 (d, J = 2.4, 4H), 3.96 (m, 4H), 3.57 (s, 12H), 1.48 (s, 36H), 1.37 (s, 36H) ppm.; $^{13}C\{^{1}H\}\{^{31}P\}$ NMR (126 MHz, CD_2Cl_2) δ 147.1, 146.3, 140.4, 133.0, 126.8, 124.8, 71.1, 71.0, 70.9, 64.3, 35.7, 34.9, 31.7, 31.2 ppm.; $^{31}P\{^{1}H\}$ NMR (202 MHz, CD_2Cl_2) δ 139.1 ppm.; IR (neat): 2955, 2905, 2868, 1595, 1437, 1394, 1361, 1281, 1229, 1201, 1173, 1124, 1090, 1034, 941, 914, 869, 851, 803, 777, 764, 697, 616 cm^{-1}.; HRMS (ESI^+) m/z calcd. for $C_{64}H_{97}O_9P_2^+$ $[M+H]^+$ 1071.6602, found 1071.6597. Melting point: 92 °C.

2.5.3. Synthesis of supramolecular bisphosphite ligand L47

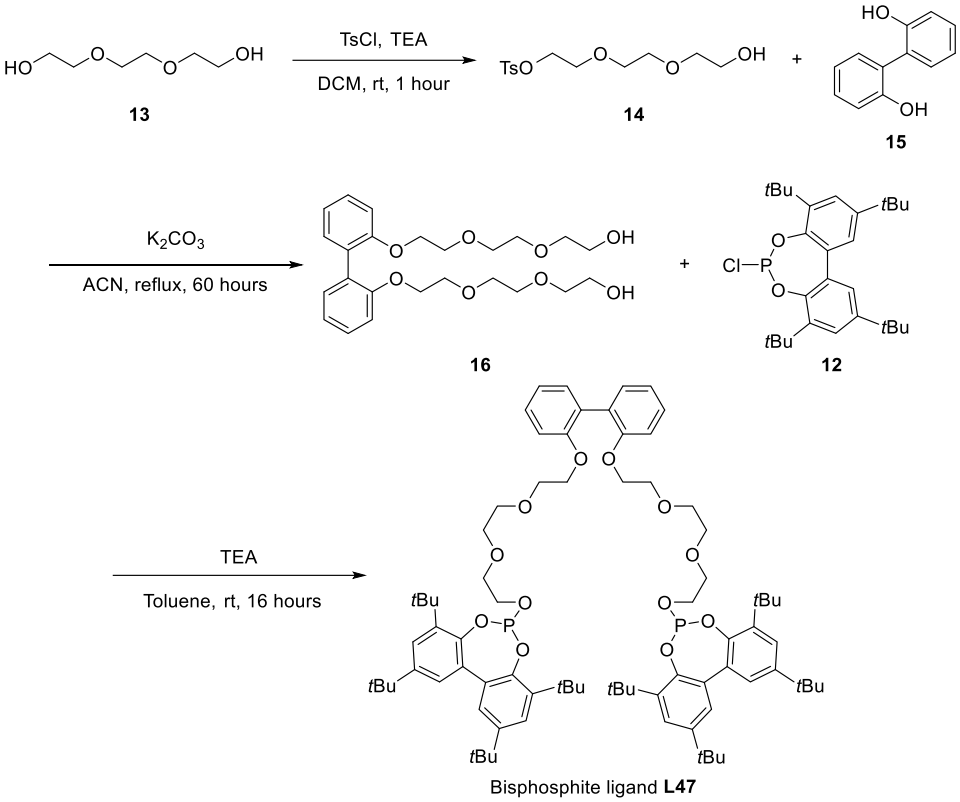

Scheme 46. Synthetic route towards bisphosphite ligand **L47**.

2.5.3.1. Synthesis of 2-(2-(2-hydroxyethoxy)ethoxy)ethyl 4-methylbenzenesulfonate (14)

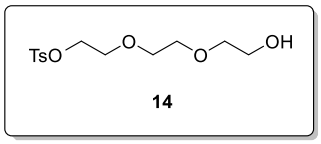

The monotosylated product **14** was prepared from a solution of triethylene glycol **13** (7.83 mL, 55.5 mmol, 1 equiv.) and triethylamine (4.0 mL, 28.5 mmol, 0.514 equiv.) were dissolved in CH_2Cl_2 (100 mL). Then, tosyl chloride (2.71 g, 13.9 mmol, 0.251 equiv.) was added in one portion. The resulting mixture was stirred for two hours at room temperature. After washing with 100 mL of 1 M $KHSO_4$ and 5% $NaHCO_3$ and drying over Na_2SO_4, the product was obtained by purification by flash column chromatography over SiO_2 using AcOEt as eluent. The pure monotosylated product **14** was obtained as a clear, colorless oil (2.68 g, 16% isolated yield). Spectroscopic data for this compound were in agreement with the reported ones.[9797] ^{1}H NMR (400 MHz, $CDCl_3$) δ 7.78 (d, J = 7.9 Hz, 2H), 7.33 (d, J = 7.9 Hz, 2H), 4.15 (t, J = 4.8 Hz, 2H), 3.68 (t, J = 4.7 Hz, 4H), 3.59 (s, 4H), 3.55 (t, J = 4.6 Hz, 2H), 2.43 (s, 3H), 2.35 (br s, 1H).

2.5.3.2. Synthesis of 2,2'-(((((([1,1'-biphenyl]-2,2'-diylbis(oxy))bis(ethane-2,1-diyl))bis(oxy))bis(ethane-2,1-diyl))bis(oxy))bis(ethan-1-ol) (16)

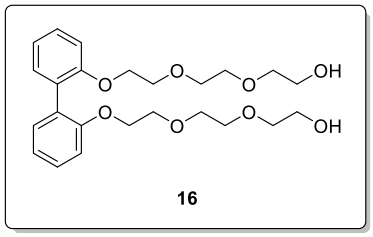

16

[1,1'-Biphenyl]-2,2'-diol **15** (0.934 g, 4.96 mmol, 1 equiv.) and the monotosylated triethyleneglycol **14** (3.02 g, 9.93 mmol, 2 equiv.), a K_2CO_3 (2.98 g, 21.3 mmol). were introduced into an oven-dried 100 mL two-necked flask. Then, a condenser was connected to the flask and three vacuum-nitrogen cycles were performed. Anhydrous acetonitrile (46 mL) was syringed to the flask under nitrogen atmosphere. The resulting reaction mixture was heated at reflux and stirred for 60h. Then, the reaction mixture was cooled, allowed to reach room temperature, and concentrated *in vacuo*. The resulting residue was finally purified by flash column chromatography on SiO_2 using cyclohexane/acetone as eluent (50:50 to 30:70) to yield the desired product **16** as a colourless viscous oil (2.1 g, 94% isolated yield). Spectroscopic data for this compound were in agreement with the reported ones.[97] ^{1}H NMR (400 MHz, $CDCl_3$) δ 7.32 – 7.28 (m, 2H), 7.28 – 7.23 (m, 2H), 7.00 (td, *J* = 7.4, 1.2 Hz, 2H), 6.95 (dd, *J* = 8.2, 1.1 Hz, 2H), 4.09 (dd, *J* = 5.8, 4.1 Hz, 4H), 3.75 – 3.65 (m, 8H), 3.58 – 3.46 (m, 12H), 2.87 (s, 2H).

2.5.3.3. Synthesis of bisphosphite ligand L47

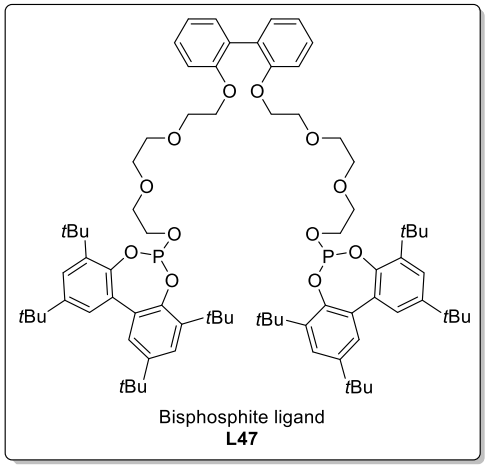

Bisphosphite ligand
L47

In a flame dried Schlenk, a solution of the corresponding chlorophosphite **12** (2.61 g, 5.49 mmol, 2.17 equiv.) in 35 mL of anhydrous toluene (SPS) was prepared. Triethylamine (1.07 mL, 7.59 mmol, 3 equiv.) was then added dropwise. In another flame dried Schlenk, a solution of diol 6 (1.14 g, 2.53 mmol, 1.0 equiv.), previously azeotropically dried with toluene (3 x 5 mL), in 35 mL anhydrous toluene (SPS) was prepared. The diol **16** was slowly added via cannula to the chlorophosphite solution (*ca.* 30 min) at room temperature. Then, the mixture was stirred for 18 hours. After this, the turbid reaction mixture was filtered through celite® and the filtrate was evaporated to dryness to give the crude as a white-yellow solid. The product was then purified by filtration through a pad of basic alumina, using dichloromethane as the solvent, to give the pure bisphosphite **L47** a white solid (2.98 g, 89%

isolated yield). ^{1}H NMR (500 MHz, CD_2Cl_2) δ 7.49 (d, *J* = 2.4 Hz, 4H), 7.26 (m, 4H), 7.21 (d, *J* = 2.4 Hz, 4H), 6.98 (m, 4H), 4.08 (t, *J* = 4.9 Hz, 4H), 3.95 (m, 4H), 3.67 (t, *J* = 4.9 Hz, 4H), 3.53 (t, J = 5.0 Hz, 4H), 3.49 (s, 8H), 1.51 (s, 36H), 1.39 (s, 36H) ppm.; ^{13}C{^{1}H}{^{31}P} NMR (126 MHz, CD_2Cl_2) δ 156.3, 146.7, 145.9, 140.0, 132.6, 131.5, 126.4, 124.3, 120.4, 112.3, 70.7, 70.6, 70.5, 69.6, 68.3, 35.3, 34.5, 31.3, 30.8, ppm; ^{31}P{^{1}H} NMR (202 MHz, CD_2Cl_2) δ 139.0 ppm.; IR (neat): 2955, 2905, 2868, 1594, 1504, 1437, 1394, 1361, 1281, 1261, 1228, 1124, 1090, 1034, 928, 868, 850, 777, 750, 696, 614 cm^{-1}; HRMS (ESI^{+}) *m/z* calcd. for $C_{80}H_{112}NaO_{12}P_2^{+}$ $[M+Na]^{+}$ 1349.7521, found 1349.7527. Melting point: 81 °C.

2.5.4. Synthesis of substrates for rhodium hydroformylation reaction

2.5.4.1. Synthesis of the substrate (3-methylbut-3-en-1-yl)benzene (S56)

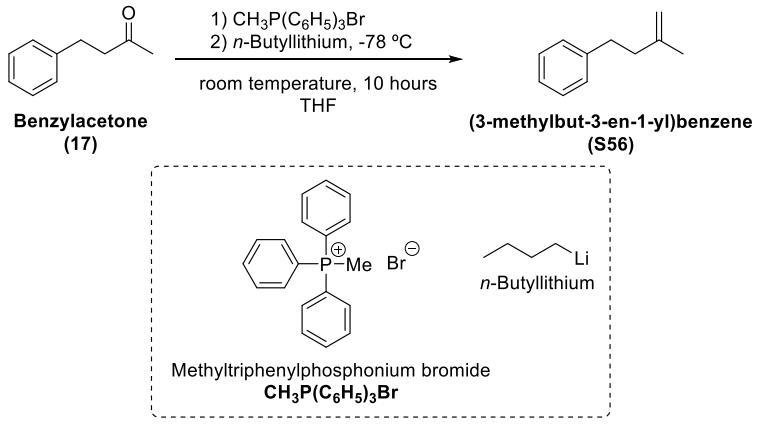

Scheme 47. Synthetic route towards substrate **S12**.

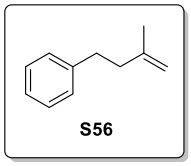

Methyltriphenylphosphonium bromide (2.92 g, 8 mmol) in anhydrous THF (10 mL) was cooled down to -78 ºC and *n*-butyllitihium (1.6M in hexanes, 5 mL, 8 mmol) was added dropwise. The achieved reddish solution was stirred at room temperature for 1 hour. Benzylacetone (**17**) (0.758 mL, 5 mmol) in anhydrous THF (10 mL) was added to this solution dropwise. The achieved yellow suspension was stirred at room temperature for 10 hours and quenched with water. The aqueous layer was extracted with petroleum ether. The combined organic layers were washed with brine, dried over Na_2SO_4, and concentrated. The crude was purified by flash column chromatography over SiO_2 using Cy/AcOEt (95:5) as eluent to give the desired product **S56** (600 mg, 82% isolated yield). Spectroscopic data for this compound were in agreement with the reported ones.[164] ^{1}H NMR (400 MHz, $CDCl_3$) δ 7.33 – 7.26 (m, 2H), 7.23 – 7.16 (m, 3H), 4.78 – 4.68 (m, 2H), 2.81 – 2.72 (m, 2H), 2.37 – 2.28 (m, 2H), 1.78 (s, 3H).

2.5.4.2. Synthesis of the substrate 1-((2-methylallyl)oxy)octane (S57)

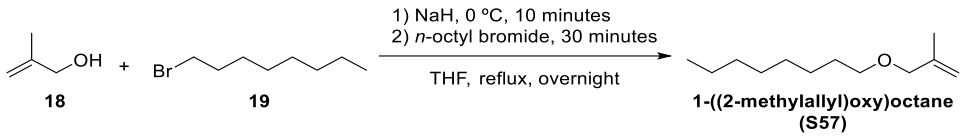

18 **19** **1-((2-methylallyl)oxy)octane (S57)**

Scheme 48. Synthetic route towards substrate **S57**.

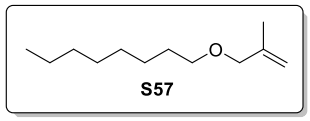

S57

Sodium hydride (0.676 mg, 16.9 mmol) was added to a solution of 2-methylprop-2-en-1-ol (**18**) (1.45 mL, 16.9 mmol) in dry THF under an atmosphere of nitrogen at 0 °C. The mixture was stirred at 0 °C for 10 minutes before adding *n*-octyl bromide dropwise (**19**) (2.0 mL, 11.3 mmol). The reaction was stirred at room temperature for 30 minutes and was refluxed overnight (68 °C). The reaction was quenched by the addition of saturated ammonium chloride solution (15 mL). The mixture was then extracted with diethyl ether (3 x 25 mL) and the organic phase was washed with water (25 mL), brine (25 mL) and dried over Na_2SO_4 and concentrated in vacuo. The crude was purified by flash column chromatography over SiO_2 using pentane/Et_2O (99.5:0.5) as eluent to give the desired product **S57** as a colourless oil (803 mg, 37% isolated yield). Spectroscopic data for this compound were in agreement with the reported ones.[204] ^{1}H NMR (400 MHz, $CDCl_3$) δ 4.95 (m, 1H), 4.87 (m, 1H), 3.89 – 3.84 (m, 2H), 3.38 (t, J = 6.7 Hz, 2H), 1.73 (dd, J = 1.5, 0.9 Hz, 3H), 1.64 – 1.52 (m, 2H), 1.39 – 1.20 (m, 10H), 0.94 – 0.83 (m, 3H).

[204] a) Smith, C. M.; Boden, R. M. Preparation of aldehydes for fragrances. US20080319088, **2008**. b) Crivello, J. V.; Kong, S. *J. Org. Chem.* **1998**, *63*, 6745-6748.

2.5.4.3. Synthesis of the substrate 1-isopropyl-3-(prop-1-en-2-yl)benzene (S58)

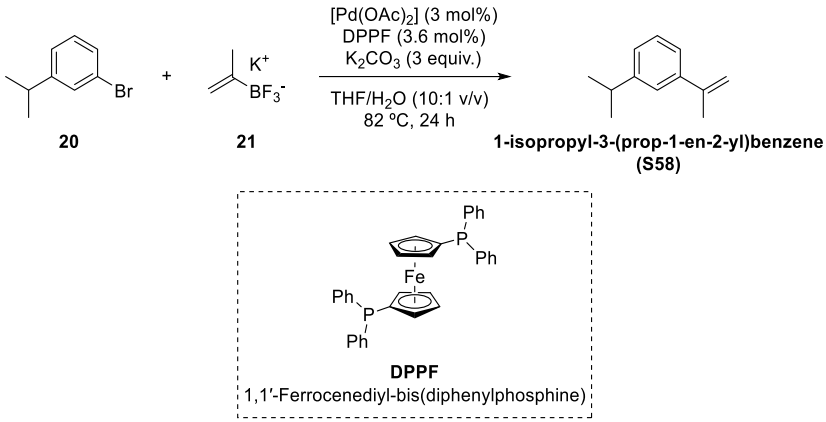

Scheme 49. Synthetic route towards substrate **S58**.

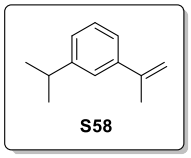

A 10 mL flame-dried three-neck-round bottom flask was charged with $[Pd(OAc)_2]$ (3.4 mg, 0.015 mmol, 3 mol%), 1,1′-bis(di-*tert*-butylphosphino)ferrocene (DPPF) (10.3 mg, 0.018 mmol, 3.6 mol%), potassium trifluoro(prop-1-en-2-yl)borate (**21**) (189 mg, 1.25 mmol), and K_2CO_3 (209 mg, 1.5 mmol). A dried dimroth condenser was joined to the flask and 3 cycles of vacuum-nitrogen were performed to the system. THF (5 mL), H_2O (0.5 mL), and 3-bromocumene (**20**) (79 µL, 0.5 mmol) were added. The mixture was refluxed at 82 ºC for 24 hours. After, the reaction mixture was allowed to reach room temperature, quenched by adding 1N HCl (10 ml) and extracted with DCM (3 x 10 mL). The combined organic phases were washed with H_2O (10 mL), brine (10 mL) and dried over $NaSO_4$. The solvent was evaporated under reduced pressure and the crude was purified by flash column chromatography over SiO_2 using hexane as eluent to give the desired product **S58** (52 mg, 65% isolated yield). Spectroscopic data for this compound were in agreement with the reported ones.[205] ^{1}H NMR (400 MHz, $CDCl_3$) δ 7.34 (m, 1H), 7.33 – 7.23 (m, 2H), 7.16 (m, 1H), 5.37 (bs, 1H), 5.08 (bs, 1H), 3.09 – 2.72 (m, 1H), 2.22 – 2.13 (m, 3H), 1.29 (d, J = 0.8 Hz, 3H), 1.27 (d, J = 0.8 Hz, 3H).

[205] Paganelli, S.; Ciappa, A.; Marchetti, M.; Scrivanti, A.; Matteoli, U. *J. Mol. Catal. A: Chem.* **2006**, *247*, 138-144.

2.5.4.4. Synthesis of the substrate hex-1-yn-1-ylbenzene (S64)

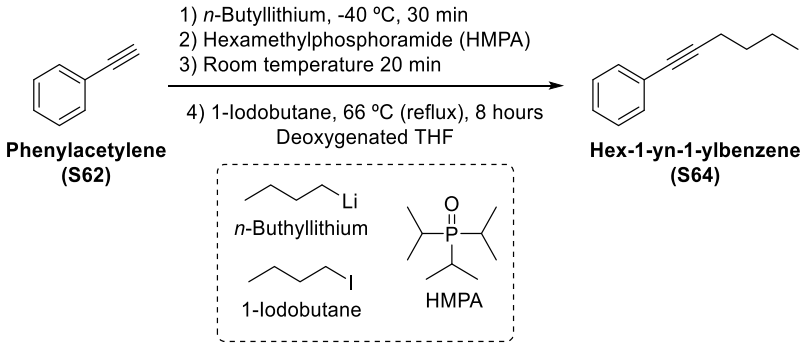

Scheme 50. Synthetic route towards substrate **S65**.

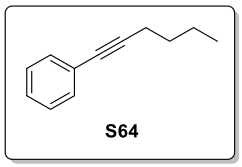

Phenylacetylene (**S63**) (2.2 mL, 19.6 mmol) in THF (30 mL) was deoxygenated by passing a stream of nitrogen for 30 minutes, then cooled down to -40 ºC, followed by dropwise addition of *n*-butyllithium (1.6 M in hexanes, 15 mL, 24.1 mmol) at -40 ºC. After stirring for 30 min, HMPA (1.03 mL, 5.73 mmol) was added. The reaction mixture was allowed to warm to room temperature for 20 minutes. To this mixture, 1-iodobutane (3.43 mL, 29.7 mmol) was added. The reaction mixture was heated to reflux (66ºC) for 8 hours. The solvent was evaporated under vacuum and the crude was purified by column chromatography over SiO_2 using cyclohexane as eluent to obtain the desired product **S64** as colourless oil (2.89 g, 93% isolated yield). Spectroscopic data for this compound were in agreement with the reported ones.[175] ^{1}H NMR (400 MHz, $CDCl_3$) δ 7.42 (d, J = 4.6 Hz, 2H), 7.30 (d, J = 5.3 Hz, 3H), 2.44 (t, J = 7.0 Hz, 3H), 1.62 (m, 2H), 1.50 (m, 2H), 0.98 (t, J = 7.2 Hz, 3H).

2.5.4.5. Synthesis of the substrate 7-vinylidenetridecane (S66)

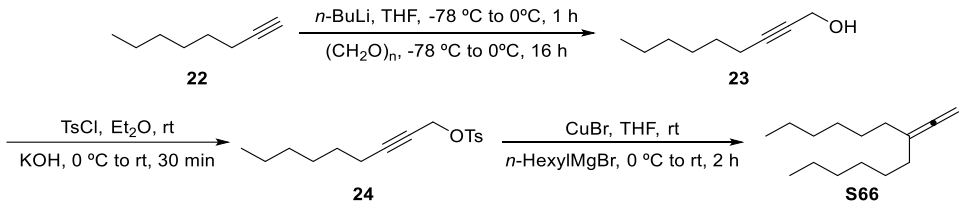

Scheme 51. Synthetic route towards substrate **S66**.

2.5.4.5.1. Synthesis of non-2-yn-1-ol (23)

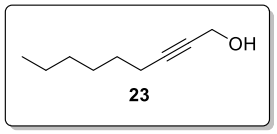

A mixture of oct-1-yne (**22**) (4.5 mL, 30.50 mmol) and THF (24.4 mL) was stirred and cooled to –78 °C. To the stirred solution, *n*-BuLi (1.6 M in hexane, 23.3 mL, 37.20 mmol) was added dropwise. The reaction

mixture was allowed to warm up to 0 °C and was stirred for 1 h. The reaction mixture was cooled down again to –78 °C and added *via* cannula over paraformaldehyde (1.1 g, 36.60 mmol). The reaction mixture was allowed to reach room temperature and stirred for 16 hours, quenched by adding a saturated aqueous solution of NH_4Cl (18.3 mL) and extracted with Et_2O (3 x 16 mL). The combined organic phases were washed with brine (16 mL), dried over $MgSO_4$ and the solvent was evaporated under reduced pressure. After purification by column chromatography over SiO_2 using DCM as eluent, non-2-yl-1-ol (**23**) was obtained as a colorless oil (4.2 g, 98% yield). Spectroscopic data for this compound were in agreement with the reported ones.[206] ^{1}H NMR (500 MHz, $CDCl_3$) δ 4.24 (bs, 2H), 2.19 (tt, *J* = 10.7, 2.2 Hz, 2H), 1.73 (bs, 1H), 1.52–1.46 (m, 2H), 1.40–1.23 (m, 6H), 0.88 (t, *J* = 7.0 Hz, 3H) ppm.^{13}C{^{1}H} NMR (126 MHz, $CDCl_3$) δ 86.8, 78.4, 51.5, 31.5, 28.70, 28.67, 22.7, 18.9, 14.2 ppm.

2.5.4.5.2. Synthesis of 1-(4-methylbenzenesulfonate)-2-nonyn-1-ol (24)

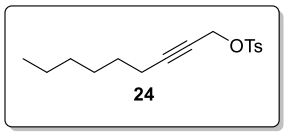

To a stirred solution of non-2-yl-1-ol (**23**) (4.4 g, 31.40 mmol) in Et_2O (50.2 mL) *p*-toluenesulfonyl chloride (6.6 g, 34.50 mmol) was added and the reaction mixture was cooled down to 0 °C. Then, freshly grounded KOH (8.8 g, 158.00 mmol) was added in small portions over ten minutes. The resulting mixture was allowed to reach room temperature and stirred for 30 minutes, quenched by pouring the crude mixture into iced H_2O (8 mL). The aqueous phase was extracted with Et_2O (3 x 20 mL) and the combined organic phases were washed with brine (30 mL), dried over $MgSO_4$ and solvent was evaporated under reduced pressure. After purification by column chromatography over SiO_2 using Cy/AcOEt 97:3, 1-(4-methylbenzenesulfonate)-2-nonyn-1-ol (**24**) was obtained as a yellowish oil (6.1 g, 66% yield). Spectroscopic data for this compound were in agreement with the reported ones.[176] ^{1}H NMR (400 MHz $CDCl_3$) δ 7.81 (d, *J* = 8.3 Hz, 2H), 7.33 (d, *J* = 8.0 Hz, 2H), 4.70 (t, *J* = 2.2 Hz, 2H), 2.44 (s, 3H), 2.05 (tt, *J* = 7.1, 2.2 Hz, 2H), 1.39–1.21 (m, 8H), 0.88 (t, *J* = 7.0 Hz, 3H) ppm.^{13}C{^{1}H} NMR (101 MHz, $CDCl_3$) δ 144.9, 133.6, 129.8, 128.3, 90.8, 71.9, 58.9, 31.4, 28.6, 28.2, 22.6, 21.8, 18.8, 14.2 ppm.

2.5.4.5.3. Synthesis of 7-vinylidenetridecane (S66)

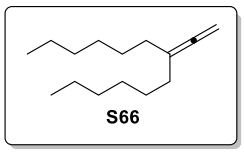

A mixture of CuBr (129 mg, 0.90 mmol), 1-(4-methylbenzenesulfonate)-2-nonyn-1-ol (**24**) (2.6 g, 9.00 mol) in THF (18 mL) was cooled down to 0 °C. *n*-Hexylmagnesium bromide (11.3 mL, 1 M in THF, 11.30 mmol) was added dropwise. The reaction mixture was allowed to reach room temperature and stirred for 2 h, quenched by adding a sat. solution of NH_4Cl (9.5 mL) and the aqueous layer was extracted

[206] Yamamoto, H.; Nishiyama, M.; Imagawa, H.; Nishizawa, M. *Tetrahedron Lett.* **2006**, *47*, 8369-8373.

with Et_2O (3 x 6 mL). The combined organic phases were washed with brine (30 mL), dried over $MgSO_4$ and the solvent was evaporated under reduced pressure. After purification by column chromatography over SiO_2 using pentane, 7-vinylidenetridecane (**S66**) was obtained as a colourless oil (1.1 g, 56% yield). Spectroscopic data for this compound were in agreement with the reported ones.[176] ^{1}H NMR (400 MHz, $CDCl_3$) δ 4.62 (q, *J*= 3.2 Hz, 2H), 1.94–1.89 (m, 4H), 1.43–1.38 (m, 4H), 1.31–1.26 (m, 12H), 0.90–0.87 (m, 6H) ppm.^{13}C{^{1}H} NMR (101 MHz, $CDCl_3$) δ 205.9, 103.5, 75.3, 32.3, 31.9, 29.2, 27.7, 22.8, 14.2 ppm.

2.5.5. General procedure for the rhodium mediated hydroformylations

In a vial with a magnetic bar, stock solutions of bisphosphite ligands **L46**, or **L47** (1.20 mol%), BArF salt (1.56 mol%), and [Rh(κ^2*O*,*O'*-acac)$(CO)_2$] (1.0 mol%) were added. The corresponding substrate (1 mmol), dodecane (30 mol%, internal standard) and toluene/THF (97:3 v/v) were charged to provide the desired final concentration of 0.26 M.

Once the reaction mixture had been loaded, the vial vessel was then placed into one of the holes of a steel autoclave reactor (HEL Cat-24 parallel pressure multireactor) and taken out of the glove box. The autoclave was purged three times with H_2/CO (1:1) (pressure not higher than 10 bar) and finally, the autoclave was pressurized with H_2/CO (1:1) to the desired pressure (10 bar). The reaction mixture was stirred at 35, 40, 60 or 100 °C for 18 hours. The reaction was cooled, and the pressure was carefully released in a well-ventilated hood. Conversion, chemo- , regio-selectivity and yield of the products arising from hydroformylation reaction conditions were determined by GC analysis on an achiral stationary phase (HP-5) using dodecane as the internal standard. ^{1}H NMR using 1,3,5-trimethoxybenzene or dimethyl sulfone as internal standards was also used to determine the conversion, chemo-, regio-selectivity and yield.

2.5.6. Results of catalysis of the hydroformylation of oct-1-ene (S31a)

Table 25. Supramolecularly regulated hydroformylation of oct-1-ene (**S31a**)

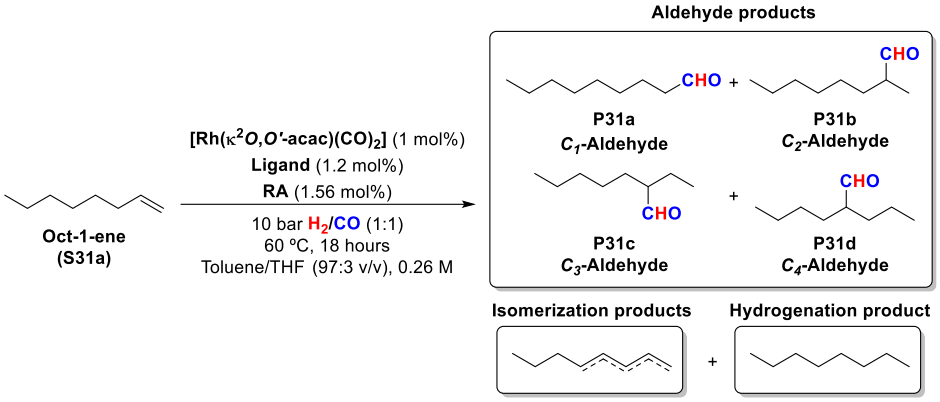

Entry	RA	Ligand	Conv. (%)	Select. (%)[a]		$C_1/C_2/C_3/C_4$ ratio (%)	$C_1/C_2/C_3/C_4$ yield (%)
				Isom.	Hydrog.		
1	None	L46	98	3	2	62:38:0:0	58:35:0:0
2	LiBArF	L46	99	2	1	61:39:0:0	59:37:0:0
3	NaBArF	L46	98	7	8	94:6:0:0	78:5:0:0
4	KBArF	L46	98	8	14	97:3:0:0	74:2:0:0
5	RbBArF	L46	98	6	10	94:6:0:0	77:5:0:0
6	CsBArF	L46	99	4	5	86:14:0:0	77:13:0:0
7	None	L47	99	2	0.3	60:38:2:0	58:37:2:0
8	LiBArF	L47	99	2	0.3	61:34:4:1	59:33:4:1
9	NaBArF	L47	99	2	0.3	61:34:4:1	59:33:4:1
10	KBArF	L47	99	2	0.5	66:30:3:1	64:29:3:1
11	RbBArF	L47	99	2	1	73:24:3:0	70:23:3:0
12	CsBArF	L47	99	2	1	75:22:3:0	72:21:3:0

The HF was performed in a parallel autoclave. Reaction conditions: [substrate] = 0.26 M; stirring rate = 800 rpm; 10 bar H_2/CO (1:1); 60 °C, 18h. Conversion was determined by GC using dodecane as an internal standard. Selectivity, ratio, and yield were determined by the area% values of the peaks in the GC chromatogram. [a] Selectivity of the isomerisation (Isom.) and hydrogenation (Hydrog.) processes.

Selected GC chromatogram and ^{1}H NMR spectrum for octenes S31a, (*E*)-S31b, (*Z*)-S31b, (*E*)-S31c, (*E*)-S31d, (*Z*)-S31d, and octenes mixture

Representative example of a GC chromatogram of the mixtures derived from oct-1-ene or its isomers under rhodium-catalysed hydroformylation reaction conditions.

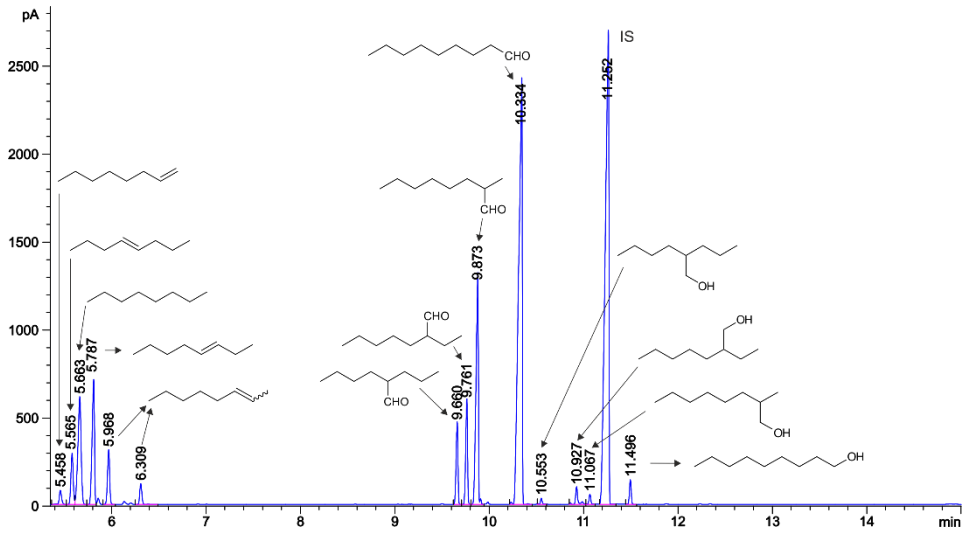

Figure 51. GC chromatogram of the mixtures derived from octenes after hydroformylation.

GC analysis conditions for hydroformylation reaction of oct-1-ene, (*Z*)-oct-2-ene, (*E*)-oct-2-ene, (*E*)-oct-3-ene, (*E*)-oct-4-ene, (*Z*)-oct-4-ene and their equimolar mixture: Conversion, chemo- and regio-selectivity in the mixtures arising from hydroformylation reaction conditions were determined by GC-FID analysis with a HP-5 column (5% phenyl methyl siloxane; 30 m x 320 µm x 0.25 µm). Flow rate: 2.3 mL/min. Temperature program: 35 °C for 5 min, then up to 150 °C at 20 °C/min and 10 min at 150 °C, then up to 320 °C at 20 °C/min and 5 min at 320 °C. Retention times: 5.46 min for oct-1-ene, 5.56 min for (*E*)-oct-4-ene, 5.66 min for octane, 5.78 min for (*E*)-oct-3-ene, 5.87 min for (*Z*)-oct-4-ene, 5.97 min for (*E*)-oct-2-ene, 6.31 min for (*Z*)-oct-2-ene, 9.66 min for 2-propylhexanal (**P31d**), 9.76 min for 2-ethylheptanal (**P31c**), 9.87 min for 2-methyloctanal (**P31b**), 10.33 min for nonanal (**P45a**), 10.55 min for (2-propyl-hexan-1-ol), 10.93 min for (2-ethyl-heptan-1-ol), 10.07 min for (2-methyl-octan-1-ol), 11.25 min for the IS (dodecane), 11.50 min for 3a (nonan-1-ol).

Representative example of an ^{1}H NMR spectrum of the mixtures derived from oct-1-ene or its isomers under rhodium-catalysed hydroformylation reaction conditions.

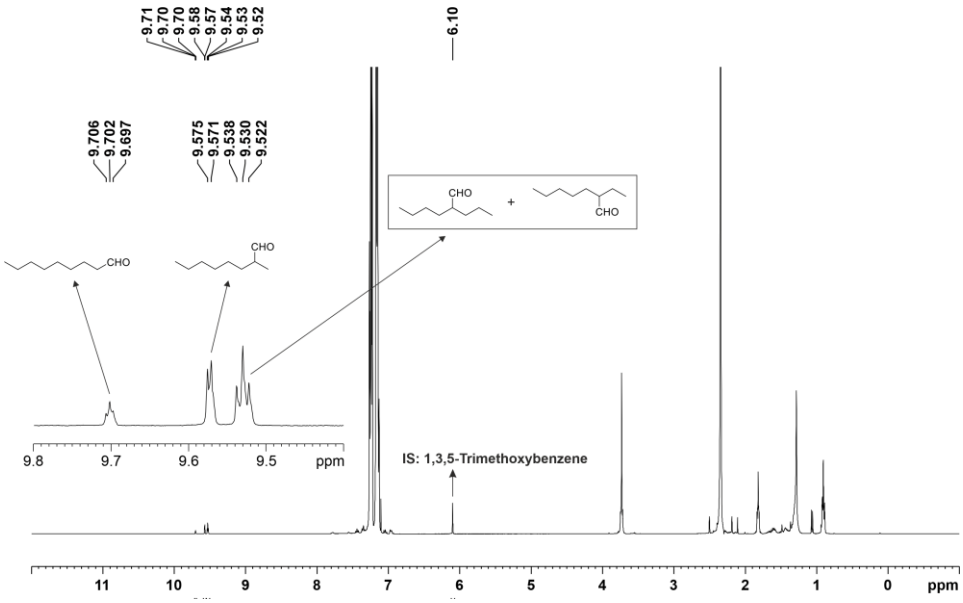

Figure 52. ^{1}H NMR of the mixtures derived from octenes after hydroformylation.

2.5.7. Results of catalysis of the hydroformylation of hept-1-ene (S46a)

Table 26. Supramolecularly regulated hydroformylation of hept-1-ene (**S46a**).

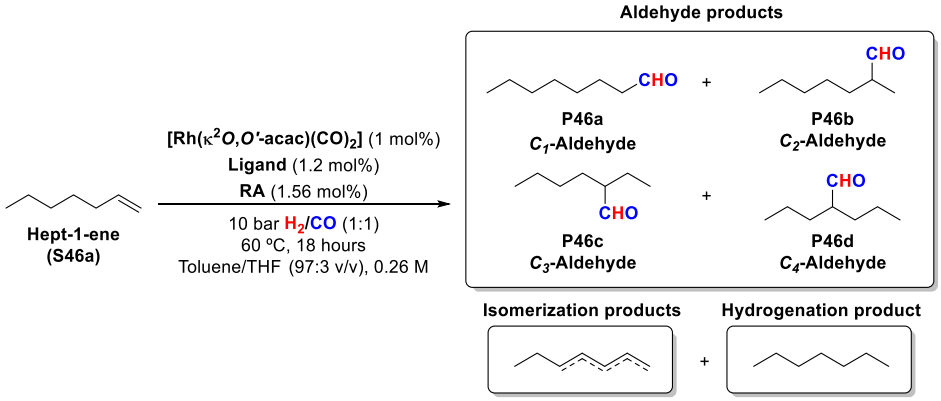

Entry	RA	Ligand	Conv. (%)	Select. (%)[a]		$C_1/C_2/C_3/C_4$ ratio (%)	$C_1/C_2/C_3/C_4$ yield (%)
				Isom.	Hydrog.		
1	**None**	**L46**	99	0	0.3	62:33:4:1	61:33:4:1
2	**LiBArF**	**L46**	99	0	0.3	57:35:6:2	56:35:6:2
3	**NaBArF**	**L46**	99	3	2	93:6:1:0	87:6:1:0
4	**KBArF**	**L46**	99	5	4	92:6:2:0	82:5:2:0
5	**RbBArF**	**L46**	99	1	2	81:13:5:1	78:12:5:1
6	**CsBArF**	**L46**	99	0	1	71:20:7:2	70:20:7:2

The HF was performed in a parallel autoclave. Reaction conditions: [substrate] = 0.26 M; stirring rate = 800 rpm; 10 bar H_2/CO (1:1); 60 °C, 18h. Conversion was determined by GC using dodecane as an internal standard. Selectivity, ratio, and yield were determined by the area% values of the peaks in the GC chromatogram. [a] Selectivity of the isomerisation (Isom.) and hydrogenation (Hydrog.) processes.

Selected GC chromatogram and ^{1}H NMR spectrum for hept-1-ene (S46a) and heptenes mixture

Representative example of a GC chromatogram of the mixtures derived from hept-1-ene under rhodium-catalysed hydroformylation reaction conditions.

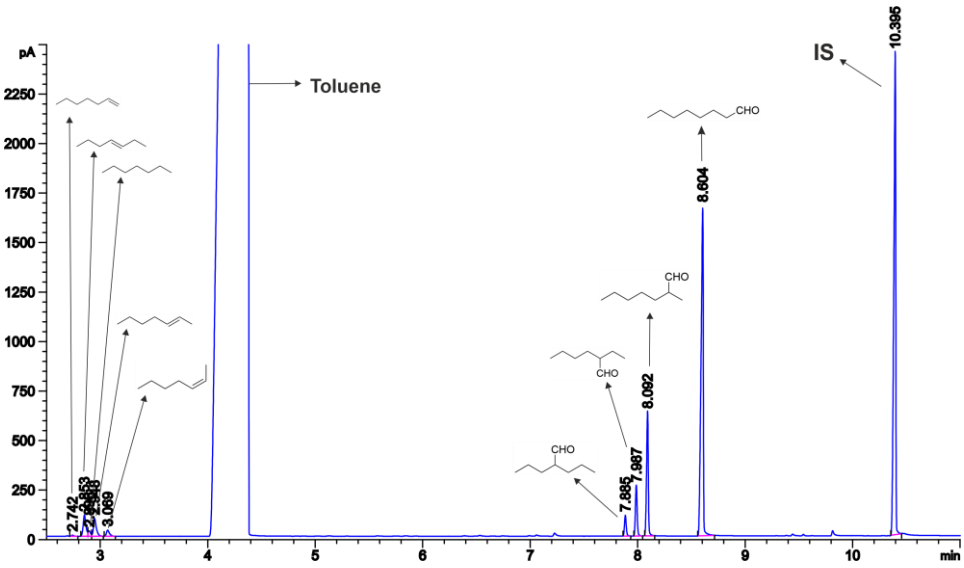

Figure 53. GC chromatogram of the mixtures derived from hept-1-ene after hydroformylation.

GC analysis conditions for hydroformylation reaction of hept-1-ene and the mixture of hept-1-ene, (*Z*)-hept-2-ene, (*E*)-hept-2-ene, (*E*)-hept-3-ene: Conversion, chemo- and regio-selectivity in the mixtures arising from hydroformylation reaction conditions were determined by GC-FID analysis with a HP-5 column (5% phenyl methyl siloxane; 30 m x 320 µm x 0.25 µm). Flow rate: 2.6 mL/min. Temperature program: 40 °C for 5 min, then up to 150 °C at 20 °C/min and 10 min at 150 °C, then up to 275 °C at 20 °C/min and 5 min at 275 °C. Retention times: 2.74 min for hept-1-ene, 2.06 min for (*E*)-hept-3-ene, 2.89 min for heptane, 2.95 min for (*E*)-hept-2-ene, 3.07 min for (*Z*)-hept-2-ene, 7.88 min for 2-propylpentanal (**P46d**), 7.98 min for 2-ethylhexanal (**P46c**), 8.09 min for 2-methylheptanal (**P46b**), 8.60 min for octanal (**P46a**), 10.39 min for the IS (dodecane).

Representative example of an ^{1}H NMR spectrum of the mixtures derived from hept-1-ene under rhodium-catalysed hydroformylation reaction conditions.

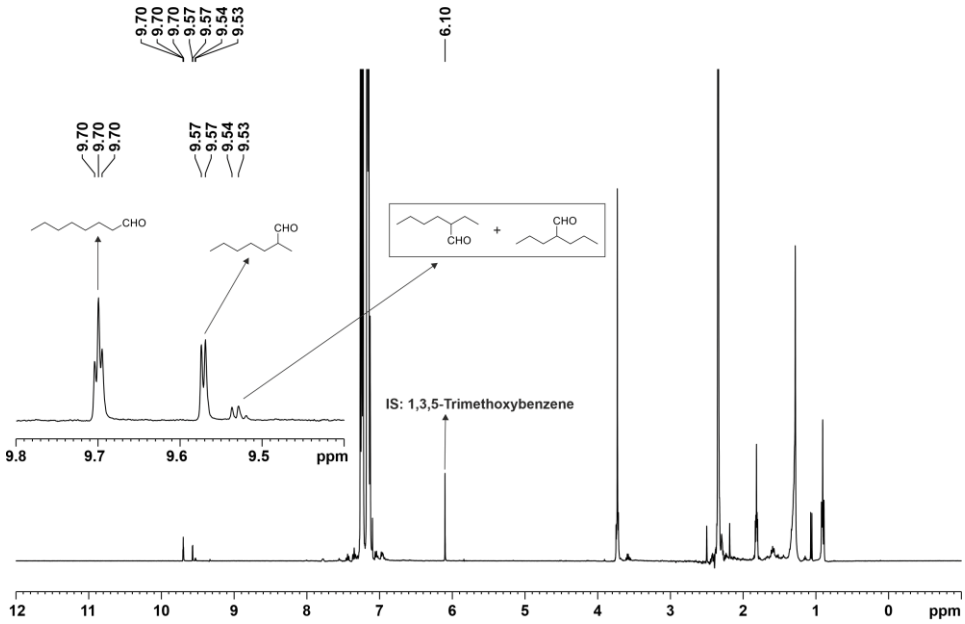

Figure 54. ^{1}H NMR of the mixtures derived from hept-1-ene after hydroformylation.

2.5.8. Results of catalysis of the hydroformylation of hex-1-ene (S47a)

Table 27. Supramolecularly regulated hydroformylation of hex-1-ene (**S57a**).

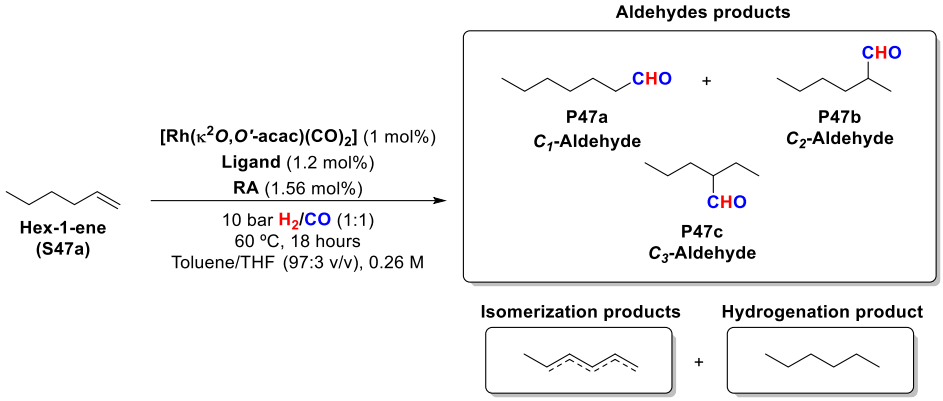

Entry	RA	Ligand	Conv. (%)	Select. (%)[a]		$C_1/C_2/C_3$ ratio (%)	$C_1/C_2/C_3$ yield (%)
				Isom.	Hydrog.		
1	None	L46	99	1	1	61:37:2	59:36:2
2	LiBArF	L46	99	1	1	61:36:3	59:35:3
3	NaBArF	L46	99	6	1	98:2:0	90:2:0
4	KBArF	L46	99	14	2	98:2:0	81:2:0
5	RbBArF	L46	99	11	2	93:6:1	80:5:1
6	CsBArF	L46	99	4	1	85:12:3	80:11:3

The HF was performed in a parallel autoclave. Reaction conditions: [substrate] = 0.26 M; stirring rate = 800 rpm; 10 bar H_2/CO (1:1); 60 °C, 18h. Conversion was determined by GC using dodecane as an internal standard. Selectivity, ratio, and yield were determined by the area% values of the peaks in the GC chromatogram. [a] Selectivity of the isomerisation (Isom.) and hydrogenation (Hydrog.) processes.

Selected GC chromatogram and ^{1}H NMR spectrum for hex-1-ene (S47a) and hexenes mixture.

Representative example of a GC chromatogram of the mixtures derived from hex-1-ene under rhodium-catalysed hydroformylation reaction conditions.

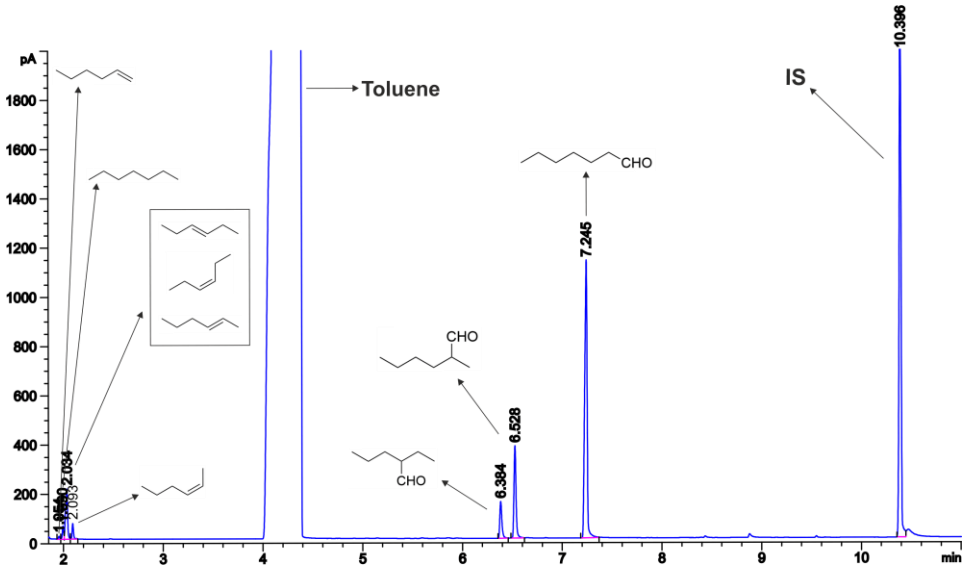

Figure 55. GC chromatogram of the mixtures derived from hex-1-ene after hydroformylation.

GC analysis conditions for hydroformylation reaction of hex-1-ene and the mixtures of hex-1-ene, (*Z*)-hex-2-ene, (*E*)-hex-2-ene, (*E*)-hex-3-ene, (*Z*)-hex-3-ene: Conversion, chemo- and regio-selectivity in the mixtures arising from hydroformylation reaction conditions were determined by GC-FID analysis with a HP-5 column (5% phenyl methyl siloxane; 30 m x 320 µm x 0.25 µm). Flow rate: 2.6 mL/min. Temperature program: 40 °C for 5 min, then up to 150 °C at 20 °C/min and 10 min at 150 °C, then up to 275 °C at 20 °C/min and 5 min at 275 °C. Retention times: 1.95 min for hex-1-ene, 1.99 min for hexane, 2.03 min for (*E*)-hex-2-ene, (*Z*)-hex-3-ene, (*E*)-hex-3-ene, 2.09 min for (*Z*)-hex-2-ene), 6.38 min for 2-ethylpentanal (**P47c**), 6.52 min for 2-methylhexanal (**P47b**), 7.24 min for heptanal (**P47a**), 10.39 min for the IS (dodecane).

Representative example of an ^{1}H NMR spectrum of the mixtures derived from hex-1-ene under rhodium-catalysed hydroformylation reaction conditions.

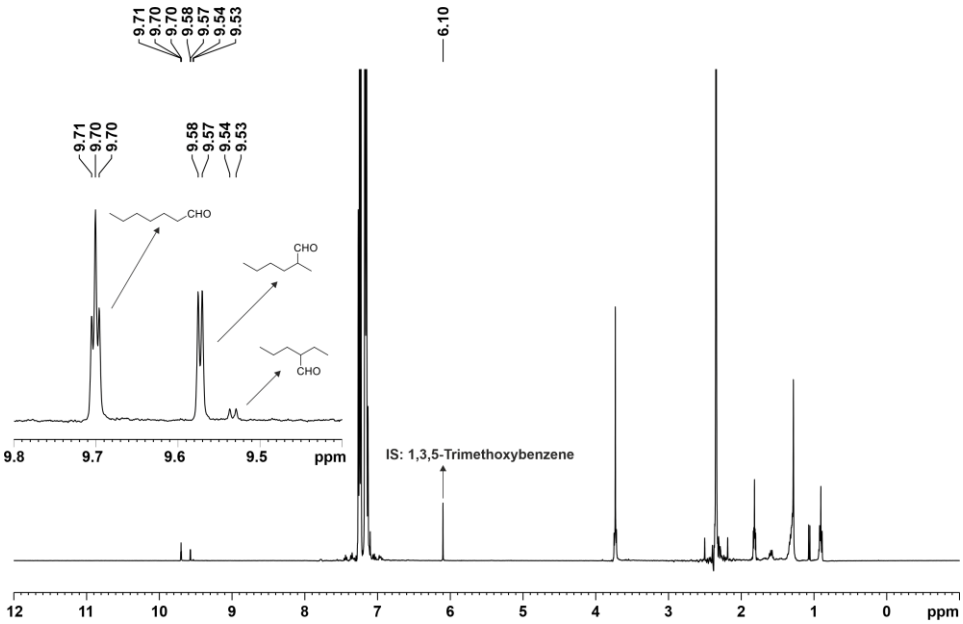

Figure 56. ^{1}H NMR of the mixtures derived from hex-1-ene after hydroformylation.

2.5.9. Results of catalysis of the hydroformylation of undec-1-ene (S48)

Table 28. Supramolecularly regulated hydroformylation of undec-1-ene (**S48**).

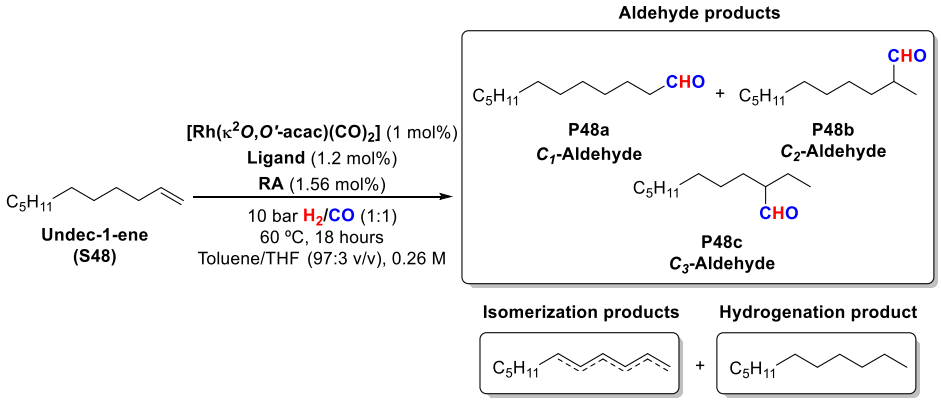

Entry	RA	Ligand	Conv. (%)	Select. (%)[a]		$C_1/C_2/C_3$ ratio (%)	$C_1/C_2/C_3$ yield (%)
				Isom.	Hydrog.		
1	None	L46	95	5	2	62:35:3	55:31:3
2	LiBArF	L46	95	5	1	61:35:4	54:31:4
3	NaBArF	L46	95	8	6	95:5:0	78:4:0
4	KBArF	L46	96	15	10	96:3:1	69:2:1
5	RbBArF	L46	94	9	6	90:8:2	72:6:2
6	CsBArF	L46	96	5	1	83:14:3	75:13:3

The HF was performed in a parallel autoclave. Reaction conditions: [substrate] = 0.26 M; stirring rate = 800 rpm; 10 bar H_2/CO (1:1); 60 °C, 18h. Conversion was determined by ^{1}H NMR using 1,3,5-trimethoxybenzene as internal standard. Selectivity, ratio, and yield were determined by the area% values of the peaks in the GC chromatogram. [a] Selectivity of the isomerisation (Isom.) and hydrogenation (Hydrog.) processes.

Selected GC chromatogram and ^{1}H NMR spectrum for undec-1-ene (S48)

Representative example of a GC chromatogram of the mixtures derived from undec-1-ene under rhodium-catalysed hydroformylation reaction conditions.

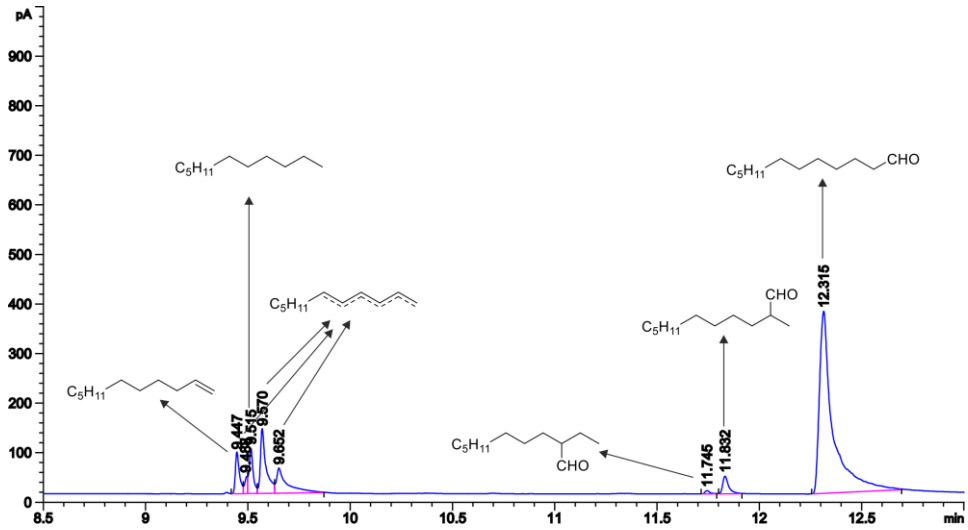

Figure 57. GC chromatogram of the mixtures derived from undec-1-ene after hydroformylation.

GC analysis conditions for hydroformylation reaction of undec-1-ene: Chemo- and regio-selectivity in the mixtures arising from hydroformylation reaction conditions were determined by GC-FID analysis with a HP-5 column (5% phenyl methyl siloxane; 30 m x 320 μm x 0.25 μm). Flow rate: 2.3 mL/min. Temperature program: 40 °C for 5 min, then up to 150 °C at 20 °C/min and 10 min at 150 °C, then up to 320 °C at 20 °C/min and 5 min at 320 °C. Retention times: 9.45 min for undec-1-ene, 9.51 min for undecane 9.48, 9,57 and 9.65 min for undecane isomers, 11.74 min for 2-ethyldecanal (**P48c**), 11.83 min for 2-methylundecanal (**P48b**), 12.31 min for dodecanal (**P48a**).

Representative example of an ^{1}H NMR spectrum of the mixtures derived from undec-1-ene under rhodium-catalysed hydroformylation reaction conditions.

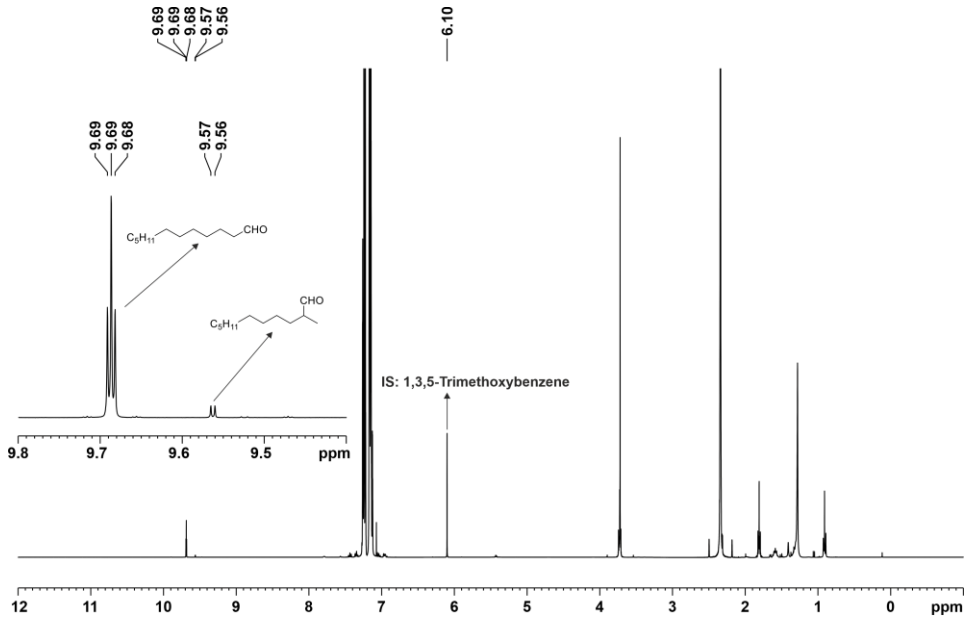

Figure 58. ^{1}H NMR of the mixtures derived from undec-1-ene after hydroformylation.

2.5.10. Results of catalysis of the hydroformylation of allyloxytrimethylsilane (S49)

Table 29. Supramolecular regulated hydroformylation of allyloxytrimethylsilane (**S49**).

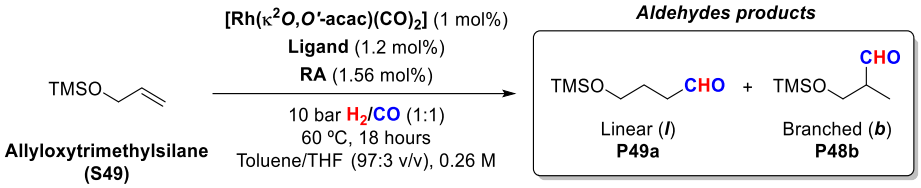

Entry	RA	Ligand	Conv. (%)	Select. (%)[a]		*l/b* ratio (%)	*l/b* yield (%)
				Isom.	Hydrog.		
1	None	L46	99	-	-	41:59	37:54
2	LiBArF	L46	99	-	-	37:63	26:44
3	NaBArF	L46	99	-	-	54:46	40:34
4	KBArF	L46	99	-	-	87:13	67:10
5	RbBArF	L46	99	-	-	69:31	40:18
6	CsBArF	L46	99	-	-	58:42	44:32
7	$EtNH_3BArF$	L46	99	-	-	41:59	32:47
8	None	L47	99	-	-	47:53	41:36
9	LiBArF	L47	99	-	-	30:70	18:41
10	NaBArF	L47	99	-	-	48:52	39:42
11	KBArF	L47	99	-	-	45:55	33:39
12	RbBArF	L47	99	-	-	44:56	36:47
13	CsBArF	L47	99	-	-	43:57	37:50
14	$EtNH_3BArF$	L47	99	-	-	42:58	34:46

The HF was performed in a parallel autoclave. Reaction conditions: [substrate] = 0.26 M; stirring rate = 800 rpm; 10 bar H_2/CO (1:1); 60 °C, 18h. Conversion, ratio, selectivity, and yield were determined by ^{1}H NMR using 1,3,5-trimethoxybenzene as internal standard. [a] Selectivity of the isomerisation (Isom.) and hydrogenation (Hydrog.) processes.

Selected ^{1}H NMR spectrum for allyloxytrimethylsilane (S49)

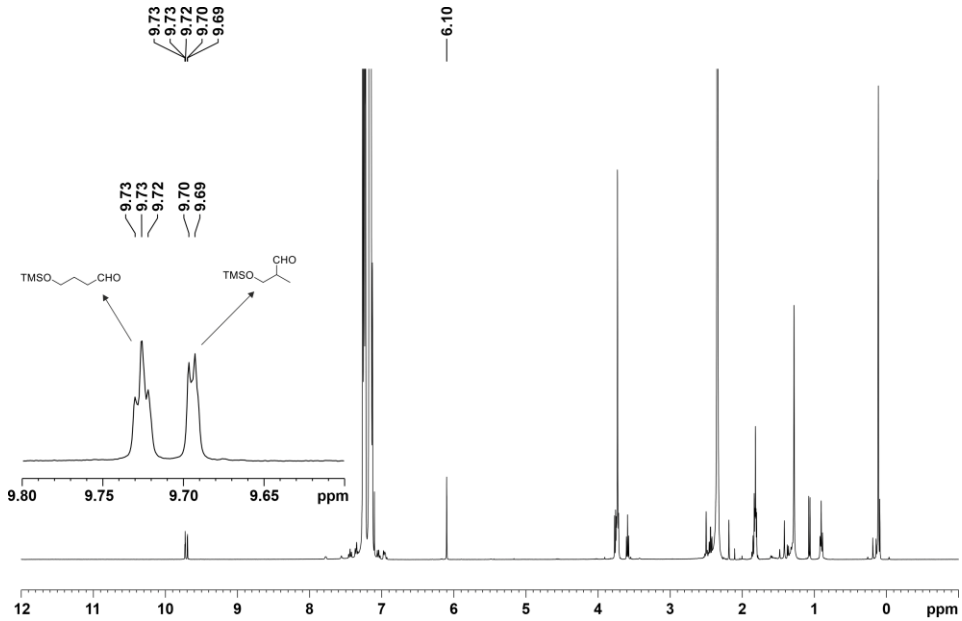

Figure 59. ^{1}H NMR of the mixtures derived from allyloxytrimethylsilane after hydroformylation.

2.5.11. Results of catalysis of the hydroformylation of 2-ethyl-2-vinyl-1,3-dioxolane (S50)

Table 30. Supramolecularly regulated hydroformylation of 2-ethyl-2-vinyl-1,3-dioxolane (**S50**).

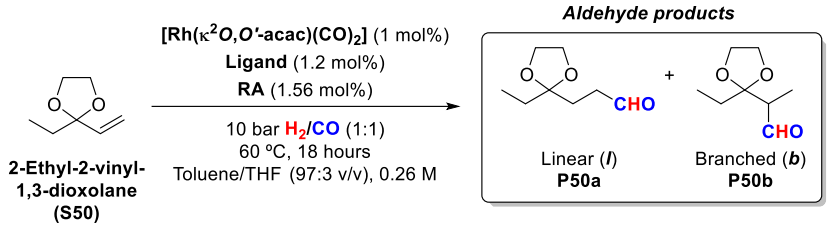

Entry	RA	Ligand	Conv. (%)	Select. (%)[a]		*l*/*b* ratio (%)	*l*/*b* NMR yield (%)
				Isom.	Hydrog.		
1	None	L46	19	-	-	76:24	7:2
2	LiBArF	L46	99	-	-	76:24	61:19
3	NaBArF	L46	67	-	-	94:6	44:3
4	KBArF	L46	84	-	-	96:4	57:3
5	RbBArF	L46	95	-	-	92:8	82:7
6	CsBArF	L46	99	-	-	87:13	68:10
7	$EtNH_3BArF$	L46	10	-	-	84:16	2:0
8	None	L47	24	-	-	74:26	6:2
9	LiBArF	L47	99	-	-	86:14	62:10
10	NaBArF	L47	99	-	-	84:16	60:11
11	KBArF	L47	99	-	-	83:17	56:11
12	RbBArF	L47	99	-	-	82:18	59:13
13	CsBArF	L47	99	-	-	82:18	59:13
14	$EtNH_3BArF$	L47	99	-	-	87:13	55:7

The HF was performed in a parallel autoclave. Reaction conditions: [substrate] = 0.26 M; stirring rate = 800 rpm; 10 bar H_2/CO (1:1); 60 °C, 18h. Conversion, ratio, selectivity, and yield were determined by ^{1}H NMR using 1,3,5-trimethoxybenzene as internal standard. [a] Selectivity of the isomerisation (Isom.) and hydrogenation (Hydrog.) processes.

Selected ^{1}H NMR spectrum for 2-ethyl-2-vinyl-1,3-dioxolane (S50)

Representative example of an ^{1}H NMR spectrum of the mixtures derived from 2-ethyl-2-vinyl-1,3-dioxolane under rhodium-catalysed hydroformylation reaction conditions.

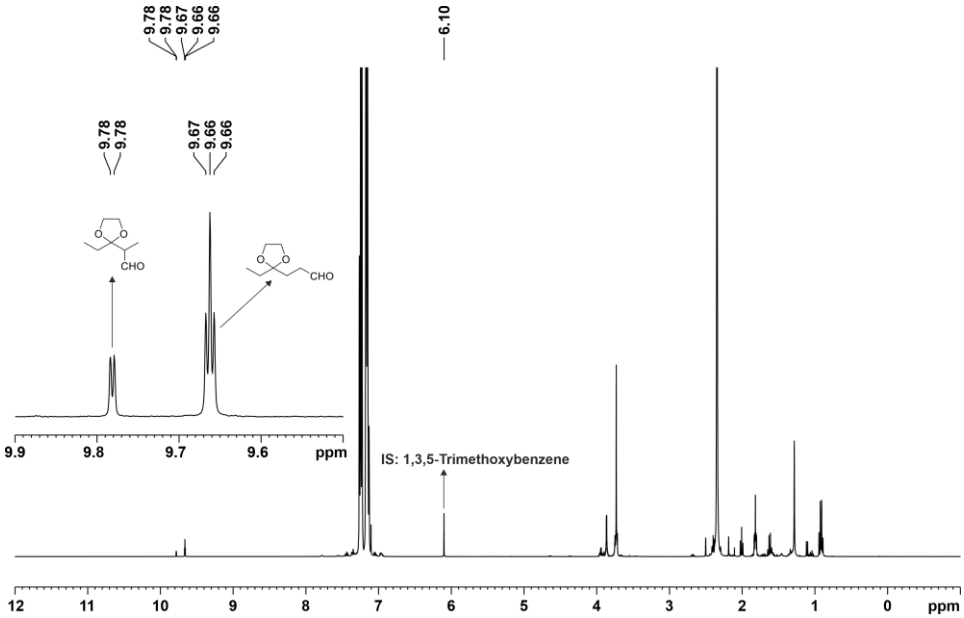

Figure 60. ^{1}H NMR of the mixtures derived from ethyl-2-vinyl-1,3-dioxolane after hydroformylation.

2.5.12. Results of catalysis of the hydroformylation of allylbenzene (S51)

Table 31. Supramolecularly regulated hydroformylation of allylbenzene (**S51**)

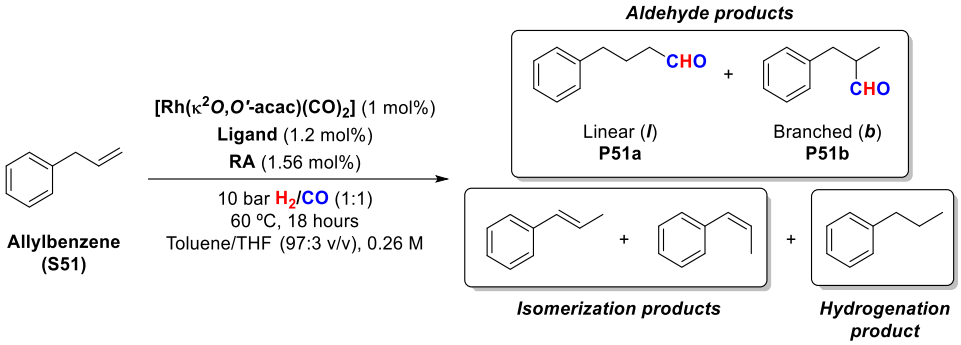

Entry	RA	Ligand	Conv. (%)	Select. (%)[a]		*l*/*b* ratio (%)	*l*/*b* yield (%)
				Isom.	Hydrog.		
1	None	L46	99	0	0	52:48	51:48
2	LiBArF	L46	98	1	0	56:44	54:43
3	NaBArF	L46	99	3	1	87:13	83:12
4	KBArF	L46	99	2	6	95:5	87:5
5	RbBArF	L46	99	4	1	93:7	87:7
6	CsBArF	L46	99	3	1	91:9	86:9

The HF was performed in a parallel autoclave. Reaction conditions: [substrate] = 0.26 M; stirring rate = 800 rpm; 10 bar H_2/CO (1:1); 60 °C, 18h. Conversion was determined by GC using dodecane as an internal standard. Selectivity, ratio, and yield were determined by the area% values of the peaks in the GC chromatogram. [a] Selectivity of the isomerisation (Isom.) and hydrogenation (Hydrog.) processes.

Selected GC chromatogram and ^{1}H NMR spectrum for allylbenzene (S51) and allylbenzenes mixture

Representative example of a GC chromatogram of the mixtures derived from allylbenzene under rhodium-catalysed hydroformylation reaction conditions.

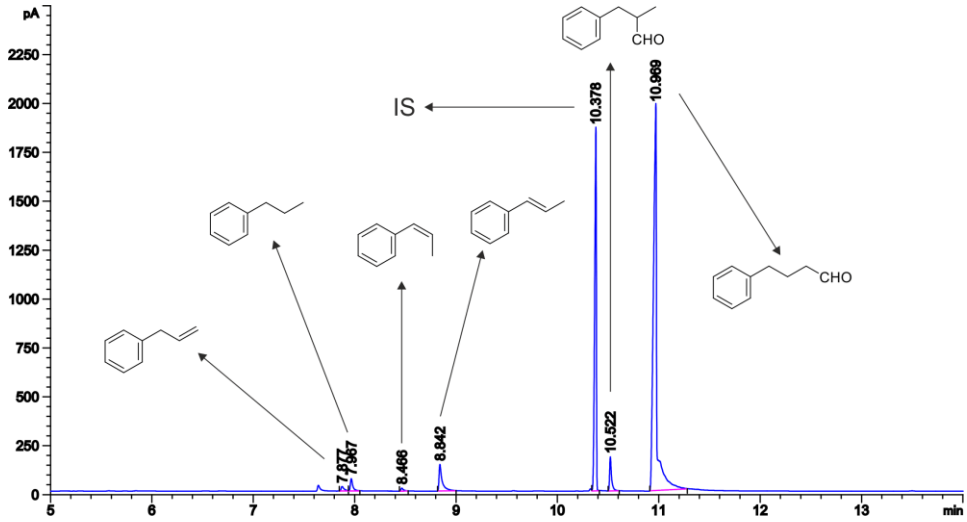

Figure 61. GC chromatogram of the mixtures derived from hept-1-ene after hydroformylation.

GC analysis conditions for hydroformylation reaction mixtures of allylbenzene: Conversion, chemo- and regio-selectivity in the mixtures arising from hydroformylation reaction conditions were determined by GC-FID analysis with a HP-5 column (5% phenyl methyl siloxane; 30 m x 320 μm x 0.25 μm). Flow rate: 2.6 mL/min. Temperature program: 40 °C for 5 min, then up to 150 °C at 20 °C/min and 10 min at 150 °C, then up to 275 °C at 20 °C/min and 5 min at 275 °C. Retention times: 7.88 min for allylbenzene, 7.97 min for propylbenzene, 8.47 min for (*Z*)-prop-1-en-1-ylbenzene, 8.84 min for (*E*)-prop-1-en-1-ylbenzene, 10.38 min for the IS (dodecane), 10.52 min for 2-methyl-3-phenylpropanal (**P51b**), 10.97 min for 4-phenylbutanal (**P51a**).

Representative example of an ^{1}H NMR spectrum of the mixtures derived from allylbenzene under rhodium-catalysed hydroformylation reaction conditions.

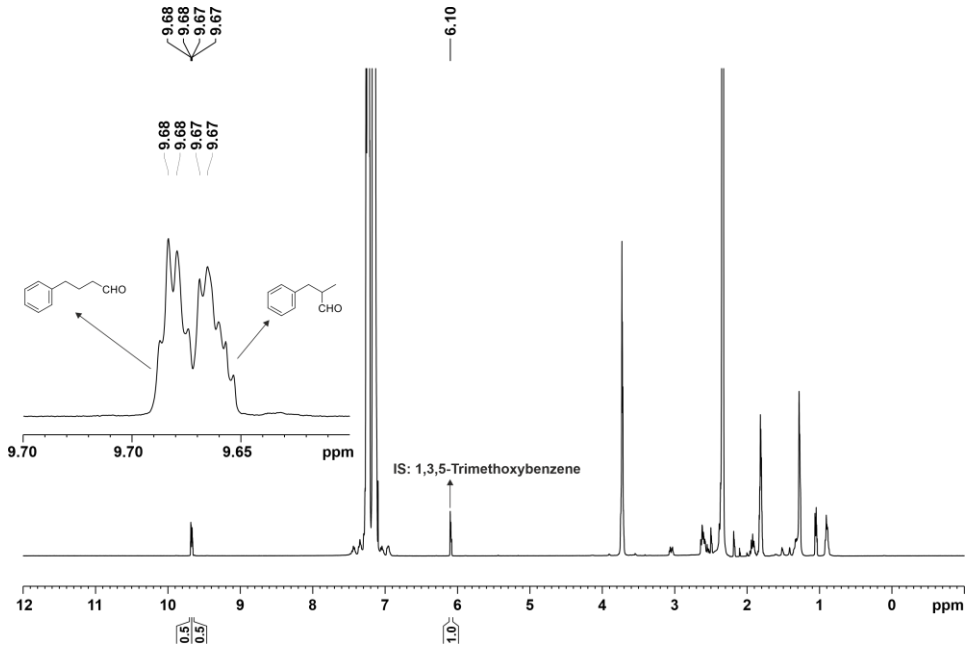

Figure 62. ^{1}H NMR of the mixtures derived from allylbenzene after hydroformylation.

2.5.13. Results of catalysis of the hydroformylation of 2,4,4-trimethylpent-1-ene (S52)

Table 32. Supramolecularly regulated hydroformylation of 2,4,4-trimethylpent-1-ene (**S52**).

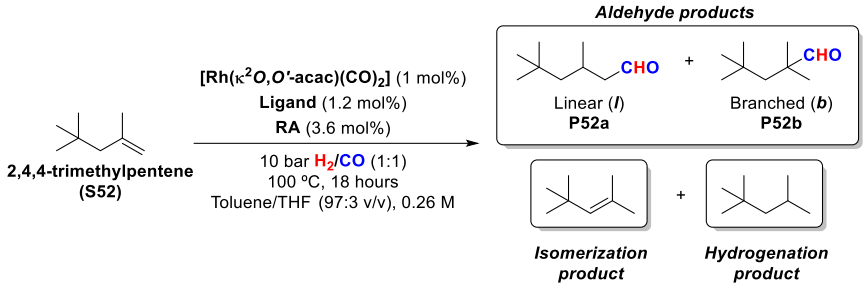

Entry	RA	Ligand	Conv. (%)	Select. (%)[a]		*l*/*b* ratio (%)	*l*/*b* yield (%)
				Isom.	Hydrog.		
1	None	L46	98	2	1	>99:<1	95:0
2	LiBArF	L46	96	1	5	>99:<1	90:0
3	NaBArF	L46	59	1	10	>99:<1	53:0
4	KBArF	L46	46	3	15	>99:<1	38:0
5	RbBArF	L46	73	1	8	>99:<1	66:0
6	CsBArF	L46	88	1	8	>99:<1	80:0

The HF was performed in a parallel autoclave. Reaction conditions: [substrate] = 0.26 M; stirring rate = 800 rpm; 10 bar H_2/CO (1:1); 60 °C, 18h. Conversion was determined by GC using dodecane as an internal standard. Selectivity, ratio, and yield were determined by the area% values of the peaks in the GC chromatogram. [a] Selectivity of the isomerisation (Isom.) and hydrogenation (Hydrog.) processes.

Selected GC chromatogram and ^{1}H NMR spectrum for 2,4,4-trimethylpent-1-ene (S52)

Representative example of a GC chromatogram of the mixtures derived from 2,4,4-trimethylpent-1-ene under rhodium-catalysed hydroformylation reaction conditions.

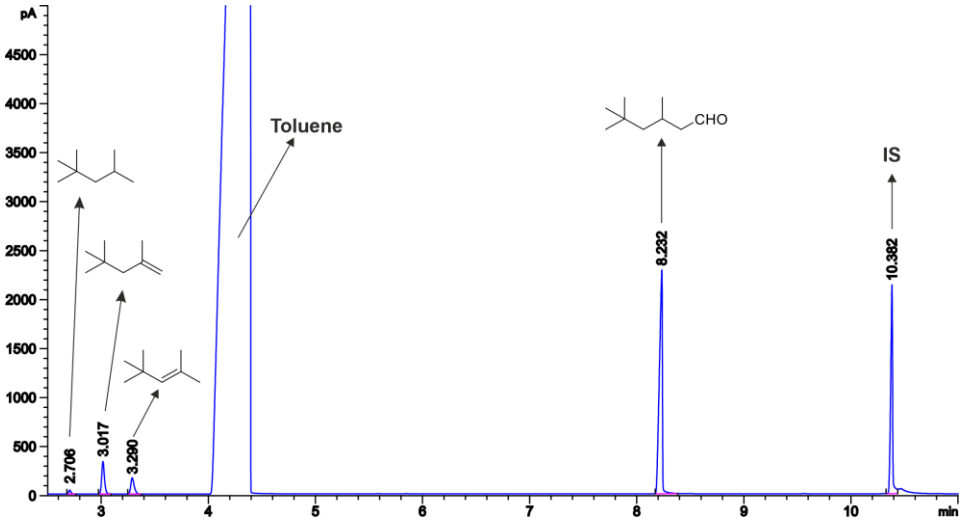

Figure 63. GC chromatogram of the mixtures derived from 2,4,4-trimethylpent-1-ene after hydroformylation.

GC analysis conditions for hydroformylation reaction mixtures of 2,4,4-trimethylpent-1-ene: Conversion, chemo- and regio-selectivity in the mixtures arising from hydroformylation reaction conditions were determined by GC-FID analysis with a HP-5 column (5% phenyl methyl siloxane; 30 m x 320 μm x 0.25 μm). Flow rate: 2.6 mL/min. Temperature program: 40 °C for 5 min, then up to 150 °C at 20 °C/min and 10 min at 150 °C, then up to 275 °C at 20 °C/min and 5 min at 275 °C. Retention times: 2.71 min for 2,4,4-trimethylpentane, 3.02 min for 2,4,4-trimethylpent-1-ene, 3.29 min for 2,4,4-trimethylpent-2-ene, 8.23 min for 3,5,5-trimethylhexanal (**S52a**), 10.38 min for the IS (dodecane).

Representative example of an ^{1}H NMR spectrum of the mixtures derived from 2,4,4-trimethylpent-1-ene under rhodium-catalysed hydroformylation reaction conditions.

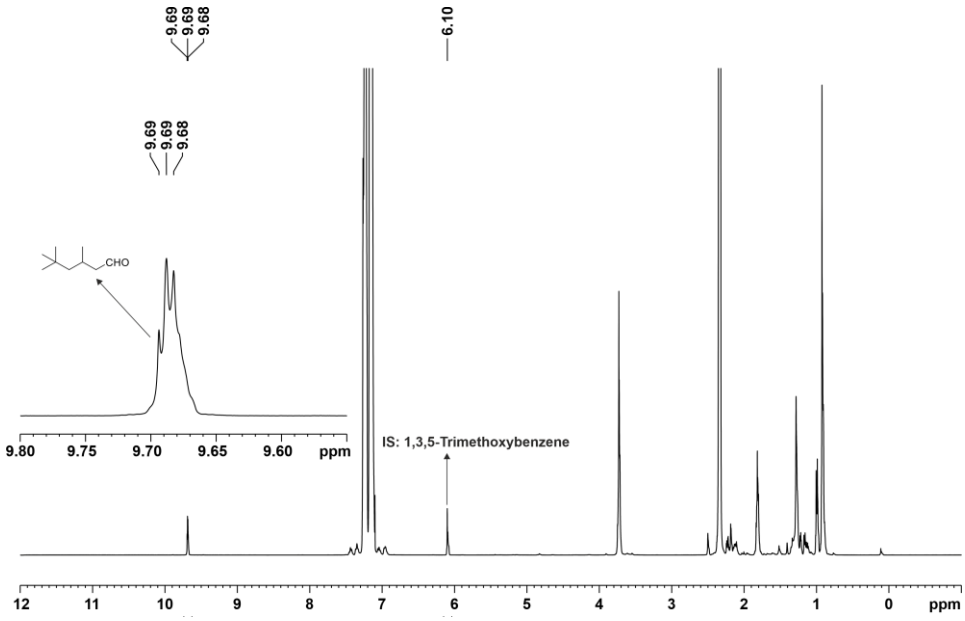

Figure 64. ^{1}H NMR of the mixtures derived from 2,4,4-trimethylpent-1-ene after hydroformylation.

2.5.14. Results of catalysis of the hydroformylation of (+)-β-citronellene (S53)

Table 33. Supramolecularly regulated hydroformylation of (+)-β-citronellene (**S53**).

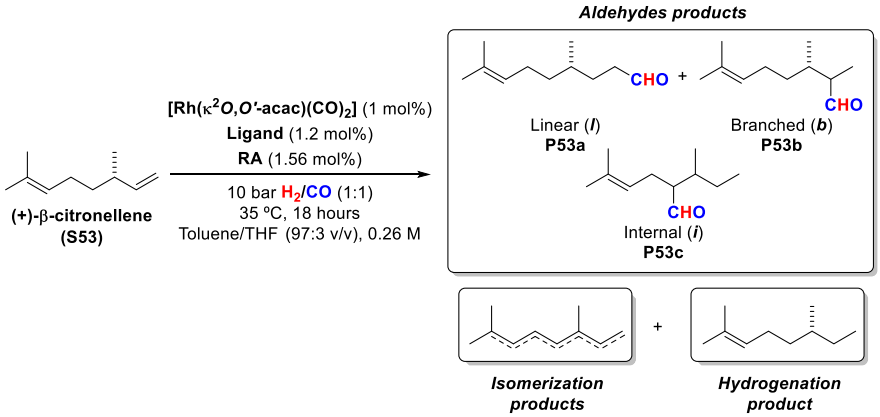

Entry	RA	Ligand	Conv. (%)	Select. (%)[a]		*l*/*b*/*i* ratio (%)	*l*/*b*/*i* yield (%)
				Isom.	Hydrog.		
1	**None**	**L46**	15	1	<1	76:14:10	11:2:1
2	**LiBArF**	**L46**	89	2	1	76:14:10	66:12:9
3	**NaBArF**	**L46**	28	<1	<1	>99:<1:0	27:0:0
4	**KBArF**	**L46**	52	6	3	>99:<1:0	47:0:0
5	**RbBArF**	**L46**	75	3	3	>99:<1:0	71:0:0
6	**CsBArF**	**L46**	88	3	2	95:3:2	79:3:2

The HF was performed in a parallel autoclave. Reaction conditions: [substrate] = 0.26 M; stirring rate = 800 rpm; 10 bar H_2/CO (1:1); 60 °C, 18h. Conversion was determined by ^{1}H NMR using 1,3,5-trimethoxybenzene as internal standard. Selectivity, ratio, and yield were determined by the area% values of the peaks in the GC chromatogram. [a] Selectivity of the isomerisation (Isom.) and hydrogenation (Hydrog.) processes.

Selected GC chromatogram and ^{1}H NMR spectrum for (+)-β-citronellene (S53)

Representative example of a GC chromatogram of the mixtures derived from (+)-β-citronellene under rhodium-catalysed hydroformylation reaction conditions.

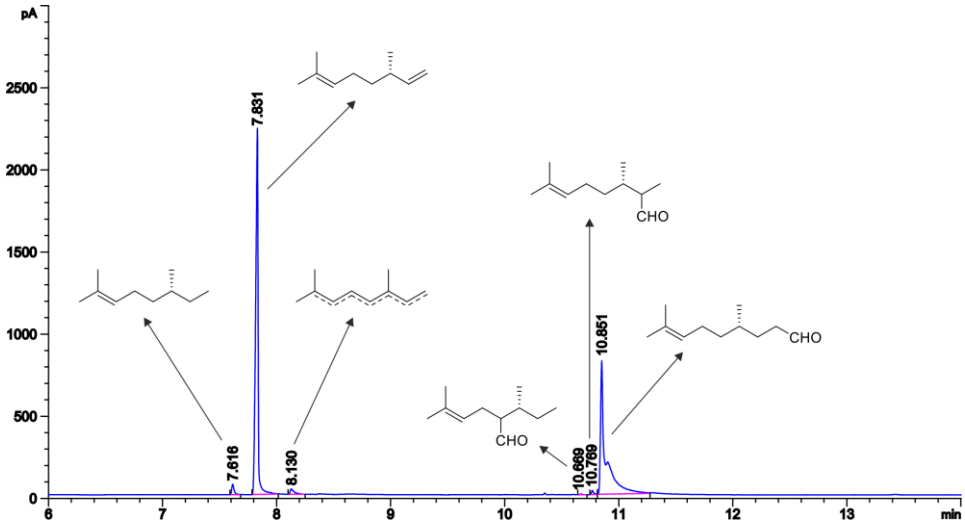

Figure 65. GC chromatogram of the mixtures derived from (+)-β-citronellene after hydroformylation.

GC analysis conditions for hydroformylation reaction mixtures of (+)-β-citronellene: Chemo- and regio-selectivity in the mixtures arising from hydroformylation reaction conditions were determined by GC-FID analysis with a HP-5 column (5% phenyl methyl siloxane; 30 m x 320 µm x 0.25 µm). Flow rate: 2.6 mL/min. Temperature program: 40 °C for 5 min, then up to 150 °C at 20 °C/min and 10 min at 150 °C, then up to 275 °C at 20 °C/min and 5 min at 275 °C. Retention times: 7.61 min for (*R*)-2,6-dimethyloct-2-ene, 7.83 min for (+)-β-citronellene, 8.13 min for (+)-β-citronellene isomers, 10.67 min for 2-((*R*)-*sec*-butyl)-5-methylhex-4-enal (**P53c**), 10.77 min for (3*S*)-2,3,7-trimethyloct-6-enal (**P53b**), 10.85 min for (*S*)-4,8-dimethylnon-7-enal (**P53a**).

Representative example of an ^{1}H NMR spectrum of the mixtures derived from (+)-β-citronellene under rhodium-catalysed hydroformylation reaction conditions.

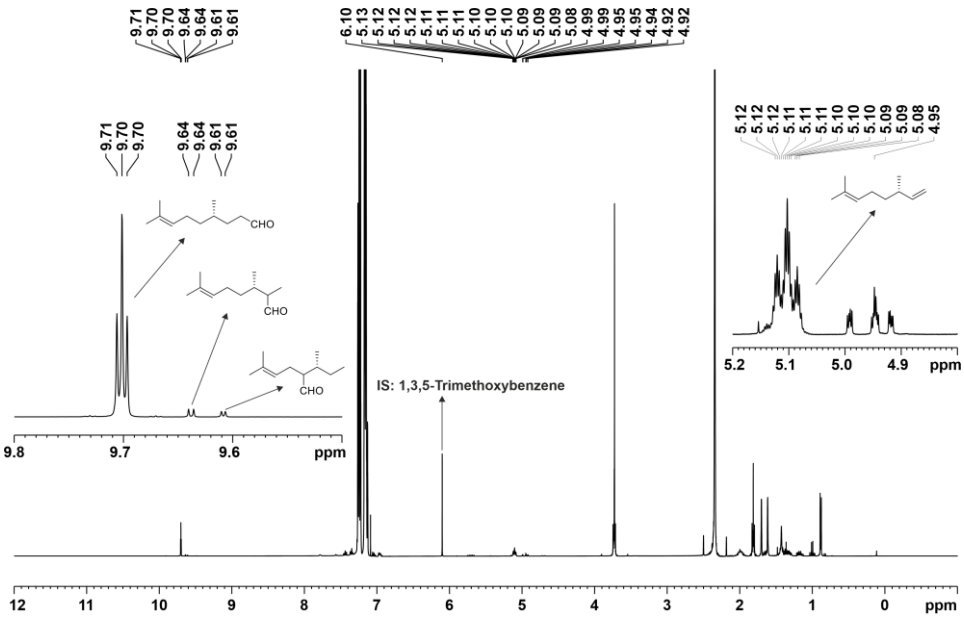

Figure 66. ^{1}H NMR of the mixtures derived from (+)-β-citronellene after hydroformylation.

2.5.15. Results of catalysis of the hydroformylation of eugenol (S54)

Table 34. Supramolecularly regulated hydroformylation of eugenol (**S54**).

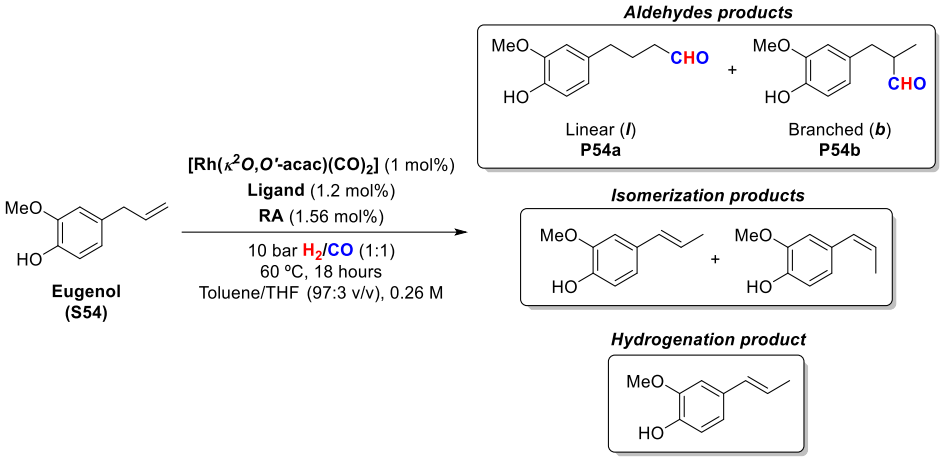

Entry	RA	Ligand	Conv. (%)	Select. (%)[a]		*l*/*b* ratio (%)	*l*/*b* yield (%)
				Isom.	Hydrog.		
1	None	L46	99	4	0	52:48	49:46
2	LiBArF	L46	99	2	0	44:56	43:54
3	NaBArF	L46	99	5	6	81:19	71:17
4	KBArF	L46	94	6	11	92:8	72:6
5	RbBArF	L46	99	4	5	91:9	82:8
6	CsBArF	L46	99	2	0	53:47	51:46

The HF was performed in a parallel autoclave. Reaction conditions: [substrate] = 0.26 M; stirring rate = 800 rpm; 10 bar H_2/CO (1:1); 60 °C, 18h. Conversion was determined by ^{1}H NMR using 1,3,5-trimethoxybenzene as internal standard. Selectivity, ratio, and yield were determined by the area% values of the peaks in the GC chromatogram. [a] Selectivity of the isomerisation (Isom.) and hydrogenation (Hydrog.) processes.

Selected GC chromatogram and ^{1}H NMR spectrum for eugenol (S54)

Representative example of a GC chromatogram of the mixtures derived from eugenol under rhodium-catalysed hydroformylation reaction conditions.

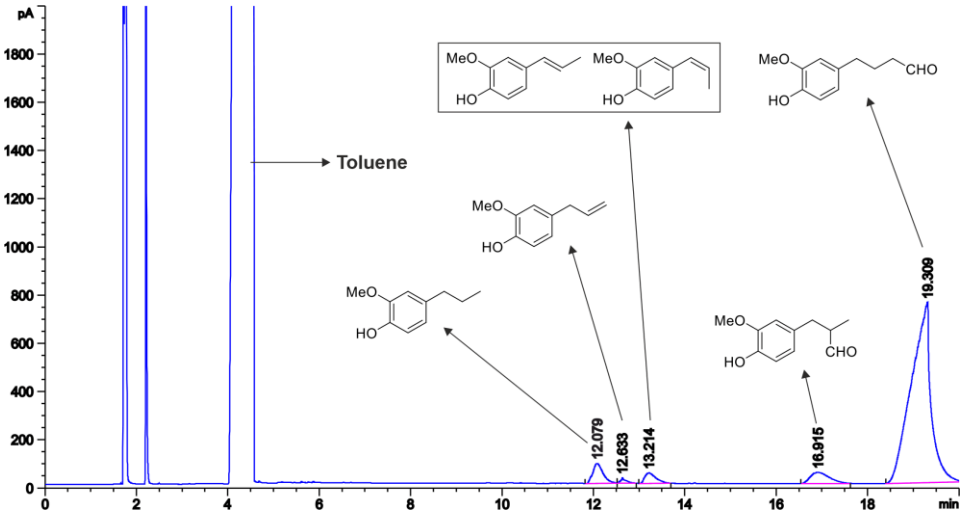

Figure 67. GC chromatogram of the mixtures derived from (+)-β-citronellene after hydroformylation.

GC analysis conditions for hydroformylation reaction mixtures of eugenol: Chemo- and regio-selectivity in the mixtures arising from hydroformylation reaction conditions were determined by GC-FID analysis with a HP-5 column (5% phenyl methyl siloxane; 30 m x 320 μm x 0.25 μm). Flow rate: 2.6 mL/min. Temperature program: 40 °C for 5 min, then up to 150 °C at 20 °C/min and 10 min at 150 °C, then up to 275 °C at 20 °C/min and 5 min at 275 °C. Retention times: 12.08 min for 2-methoxy-4-propylphenol, 12.63 min for eugenol, 13.21 min for (*E*)-2-methoxy-4-(prop-1-en-1-yl)phenol and (*Z*)-2-methoxy-4-(prop-1-en-1-yl)phenol, 16.92 min for 3-(4-hydroxy-3-methoxyphenyl)-2-methylpropanal (**P54b**), 19.31 min for 4-(4-hydroxy-3-methoxyphenyl)butanal (**P54a**).

Representative example of an ^{1}H NMR spectrum of the mixtures derived from eugenol under rhodium-catalysed hydroformylation reaction conditions.

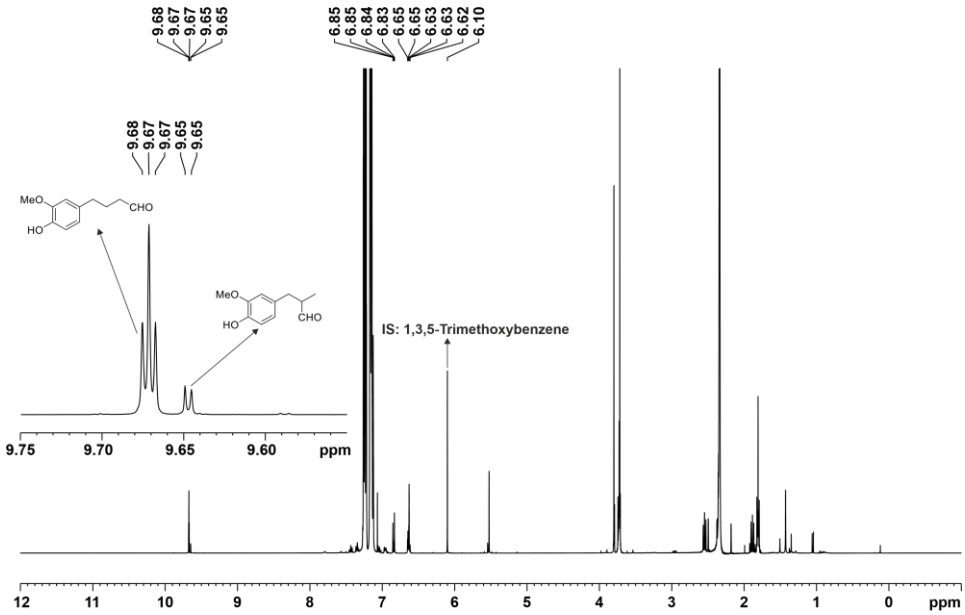

Figure 68. ^{1}H NMR of the mixtures derived from eugenol after hydroformylation.

2.5.16. Results of catalysis of the hydroformylation of (*R*)-limonene (S55)

Table 35. Supramolecularly regulated hydroformylation of (*R*)-limonene (**S55**).

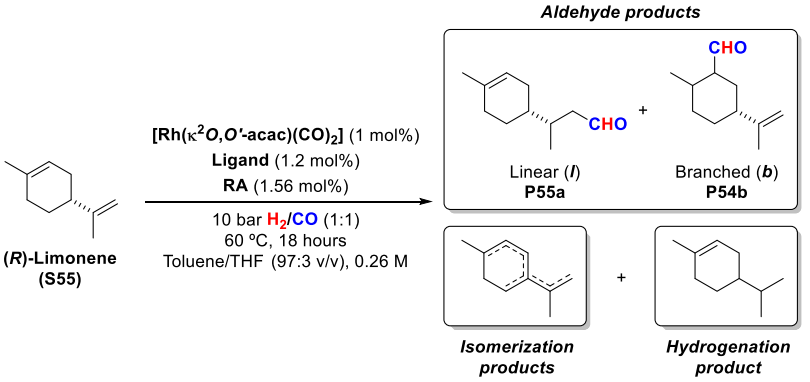

Entry	RA	Ligand	Conv. (%)	Select. (%)[a]		*l*/*b* ratio (%)	*l*/*b* yield (%)
				Isom.	Hydrog.		
1	**None**	**L46**	97	11	28	99:1	59:1
2	**LiBArF**	**L46**	78	18	0.8	99:1	63:1
3	**NaBArF**	**L46**	96	14	1	99:1	81:1
4	**KBArF**	**L46**	58	32	1.2	99:1	38:0
5	**RbBArF**	**L46**	81	20	1.2	99:1	63:1
6	**CsBArF**	**L46**	93	15	1.1	99:1	77:1

The HF was performed in a parallel autoclave. Reaction conditions: [substrate] = 0.26 M; stirring rate = 800 rpm; 10 bar H_2/CO (1:1); 60 °C, 18h. Conversion was determined by ^{1}H NMR using 1,3,5-trimethoxybenzene as internal standard. Selectivity, ratio, and yield were determined by the area% values of the peaks in the GC chromatogram. [a] Selectivity of the isomerisation (Isom.) and hydrogenation (Hydrog.) processes.

Selected GC chromatogram and ^{1}H NMR spectrum for (*R*)-limonene (S55)

Representative example of a GC chromatogram of the mixtures derived from (*R*)-limonene under rhodium-catalysed hydroformylation reaction conditions.

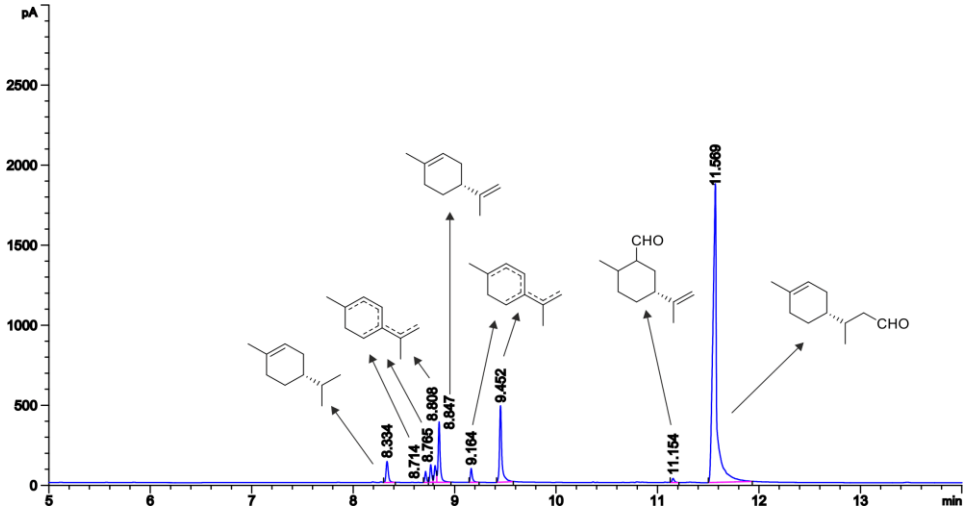

Figure 69. GC chromatogram of the mixtures derived from (*R*)-limonene after hydroformylation.

GC analysis conditions for hydroformylation reaction mixtures of (*R*)-limonene: Chemo- and regio-selectivity in the mixtures arising from hydroformylation reaction conditions were determined by GC-FID analysis with a HP-5 column (5% phenyl methyl siloxane; 30 m x 320 µm x 0.25 µm). Flow rate: 2.6 mL/min. Temperature program: 40 °C for 5 min, then up to 150 °C at 20 °C/min and 10 min at 150 °C, then up to 275 °C at 20 °C/min and 5 min at 275 °C. Retention times: 8.33 min for (*R*)-4-isopropyl-1-methylcyclohex-1-ene, 8.71, 8.77, 8.01, 9.16 and 9.45 min for (*R*)-limonene isomers, 8.85 min for (*R*)-limonene, 11.15 min for (*R*)-2-methyl-5-(prop-1-en-2-yl)cyclohex-1-ene-1-carbaldehyde (**P55b**), 11.57 min for 3-((*R*)-4-methylcyclohex-3-en-1-yl)butanal (**P55a**).

Representative example of an ^{1}H NMR spectrum of the mixtures derived from (*R*)-limonene under rhodium-catalysed hydroformylation reaction conditions.

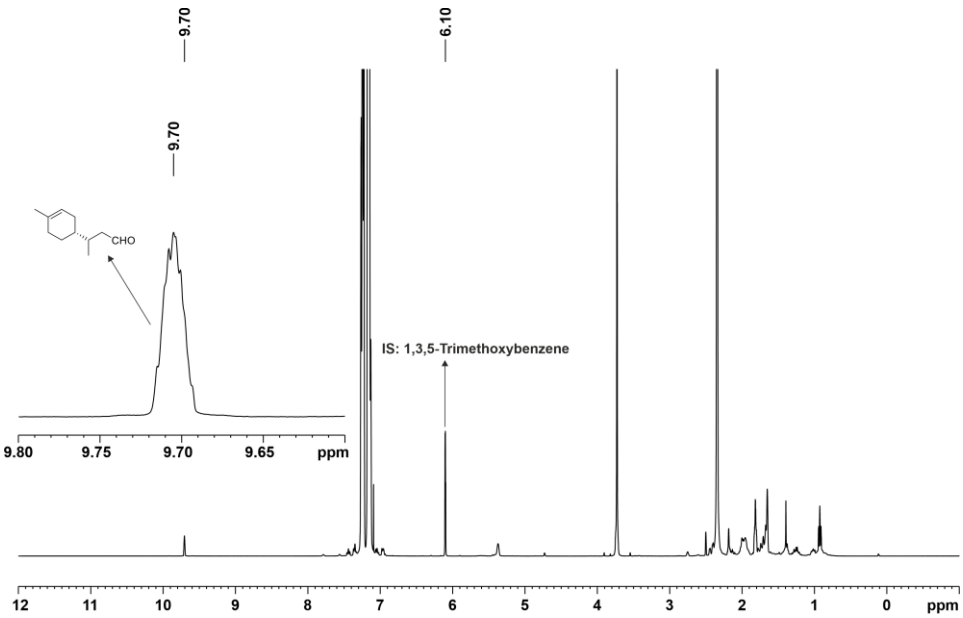

Figure 70. ^{1}H NMR of the mixtures derived from (*R*)-limonene after hydroformylation.

2.5.17. Results of catalysis of the hydroformylation of (3-methylbut-3-en-1-yl)benzene (S56)

Table 36. Supramolecularly regulated hydroformylation of (3-methylbut-3-en-1-yl)benzene (**S56**).

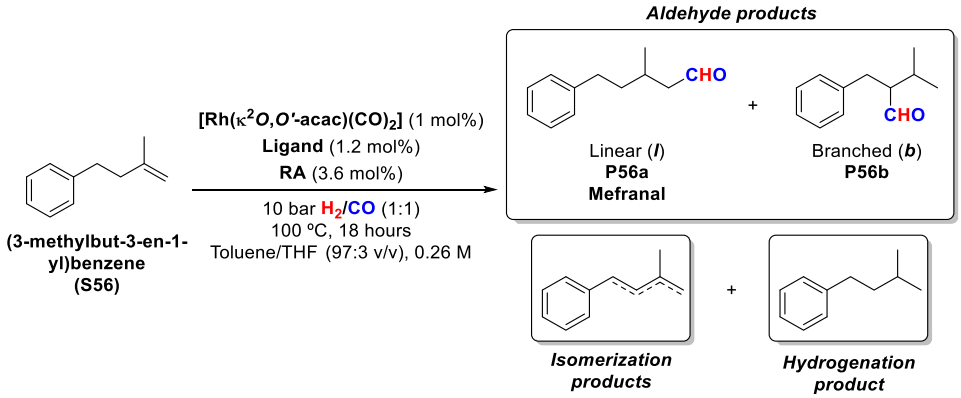

Entry	RA	Ligand	Conv. (%)	Select. (%)[a]		*l*/*b* ratio (%)	*l*/*b* yield (%)
				Isom.	Hydrog.		
1	None	L46	97	6	5	96:4	83:3
2	LiBArF	L46	97	10	9	95:5	75:4
3	NaBArF	L46	97	25	10	92:8	58:5
4	KBArF	L46	97	30	4	99:1	63:1
5	RbBArF	L46	98	15	6	98:2	76:2
6	CsBArF	L46	98	10	5	98:2	82:2

The HF was performed in a parallel autoclave. Reaction conditions: [substrate] = 0.26 M; stirring rate = 800 rpm; 10 bar H_2/CO (1:1); 60 °C, 18h. Conversion was determined by ^{1}H NMR using 1,3,5-trimethoxybenzene as internal standard. Selectivity, ratio, and yield were determined by the area% values of the peaks in the GC chromatogram. [a] Selectivity of the isomerisation (Isom.) and hydrogenation (Hydrog.) processes.

Selected GC chromatogram and ^{1}H NMR spectrum for (3-methylbut-3-en-1-yl)benzene (S56)

Representative example of a GC chromatogram of the mixtures derived from (3-methylbut-3-en-1-yl)benzene under rhodium-catalysed hydroformylation reaction conditions.

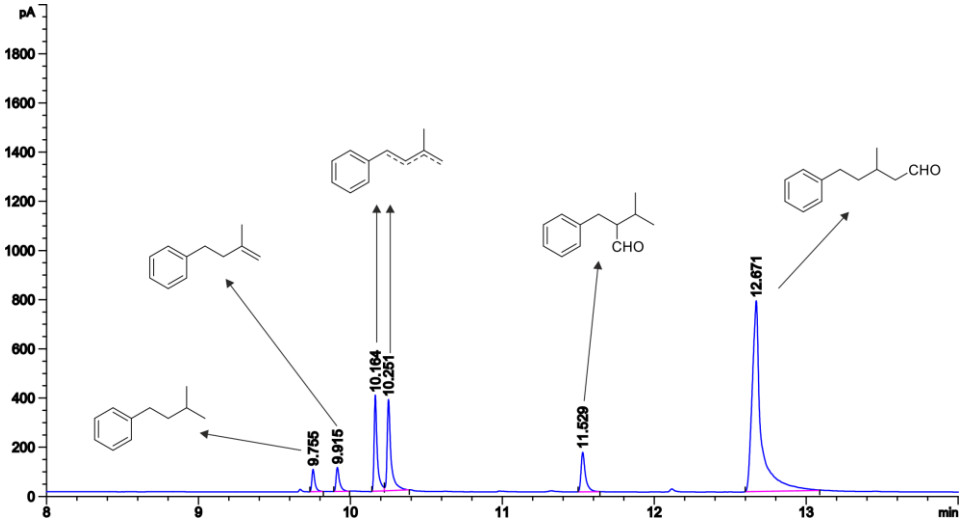

Figure 71. GC chromatogram of the mixtures derived from (3-methylbut-3-en-1-yl)benzene after hydroformylation catalysis.

GC analysis conditions for hydroformylation reaction mixtures of (3-methylbut-3-en-1-yl)benzene: Chemo- and regio-selectivity in the mixtures arising from hydroformylation reaction conditions were determined by GC-FID analysis with a HP-5 column (5% phenyl methyl siloxane; 30 m x 320 µm x 0.25 µm). Flow rate: 2.6 mL/min. Temperature program: 40 °C for 5 min, then up to 150 °C at 20 °C/min and 10 min at 150 °C, then up to 275 °C at 20 °C/min and 5 min at 275 °C. Retention times: 9.76 min for isopentylbenzene, 9.92 min for (3-methylbut-3-en-1-yl)benzene, 10.16 and 10.25 min for (3-methylbut-3-en-1-yl)benzene isomers, 11.53 min for 2-benzyl-3-methylbutanal (**P56b**), 12.67 min for mefranal (3-methyl-5-phenylpentanal) (**P56a**).

Representative example of an ^{1}H NMR spectrum of the mixtures derived from (3-methylbut-3-en-1-yl)benzene under rhodium-catalysed hydroformylation reaction conditions.

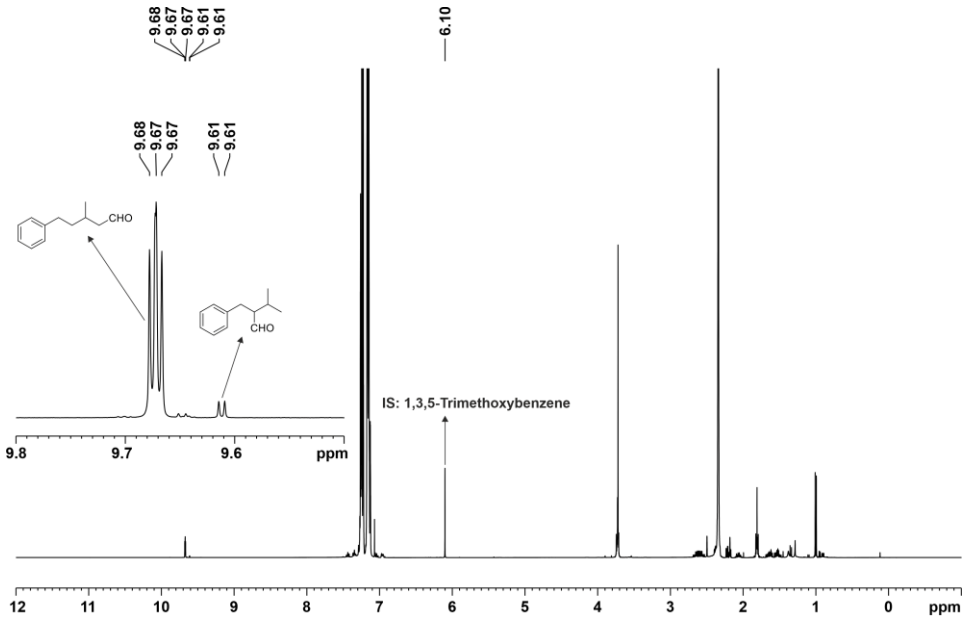

Figure 72. ^{1}H NMR of the mixtures derived from (3-methylbut-3-en-1-yl)benzene after hydroformylation.

2.5.18. Results of catalysis of the hydroformylation of 1-((2-methylallyl)oxy)octane (S57)

Table 37. Supramolecular regulated hydroformylation of 1-((2-methylallyl)oxy)octane (**S57**).

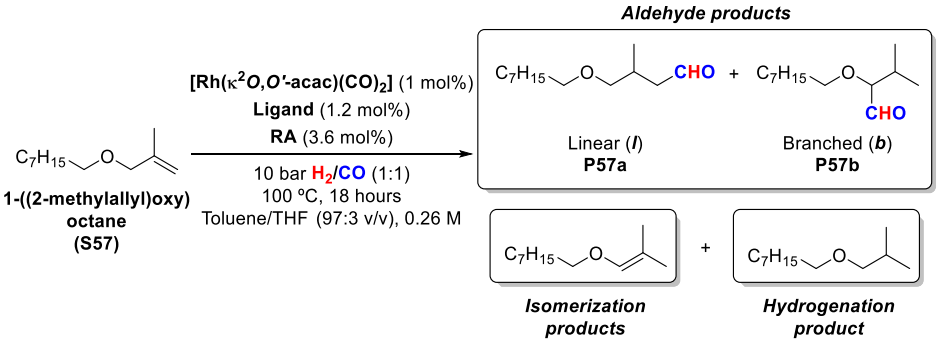

Entry	RA	Ligand	Conv. (%)	Select. (%)[a]		*l*/*b* ratio (%)	*l*/*b* yield (%)
				Isom.	Hydrog.		
1	None	L46	99	17	3	93:7	74:6
2	LiBArF	L46	99	42	4	94:6	50:3
3	NaBArF	L46	99	69	2	94:6	27:2
4	KBArF	L46	99	57	2	98:2	40:1
5	RbBArF	L46	99	54	4	99:1	41:0
6	CsBArF	L46	99	31	5	99:1	63:1

The HF was performed in a parallel autoclave. Reaction conditions: [substrate] = 0.26 M; stirring rate = 800 rpm; 10 bar H_2/CO (1:1); 60 °C, 18h. Conversion was determined by ^{1}H NMR using 1,3,5-trimethoxybenzene as internal standard. Selectivity, ratio, and yield were determined by the area% values of the peaks in the GC chromatogram. [a] Selectivity of the isomerisation (Isom.) and hydrogenation (Hydrog.) processes.

Selected GC chromatogram and ^{1}H NMR spectrum for 1-((2-methylallyl)oxy)octane (S57)

Representative example of a GC chromatogram of the mixtures derived from 1-((2-methylallyl)oxy)octane under rhodium-catalysed hydroformylation reaction conditions.

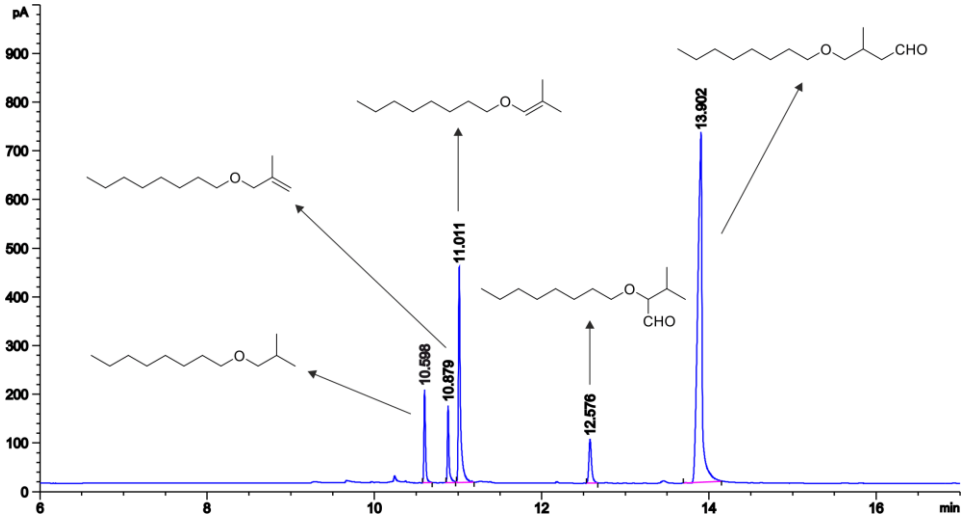

Figure 73. GC chromatogram of the mixtures derived from 1-((2-methylallyl)oxy)octane after hydroformylation.

GC analysis conditions for hydroformylation reaction mixtures of 1-((2-methylallyl)oxy)octane: Chemo- and regio-selectivity in the mixtures arising from hydroformylation reaction conditions were determined by GC-FID analysis with a HP-5 column (5% phenyl methyl siloxane; 30 m x 320 µm x 0.25 µm). Flow rate: 2.6 mL/min. Temperature program: 40 °C for 5 min, then up to 150 °C at 20 °C/min and 10 min at 150 °C, then up to 275 °C at 20 °C/min and 5 min at 275 °C. Retention times: 10.59 min for 1-isobutoxyoctane, 10.88 min for 1-((2-methylallyl)oxy)octane, 10.01 1-((2-methylprop-1-en-1-yl)oxy)octane, 12.57 min for 3-methyl-2-(octyloxy)butanal (**P57b**), 13.90 min for 3-methyl-4-(octyloxy)butanal (**P57a**).

Representative example of an ^{1}H NMR spectrum of the mixtures derived from 1-((2-methylallyl)oxy)octane under rhodium-catalysed hydroformylation reaction conditions.

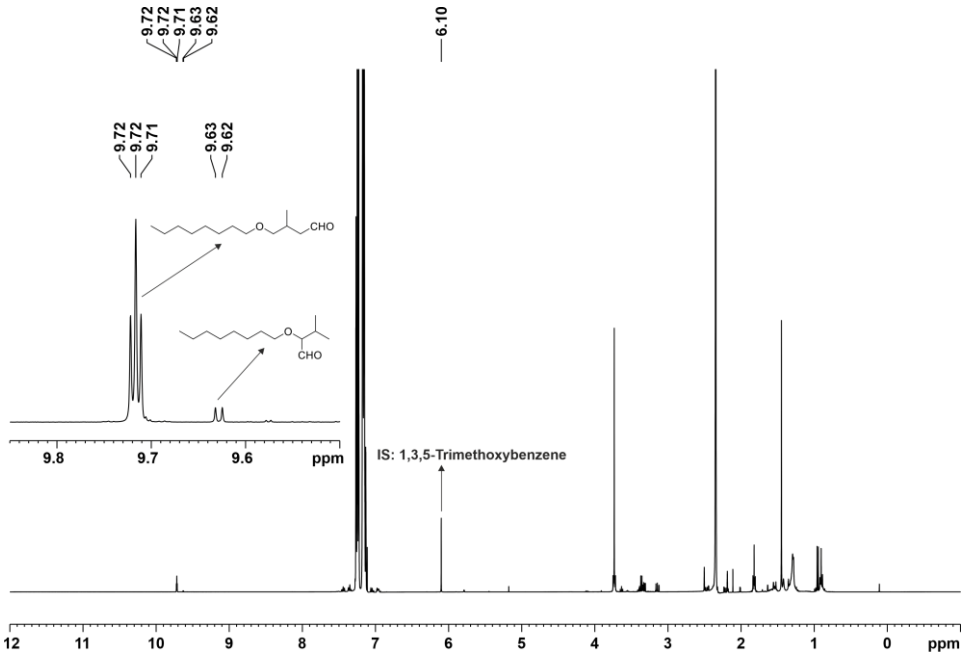

Figure. ^{1}H NMR of the mixtures derived from (3-methylbut-3-en-1-yl)benzene after hydroformylation.

2.5.19. Results of catalysis of the hydroformylation of 1-isopropyl-3-(prop-1-en-2-yl)benzene (S58)

Table 38. Supramolecularly regulated hydroformylation of 1 isopropyl 3-(prop-1-en-2-yl)benzene (**S58**).

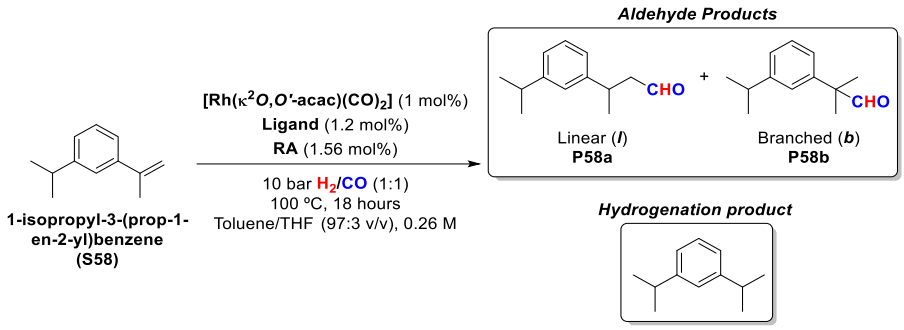

Entry	RA	Ligand	Conv. (%)	Select. (%)[a]		*l/b* ratio (%)	*l/b* yield (%)
				Isom.	Hydrog.		
1	**None**	**L46**	98	-	5	>99:<1	93:0
2	**LiBArF**	**L46**	92	-	3	>99:<1	89:0
3	**NaBArF**	**L46**	43	-	4	>99:<1	41:0
4	**KBArF**	**L46**	59	-	4	>99:<1	57:0
5	**RbBArF**	**L46**	60	-	4	>99:<1	58:0
6	**CsBArF**	**L46**	68	-	4	>99:<1	65:0

The HF was performed in a parallel autoclave. Reaction conditions: [substrate] = 0.26 M; stirring rate = 800 rpm; 10 bar H_2/CO (1:1); 60 °C, 18h. Conversion was determined by ^{1}H NMR using 1,3,5-trimethoxybenzene as internal standard. Selectivity, ratio, and yield were determined by the area% values of the peaks in the GC chromatogram. [a] Selectivity of the isomerisation (Isom.) and hydrogenation (Hydrog.) processes.

Selected GC chromatogram and ^{1}H NMR spectrum for 1-isopropyl-3-(prop-1-en-2-yl)benzene (S58)

Representative example of a GC chromatogram of the mixtures derived from 1-isopropyl-3-(prop-1-en-2-yl)benzene under rhodium-catalysed hydroformylation reaction conditions.

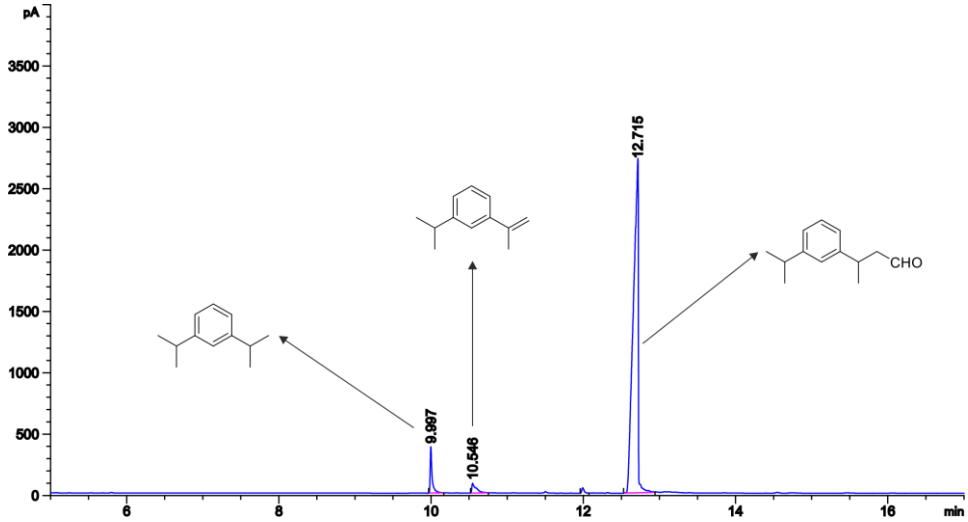

Figure 74. GC chromatogram of the mixtures derived from 1-isopropyl-3-(prop-1-en-2-yl)benzene after hydroformylation.

GC analysis conditions for hydroformylation reaction mixtures of 1-isopropyl-3-(prop-1-en-2-yl)benzene: Chemo- and regio-selectivity in the mixtures arising from hydroformylation reaction conditions were determined by GC-FID analysis with a HP-5 column (5% phenyl methyl siloxane; 30 m x 320 µm x 0.25 µm). Flow rate: 2.6 mL/min. Temperature program: 40 °C for 5 min, then up to 150 °C at 20 °C/min and 10 min at 150 °C, then up to 275 °C at 20 °C/min and 5 min at 275 °C. Retention times: 9.99 min for 1,3-diisopropylbenzene, 10.55 min for 1-isopropyl-3-(prop-1-en-2-yl)benzene, 12.72 min for 3-(3-isopropylphenyl)butanal (**P58a**).

Representative example of an ^{1}H NMR spectrum of the mixtures derived from 1-isopropyl-3-(prop-1-en-2-yl)benzene under rhodium-catalysed hydroformylation reaction conditions.

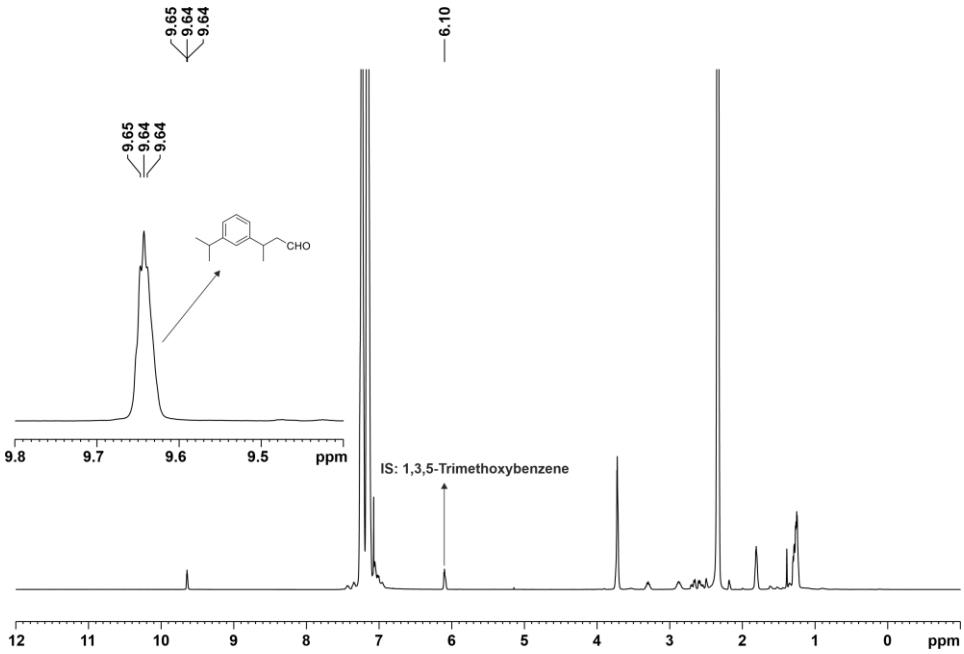

Figure 75. ^{1}H NMR of the mixtures derived from 1-isopropyl-3-(prop-1-en-2-yl)benzene after hydroformylation.

2.5.20. Results of catalysis of the hydroformylation of vinyl acetate (S1)

Table 39. Supramolecularly regulated hydroformylation of vinyl acetate (**S1**).

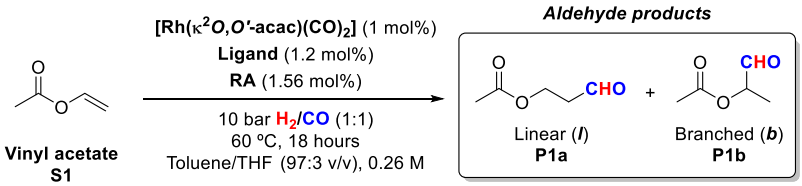

Entry	RA	Ligand	Conv. (%)	Select. (%)		*l*/*b* ratio (%)	*l*/*b* yield (%)
				Isom.	Hydrog.		
1	None	L46	99	-	-	9:91	8:78
2	LiBArF	L46	54	-	-	14:86	5:28
3	NaBArF	L46	95	-	-	10:90	8:70
4	KBArF	L46	31	-	-	22:78	1:5
5	RbBArF	L46	32	-	-	26:74	2:6
6	CsBArF	L46	84	-	-	15:85	9:51
7	None	L47	99	-	-	6:94	5:79
8	LiBArF	L47	76	-	-	8:92	4:53
9	NaBArF	L47	99	-	-	8:92	6:78
10	KBArF	L47	99	-	-	6:94	6:84
11	RbBArF	L47	99	-	-	5:95	5:84
12	CsBArF	L47	99	-	-	5:95	4:80

The HF was performed in a parallel autoclave. Reaction conditions: [substrate] = 0.26 M; stirring rate = 800 rpm; 10 bar H_2/CO (1:1); 60 °C, 18h. Conversion, ratio, selectivity, and yield were determined by ^{1}H NMR using 1,3,5-trimethoxybenzene as internal standard.

Selected ^{1}H NMR spectrum for vinyl acetate (S1)

Representative example of an ^{1}H NMR spectrum of the mixtures derived from vinyl acetate under rhodium-catalysed hydroformylation reaction conditions.

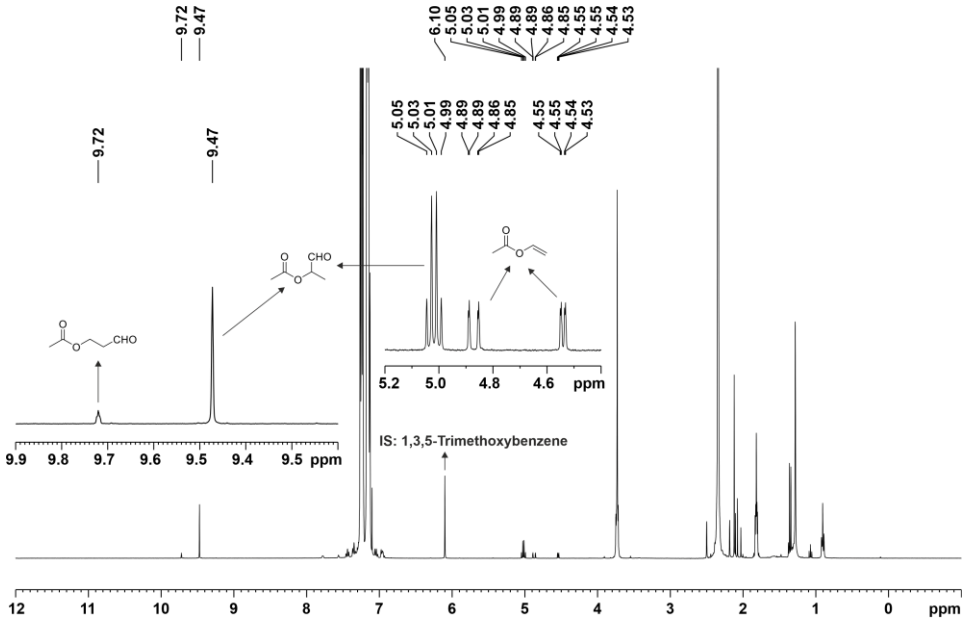

Figure 76. ^{1}H NMR of the mixtures derived from vinyl acetate after hydroformylation.

2.5.21. Results of catalysis of the hydroformylation of styrene (S59)

Table 40. Supramolecular regulated hydroformylation of styrene (**S59**).

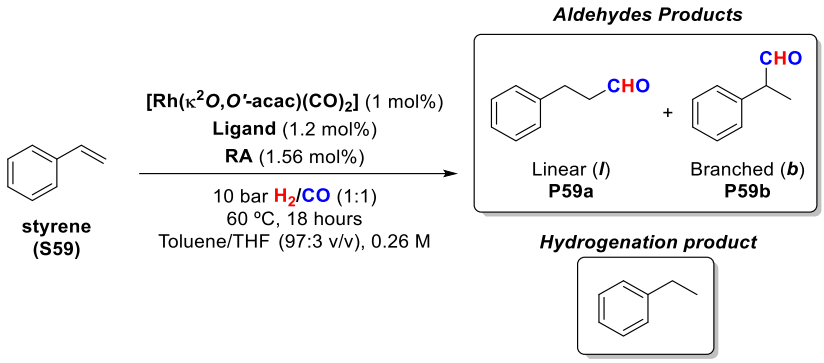

Entry	RA	Ligand	Conv. (%)	Select. (%)[a]		*l*/*b* ratio (%)	*l*/*b* yield (%)
				Isom.	Hydrog.		
1	None	L46	99	-	0.4	8:92	8:91
2	LiBArF	L46	99	-	0.4	7:93	7:92
3	NaBArF	L46	95	-	0.5	16:84	15:79
4	KBArF	L46	99	-	1	23:77	23:75
5	RbBArF	L46	99	-	0.9	25:75	25:74
6	CsBArF	L46	99	-	0.6	21:79	21:78
7	None	L47	99	-	0.4	10:90	10:89
8	LiBArF	L47	99	-	0.5	11:89	11:88
9	NaBArF	L47	99	-	0.6	14:86	14:85
10	KBArF	L47	99	-	0.5	11:89	11:88
11	RbBArF	L47	99	-	0.4	12:88	12:87
12	CsBArF	L47	99	-	0.4	11:89	11:88

The HF was performed in a parallel autoclave. Reaction conditions: [substrate] = 0.26 M; stirring rate = 800 rpm; 10 bar H_2/CO (1:1); 60 °C, 18h. Conversion was determined by GC using dodecane as an internal standard. Selectivity, ratio, and yield were determined by the area% values of the peaks in the GC chromatogram. [a] Selectivity of the isomerisation (Isom.) and hydrogenation (Hydrog.) processes.

Selected GC chromatogram and ^{1}H NMR spectrum for styrene (S59).

Representative example of a GC chromatogram of the mixtures derived from styrene under rhodium-catalysed hydroformylation reaction conditions.

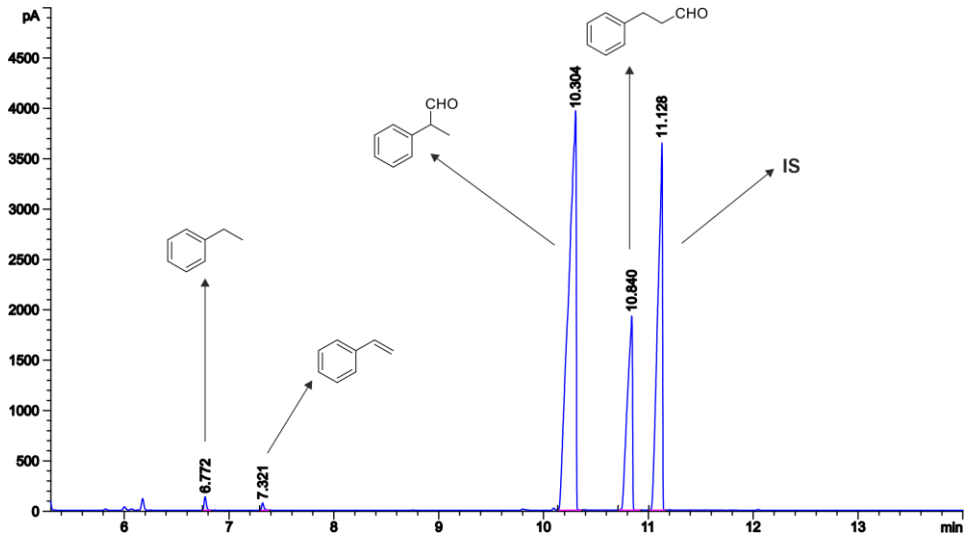

Figure 77. GC chromatogram of the mixtures derived from styrene after hydroformylation.

GC analysis conditions for hydroformylation reaction of styrene: Conversion, chemo- and regio-selectivity in the mixtures arising from hydroformylation reaction conditions were determined by GC-FID analysis with a HP-5 column (5% phenyl methyl siloxane; 30 m x 320 µm x 0.25 µm). Flow rate: 2.3 mL/min. Temperature program: 35 °C for 5 min, then up to 150 °C at 20 °C/min and 10 min at 150 °C, then up to 320 °C at 20 °C/min and 5 min at 320 °C. Retention times: 6.8 min for ethylbenzene, 7.3 min for styrene, 10.3 min for 2-phenylpropanal (**P60b**), 10.8 min for 3-phenylpropanal (**P60a**), 11.1 min for the IS (dodecane).

Representative example of an ^{1}H NMR spectrum of the mixtures derived from styrene under rhodium-catalysed hydroformylation reaction conditions.

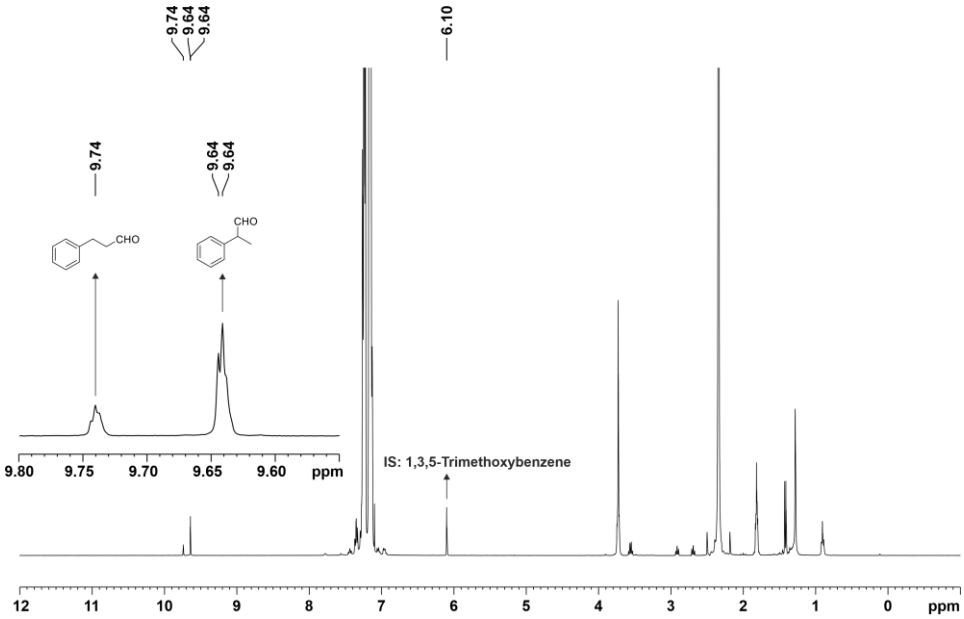

Figure 78. ^{1}H NMR of the mixtures derived from styrene after hydroformylation.

2.5.22. Results of catalysis of the hydroformylation of *N*-vinylphthalimide (S60)

Table 41. Supramolecularly regulated hydroformylation of *N*-vinylphthalimide (**S60**).

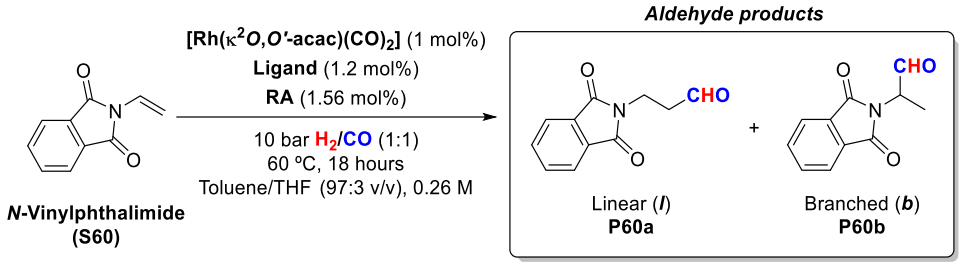

Entry	RA	Ligand	Conv. (%)	Select. (%)		*l*/*b* ratio (%)	*l*/*b* yield (%)
				Isom.	Hydrog.		
1	**None**	**L46**	87	-	-	4:96	3:73
2	**LiBArF**	**L46**	78	-	-	5:95	3:61
3	**NaBArF**	**L46**	38	-	-	22:78	6:22
4	**KBArF**	**L46**	78	-	-	11:89	7:57
5	**RbBArF**	**L46**	91	-	-	9:91	7:71
6	**CsBArF**	**L46**	89	-	-	6:94	4:66
7	**None**	**L47**	97	-	-	4:96	3:85
8	**LiBArF**	**L47**	95	-	-	3:97	3:81
9	**NaBArF**	**L47**	96	-	-	4:96	3:85
10	**KBArF**	**L47**	95	-	-	3:97	3:85
11	**RbBArF**	**L47**	95	-	-	3:97	2:88
12	**CsBArF**	**L47**	97	-	-	2:98	2:84

The HF was performed in a parallel autoclave. Reaction conditions: [substrate] = 0.26 M; stirring rate = 800 rpm; 10 bar H_2/CO (1:1); 60 °C, 18h. Conversion, ratio, selectivity, and yield were determined by ^{1}H NMR using dimethyl sulfone ($(CH_3)_2SO_2$) as internal standard.

Selected ^{1}H NMR spectrum for *N*-vinylphthalimide (S60)

Representative example of an ^{1}H NMR spectrum of the mixtures derived from *N*-vinylphthalimide under rhodium-catalysed hydroformylation reaction conditions.

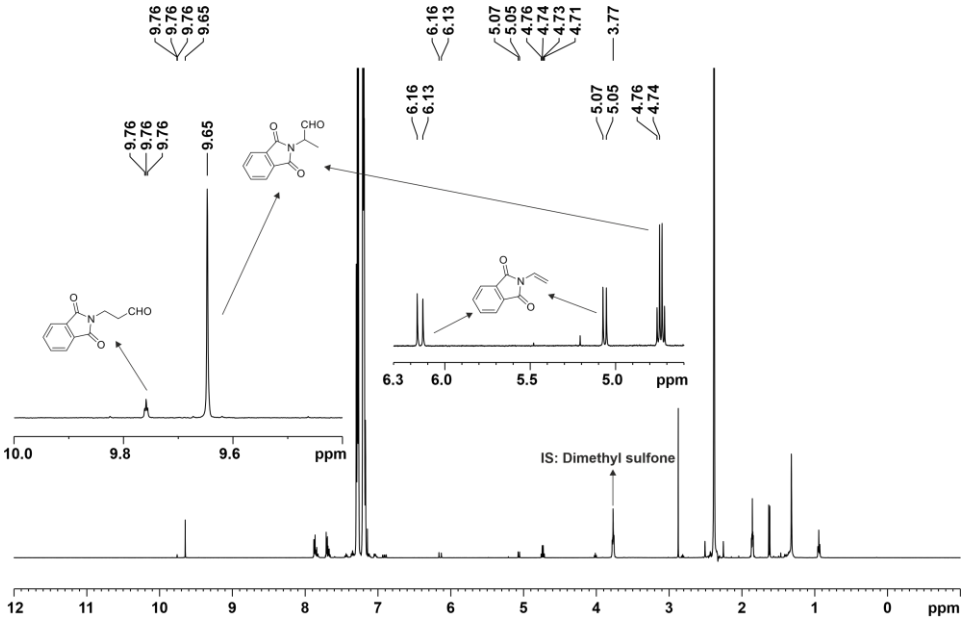

Figure 79. ^{1}H NMR of the mixtures derived from *N*-vinylphthalimide after hydroformylation.

2.5.23. Results of catalysis of the hydroformylation of 1-(*tert*-butyl)-4-vinylbenzene (S61)

Table 42. Supramolecularly regulated hydroformylation of 1-(*tert*-butyl)-4-vinylbenzene (**S61**).

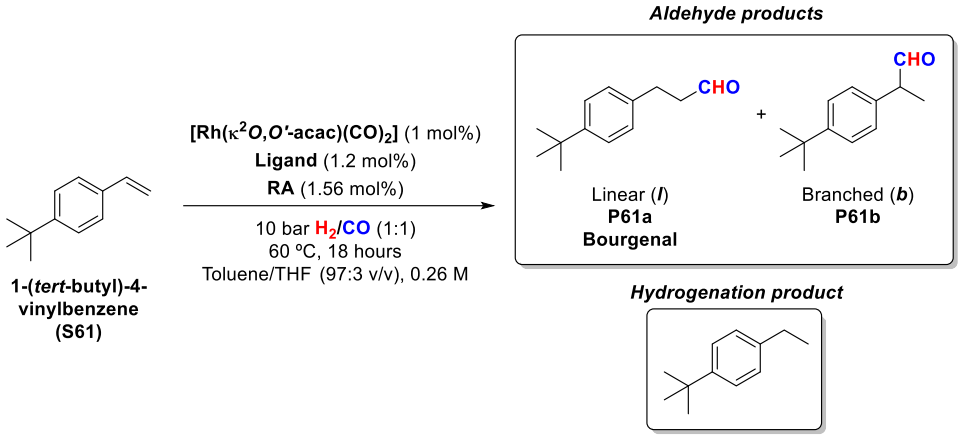

Entry	RA	Ligand	Conv. (%)	Select. (%)[a]		*l*/*b* ratio (%)	*l*/*b* yield (%)
				Isom.	Hydrog.		
1	**None**	**L46**	95	-	2	13:87	12:81
2	**LiBArF**	**L46**	95	-	1	9:91	8:86
3	**NaBArF**	**L46**	97	-	1	20:80	19:77
4	**KBArF**	**L46**	96	-	1	33:67	31:64
5	**RbBArF**	**L46**	95	-	2	34:66	32:61
6	**CsBArF**	**L46**	96	-	2	28:72	26:68

The HF was performed in a parallel autoclave. Reaction conditions: [substrate] = 0.26 M; stirring rate = 800 rpm; 10 bar H_2/CO (1:1); 60 °C, 18h. Conversion was determined by ^{1}H NMR using 1,3,5-trimethoxybenzene as internal standard. Selectivity, ratio, and yield were determined by the area% values of the peaks in the GC chromatogram. [a] Selectivity of the isomerisation (Isom.) and hydrogenation (Hydrog.) processes.

Selected GC chromatogram and ^{1}H NMR spectrum for 1-(*tert*-butyl)-4-vinylbenzene (S61)

Representative example of a GC chromatogram of the mixtures derived from 1-(*tert*-butyl)-4-vinylbenzene under rhodium-catalysed hydroformylation reaction conditions.

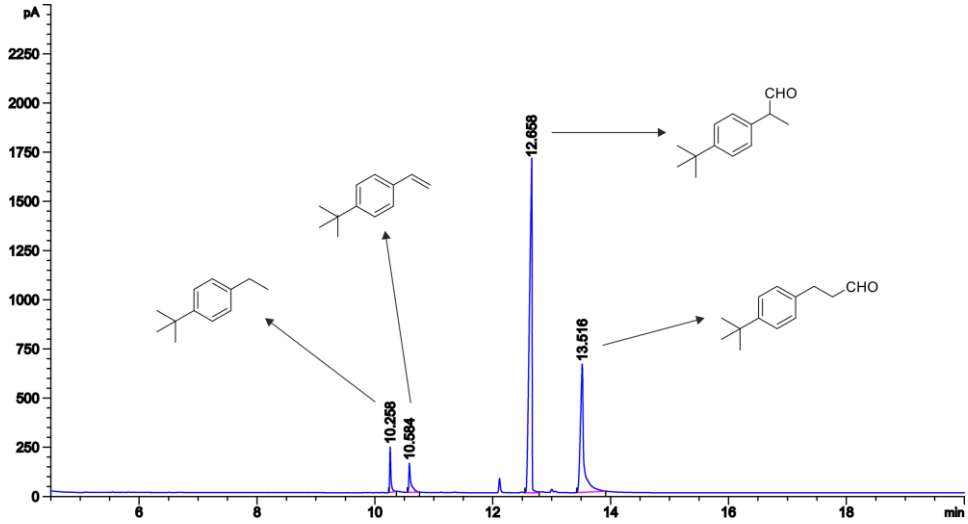

Figure 80. GC chromatogram of the mixtures derived from 1-(*tert*-butyl)-4-vinylbenzene after hydroformylation catalysis.

GC analysis conditions for hydroformylation reaction mixtures of 1-(*tert*-butyl)-4-vinylbenzene: Chemo- and regio-selectivity in the mixtures arising from hydroformylation reaction conditions were determined by GC-FID analysis with a HP-5 column (5% phenyl methyl siloxane; 30 m x 320 µm x 0.25 µm). Flow rate: 2.6 mL/min. Temperature program: 40 °C for 5 min, then up to 150 °C at 20 °C/min and 10 min at 150 °C, then up to 275 °C at 20 °C/min and 5 min at 275 °C. Retention times: 10.26 min for 1-(*tert*-butyl)-4-ethylbenzene, 10.58 min for 1-(*tert*-butyl)-4-vinylbenzene, 12.66 min for 2-(4-(*tert*-butyl)phenyl)propanal (**P61b**), 13.52 min for bourgenal (3-(4-(*tert*-butyl)phenyl)propanal) (**P61a**).

Representative example of an ^{1}H NMR spectrum of the mixtures derived from 1-(*tert*-butyl)-4-vinylbenzene under rhodium-catalysed hydroformylation reaction conditions.

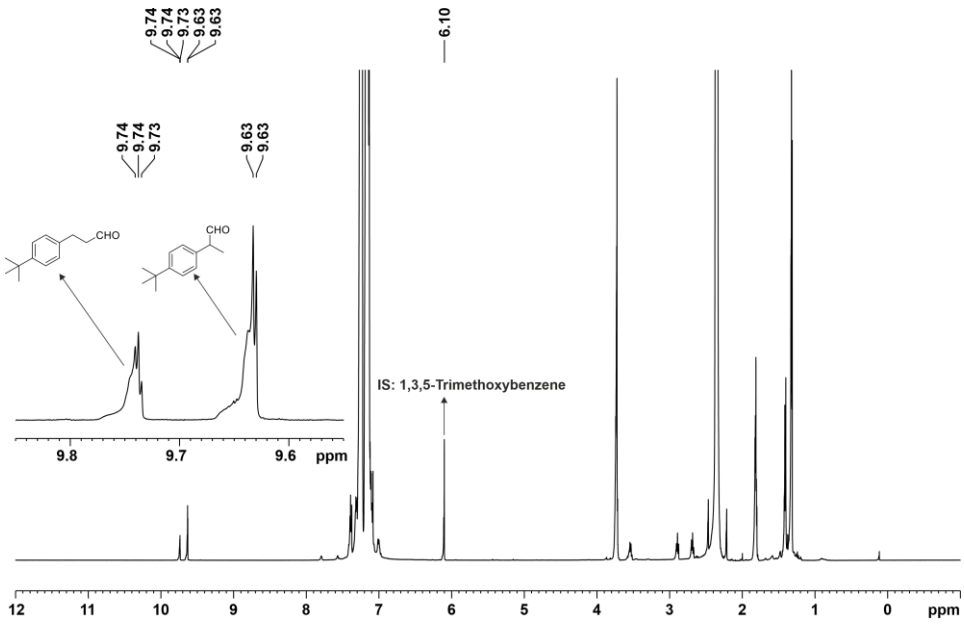

Figure 81. ^{1}H NMR of the mixtures derived from 1-(*tert*-butyl)-4-vinylbenzene after hydroformylation.

2.5.24. Results of catalysis of the hydroformylation of phenylacetylene (S62)

Table 43. Supramolecular regulated hydroformylation of phenylacetylene (**S62**).

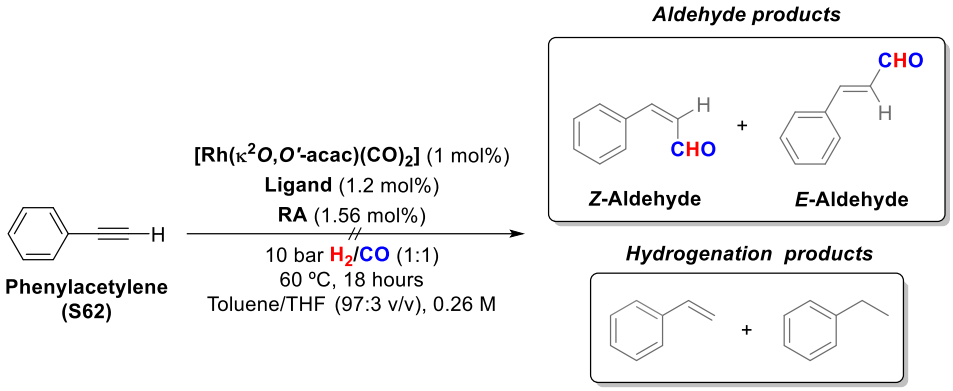

Entry	RA	Ligand	Conv. (%)	Select. (%)		*Z*/*E* isomers ratio (%)	*Z* isomer yield (%)
				A	B		
1	None	L46	0	-	-	-	-
2	LiBArF	L46	0	-	-	-	-
3	NaBArF	L46	0	-	-	-	-
4	KBArF	L46	0	-	-	-	-
5	RbBArF	L46	0	-	-	-	-
6	CsBArF	L46	0	-	-	-	-

The HF was performed in a parallel autoclave. Reaction conditions: [substrate] = 0.26 M; stirring rate = 800 rpm; 10 bar H_2/CO (1:1); 60 °C, 18h. Conversion was determined by GC using dodecane as an internal standard. Selectivity, ratio, and yield were determined by the area% values of the peaks in the GC chromatogram. [a] Selectivity of the isomerisation (Isom.) and hydrogenation (Hydrog.) processes.

2.5.25. Results of catalysis of the hydroformylation of 1,2-diphenylethyne (S63)

Table 44. Supramolecularly regulated hydroformylation of 1,2-diphenylethyne (**S63**).

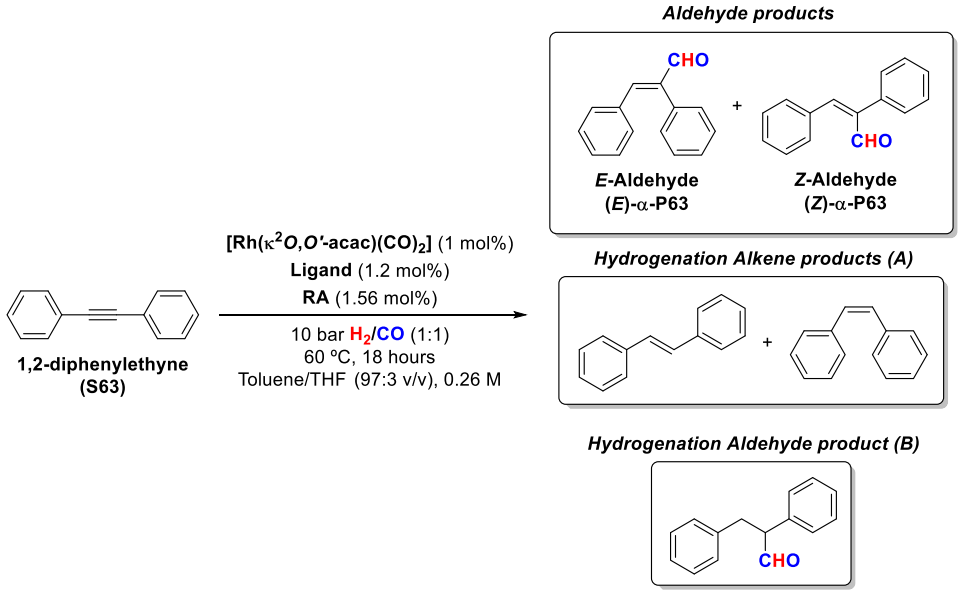

Entry	RA	Ligand	Conv. (%)	Select. (%)[a]		*E*/*Z* isomer ratio (%)	*E*/*Z* isomer yield (%)
				A	B		
1	None	L46	99	70	8	98:2	21:0
2	LiBArF	L46	89	40	2	99:1	51:1
3	NaBArF	L46	99	3	0	98:2	94:2
4	KBArF	L46	99	6	0	98:2	91:2
5	RbBArF	L46	99	19	1	99:1	78:1
6	CsBArF	L46	99	40	2	98:2	56:1

The HF was performed in a parallel autoclave. Reaction conditions: [substrate] = 0.26 M; stirring rate = 800 rpm; 10 bar H_2/CO (1:1); 60 °C, 18h. Conversion was determined by GC using dodecane as an internal standard. Selectivity, ratio, and yield were determined by the area% values of the peaks in the GC chromatogram. [a] Selectivity of the isomerisation (Isom.) and hydrogenation (Hydrog.) processes.

Selected GC chromatogram and ^{1}H NMR spectrum for 1,2-diphenylethyne (S63)

Representative example of a GC chromatogram of the mixtures derived from 1,2-diphenylethyne under rhodium-catalysed hydroformylation reaction conditions.

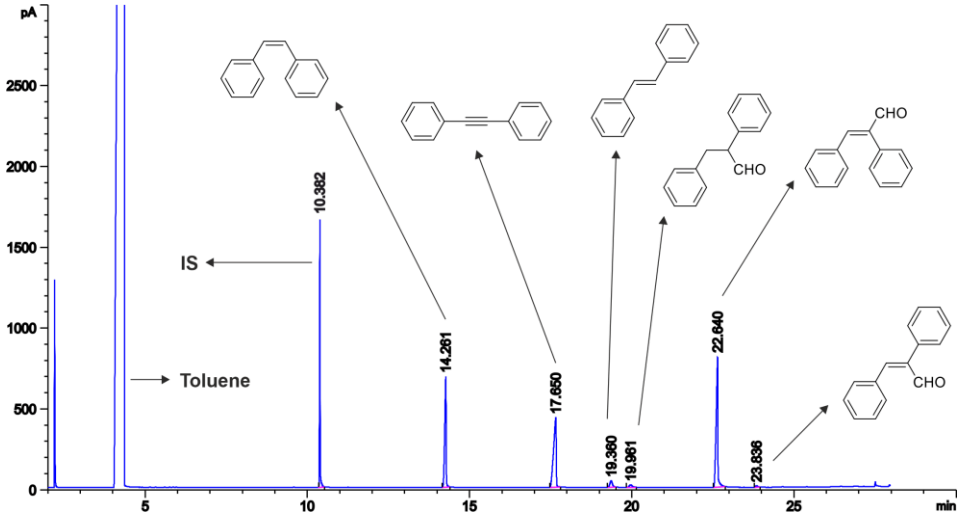

Figure 82. GC chromatogram of the mixtures derived from 1,2-diphenylethyne after hydroformylation.

GC analysis conditions for hydroformylation reaction mixtures of 1,2-diphenylethyne: Conversion, chemo- and regio-selectivity in the mixtures arising from hydroformylation reaction conditions were determined by GC-FID analysis with a HP-5 column (5% phenyl methyl siloxane; 30 m x 320 µm x 0.25 µm). Flow rate: 2.6 mL/min. Temperature program: 40 °C for 5 min, then up to 150 °C at 20 °C/min and 10 min at 150 °C, then up to 275 °C at 20 °C/min and 5 min at 275 °C. Retention times: 10.38 for IS (dodecane), 14.26 min for (*Z*)-1,2-diphenylethene, 17.65 min for 1,2-diphenylacetylene, 19.36 min for (*E*)-1,2-diphenylethene, 19.96 min for 2,3-diphenylpropanal, 22.64 min for (*E*)-2,3-diphenylacrylaldehyde (**(*E*)-α-P63**), 23.84 min for (*Z*)-2,3-diphenylacrylaldehyde (**(*Z*)-α-P63**).

Representative example of an ^{1}H NMR spectrum of the mixtures derived from 1,2-diphenylethyne under rhodium-catalysed hydroformylation reaction conditions.

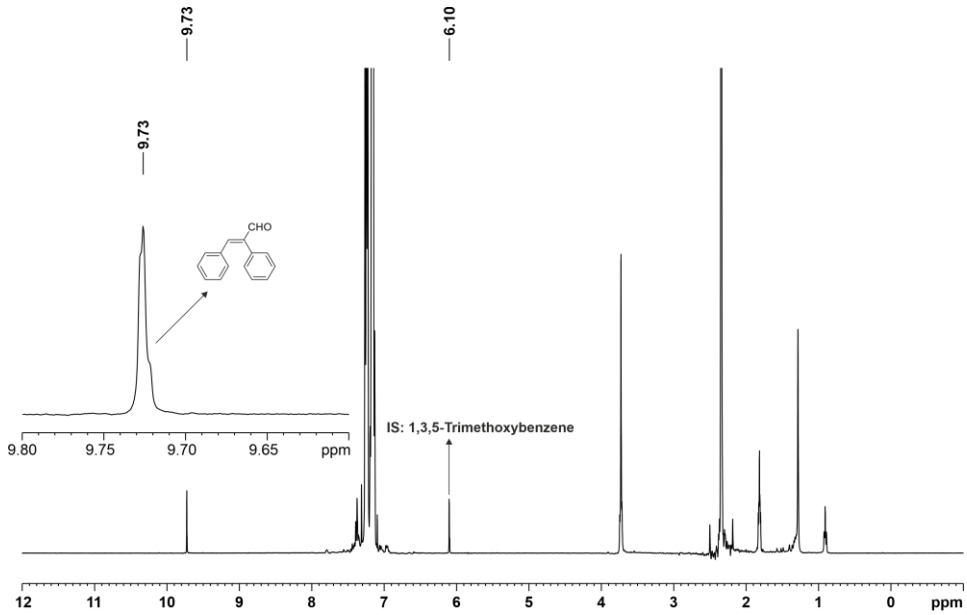

Figure 83. ^{1}H NMR of the mixtures derived from 1,2-diphenylacetylene after hydroformylation.

2.5.26. Results of catalysis of the hydroformylation of hex-1-yn-1-ylbenzene (S64)

Table 45. Supramolecularly regulated hydroformylation of hex-1-yn-1-ylbenzene (**S64**).

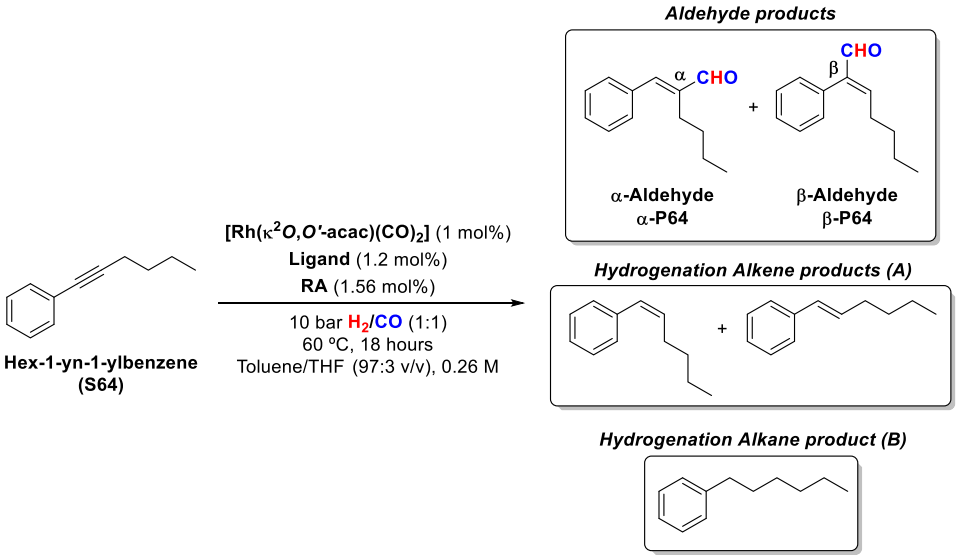

Entry	RA	Ligand	Conv. (%)	Select. (%)[a]		α/β isomer ratio (%)	α/β isomer yield (%)
				A	B		
1	None	L46	66	28	4	74:26	33:12
2	LiBArF	L46	40	20	16	73:27	19:7
3	NaBArF	L46	90	0	1	78:22	69:20
4	KBArF	L46	99	2	0	76:24	74:23
5	RbBArF	L46	99	2	1	77:23	74:22
6	CsBArF	L46	97	5	3	78:22	70:20

The HF was performed in a parallel autoclave. Reaction conditions: [substrate] = 0.26 M; stirring rate = 800 rpm; 10 bar H_2/CO (1:1); 60 °C, 18h. Conversion was determined by GC using dodecane as an internal standard. Selectivity, ratio, and yield were determined by the area% values of the peaks in the GC chromatogram. [a] Selectivity of hydrogenation of alkenes product (A) and hydrogenation of alkane product (B).

Selected GC chromatogram and ^{1}H NMR spectrum for hex-1-yn-1-ylbenzene (S64).

Representative example of a GC chromatogram of the mixtures derived from hex-1-yn-1-ylbenzene under rhodium-catalysed hydroformylation reaction conditions.

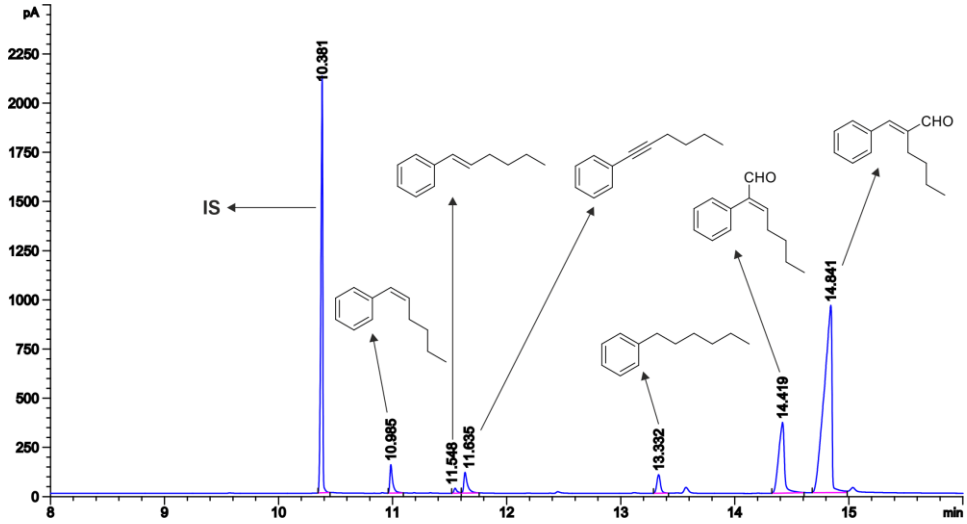

Figure 84. GC chromatogram of the mixtures derived from hex-1-yn-1-ylbenzene after hydroformylation.

GC analysis conditions for hydroformylation reaction mixtures of 1,2-diphenylethyne: Conversion, chemo- and regio-selectivity in the mixtures arising from hydroformylation reaction conditions were determined by GC-FID analysis with a HP-5 column (5% phenyl methyl siloxane; 30 m x 320 µm x 0.25 µm). Flow rate: 2.6 mL/min. Temperature program: 40 °C for 5 min, then up to 150 °C at 20 °C/min and 10 min at 150 °C, then up to 275 °C at 20 °C/min and 5 min at 275 °C. Retention times: 10.38 for IS (dodecane), 10.98 min for (*Z*)-hex-1-en-1-ylbenzene, 11.55 min for (*E*)-hex-1-en-1-ylbenzene, 11.63 min for hex-1-yn-1-ylbenzene, 13.33 min for hexylbenzene, 14.42 min for (*E*)-2-phenylhept-2-enal (**β-P64**), 14.84 min for (*E*)-2-benzylidenehexanal (**α-P64**).

Representative example of an ^{1}H NMR spectrum of the mixtures derived from hex-1-yn-1-ylbenzene under rhodium-catalysed hydroformylation reaction conditions.

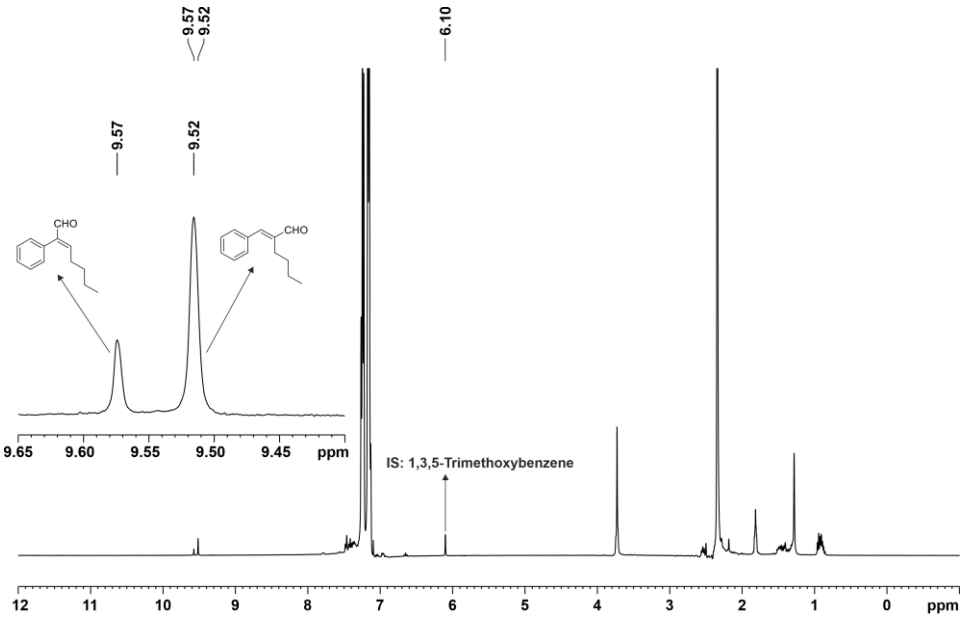

Figure 85. ^{1}H NMR of the mixtures derived from hex-1-yn-1-ylbenzene after hydroformylation.

2.5.27. Results of catalysis of the hydroformylation of ethyl 3-phenylpropiolate (S65)

Table 46. Supramolecularly regulated hydroformylation of ethyl 3-phenylpropiolate (**S65**).

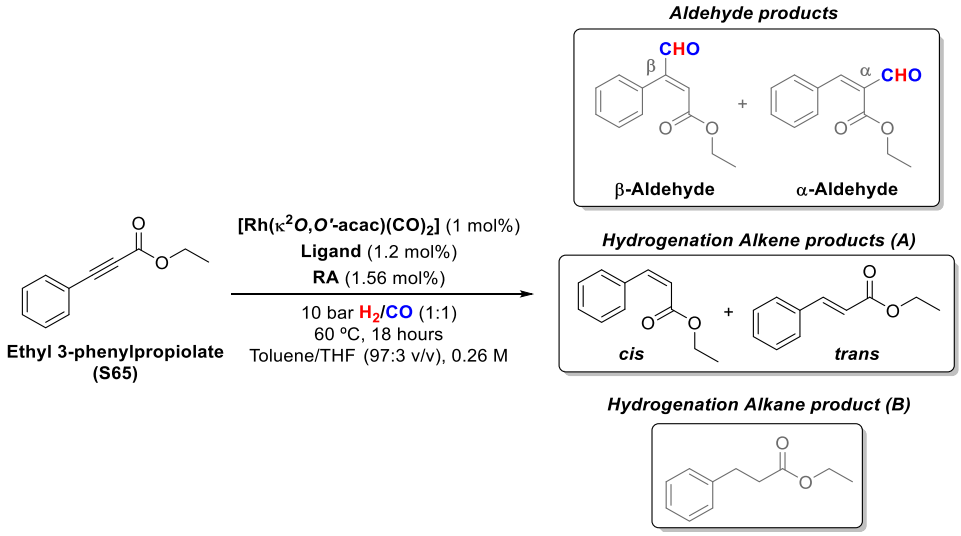

Entry	RA	Ligand	Conv. (%)	Select. (%)[a]		*cis*/*trans* isomer ratio (%)	*cis*/*trans* isomer yield (%)
				A	B		
1	None	L46	16	99	0	44:56	7:9
2	LiBArF	L46	68	99	0	75:25	50:17
3	NaBArF	L46	23	99	0	78:22	18:5
4	KBArF	L46	69	99	0	60:40	41:27
5	RbBArF	L46	54	99	0	54:46	29:25
6	CsBArF	L46	45	99	0	54:46	24:20

The HF was performed in a parallel autoclave. Reaction conditions: [substrate] = 0.26 M; stirring rate = 800 rpm; 10 bar H_2/CO (1:1); 60 °C, 18h. Conversion was determined by GC using dodecane as an internal standard. Selectivity, ratio, and yield were determined by the area% values of the peaks in the GC chromatogram. [a] Selectivity of Hydrogenation of alkenes product (A) and Hydrogenation of alkane product (B).

Selected GC chromatogram and ^{1}H NMR spectrum for ethyl 3-phenylpropiolate (S65)

Representative example of a GC chromatogram of the mixtures derived from ethyl 3-phenylpropiolate under rhodium-catalysed hydroformylation reaction conditions.

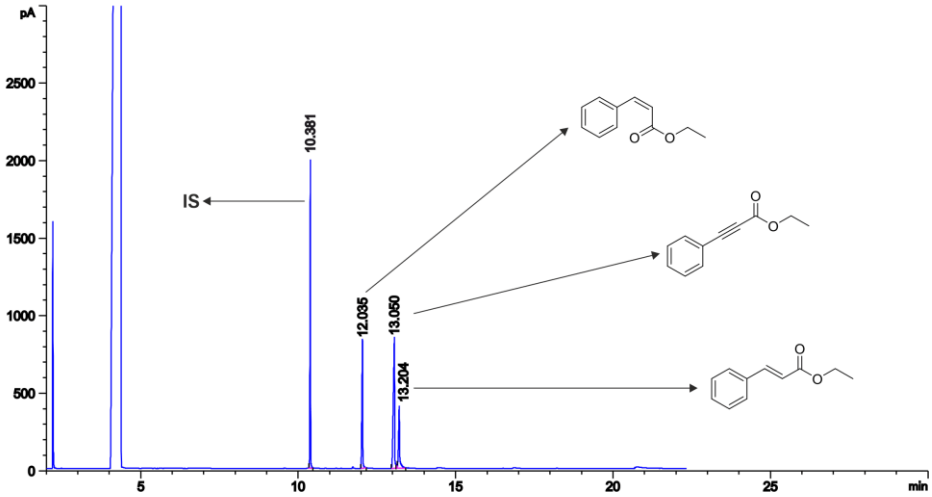

Figure 86. GC chromatogram of the mixtures derived from ethyl 3-phenylpropiolate after hydroformylation.

GC analysis conditions for hydroformylation reaction mixtures of ethyl 3-phenylpropiolate: Conversion, chemo- and regio-selectivity in the mixtures arising from hydroformylation reaction conditions were determined by GC-FID analysis with a HP-5 column (5% phenyl methyl siloxane; 30 m x 320 µm x 0.25 µm). Flow rate: 2.6 mL/min. Temperature program: 40 °C for 5 min, then up to 150 °C at 20 °C/min and 10 min at 150 °C, then up to 275 °C at 20 °C/min and 5 min at 275 °C. Retention times: 10.38 for IS (dodecane), 10.98 min for (*Z*)-hex-1-en-1-ylbenzene, 12.03 min for ethyl (*Z*)-3-phenylacrylate, 13.05 min for ethyl 3-phenylpropiolate, 13.20 min for ethyl cinnamate.

Representative example of an ^{1}H NMR spectrum of the mixtures derived from ethyl 3-phenylpropiolate under rhodium-catalysed hydroformylation reaction conditions.

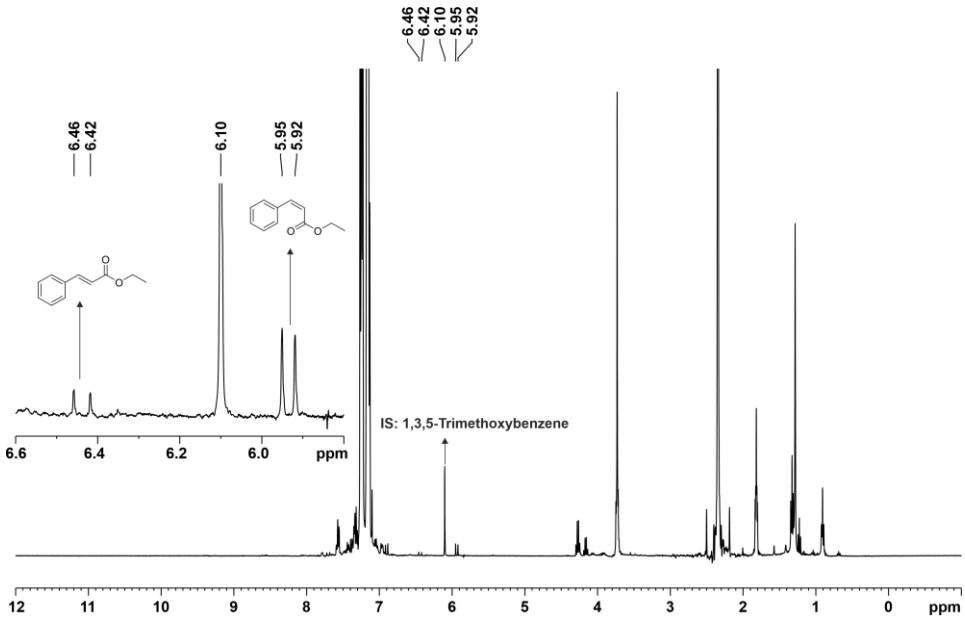

Figure 87. ^{1}H NMR of the mixtures derived from ethyl 3-phenylpropiolate after hydroformylation.

2.5.28. Results of catalysis of the hydroformylation of 7-vinylidenetridecane (S66)

Table 47. Supramolecularly regulated hydroformylation of 7-vinylidenetridecane (**S66**).

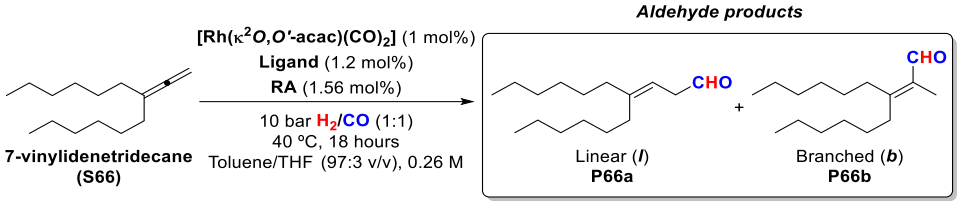

Entry	RA	Ligand	Conv. (%)	Select. (%)[a]		*l*/*b* ratio (%)	*l*/*b* yield (%)
				Isom.	Hydrog.		
1	None	L46	99	-	-	>99:<1	9:0
2	LiBArF	L46	99	-	-	>99:<1	11:0
3	NaBArF	L46	99	-	-	>99:<1	62:0
4	KBArF	L46	99	-	-	>99:<1	69:0
5	RbBArF	L46	99	-	-	>99:<1	43:0
6	CsBArF	L46	99	-	-	>99:<1	11:0
7	None	L47	99	-	-	>99:<1	5:0
8	LiBArF	L47	99	-	-	>99:<1	7:0
9	NaBArF	L47	99	-	-	>99:<1	7:0
10	KBArF	L47	99	-	-	>99:<1	6:0
11	RbBArF	L47	99	-	-	>99:<1	7:0
12	CsBArF	L47	99	-	-	>99:<1	7:0

The HF was performed in a parallel autoclave. Reaction conditions: [substrate] = 0.26 M; stirring rate = 800 rpm; 10 bar H_2/CO (1:1); 40 °C, 18h. Conversion, ratio and yield were determined by ^{1}H NMR using 1,3,5-trimethoxybenzene as internal standard.

Selected ^{1}H NMR spectrum for 7-vinylidenetridecane (S66)

Representative example of an ^{1}H NMR spectrum of the mixtures derived from 7-vinylidenetridecane under rhodium-catalysed hydroformylation reaction conditions.

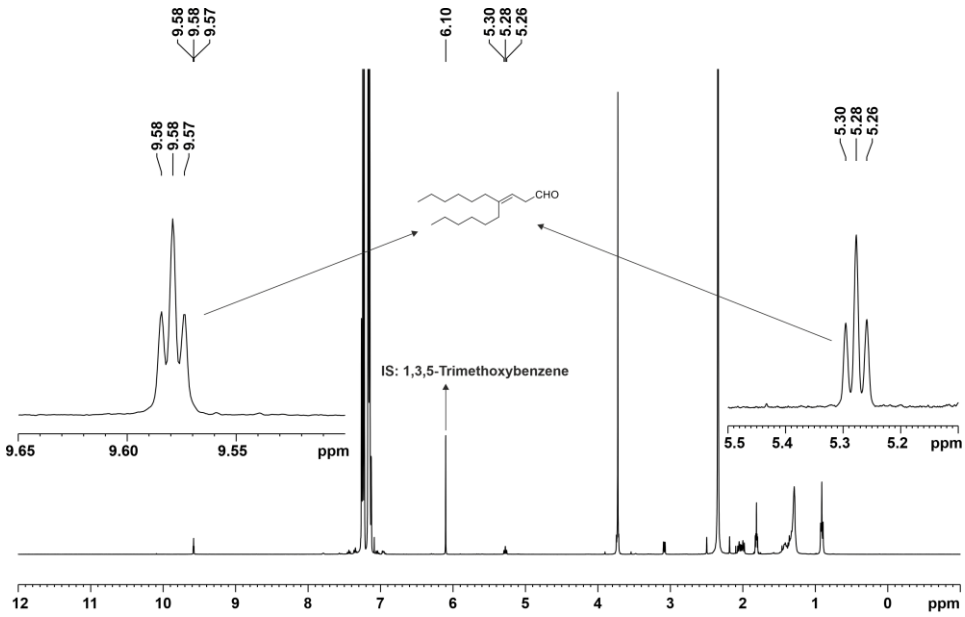

Figure 88. ^{1}H NMR of the mixtures derived from 7-vinylidenetridecane after hydroformylation.

2.5.29. Results of catalysis of the hydroformylation of (*E*)-oct-2-ene ((*E*)-S31b)

Table 48. Supramolecularly regulated hydroformylation of (*E*)-oct-2-ene (**(*E*)-S31b**).

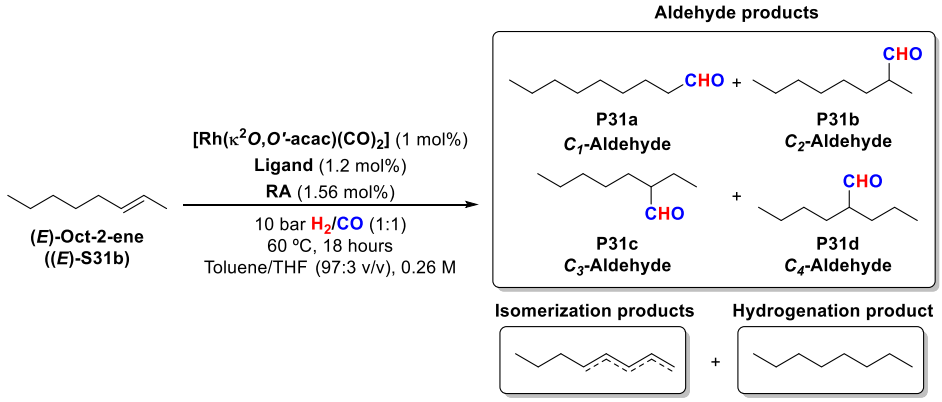

Entry	RA	Ligand	Conv. (%)	Select. (%)[a]		$C_1/C_2/C_3/C_4$ ratio (%)	$C_1/C_2/C_3/C_4$ yield (%)
				Isom.	Hydrog.		
1	**None**	**L46**	99	2	0.3	3:54:32:11	3:52:31:11
2	**LiBArF**	**L46**	98	42	6	2:56:36:6	1:29:18:3
3	**NaBArF**	**L46**	99	8	3	7:50:29:14	6:44:26:12
4	**KBArF**	**L46**	99	7	3	7:51:28:14	6:45:25:12
5	**RbBArF**	**L46**	99	3	1	8:51:27:14	8:48:26:13
6	**CsBArF**	**L46**	99	3	1	7:52:27:14	7:49:26:13
7	**None**	**L47**	99	2	0.2	3:54:32:11	3:52:31:11
8	**LiBArF**	**L47**	99	2	0.4	5:53:29:13	5:51:28:13
9	**NaBArF**	**L47**	99	2	0.2	5:53:29:13	5:51:28:13
10	**KBArF**	**L47**	99	3	1	5:53:29:13	5:50:28:12
11	**RbBArF**	**L47**	99	3	1	6:52:29:13	6:49:28:12
12	**CsBArF**	**L47**	99	2	0.4	6:52:29:13	6:50:28:13

The HF was performed in a parallel autoclave. Reaction conditions: [substrate] = 0.26 M; stirring rate = 800 rpm; 10 bar H_2/CO (1:1); 60 °C, 18h. Conversion was determined by GC using dodecane as an internal standard. Selectivity, ratio, and yield were determined by the area% values of the peaks in the GC chromatogram. [a] Selectivity of the isomerisation (Isom.) and hydrogenation (Hydrog.) processes.

2.5.30. Results of catalysis of the hydroformylation of (*Z*)-oct-2-ene ((*Z*)-S31b)

Table 49. Supramolecularly regulated hydroformylation of (*Z*)-oct-2-ene (**(*Z*)-S31b**).

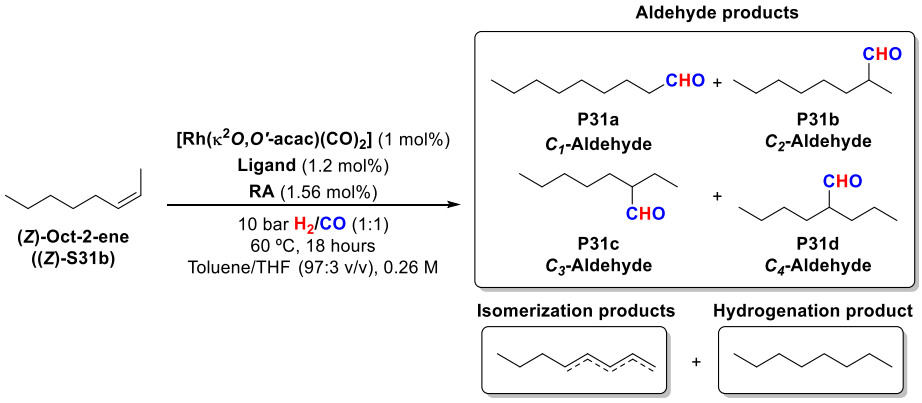

Entry	RA	Ligand	Conv. (%)	Select. (%)[a]		$C_1/C_2/C_3/C_4$ ratio (%)	$C_1/C_2/C_3/C_4$ yield (%)
				Isom.	Hydrog.		
1	**None**	**L46**	99	1	2	3:58:32:7	3:56:31:7
2	**LiBArF**	**L46**	98	14	5	2:60:34:4	2:48:27:3
3	**NaBArF**	**L46**	99	8	6	6:54:30:10	5:46:26:9
4	**KBArF**	**L46**	99	8	12	8:56:26:10	6:44:21:8
5	**RbBArF**	**L46**	99	4	8	8:55:26:11	7:48:23:10
6	**CsBArF**	**L46**	99	6	9	7:57:27:9	6:48:23:8
7	**None**	**L47**	99	0.5	2	3:57:32:8	3:55:31:8
8	**LiBArF**	**L47**	99	0.6	2	5:56:28:11	5:54:27:11
9	**NaBArF**	**L47**	99	0.5	2	5:56:28:11	5:54:27:11
10	**KBArF**	**L47**	99	2	4	5:57:29:9	5:53:27:8
11	**RbBArF**	**L47**	99	3	5	5:56:30:9	5:51:27:8
12	**CsBArF**	**L47**	99	2	3	6:56:29:9	6:53:27:8

The HF was performed in a parallel autoclave. Reaction conditions: [substrate] = 0.26 M; stirring rate = 800 rpm; 10 bar H_2/CO (1:1); 60 °C, 18h. Conversion was determined by GC using dodecane as an internal standard. Selectivity, ratio, and yield were determined by the area% values of the peaks in the GC chromatogram. [a] Selectivity of the isomerisation (Isom.) and hydrogenation (Hydrog.) processes.

2.5.31. Results of catalysis of the hydroformylation of (*E*)-oct-3-ene ((*E*)-S31c)

Table 50. Supramolecularly regulated hydroformylation of (*E*)-oct-3-ene (**(*E*)-S31c**).

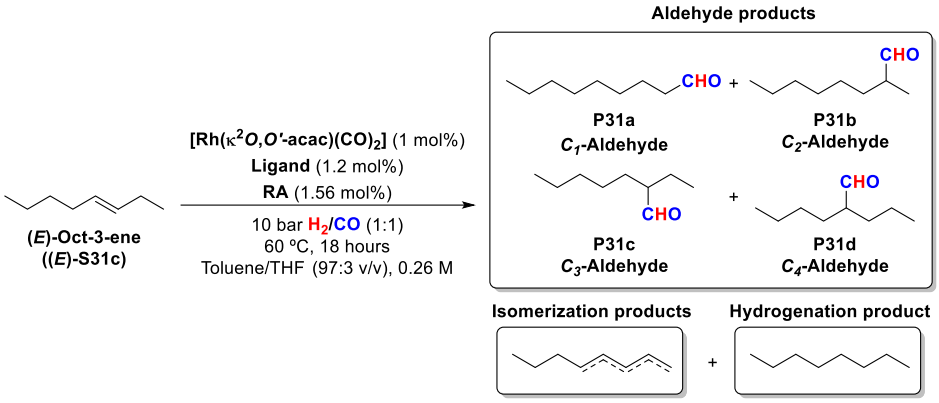

Entry	RA	Ligand	Conv. (%)	Select. (%)[a]		$C_1/C_2/C_3/C_4$ ratio (%)	$C_1/C_2/C_3/C_4$ yield (%)
				Isom.	Hydrog.		
1	**None**	**L46**	99	1	0.3	3:19:37:41	3:19:36:40
2	**LiBArF**	**L46**	96	8	10	1:13:42:44	1:10:33:35
3	**NaBArF**	**L46**	99	2	0.1	5:24:34:37	5:23:33:36
4	**KBArF**	**L46**	99	1	0.1	6:27:32:35	6:26:31:34
5	**RbBArF**	**L46**	99	2	0.1	7:28:31:34	7:27:30:33
6	**CsBArF**	**L46**	99	0	0.1	7:29:31:33	7:29:31:33
7	**None**	**L47**	99	0	0	3:21:36:40	3:21:36:40
8	**LiBArF**	**L47**	99	2	0	4:22:36:38	4:21:35:37
9	**NaBArF**	**L47**	99	1	0	7:28:31:34	7:27:30:33
10	**KBArF**	**L47**	99	2	0	7:28:31:34	7:27:30:33
11	**RbBArF**	**L47**	99	1	0	6:27:32:35	6:26:31:34
12	**CsBArF**	**L47**	99	1	0	6:27:32:35	6:26:31:34

The HF was performed in a parallel autoclave. Reaction conditions: [substrate] = 0.26 M; stirring rate = 800 rpm; 10 bar H_2/CO (1:1); 60 °C, 18h. Conversion was determined by GC using dodecane as an internal standard. Selectivity, ratio, and yield were determined by the area% values of the peaks in the GC chromatogram. [a] Selectivity of the isomerisation (Isom.) and hydrogenation (Hydrog.) processes.

2.5.32. Results of catalysis of the hydroformylation of (*E*)-oct-4-ene ((*E*)-S31d)

Table 51. Supramolecular regulated hydroformylation of (*E*)-oct-4-ene (**(*E*)-S31d**).

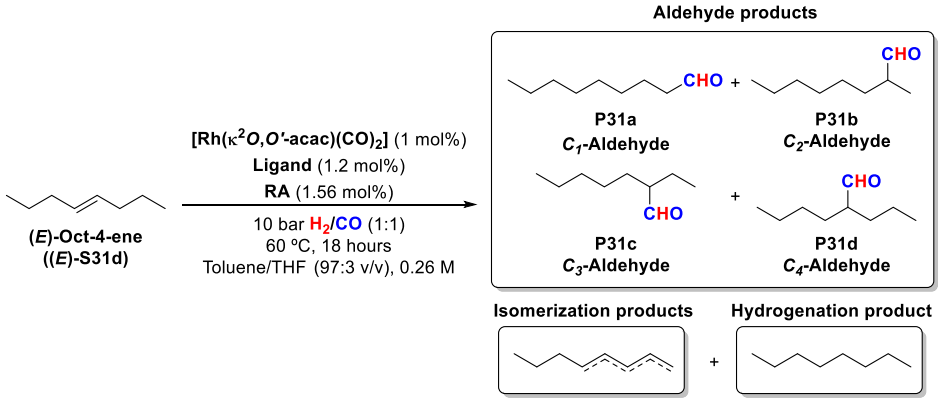

Entry	RA	Ligand	Conv. (%)	Select. (%)[a]		$C_1/C_2/C_3/C_4$ ratio (%)	$C_1/C_2/C_3/C_4$ yield (%)
				Isom.	Hydrog.		
1	**None**	**L46**	99	1	0.7	0:6:22:72	0:6:21:70
2	**LiBArF**	**L46**	87	34	1	0:1:13:86	0:1:7:49
3	**NaBArF**	**L46**	95	6	3	1:9:27:63	1:8:23:54
4	**KBArF**	**L46**	98	3	1	1:12:28:59	1:11:26:56
5	**RbBArF**	**L46**	99	2	0.3	1:14:28:57	1:14:27:55
6	**CsBArF**	**L46**	99	2	0.2	1:14:28:57	1:14:27:55
7	**None**	**L47**	99	2	0	0:6:23:71	0:6:22:69
8	**LiBArF**	**L47**	98	4	1	0:7:25:68	0:7:23:63
9	**NaBArF**	**L47**	99	2	0	1:12:27:60	1:12:26:58
10	**KBArF**	**L47**	99	2	0.1	1:13:27:59	1:13:26:57
11	**RbBArF**	**L47**	99	1	0.1	1:13:27:59	1:13:26:58
12	**CsBArF**	**L47**	99	2	0	1:12:27:60	1:12:26:58

The HF was performed in a parallel autoclave. Reaction conditions: [substrate] = 0.26 M; stirring rate = 800 rpm; 10 bar H_2/CO (1:1); 60 °C, 18h. Conversion was determined by GC using dodecane as an internal standard. Selectivity, ratio, and yield were determined by the area% values of the peaks in the GC chromatogram. [a] Selectivity of the isomerisation (Isom.) and hydrogenation (Hydrog.) processes.

2.5.33. Results of catalysis of the hydroformylation of (*Z*)-oct-4-ene ((*Z*)-S31d)

Table 52. Supramolecular regulated hydroformylation of (*E*)-oct-4-ene (**(*E*)-S31d**).

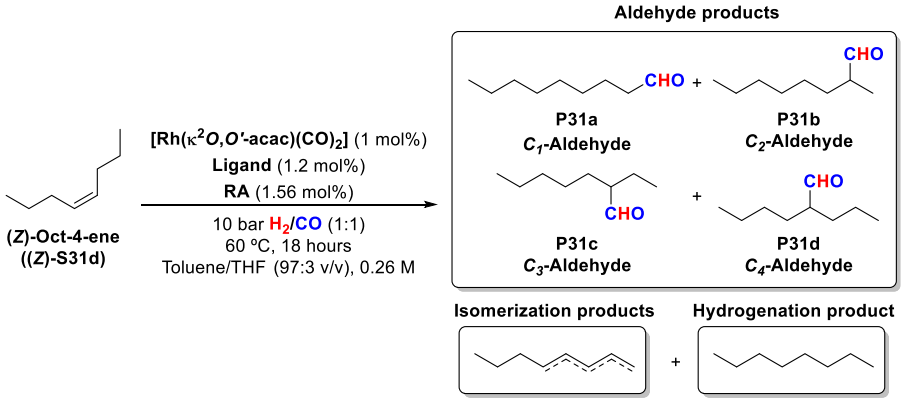

Entry	RA	Ligand	Conv. (%)	Select. (%)[a]		$C_1/C_2/C_3/C_4$ ratio (%)	$C_1/C_2/C_3/C_4$ yield (%)
				Isom.	Hydrog.		
1	**None**	**L46**	99	1	2	3:20:28:49	3:19:27:4
2	**LiBArF**	**L46**	99	2	2	7:28:28:37	7:27:27:35
3	**NaBArF**	**L46**	99	2	2	14:35:25:26	13:33:24:25
4	**KBArF**	**L46**	99	2	2	11:34:26:29	10:32:25:28
5	**RbBArF**	**L46**	99	1	1	9:31:27:33	9:30:26:32
6	**CsBArF**	**L46**	99	2	2	11:33:25:31	10:31:24:29
7	**None**	**L47**	99	3	0	4:20:28:48	4:19:27:46
8	**LiBArF**	**L47**	99	3	0	7:28:27:38	7:27:26:36
9	**NaBArF**	**L47**	99	3	0	16:36:23:25	15:35:22:24
10	**KBArF**	**L47**	99	3	0	14:35:24:27	13:34:23:26
11	**RbBArF**	**L47**	99	4	0	13:34:24:29	12:32:23:28
12	**CsBArF**	**L47**	99	3	0	12:34:25:29	12:33:24:28

The HF was performed in a parallel autoclave. Reaction conditions: [substrate] = 0.26 M; stirring rate = 800 rpm; 10 bar H_2/CO (1:1); 60 °C, 18h. Conversion was determined by GC using dodecane as an internal standard. Selectivity, ratio, and yield were determined by the area% values of the peaks in the GC chromatogram. [a] Selectivity of the isomerisation (Isom.) and hydrogenation (Hydrog.) processes.

2.5.34. Results of catalysis of the hydroformylation under partial pressures of H_2/CO

Table 53. Supramolecularly regulated hydroformylation of substrates **S31a**, **S49**, **S50** and **S51**.

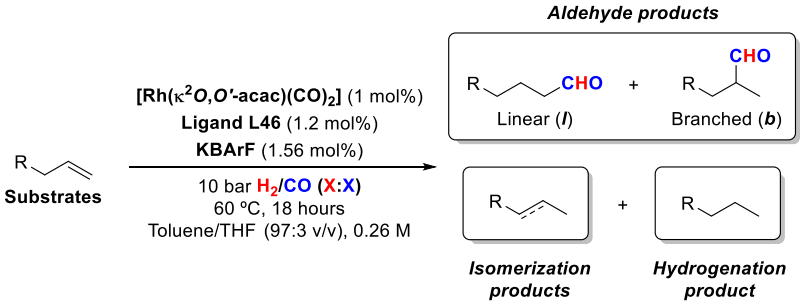

Entry	Substrate	Pressure H_2/CO (X:X)	Conv. (%)	Select. (%)[a]		*l/b* ratio (%)	*l/b* yield (%)
				Isom.	Hydrog.		
1	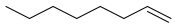 S31a	(1:1)	98	8	14	97:3	74:2
2		(3:7)	99	3	14	97:3	80:2
3		(7:3)	99	5	19	98:2	74:2
4	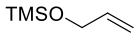 S49	(1:1)	99	-	-	87:13	67:10
5		(3:7)	99	-	-	86:14	68:11
6		(7:3)	99	-	-	89:11	70:9
7	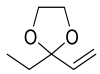 S50	(1:1)	84	-	-	96:4	57:3
8		(3:7)	87	-	-	96:4	76:4
9		(7:3)	99	-	-	97:3	89:3
10	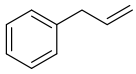 S51	(1:1)	99	2	6	95:5	87:5
11		(3:7)	99	2	6	96:4	87:4
12		(7:3)	99	6	9	98:2	82:2

The HF was performed in a parallel autoclave. Reaction conditions: [substrate] = 0.26 M; stirring rate = 800 rpm; 10 bar H_2/CO (X:X); 60 °C, 18h. For substrates **S31a** and **S51**, the conversion was determined by GC using dodecane as an internal standard. Selectivity, ratio, and yield were determined by the area% values of the peaks in the GC chromatogram. For the substrates **S49** and **S50**, the conversion, ratio, selectivity, and yield were determined by ^1H NMR using 1,3,5-trimethoxybenzene as internal standard. [a] Selectivity of the isomerisation (Isom.) and hydrogenation (Hydrog.) processes.

2.5.35. General procedure for the isomerisation-hydroformylation tandem reaction

The Pd-mediated isomerisation Rh-mediated asymmetric hydroformylation tandem reaction of an equimolecular mixture of octenes, heptenes, hexenes and allylbenzenes was performed by adding stock solutions of bisphosphite ligand **L46** (1.20 mol%), KBArF salt (3.6 – 10.0 mol%), [Rh(κ^2*O*,*O'*-acac)(CO)$_2$] (1.0 mol%), [{Pd(μ-Br)(*t*Bu$_3$P)}$_2$] (1.0 mol %), [Pd(*t*Bu$_3$P)$_2$] (0.5 – 3.0 mol%) and PdI_2 (0.5 mol%) in a vial with a magnetic bar. The corresponding mixture of alkenes (overall molar amount of octenes, heptenes, hexenes or allylbenzenes = 1 mmol), dodecane (30 mol%, internal standard) and toluene/THF (97:3 v/v) were charged to provide the desired final concentration of 0.26 M.

Once the reaction mixture was loaded, the vial vessel was then placed into one of the holes of a steel autoclave reactor (HEL Cat-24 parallel pressure multireactor) and taken out of the glove box. The autoclave was purged three times with H_2/CO (1:1) (pressure not higher than 10 bar) and finally, the autoclave was pressurized with H_2/CO (1:1) to the desired pressure (10 bar). The reaction mixture was stirred at 60 or 100 °C for 18 hours. The reaction was cooled, and the pressure was carefully released in a well-ventilated hood. Conversion, chemo- , regio-selectivity and yield of the products arising from hydroformylation reaction conditions were determined by GC analysis on an achiral stationary phase (HP-5) using dodecane as the internal standard.

2.5.36. Results of isomerisation-hydroformylation tandem reactions

Table 54. Screening of isomerisation-hydroformylation tandem reactions of an equimolar mixture of octenes (selectivity of aldehydes).

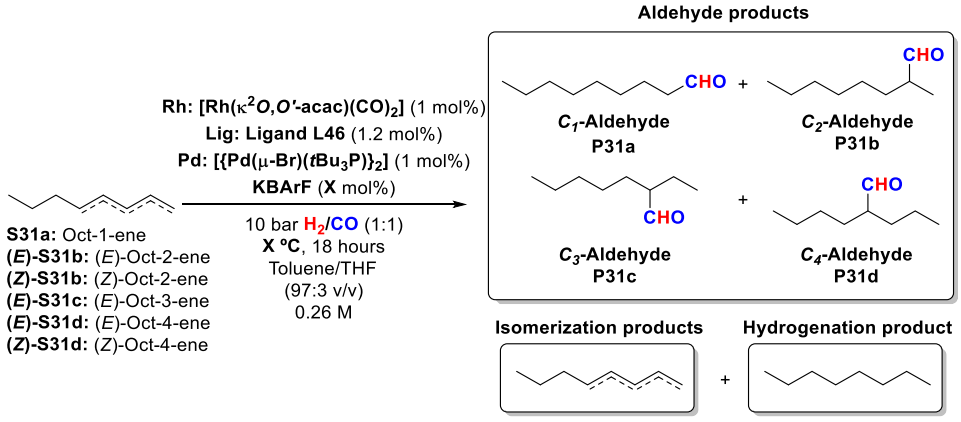

Entry	Rh	Lig	Pd	KBArF	Temp. (°C)	Select. Aldehydes (%)	P31 $C_1/C_2/C_3/C_4$ ratio (%)
1	✓	✓	-	-	60	98	8:31:26:34
2	✓	✓	-	1.56	60	94	11:32:27:30
3	✓	✓	✓	-	60	-	-
4	✓	✓	✓	-	100	-	-
5	✓	✓	✓	1.56	60	7	42:44:6:8
6	✓	✓	✓	3.6	100	7	39:39:11:11
7	-	-	✓	-	60	-	-
8	-	-	✓	-	100	-	-

The isomerisation-hydroformylation tandem reaction was performed in a parallel autoclave. Reaction conditions: [substrate] = 0.26 M; stirring rate = 800 rpm; 10 bar H_2/CO (1:1); 18h. Selectivity and ratio were determined by GC using dodecane as an internal standard.

Table 55. Screening of isomerisation-hydroformylation tandem reactions of an equimolar mixture of octenes (selectivity of alkenes).

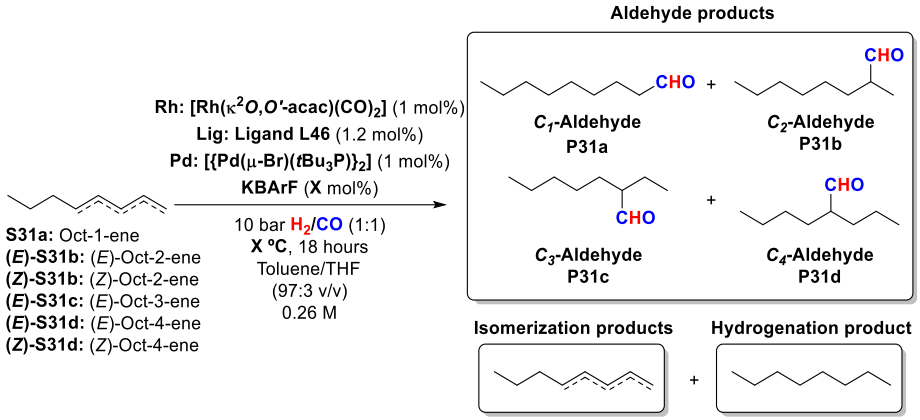

Entry	Rh	Lig	Pd	KBArF (mol%)	Temp. (°C)	Molar amounts of unreacted alkene (%)[a]				
						S31a	(*E*)-S31b	(*Z*)-S31b	(*E*)-S31c + (*E*)-S31d	(Z)-S31d
1	✓	✓	-	-	60	-	-	-	2	-
2	✓	✓	-	1.56	60	1	1	-	3	1
3	✓	✓	✓	-	60	3	30	17	34	16
4	✓	✓	✓	-	100	2	28	11	41	18
5	✓	✓	✓	1.56	60	3	21	17	35	17
6	✓	✓	✓	3.6	100	1	25	9	39	18
7	-	-	✓	-	60	1	30	10	40	19
8	-	-	✓	-	100	2	28	11	41	18

The HF was performed in a parallel autoclave. Reaction conditions: [substrate] = 0.26 M; stirring rate = 800 rpm; 10 bar H_2/CO (1:1); 18h. Selectivity was determined by GC using dodecane as an internal standard. [a] Molar amounts of unreacted alkene **S31a**: oct-1-ene; **(*E*)-S31b**: (*E*)-oct-2-ene; **(*Z*)-S31b**: (*Z*)-oct-2-ene; **(*E*)-S31c**: (*E*)-oct-3-ene; **(*E*)-S31d**: (*E*)-oct-4-ene; **(*Z*)-S31d**: (*Z*)-oct-4-ene.

Table 56. Screening of isomerisation-hydroformylation tandem reactions of an equimolar mixture of octenes

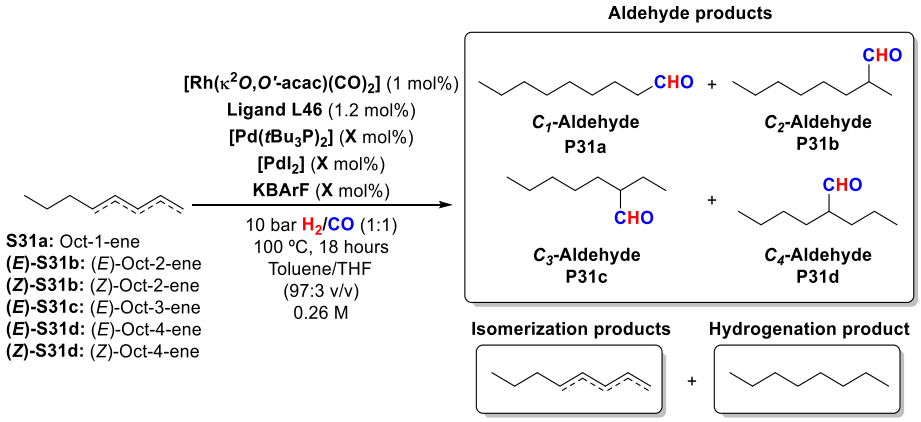

Entry	Pd(*t*Bu₃P)₂ (mol%)	PdI₂ (mol%)	KBArF (mol%)	Select. Hydrog. (%)	Select. Aldehydes (%)	P31 $C_1/C_2/C_3/C_4$ ratio (%)
1	0.5	0.5	3.6	0	78	37:36:14:13
2	1	0	3.6	0	97	21:34:21:24
3	2.5	0	4.6	0	90	33:26:18:22
4	2.5	0.5	3.6	0	91	31:31:18:20
5	3	0	10	0	76	41:22:17:21
6	3	0.5	3.6	0	96	24:31:21:24

Entry	Pd(*t*Bu₃P)₂ (mol%)	PdI₂ (mol%)	KBArF (mol%)	Molar amounts of unreacted alkene (%)[a]				
				S31a	(*E*)-S31b	(*Z*)-S31b	(*E*)-S31c + (*E*)-S31d	(*Z*)-S31d
7	0.5	0.5	3.6	1	5	2	10	4
8	1	0	3.6	1	-	-	2	-
9	2.5	0	4.6	3	1	-	5	1
10	2.5	0.5	3.6	3	1	-	4	1
11	3	0	10	4	3	1	11	5
12	3	0.5	3.6	1	1	-	2	-

The HF was performed in a parallel autoclave. Reaction conditions: [substrate] = 0.26 M; stirring rate = 800 rpm; 10 bar H_2/CO (1:1); 100 °C, 18h. Selectivity and ratio were determined by GC using dodecane as an internal standard. [a] Molar amounts of unreacted alkene **S31a**: oct-1-ene; **(*E*)-S31b**: (*E*)-oct-2-ene; **(*Z*)-S31b**: (*Z*)-oct-2-ene; **(*E*)-S31c**: (*E*)-oct-3-ene; **(*E*)-S31d**: (*E*)-oct-4-ene; **(*Z*)-S31d**: (*Z*)-oct-4-ene.

Table 57. Isomerisation-hydroformylation reactions of an equimolar mixture of hexenes.

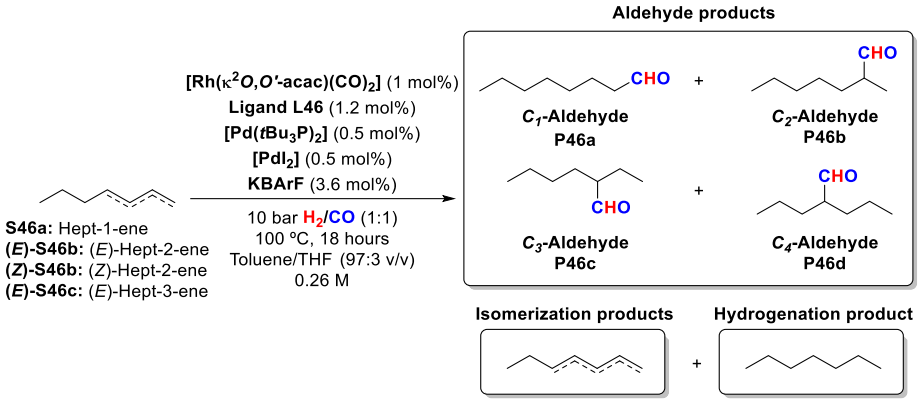

Entry	Molar amounts of unreacted alkene (%)[a]				Selectivity (%)[b]		P46 $C_1/C_2/C_3/C_4$ ratio (%)
	(*E*)-S46a	(*E*)-S46b	(*Z*)-S46b	(*E*)-S46c	Hydrog.	Aldehydes	
1	1	5	4	1	1	89	46:33:15:6

The HF was performed in a parallel autoclave. Reaction conditions: [substrate] = 0.26 M; stirring rate = 800 rpm; 10 bar H_2/CO (1:1); 100 °C, 18h. Selectivity and ratio were determined by GC using dodecane as an internal standard. [a] Molar amounts of unreacted alkene **S46a**: hept-1-ene; **(*E*)-S46b**: (*E*)-hept-2-ene; **(*Z*)-S46b**: (*Z*)-hept-2-ene; **(*E*)-S46c**: (*E*)-hept-3-ene. [b] Selectivity of the hydrogenation product and aldehydes.

Table 58. Isomerisation-hydroformylation reactions of an equimolar mixture of hexenes.

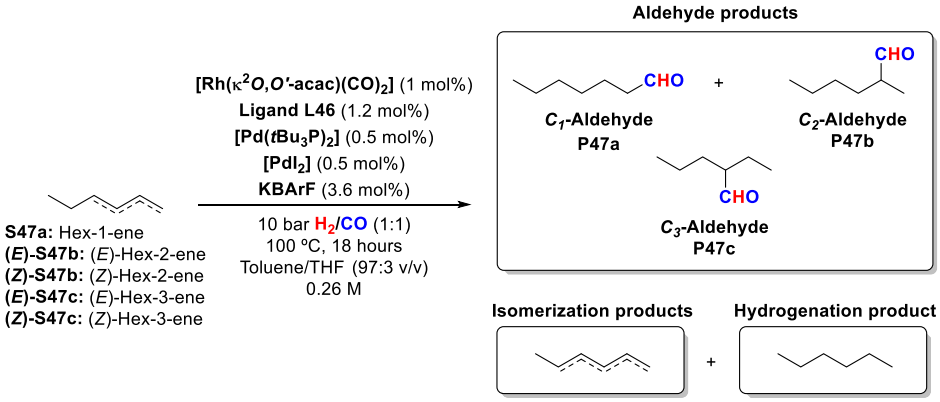

Entry	Molar amounts of unreacted alkene (%)[a]			Selectivity (%)[a]		P47 $C_1/C_2/C_3$ ratio (%)
	S47a	(*E*)-S47b + (*E*)-S47c + (*E*)-S47c	(*Z*)-S47b	Hydrog.	Aldehydes	
1	0.5	8	2.5	2	87	58:28:14

The HF was performed in a parallel autoclave. Reaction conditions: [substrate] = 0.26 M; stirring rate = 800 rpm; 10 bar H_2/CO (1:1); 100 °C, 18h. Selectivity and ratio were determined by GC using dodecane as an internal standard. [a] Molar amounts of unreacted alkene **S47a**: Hex-1-ene; **(*E*)-S47b**: (*E*)-Hex-2-ene; **(*Z*)-S47b**: (*Z*)-hex-2-ene; **(*E*)-S47c**: (*E*)-hex-3-ene; **(*E*)-S47c**: (*Z*)-hex-3-ene. [b] Selectivity of the hydrogenation product and aldehydes.

Table 59. Isomerisation-hydroformylation reactions of an equimolar mixture hexenes.

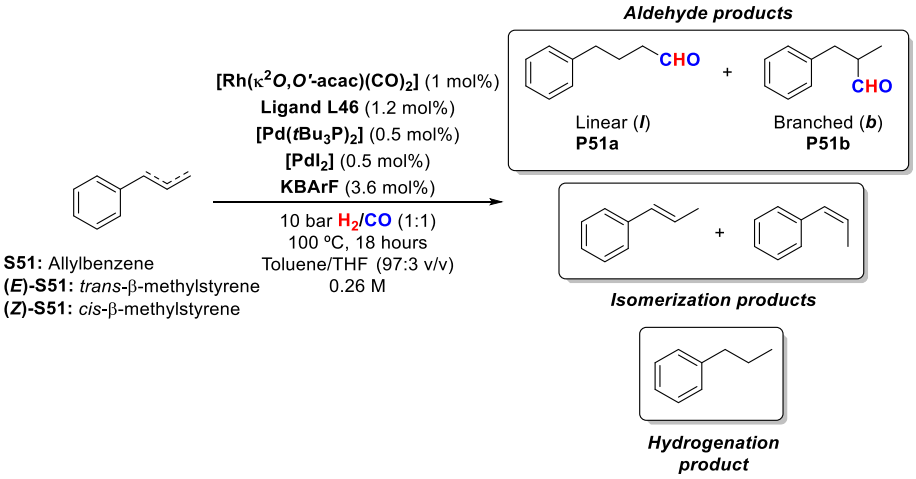

Entry	Molar amounts of unreacted alkene (%)[a]			Selectivity (%)[b]		*l*/*b* ratio (%)
	S51	(*E*)-S51	(*Z*)-S51	Hydrog.	Aldehydes	
1	3	50	15	2	30	86:14

The HF was performed in a parallel autoclave. Reaction conditions: [substrate] = 0.26 M; stirring rate = 800 rpm; 10 bar H_2/CO (1:1); 100 °C, 18h. Selectivity and ratio were determined by GC using dodecane as an internal standard. [a] Molar amounts of unreacted alkene **S51**: allylbenzene; **(*E*)-S51**: *trans*-β-methylstyrene; **(*Z*)-S51**: *cis*-β-methylstyrene. [b] Selectivity of the hydrogenation product and aldehydes.

2.5.37. NMR spectrum of ligands L46, L47 and substrates

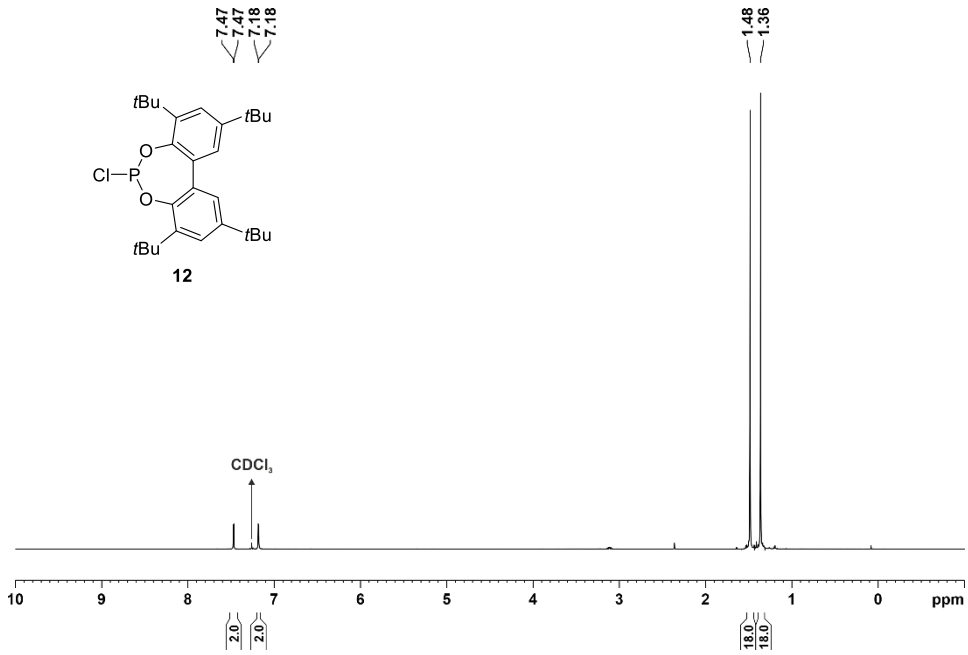

Figure 89. ^{1}H NMR (400 MHz, $CDCl_3$) of isolated compound 3,3',5,5'-tetra-*tert*-butylbiphenyl-2,2'-diyl chlorophosphite (**12**).

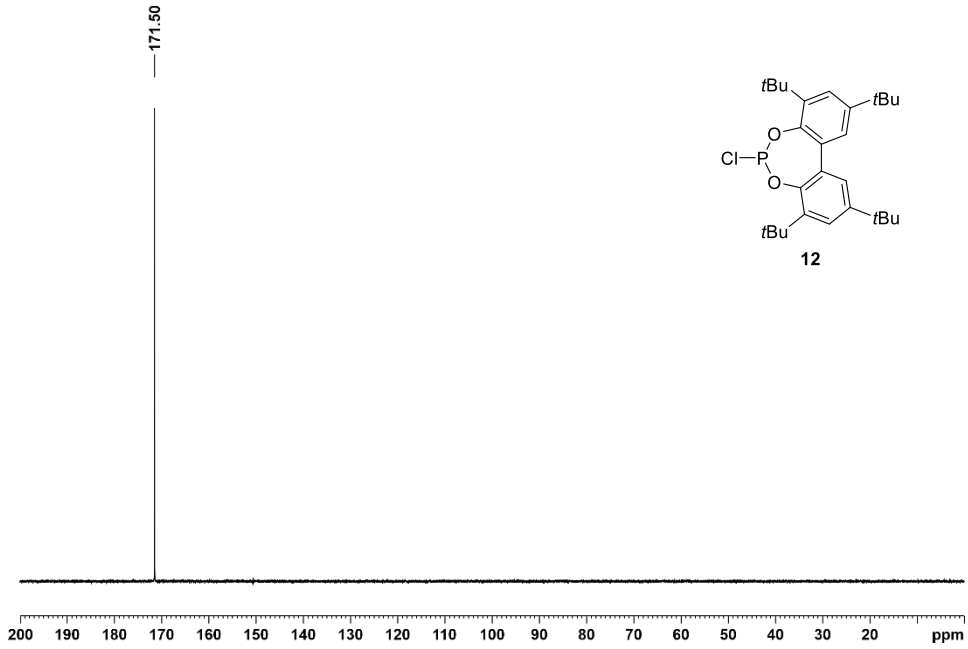

Figure 90. $^{31}P\{^{1}H\}$ NMR (162 MHz, $CDCl_3$) of isolated compound 3,3',5,5'-tetra-*tert*-butylbiphenyl-2,2'-diyl chlorophosphite (**12**).

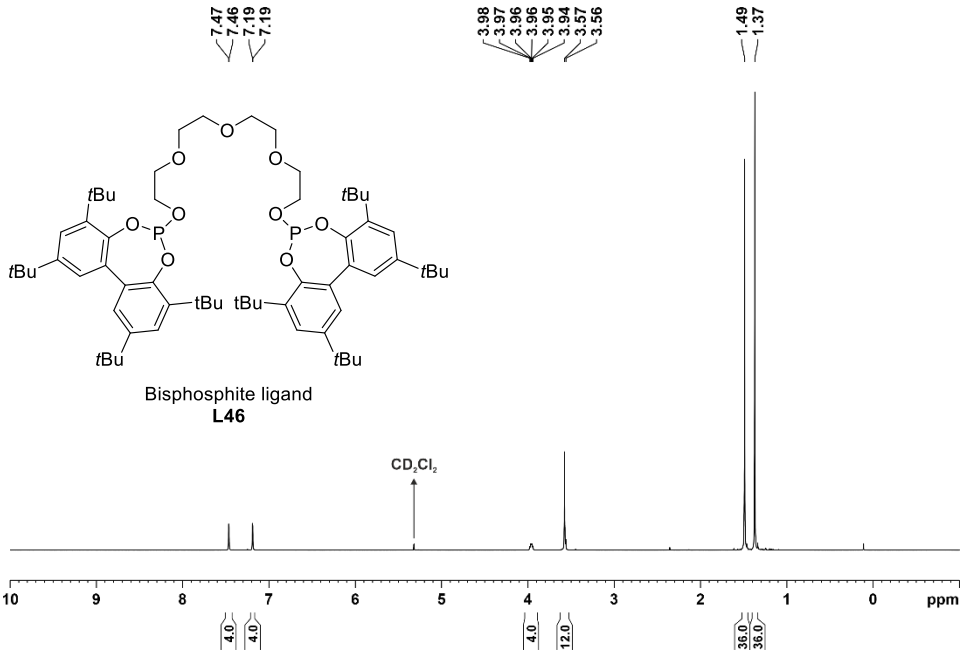

Figure 91. ^{1}H NMR (500 MHz, CD_2Cl_2) of isolated compound bisphosphite ligand **L46**.

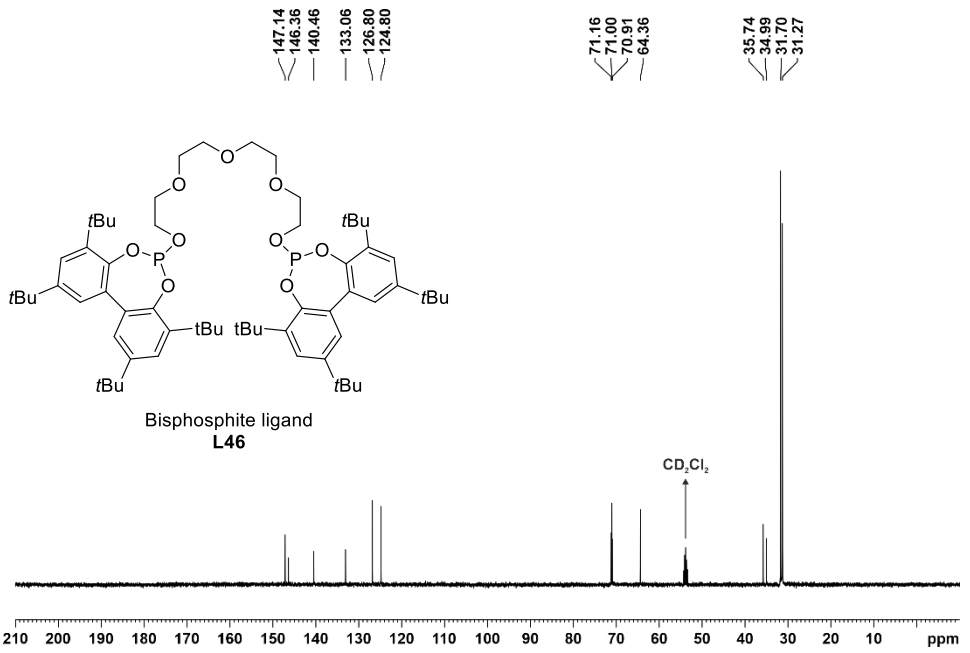

Figure 92. $^{13}C\{^{1}H\}\{^{31}P\}$ NMR (126 MHz, CD_2Cl_2) of isolated compound bisphosphite ligand **L46**.

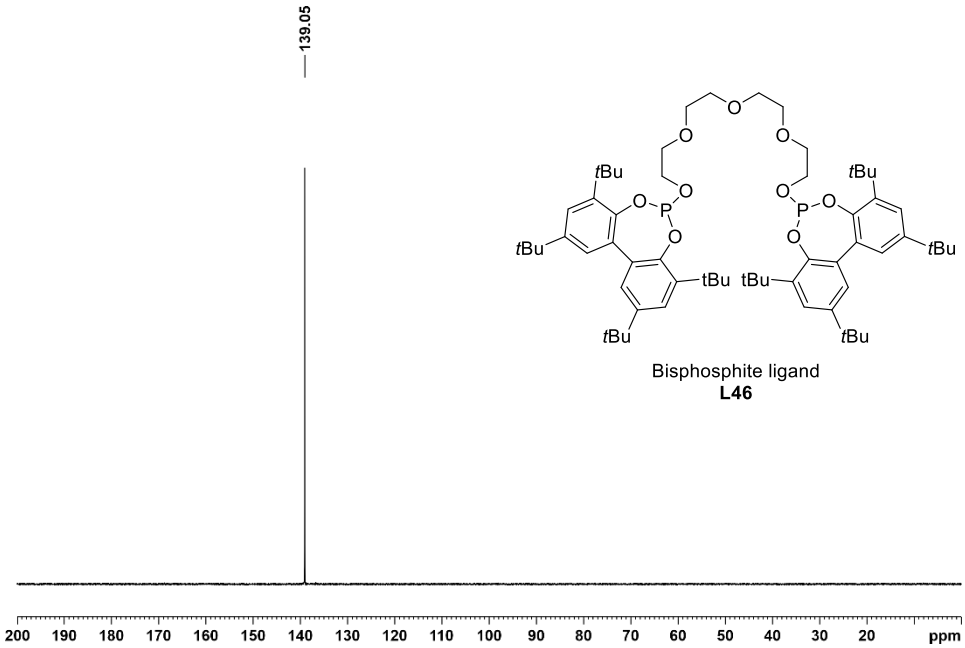

Figure 93. $^{31}P\{^{1}H\}$ NMR (202 MHz, CD_2Cl_2) of isolated compound bisphosphite ligand **L46**.

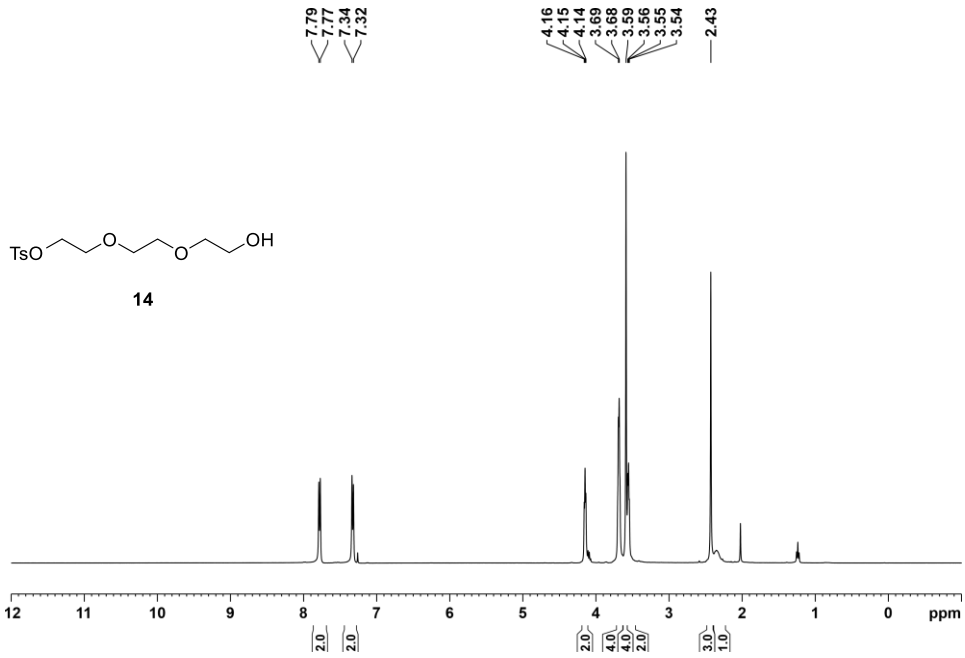

Figure 94. ^{1}H NMR (400 MHz, $CDCl_3$) of the isolated compound **14**.

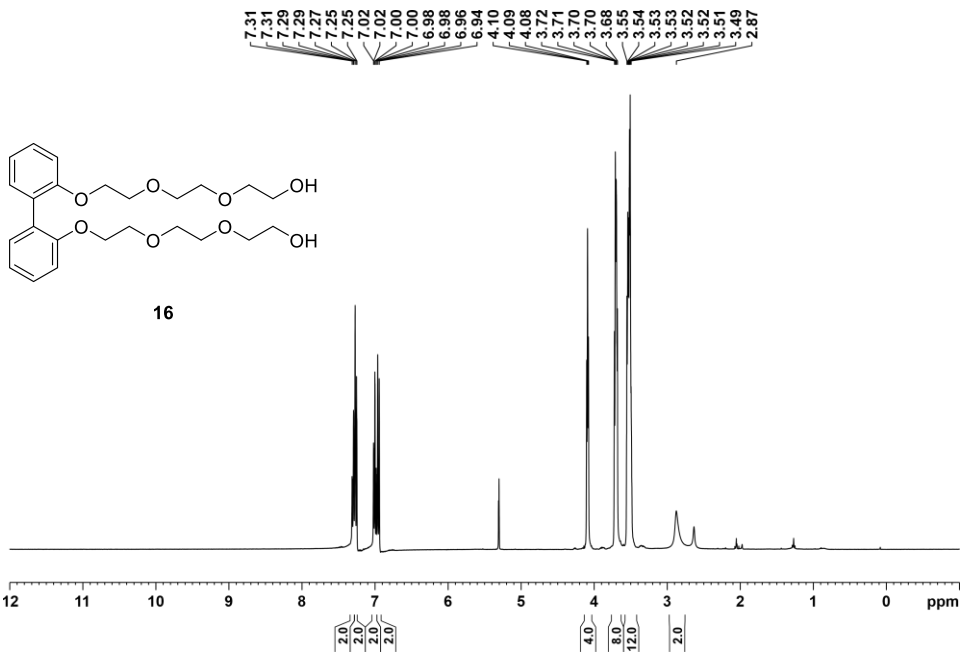

Figure 95. ^{1}H NMR (400 MHz, $CDCl_3$) of isolated compound **16**.

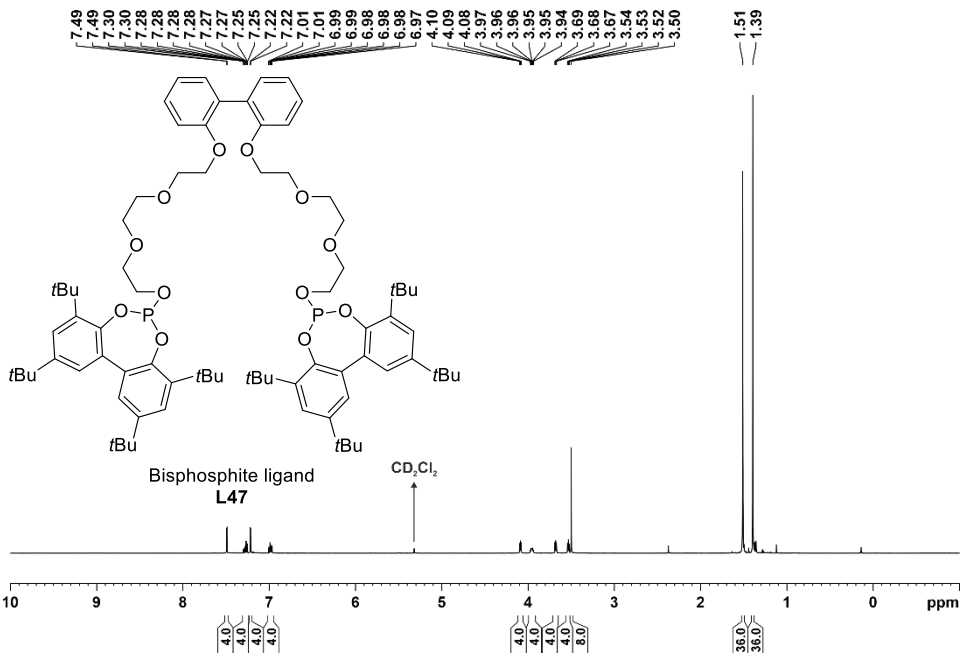

Figure 96. ^{1}H NMR (500 MHz, CD_2Cl_2) of isolated compound bisphosphite ligand **L47**.

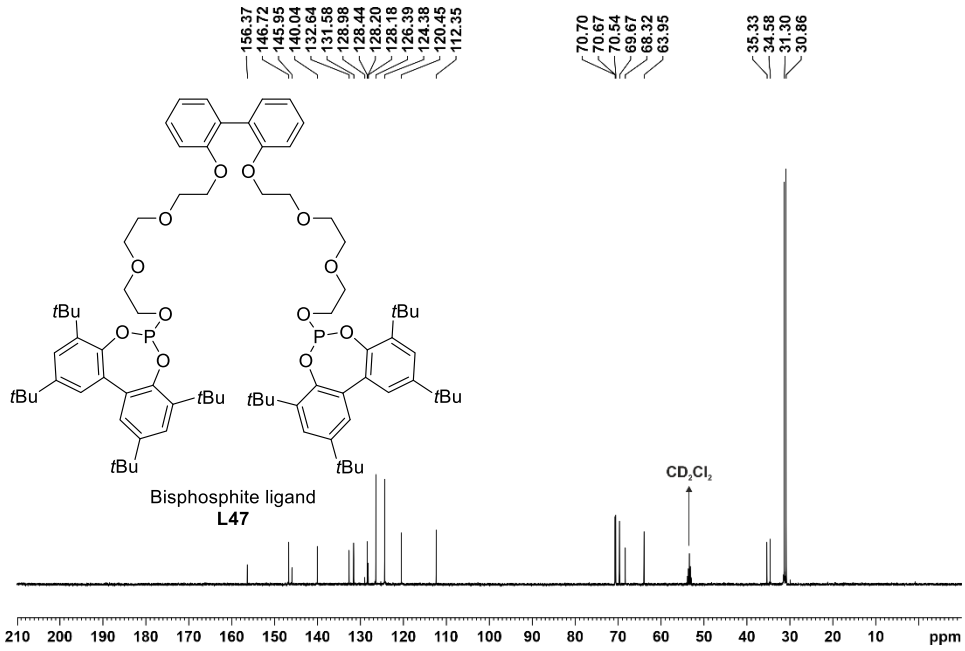

Figure 97. $^{13}C\{^{1}H\}\{^{31}P\}$ NMR (126 MHz, CD_2Cl_2) of isolated compound bisphosphite ligand **L47**.

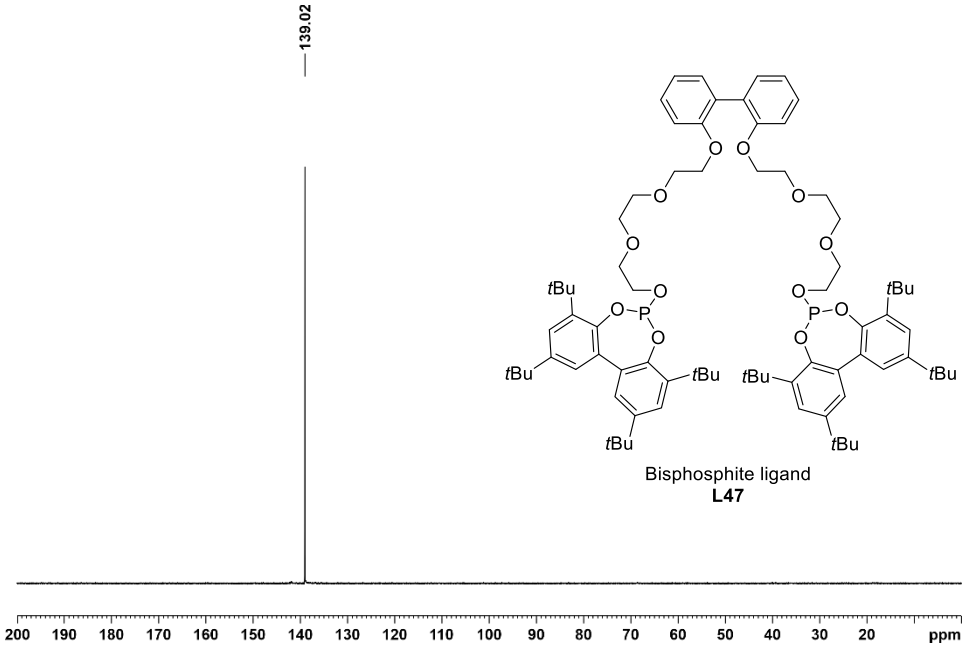

Figure 98. $^{31}P\{^{1}H\}$ NMR (202 MHz, CD_2Cl_2) of isolated compound bisphosphite ligand **L47**.

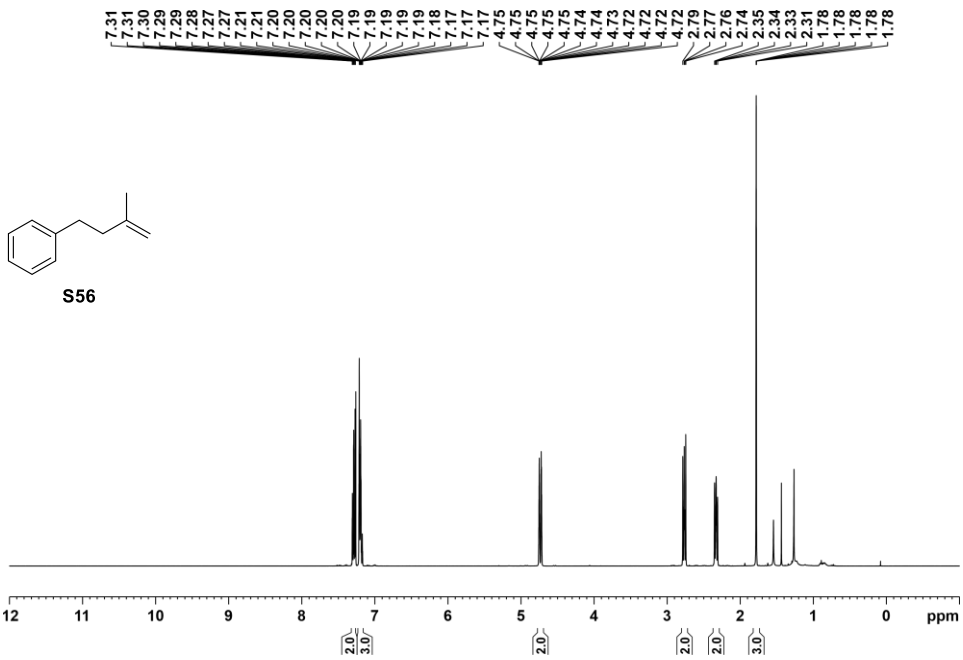

Figure 99. ^{1}H NMR (400 MHz, $CDCl_3$) of isolated substrate **S56**.

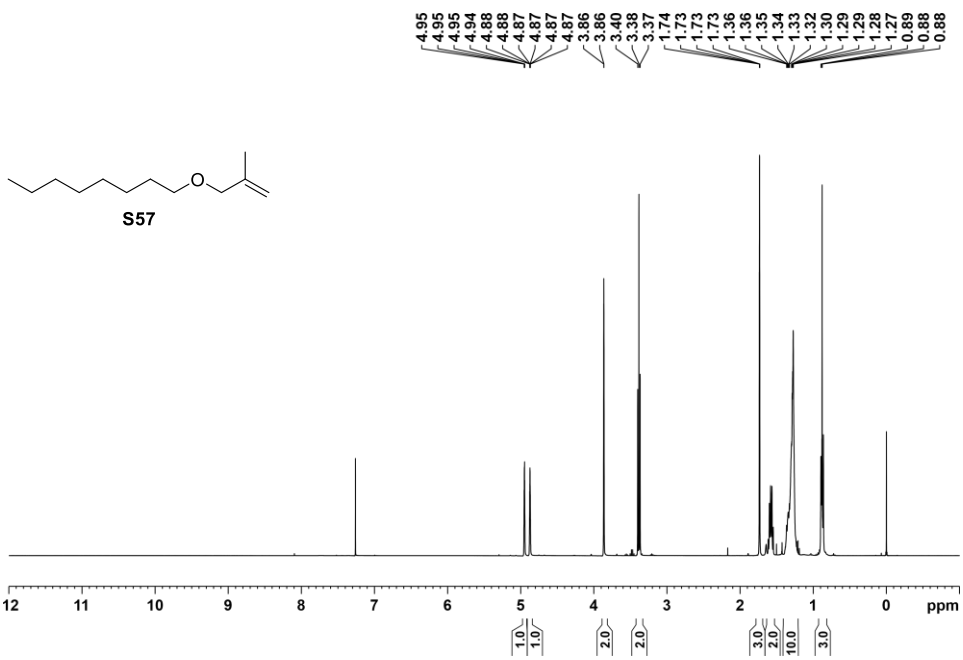

Figure 100. ^{1}H NMR (400 MHz, $CDCl_3$) of isolated substrate **S57**.

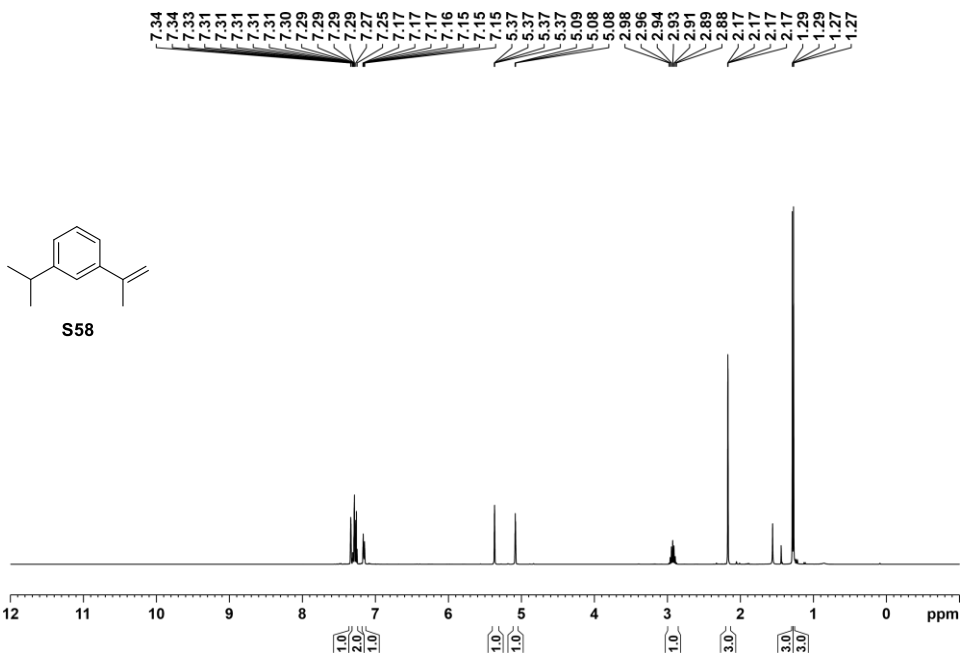

Figure 101. ^{1}H NMR (400 MHz, $CDCl_3$) of isolated substrate **S58**.

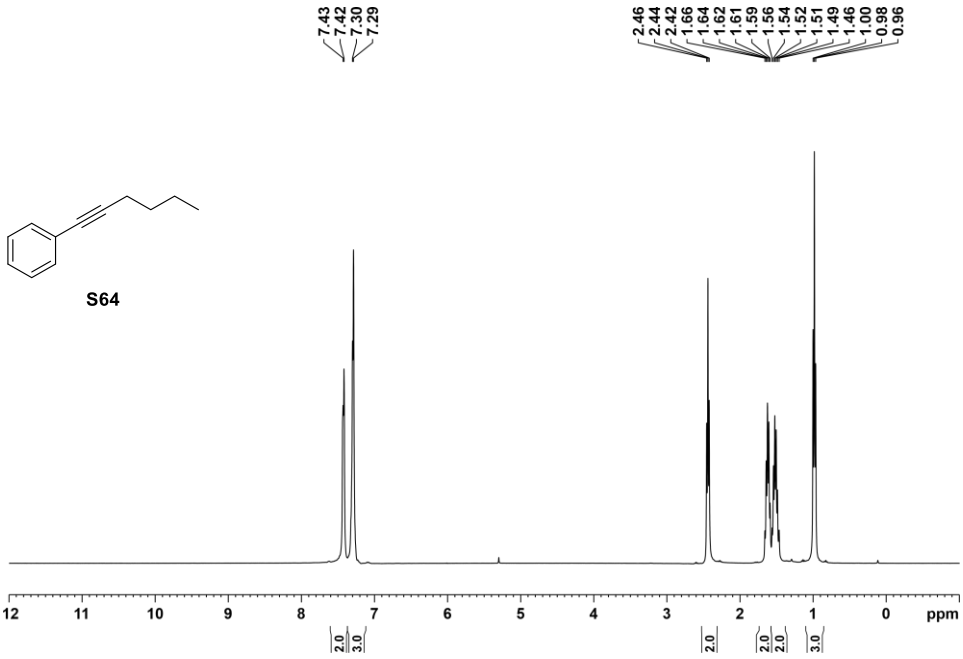

Figure 102. ^{1}H NMR (400 MHz, $CDCl_3$) of isolated substrate **S64**.

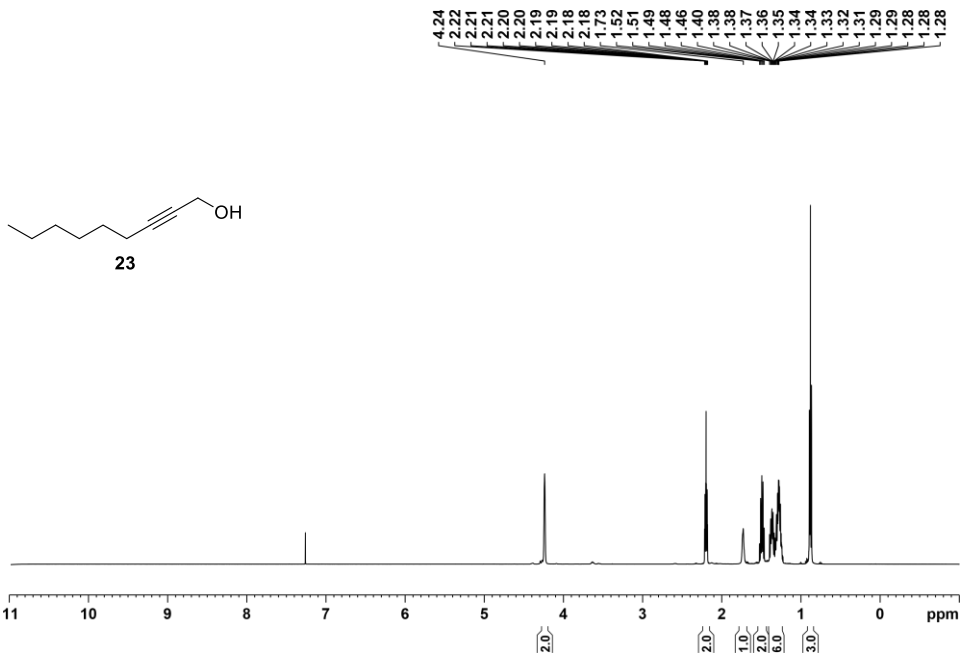

Figure 103. ^{1}H NMR (400 MHz, $CDCl_3$) of isolated compound **23**.

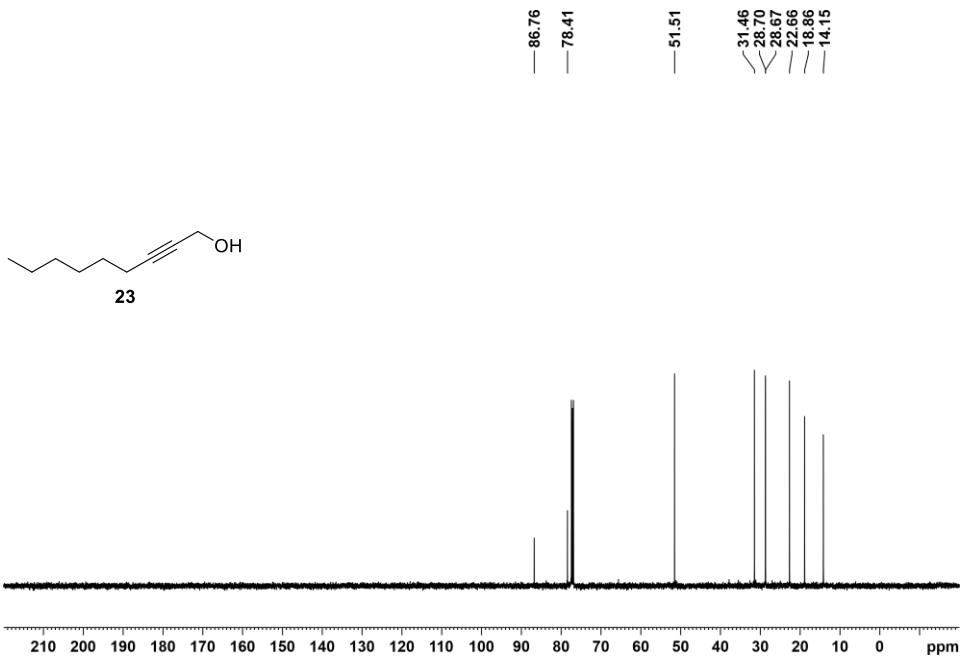

Figure 104. $^{13}C\{^{1}H\}$ NMR (101 MHz, $CDCl_3$) of isolated compound **23**.

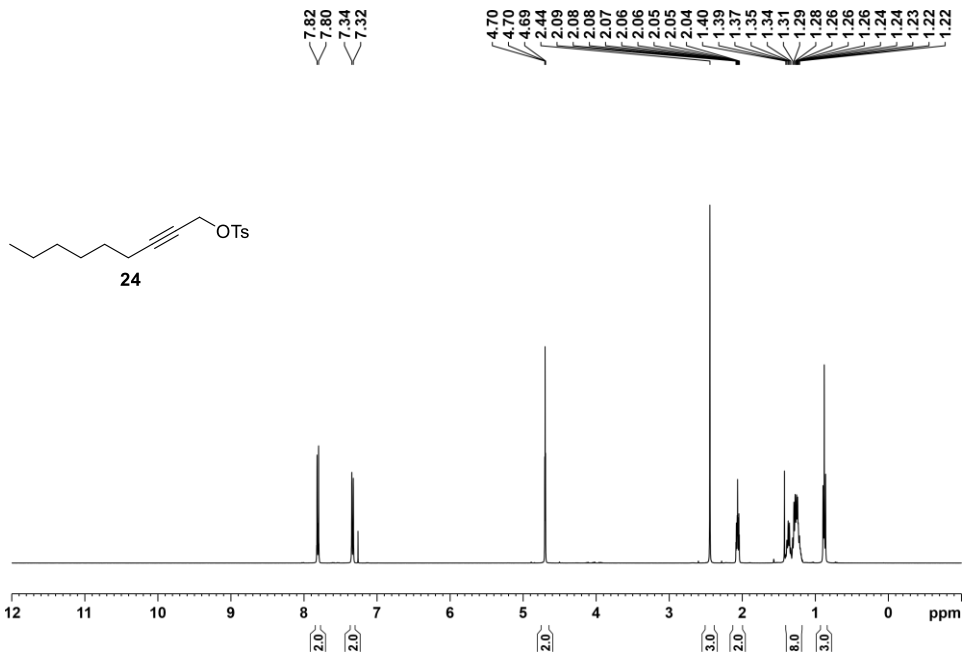

Figure 105. ^{1}H NMR (400 MHz, $CDCl_3$) of isolated substrate **24**.

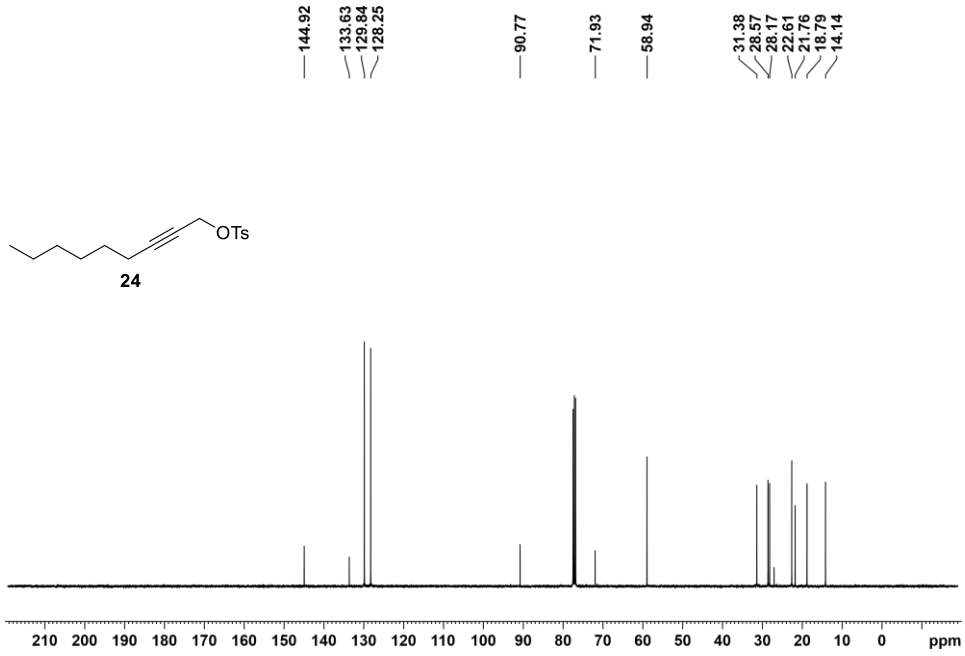

Figure 106. $^{13}C\{^{1}H\}$ NMR (101 MHz, $CDCl_3$) of isolated substrate **24**.

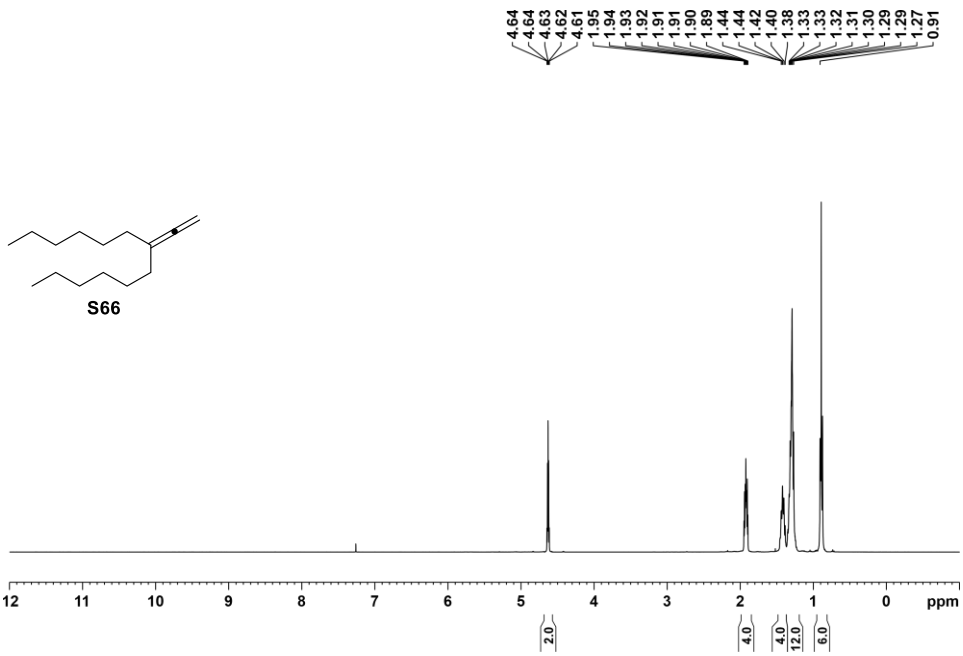

Figure 107. ^{1}H NMR (400 MHz, $CDCl_3$) of isolated substrate **S66**.

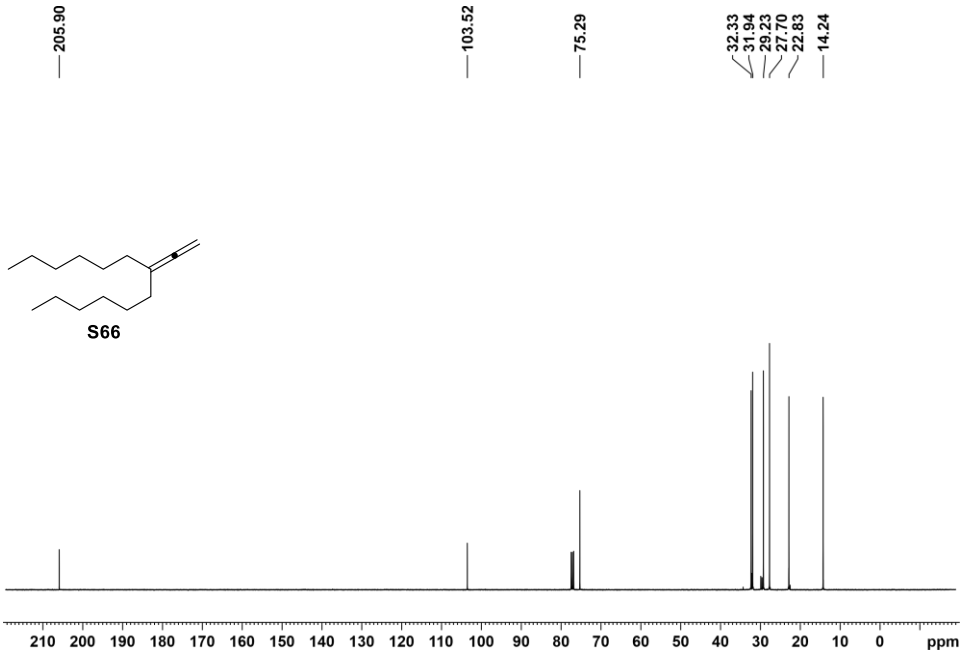

Figure 108. $^{13}C\{^{1}H\}$ NMR (101 MHz, $CDCl_3$) of isolated substrate **S66**.

2.5.38. Copies of IR spectra of the bisphosphite ligands L46 and L47

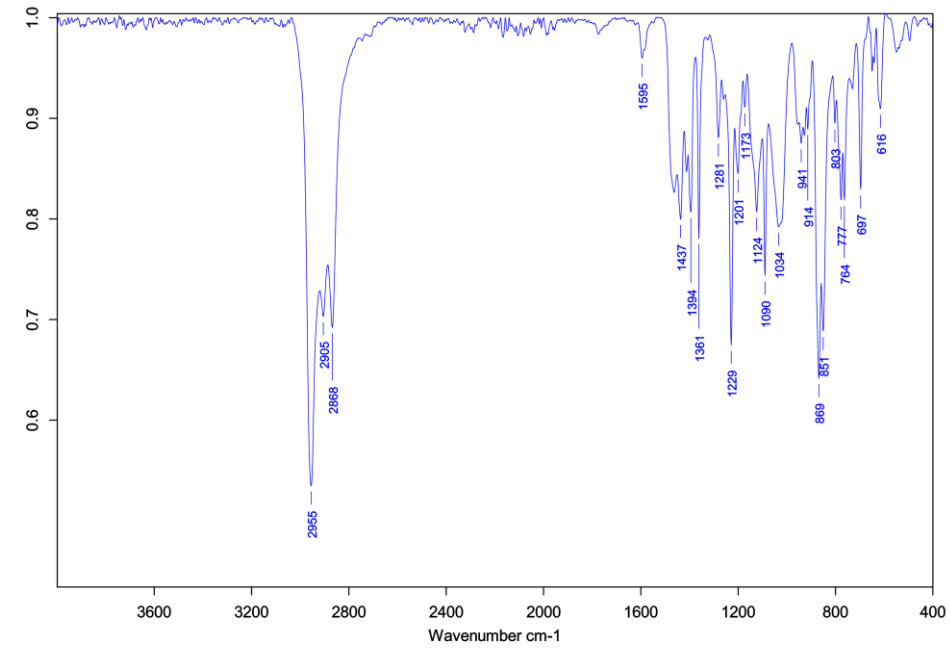

Figure 109. IR spectrum of isolated compound bisphosphite ligand **L46**.

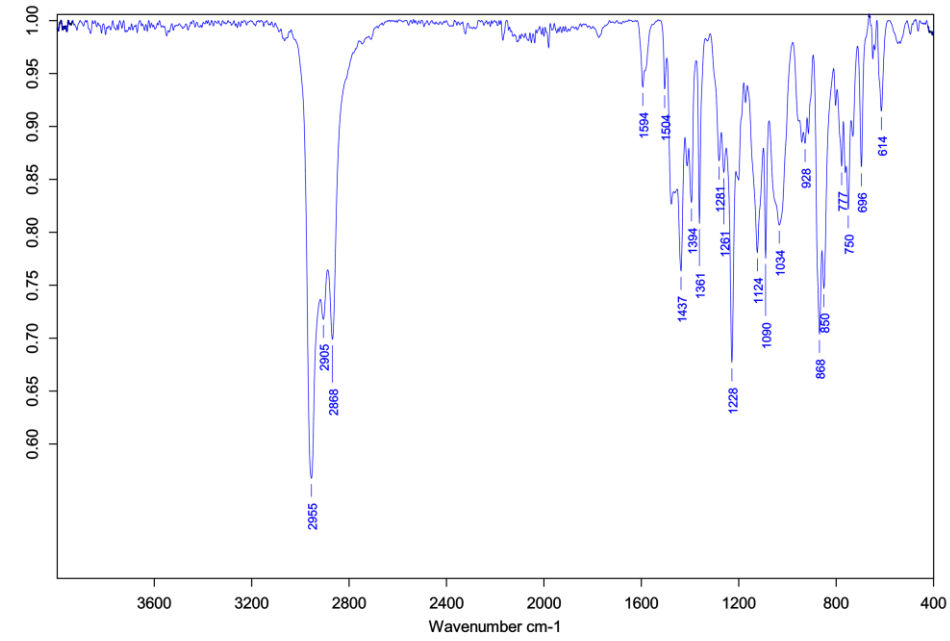

Figure 110. IR spectrum of isolated compound bisphosphite ligand **L47**.

2.5.39. Coordination studies of the bisphosphite L46 in absence of RA: [Rh(CO)$_2$H(κ^2*P*,*P*-L46)]

A 50 mM solution of bisphosphite ligand **L46** (1 equiv.) and [Rh(κ^2*O*,*O'*-acac)(CO)$_2$] (1 equiv.) in PhMe-d_8/THF-d_8 (97:3 v/v) was transferred to a 25 mL autoclave reactor, which was pressurized at 10 bar of H_2/CO (1:1) and heated at 60 °C. The mixture was allowed to stir for 18 hours. The reactor was cooled to room temperature, depressurized in a well-ventilated fume hood and the reaction mixture was transferred to 5 mm HP-NMR sapphire tube. The tube was pressurized at 10 bar H_2/CO (1:1) and the HP-NMR spectrum were collected at 298 K. Mass Spectroscopy samples were immediately recorded under N_2 after depressurizing the autoclave. Spectroscopic data obtained from this solution were in agreement with the quantitative formation of [Rh(CO)$_2$H(κ^2*P*,*P*-**L46**)]. ^{1}H NMR (500 MHz, PhMe-d_8/THF-d_8 (97:3 v/v)) δ 7.57 (d, J = 2.4 Hz, 4H), 7.27 (d, J = 2.4 Hz, 4 H), 4.25 (bs, 4H), 3.61 (t, J = 5.7 Hz, 4H), 3.35 (bs, 8H), 1.65 (s, 36H), 1.25 (s, 36H), -10.08 (td, $^1J_{H\text{-}Rh}$ = 3.46 Hz, $^2J_{H\text{-}P}$ = 12.82 Hz, 1H) ppm;). ^{1}H{^{31}P} NMR (500 MHz, PhMe-d_8/THF-d_8 (97:3 v/v)) δ 7.58 (d, J = 2.5 Hz, 4H), 7.27 (d, J = 2.2 Hz, 4 H), 4.25 (t, J = 5.7 Hz, 4H), 3.61 (t, J = 5.7 Hz, 4H), 3.35 (bs, 8H), 1.65 (s, 36H), 1.25 (s, 36H), -10.08 (d, $^1J_{H\text{-}Rh}$ = 3.61 Hz, 1H) ppm; ^{13}C{^{1}H} NMR (126 MHz, PhMe-d_8/THF-d_8 (97:3 v/v)) δ 190.9, 147.4, 146.5, 140.13, 132.7, 127.4, 71.6, 70.6, 66.4, 36.0, 34.6, 32.2, 31.5, 24.3 ppm; ^{31}P NMR (202 MHz, PhMe-d_8/THF-d_8 (97:3 v/v)) δ 150.4 (dd, $^1J_{P\text{-}Rh}$ = 233.7 Hz, $^2J_{P\text{-}H}$ = 11.1 Hz) ppm; ^{31}P{^{1}H} NMR (202 MHz, PhMe-d_8/THF-d_8 (97:3 v/v)) δ 150.4 (d, $^1J_{P\text{-}Rh}$ = 233.8 Hz) ppm; HRMS (MALDI-TOF) *m/z* calcd. for $C_{64}H_{96}O_9P_2Rh^+$ [M-2CO-H]$^+$ 1173.5579, found 1173.5569.

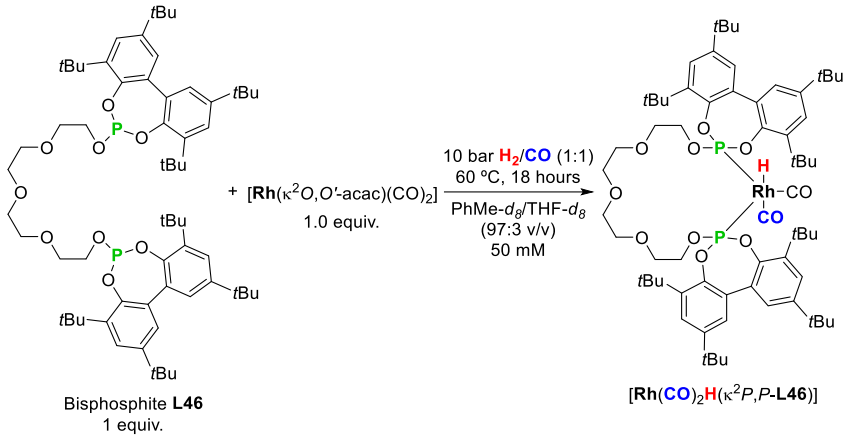

Scheme 52. Coordination of [Rh]/**L46** (1:1) under 10 bar H_2/CO (1:1) at 60 °C for 18 hours.

NMR spectrum of the High-Pressure experiment:

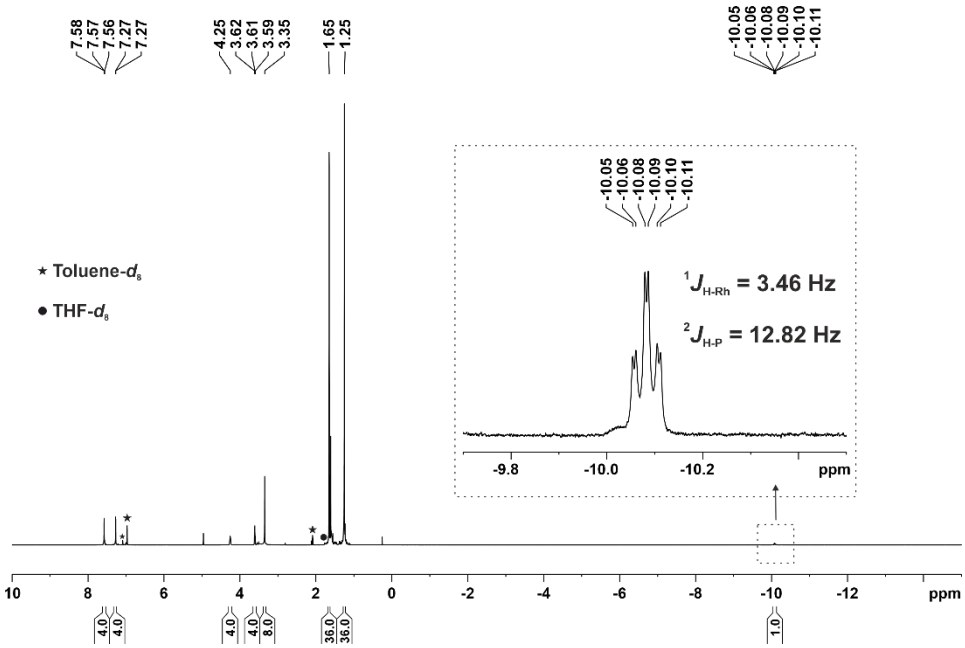

Figure 111. High-Pressure ^{1}H NMR (500 MHz, PhMe-d_8/THF-d_8 (97:3 v/v)) of [Rh(CO)$_2$H(κ^2*P*,*P*-**L46**)].

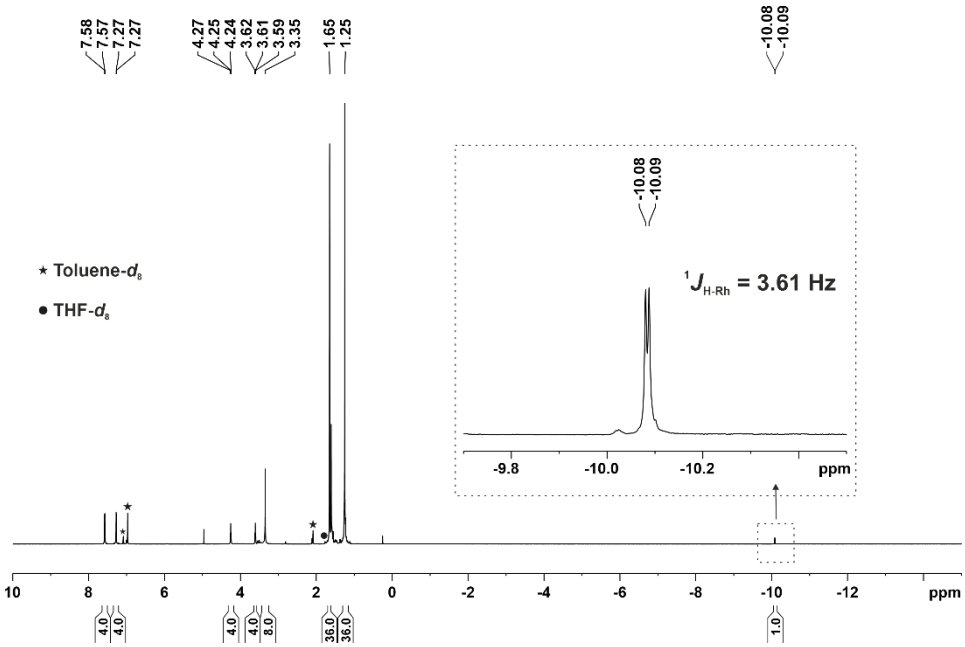

Figure 112. High-Pressure $^{1}H\{^{31}P\}$ NMR (500 MHz, PhMe-d_8/THF-d_8 (97:3 v/v)) of [Rh(CO)$_2$H(κ^2*P*,*P*-**L46**)].

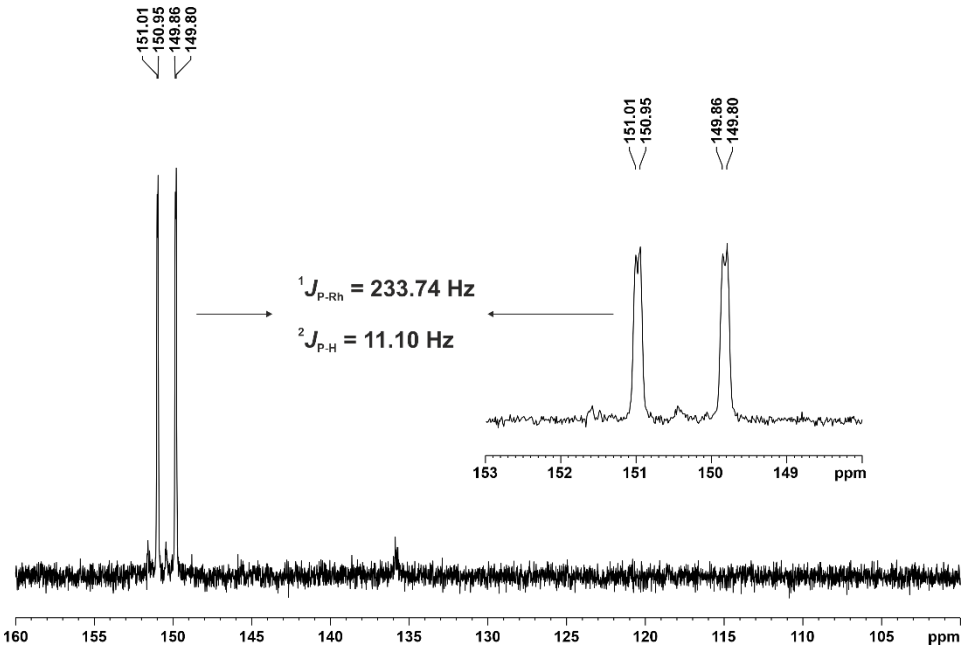

Figure 113. High-Pressure ^{31}P NMR (202 MHz, PhMe-d_8/THF-d_8 (97:3 v/v)) of [Rh(CO)$_2$H(κ^2*P*,*P*-**L46**)].

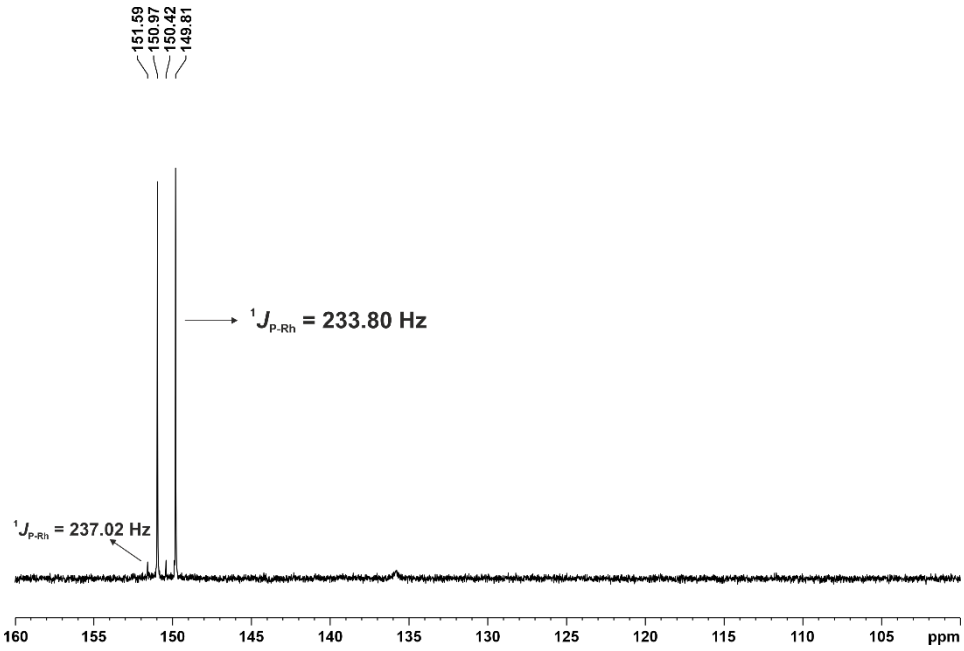

Figure 114. High-Pressure ^{31}P{^{1}H} NMR (202 MHz, PhMe-d_8/THF-d_8 (97:3 v/v)) of [Rh(CO)$_2$H(κ^2*P*,*P*-**L46**)].

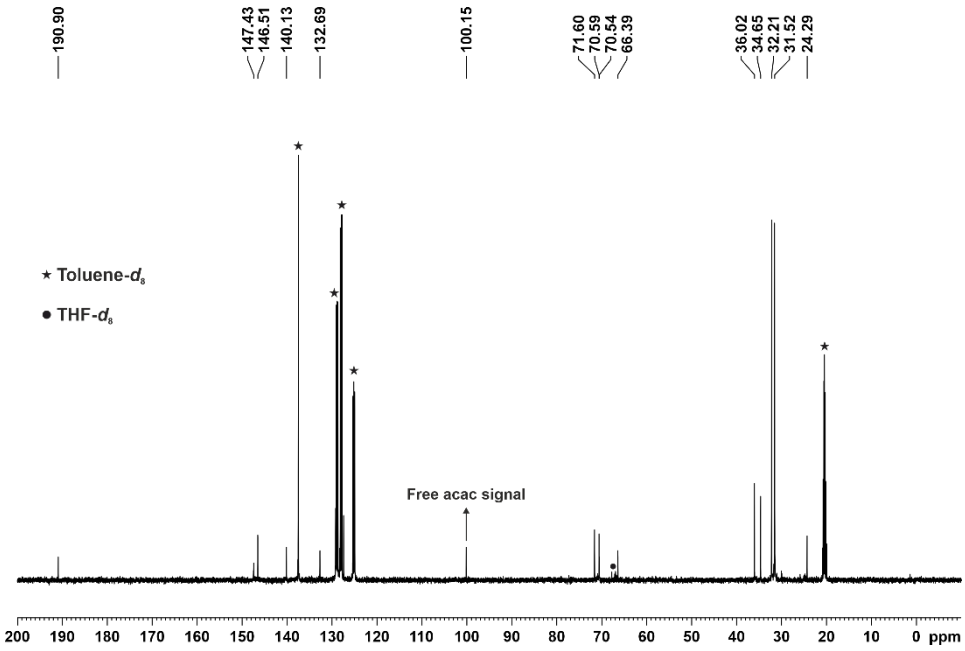

Figure 115. High-Pressure $^{13}C\{^{1}H\}$ NMR (126 MHz, PhMe-d_8/THF-d_8 (97:3 v/v)) of [Rh(CO)$_2$H(κ^2*P*,*P*-**L46**)].

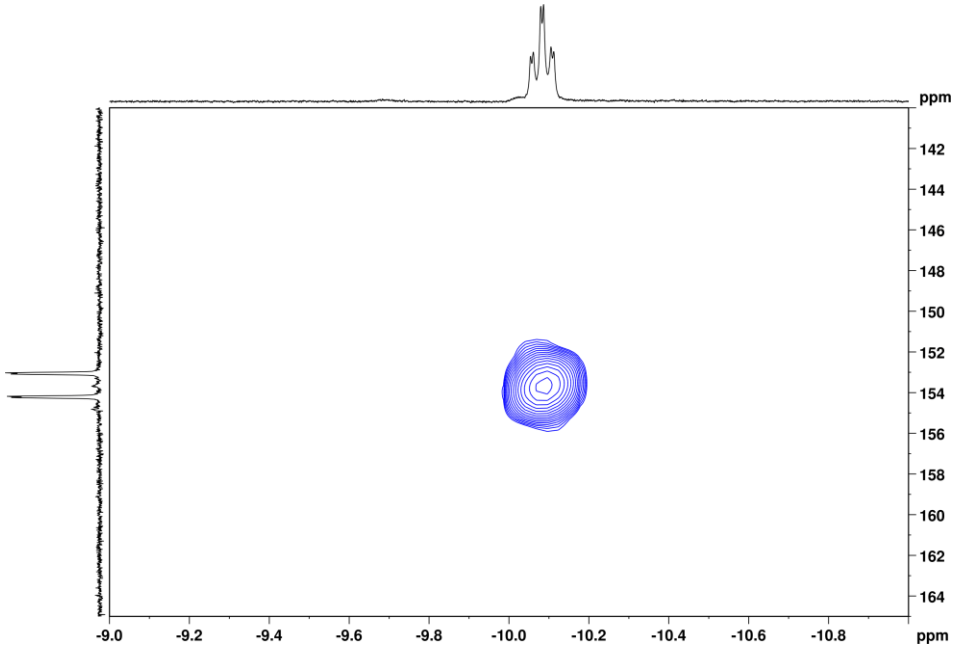

Figure 116. High-Pressure ^{1}H–^{31}P HMBC spectrum of the complex of [Rh(CO)$_2$H(κ^2*P*,*P*-**L46**)] in PhMe-d_8/THF-d_8 (97:3 v/v).

2.5.40. Coordination studies of the bisphosphite ligand L46 and KBArF as the RA: [Rh(CO)$_2$H(κ^2*P*,*P*-L46•KBArF)]

A 50 mM solution of bisphosphite ligand **L46** (1 equiv.), KBArF (1.3 equiv.) and [Rh(κ^2*O*,*O*'-acac)(CO)$_2$] (1 equiv.) in PhMe-d_8/THF-d_8 (97:3 v/v) was transferred to a 25 mL autoclave reactor, which was pressurized at 10 bar H_2/CO (1:1) and heated at 60 °C. The mixture was allowed to stir for 18 hours. The reactor was cooled to room temperature, depressurized in a well-ventilated fume hood and the reaction mixture was transferred to 5 mm HP-NMR sapphire tube. The tube was pressurized at 10 bar H_2/CO (1:1) and the HP-NMR spectrum were collected at 298 K. MS samples were immediately recorded under N_2 after depressurizing the autoclave. Spectroscopic data obtained from this solution were in agreement with the quantitative formation of [Rh(CO)$_2$H(κ^2*P*,*P*-**L46**•KBArF)]. ^{1}H NMR (500 MHz, PhMe-d_8/THF-d_8 (97:3 v/v)) δ 7.59 (d, J = 2.0 Hz, 4H), 7.27 (d, J = 2.1 Hz, 4 H), 3.92 (bs, 4H), 2.99 (bs, 8H), 2.94 (bs, 4H), 1.53 (s, 36H), 1.23 (s, 36H), -11.21 (d, $^1J_{H\text{-}Rh}$ = 4.3 Hz, 1H) ppm; ^{1}H{^{31}P} NMR (500 MHz, PhMe-d_8/THF-d_8 (97:3 v/v)) δ 7.59 (d, J = 1.4 Hz, 4H), 7.27 (d, J = 1.4 Hz, 4 H), 3.92 (bs, 4H), 2.99 (bs, 8H), 2.94 (bs, 4H), 1.52 (s, 36H), 1.23 (s, 36H), -11.21 (d, $^1J_{H\text{-}Rh}$ = 4.3 Hz, 1H) ppm; ^{13}C{^{1}H} NMR (126 MHz, PhMe-d_8/THF-d_8 (97:3 v/v)) δ 191.4, 147.9, 146.9, 139.5, 131.6, 126.3, 70.0, 69.6, 69.4, 35.8, 34.7, 32.2, 31.7, 24.3 ppm; ^{31}P NMR (202 MHz, PhMe-d_8/THF-d_8 (97:3 v/v)) δ 138.2 (d, $^1J_{P\text{-}Rh}$ = 248.2 Hz) ppm; ^{31}P{^{1}H} NMR (202 MHz, PhMe-d_8/THF-d_8 (97:3 v/v)) δ 138.2 (d, $^1J_{P\text{-}Rh}$ = 248.2 Hz) ppm; HRMS (MALDI-TOF) *m/z* calcd. for $C_{64}H_{96}O_9P_2Rh^+$ [M-KBArF-2CO-H]$^+$ 1173.5579, found 1173.5584.

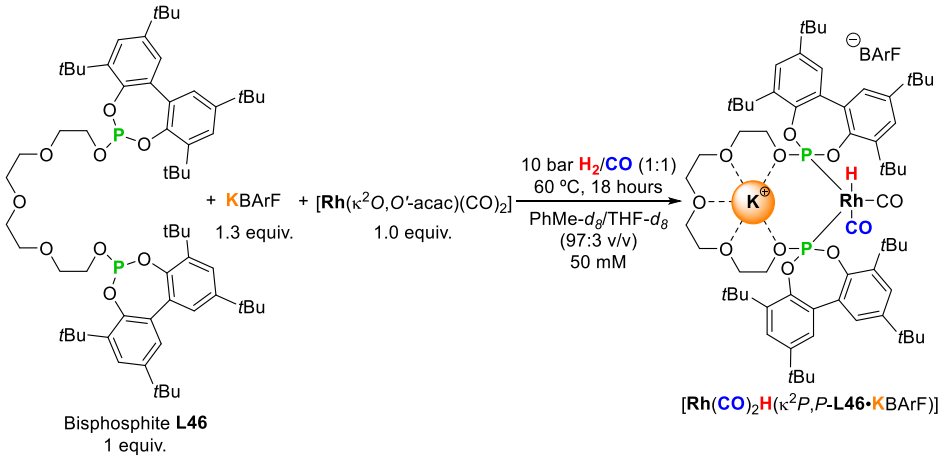

Scheme 53. Coordination of [Rh]/**L46**/KBArF (1:1:1.3) under 10 bar H_2/CO (1:1) at 60 °C for 18 hours.

NMR spectrum of the High-Pressure experiment:

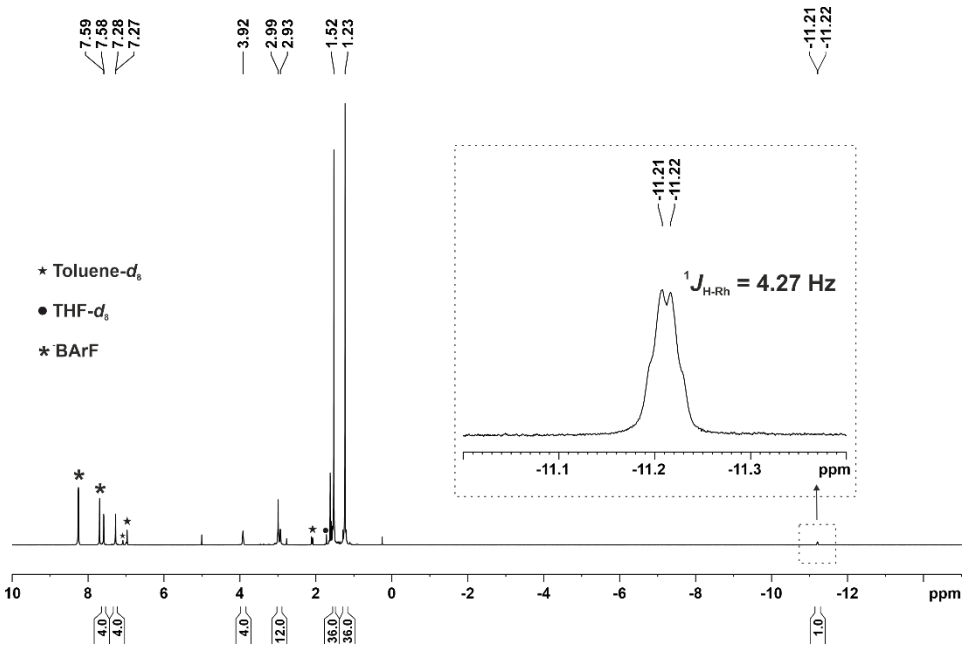

Figure 117. High-Pressure ^{1}H NMR (500 MHz, PhMe-d_8/THF-d_8 (97:3 v/v)) of [Rh(CO)$_2$H(κ^2*P*,*P*-**L46**•KBArF)].

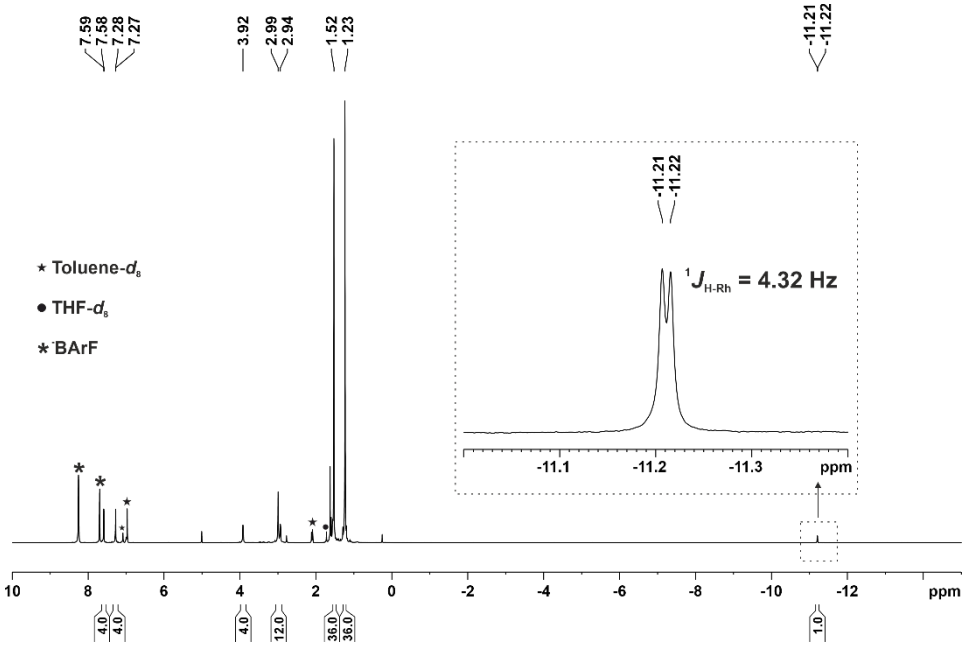

Figure 118. High-Pressure ^{1}H{^{31}P} NMR (500 MHz, PhMe-d_8/THF-d_8 (97:3 v/v)) of [Rh(CO)$_2$H(κ^2*P*,*P*-**L46**•KBArF)].

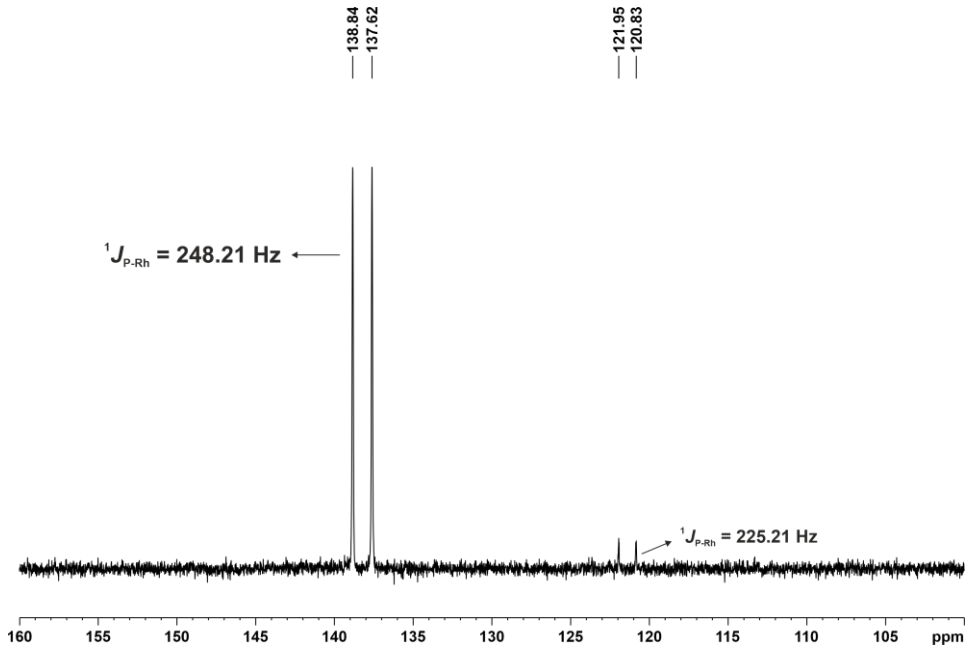

Figure 119. High-Pressure ^{31}P NMR (202 MHz, PhMe-d_8/THF-d_8 (97:3 v/v)) of [Rh(CO)$_2$H(κ^2*P,P*-**L46**•KBArF)].

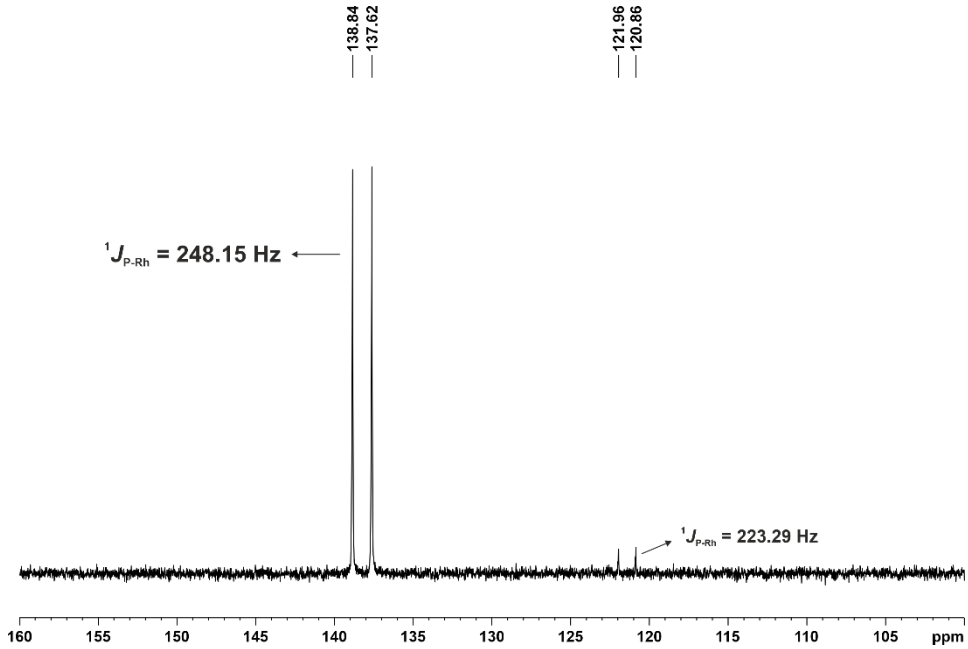

Figure 120. High-Pressure ^{31}P{^{1}H} NMR (202 MHz, PhMe-d_8/THF-d_8 (97:3 v/v)) of [Rh(CO)$_2$H(κ^2*P,P*-**L46**•KBArF)].

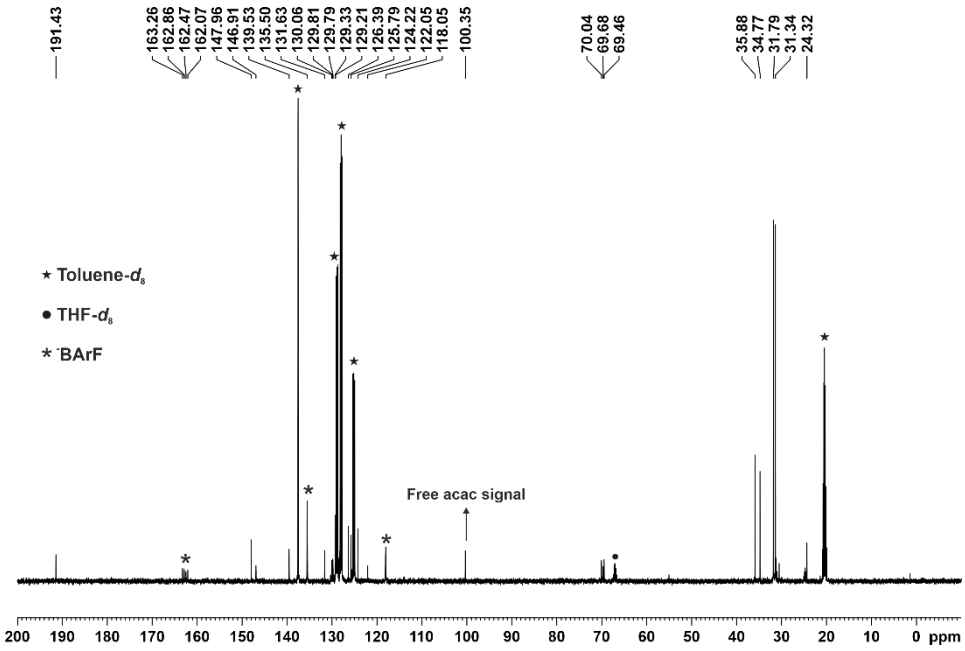

Figure 121. High-Pressure $^{13}C\{^{1}H\}$ NMR (126 MHz, PhMe-d_8/THF-d_8 (97:3 v/v)) of [Rh(CO)$_2$H(κ^2*P*,*P*-**L46**•KBArF)].

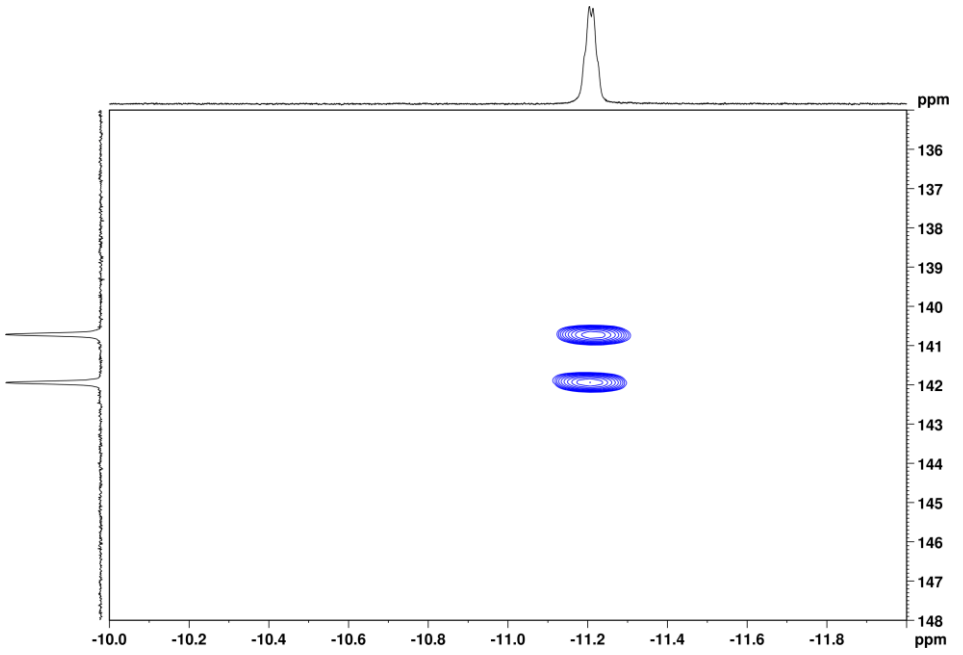

Figure 122. High-Pressure $^{1}H-^{31}P$ HMBC spectrum of the complex of [Rh(CO)$_2$H(κ^2*P*,*P*-**L46**•KBArF)] in PhMe-d_8/THF-d_8 (97:3 v/v).

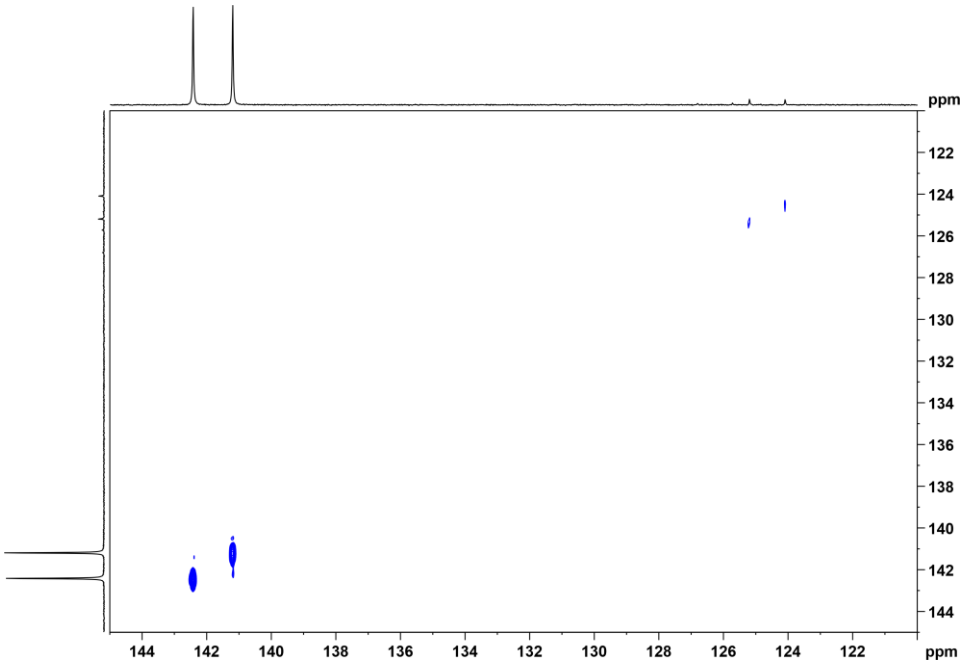

Figure 123. High-Pressure $^{31}P–^{31}P$ EXSY spectrum of the complex of [Rh(CO)$_2$H(KBArF·**L46**)] in PhMe-d_8/THF-d_8 (97:3 v/v).

2.5.41. Coordination studies of the bisphosphite ligand L46 with CsBArF as the RA: [Rh(CO)$_2$H(κ^2*P*,*P*-L46•CsBArF)]

A 50 mM solution of bisphosphite ligand **L46** (1 equiv.), CsBArF (1.3 equiv.) and [Rh(κ^{2}O,O′-acac)(CO)$_2$] (1 equiv.) in PhMe-d_8/THF-d_8 in (97:3 v/v) was transferred to a 25 mL autoclave reactor, which was pressurized at 10 bar H_2/CO (1:1) and heated at 60 °C. The mixture was allowed to stir for 18 hours. The reactor was cooled to room temperature, depressurized in a well-ventilated fume hood and the reaction mixture was transferred to 5 mm HP-NMR sapphire tube. The tube was pressurized at 10 bar H_2/CO (1:1) and the HP-NMR spectrum were collected at 298 K. MS samples were immediately recorded under N_2 after depressurizing the autoclave. Spectroscopic data obtained from this solution were in agreement with the quantitative formation of the [Rh(CO)$_2$H(κ^2*P*,*P*-**L46**•CsBArF)]. ^{1}H NMR (500 MHz, PhMe-d_8/THF-d_8 (97:3 v/v)) δ 7.59 (d, J = 2.3 Hz, 4H), 7.28 (d, J = 2.2 Hz, 4 H), 3.86 (bs, 4H), 3.01 (bd, 8H), 2.87 (bs, 4H), 1.53 (s, 36H), 1.24 (s, 36H), -11.20 (d, $^1J_{H\text{-}Rh}$ = 2.8 Hz, 1H) ppm; ^{1}H{^{31}P} NMR (500 MHz, PhMe-d_8/THF-d_8 (97:3 v/v)) δ 7.59 (d, J = 2.2 Hz, 4H), 7.27 (d, J = 1.9 Hz, 4 H), 3.86 (bs, 4H), 3.01 (bd, 8H), 2.87 (bs, 4H), 1.53 (s, 36H), 1.24 (s, 36H), -11.20 (d, $^1J_{H\text{-}Rh}$ = 3.9 Hz, 1H) ppm; ^{13}C{^{1}H} NMR (126 MHz, PhMe-d_8/THF-d_8 (97:3 v/v)) δ 191.2, 147.8, 147.1, 139.4, 131.7, 126.4, 70.0, 69.7, 68.9, 35.9, 34.7, 31.9, 31.3, 24.3 ppm; ^{31}P NMR (202 MHz, PhMe-d_8/THF-d_8 (97:3 v/v)) δ 138.3 (d, $^1J_{P\text{-}Rh}$ = 246.9 Hz) ppm; ^{31}P{^{1}H} NMR (202 MHz, PhMe-d_8/THF-d_8 (97:3 v/v)) δ 138.3 (d, $^1J_{P\text{-}Rh}$ = 246.9 Hz) ppm; HRMS (MALDI-TOF) *m/z* calcd. for $C_{64}H_{96}O_9P_2Rh^+$ [M-CsBArF-2CO-H]$^+$ 1173.5579, found 1173.5583. Attempts to isolate this rhodium complex in analytically pure form failed.

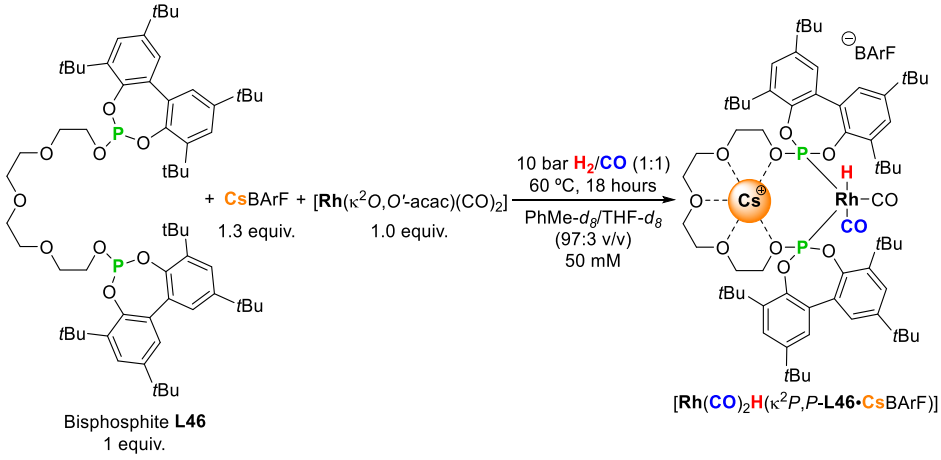

Scheme 54. Coordination of [Rh]/**L46**/CsBArF (1:1:1.3) under 10 bar H_2/CO (1:1) at 60 ºC for 18 hours.

NMR spectrum of High-Pressure experiment:

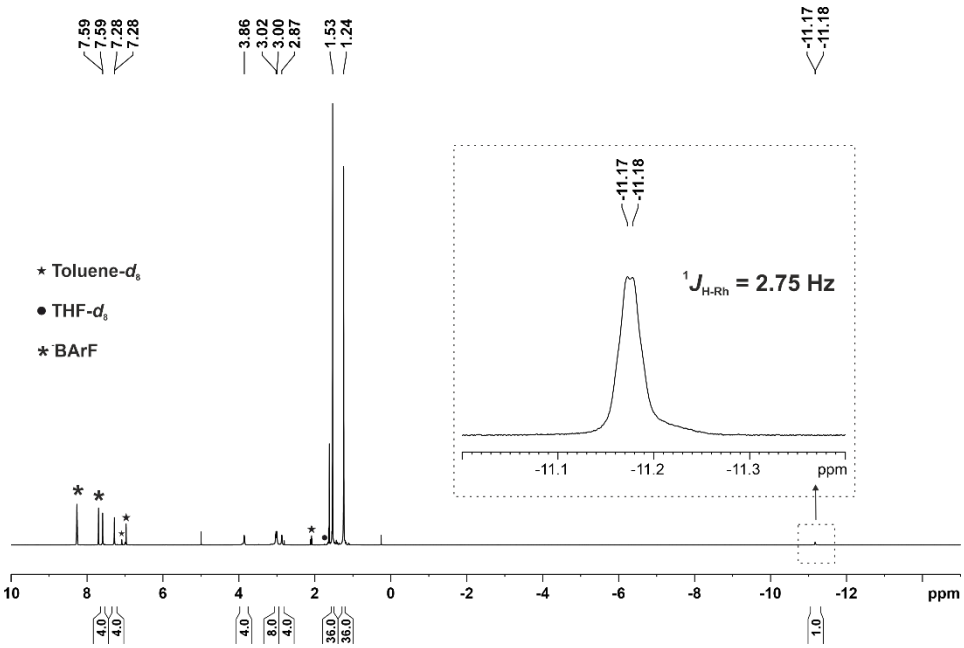

Figure 124. High-Pressure ^{1}H NMR (500 MHz, PhMe-d_8/THF-d_8 (97:3 v/v)) of [Rh(CO)$_2$H(κ^2*P*,*P*-**L46**•CsBArF)].

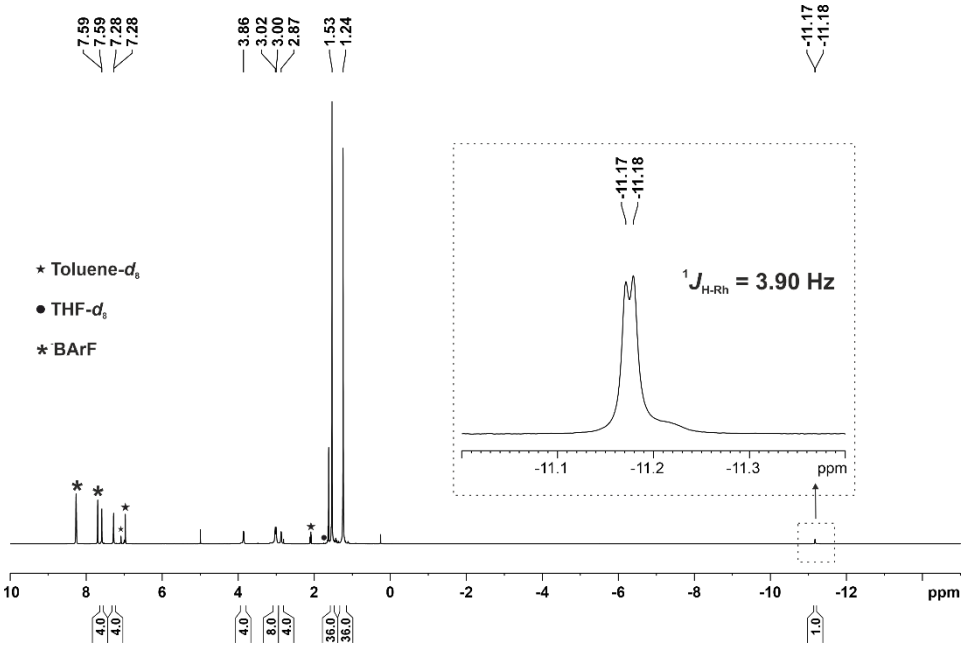

Figure 125. High-Pressure ^{1}H{^{31}P} NMR (500 MHz, PhMe-d_8/THF-d_8 (97:3 v/v)) of [Rh(CO)$_2$H(κ^2*P*,*P*-**L46**•CsBArF)].

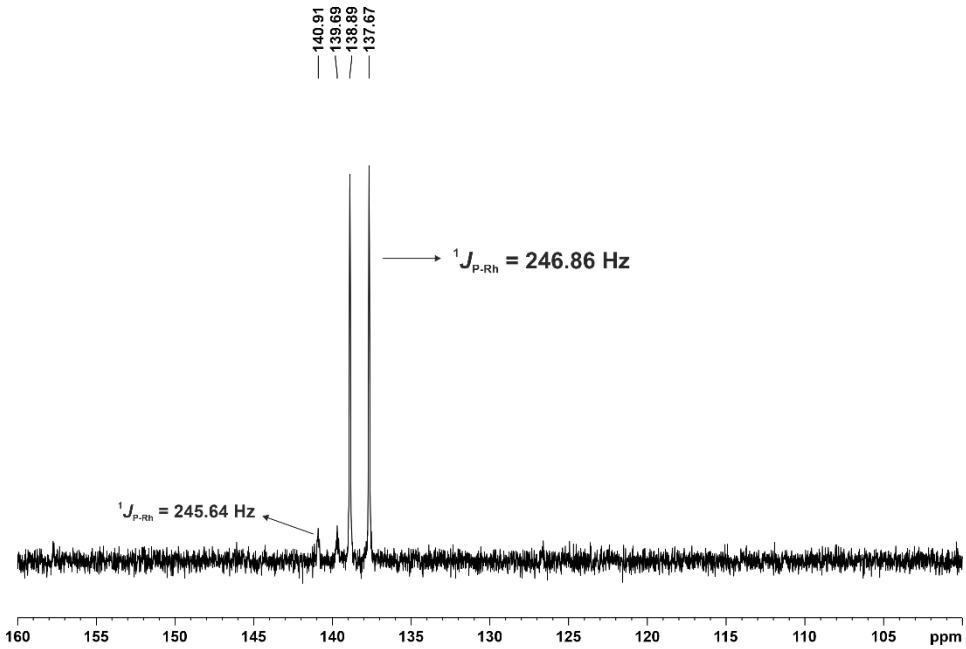

Figure 126. High-Pressure ^{31}P NMR (202 MHz, PhMe-d_8/THF-d_8 (97:3 v/v)) of [Rh(CO)$_2$H(κ^2*P*,*P*-**L46**•CsBArF)].

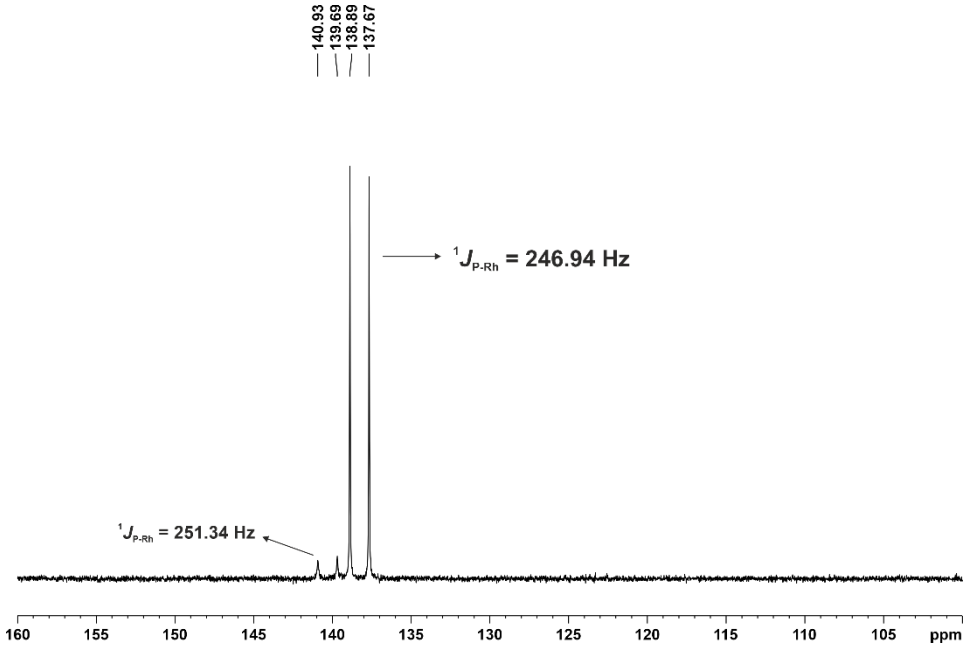

Figure 127. High-Pressure ^{31}P{^{1}H} NMR (202 MHz, PhMe-d_8/THF-d_8 (97:3 v/v)) of [Rh(CO)$_2$H(κ^2*P*,*P*-**L46**•CsBArF)].

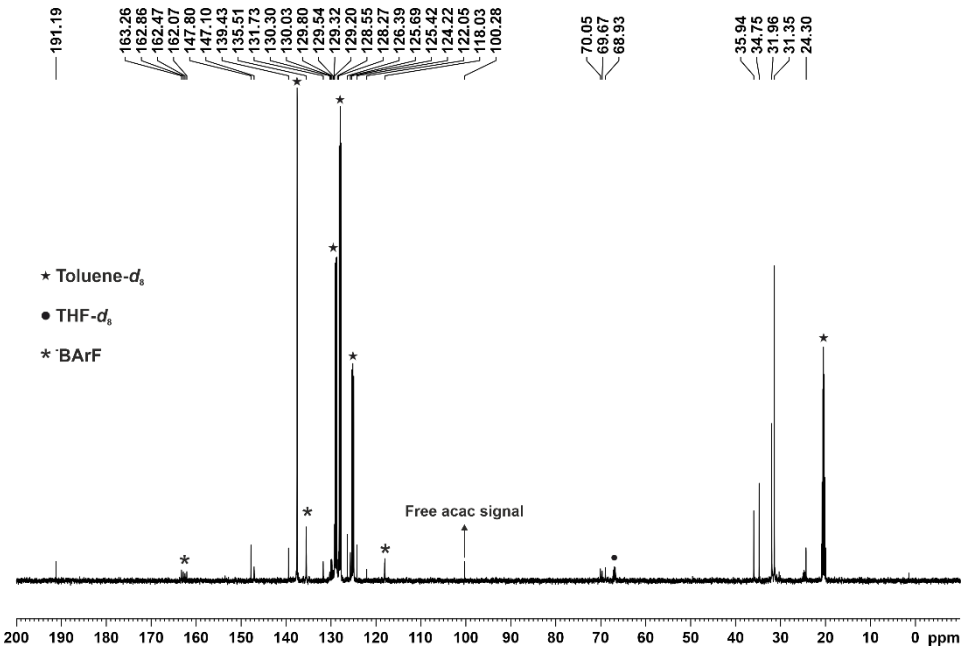

Figure 128. High-Pressure $^{13}C\{^1H\}$ NMR (126 MHz, PhMe-d_8/THF-d_8 (97:3 v/v)) of [Rh(CO)$_2$H(κ^2*P*,*P*-**L46**•CsBArF)].

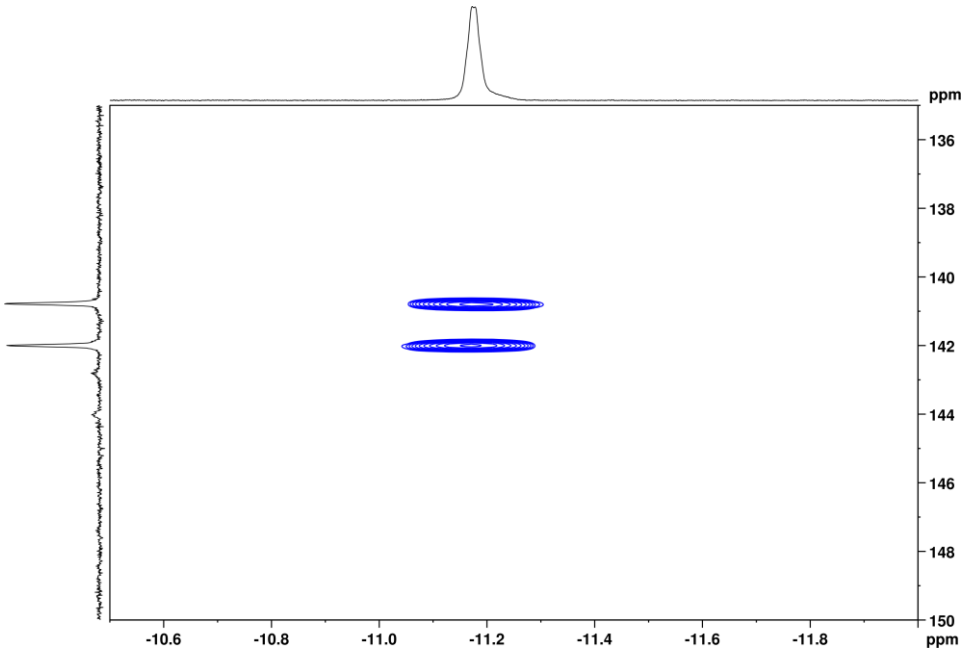

Figure 129. High-Pressure ^1H–^{31}P HMBC spectrum of the complex of [Rh(CO)$_2$H(κ^2*P*,*P*-**L46**•CsBArF)] in PhMe-d_8/THF-d_8 (97:3 v/v).

2.5.42. Coordination studies of [Rh(CO)$_2$H(κ^2*P*,*P*-L46)] with KBArF as the RA: [Rh(CO)$_2$H(κ^2*P*,*P*-L46•KBArF)]

A 50 mM solution of bisphosphite ligand **L46** (1 equiv.) and [Rh(κ^2*O*,*O*′-acac)(CO)$_2$] (1 equiv.) in PhMe-d_8/THF-d_8 in (97:3 v/v) was transferred to a 25 mL autoclave reactor, which was pressurized at 10 bar H_2/CO (1:1) and heated at 60 °C. The mixture was allowed to stir for 18 hours. The reactor was cooled to room temperature, depressurized in a well-ventilated fume hood and the reaction mixture was transferred to 5 mm NMR tube. The tube was pressurized at 1 bar H_2/CO (1:1) and the NMR spectrum were collected at 298 K. The NMR tube was transfer to the glove box and the solution was added over KBArF (1.3 equiv.). The solution was transferred to 5 mm NMR tube. The tube was pressurized at 1 bar H_2/CO (1:1) and the NMR spectrum were collected at 298 K. Spectroscopic data obtained from this solution were in agreement with the quantitative formation of [Rh(CO)$_2$H(κ^2*P*,*P*-L46•KBArF)]. Spectroscopic data were in agreement with those already reported in the section 2.5.40.

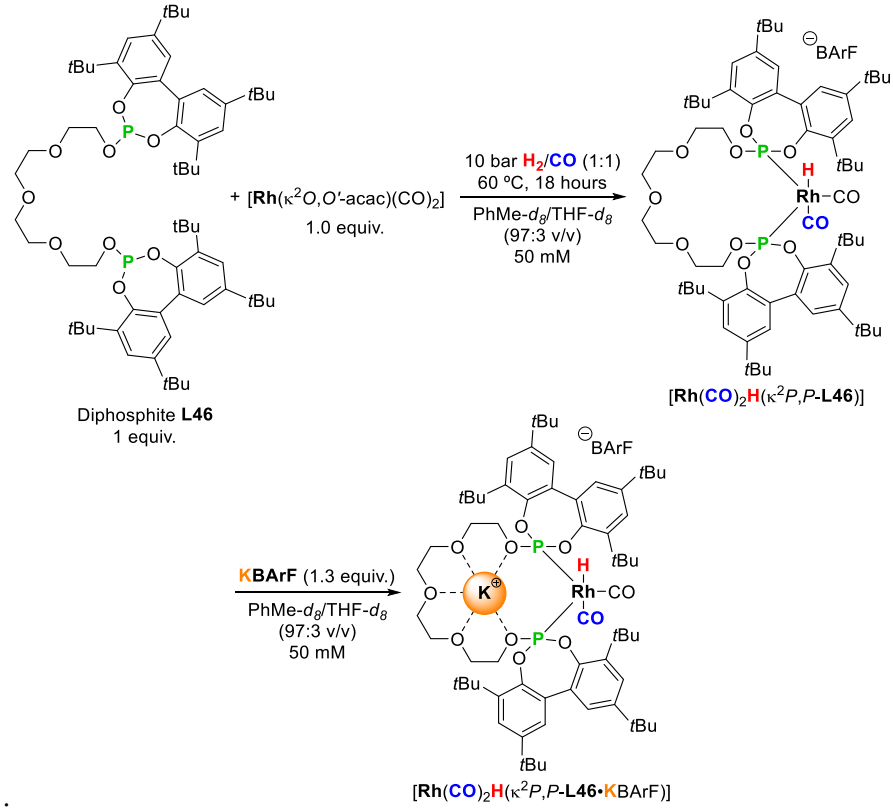

Scheme 55. Coordination of [Rh]/**L46**/KBArF (1:1:1.3).

NMR spectrum of High-Pressure experiment:

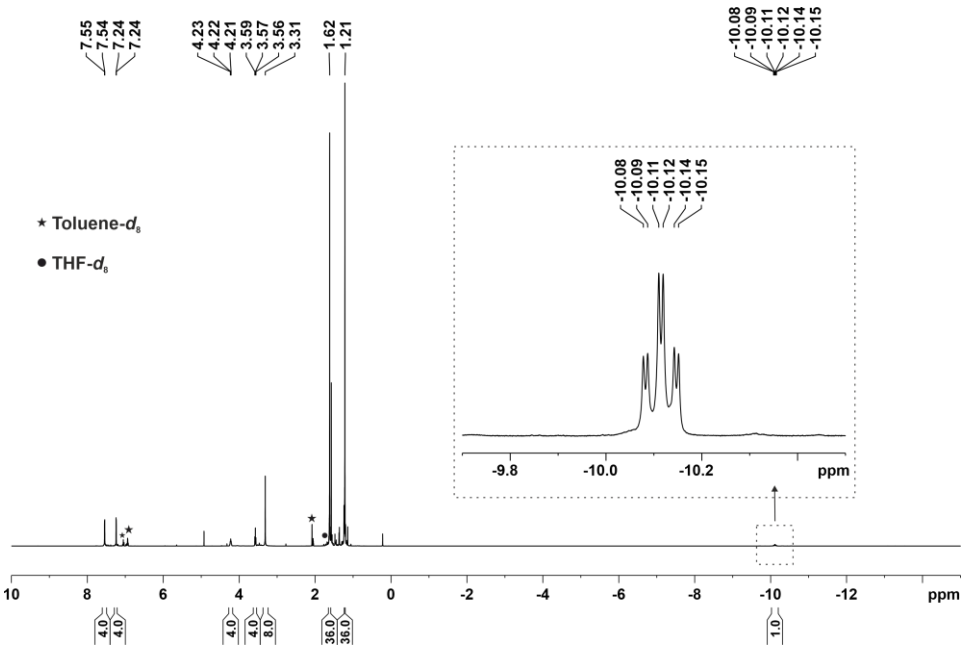

Figure 130. ^{1}H NMR (400 MHz, PhMe-d_8/THF-d_8 (97:3 v/v)) of [Rh(CO)$_2$H(κ^2*P*,*P*-**L46**)].

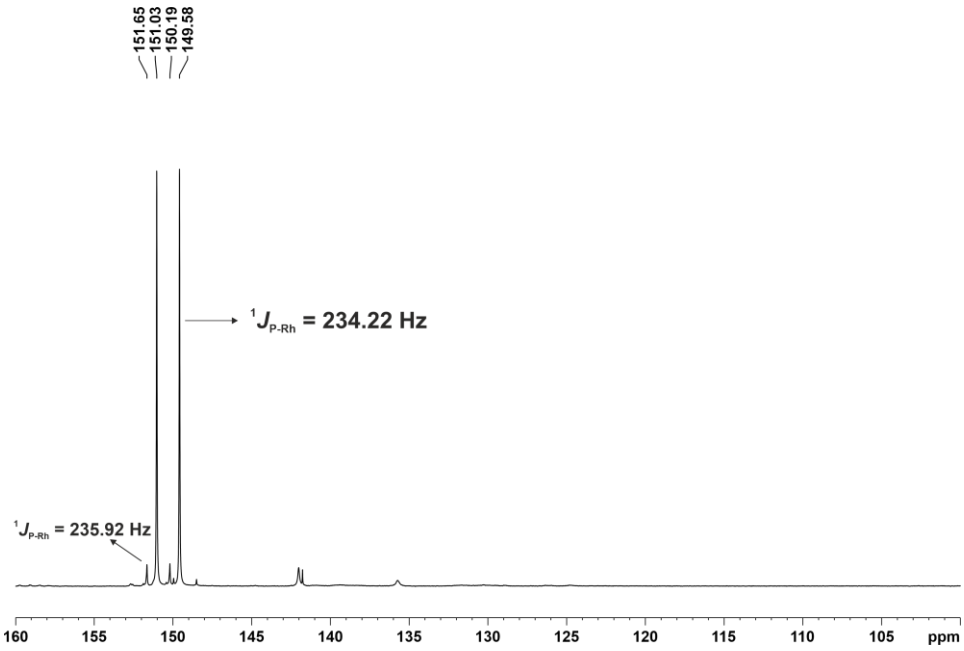

Figure 131. ^{31}P NMR (162 MHz, PhMe-d_8/THF-d_8 (97:3 v/v)) of [Rh(CO)$_2$H(κ^2*P*,*P*-**L46**)].

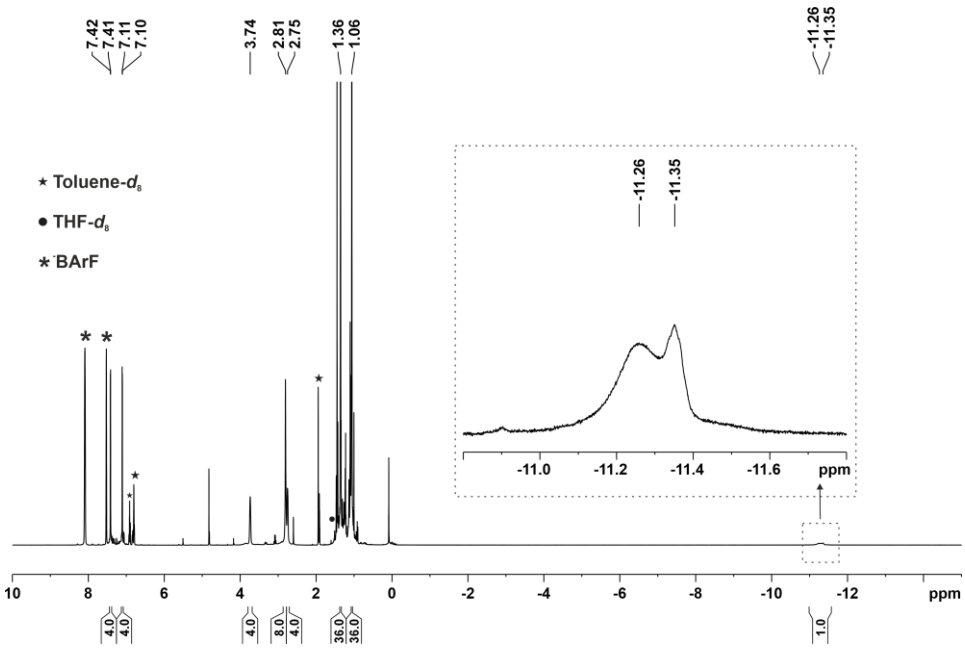

Figure 132. ^{1}H NMR (400 MHz, PhMe-d_8/THF-d_8 (97:3 v/v)) of [Rh(CO)$_2$H(κ^2*P*,*P*-**L46**•KBArF)].

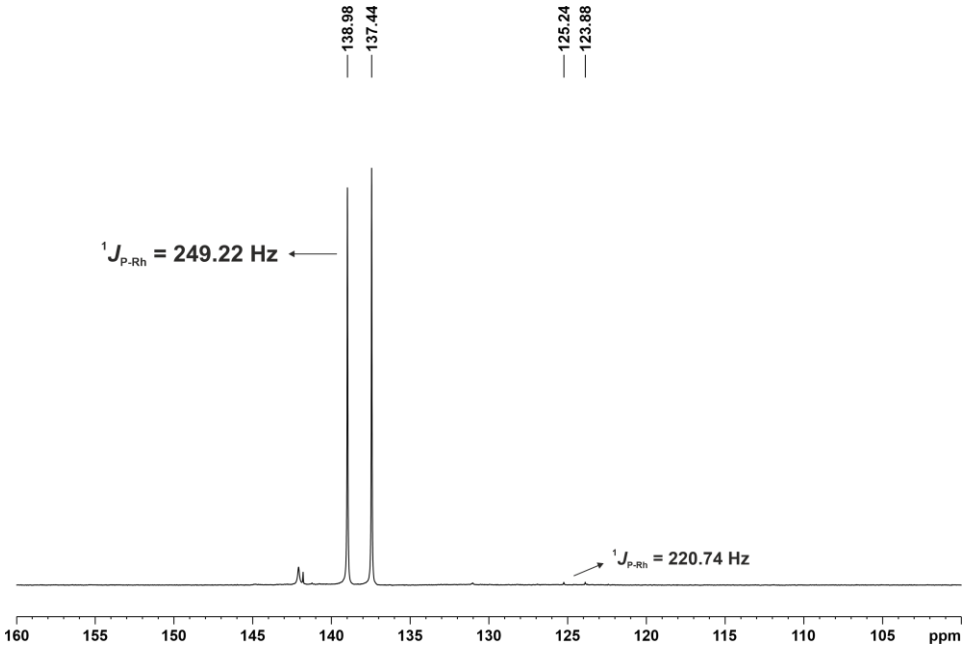

Figure 133. ^{31}P NMR (162 MHz, PhMe-d_8/THF-d_8 (97:3 v/v)) of [Rh(CO)$_2$H(κ^2*P*,*P*-**L46**•KBArF)].

2.5.43. Preparation of the catalyst precursor for Rh-catalysed hydroformylation in FlowNMR experiments

General procedure for the FlowNMR monitoring at DReaM facility of Rh-catalysed hydroformylation of hex-1-ene (**S47a**).

The hydroformylation of hex-1-ene was carried out in a pressure reactor made of glass with a stainless-steel lid connected to the FlowNMR apparatus. A micro-annular gear pump (mzr-6355from HNP Mikrosysteme GmbH) was used to circulate the reaction mixture through the 1/16" polyether ether ketone (PEEK, Upchurch Scientific) tubing with 0.76 mm i.d. connected to an InsightMR flow tube (Bruker) placed in the probe of the spectrometer. The inner volume of the flow system was approximately 7 mL. NMR spectra were recorded on a Bruker 500 MHz Advance II+ Ultrashield equipped with a nitrogen cooled BBO Prodigy CryoProbe. ^{1}H NMR chemical shifts are referenced against TMS (99.5 % purity in $CDCl_3$) and ^{31}P NMR shifts are referenced to 85% H_3PO_4. The reaction monitoring software used was InsightMR, and data processing was performed with TopSpin 4.0.6 and DynamicCenter 2.5.6.

In a glove box filled with argon, the following solutions were prepared:

Solution A: Ligand **L46** (50.1 mg, 46.8 µmol), CsBArF (60.6 mg, 60.84 µmol) in 450 µL of THF-d_8, [Rh(κ^2*O*,*O*′-acac)(CO)$_2$] (10.1 mg, 39.1 µmol) and PhMe-d_8 were mixed until a total volume of 10 mL.

Solution B: Hex-1-ene (**S47a**) (487.7 µL, 328.22 mg, 3.9 mmol), 1,3,5-trimethoxybenzene (62.9 mg, purity 99%, 0.37 mmol), triphenyl phosphate (100.7 mg, purity 97%, 0.30 mmol) and PhMe-d_8 were mixed until a total volume of 5 mL.

The solution A was added into the 50 ml glass-autoclave followed by the solution B inside the glovebox (argon atmosphere). The reactor was then taken out from the glove box.

The reactor was connected to the pressure system and was leak-checked, vacuum-argon cycled three times at room temperature in one of the lines. The valve was then opened and kept under argon. The inlet of the flow tube was then moved into a separate Schlenk flask that contained dry toluene under argon with the outlet being connected to the waste bottle. Dry toluene was then pumped through the flow tube for 5 minutes to leave the transfer lines, pump and flow tube filled with dry solvent (7 mL). Thereafter, both flow tube ends were reconnected to the reactor which was topped up with the reaction mixture against a flow of argon. The NMR tube and tip were then inserted into the spectrometer, the stirring was started, and the reaction mixture was pumped through the system at 4 mL/min. NMR spectra were recorded while

flowing under argon atmosphere. The reactor, heat exchanger and NMR probe were heated to 60 °C and, once the temperature had stabilised throughout the system, the NMR spectrometer lock was turned off, shimmed on ^{1}H peaks and tuned to proton and phosphorus. Spectra of the reagents were recorded both statically and at 4 mL/min. Acquisition parameters for interleaved ^{1}H, selectively excited ^{1}H and $^{31}P\{^{1}H\}$ NMR measurements were entered, and the sequence was initiated to start the FlowNMR reaction monitoring. After acquisition of at least one sequence of measurements under argon, the system was purged three times with less than 5 bar with CO. Once purged, the reservoir was pressurised with 7 bar of CO and after with 14 bar of H_2 in order to have 14 bar of syngas (H_2/CO in a 1:1 ratio) in the reservoir. The reservoir was connected to a 50 mL glass pressure reactor, which was pressurised at 10 bar of H_2/CO (1:1). When the pressure of the reactor decreased, it was pressurised again at 10 bar of H_2/CO (1:1) in order to keep the pressure stable during the reaction monitoring. The stirring rate was set to 800 rpm. At the end of the reaction, additional calibration spectra with and without flow were recorded. Once the experiment was finished, the H_2 and CO cylinders were closed, and the pressure system was depressurized. The thermostat, NMR spectrometer and heating plate were switched off, the crude mixture was removed from the reactor when it reached room temperature and the sample lines were cleaned. Conversion, concentrations and linear to branched ratio for the products derived from the hydroformylations were determined by NMR analyses using 1,3,5-trimethoxybenzene and triphenyl phosphate as internal standards for ^{1}H and ^{31}P NMR, respectively.

CHAPTER III

Anionic Supramolecular Regulation for Rhodium-Catalysed Hydroformylations

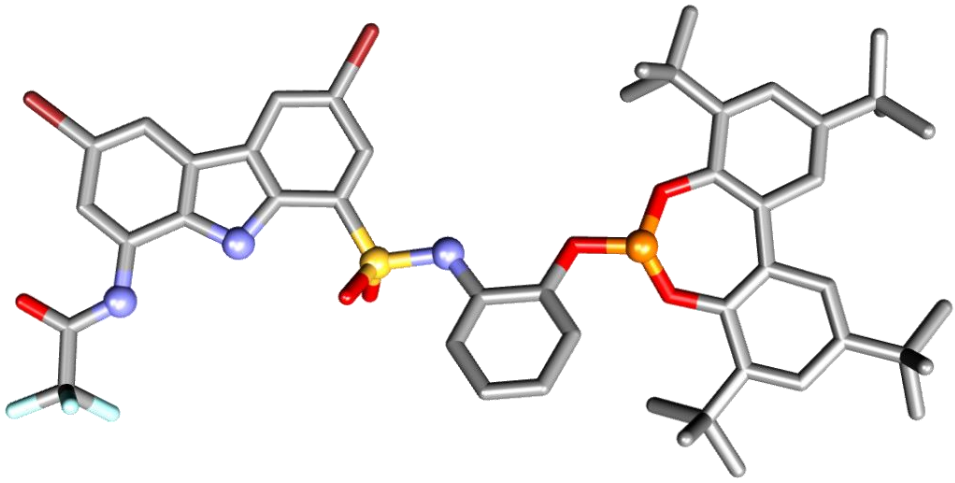

Anionic Supramolecular Regulation for Rhodium-Catalysed Hydroformylations

Unpublished work

Andrés Romero-Navarro,[a,b] and Anton Vidal-Ferran[b,c,d*]

[a] Institute of Chemical Research of Catalonia (ICIQ), Av. Països Catalans 16, 43007 Tarragona, Spain.

[b] Department of Inorganic and Organic Chemistry, University of Barcelona, C. Martí i Franquès 1-11, 08028 Barcelona, Spain.

[c] Institut de Nanociència i Nanotecnologia (IN2UB), Universitat de Barcelona, 08028 Barcelona, Spain.

[d] Institució Catalana de Recerca i Estudis Avançats (ICREA), Pg. Lluís Companys 23, 08010 Barcelona, Spain.

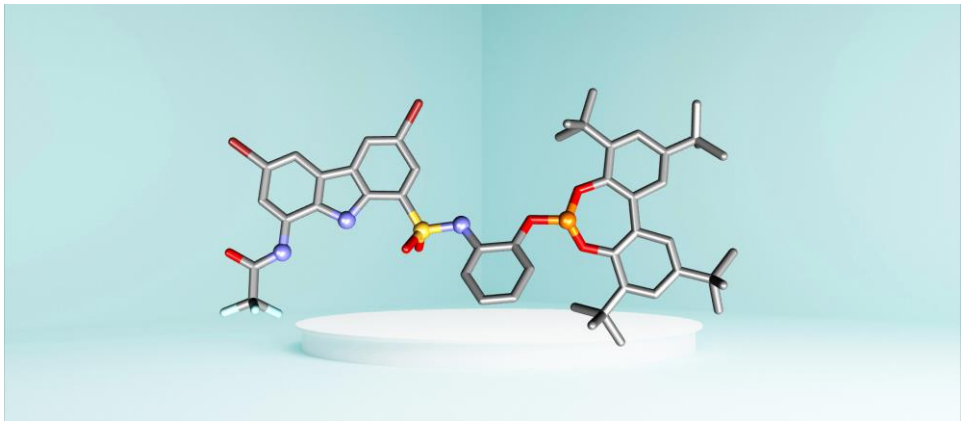

3.1. ABSTRACT

Herein we report the design and synthesis of a monophosphite ligand based on a carbazole scaffold. The purpose of synthesising this ligand was to supramolecularly control the activity and regioselectivity in hydroformylation reactions employing anionic regulation agents. In an analogous manner to the regulation strategy developed in our group involving cation recognition, we hypothesised that the combined use of a suitably designed monophosphite ligand **L50**, a rhodium precursor for hydroformylation reactions and an anionic regulation agent would lead to rhodium complexes with a catalytic site whose geometry, rigidity and/or conformational flexibility would depend on the size and shape of the regulation agent used. The ultimate goal of this approach was to maximise the activity and/or selectivity of the hydroformylation catalyst by the choice of the RA. The synthesis of a first

generation of supramolecularly regulated catalysts derived from the 2-((8-amino-9*H*-carbazole)-1-sulfonamido)phenyl phosphite ligand **L50**, the preliminary studies on the hydroformylation of two benchmark alkenes and the effects of anionic regulation are described herein.

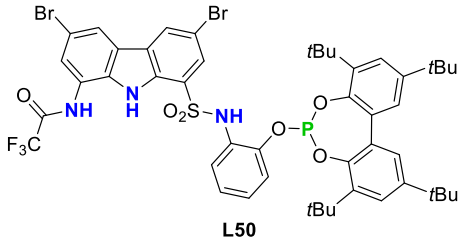

Figure 134. Supramolecular ligand **L50**.

3.2. INTRODUCTION

The hydroformylation reaction has become one of the most important industrially exploited homogeneously catalysed processes since Otto Roelen discovered this chemistry in 1938.[3,4] This transformation is an efficient and economic route to create high-value aldehydes as organic intermediates or final products for the fragrance and pharmaceutical industry.[9,10] As already mentioned, hydroformylation entails the addition of an hydrogen (H) and a formyl group (CHO) across an unsaturated C–C bond in the presence of a catalyst under H_2/CO atmosphere. The most common catalysts used in this transformation are cobalt (Co) and rhodium (Rh) complexes. Although rhodium catalysts are economically less favoured than the cobalt ones, they can be used under milder reaction conditions.[11,116]

Since hydroformylation was discovered, the main goal has been to control the chemoselectivity of the reaction towards the aldehydes, and also the regioselectivity towards the selective formation of either linear or the branched aldehydes.[5,11]

Therefore, the design and synthesis of new catalysts to control the activity, regio- and/or enantio-selectivity in hydroformylation reactions are still cutting-edge goals in this chemistry. One attractive and underdeveloped area of research is the development of supramolecularly regulated catalysts involving the recognition of anions.[207]

[207] a) Gale, P. A.; Dehaen, W. *Anion Recognition in Supramolecular Chemistry*; Springer GmbH, 2010. b) Bowman-James, K.; Bianchi, A.; García-España, E. *Anion Coordination Chemistry*; Wiley-VCH Verlag GmbH & Co. KGaA, 2012.

During the last years, the design and development of organocatalysts incorporating anion-binding motifs has flourished.[208] Jacobsen and co-workers pioneered the use of anion binding in asymmetric catalysis.[209] On the other hand, the design and development of anion receptors applied in organometallic catalysis, such as hydrogenations or hydroformylation reactions has also been reported.

Reek *et al.* have applied a supramolecular regulation strategy using an anionic regulation agent (or cofactor as named by the authors), which interacts with the supramolecular ligand. The previously mentioned authors used the di(1*H*-indol-2-yl)methane-based bisphosphane ligand **L44** (Scheme 56) in combination with and enantiopure carboxylic acid derivative, as for instance **4**•DIPEA (generated *in situ* from the acid and DIPEA). Additionally, the thiourea group of the RA **4** served also to interact with the substrate, leading to very high yields and enantiomeric excesses in the hydrogenation of a set of *N*-acyl enamines.[109]

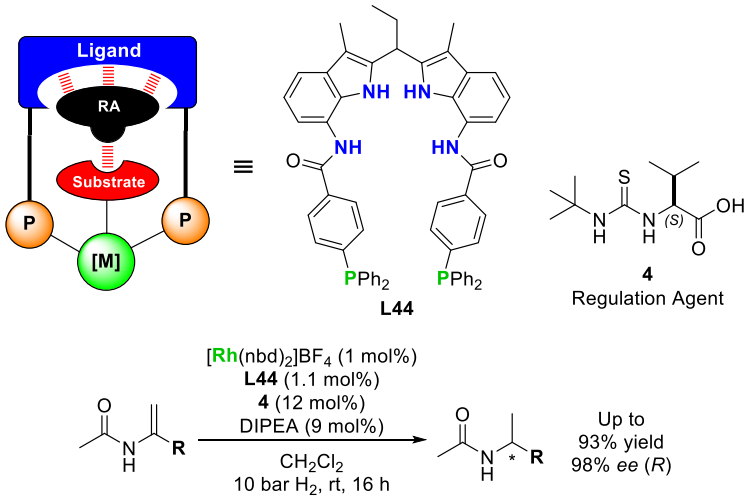

Scheme 56. Supramolecular anionic regulation in asymmetric hydrogenation.

In this work, we present the design and synthesis of a new supramolecular phosphorus-ligand incorporating a regulation site with anion recognition motifs. We also describe preliminary studies on its application in hydroformylation reactions. The design of the regulation site was inspired in the work of Caballero *et al.* and Molina *et al.*,[210] who have demonstrated the

[208] a) Busschaert, N.; Caltagirone, C.; van Rossom, W.; Gale, P. A. *Chem. Rev. (Washington, DC, U. S.)* **2015**, *115*, 8038-8155. b) Zhao, J.; Yang, D.; Yang, X.-J.; Wu, B. *Coord. Chem. Rev.* **2019**, *378*, 415-444.
[209] Brak, K.; Jacobsen, E. N. *Angew. Chem. Int. Ed.* **2013**, *52*, 534-561.
[210] a) Belén Jiménez, M.; Alcázar, V.; Peláez, R.; Sanz, F.; Fuentes de Arriba, Á. L.; Caballero, M. C. *Org. Biomol. Chem.* **2012**, *10*, 1181-1185 b) Sanchez, G.; Espinosa, A.; Curiel, D.; Tarraga, A.; Molina, P. *J. Org. Chem.* **2013**, *78*, 9725-9737.

ability of the *N*,*N*'-(9*H*-carbazole-1,8-diyl)diacyl motif to form highly stable complexes with anions.

Our ligand design is shown in Scheme 57. We hypothesized that the combined use of monophosphite ligand **L50**, a rhodium precursor for hydroformylation reactions and an anionic regulation agent would lead to rhodium complexes derived from a supramolecular bisphosphite with a catalytic site whose geometry, rigidity and/or conformational flexibility would depend on the size and shape of the regulation agent used. Moreover, we envisaged that the solubility of the catalyst could be modulated with the optimal choice of the R substituent.

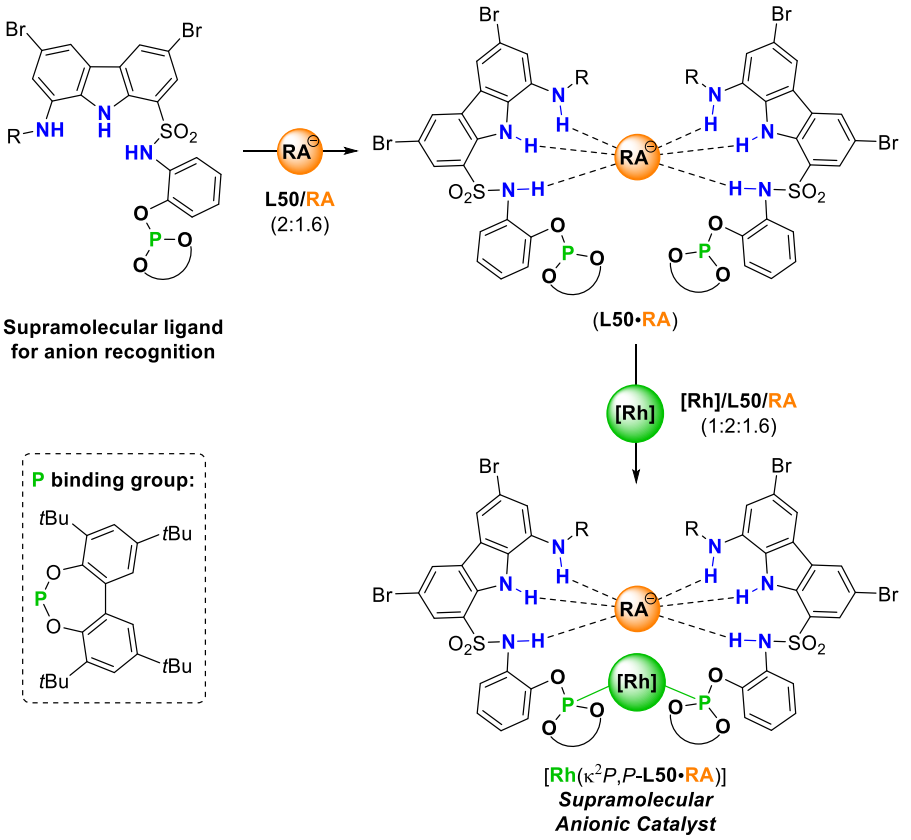

Scheme 57. Design of the supramolecularly regulated catalysts employing anionic regulation agents within this doctoral thesis

3.3. RESULTS AND DISCUSSION

The synthesis of the monophosphite ligand that was designed for our studies (*i.e.*, **L50**) consisted of seven synthetic steps (Scheme 58). The first step was the nitration with 65% HNO_3 of dibromo-9*H*-carbazole (**27**), which is commercially available. The mononitration at the *ortho*-position of the nitrogen in the five-membered ring was selectively achieved in 91% yield employing 1.25 equiv. of 65% nitric acid in boiling acetic acid (for the structure of the mono-nitrated carbazole **26**, see Scheme 58A). The second step consisted of the sulfonation of **26** using chlorosulfonic acid. The product **27** was isolated as the sodium sulfonate in 94% yield after a basic aqueous work-up with sodium bicarbonate (Scheme 58B). The third step consisted of the transformation of the sodium sulfonate into the chlorosulfonic group using PCl_5. The transformation proceeded smoothly in a dichloromethane solution at room temperature and the product **28** was isolated from the reaction mixture in 99% yield (Scheme 58C). Derivatization of the chlorosulfonic acid derivative with *ortho*-aminophenol in the presence of pyridine as the auxiliary base led to the compound **29** in 90% yield (Scheme 58D). The fifth step consisted of the reduction of the nitro group with $SnCl_2{\cdot}H_2O$. The reaction proceeded smoothly and the target product **30** was obtained in 81% yield (Scheme 58E). The sixth step involved the trifluoromethylation of the free amino group in **31** using trifluoroacetic anhydride and triethylamine as auxiliary base (Scheme 58F). The reaction product was obtained in high yield (90%) after purification by column chromatography. The last step of the synthesis of the ligand consisted of the *O*-phosphorylation of the phenolic OH group with chlorophosphite **12**. An excess of triethylamine (5 equiv.) was used to obtain the target monophosphite ligand **L50** (33% yield, Scheme 58G). The overall yield for the 7 steps was 19%, which corresponds to an 83% of average yield for each step. The lowest yielding step was the *O*-phosphorylation, which certainly needs further optimization efforts in the future. Perhaps, the use of alternative auxiliary bases such as pyridine[211] or DMAP[212] (alone[213] or catalytic amounts combined with triethylamine[214]) may lead to higher yields for this transformation. Other options to consider are changes in the reaction

[211] a) Diéguez, M.; Pàmies, O. *Chem. Eur. J.* **2008**, *14*, 3653-3669. b) Diéguez, M.; Pàmies, O.; Ruiz, A.; Claver, C. *New J. Chem.* **2002**, *26*, 827-833 b) Biosca, M.; Magre, M.; Coll, M.; Pàmies, O.; Diéguez, M. *Adv. Synth. Catal.* **2017**, *359*, 2801-2814. d) Diéguez, M.; Pàmies, O.; Net, G.; Ruiz, A.; Claver, C. *J. Mol. Catal. A: Chem.* **2002**, *185*, 11-16. e) la Cruz-Sánchez, P. d.; Faiges, J.; Mazloomi, Z.; Borràs, C.; Biosca, M.; Pàmies, O.; Diéguez, M. *Organometallics* **2019**, *38*, 4193-4205.
[212] DMAP is an acronym that refers to *N*,*N*-dimethylpyridin-4-amine.
[213] a) Park, H.; RajanBabu, T. V. *J. Am. Chem. Soc.* **2002**, *124*, 734-735. b)Park, H.; Kumareswaran, R.; RajanBabu, T. V. *Tetrahedron* **2005**, *61*, 6352-6367.
[214] a) Iuliano, A.; Facchetti, S.; Uccello-Barretta, G. *J. Org. Chem.* **2006**, *71*, 4943-4950. b) Piras, I.; Jennerjahn, R.; Jackstell, R.; Baumann, W.; Spannenberg, A.; Franke, R.; Wiese, K.-D.; Beller, M. *J. Organomet. Chem.* **2010**, *695*, 479-486.

conditions, such as an increase in the reaction temperature up to 80 or 100 ºC, which we believe may lead to a higher yield.[211b,e]

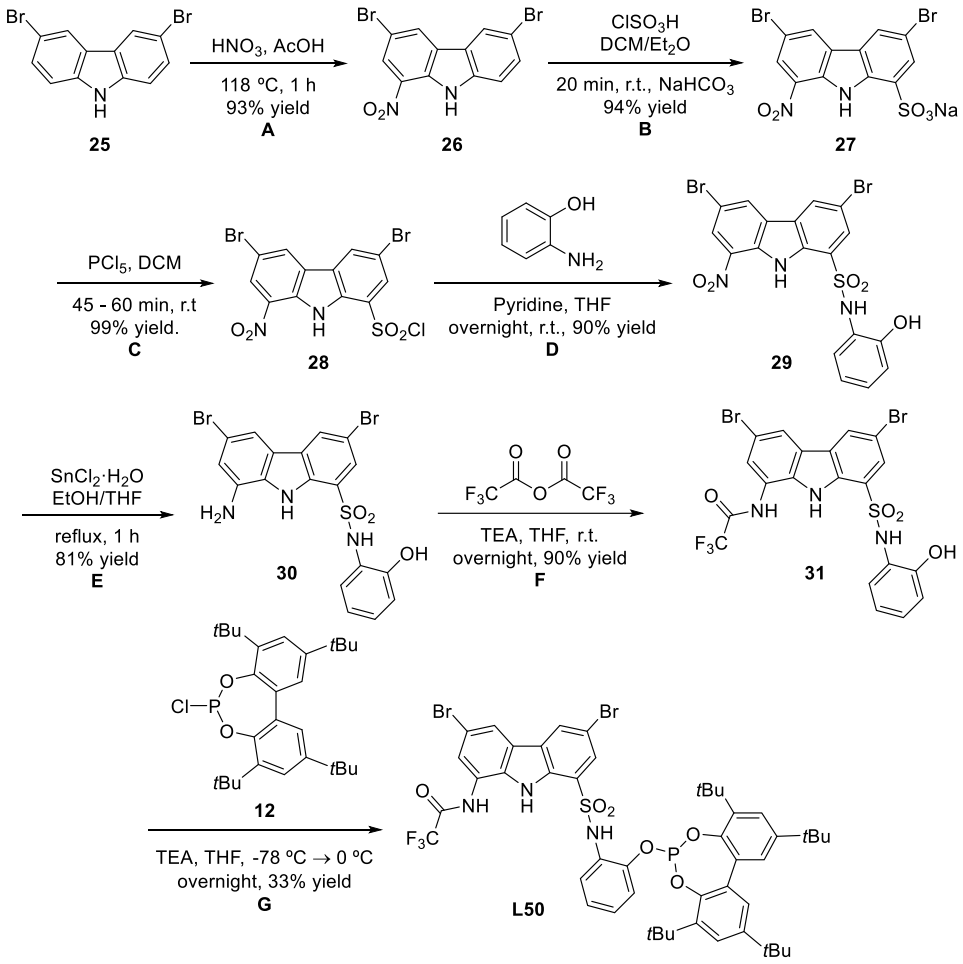

Scheme 58. Synthesis of the ligand **L50**: A) HNO_3, AcOH, 118 ºC, 1 hour (91% yield).B) $ClSO_3H$, DCM/EtOH, room temperature, 20 min, $NaHCO_3$ (94% yield). C) PCl_5, DCM, room temperature, 30 min (99% yield). D) *ortho*-Aminophenol, pyridine, THF, room temperature, overnight (90% yield). E) $SnCl_2{\cdot}H_2O$, EtOH/THF, reflux, 1 hour (81% yield). F) Trifluoroacetic anhydride, TEA, THF, room temperature, overnight (90% yield). G) Chlorophosphite (**12**), TEA, THF, -78 ºC → 0 ºC, overnight (33% yield).

Studies aimed at synthesizing suitable rhodium complexes derived from monophosphite **L50** for hydroformylation followed. A complexation study between [Rh(κ^2*O*,*O'*-acac)(CO)$_2$] and the ligand **L50** was performed in order to investigate the coordination mode of **L50** with the above-mentioned rhodium complex. The experiment was performed with the addition of a solution of **L50** onto another solution of [Rh(κ^2*O*,*O'*-acac)(CO)$_2$] in a ratio of 2:1, respectively, under inert atmosphere. This led to the displacement of one

of the CO groups of the starting rhodium complex by one phosphite-binding group as the major ongoing reaction, with formation of complex [Rh(κ²*O*,*O'*-acac)(CO)(κ*P*-**L50**)].

The structure of the monodentate complex was confirmed by $^{31}P\{^{1}H\}$ NMR spectroscopy (Figure 135a), which revealed a singlet at δ = 137.9 ppm and a doublet centred at δ = 128.3 ppm ($^{1}J_{P-Rh}$ = 306.3 Hz). The doublet was assigned to the bound phosphite group, and the singlet was assigned to the free ligand, which remained unreacted (see the $^{31}P\{^{1}H\}$ NMR spectra in Figure 135b, which also includes the $^{31}P\{^{1}H\}$ NMR of the free ligand to aid comparison).

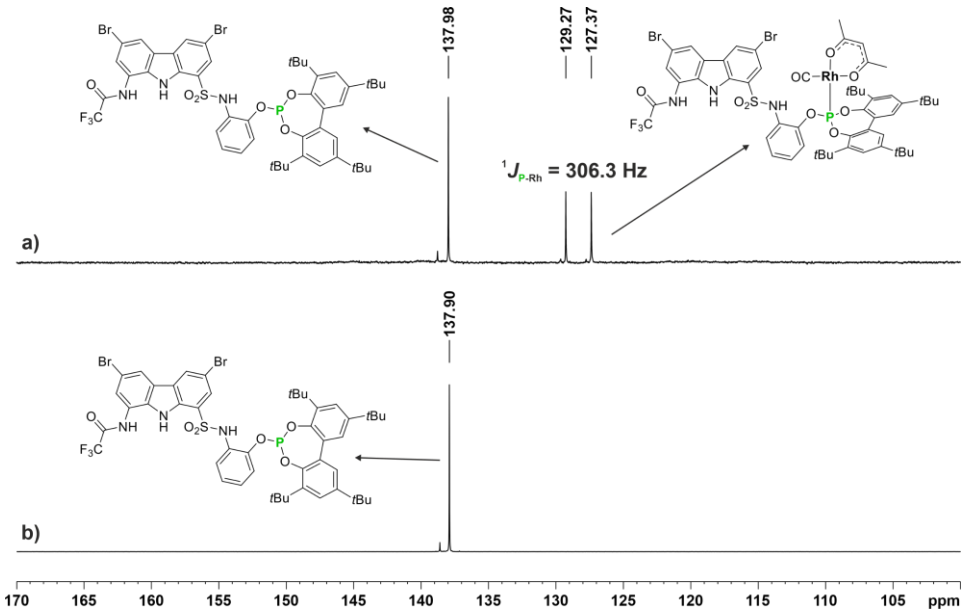

Figure 135. a) $^{31}P\{^{1}H\}$ NMR of the complexation between the ligand **L50** and [Rh(κ²*O*,*O'*-acac)(CO)₂]. b) $^{31}P\{^{1}H\}$ NMR of the free ligand **L50**.

With the aim of studying the generation of hydrido-carbonyl rhodium complexes derived from **L50** that could act as catalysts in hydroformylations (see Figure 136 for a 3D representation of the expected hydrido-dicarbonyl rhodium complex derived from **L50** with the BF_4^- anion bound to the anionic recognition motifs), the reaction mixture arising from the complexation between ligand **L50** and [Rh(κ²*O*,*O'*-acac)(CO)₂] was heated at 60 ºC, under 10 bar H_2/CO (1:1), in the presence or absence of NMe_4BF_4 as a model anionic regulation agent. Unfortunately, the performed $^{31}P\{^{1}H\}$ NMR spectroscopic analysis on the reaction mixtures were not conclusive and did not allow either to confirm or rule out the formation of hydrido-carbonyl rhodium complexes.

a) 3D representations of [Rh(CO)$_2$H(κ^2*P*,*P*-(**(*Ra*,*Ra*)-L50**•BF_4)]

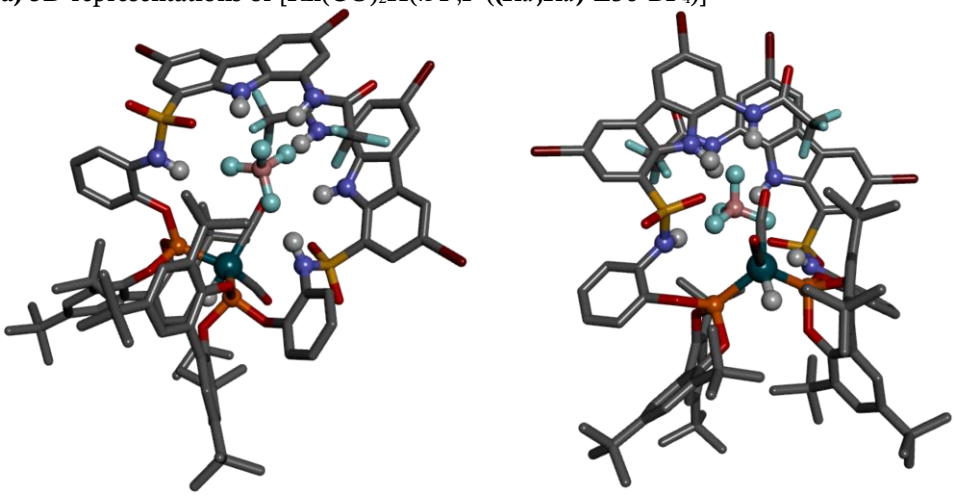

b) 3D representations of [Rh(CO)$_2$H(κ^2*P*,*P*-(**(*Ra*,*Sa*)-L50**•BF_4)]

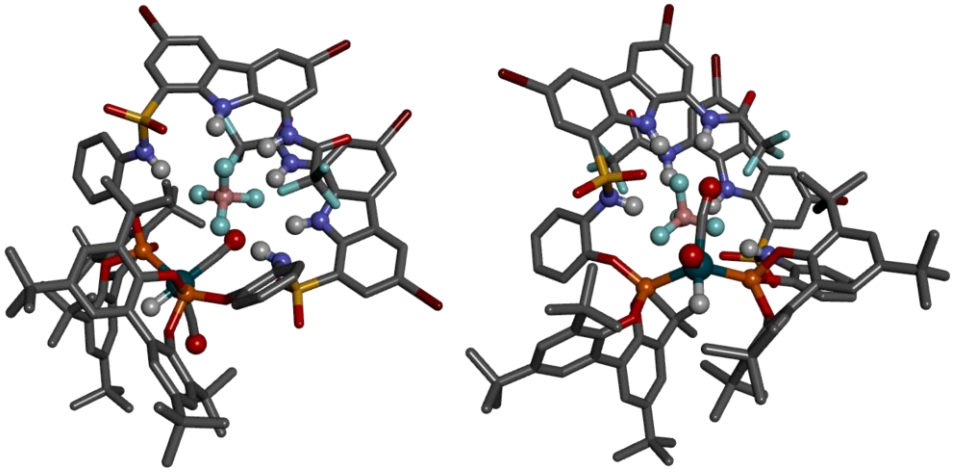

Figure 136. 3D representations of the expected hydrido-dicarbonyl rhodium complex derived from **L50** with the BF_4^- anion bound to the anionic recognition motifs.

Despite this fact, rhodium complexes derived from **L50** were applied in the hydroformylation of styrene in order to evaluate their performance as supramolecular ligand with the presence and absence of an anion as a regulation agent (RA). The results of the preliminary catalytic studies are summarised in Table 60. Standard screening conditions were performed with [Rh(κ^2*O*,*O'*-acac)(CO)$_2$] (1.0 mol%) as the metal precursor and the corresponding monophosphite ligand **L50** (2.0 mol%) at 60 °C under 10 bar H_2/CO (1:1) for 18 hours in toluene, with the minimum amount of THF to solubilize NMe_4BF_4 (1.6 mol%) as the regulation agent in the case it was used.

Table 60. Results of hydroformylation using the supramolecular ligand **L50**.

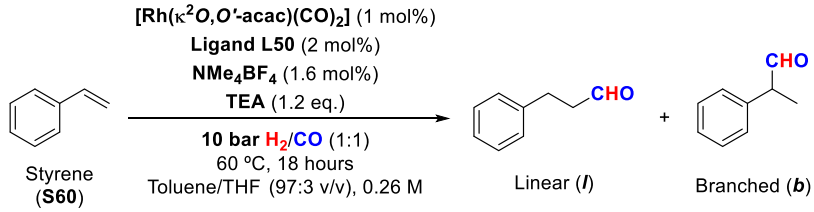

Entry	Subs.	NMe_4BF_4	Conv. (%)	Select. (%)[a]		*l*/*b* ratio (%)	*l*/*b* yield (%)
				Isom.	Aldehydes		
1	**S60**	-	99	<1	99	33:67	24:49
2	**S60**	✓	99	<1	99	34:66	30:54

Reaction conditions: [substrate] = 0.26 M; stirring rate= 800 rpm; 10 bar H_2/CO (1:1); 60 °C, 18h. Conversion, ratio, selectivity, and yields were determined by ^{1}H NMR using 1,3,5-trimethoxybenzene as internal standard. [a] Selectivity of isomerisation (Isom.) and aldehydes products.

The results of this preliminary study on the activity of rhodium complexes derived from **L50** in hydroformylation reactions are summarised in Table 60. Styrene (**S60**) was hydroformylated under the previously mentioned conditions in the presence and absence of an anionic RA, in this case the anionic component of NMe_4BF_4. The addition of this RA had no effects in the outcome of the reaction, with the same activity and regioselectivity being obtained within experimental error. Due to time constraints, no further experiments in this area of research (such as performing more conclusive coordination studies with **L50**, using other anionic regulation agents, studying other substrates, etc.) could be performed.

3.4. CONCLUSIONS

The supramolecular ligand **L50** containing a recognition motif for anions was successfully synthesised through a seven-step synthetic route. All the transformations on the starting carbazole framework took place in very high yield, with the exception of the *O*-phosphorylation reaction (33% yield) that will require further optimization studies in the future. The average yield for each step was 83%.

The monophosphite **L50** was coordinated to the standard rhodium precursor in hydroformylations (*i.e.*, [Rh(κ²*O*,*O'*-acac)$(CO)_2$] employing a 2:1 molar ratio (**L50**/[Rh]), with the formation of the rhodium complex [Rh(κ²*O*,*O'*-acac)(CO)(κ*P*-**L50**)] being observed. The structure of the final complex was established by ^{31}P NMR studies, which confirmed that only one of the CO groups from the starting rhodium complex was displaced by the phosphite ligating group of **L50**. The formation of active rhodium complexes

in hydroformylation derived from **L50** and [Rh(κ^2*O,O'*-acac)(CO)$_2$] under H_2/CO atmosphere could not be confirmed.

Ligand **L50** was tested in hydroformylation obtaining high conversions and selectivities for styrene. However, the regioselectivities observed were moderate and the few performed experiments did not prove any regulation effect mediated by the only RA studied (NMe_4BF_4). Further work is required in the future to establish the potential of the use of anionic regulation agents in hydroformylation chemistry.

3.5. EXPERIMENTAL SECTION

3.5.1. General remarks

All syntheses were carried out using chemicals purchased from commercial sources unless otherwise cited. Air- and moisture-sensitive manipulations and hydroformylation reactions were performed under inert atmosphere, either in a N_2-filled glove box or with standard Schlenk techniques. Hazards: Carbon monoxide (CO) is a very toxic gas by inhalation and this reagent or metal carbonyl complexes were always used in well-ventilated hoods. Glassware was dried in vacuo before use with a hot air gun. All solvents were dried by using a Solvent Purification system (SPS). SiO_2 (230-400 mesh) was used for column chromatography. NMR spectra were recorded in DMSO-d_6, THF-d_8, CD_2Cl_2 and $CDCl_3$ and unless otherwise cited, on a Bruker Avance 400 MHz or 500 MHz Ultrashield spectrometers. ^{1}H NMR and ^{13}C{^{1}H} NMR chemical shifts are quoted in ppm relative to residual solvent peaks. ^{31}P{^{1}H} NMR chemical shifts are quoted in ppm relative to 85% phosphoric acid in water. High-resolution mass spectrum (HRMS) and nominal mass were recorded by using ESI as ionization method in positive or negative mode, unless otherwise stated. Selectivity of hydrogenation and isomerisation of the octenes substrates were determined by GC with a FID detector using achiral stationary phase, HP-5. Conversions, *l*/*b* ratio and NMR yield were determined by ^{1}H NMR using 1,3,5-trimethoxybenzene as internal standard.

3.5.2. Synthesis of monophosphite ligand L50.

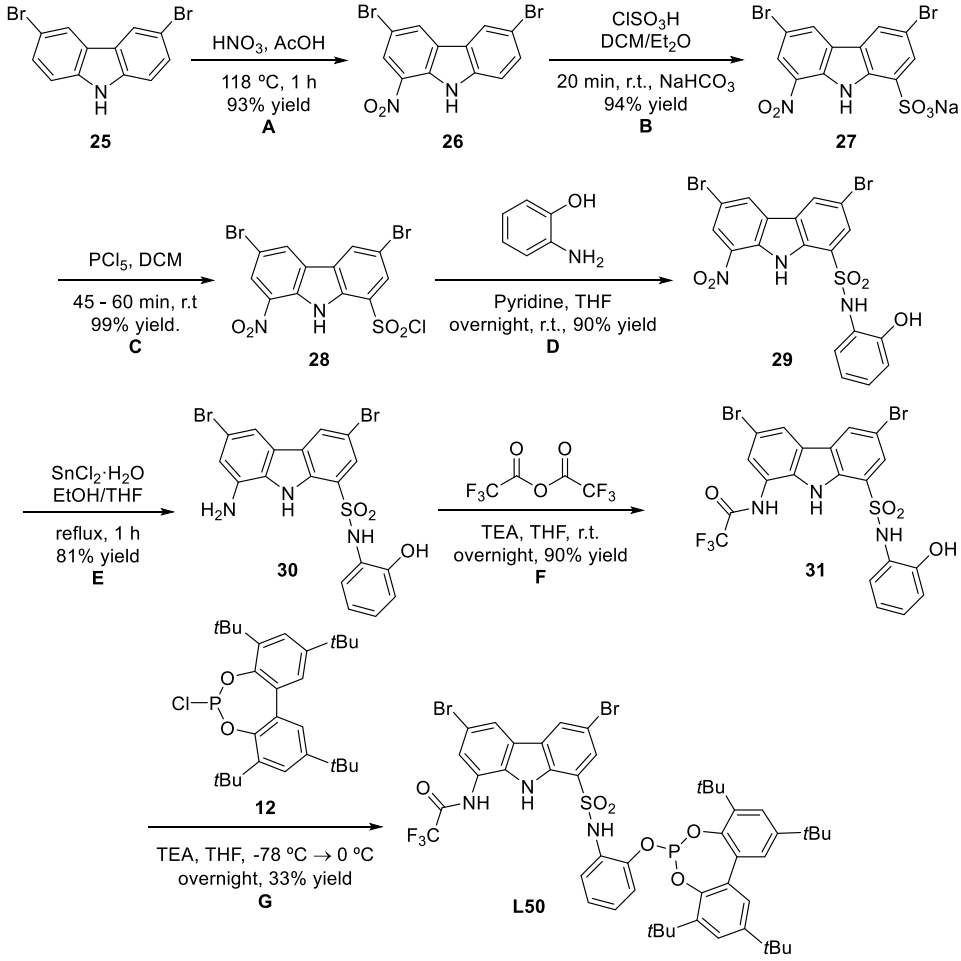

Scheme 59. Synthesis of **L50**.

Step A: Synthesis of the compound **26** (3,6-dibromo-1-nitro-9*H*-carbazole).

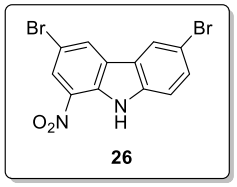

3,6-Dibromo-9*H*-carbazole (**25**) (30.2 mmol, 10 g) was dissolved in acetic acid (131 mL, 0.23 M) in a two-necked round flask with a reflux condenser. The mixture was heated to reflux (118ºC), at which time nitric acid (37.5 mmol, 2.6 mL, 65%) was added with a dropping funnel. After having added 2/3 of the total amount of nitric acid was added, a flocculent yellow precipitate deposited. After adding all nitric acid, the mixture was stirred at 118ºC for one additional hour. Then, the mixture was cooled to 0ºC in an ice bath and filtered. The 3,6-dibromo-1-nitro-9*H*-carbazole (**26**) (28.2 mmol, 10.44 g, yield: 93 %) was obtained as a yellow solid. ^{1}H NMR (400 MHz, DMSO-d_6) δ 12.31 (s, 1H), 8.84 (d, J = 1.8

Hz, 1H), 8.48 (s, 1H), 8.33 (d, J = 1.9 Hz, 1H), 7.67 (s, 2H). ^{13}C NMR (101 MHz, DMSO-d_6) δ 139.77, 132.04, 132.00, 130.79, 130.49, 127.68, 124.02, 123.76, 122.43, 114.59, 113.00, 109.33. HRMS (ESI$^-$) *m/z* calcd. for $C_{12}H_5Br_2N_2O_2$ [M–H]$^-$ 366.8718, found 366.8731.

Step B: Synthesis of the compound **27** (sodium 3,6-dibromo-8-nitro-9*H*-carbazole-1-sulfonate).

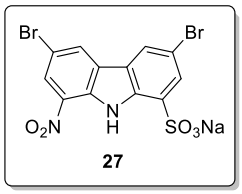

27

3,6-Dibromo-1-nitro-9*H*-carbazole (**26**) (16.2 mmol, 6.0 g) was suspended in a mixture of DCM (125 mL) and Et_2O (4.8 mL) and a solution of chlorosulfonic acid (154 mmol, 10.2 mL) in DCM (43.5 mL) was added dropwise to the strongly stirred solution at room temperature. After 20 min, the reaction was poured onto ice and filtered. The organic layer was extracted with DCM and sodium bicarbonate was added into the aqueous layer until pH 7 and a precipitated appeared. The solid was filtered and product **27** was isolated as a yellow-green solid (15.3 mmol, 7.2 g, 94% yield). ^{1}H NMR (500 MHz, DMSO-d_6) δ 11.16 (s, 1H), 9.01 (d, J = 1.8 Hz, 1H), 8.64 (s, 1H), 8.46 (d, J = 1.8 Hz, 1H), 7.77 (d, J = 1.9 Hz, 1H). ^{13}C NMR (126 MHz, DMSO-d_6) δ 134.65, 133.18, 132.33, 131.78, 131.47, 127.56, 127.23, 124.88, 124.59, 123.33, 112.64, 110.17. Nominal Mass (ESI$^-$) *m/z* calcd. for $C_{12}H_4Br_2N_2O_5S^-$ [M–Na–H]$^-$ 448.04, found 448.70.

Step c: Synthesis of the compound **28** (3,6-dibromo-8-nitro-9*H*-carbazole-1-sulfonyl chloride).

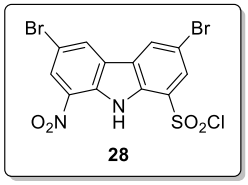

28

The compound **27** (8.47 mmol, 4.0 g) was dissolved in dry DCM (74 mL) and treated with PCl_5 (18.6 mmol, 3.96 g) under nitrogen atmosphere. Once gas evolution ceased (45 - 60 min), the mixture was evaporated and product **28** was obtained as a green-yellow solid (0.958 mmol, 3.92 g, 99% yield). ^{1}H NMR (500 MHz, DMSO-d_6) δ 11.15 (s, 1H), 9.00 (d, *J* = 1.8 Hz, 1H), 8.63 (d, *J* = 1.9 Hz, 1H), 8.44 (d, *J* = 1.9 Hz, 1H), 7.77 (d, *J* = 1.9 Hz, 1H). ^{13}C NMR (126 MHz, DMSO-d_6) δ 134.65, 133.21, 132.35, 131.80, 131.50, 127.56, 127.25, 124.91, 124.61, 123.35, 112.65, 110.18. Nominal Mass (ESI$^-$) *m/z* calcd. for $C_{12}H_4Br_2ClN_2O_4S^-$ [M–H]$^-$ 467.49, found 467.50.

Step D: Synthesis of the compound **29** (3,6-dibromo-*N*-(2-hydroxyphenyl)-8-nitro-9*H*-carbazole-1-sulfonamide).

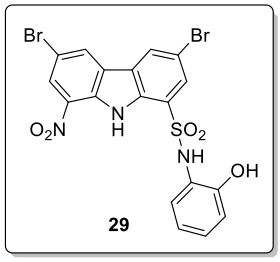

Pyridine (0.165 mL, 2.03 mmol) was added to *ortho*-aminophenol (0.892 mmol, 98.3 mg) in THF (6 mL) under nitrogen atmosphere. Following, compound **29** (0.406 mmol, 95% pure, 200 mg) was added to the above-mentioned solution and the mixture was stirred under nitrogen atmosphere overnight (16h). The solvent was evaporated under reduced pressure. The solid was washed with 10 mL of HCl 1N and extracted with AcOEt (3 x 10 mL). The organic layer was dried over $NaSO_4$ and filtered. The crude was purified by flash column chromatography over SiO_2 using Cy/AcOEt (50:50) as eluent. A yellow solid was obtained (0.406 mmol, 197 mg, 90% yield). ^{1}H NMR (500 MHz, DMSO-d_6) δ 10.80 (s, 1H), 10.13 (s, 1H), 9.37 (s, 1H), 8.98 (s, 1H), 8.83 (s, 1H), 8.45 (s, 1H), 7.73 (d, J = 1.8 Hz, 1H), 7.23 (dd, J = 7.9, 1.7 Hz, 1H), 6.93 (td, J = 7.7, 1.7 Hz, 1H), 6.73 (td, J = 7.6, 1.4 Hz, 1H), 6.55 (dd, J = 8.1, 1.5 Hz, 1H). ^{13}C NMR (126 MHz, DMSO-d_6) δ 151.57, 134.62, 132.40, 131.74, 131.53, 129.04, 128.76, 127.58, 127.13, 126.36, 125.33, 125.04, 124.39, 122.56, 119.12, 115.42, 112.11, 111.09. Nominal Mass (ESI$^-$) m/z calcd. for $C_{18}H_9Br_2N_3O_5S^{-2}$ $[M–2H]^-$ 539.16, found 539.50.

Step E: Synthesis of the compound **30** (8-amino-3,6-dibromo-*N*-(2-hydroxyphenyl)-9*H*-carbazole-1-sulfonamide).

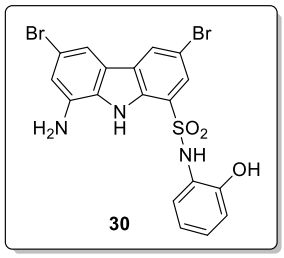

The compound **29** (7.35 mmol, 3.98 g) was suspended in a mixture of EtOH (20.9 mL), THF (17.3 mL) and $SnCl_2{\cdot}2H_2O$ (23.2 mmol, 5.22 g). The resulting reaction mixture was refluxed for 1 hour. Then, it was cooled down and AcOEt (30 mL) and water (8 mL) were added. Solid sodium carbonate was added until the reaction mixture showed a neutral pH. Filtration of the tin salts followed by extraction of the filtrated with AcOEt (3 x 50mL), drying of the solution over $NaSO_4$ and evaporation of the organic solvents led to a solid residue, which was purified by column chromatography over SiO_2 using cyclohexane/ethyl acetate (70:30). The desired product was obtained as a brown solid (3.05 g, 81% yield). ^{1}H NMR (500 MHz, DMSO-d_6) δ 11.01 (s, 1H), 9.73 (s, 1H), 9.36 (s, 1H), 8.60 (d, J = 1.9 Hz, 1H), 7.77 (d, J = 1.9 Hz, 1H), 7.20 (dd, J = 8.0, 1.6 Hz, 1H), 6.89 (td, J = 7.7, 1.7 Hz, 1H), 6.87 (d, J = 1.8 Hz, 1H), 6.73 – 6.62 (m, 2H), 5.90 (s, 2H). ^{13}C NMR (126 MHz, DMSO-d_6) δ 149.71, 135.88, 133.22, 127.99, 127.80, 126.96, 126.54, 126.27, 123.68, 123.55, 122.55,

119.05, 115.35, 113.52, 112.71, 110.57, 109.24. HRMS (ESI^-) *m/z* calcd. for $C_{18}H_{12}Br_2N_3O_3S^-$ $[M–H]^-$ 509.8972, found 509.8792.

Step F: Synthesis of the compound **31** (*N*-(3,6-dibromo-8-(*N*-(2-hydroxyphenyl)sulfamoyl)-9*H*-carbazol-1-yl)-2,2,2-trifluoroacetamide).

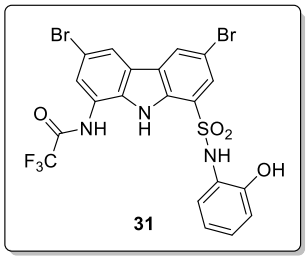

31

To a stirred solution of the compound **32** (1.91 mmol, 998 mg) and triethylamine (7.65 mmol 1.075 ml,) in THF (6.5 mL), trifluoroacetic anhydride (2.3 mmol, 323 µL) in THF (1 mL) was added dropwise at 0° C. The reaction was stirred overnight at room temperature. Then, the mixture was diluted with H_2O (5 ml), the organic layer was extracted with EtOAc (3 x 10 mL) and washed with brine (5 mL). The organic solution was dried over Na_2SO_4 and concentrated under reduced pressure. The crude was purified by flash column chromatography over SiO_2 with hexane/ethyl acetate (80:20) as eluent yielding the desired product as a solid (1.05 g, 90% yield). ^1H NMR (400 MHz, THF-d_8) δ 10.68 (s, 1H), 10.15 (s, 1H), 8.88 (s, 1H), 8.48 (d, *J* = 1.2 Hz, 1H), 8.42 (s, 1H), 8.23 (d, *J* = 1.6 Hz, 0H), 8.00 (d, *J* = 1.8 Hz, 1H), 7.88 (d, *J* = 1.9 Hz, 1H), 7.35 (dd, *J* = 7.9, 1.7 Hz, 1H), 6.86 (td, *J* = 7.7, 1.7 Hz, 1H), 6.70 (td, *J* = 7.7, 1.4 Hz, 1H), 6.47 (dd, *J* = 8.1, 1.4 Hz, 1H) ppm. ^{13}C NMR (101 MHz, THF-d_8) δ 156.23 (q, *J* = 37.6 Hz), 151.73, 135.98, 132.40, 129.44, 128.34, 127.97, 127.18, 126.66, 125.79, 125.62, 124.98, 124.76, 122.50, 122.22, 120.25, 115.84, 113.05, 112.05 ppm. ^{19}F NMR (376 MHz, THF-d_8) δ -75.87 ppm. HRMS (ESI^+) *m/z* calcd. for $C_{20}H_{16}Br_2F_3N_4O_4S^+$ $[M+NH_4]^+$ 622.9211, found 622.9202.

Step G: Synthesis of the 3,3',5,5'-tetra-*tert*-butylbiphenyl-2,2'-diyl chlorophosphite (**12**) and the ligand **L48**.

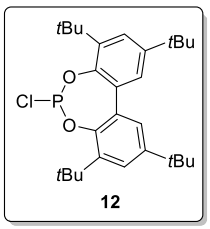

12

The preparation of 3,3',5,5'-tetra-*tert*-butylbiphenyl-2,2'-diyl chlorophosphite (**12**) was performed by slightly varying a reported procedure.[202] In a flame-dried Schlenk flask, 3,3',5,5'-tetra-*tert*-butyl-2,2'-dihydroxybiphenyl (**11**) (2.01 g, 4.8 mmol, 1.01 equiv.) was weighted, and then azeotropically dried with toluene (3 x 10 mL). 30 mL of anhydrous toluene (SPS[203]) were added to the flask. Another flame-dried Schlenk flask was placed in the glove box, and 0.51 mL of PCl_3 (5.82 mmol, 1.22 equiv.) were transferred to the flask. 30 mL of anhydrous toluene were also added to the Schlenk flask. Finally, triethylamine (1.75 mL, 12.6 mmol, 2.64 equiv.) was syringed into the solution. The "BIPOL" solution at room temperature was slowly (*ca.* 45-60 min) cannulated to the PCl_3 solution (0°C). Then, the mixture was stirred for 16 h at room temperature. After this, the reaction mixture was filtered with a cannula filter to another flame-dried Schlenk flask. The filtrate was evaporated to dryness

by vacuum to give a yellow solid (1.97 g, quantitative yield). This chlorophosphite (**12**) was used with no purification in the next synthesis step. Spectroscopic data for this compound were in agreement with those already reported in the literature.[102] ^{1}H NMR (400 MHz, $CDCl_3$) δ 7.47 (d, J = 2.4 Hz, 4H), 7.18 (d, J = 2.4, 4H), 1.48 (s, 18H), 1.36 (s, 18H) ppm; ^{31}P{^{1}H} NMR (162 MHz, $CDCl_3$) δ 171.5 ppm.

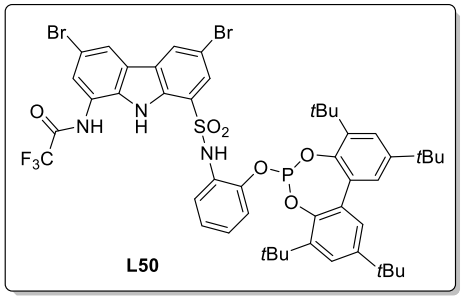

All glassware was oven-dried or flame-dried under vacuum. All solvents and reagents were dry. Compound **31** was azeotropically dried prior to use, by co-evaporation with dry toluene three times. To the solution of phenol (150 mg, 0.247 mmol) and triethylamine (173 µl, 1.24 mmol) in THF (3 ml) and 4Å molecular sieves, the freshly prepared solution of chlorophosphite **12** (1.2 mmol) in THF (3 ml; previously dried under 4Å molecular sieves) was added dropwise at -78°C. After 30 minutes, the cooling bath was removed, and the mixture was allowed to continue stirring overnight. The turbid reaction mixture was transferred to a flame-dried flask through a cannula filter with celite® at one of its ends and the filtrate was evaporated to dryness to give the crude as an orange-brown solid. This product was then purified by column chromatography over SiO_2 inside of the glove box using hexane/DCM (50:50) as eluent yielding the desired monophosphite **L50** as a yellow solid (91 mg, 94% pure, 30% yield). ^{1}H NMR (500 MHz, CD_2Cl_2) δ 9.72 (s, 1H), 8.46 (s, 1H), 8.10 (dd, J = 1.9, 0.6 Hz, 1H), 7.83 (dd, J = 1.7, 0.6 Hz, 1H), 7.64 (d, J = 1.7 Hz, 1H), 7.54 (dd, J = 8.1, 1.5 Hz, 1H), 7.47 (d, J = 2.5 Hz, 2H), 7.37 (d, J = 1.7 Hz, 1H), 7.25 (d, J = 2.5 Hz, 2H), 7.05 (s, 1H), 6.98 (td, J = 7.7, 1.9 Hz, 1H), 6.92 – 6.82 (m, 2H), 1.38 (s, 18H), 1.29 (s, 18H) ppm. ^{19}F NMR (471 MHz, CD_2Cl_2) δ -75.02 (d, J = 1.1 Hz) ppm.^{31}P NMR (202 MHz, CD_2Cl_2) δ 137.91 ppm. HRMS (ESI^+) m/z calcd. for $C_{48}H_{52}Br_2F_3N_3O_6PS^+$ $[M+H]^+$ 1044.11628, found 1044.1666.

3.5.3. General procedure for the Rh-mediated hydroformylation

The monophosphite ligand **L50** (2.0 mol%) was placed under nitrogen into a vial with a magnetic bar. Then, NMe_4BF_4 (1.6 mol%) and TEA (1.2 mol%) were added when required. [Rh(κ²*O,O'*-acac)$(CO)_2$] (1.0 mol%), substrate (260 μmol) and toluene/THF (97:3 v/v) were charged to provide the desired final solution of 0.26 M. Once the reaction mixture had been loaded, the vial vessel was then placed into one of the holes of a steel autoclave reactor (HEL Cat-24 parallel pressure multi-reactor) and taken out of the glove box. The autoclave was purged three times with syngas (1:1 H_2/CO at a pressure not higher than 10 bar) and finally, the autoclave was pressurized with syngas to the desired pressure (10 bar). The reaction mixture was stirred at 60 °C for 18 hours. The reaction was cooled, and the pressure was carefully released in a well-ventilated hood. Conversion, selectivity, linear-to-branched ratio (*b/l* ratio), and yield were calculated by ^{1}H NMR analysis of the reaction mixtures using 1,3,5-trimethoxybenzene as internal standard (30%).

3.5.4. Results of catalysis in hydroformylation using the ligand L50

Table 61. Results of hydroformylation catalysis using the anionic supramolecular ligand **L50**.

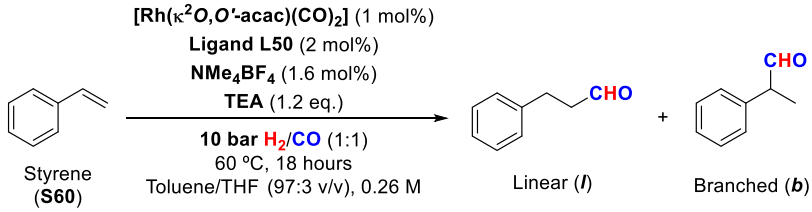

Entry	Subs.	NMe_4BF_4	Conv. (%)	Select. (%)[a]		*l/b* ratio (%)	*l/b* yield (%)
				Isom.	Aldehydes		
1	S60	-	99	<1	99	33:67	24:49
2	S60	✓	99	<1	99	34:66	30:54

Reaction conditions: [substrate] = 0.26 M; stirring rate= 800 rpm; 10 bar H_2/CO (1:1); 60 °C, 18h. Conversion, ratio, selectivity, and yields were determined by ^{1}H NMR using 1,3,5-trimethoxybenzene as internal standard. [a] Selectivity of Isomerisation (Isom.) and Aldehydes products.

3.5.5. NMR spectrum data

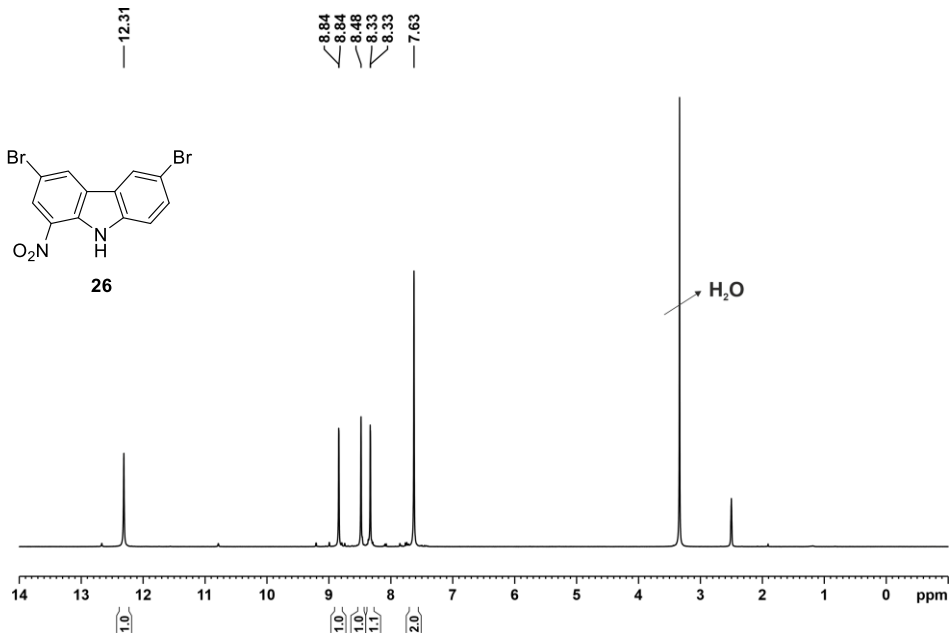

Figure 137. [1]H NMR (400 MHz, DMSO-d_6) of the compound **26** (3,6-dibromo-1-nitro-9*H*-carbazole).

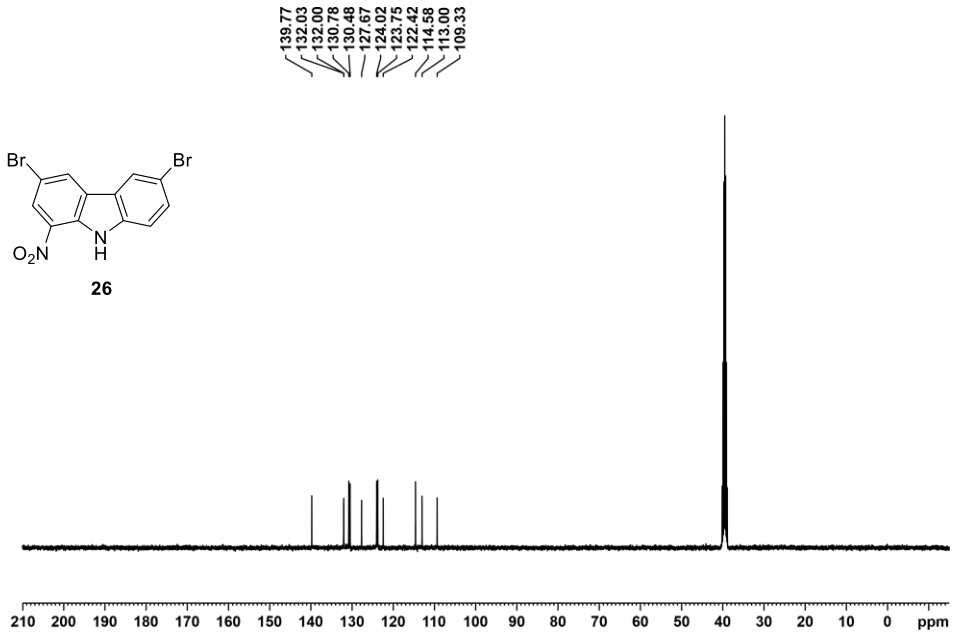

Figure 138. [13]C NMR (101 MHz, DMSO-d_6) of the compound **26** (3,6-dibromo-1-nitro-9*H*-carbazole).

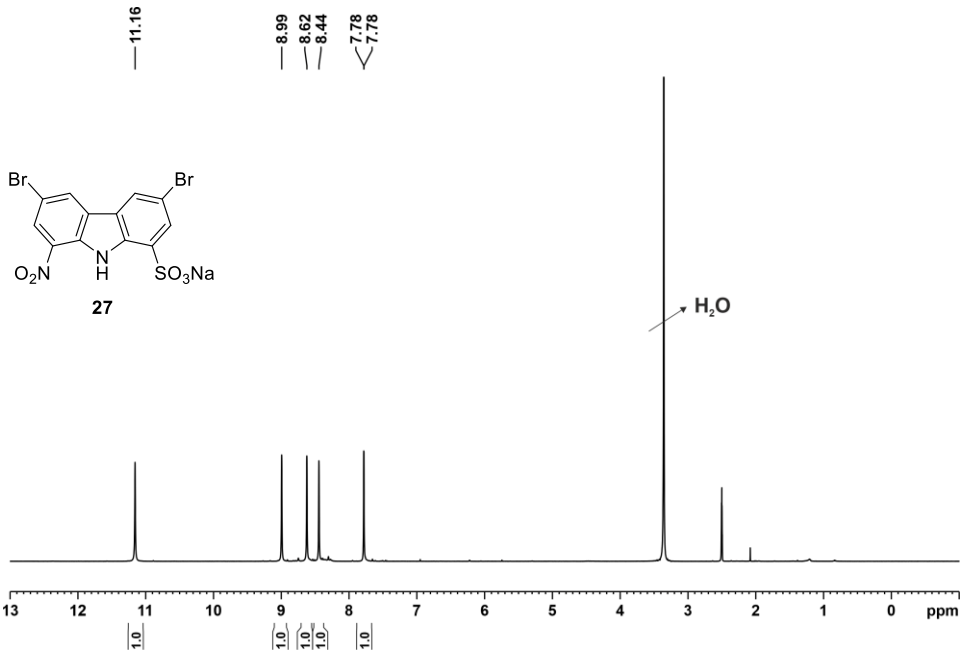

Figure 139. ^{1}H NMR (500 MHz, DMSO-d_6) of the compound **27** (sodium-3,6-dibromo-8-nitro-9*H*-carbazole-1-sulfonate).

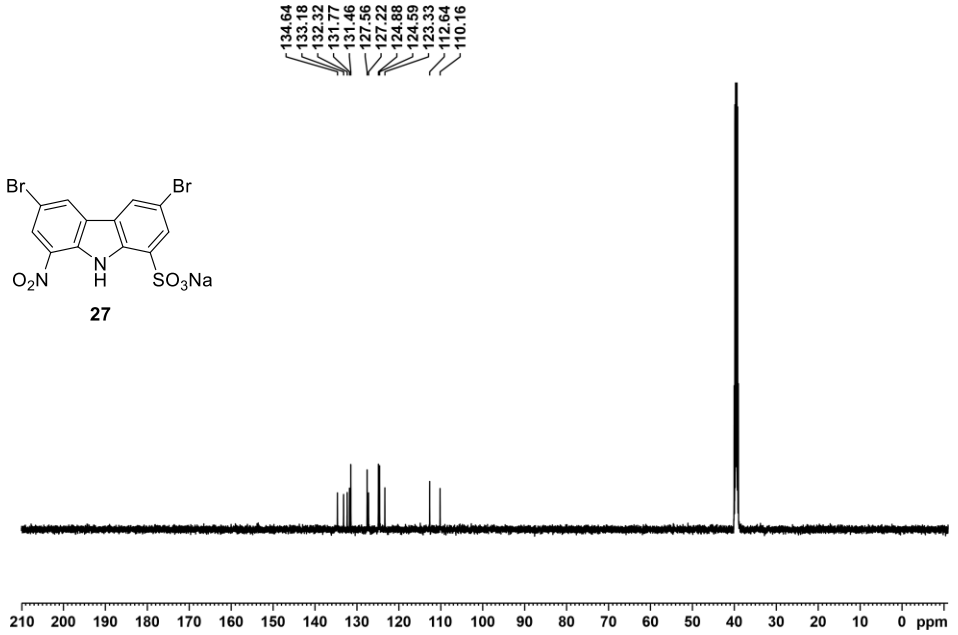

Figure 140. ^{13}C NMR (126 MHz, DMSO-d_6) of the compound **27** (sodium-3,6-dibromo-8-nitro-9*H*-carbazole-1-sulfonate).

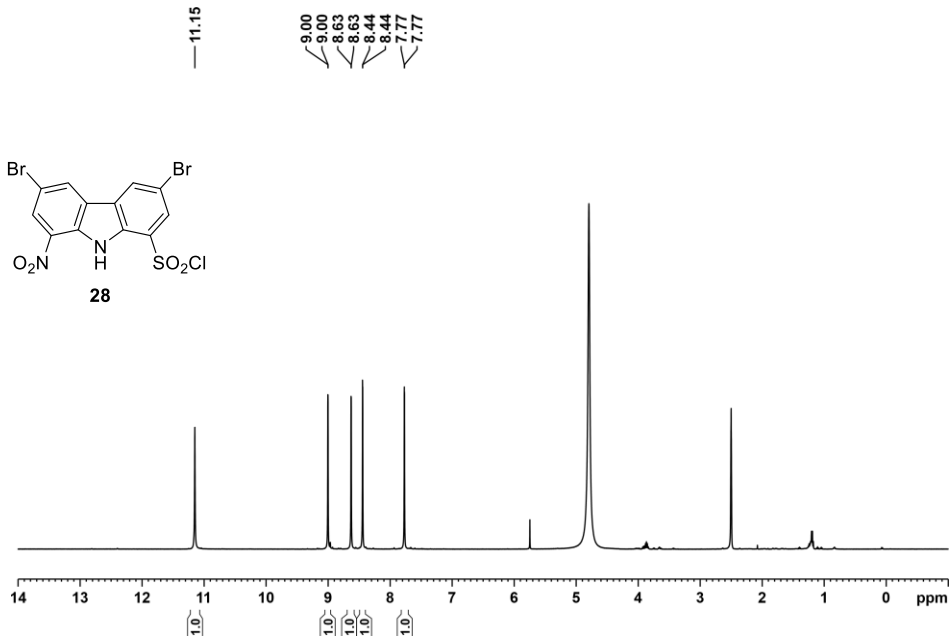

Figure 141. ^{1}H NMR (500 MHz, DMSO-d_6) of the compound **28** (3,6-dibromo-8-nitro-9*H*-carbazole-1-sulfonyl chloride).

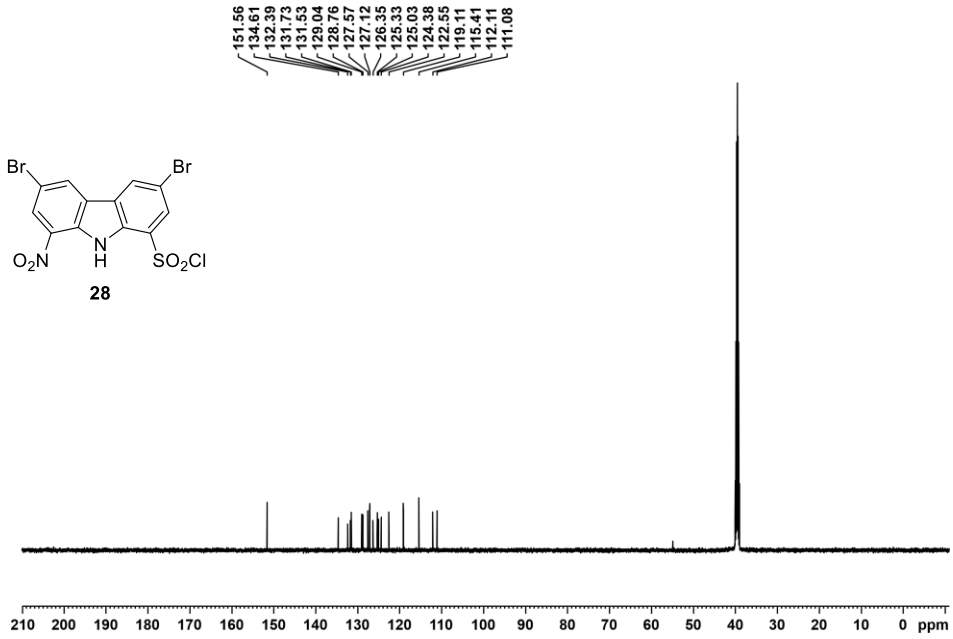

Figure 142. ^{13}C NMR (126 MHz, DMSO-d_6) of the compound **28** (3,6-dibromo-8-nitro-9*H*-carbazole-1-sulfonyl chloride).

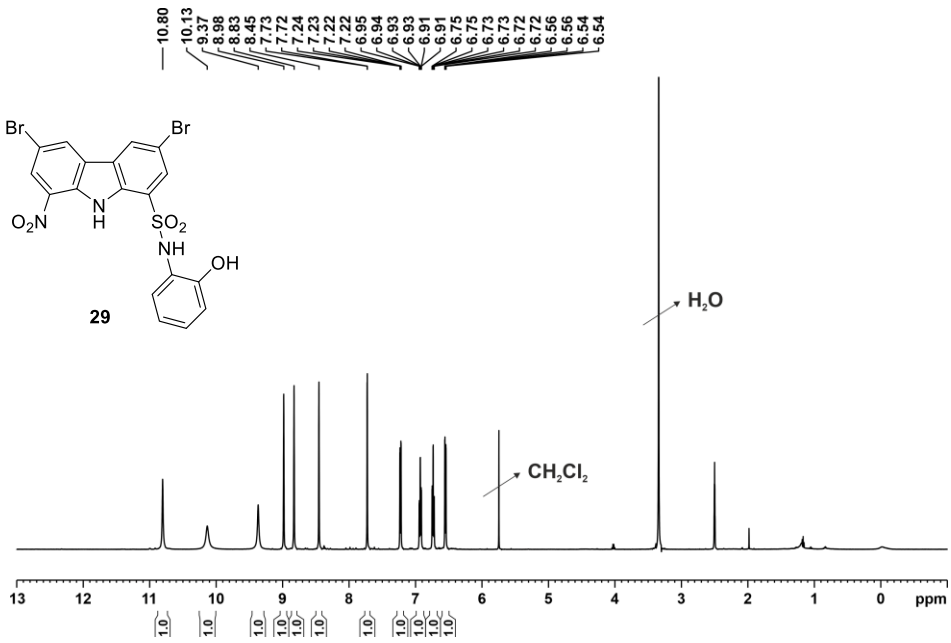

Figure 143. ^{1}H NMR (500 MHz, DMSO-d_6) of the compound **29** (3,6-dibromo-*N*-(2-hydroxyphenyl)-8-nitro-9*H*-carbazole-1-sulfonamide).

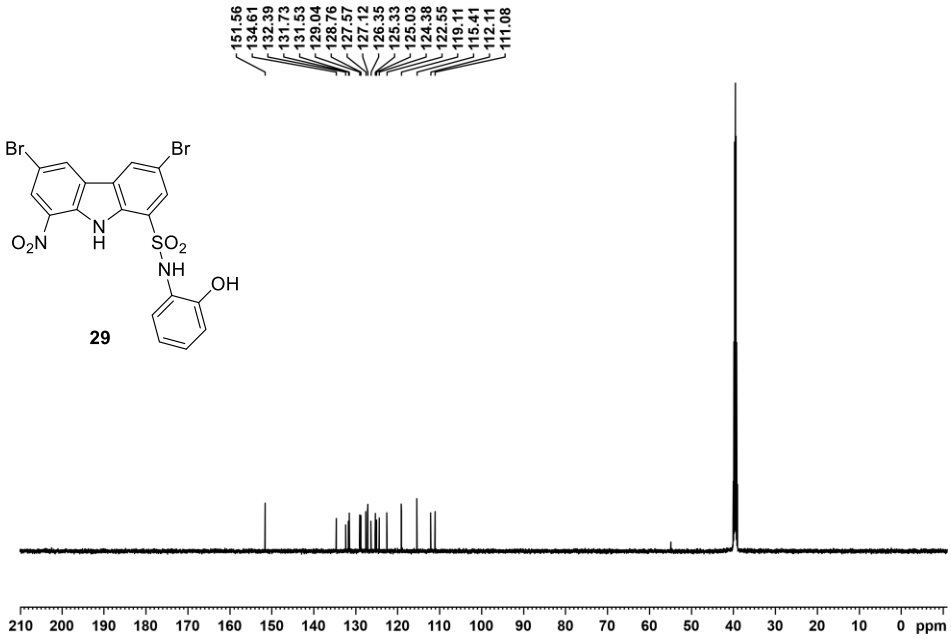

Figure 144. ^{13}C NMR (126 MHz, DMSO-d_6) of the compound **29** (3,6-dibromo-*N*-(2-hydroxyphenyl)-8-nitro-9*H*-carbazole-1-sulfonamide).

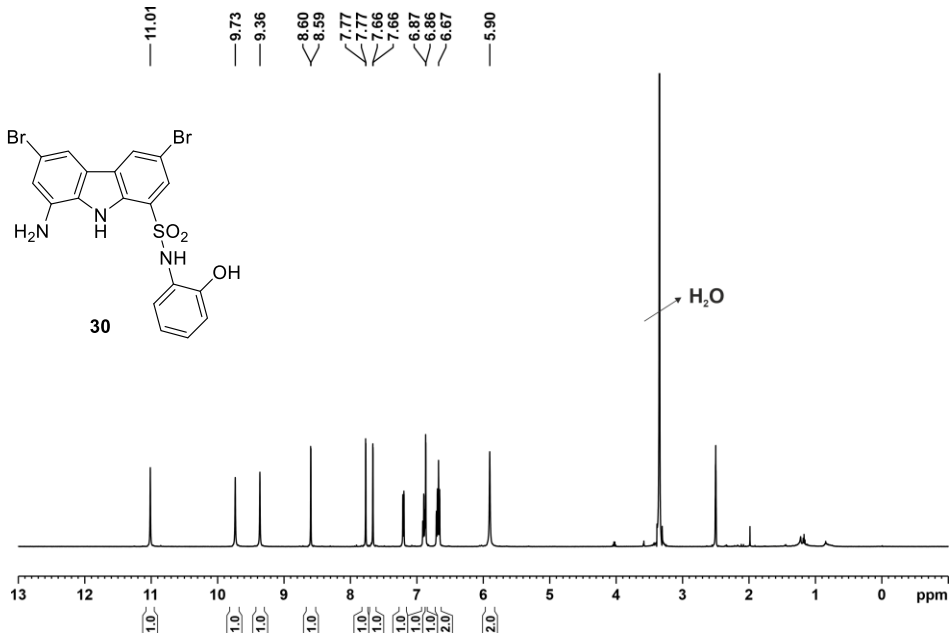

Figure 145. ^{1}H NMR (500 MHz, THF-d_8) of the compound **30** (8-amino-3,6-dibromo-*N*-(2-hydroxyphenyl)-9*H*-carbazole-1-sulfonamide).

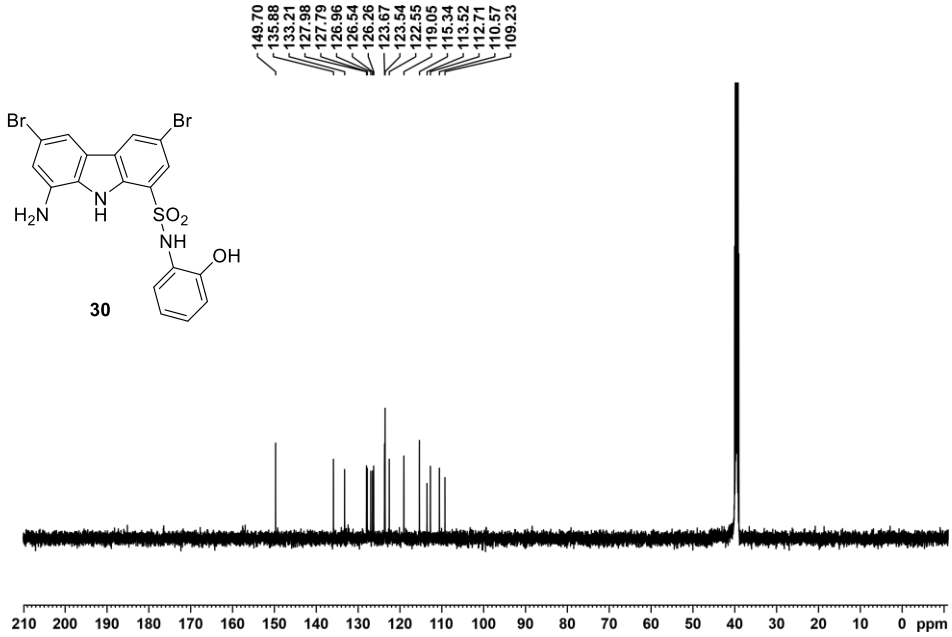

Figure 146. ^{13}C NMR (126 MHz, THF-d_8) of the compound **30** (8-amino-3,6-dibromo-*N*-(2-hydroxyphenyl)-9*H*-carbazole-1-sulfonamide).

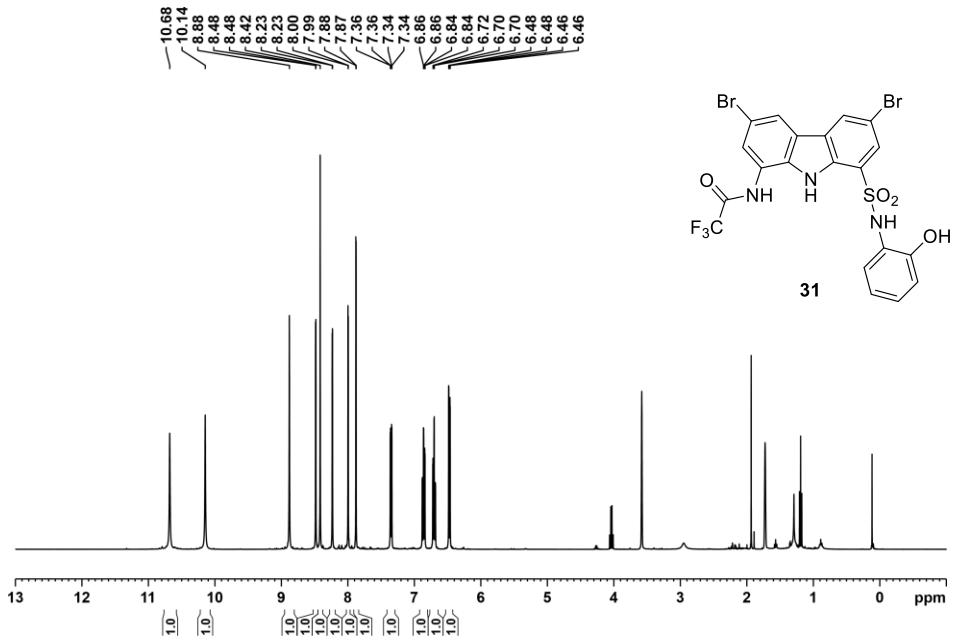

Figure 147. ^{1}H NMR (400 MHz, THF-d_8) of the compound **31** (*N*-(3,6-dibromo-8-(*N*-(2-hydroxyphenyl)sulfamoyl)-9*H*-carbazol-1-yl)-2,2,2-trifluoroacetamide).

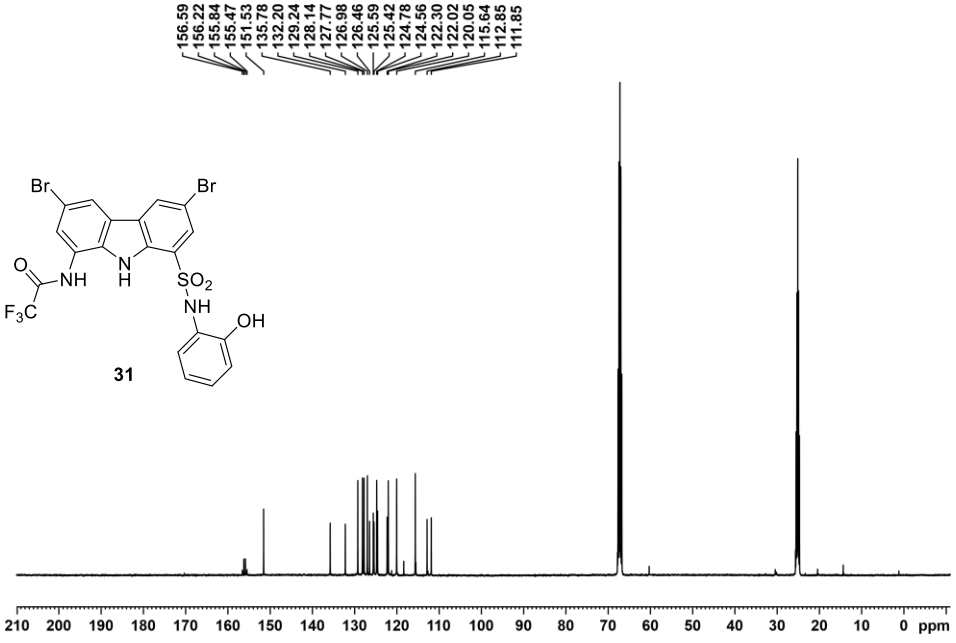

Figure 148. ^{13}C NMR (101 MHz, THF-d_8) of the compound **31** (*N*-(3,6-dibromo-8-(*N*-(2-hydroxyphenyl)sulfamoyl)-9*H*-carbazol-1-yl)-2,2,2-trifluoroacetamide).

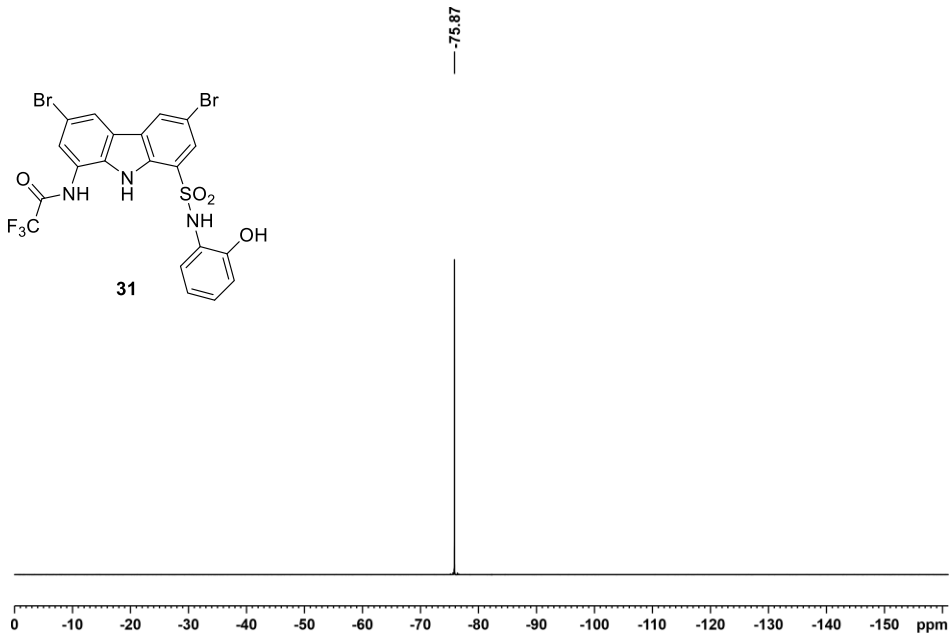

Figure 149. ^{19}F NMR (376 MHz, THF-d_8) of the compound **31** (*N*-(3,6-dibromo-8-(*N*-(2-hydroxyphenyl)sulfamoyl)-9*H*-carbazol-1-yl)-2,2,2-trifluoroacetamide).

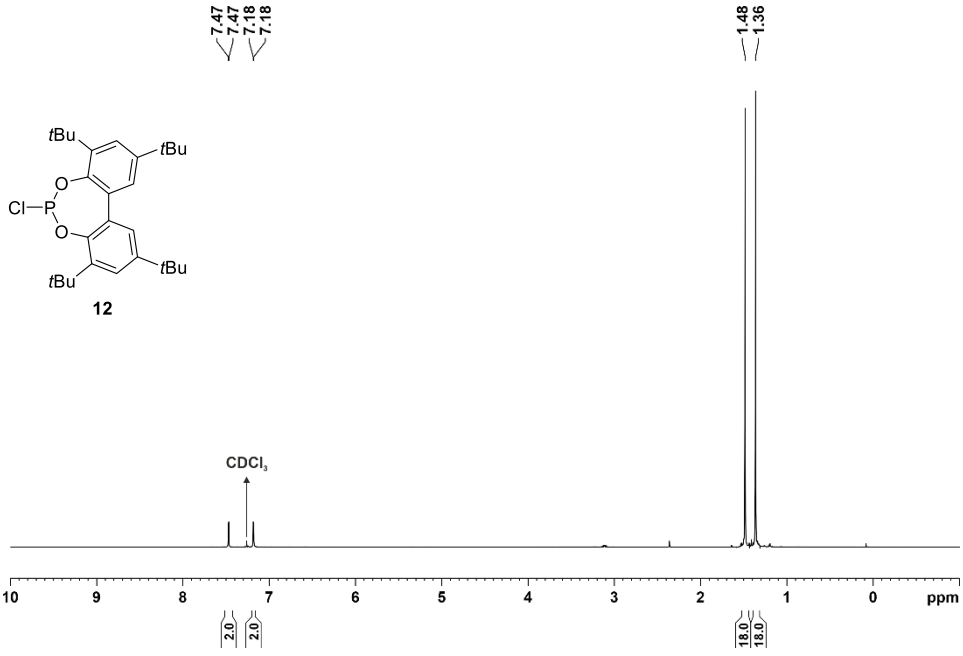

Figure 150. ^{1}H NMR (400 MHz, $CDCl_3$) of chlorophosphite **12**.

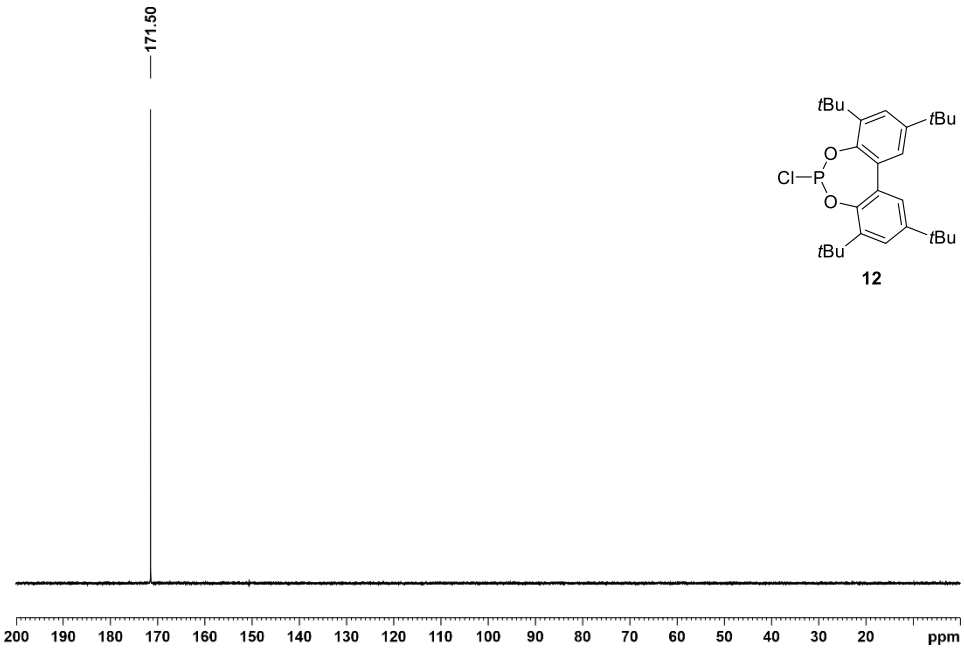

Figure 151. $^{31}P\{^{1}H\}$ NMR (162 MHz, $CDCl_3$) of chlorophosphite **12**.

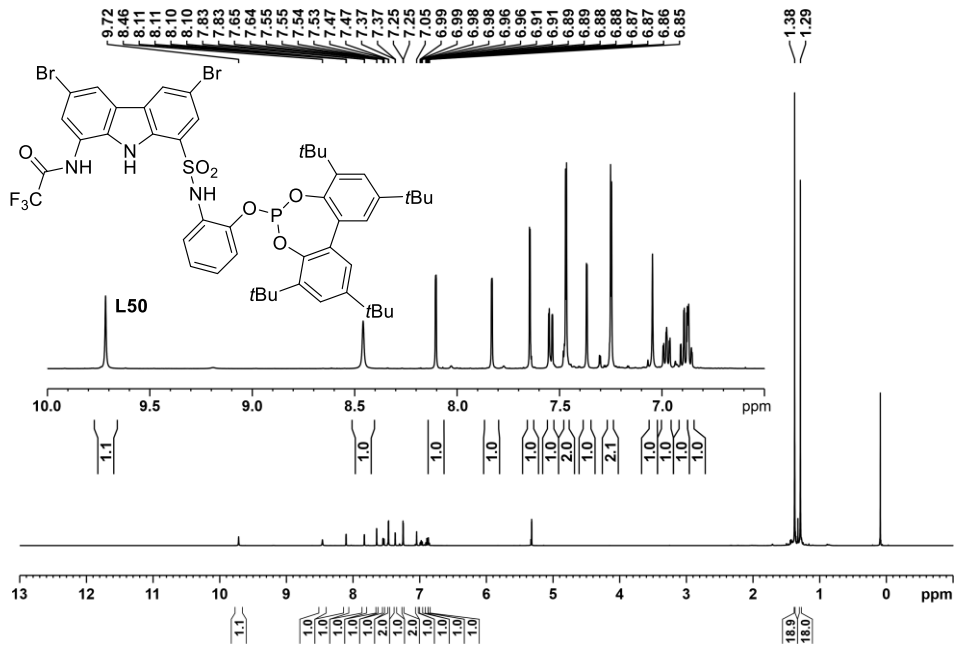

Figure 152. ^{1}H NMR (500 MHz, CD_2Cl_2) of the monophosphite **L50**.

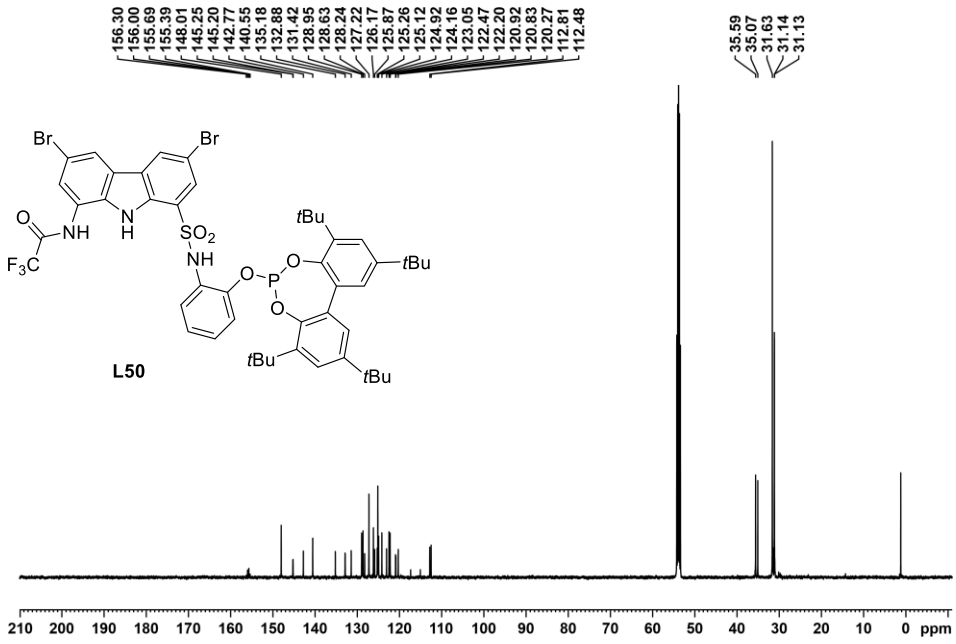

Figure 153. ^{13}C NMR (126 MHz, CD_2Cl_2) of the monophosphite **L50**.

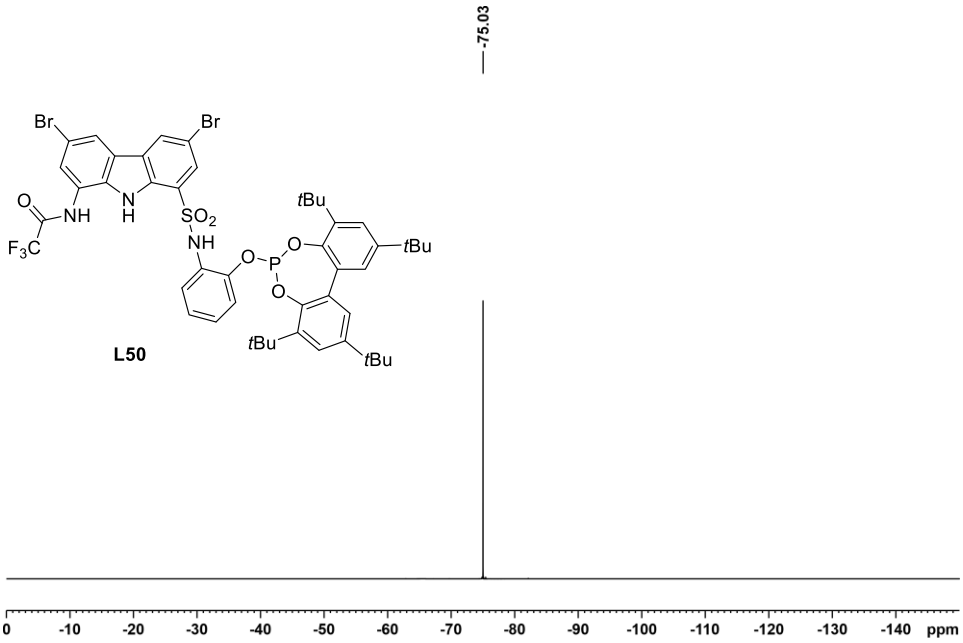

Figure 154. ^{19}F NMR (471 MHz, CD_2Cl_2) of the monophosphite **L50**.

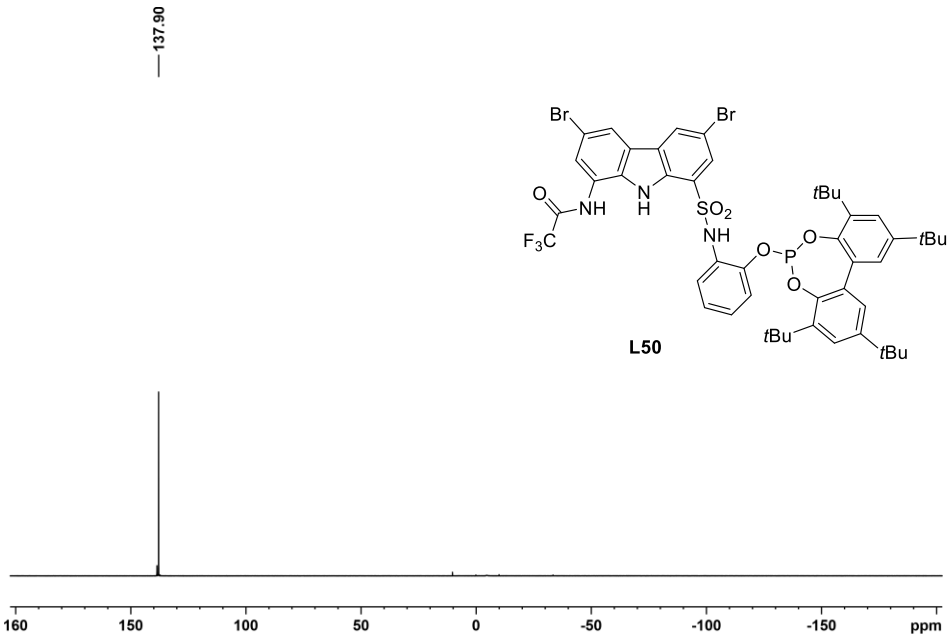

Figure 155. ^{31}P NMR (202 MHz, CD_2Cl_2) of the monophosphite **L50**.

3.5.6. NMR spectrum data of the crudes of the substrates after hydroformylation reaction.

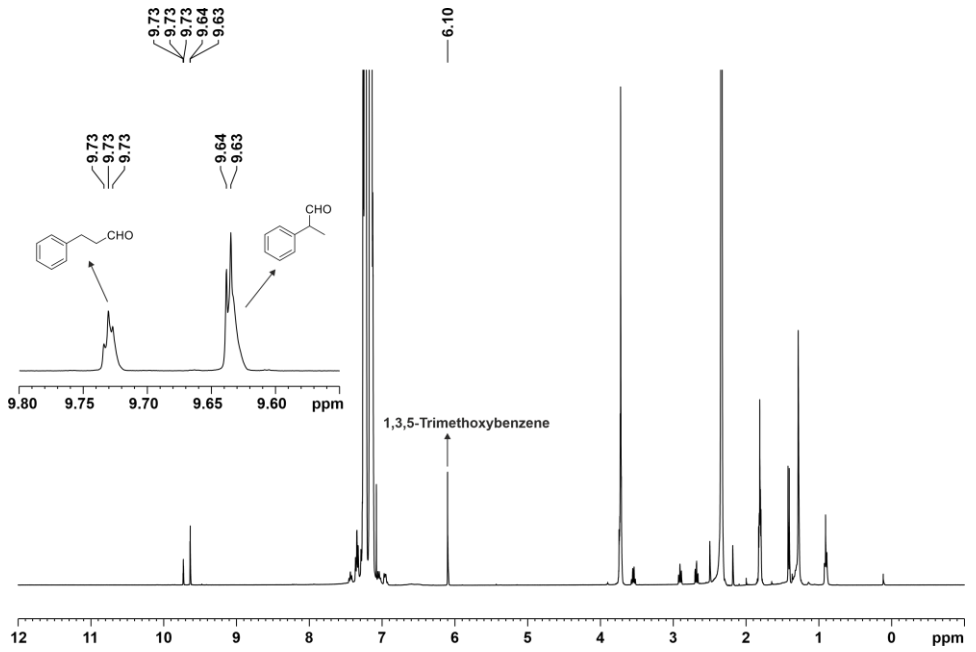

Figure 156. ^{1}H NMR of the mixtures derived from styrene after hydroformylation.

CONCLUSIONS

1. Cobalt complexes $[Co(CO)_2H(\kappa^2P,P\text{-Xantphos})]$ (**C10**) and $[(OC)_3Co(\mu\text{-}CO)_2Co(CO)(\kappa^2P,P\text{-Xantphos})]$ (**C11**) were efficiently synthesised and characterised for their application in the hydroformylation of an array of structurally diverse alkenes, differing in the position of the unsaturation and the geometry of the C=C double bond. Complexes **C10** and **C11** showed high performance as catalysts in terms of conversion and selectivity towards aldehydes in the hydroformylation of alkenes. Comparative studies employing the preformed **C11,** or complexes formed *in situ* from Xantphos and $[Co_2(CO)_8]$, indicated that the results obtained in the hydroformylation reactions were comparable, therefore demonstrating that the two strategies for the preparation of the catalysts were equally valid (*i.e.* synthesis of cobalt catalysts in advance or *in situ* generation).

The cobalt-catalysed hydroformylation of oct-1-ene employing Xantphos as a ligand was highly selective towards aldehydes under the optimised catalytic reaction conditions (**C11** or *in situ* generated catalyst with an **L5**/[Co] ratio of 0.5:1, 140 °C and 40 bar of H_2/CO at a 1:1 ratio). Furthermore, the formation of hydrogenated products, non-hydroformylated alkenes arising from the C=C isomerisation processes in the starting material and alcohol derivatives was minimised. Hydroformylations of other octenes were successfully carried out. High aldehyde selectivities were observed in all the cases. Regioselectivities for all the studied linear octene isomers remained practically constant, irrespective of the position and geometry of the double bond. These results lead us to suggest that under the effects of our Xantphos-cobalt-based catalyst, a tandem isomerisation-hydroformylation process takes place, with the isomerisation mediator $[Co(CO)_4H]$ being formed in the reaction mixture from **C11** or Xantphos/$[Co_2(CO)_8]$. We also demonstrated that this chemistry is an interesting strategy for valorising mixtures of linear hexenes, heptenes or octenes by transforming the initial mixture into one major aldehyde (addition of a CHO group to the C_1 carbon of the alkene skeleton, up to 73% selectivity).

2. Rhodium catalysts derived from supramolecular bisphosphite ligand **L46** were successfully used for linear selective hydroformylations of an array of structurally diverse alkenes and provided excellent linear ratios for terminal alkenes with aliphatic substituents (*l*/*b* ratios up to 99:1). For most of the alkenes studied, the use of a regulation agent (RA) maximised the regioselectivities of the hydroformylations (*l*/*b* ratios up to 98:2 for

hex-1-ene with NaBArF as the RA). The benefits of our regulation approach, which consists of screening a set of regulation agents to obtain the highest yield and/or selectivity for the substrate of interest, has been demonstrated in this work: the optimal catalytic system to a particular substrate was easily tailored by the choice of the regulation agent. In this work, relevant aldehydes for the fragrance industry were prepared employing supramolecular catalysts derived from ligand **L46**. Such aldehydes comprise, lauric aldehyde (**P48a**), mefranal® (**P56a**), florhydral® (**P58a**), and bourgeonal® (**P61a**). For the case of alkenes with a strong preference towards branched hydroformylation products, the linear selectivity was moderate with an increase in the linear-selectivity due to the effects of the regulation agent. The hydroformylation of internal alkynes was also achieved with supramolecularly regulated catalysts derived from **L46** with decreased amounts of the hydrogenation products and increased yield of the α,β-unsaturated aldehyde being observed with the optimal catalyst. Finally, the abovementioned supramolecularly regulated catalyst was tested in the hydroformylation of a representative allene. The addition of KBArF as regulation agent provided a remarkable maximisation in the yield of the corresponding β,γ-unsaturated aldehyde (up to 60% increase), being the formation of side-products suppressed.

The linear selective hydroformylation catalysed by supramolecular complexes derived from **L46** was successfully combined with palladium(0)-based isomerisation catalysts in order to develop an isomerisation-hydroformylation tandem reaction. With the use of only 0.5 mol% of [Pd(*t*Bu$_3$P)$_2$] and PdI$_2$, a considerable increase of the linear selectivity (up to 86%) was observed for the mixtures of i) octenes, ii) heptenes, iii) hexenes and iv) allylbenzenes.

NMR studies of the hydroformylation reaction mixtures revealed the structure of the active complex [Rh(CO)$_2$H(κ^2*P*,*P*-**L46**•RA], with the RA supramolecularly interacting with the polyether chain and the two phosphite-ligating groups being coordinated at bis-equatorial positions of the trigonal bipyramidal rhodium centre.

The monitoring of the progress of the hydroformylation reaction of hex-1-ene employing the supramolecularly regulated catalyst derived from **L46** and CsBArF by FlowNMR allowed for the determination of the structure of relevant rhodium complexes in the hydroformylation of hex-1-ene. These studies also revealed that Rh-active complexes are stable throughout the hydroformylation process.

3. The supramolecular ligand **L50** containing a recognition motif for anions was successfully synthesised through a seven-step synthetic route. All the

transformations on the starting carbazole framework took place in very high yield, with the exception of the *O*-phosphorylation reaction (33% yield) that will require further optimization studies in the future. The average yield for each step was 83%.

The monophosphite **L50** was coordinated to the standard rhodium precursor in hydroformylations (*i.e.*, [Rh(κ^2*O*,*O'*-acac)(CO)$_2$] employing a 2:1 molar ratio (**L50**/[Rh])), with the formation of the rhodium complex [Rh(κ^2*O*,*O'*-acac)(CO)(κ*P*-**L50**)] being observed. The structure of the final complex was established by ^{31}P NMR studies, which confirmed that only one of the CO groups from the starting rhodium complex was displaced by the phosphite ligating group of **L50**. The formation of active rhodium complexes in hydroformylation derived from **L50** and [Rh(κ^2*O*,*O'*-acac)(CO)$_2$] under H_2/CO atmosphere could not be confirmed.

Ligand **L50** was tested in hydroformylation obtaining high conversions and selectivities for styrene. However, the regioselectivities observed were moderate and the few performed experiments did not prove any regulation effect mediated by the only RA studied (NMe_4BF_4). Further work is required in the future to establish the potential of the use of anionic regulation agents in hydroformylation chemistry.

SUMMARY

The present doctoral thesis is focused on the design, synthesis and application of phosphorus-based complexes and supramolecular ligands in hydroformylation reactions. The reaction is the transformation of alkenes into aldehydes, which are high-value compounds that act as intermediates in organic synthesis. Aldehydes are important compounds for the fragrance and pharmaceutical industries, and hydroformylation reaction is one of the most important homogeneous catalytic reactions applied at the industrial scale. The main objective of the present research is to control the activity, chemo- and regio-selectivity towards the linear aldehydes due to their high value odour properties as fragrances.

The thesis is divided into four sections. An introduction about the hydroformylation reaction, and three chapters about the research performed during the doctoral thesis. Each chapter is divided into an abstract, introduction, results, discussion, conclusions, and experimental section. The references can be found as footnotes.

The **introduction** briefly explains the history of the hydroformylation reaction since its discovery in 1938 by Otto Roelen. It is focused on the research using cobalt and rhodium as metal precursors, and the importance of the discovery of new phosphorus-based ligands to control the activity, chemo-, regio- and enantio-selectivity of the reaction. The supramolecular regulation catalysis in hydroformylations is also explained, and other catalytic reactions are also shown applying the same supramolecular catalysis approach.

Chapter I describes the synthesis, characterization, and application cobalt catalysts bearing the Xantphos ligand (**L5**) in the hydroformylation of pure linear alkenes or their mixtures. The preformed complex $[(OC)_3Co(\mu\text{-}CO)_2Co(CO)(\kappa^2P,P\text{-Xantphos})]$ (**C11**) showed similar reactivity and selectivity towards aldehydes as the active catalyst formed *in situ* from equimolar amounts of $[Co_2(CO)_8]$ and Xantphos (**L5**). In the case of oct-1-ene, the linear aldehyde was obtained with good chemo- and regio-selectivity (linear to branched ratio was up to 75:25). For all octene isomers, tandem isomerisation-hydroformylation processes took place. Regioselectivities for all the studied octene isomers remained practically constant, independently of the position or geometry of the C=C double bond in the starting material. Moreover, by-products were formed in similarly small amounts for all the octene isomers. We also demonstrated that this chemistry is an interesting strategy for valorising mixtures of linear hexenes, heptenes or octenes by transforming the initial mixture into one major aldehyde (addition of a CHO

group to the C_1 carbon of the alkene skeleton, up to 73% selectivity). Moreover, these mixtures of alkenes were hydroformylated with low final amounts of non-hydroformylated alkenes, hydrogenated alkenes, and alcohols.

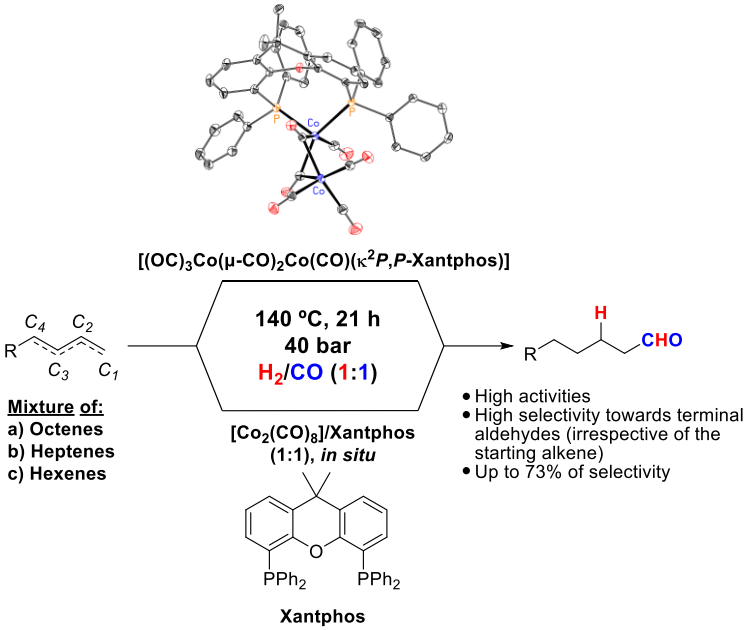

Scheme 60. Cobalt-Xantphos catalyst for isomerisation-hydroformylation tandem reactions.

Chapter II discloses the use of rhodium hydroformylation catalysts derived from supramolecular bisphosphite ligand (**L46**), with a polyether chain as the regulation side, combined with an alkali metal BArF salt as the regulation agent (RA). The use of the matched RA for a given substrate led to excellent activity and maximised regioselectivity towards the linear aldehyde (linear to branched ratios up to 99%). The supramolecular regulation catalyst was also applied to obtain value-added aldehydes for the fragrance industries, such as lauric aldehyde, mefranal®, florhydral® and bourgenal® (Scheme 61). In addition, the supramolecular catalyst was combined with Pd(0) catalysts leading to efficient conditions for a tandem isomerisation-hydroformylation process in a mixture of alkenes such as octenes, heptenes, hexenes, or allylbenzenes (37%, 46%, 57% and 86% of linear aldehyde, respectively). The catalytic species, which are present in the catalytic cycle, as well as conversion curves for the hydroformylations of hex-1-ene, have been studied by High-Pressure NMR complexation studies and by FlowNMR *operando* spectroscopy.

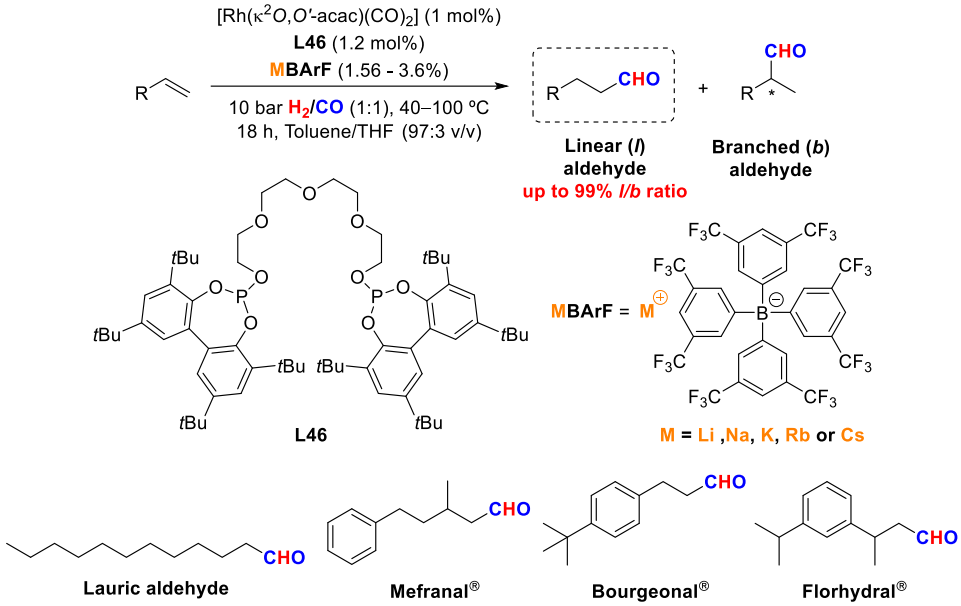

Scheme 61. Supramolecularly regulated hydroformylation towards the linear aldehyde.

Chapter III describes the design and synthesis of a monophosphite ligand based on a carbazole scaffold. The purpose of synthesising this ligand was to supramolecularly control the activity and regioselectivity in hydroformylation reactions employing anionic regulation agents. In an analogous manner to the regulation strategy developed in our group involving cation recognition, we hypothesised that the combined use of a suitably designed monophosphite ligand **L50** (Figure 158), a rhodium precursor for hydroformylation reactions and an anionic regulation agent would lead to rhodium complexes with a catalytic site whose geometry, rigidity and/or conformational flexibility would depend on the size and shape of the regulation agent used. The ultimate goal of this approach was to maximise the activity and/or selectivity of the hydroformylation catalyst by the choice of the RA. The synthesis of a first generation of supramolecularly regulated catalysts derived from the 2-((8-amino-9*H*-carbazole)-1-sulfonamido)phenyl phosphite ligand **L50**, the preliminary studies on the hydroformylation of one benchmark alkene and the effects of anionic regulation are described herein.

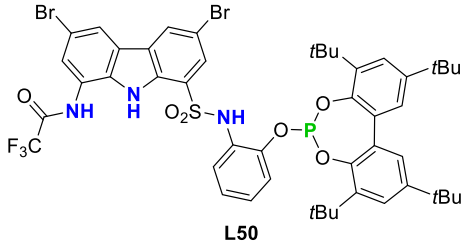

L50

Figure 157. Supramolecular ligand **L50**.

RESUMEN

La presente tesis doctoral se centra en el diseño, síntesis y aplicación de complejos basados en fósforo y ligandos supramoleculares para reacciones de hidroformilación. Dicha reacción consiste en la transformación de alquenos en aldehídos, los cuales son compuestos orgánicos de alto valor que actúan como intermedios en síntesis orgánica. Los aldehídos también son compuestos importantes para la industria farmacéutica y de fragancias. La hidroformilación es una de las reacciones de catálisis homogéneas más importantes aplicadas a escala industrial. El principal objetivo de la presente investigación es controlar la actividad, quimio- y regio-selectividad hacia los aldehídos lineales debido a sus propiedades olfativas de alto valor para fragancias.

La tesis está dividida en cuatro capítulos. Una introducción general sobre la reacción de hidroformilación y tres capítulos sobre la investigación realizada durante la presente tesis doctoral. Cada capítulo se divide en las siguientes secciones: resumen, introducción, resultados, discusión, conclusiones y sección experimental. Las referencias se pueden encontrar como notas a pie de página.

En la introducción se explica brevemente la historia de la reacción de hidroformilación desde su descubrimiento en 1938 por Otto Roelen. Se centra en la investigación utilizando cobalto y rodio como precursores metálicos, y la importancia del descubrimiento de nuevos ligandos basados en fósforo para controlar la actividad, quimio-, regio- y enantio-selectividad de la reacción. También se explica la catálisis regulada supramolecularmente para la reacción de hidroformilación, y también se muestran otras reacciones catalíticas aplicando la misma estrategia de catálisis regulada supramolecularmente.

En el **capítulo I** se describe la síntesis, caracterización y aplicación de catalizadores activos derivados del cobalto y el ligando Xantphos (**L5**) en la hidroformilación de alquenos lineales puros o sus mezclas. Se observó que el complejo preformado $[(OC)_3Co(\mu\text{-}CO)_2Co(CO)(\kappa^2\textit{P},\textit{P}\text{-Xantphos})]$ (**C11**) mostraba una reactividad y selectividad similares hacia los aldehídos que el catalizador activo generado *in situ* a partir de cantidades equimolares de $[Co_2(CO)_8]$ y Xantphos (**L5**). En el caso del 1-octeno, el aldehído lineal se obtuvo con buena quimio y regio-selectividad (la relación *l*/*b* fue de hasta 75:25). Para todos los isómeros de octeno, se llevaron a cabo reacciones en tándem de isomerización-hidroformilación. Las regioselectividades para todos los isómeros del octeno estudiados permanecieron prácticamente constantes, independientemente de la posición o geometría del doble enlace

C=C del sustrato de partida. Además, se formaron subproductos en cantidades igual de escasas para todos los isómeros de octeno. También demostramos que esta química es una estrategia interesante para valorizar mezclas de hexenos, heptenos u octenos lineales mediante la transformación de la mezcla inicial en un aldehído mayoritario (adición de un grupo CHO al carbono C_1 de la estructura del alqueno, hasta un 73 % de selectividad). Además, estas mezclas de alquenos se hidroformilaron con bajas cantidades finales de alquenos no hidroformilados, alquenos hidrogenados y alcoholes (Esquema 62).

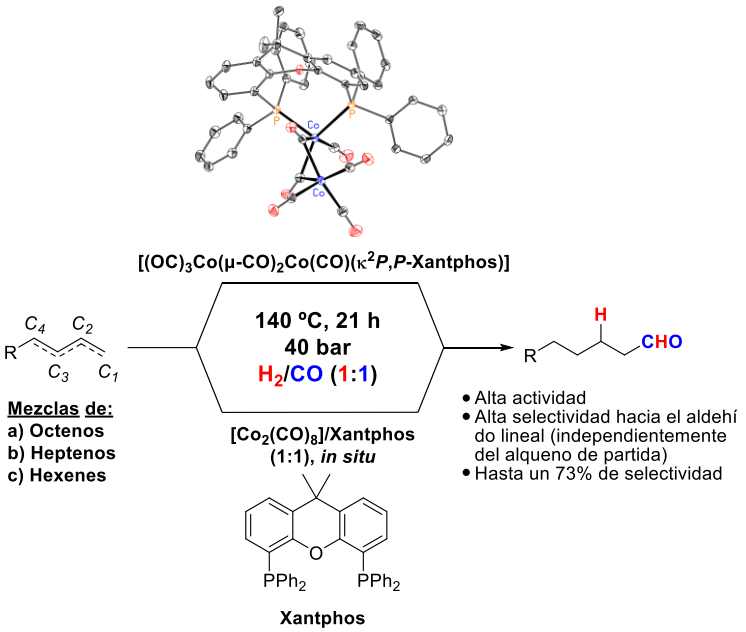

Esquema 62. Catalizador de cobalto-Xantphos para reacciones en tándem de isomerización/hidroformilación.

En el **capítulo II** se describe el uso de catalizadores de hidroformilación de rodio derivados de un ligando bisfosfito supramolecular (**L46**), con un centro de regulación alejado del centro catalítico, combinados con una sal BArF de metales alcalinos como agentes de regulación (RA). El uso de un agente de regulación específico para cada sustrato dio lugar a una excelente actividad y maximizó la regioselectividad hacia el aldehído lineal (relación *l/b* de hasta un 99%). El catalizador de regulación supramolecular también se aplicó para obtener aldehídos de interés para la industria de fragancias, tales como el aldehído láurico, el mefranal®, el florhydral® y el bourgenal® (Esquema 63). Además, el catalizador supramolecular se combinó con catalizadores de Pd(0) que dieron lugar a condiciones eficientes para un proceso en tándem de isomerización-hidroformilation de una mezcla de alquenos como por ejemplo

octenos, heptenos, hexenos o alilbencenos (37%, 46%, 57% y 86% de aldehído lineal, respectivamente). Las especies catalíticas, que están presentes en el ciclo catalítico, así como las curvas de conversión para la hidroformilación del 1-hexeno, fueron estudiadas por estudios de complejación de RMN a alta presión y por espectroscopía *operando* de RMN en flujo.

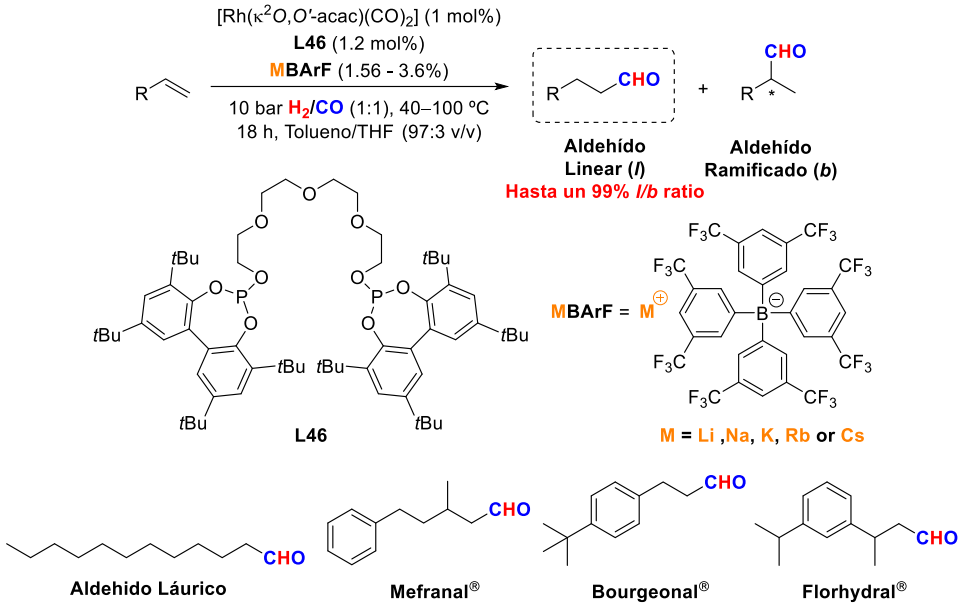

Esquema 63. Hidroformilaciones reguladas supramolecularmente hacia el aldehído lineal.

El **capítulo III** describe el diseño y la síntesis de un ligando monofosfito basado en la estructura del carbazol. El propósito de sintetizar este ligando fue controlar supramolecularmente la actividad y regioselectividad en reacciones de hidroformilación empleando agentes de regulación aniónicos. De manera análoga a la estrategia de regulación desarrollada en nuestro grupo que involucra el reconocimiento de cationes, planteamos la hipótesis de que el uso combinado del ligando monofosfito **L50** (Figura 159) adecuadamente diseñado, junto con un precursor de rodio para reacciones de hidroformilación y un agente de regulación aniónico conduciría a complejos de rodio con un sitio catalítico cuya geometría, rigidez y/o flexibilidad conformacional dependería del tamaño y forma del agente de regulación utilizado. El objetivo final de esta aproximación era maximizar la actividad y/o selectividad del catalizador de hidroformilación mediante la elección del agente de regulación idóneo. En esta sección se describe la síntesis de una primera generación de catalizadores regulados supramolecularmente derivados del ligando **L50** 2-((8-amino-9*H*-carbazol)-1-sulfonamido)fenil fosfito, los estudios

preliminares sobre la hidroformilación de un alqueno de referencia y los efectos de la regulación aniónica.

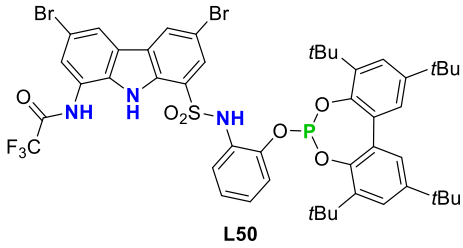

L50

Figura 159. Ligando supramolecular **L50**.

RESUM

Aquesta tesi doctoral es centra en el disseny, la síntesi i l'aplicació de complexos basats en fòsfor i lligands supramoleculars per reaccions d'hidroformilació. Aquesta reacció consisteix en la transformació d'alquens en aldehids, els quals són compostos d'alt valor com a intermedis a síntesi orgànica. Els aldehids també són compostos importants a la indústria farmacèutica i de fragàncies. La hidroformilació és una de les reaccions de catàlisis homogènia més importants aplicades a escala industrial. El principal objectiu de la present investigació és controlar l'activitat, quimio- i regio-selectivitat cap als aldehids lineals a causa de les seves propietats olfactives d'alt valor per fragàncies.

La tesi està dividida en quatre capítols. Una introducció general sobre la reacció d'hidroformilació i tres capítols sobre la investigació realitzada durant aquesta tesi doctoral. Cada capítol es divideix en les seccions següents: resum, introducció, resultats, discussió, conclusions i secció experimental. Les referències es poden trobar com a notes a peu de pàgina.

A la introducció s'explica breument la història de la reacció d'hidroformilació des del seu descobriment el 1938 per Otto Roelen. Se centra en la recerca utilitzant cobalt i rodi com a precursors metàl·lics, i la importància del descobriment de nous lligands basats en fòsfor per controlar l'activitat, quimio-, regio- i enantio-selectivitat de la reacció. També s'explica la catàlisi regulada supramolecularment per a la reacció d'hidroformilació i també es mostren altres reaccions catalítiques aplicant la mateixa estratègia de catàlisi regulada supramolecularment.

Al **capítol I** es descriu la síntesi, caracterització i aplicació de catalitzadors actius derivats del cobalt i el lligand Xantphos (**L5**) en la hidroformilació d'alquens lineals purs o les seves barreges. Es va observar que el complex preformat $[(OC)_3Co(\mu\text{-}CO)_2Co(CO)(\kappa^2P,P\text{-Xantphos})]$ (**C11**) mostrava una reactivitat i selectivitat similars cap als aldehids que el catalitzador actiu generat *in situ* a partir de quantitats equimolars de $[Co_2(CO)_8]$ i Xantphos (**L5**). En el cas de l'1-octè, l'aldehid lineal es va obtenir amb bona quimio- i regio-selectivitat (la relació *l*/*b* va ser de fins a 75:25). Per a tots els isòmers d'octè, es van dur a terme reaccions en tàndem d'isomerització-hidroformilació. Les regioselectivitats per a tots els isòmers d'octè estudiats es van mantenir pràcticament constants, independentment de la posició o geometria del doble enllaç C=C del substrat de partida. A més, es van generar subproductes en quantitats igual d'escasses per tots els isòmers de l'octè. També demostrem que aquesta química és una estratègia interessant per valoritzar barreges

d'hexens, heptens o octens lineals mitjançant la transformació de la barreja inicial en un aldehid majoritari (addició d'un grup CHO al carboni C_1 de l'estructura de l'alquè, fins a un 73% de selectivitat). A més, aquestes barreges d'alquens es van hidroformilar amb baixes quantitats finals d'alquens no hidroformilats, alquens hidrogenats i alcohols (Esquema 64).

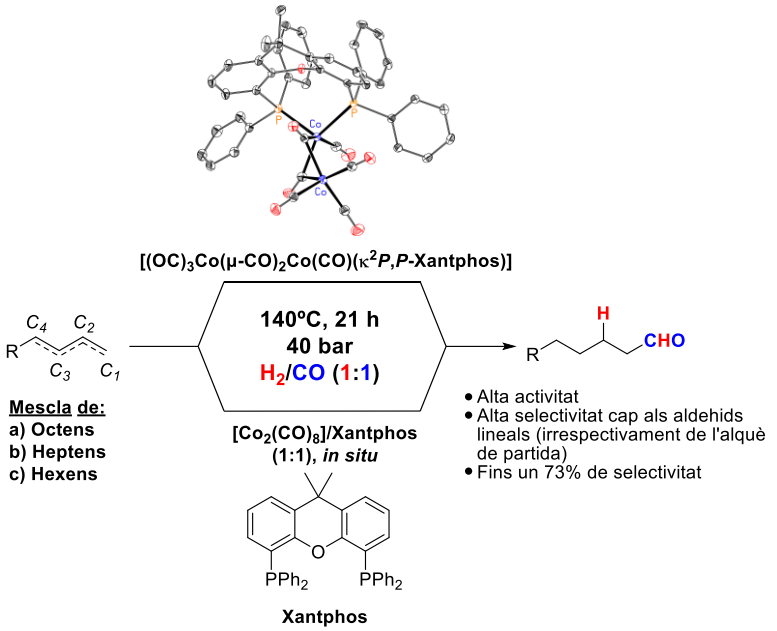

Esquema 64. Catalitzador de cobalt-Xantphos per reaccions en tàndem d'isomerització/hidroformilació.

Al **capítol II** es descriu l'ús de catalitzadors d'hidroformilació de rodi derivats d'un lligand bisfosfit supramolecular (**L46**), amb un centre de regulació allunyat del centre catalític, combinats amb una sal BArF de metalls alcalins com a agents de regulació (RA). L'ús d'un agent de regulació específic per a cada substrat va donar lloc a una activitat excel·lent i va maximitzar la regioselectivitat cap a l'aldehid lineal (relació *l/b* de fins un 99%). El catalitzador de regulació supramolecular també es va aplicar per obtenir aldehids d'interès per a la indústria de fragàncies, com ara l'aldehid làuric, el mefranal®, el florhydral® i el bourgenal® (Esquema 65). A més, el catalitzador supramolecular es va combinar amb catalitzadors de Pd(0) que van donar lloc a condicions eficients per a un procés en tàndem d'isomerització-hidroformilació d'una barreja d'alquens com ara octens, heptens, hexens o alilbenzens (37%, 46% , 57% i 86% d'aldehid lineal, respectivament). Les espècies catalítiques, que són presents en el cicle catalític, així com les corbes de conversió per a la hidroformilació de l'1-hexè, van ser estudiades per estudis

de complexació de RMN a alta pressió i per espectroscòpia *operando* de RMN en flux.

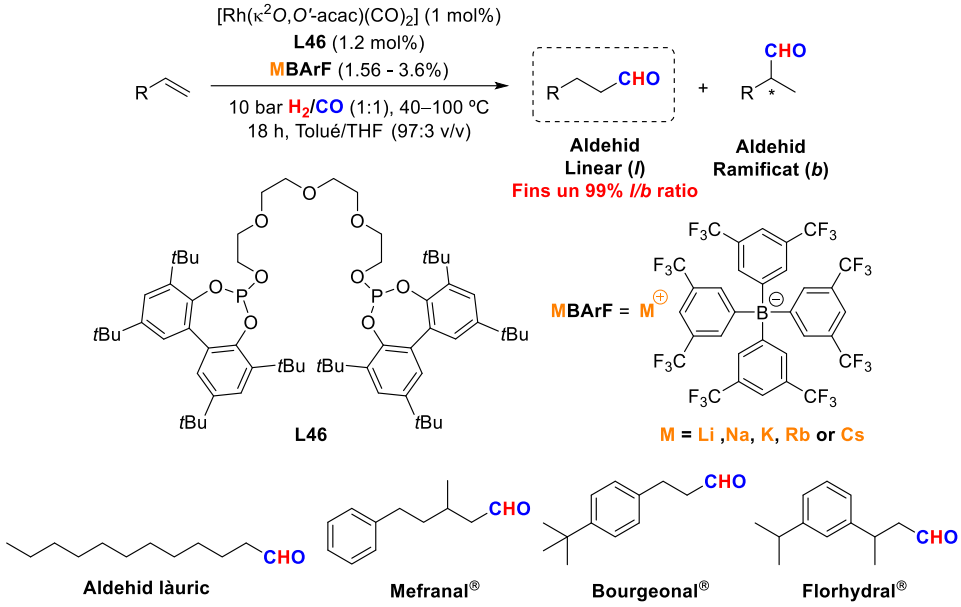

Esquema 65. Hidroformilacions regulades supramolecularment cap a l'aldehid lineal.

El **capítol III** descriu el disseny i la síntesi d'un lligand monofosfit basat en l'estructura del carbazole. El propòsit de sintetitzar aquest lligand va ser controlar supramolecularment l'activitat i la regioselectivitat en reaccions d'hidroformilació emprant agents de regulació aniònics. De manera anàloga a l'estratègia de regulació desenvolupada al nostre grup que involucra el reconeixement de cations, plantegem la hipòtesi que l'ús combinat del lligand monofosfit **L50** (Figura 160) adequadament dissenyat, un precursor de rodi per a reaccions d'hidroformilació i un agent de regulació aniònic conduiria a complexos de rodi amb un lloc catalític la geometria del qual, rigidesa i/o flexibilitat conformacional dependria de la grandària i forma de l'agent de regulació utilitzat. L'objectiu final d'aquesta estratègia era maximitzar l'activitat i/o selectivitat del catalitzador d'hidroformilació mitjançant l'elecció idònia de l'agent de regulació. En aquest capítol es descriu la síntesi d'una primera generació de catalitzadors regulats supramolecularment derivats del lligand **L50** 2-((8-amino-9*H*-carbazole)-1-sulfonamido)fenil fosfit,

els estudis preliminars sobre la hidroformilació de un alquè de referència i els efectes de la regulació aniònica.

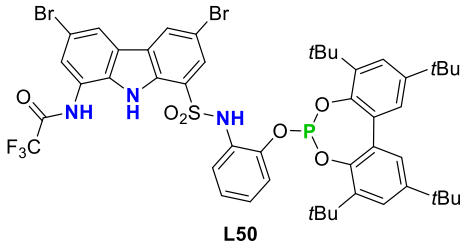

L50

Figura 160. Lligand supramolecular **L50**.

UNIVERSITAT
ROVIRA i VIRGILI

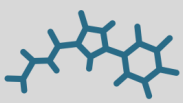

ICIQ

Institute of Chemical
Research of Catalonia